



**ISTITUTO NAZIONALE DI FISICA NUCLEARE**  
**Laboratori Nazionali di Frascati**

**FRASCATI PHYSICS SERIES**



Proceedings of  
**HEAVY QUARKS AND LEPTONS 2004**

Editor  
**A. López**

Proceedings of  
**HEAVY QUARKS AND LEPTONS 2004**

FRASCATI PHYSICS SERIES

Series Editor  
*Stefano Bianco*

Technical Editor  
*Luigina Invidia*

---

Volume XXXV

---

Istituto Nazionale di Fisica Nucleare – Laboratori Nazionali di Frascati  
Divisione Ricerca – SIS – Ufficio Pubblicazioni  
P.O. Box 13, I-00044 Frascati (Roma) Italy



FRASCATI PHYSICS SERIES

Proceedings of the  
**HEAVY QUARKS AND LEPTONS 2004**

Copyright © 2004, by INFN

*All rights reserved. No part of this publication may be reproduced, stored in a retrieval system or transmitted, in any form or by any means, electronic, mechanical, photocopying, recording or otherwise, without the prior permission of the copyright owner.*

ISBN-88 -86409-43-5

Printed in Italy  
Poligrafica Laziale, Frascati (Roma) Italia

FRASCATI PHYSICS SERIES

Volume XXXV

**HEAVY QUARKS AND LEPTONS 2004**

Editor  
Angel López



University of Puerto Rico at Mayagüez  
San Juan, Puerto Rico, 1-5 June 2004

*International Advisory Committee*

Angel López	<i>University of Puerto Rico, PR</i>
Ikaros Bigi	<i>University of Notre Dame, USA</i>
Brad Cox	<i>University of Virginia, USA</i>
Stephan Paul	<i>T.U. Muenchen, Germany</i>
Stefano Bianco	<i>INFN-Frascati, Italy</i>
Konrad Kleinknecht	<i>University of Mainz, Germany</i>
Giancarlo D'Ambrosio	<i>INFN-Napoli, Italy</i>
Franco L. Fabbri	<i>INFN-Frascati, Italy</i>
Alberto Reis	<i>CBPF, Brazil</i>
Gianpaolo Bellini	<i>University of Milano, Italy</i>
Joel Butler	<i>Fermilab, USA</i>
Peter Dornan	<i>Imperial College London, UK</i>
Vera Luth	<i>SLAC, USA</i>
Hitoshi Yamamoto	<i>Tohoku University, Japan</i>
Ritchie Patterson	<i>Cornell University, USA</i>
Adam Para	<i>Fermilab, USA</i>
Franco Grancagnolo	<i>INFN-Lecce, Italy</i>

*Local Organizing Committee*

Héctor Mendez	<i>University of Puerto Rico</i>
Eduardo Ramirez	<i>University of Puerto Rico</i>
Jose Nieves	<i>University of Puerto Rico</i>
Sandra Troche	<i>University of Puerto Rico</i>

*Conference Chairman*

Angel M. López	<i>University of Puerto Rico</i>
----------------	----------------------------------

*Secretariat*

Sandra Troche

*Sponsor*

University of Puerto Rico  
U.S. Department of Energy  
P.R. Tourism Office

## CONTENTS

<b>Opening</b> .....	1
H. R. Quinn      Opening Talk for Heavy Quarks and Lepton 2004 .....	3
<b>SESSION I – Neutrinos</b> .....	<b>23</b>
S. Parke      Neutrino Oscillations Phenomenology .....	25
J. Link      Using Reactor Neutrinos to Study Neutrino Oscillations .....	24
J. Bonn      Neutrino Mass Limits from Tritium Beta Decay, Present Limits and Perspectives for KATRIN .....	29
A. Giuliani      Search for Neutrinoless Double Beta Decay: Present and Future .....	41
P. Langacker      Neutrinos and Astrophysics .....	51
T. Kajita      Neutrinos Atmospheric: Past, Present and Future .....	53
I. Stancu      The LSND Signal: Past, Present and Future.....	63
A. Ereditato      Present Status and Prospects of Neutrino Oscillation Experiments .....	73
M. V. Diwan      The Case for a Super Neutrino Beam .....	89
<b>SESSION II – CP Violation I – B Decays</b> .....	<b>111</b>
H. Yamamoto      Search for new CP violating phases by Belle .....	113
M. C. Simani      Measurements Related to the CKM Angle $\beta/\phi_1$ from BABAR .....	115
K. E. Ford      Measurement of the CKM Angles $\alpha$ and $\gamma$ at the BABAR Experiment .....	125
R. Itoh      Measurements of $\phi_3/\gamma$ with $B \rightarrow D^{(*)} K$ and $B \rightarrow D^{(*)} \pi$ at Belle.....	135
<b>SESSION III – CP Violation II – Strange and Charm Sectors</b> .....	<b>137</b>
A. Maier      Charged Kaon Decays at NA48: Current Status and Future Plans .....	139
A. Ledovskoy      KTeV Results on CP Violation in $K_L \rightarrow \pi^+ \pi^- e^+ e^-$ .....	141
K. Nelson      Search for CP violation in Hyperon Decays and Measurement of Hyperon Decay Parameters .....	149
D. Asner      CP Violation Results in Charm .....	151
K. Flood      Review of Charm Mixing .....	163

<b>SESSION IV – Searches for Pentaquarks .....</b>	<b>175</b>
H. J. Lipkin	The Theory of Pentaquarks ..... 177
L. Stanco	Pentaquark Searches at HERA ..... 187
D. J. Tedeschi	Pentaquark Searches with Intermediate Energy Probes ..... 189
<b>SESSION V – CKM Matrix Elements from D and B Decays .....</b>	<b>197</b>
A. Gray	Unquenched Lattice Gauge Theory Calculations for Semileptonic $B, D$ Decays ..... 199
J. Wiss	Review of Charm Semileptonic Decays..... 209
C.W. Bauer	Inclusive Determinations of $ V_{ub} $ and $ V_{cb} $ ..... 221
D. Fortin	Measurement of $ V_{cb} $ and HQE Parameters from Semileptonic B Decays ..... 231
C. Schwanda	New Methods for $ V_{ub} $ Determination ..... 241
C. Stepaniak	Spectral moments from B Decays at CLEO ..... 243
<b>SESSION VI – CKM Matrix Elements from K Decays .....</b>	<b>245</b>
P. Talavera	Extraction of CKM Parameters - K Decays ..... 247
A. Antonelli	$V_{us}$ From $K^0$ Semileptonic Decays at KLOE ..... 249
K. Kleinknecht	Mesurement of the Branching Ratio of the Decay $K_L \rightarrow \pi^\pm e^\mp \nu$ and the Coupling Constant $V_{us}$ ..... 259
A. Sher	Measurement of the $K^+ \rightarrow \pi^0 e^+ \nu (K_{e3}^+)$ Branching Ratio by E865 at Brookhaven National Laboratory ..... 273
R. Kessler	KTev Determination of the CKM Parameter $ V_{us} $ ..... 281
<b>SESSION VII – Heavy Quark Decays .....</b>	<b>291</b>
G. Boca	Beauty and Charm Lifetimes. An Experimental Review ..... 293
L. Moroni	Dalitz Plot Analysis of D Decays ..... 303
<b>SESSION VIII – Heavy Quark Production .....</b>	<b>317</b>
G. Gómez-Ceballos	Heavy Quark Production at the Tevatron ..... 319
F. Di Capua	Study of Neutrino Induced Charm-Production with the Chorus Experiment ..... 329
F. Sefkow	Heavy Quark Production in Electron-Proton Collisions at HERA..... 343

<b>SESSION IX – Onia States .....</b>	<b>345</b>	
J. M. Yelton	First Results from CLEO-c .....	347
Z. Metreveli	Heavy Quarkonia .....	357
<b>SESSION X – Rare Decays .....</b>	<b>367</b>	
M. M. Velasco	Latest Results from NA48 on $K_L$ & $K_S$ CP Violating Related Rare Decays .....	369
E. Cheu	KTeV Results on Rare Kaon Decays .....	379
D. E. Jaffe	E949 $K^+ \rightarrow \pi^+ \nu \bar{\nu}$ Results .....	387
D. Nicolò	Status and Perspectives in $\mu \rightarrow e \gamma$ Decay Search .....	393
M.-C. Chuan	New Results on $B \rightarrow VV$ and $PV$ Modes .....	401
P. D. Jackson	Rare B Decays.....	411
<b>SESSION XI – D Meson Spectroscopy .....</b>	<b>421</b>	
T. Barnes	Recent Developments in Charm Spectroscopy: $X(3872)$ , $D^*_{sJ}(2317)^+$ and $D_{sJ}(2463)^+$ .....	423
H. Guler	What Are the $X(3872)$ and $D_{sJ}$ Particles? .....	435
R. K. Kutschke	Charmed Meson Spectroscopy .....	445
<b>SESSION XII – Leptons .....</b>	<b>453</b>	
W. M. Morse	IMPLICATIONS OF THE NEW RESULTS ON g-2 .....	455
I. Logashenko	Mesurement of the Total Hadronic Cross-Section at $e^+e^-$ Machines .....	457
W. M. Morse	Electric Dipole Moment Measurements in a Storage Ring .....	467



## ***Opening***

*H.R. Quinn    Opening Talk for Heavy Quarks and Leptons 2004*



Frascati Physics Series Vol. XXXV (2004), pp. 3–22  
HEAVY QUARKS AND LEPTONS - San Juan, Puerto Rico, June 1-5, 2004

## OPENING TALK FOR HEAVY QUARKS AND LEPTONS 2004

Helen R. Quinn  
*Stanford Linear Accelerator Center*  
*2575 Sand Hill Road, Menlo Park, California 94025*

### ABSTRACT

Before preparing this talk I asked our host Angel Lopez what he wanted from an opening talk—his response was that I should set the context for what follows, to get the audience to think about the future of this subfield of physics, and give some of my own opinions on this area of physics. So that is what this talk does. It highlights a biased selection of topics; there is much more in the week of lectures than I can cover in this introductory talk.

### 1 What are the deep questions in this field?

A few questions are mentioned often as the deep puzzles of flavor physics, questions such as

- Why are there multiple generations?

- Do the patterns of mass and mixing tell us anything?
- Can we understand the CP asymmetry of the Universe?

Let us begin by talking about these for a while.

My own reaction to the first question is to remark that in our science we never actually answer the question “Why?” in the conventional sense. In everyday situations any answer to that question is a description of a mechanism that occurs at some smaller scale and explains the behavior seen at the scale where the question was asked. Most of us think it is likely that quarks and leptons have no smaller scale structure, because attempts to answer the above questions via substructure for quarks and leptons have failed miserably. Once we are dealing with elementary particles there can be no mechanism at a smaller scale to provide reasons for an observed behavior or pattern. Thus all we can do is find the underlying mathematical theory that describes what we observe and can predict future results. We convert “why?” into questions like the following:

- What underlying symmetry or conservation law that forbids this process?
- What mathematical structures can be predictive about these features of the physics?

The Standard Model describes the physics of flavor, though it must be extended to encompass neutrino masses. The deep questions about flavor are not addressed by its mathematical structures. It allows, but does not require, multiple generations. The Yukawa couplings of the fermions to the Higgs field give all the flavor structure we observe. We have a set of arbitrary parameter choices, not an explanation in even the limited sense discussed above.

One might be tempted to argue that the observed CP violation in the quark sector of the Standard Model requires three quark generations<sup>1)</sup>. That is not strictly true, one could equally well have violation with two generations and two complex Higgs-type multiplets<sup>2)</sup>. We do not know yet whether nature uses both of these possibilities for CP violation, or only one of them. The success of the CKM picture shows that the weak-coupling phases are non-trivial and dominate the CP violation so far observed. Even if this is the dominant source of CP violation, we cannot call it an “explanation” for the existence of three generations.

Neutrinos have mass, even though they are not “heavy” in the traditional sense of this conference series. Thus they are an important part of the physics of flavor and should be a major part of this meeting’s agenda, as indeed they are. (Perhaps the series title should change to “the Physics of Flavor”.) Neutrino masses can be accommodated by extending the Standard Model a little, at the price of a larger set of arbitrary Yukawa coupling parameters. In addition we need an arbitrary large Majorana-type mass term to generate the small neutrino masses via a see-saw mechanism.

Even when we extend the Standard Model to a grand unified theory, or add supersymmetry we get no real answer to our questions about flavor structure. Many such extensions do have the benefit of making the additional neutrino states needed for a massive neutrino theory unavoidable, rather than an arbitrary, and somewhat uncomfortable, addition to the theory. We also gain relationships between quark and lepton parameters from the multiplet structure of a Grand Unified theory. However, the predictions with a single multiplet type do not fit the observed mass and mixing patterns, so different in the quark sector and the neutrino sector. Grand unified theories with no  $B-L$  violating terms predict similar patterns in the two sectors. I think it is a fair statement of history to say that it was only after the data pointed the way that the focus turned to theories that accommodate two very different patterns. So these patterns were not a prediction, but they can be fit by some choice of representation content and possibly some added  $U(1)$  symmetry that distinguishes the generations <sup>3)</sup>.

Some attempts to explain mass and mixing patterns use an approach known as “textures” where a particular pattern of zeros in the coupling matrix is assumed. If this approach can give an acceptable set of physical parameters, one then needs some deeper reason for the texture, coming from a symmetry or an underlying theory. An added  $U(1)$  flavor-distinguishing symmetry such as mentioned above can perhaps provide this. Then the apparently symmetry-breaking mass terms can arise in an effective field theory as higher-dimensional products of fields, with some powers of a gauge-group singlet field that carries one unit of the flavor charge. Such terms are assumed to be suppressed by denominator powers of a large mass.

One of the initial great hopes of string theory was that, in addition to solving the problem of formulating a finite theory of quantum gravity, it would

be predictive about the number of generations and the parameters of the flavor sector. This does not seem to be the case. One can find ways to wrap branes on the topological cycles of the extra six dimensional (Calabi-Yau) manifold so that the resulting theory has three chiral generations<sup>4)</sup>. Other approaches use different distributions of fermion states in the additional (extended) dimensions to obtain a variety of coupling strengths to a Higgs field that exists on the 3+1 dimensional brane<sup>5)</sup>. In these approaches one relates the parameters of the field theory to the way the various flavors of quarks populate the additional dimensions, or to the overlaps of the various branes. Any theory that gives the Standard Model as its low energy realization is one option among many similar possibilities. We choose the parameters of the string theory to get the right parameters for the field theory. This would not “explain” the generation structure or the pattern of masses and mixings. Perhaps my second question gets an answer here, in a strange reversed fashion—what the patterns of masses and mixing may tell us is how we must choose the extra six-dimensional manifold and what branes we need to wrap it up with to give us our observed world of particles.

As for the matter-antimatter asymmetry of the Universe,<sup>6)</sup> the Standard Model alone seems to be inadequate to answer this question. However there are many possible extensions of it which give the observed asymmetry starting from CP-violating effects in either from the lepton sector (leptogenesis)<sup>7)</sup> or the quark sector (baryogenesis)<sup>8)</sup>. No one scenario is, as yet, compelling. Perhaps more data will rule out one or the other possibility; as long as both remain viable it is difficult to choose between them.

The third possible answer to the question of matter-antimatter asymmetry of the Universe is that it arises as an initial condition on the Universe. In this regard, Pauli, writing to Heisenberg in 1933 (after the discovery of positrons), said “I do not believe in the hole theory, since I would like to have the asymmetry between positive and negative electricity in the laws of nature (**it does not satisfy me to shift the empirically established asymmetry to one of the initial state**)”<sup>9)</sup>. I have highlighted here Pauli’s parenthetical remark, which I find remarkable. As far as I know, until the experimental discovery of CP violation in 1964, Pauli was the only person to object to the fact that the equations of nature appeared to be symmetric between matter and antimatter, while the Universe does not, and to reject the idea that the observed imbalance

arises from an initial condition.

I share Pauli's prejudice against a finely-tuned initial condition. If you give me one, why not many? Why not a young universe with initial conditions tuned to create all the data that we interpret as evidence of its evolution and its age? I think we all find that idea absurd. In addition to this philosophical objection, there is a physical reason to doubt this answer. Initial conditions cannot be maintained without a conservation law to protect them. Thermal equilibrium between matter and antimatter would give equal populations, because of their CPT-required equal masses. If no conservation laws protect an imbalance, it would be wiped out by the progression to thermal equilibrium. We do not know that such a conservation law applies in the high-energy environment of the early Universe.

In the Standard Model at high temperature there are processes that violate both lepton number and baryon number, although they preserve  $B-L$ . Many extensions of the theory to a grand unified theory do not conserve that quantity; indeed to get the different lepton and quark mass patterns it seems one needs to distinguish quarks from leptons in ways that tend to break this symmetry. It thus seems to me unlikely that the answer to the CP asymmetry of the Universe lies in a conserved initial condition of matter-antimatter imbalance.

## 2 Turning to the detailed questions

It seems we have no good answers to any of my "big" questions, nor much hope of answering any of them soon. However the current Standard Model is almost surely incomplete, even when we extend it to include neutrino masses. It gives us no candidate particles to be the dark matter that we know pervades the Universe; CP conservation of the strong interactions appears to be an accident (or a fine-tuning); and the theory as it stands does not give a good scenario for the generation of the matter-antimatter asymmetry of the Universe. Beyond these obvious problems there are the problems of unification with gravity and the existence of either dark energy or a cosmological constant. These are total mysteries, problems that are not even addressable, in the Standard Model.

One might add the hierarchy problem, namely the fine-tuning required to have the scale of physics where electroweak symmetry breaking occurs so small compared to the scale of grand unified symmetry breaking. Solutions to

this issue via supersymmetry suggest new particles and also new interactions of the Standard Model particles. At least some evidence of these should appear around the TeV scale. Very possibly there is more than one “new physics” scale. No one new mechanism fixes all the problems listed above.

If there is physics beyond the Standard Model, perhaps we cannot answer the big questions because we do not know enough as yet to be asking them. Einstein failed in his quest for a Unified theory of matter and gravity. At least in part, his failure was surely because he did not know enough about the fundamental structure of matter. He was trying to unify gravity with the wrong ideas about matter. He may have been asking the right question, but so far ahead of its time that it was the wrong question. Perhaps we too are making this mistake when we ask the above “deep” questions. Perhaps when we know more about the physics beyond the Standard Model we will see why these are simply the wrong questions.

The path to knowledge is thus the usual path of science, via experiment. We need to test the predictions of our current theory in further detail, to hunt for clues about physics beyond the Standard Model. One way to do this is to search directly for new particles with new higher energy machines. A second way, the way of flavor physics, is to search for those places where new physics effects cause inconsistencies with precision predictions of the Standard Model.

Weak interactions can yield precision physics. Perturbative calculations of weak decays in the Standard Model quark sector are governed by the masses of the W and Z mesons, the electromagnetic coupling constant, the Weinberg angle, and the four parameters of the flavor sector, those that determine the CKM matrix of weak decays<sup>10)</sup>, and the quark masses. The first four of these are by now well measured. We can obtain multiple independent measurements of the four CKM quantities (one of which is CP violating) and the heavy quark masses, by exploring many different weak decay processes. New physics effects may impact these measurements differently and thereby cause us to get inconsistent results for the Standard Model parameters.

New physics can enter these decays through new heavy particles in intermediate states. Tree diagrams with such particles are typically very suppressed by the large mass of the new intermediate particles. The chief impact of such particles thus comes from loop diagrams; with high momentum in the loop the large mass is less of a suppressing factor. Even so loop diagrams do not

give large effects. Thus the places where we are most likely to be sensitive to these effects are those places where the Standard Model predicts a null result, or where the Standard Model process is itself rare, either because it is a loop process or because it is suppressed by Standard Model approximate symmetries.

The challenge in testing the Standard Model is not just for the experiments to obtain precision data. In most cases there is also a theoretical challenge to obtain precision predictions. The relationships between measurements and Standard Model parameters are seldom free of corrections to the quark-level weak decay because what we observe are not quarks but hadrons. Hence strong interaction physics plays a role. This complicates the situation. The challenge to theorists is to determine the impact of strong interaction effects and the residual uncertainties in the extraction of weak interaction parameters that arise because of uncertainties in these effects. Before turning to my own special interest of  $B$  physics, I want to make a few comments on how these issues play out in some of the other areas of physics that will be discussed in this meeting.

### 3 Rare Processes

One way that new physics could be obvious even in the face of order 1 uncertainties from hadronic physics, is if a decay that is very rare in the Standard Model is found at a level orders of magnitude above its prediction. Then we do not need a precision calculation to see that new physics is playing a role. This was the hope in, for example, the search for rare  $K$  decays, or for  $D^0 - \bar{D}^0$  mixing. Once these searches are close to the Standard Model level then the question of Standard Model precision again becomes a challenge for the search for new physics. Some particular channels such as  $K^0 \nu \bar{\nu}$  are cleanly predicted, but very difficult to measure. Other channels have experimental limits still well above Standard Model estimates and in these cases a detection that would signal new physics is still a possibility.

Sometimes early optimism about a test for new physics is tempered by more careful examination of the uncertainties in the Standard Model prediction. In the case of  $D^0 - \bar{D}^0$  mixing there is at present a very large theory uncertainty in the Standard Model prediction. In the Standard Model, in the  $SU(3)$  limit, the effect is expected to be tiny, partly because of an  $SU(3)$  cancellation (or GIM

suppression) of the leading graphs. However the actual  $s$  and  $d$  quark masses are quite different. Thus  $SU(3)$  breaking terms can significantly enhance the effect. It has been argued that significant differences in the phase space for multiparticle states which differ only in  $K$  and  $\pi$  content can give a substantial the imaginary part of the  $D$  mixing amplitude (and by analyticity, this also enhances the real part) <sup>11, 12, 13</sup>). This gives an uncertainty in the Standard Model prediction comparable to the magnitude of the current limits on the effect, so it ceases to be a good place to search for new physics. One possible exception is if the real part is found to be large compared to the imaginary part. Thus the challenge to experiment is not just to measure this effect but to untangle the real and imaginary parts.

In the case of neutrinos the challenges are still chiefly on the experimental side, although there too theoretical uncertainties can plague certain measurements. Since the next talk will cover this area I will not dwell on it further <sup>14</sup>). Neutrino masses also induce tiny Standard Model flavor violations in charged lepton decays. Searches for these rare processes are another way to search for new physics, which could possibly amplify these effects to an observable level.

#### 4 Heavy Quark Spectroscopy

In the past year or so considerable excitement has been generated by observations of some states that, while not entirely unexpected, were not a good match to predictions. Two classes of states have emerged, new charm-strange mesons <sup>15</sup>) and the so-called “pentaquarks” <sup>16</sup>). The first are probably more solid experimentally; their interest stems from the fact that the potential models for heavy-light bound states did not predict the masses and widths that are found <sup>17</sup>). Since the charm quark is not so very heavy and the strange quark is not so very light, perhaps this discrepancy should not be so surprising. Furthermore, any potential model is at best an approximation to the full QCD theory. We learn from these states something about what was missing in those approximations.

The case of pentaquarks is even muddier, here there are apparently discrepant experiments as well as a wealth of ideas as to how to describe the inner working of the claimed states. Given the current mixed-bag of the data, we can only wait and see what survives with higher statistics. We will hear some reports on the current status at this meeting <sup>16</sup>). From the theory side, my

own attitude to these things is that none of them can tell us anything about physics beyond the Standard Model. While weak decays have uncertainties due to strong interaction corrections, spectroscopy is strong interactions from the start. We calculate none of it from first principles. Hence when results and calculations do not match we do not have to suspect our underlying QCD theory, we only have to modify our approximations to it. We can learn how to model the physics better, but I think it is very unlikely that the study of these states can reveal any fundamental flaws in the underlying theory.

One thing further that puzzles me is the very classical “either it is this or it is that” discussion which often occurs here. These states are quantum states, there is no reason why a single static substructure configuration dominates. Configurations of the constituents for a pentaquark state, such as two di-quarks and an antiquark, rather than a state that is effectively (spatially) a baryon plus a meson in a bound configuration, are suggested. The true states are likely to be quantum superpositions of both these “pictures” and more. Perhaps the various configurations can give us some insight as to why the state is narrow (if indeed it is), but, in all probability, no one of them a full description of the interacting quantum system of four quarks plus one antiquark of a distinct flavor<sup>18</sup>).

## 5 B Physics—Generalities

In  $B$  decays too, the search for new physics is most likely to succeed in cases where the Standard Model contribution is suppressed or null. Alternatively we look for multiple measurements of the same set of CKM parameters to see if new physics effects give inconsistent values from the Standard Model interpretation. There are now many papers in the literature about which modes are of interest and why. The collection of analyzed data is now also growing at a formidable rate.

To test the Standard Model in  $B$  physics one must first determine the magnitudes of the CKM matrix elements  $V_{cb}$ ,  $V_{ub}$  and  $V_{td}$  which enter the predictions (along with the better known  $V_{ud}$ ,  $V_{cd}$  and  $V_{tb}$ ) as the scales for sides of the unitarity triangle that follows from the relationship

$$\sum_j V_{jb} V_{jd}^* = 0 . \tag{1}$$

This relationship is one of several given by the requirement that the CKM

matrix is unitary. It is perhaps the most interesting one because all three terms in the sum are of comparable magnitude, so phase differences (weak phases) between the sides of the triangle can be large, leading to large CP violating effects.

I will not dwell here on the challenges of measuring the sides, later talks in this conference will discuss that in detail. We now have numbers for all three sides, and uncertainties in these numbers are gradually shrinking. In addition the magnitude of the CP violation seen via the decay  $K_L \rightarrow \pi\pi$  gives a constraint on a combination of parameters. In all cases, except for the ratio of  $B_s$  mixing to  $B_d$  mixing as a measure of  $V_{td}$ , the uncertainties are now dominated by theory uncertainties. We will hear about recent work, both theory and experiment, later in the week <sup>19)</sup>.

I now turn to measurement of the angles of the Unitarity triangle via CP violation studies. The basics of the subject of  $B$  decays and the study of CP violation is well described in some excellent text books <sup>20)</sup>. Here I will give only a lightening review to define a bit of the jargon of this field.  $B$  decays to two-body or quasi-two-body final states where these states are CP eigenstates (or can be separated into CP odd and CP even fractions by angular analysis of the decay) are of particular interest <sup>21)</sup>. The first situation occurs when the final four valence quarks are CP self conjugate and at least one of the final particles has zero spin. The second occurs when the quarks are self-conjugate but both particles have non-zero spin. In that case the two particles can have either odd or even relative angular momentum, and the angular analysis sorts these two cases.

For general multiparticle decays, even if the quark content is CP-self-conjugate, the final states are generally an unknown admixture of CP-odd and CP-even states. Since the sign of the most readily interpreted asymmetry effect depends on this CP quantum number, information about underlying CKM parameters comes best from two body channels.

In the electron-positron  $B$  factories the  $B^0$  and  $\bar{B}^0$  are produced in a coherent state that contains one of each particle until such time as one of them decays. Then the other evolves, because it is a superposition of mass eigenstates, until it too decays. We search for events where one  $B$  decays to the final state under study and the other to a state that tells us its flavor. This latter is called the tag decay. Any asymmetry between the rate for a  $B^0$  tag

and that for a  $\overline{B}^0$  tag is a CP violation. In the  $B$  factories, because of the coherent initial state, the most interesting CP violation effects vanish when integrated over the time difference between the decay of interest and the tag decay, so one must study the differences as a function of time.

In general there are three types of CP violation. The first, which can occur for any decay, is a difference in rate between any process and its CP conjugate process,  $|\overline{A}/A| \neq 1$ . This is known as direct CP violation, though a better name is CP violation in the decay amplitudes. (It has been observed for the kaon system in the result  $\epsilon' \neq 0$ .)

The two other types of CP violation occur only in the case of decays of the neutral but flavored pairs of mesons  $P = K, D, B$  to final states that are common to both members of the pair, and can be resolved into CP eigenstates. We denote the mass eigenstates of these mesons by  $P_{H,L} = pP^0 \pm q\overline{P}^0$ , where the subscripts H and L refer to the heavier and lighter mass states. The second type of CP violation is that which shows that these mass eigenstates cannot be CP eigenstates, namely  $|q/p| \neq 1$ . This is called CP violation in the mixing. It is seen in the decay of the long-lived neutral kaon states (which would be the CP-odd state if CP were a good quantum number) to the CP-even final states of two pions.

The third type of CP violation can occur even if both of the first two do not. The CP asymmetries in decays to CP-eigenstate final states  $f$  are all governed by the ratios

$$\lambda_f = \frac{qA(\overline{B} \rightarrow f)}{pA(B \rightarrow f)}. \quad (2)$$

The amplitude in the numerator is  $\eta_f = \pm 1$  times the CP conjugate of the amplitude in the denominator, where  $\eta_f$  is the CP quantum number of the state  $f$ . The third type of CP violation, which arises from interference between decays with and without mixing transitions, is signaled by  $\text{Im}\lambda_f \neq 0$ , namely by a difference between the weak phase of the decay amplitude ratio and the weak phase of the mixing parameter  $q/p$ . When both ratios are of unit magnitude the quantity  $\text{Im}\lambda_f$  can be directly related to the phases of a product of  $CKM$  matrix elements, that is to weak-coupling phase differences.

There is now a copious literature suggesting many channels for analysis. First among these is the ‘‘golden mode’’  $B_d \rightarrow J/\psi K_S$ . This and the related final states with other  $c\overline{c}$  states (or a  $K_L$ ) have both  $|\overline{A}/A| = 1$  and  $|q/p| = 1$

to high accuracy. The SLAC and the KEK  $B$  factories now have collected large samples and analyzed these modes in detail.

The CP-violating asymmetry that is measured is given by

$$\begin{aligned}
 a_f &= \frac{\Gamma(B^0(t) \rightarrow f) - \Gamma(\overline{B}^0(t) \rightarrow f)}{\Gamma(B^0(t) \rightarrow f) + \Gamma(\overline{B}^0(t) \rightarrow f)} \\
 &= \cos(\Delta Mt) \frac{1 - |\lambda_f|^2}{1 + |\lambda_f|^2} + \sin(\Delta Mt) \frac{2Im\lambda_f}{1 + |\lambda_f|^2} \\
 \text{for } |\lambda_f| = 1 &\rightarrow \sin(\Delta Mt) Im\lambda_f
 \end{aligned} \tag{3}$$

Here  $B^0(t)$  is time-dependent state that was (or will be) pure  $B^0$  at time  $t = 0$ . The time dependence is obvious if one recognizes that it is a superposition of the two mass eigenstates,  $B_{\text{heavy}}$  and  $B_{\text{light}}$ . The  $t$  in Eq.(3) is the time between the decay of one  $B$  to a state that labels its flavor and the decay of the other to the state  $f$  under study. (This can be either positive or negative as either decay may be the first that occurs.) The term with the cosine in time contributes if either of the first two types of CP violation are present, while the sine term contributes only if the third type occurs, whether or not the first two types are present. For the  $B_d$  system,  $|q/p| = 1$  to a good approximation. (When we study  $B_s$  decays in hadronic  $B$  production facilities we will not have this simple situation.)

One can write a generic  $B$  decay amplitude as a sum of two terms with different CKM structure. For the quark level decay,  $b \rightarrow q_1 \overline{q}_2 q_3$  two classes of diagrams can contribute, weak-interaction tree diagrams and weak-loop diagrams, (commonly called penguin diagrams). The loop diagrams give a contribution of the form

$$\delta_{12} \sum_j V_{jb} V_{jq_3}^* F(m_j) = 0 \tag{4}$$

where the sum over  $j$  runs over up-type quarks. The delta function denotes the fact that such diagrams contribute only when a matching  $q\overline{q}$  pair is produced. The function  $F(m_j)$  arises from the loop integral and depends on the mass of the up-type quark in the loop. One of the three products of CKM coefficients that appears here is the same as that for any tree-type diagram that contributes to the same final state. (Indeed there is no meaningful distinction between a tree diagram plus some final state rescattering and the long range part of a penguin loop amplitude). One can use the unitarity relationship of Eq. (1) to remove any one of the three CKM coefficients by rewriting it as the negative of

the remaining two (thereby obtaining the two terms mentioned at the beginning of this paragraph).

Amplitudes with significant contributions for two different weak phases can lead to the first type of CP violation (if they also have two different strong phases). To extract Standard Model parameters from such channels we would need to calculate the relative size and relative strong phase of the two terms. This brings in strong interaction physics, and in general leads to large uncertainties.

## 6 B Physics –the “simple” modes

Cases where a single product of CKM matrix elements dominates are thus of particular interest. Then  $|\frac{\bar{A}_f}{A_f}| = 1$ . Remember that for  $B_d$  decays the approximation  $|q/p| = 1$  is also very accurate, so in these cases  $|\lambda_f| = 1$  to a good approximation. Then the quantity  $\text{Im}\lambda_f$  directly measures a CKM phase difference.

A single term dominates the decay amplitude for the “golden mode” cases of  $\psi K_S$  and  $\psi K_L$  channels, where  $\psi$  denotes any  $c\bar{c}$  resonance. More generally, we get a single dominant term proportional to  $V_{cb}V_{cs}^*$  for any  $b \rightarrow c\bar{c}s$  decay. There are penguin graph terms with this coefficient as well as the dominant tree graph. One can use unitarity to remove the term proportional to  $V_{tb}V_{ts}^*$ . Then the remaining penguin term is proportional to  $V_{ub}V_{us}^*$ , which is suppressed by two additional powers of  $\lambda = V_{us}$ . The dominant term is also enhanced because it has the larger tree contribution as well as a penguin part, thus corrections to  $|\bar{A}_f/A_f| = 1$  are expected to be at most a few percent.<sup>1</sup>

The measured results from combining all such channels are <sup>23)</sup>

$$\begin{aligned} \text{Im}\lambda_f &= \sin(2\beta) = 0.741 \pm 0.067 \pm 0.033 && \text{BaBar} \\ \text{Im}\lambda_f &= \sin(2\beta) = 0.733 \pm 0.057 \pm 0.028 && \text{Belle} \\ \text{Im}\lambda_f &= \sin(2\beta) = 0.736 \pm 0.048 && \text{World average .} \end{aligned} \tag{5}$$

---

<sup>1</sup>A paper I wrote with Grossman, Ligeti and Nir <sup>22)</sup> defined rigorous bounds on this deviation from data on SU(3)-related channels. These bounds are much larger than the few percent quoted above. This should not be interpreted as an indication that the deviation is large, it merely shows that, at present and in this case, the data-driven bound is not a strong one.

These results give clear evidence for the third type of CP violation, furthermore they give a relative phase, here called  $\beta$ , of  $V_{cb}^*V_{cd}$  and  $V_{tb}^*V_{td}$  that agrees well with that expected from the best-fit values of the lengths of the sides of the Unitarity triangle, and the constraint from  $K_L \rightarrow \pi\pi$  decays, as can be seen in Fig. 1. This is a spectacular success for the CKM picture of CP violation.

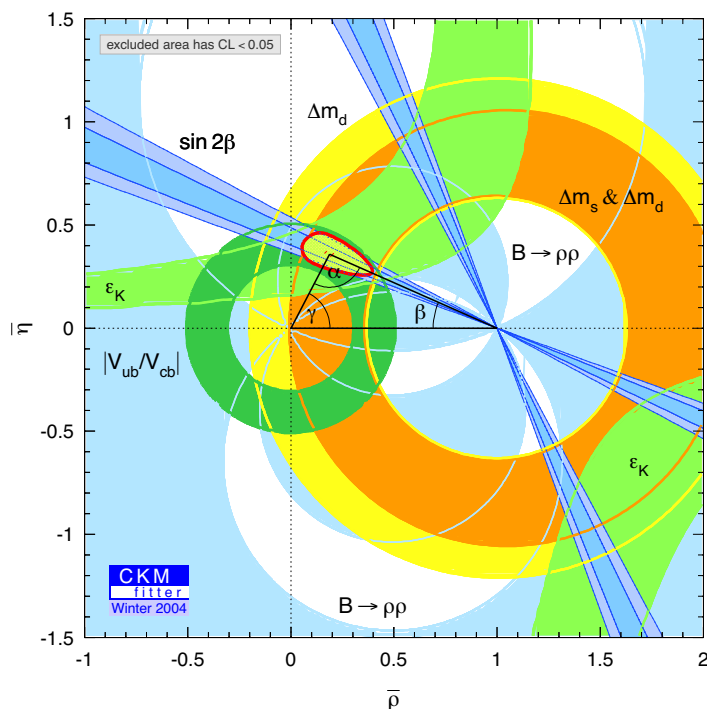


Figure 1: *Concordance of all measurements of Standard Model flavor parameters as shown by the unitarity triangle for B decays. This figure is taken from the CKM Fitter website which also provides the details of the input data used <sup>24)</sup>.*

For channels dominated by  $b \rightarrow s\bar{s}$  the same two CKM coefficients as in the  $c\bar{c}s$  case occur, although here there is no tree graph contribution to further enhance the dominant term. Thus, in the Standard Model, up to small and relatively well-estimated corrections, these channels should have the same CP-violating asymmetry as the golden mode channels. The experimental results here are, at present, a puzzle. The numbers are

$$\begin{aligned}
\text{Im}\lambda_{\psi K_S} &= 0.736 \pm 0.049 \\
\text{Im}\lambda_{\phi K_S} &= -0.96 \pm 0.50^{+0.09}_{-0.11} \quad \text{Belle} \\
\text{Im}\lambda_{\phi K_S} &= 0.47 \pm 0.34^{+0.08}_{-0.06} \quad \text{BaBar} .
\end{aligned}
\tag{6}$$

Clearly, unless someone is making a mistake in their analysis, this situation can be expected to be resolved with more data. We will just have to wait a few years to see if the tantalizing hint that there may be a new physics contribution here survives.

Any channel with three distinct quark types produced in the b-decay has only a tree-diagram contribution. For example  $b \rightarrow c\bar{u}s$  (or  $c\bar{u}d$ ) give modes such as  $D^0 K_S$  or  $D^0 \pi^0$ , where the  $D^0$  decays to a CP eigenstate. These modes give ways to extract the CKM parameter  $\gamma$  (modulo the complication of doubly CKM suppressed corrections from  $b \rightarrow u\bar{c}s$  (or  $c\bar{u}d$ ))<sup>25</sup>). We do not yet have enough data for these rare modes to make the asymmetry analysis accurate, so I will not talk further about them. Eventually they will be very interesting to study.

For  $b \rightarrow u\bar{u}s$  (and  $b \rightarrow d\bar{d}s$  channels, which cannot be experimentally separated in  $B_d$  decays), the uncertainty in the Standard Model correction is larger, because the CKM-suppressed term is enhanced by having the larger tree graph contribution, so these  $K\pi$  channels do not provide a sensitive test for new physics.

## 7 B Physics—modes with two competing terms in the amplitude

In the case of  $b \rightarrow q\bar{q}d$  decays, such as  $B \rightarrow \pi^+\pi^-$ , there are always two comparable magnitude CKM terms in the amplitude, however one of them is somewhat enhanced by having the larger tree graph contribution in addition to the penguin terms. Early papers used this argument to suggest that these channels too could give clean extraction of CKM phases, but experience has taught us that this argument is not reliable; the penguin contribution is larger than early estimates suggested. Hence one needs to use additional theoretical input to relate the measured CP asymmetries to CKM phases. In the rest of this talk I discuss some ways in which this can be done.

In these cases the quantity  $\text{Im}\lambda_f$  depends on the relative magnitudes and the strong phases of the two terms in the amplitude. These are hadronic

physics effects. Uncertainties in the interpretation of the measurement arise because we cannot readily calculate them. The theory effort is thus to find ways to reduce our ignorance to a few quantities that enter into more than one measurement, so that we can use multiple measurements to determine both the uninteresting (for our purposes) hadronic physics quantities and the weak interaction parameters that we are trying to measure.

There are two general directions to go. The first is to use strong interaction symmetries, isospin or SU(3), to determine the necessary quantities using other measurable rates. In a few cases this is all one needs. Theory uncertainties then arise from the impact of symmetry breaking effects, since these are not exact symmetries. However these uncertainties are typically smaller, and better understood, than the uncertainties that would arise from using models of hadrons to calculate the hadronic physics effects.

For example let us look at the decays  $B \rightarrow \pi\pi$ . If we can measure all such decays, including those for charged B's, we can use isospin symmetry to remove the unwanted complications and get a clean determination of the angle  $\alpha = \pi - \beta - \gamma$  at the apex of the unitarity triangle <sup>26)</sup>. We need the rates for  $B^0 \rightarrow \pi^0\pi^0$  and  $\bar{B}^0 \rightarrow \pi^0\pi^0$  separately; as yet only their average is measured. It will take over ten times the present data to get sufficiently accurate numbers to give a well-constrained answer by this method.

The same method can be applied, together with angular analysis, for  $B \rightarrow \rho\rho$ . Here the two-neutrals channel is smaller (but easier to detect); thus a method for using the combined  $B^0$  and  $\bar{B}^0$  decays to bound the correction to the value of  $\alpha$  <sup>27)</sup> gives the best determination of  $\alpha$  at present. This analysis too will be presented later in this conference <sup>28)</sup>.

The second method uses all the tools. In addition to symmetries the main theory tools are the Operator Product Expansion which allows us to expand the effects of hard gluons in powers of  $\alpha_s(m_b)$ , plus the heavy quark expansion, which organizes the calculation in powers of  $\Lambda_{QCD}/M_b$ . A more recent addition to the toolkit is a technique for grouping the effects of soft gluons and those collinear to a hard quark (Soft Collinear Effective Theory). This gives an expansion in  $\sqrt{(\Lambda_{QCD}/E)}$  where  $E$  is the energy of some final state particle, and thus is typically something of order  $M_B/2$ . The coefficients of the expansion contain a set of hadronic quantities, both operator matrix elements and quark distribution functions for mesons. These functions are particle dependent, but

process independent. The symmetries further reduce the number of unknown quantities. They can relate one matrix element or quark distribution function to others, up to some uncertainty due to symmetry breaking effects.

To make all these words a bit more concrete let me give you a couple of examples of the application of these ideas. To extract the magnitude of  $V_{ub}$  from the rate of semileptonic  $B$  decays to any final state with no charm particles we need to know the spectrum of such decays. Any method to remove backgrounds from charm decays of  $b$ -quark will also remove some fraction of the desired decays. We need the spectrum to determine what that fraction is. The theory relates the spectrum in this decay to that seen in  $B \rightarrow X_s \gamma$  where  $X_s$  is any state with non-zero strangeness. So we can use the measurement in the one case to reduce the uncertainty coming from the cut on the spectrum in the other. This methodology, together with improvement in statistics of the data, have considerably reduced the uncertainty on  $V_{ub}$ . You will hear more about this later in this conference <sup>19</sup>).

The same matrix elements that determine this spectrum, also enter in decays of a  $B$  meson to two light pseudoscalars. Furthermore the matrix elements and distribution functions that enter for decay to two pions and that to a kaon plus a pion have SU(3) symmetry relationships. The calculation of the impact of penguins in the two pion decay can be accomplished using all these tools. Note that the CKM factors do not respect SU(3) symmetry, that applies only to the hadronic part of the amplitude. The upshot is that the penguin contribution that dominates the  $B \rightarrow K\pi$  decay can be used to determine the similar penguin contribution in  $B \rightarrow \pi\pi$ , up to SU(3) corrections. The residual uncertainties are still significant, but they are smaller and better controlled than was the case before all the tools were brought to bear <sup>29</sup>).

Lattice QCD calculations are another important tool, used to determine one-particle to one particle (or one to zero) matrix elements. Here too there has been a steady advance in precision, with the biggest recent steps being the move to “unquenched” calculations (including light quark loops), and better extrapolations to the physical light-quark mass values using chiral calculations to guide the functional form of the extrapolation <sup>30</sup>). An example where this work plays a role is the extraction of  $V_{td}$  from the measurement of the  $B_d$  mixing parameters.

All this theory discussion makes it clear that we need more than im-

proved statistics to mine the physics out of the data. We also need ongoing reductions of theoretical uncertainties. Theorists tend to tackle these hard problems when theory uncertainties dominate over those from experiment in extracting a parameter that they care about. The challenge is to keep everyone honest about these uncertainties, which are often very difficult to quantify. Experience shows that theorists often underestimate them. The temptation for an experimental analysis is to use the particular theoretical input that gives the smallest quoted uncertainty. This may be overly optimistic if other similar theoretical approaches give different values for the result, or for its uncertainty.

## 8 Concluding remarks

I began this talk with some generalities, and I will end there too. We know that Standard Model extensions are needed before we can begin to address any of the deeper questions that remain. Heavy quark physics provides probes that are sensitive to many of these extensions, and can possibly distinguish between classes of ideas. The neutrino sector likewise may exhibit CP violation and lepton flavor violation, and provides another possible answer the question about the matter antimatter asymmetry of the Universe. Here there are more parameters that are as yet undetermined, some of them perhaps reachable in the next round of experiments some much harder to get at (perhaps even beyond our wildest accelerator dreams). Of course direct searches for new particles target some of same extensions of the theory. We need more data on all three fronts to make further progress. I am sure that this conference will present some interesting steps forward in this ongoing quest.

## 9 Acknowledgements

Work supported by the Department of Energy under contract number DE-AC03-76SF00515.

## References

1. M. Kobayashi and T. Maskawa, *Prog. Theor. Phys.* **49**, 652 (1973).
2. S. Weinberg, *Phys. Rev. Lett.* **37**, 657 (1976).
3. For example see J. C. Pati, J. C. Pati, arXiv:hep-ph/0204240.

4. See for example S. B. Giddings, S. Kachru and J. Polchinski, Phys. Rev. D **66**, 106006 (2002) [arXiv:hep-th/0105097].
5. For a recent example and references to earlier work see B. Lillie, JHEP **0312**, 030 (2003) [arXiv:hep-ph/0308091].
6. A. D. Sakharov, Pisma Zh. Eksp. Teor. Fiz. **5**, 32 (1967) [JETP Lett. **5**, 24 (1967 SOPUA,34,392-393.1991 UFNAA,161,61-64.1991)].
7. For a recent example and references to earlier work see M. Ibe, R. Kitano, H. Murayama and T. Yanagida, arXiv:hep-ph/0403198.
8. For a recent example and references to earlier work see A. Menon, D. E. Morrissey and C. E. M. Wagner, arXiv:hep-ph/0404184.
9. W. Pauli, letter to Heisenberg June 16, 1933 Wolfgang Pauli, Scientific Correspondence, Vol. 2 p169, Springer (1979)
10. For a commonly used parametrization see L. Wolfenstein, Phys. Rev. Lett. **51**, 1945 (1983).
11. L. Wolfenstein, Phys. Lett. B **164**, 170 (1985).
12. A. F. Falk, Y. Grossman, Z. Ligeti, Y. Nir and A. A. Petrov, arXiv:hep-ph/0402204.
13. See talk at this conference by K. Flood.
14. See talk at this conference by S. Parke and references contained therein.
15. B. Aubert *et al.* [BABAR Collaboration], Phys. Rev. Lett. **90**, 242001 (2003) [arXiv:hep-ex/0304021]. K. Abe *et al.*, Phys. Rev. Lett. **92**, 012002 (2004) [arXiv:hep-ex/0307052]. D. Besson *et al.* [CLEO Collaboration], Phys. Rev. D **68**, 032002 (2003) [arXiv:hep-ex/0305100].
16. See talks at this meeting by L. Stanco and D. Tedeschi.
17. See for example R. N. Cahn and J. D. Jackson, Phys. Rev. D **68**, 037502 (2003) [arXiv:hep-ph/0305012].
18. See for example M. Karliner and H. J. Lipkin, Phys. Lett. B **575**, 249 (2003) [arXiv:hep-ph/0402260]. R. Jaffe and F. Wilczek, arXiv:hep-ph/0401034. and the talk at this meeting by H. Lipkin.

19. See talks at this conference by J. Wiss, C. Bauer, D. Fortin, C. Schwanda and C. Stepaniak and references therein.
20. CP VIOLATION. By Gustavo Castelo Branco, Luis Lavoura, Joao Paulo Silva. Oxford Univ. Press, 1999. 511p. (The International Series of Monographs on Physics, Vol. 103) QCD161:B721:1999. CP VIOLATION. By I. I. Bigi and A. I. Sanda. Cambridge Univ. Press, 2000. 382p. (Cambridge Monographs on Particle Physics, Nuclear Physics, and Cosmology, Vol. 9)QCD161:B54:2000.
21. I. Dunietz, H. R. Quinn, A. Snyder, W. Toki and H. J. Lipkin, Phys. Rev. **D43**, 2193 (1991).
22. Y. Grossman, Z. Ligeti, Y. Nir and H. Quinn, Phys. Rev. D **68**, 015004 (2003) [arXiv:hep-ph/0303171].
23. <http://www.slac.stanford.edu/xorg/hfag/triangle/winter2004/index.shtml>  
B. Aubert *et al.* [BABAR Collaboration], Phys. Rev. Lett. **89**, 201802 (2002) [arXiv:hep-ex/0207042]. T. Browder for the Belle Experiment [http://conferences.fnal.gov/lp2003/program/S5/browder\\_s05.pdf](http://conferences.fnal.gov/lp2003/program/S5/browder_s05.pdf)
24. J. Charles *et al.* [CKMfitter Group Collaboration], arXiv:hep-ph/0406184.
25. For a recent review see D. Atwood and A. Soni, arXiv:hep-ph/0312100.
26. M. Gronau and D. London, Phys. Rev. Lett. **65**, 3381 (1990).
27. Y. Grossman and H. R. Quinn, Phys. Rev. D **58**, 017504 (1998) [arXiv:hep-ph/9712306]. M. Gronau, D. London, N. Sinha and R. Sinha, Phys. Lett. B **514**, 315 (2001) [arXiv:hep-ph/0105308].
28. See talk by K. Ford in this meeting and B. Aubert [BABAR Collaboration], arXiv:hep-ex/0404029.
29. C. W. Bauer, D. Pirjol, I. Z. Rothstein and I. W. Stewart, arXiv:hep-ph/0401188.
30. See talk in this conference by A. Gray.

## ***SESSION I - Neutrinos***

S. Parke	Neutrino Oscillations Phenomenology
J. Link	Using Reactor Neutrinos to Study Neutrino Oscillations
J. Bonn	Neutrino Mass Limits from Tritium Beta Decay, Present Limits and Perspectives for KATRIN
A. Giuliani	Search for Neutrinoless Double Beta Decay: Present and Future
P. Langacker	Neutrinos and Astrophysics
T. Kajita	Neutrinos Atmospheric: Past, Present and Future
I. Stancu	The LSND Signal: Past, Present and Future
A. Ereditato	Present Status and Prospects of Neutrino Oscillation Experiments
M. V. Diwan	The Case for a Super Neutrino Beam



Frascati Physics Series Vol. XXXV (2004), pp. 25  
HEAVY QUARKS AND LEPTONS - San Juan, Puerto Rico, June 1-5, 2004

## **NEUTRINO OSCILLATIONS PHENOMENOLOGY**

S. Parke

*FERMILAB- Fermi National Accelerator Laboratory, Batavia, Illinois, USA*

Written contribution not received



Frascati Physics Series Vol. XXXV (2004), pp. 27  
HEAVY QUARKS AND LEPTONS - San Juan, Puerto Rico, June 1-5, 2004

**USING REACTOR NEUTRINOS TO STUDY NEUTRINO  
OSCILLATIONS**

J. Link  
*Columbia University in the City of New York*  
2960 Broadway New York, NY 10027-6902

Written contribution not received



**NEUTRINO MASS LIMITS FROM TRITIUM BETA DECAY,  
PRESENT LIMITS AND PERSPECTIVES FOR KATRIN**

Jochen Bonn

*Institute of Physics, Johannes Gutenberg University, 55099 Mainz / Germany*

**ABSTRACT**

The Neutrino Mass experiments at Mainz and Troitsk investigate the endpoint region of tritium  $\beta$  decay spectrum very precisely to extract the mass of the electron antineutrino. The measurements are performed with a MAC-E-Filter, combining Magnetic Adiabatic Collimation and an Electrostatic high pass Filter. The next generation experiment KATRIN aims for an improvement of a factor of 10 in the mass limit.

**1 The Neutrino Mass Experiments**

The fingerprint of the neutrino is the shape of nuclear  $\beta$ -decay spectra. The influence of the neutrino mass is restricted to the region close to the endpoint. As the count rate is very low in the region of interest the spectrometer used has to combine high resolution, high luminosity and a low background.

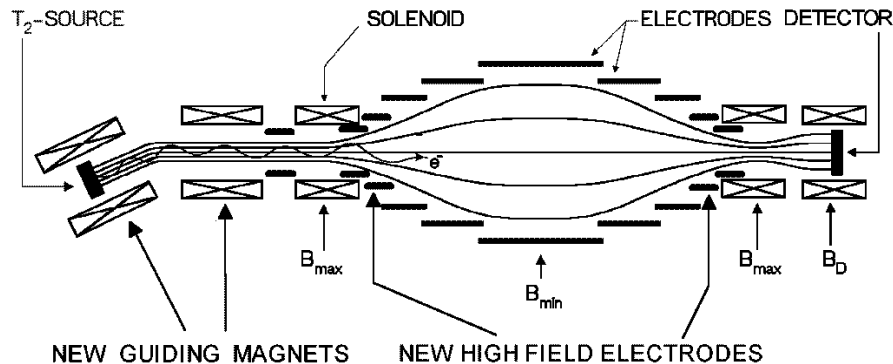


Figure 1: The setup of Mainz II is shown schematically. The distance between source and detector is about 6 m and the diameter of the vessel is 1 m.

The groups in Mainz and Troitsk independently from each other developed a new type of spectrometer to study the endpoint region of tritium  $\beta$ -decay. It is based on the principle of the MAC-E-Filter [2], which fulfils the requests mentioned above. Its principle is given in figure 1. The source is placed in a strong magnetic field guiding the decay electrons. The gradient force in the fringing field of the source solenoid transforms the energy in the cyclotron motion around the magnetic field line into energy parallel to it. By this adiabatic transformation a large parallel beam of electrons is formed that can be analysed by the electrostatic filter formed by a set of cylindrical electrodes.

The resolution is given by the ratio of the maximum magnetic field  $B_{max}$  to the minimum magnetic field  $B_{min}$  reached in the analysing plane. The luminosity can reach the full forward solid angle if the source is put into the field maximum in real experiments it is limited to around 60% to reduce energy losses.

A combination of high luminosity and high resolution in general results in a large setup. Comparing the MAC-E filters with the magnetic, momentum analysing spectrometers of similar dimensions the MAC-E filters reach a much better performance at lower demands on mechanical precision and less stringent demands on the parameters of the electric and the magnetic fields. In addition to optimising the signal the background has to be kept as low as possible. The Mainz spectrometer is shown in figure 1:

Two super conducting solenoids create a magnetic guiding field. The

$\beta$  electrons, starting from the tritium source inside the left solenoid into the forward hemisphere, are guided on a cyclotron motion around the magnetic field lines into the spectrometer with an accepted solid angle of nearly  $2\pi$ . The magnetic field strength drops from the centre of the solenoid to the centre of the spectrometer by several orders of magnitude. In the centre of the spectrometer, the analysing plane, the electron moments are almost perfectly aligned in the direction of the magnetic field lines. The energy in this motion  $E_{\parallel}$  is analysed energetically by applying an electrostatic potential formed by a system of cylindrical electrodes. All electrons with enough energy to pass the retarding potential barrier are reaccelerated onto the detector (in the right solenoid). Therefore the spectrometer works as an integrating high pass filter. The relative energy resolution of the MAC-E-filter is given by the ratio of the minimal magnetic field  $B_{min}$  in the analysing plane and the maximal magnetic field  $B_{max}$  between source and spectrometer, in case of the Mainz setup we obtain:

$$\Delta E = E \frac{B_{min}}{B_{max}} = 18600 \text{ eV} \frac{5.6^{-4} T}{1.8 T} \approx 5.8 \text{ eV} \quad (1)$$

By changing the retarding potential the  $\beta$  spectrum can be scanned. The Mainz set-up uses a solid state source realized by a film of molecular tritium quench-condensed onto a graphite substrate (HOPG). Typical source parameters are: diameter 17 mm, thickness 45 nm (measured by laser ellipsometry), activity 1 GBq.

## 2 The Mainz measurements

The Mainz II setup has a source solenoid consisting of two coils. The first coil houses the tritium film and the second one follows after a bend, so that tritium molecules evaporating from the source are trapped on the LHe cold tube. It eliminates source correlated background and allows to use a stronger source. This one stage cryogenic trap is sufficient to suppress the flow of tritium from the source into the spectrometer in case of the relatively stable quench condensed source used in Mainz. For the windowless gaseous tritium sources used in Troitsk and planned for KATRIN a highly complicated differential pumping system is needed to circulate the tritium.

The endpoint region of the Mainz 1998, 1999 data in comparison with the

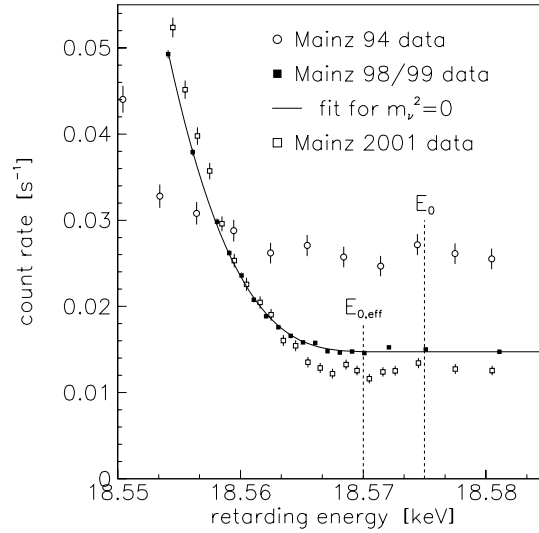


Figure 2: Averaged count rate of the 98/99 data (filled squares) with fit (line) and the 2001 data (open squares) in comparison with previous Mainz data from 94 (open circles) as function of retarding energy near the endpoint  $E_0$ , and effective endpoint  $E_{0,eff}$ . The position of the latter takes into account the width of the resolution function of the set-up.

former data from 1994 is shown in figure 2. The signal to noise ratio was improved by a factor of 10. Also shown are the data of 2001, which have a third of the statistic of the 98/99 data and even a lower background level.

This further improvement is due to very careful preparation of the whole system. Especially all parts which need refreshment from time to time were replaced. In particular: The graphite substrate for the tritium source, the oil for the high voltage divider, baking of all vacuum systems and reactivation of the non evaporable getter pumps. All these measures lead to the most stable operation ever had. The background rate was about 12 mHz over the whole period (2 month) without the necessity of high voltage conditioning during the run.

The results for fit on  $m_{\nu_e}^2$  of Mainz 2001 data as a function of the lower limit

of fit interval are shown in figure 3. All values are in good agreement with each other and with the physically allowed range. To extract a limit on the neutrino mass the interval which leads to the smallest combined statistical and systematical uncertainty (last 70 eV below endpoint) was chosen. This gives:

$$m_\nu^2 c^4 = +1.3 \pm 5.8_{\text{stat}} \pm 2.2_{\text{sys}} \text{ eV}^2 \chi^2/\text{d.o.f.} = 42/36 \text{ for the first tritium film} \quad (2)$$

$$m_\nu^2 c^4 = -1.0 \pm 6.1_{\text{stat}} \pm 1.7_{\text{sys}} \text{ eV}^2 \chi^2/\text{d.o.f.} = 41/36 \text{ for the second tritium film} \quad (3)$$

Combining these measurements with the older measurements from 98/99 [3]:

$$m_\nu^2 c^4 = -1.6 \pm 2.5_{\text{stat}} \pm 2.1_{\text{sys}} \text{ eV}^2 \chi^2/\text{d.o.f.} = 125/121 \quad (4)$$

one gets:

$$m_\nu^2 c^4 = -1.2 \pm 2.2_{\text{stat}} \pm 2.1_{\text{sys}} \text{ eV}^2 \chi^2/\text{d.o.f.} = 208/193 \quad (5)$$

. This value corresponds to an upper limit on the electron neutrino mass of:

$$m_\nu c^2 \leq 2.2 \text{ eV} \quad (95\% \text{ C.L., unif.appr.}) \quad (6)$$

In the final evaluation the neighbour exatation could be determined from the data instead of taking them from a calculation by Kolos et al. [8] The fit result is pushed up a bit the errors remain the same.

$$m_\nu^2 c^4 = -0.7 \pm 2.2_{\text{stat}} \pm 2.1_{\text{sys}} \text{ eV}^2 \chi^2/\text{d.o.f.} = 208/193 \quad (7)$$

which is compatible with a zero neutrino mass. This value corresponds to an upper limit on the electron neutrino mass of:

$$m_\nu c^2 \leq 2.3 \text{ eV} \quad (95\% \text{ C.L., unif.appr.}[9]) \quad (8)$$

### 3 The Troitsk measurements

The spectrometer in Troitsk is also a MAC-E-filter with slightly different dimensions. The Troitsk experiment started data taking in 1994 about two years after the Mainz experiment. The relevant parameters source strength, resolution and background are rather similar. The main difference in the experimental set up is the windowless gaseous tritium source used in Troitsk. This type of source

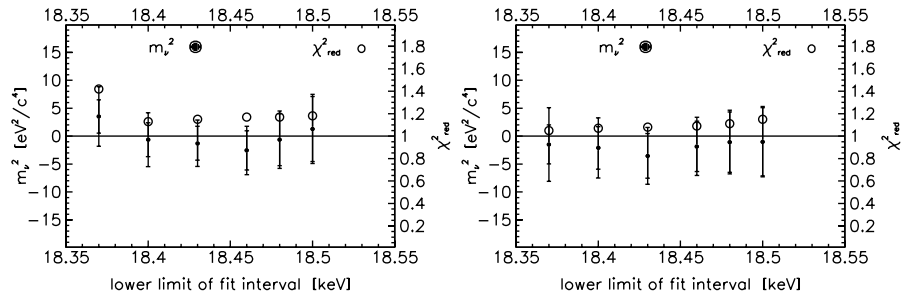


Figure 3: Mainz fit results on  $m_{\nu_e}^2$  (filled circles, left scale) as a function of the lower limit of fit interval (the upper bound is fixed at 18.66 keV, well above  $E_0$ ) for the two different tritium films of 2001. The error bars show the statistical uncertainties (inner bar) and the total uncertainties (outer bar). The corresponding values for the  $\chi_{red}^2 = \chi^2/d.o.f.$  is given on the right scale (open circles).

was pioneered by the Los Alamos experiment [6] and it was also used in the Lawrence Livermore experiment [7]. The claim is that the gaseous source has less systematic effects as compared to the quench condensed source due to the absence of solid state effects. It should however be mentioned that the tritium in the source is not a neutral gas but a charge compensated plasma. The systematic effects introduced by this plasma are absent in the quench condensed source. The two sources are thus complementary in some of their systematic effects. From their first measurement in 1994 on the Troitsk group reported about a small, but significant anomaly, the so called "Troitsk anomaly" [4] in their experimental spectrum.

To extract information on the neutrino mass from the Troitsk data the step effect has to be eliminated as it corresponds to a positive offset interpreted by the fit as a negative value for the parameter  $m_{\nu_e}^2$ . The presently best value from Troitsk was given by V.M. Lobashev at INPA 2002 conference in Hungary:

$$m_{\nu_e}^2 c^4 = -2.3 \pm 2.5_{\text{fit}} \pm 2.0_{\text{sys}} \text{ eV}^2 \pm 1.5_{\text{step}} \text{ eV}^2 \quad (9)$$

This value corresponds to an upper limit on the electron neutrino mass of:

$$m_{\nu_e} c^2 \leq 2.05 \text{ eV} \quad (95\% \text{ C.L., unif. appr.}) \quad (10)$$

and not including the additional error caused by introducing the step effect.<sup>1</sup>

There is no indication of a step like anomaly in the Mainz data of 2000 and 2001 (nor in 98/99 data). To check this two more free parameters (position below endpoint and amplitude) are introduced in the fit procedure. If this is a better description of the measured spectrum one would expect a significant improvement in  $\chi^2$  by scanning it as function of the position below endpoint. The Mainz data show no significant improvement in  $\chi^2$ , supporting clearly the assumption, that the Troitsk anomaly is caused by an unknown experimental artefact. In comparing the two experiments in Mainz and Troitsk one should use the statistical and systematic uncertainties and not the upper limit on the neutrino mass which improves if the value for  $m_\nu^2$  is getting unphysically negative. Both experiment are about equal in their sensitivity limit which they have practically reached.

#### 4 Summary of the experiments in Mainz and Troitsk

The precise measurement of the endpoint region of the  $\beta$  decay spectrum of  $T_2$  by the Mainz Neutrino Mass Experiment lead to an upper limit for the electron neutrino mass of 2.3 eV, final analysis. Troitsk claims 2.05 eV based on a a little more negative mean value. Especially the synchronous measurements at Troitsk and Mainz show that the step like Troitsk anomaly is an experimental artefact.

#### 5 The KATRIN experiment

As the Mainz Experiment almost reached its sensitivity limit it was shut down and the Mainz group focused its activities on KATRIN (KARlsruhe TRItium Neutrino experiment) [5]. The Mainz spectrometer was converted into a test facility for dedicated experiments to study background in the MAC-E filter.

The next generation tritium beta decay experiment KATRIN is presently set up at Forschungszentrum Karlsruhe (FZK) by an international collaboration. Its location inside FZK will be in the Tritiumlabor (TLK) as far as the sources are concerned and in a new hall for the spectrometer etc. The

---

<sup>1</sup>Including the additional error caused by step effect this value leads to an upper limit of 2.2 eV (95% C.L., unif. appr.).

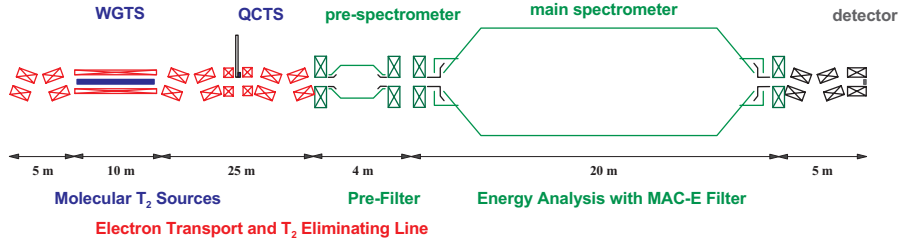


Figure 4: The setup of KATRIN is shown schematically.

main components of KATRIN are the sources, the differential transport system, the spectrometer and the detector. A schematical layout is given in figure 4. KATRIN will have two alternative tritium sources, a windowless gaseous tritium source (WGTS) and a quench condensed tritium source (QCTS). The WGTS can be somewhat stronger than the QCTS as long as the charching problem of solid tritium at low temperature is unsolved. Sensitivity limits claimed below are therefore based on WGTS operation.

The WGTS consists of a 10 m tube of a diameter of 90 mm. Tritium is fed into the center of the tube and freely streaming out at both ends. The source activity is about  $10^{11}$  Bq, the flow out at each end of the source tube is about  $10^{10}$  Bq. The main technical challanges are to provide the tritium and keep its isotopical purity at a level of  $\geq 95\%$  and to prevent tritium from migrating into the spectrometer.

The isotopic purity is guaranteed by TLK. The differential pumping system of KATRIN consists of three different sections: the active differential pumping in the inner loop with 2 differential pumping stations, the active differential pumping in the outer loop with 4 differential pumping stations and the cryogenic traps. The main difference is in the tritium handling and purification. The tritium circulating in the inner loop passes through a palladium membran back to the source tube. The gas from the outer loop is collected by the TLK tritium system and isotopically enriched before going back to the source. The tritium in the gryogenic traps is collecting for the period of a run, (typically 60 days) and then blown out into the TLK tritium system.

The differential pumping system is followed by the spectrometers. The pre-spectrometer reduces the number of electrons entering the main spectrometer to about  $10^{-6}$  of its original value thus eliminating a possible source of back-

ground. The large diameter of the KATRIN main spectrometer of 10 m will give an excellent magnetic shielding of the inner part used for data taking. At Mainz e.g. only 10 cm can be used to separate the electrode and the observed flux. The distance at Troitsk is a little wider, partly explaining the low background at a relatively bad vacuum.

Apart from electromagnetic shielding extremely good vacuum is a key to low background. Scattering with residual gas can lead to background by two processes. Electrons produced by inelastic scattering will be recorded as background if they are created on the detector side of the analysing plane. The second process is related to elastic scattering of very low energy electrons (a few eV). As this is almost isotropic it can lead to trapping of electrons. To reduce background the vacuum at the KATRIN spectrometers has a design value below  $10^{-11}$  mbar. It has been demonstrated in a test setup that this value is not unrealistic. The pumping system consists of cascaded turbo pumps, getter strips and cooling the set up to about  $-20$  °C to reduce outgasing.

The KATRIN detector system will be a segmented silicon detector with high resolution. Extreme care has to be taken to reach a detector background of about 1 mHz. The detector will be separated from the main spectrometer vacuum system by a differential pumping system.

## 6 Development and perspectives of the KATRIN projekt

To present Katrin to the international community two workshops were held at Bad Liebenzell, a summary is presented on the KATRIN homepage. The topic of first workshop on neutrino masses in the sub eV range in January 2001 was to present the project and to discuss the scientific case in relation to alternative experiments. On this workshop the letter of intend was presented.[5] The second workshop on Extreme High Vacuum in April 2003 focused on vacuum related topics.

Based on very careful simulations the collaboration claims that the sensitivity of the KATRIN set up will allow to set a limit on the neutrino mass of

$$m_\nu c^2 \leq 0.2 \text{ eV} \quad (95\% \text{ C.L., unif. appr.}) \quad (11)$$

and to detect a neutrino of

$$m_\nu c^2 \geq 0.35 \text{ eV} \quad (12)$$

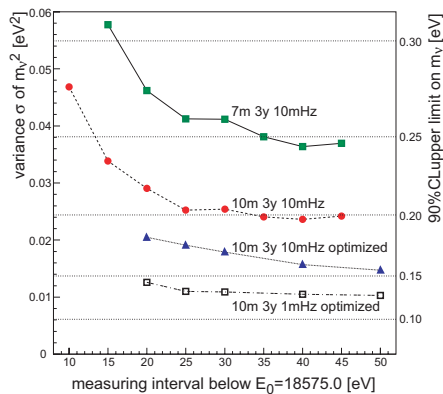


Figure 5: Sensitivity of KARTRIN versus time. Left scale: variance of  $m_\nu c^2$  including statistical and systematic uncertainties. Right scale: upper limit on the neutrino mass. The figure shows the improvement due to enlarging the set up, optimizing data taking and the influence of a 10 mHz background compared to 1 mHz.

both numbers are based on 3 years of data taking. This sensitivity allows to check the cosmologically relevant parameter space and to set the neutrino mass scale.

#### Present status of KARTRIN

Most of the main components of KARTRIN are defined. The prespectrometer is on site. The differential pumping system of the outer loop is ordered. Main spectrometer and the WGTS system will be defined and ordered in 2004. The construction of the spectrometer hall will also be finalized and construction will start in 2004. The earliest date to start measurements with the complete setup is 2007.

## 7 References

- [1] Q.R. Ahmad *et al.*, Phys. Rev. Lett. **87** (2001) 071301
- [2] A. Picard *et al.*, Nucl. Inst. Meth. **B63** (1992) 345
- [3] J. Bonn *et al.*, Nucl. Phys. **B** (Proc. Suppl.) **91** (2001) 273.
- [4] V.M. Lobashev *et al.*, Nucl. Phys. **B** (Proc. Suppl.) **91** (2001) 280.
- [5] KARTRIN letter of intent, hep-ex/0109033, (2001).

- [6] J.F. Wilkerson *et. al.*, Phys. Rev. Lett. **58** (1987) 2023
- [7] W. Stoeffl and D.J. Decman, Phys. Rev. Lett. **75** (1995) 3237
- [8] Kolos *et. al.*, Phys. Rev. **A37** (1988) 2297
- [9] C. Kraus Doctoral thesis Mainz 2004



Frascati Physics Series Vol. XXXV (2004), pp. 41-50  
HEAVY QUARKS AND LEPTONS - San Juan, Puerto Rico, June 1-5, 2004

## SEARCH FOR NEUTRINOLESS DOUBLE BETA DECAY: PRESENT AND FUTURE

Andrea Giuliani

*Department of Physics and Mathematics of the Insubria University  
and INFN-Milano, Via Valleggio 11, 22100 Como, Italy*

### ABSTRACT

After a short introduction on Double Beta Decay and its connections with neutrino properties, of paramount importance after the discovery of neutrino flavor oscillation, this paper describes the most sensitive experimental approaches to the search for this rare nuclear transition. An overview of the presently running experiments is then given and the situation about the experimental determination of the Majorana neutrino mass is discussed. Finally, the more promising future projects are briefly presented.

### 1 Introduction

Double Beta Decay (DBD) <sup>1, 2, 3)</sup> is a rare nuclear transition proposed by Göppert-Mayer <sup>4)</sup> in the far 1935. In this process, a metastable isobar changes into a more stable one by the simultaneous emission of two electrons. Such

transition can take place in principle for 35 naturally occurring even-even nuclei, whose ordinary Beta Decay is forbidden energetically or severely hindered by a large change of the nuclear spin-parity state. DBD is a second-order process of the weak interactions and has consequently a very low probability, which leads to extraordinary long lifetimes for the candidate nuclides.

Two decay modes will be discussed here. The two-neutrino process ( $2\nu$ -DBD), already observed in several nuclides, is described by

$$(A, Z) \rightarrow (A, Z + 2) + e_1^- + e_2^- + \bar{\nu}_1 + \bar{\nu}_2 \quad (1)$$

and is fully consistent with the standard model (SM) of electroweak theory. The neutrinoless channel ( $0\nu$ -DBD)

$$(A, Z) \rightarrow (A, Z + 2) + e_1^- + e_2^- \quad (2)$$

violates lepton number conservation and, if observed, would definitely imply new physics beyond the SM. The available phase space is quite larger for this process than for the  $2\nu$  channel.

### 1.1 Double Beta Decay and neutrino physics

In channel (2) neutrino does not appear explicitly but it is hidden as a virtual particle joining the two electroweak vertices. This role can be played if and only if at least one neutrino eigenstate has a non-zero mass and if neutrino is a self-conjugated ‘‘Majorana’’ particle. Search for  $0\nu$ -DBD is presently the only viable experiment which can reveal the Majorana nature of neutrino. In the so-called mass mechanism, the connection between the lifetime  $\tau$  of process (2) and the neutrino masses is expressed by

$$\frac{1}{\tau} = G_{0\nu} |M^{0\nu}|^2 \left( \frac{\langle m_\nu \rangle}{m_e} \right)^2 \quad (3)$$

where  $G_{0\nu}$  is a phase-space factor growing steeply with the Q-value of process (2),  $|M^{0\nu}|$  (the ‘‘nuclear matrix element’’) includes the nuclear physics involved in the decay, and  $\langle m_\nu \rangle$ , sometimes defined ‘‘effective Majorana mass’’, is a linear combination of the three neutrino physical masses. The coefficients of this linear combination are connected to the neutrino mass matrix, and represent therefore the bridge between flavor oscillations and  $0\nu$ -DBD. <sup>5, 6)</sup> In case of

inverted hierarchy of the neutrino mass spectrum,  $\langle m_\nu \rangle \geq 50$  meV is possible, as suggested by the oscillation results. The experimental observation of  $0\nu$ -DBD could be therefore round the corner (see section 2). Present experimental limits on  $\langle m_\nu \rangle$  are of the order of  $\sim 0.5$  eV, with a large systematics originated by the difficult computation of  $|M^{0\nu}|$ . Mechanisms other than massive Majorana neutrino exchange can induce  $0\nu$ -DBD, such as right-handed currents, heavy right-handed neutrinos, leptoquark-Higgs couplings, compositeness, supersymmetric particle exchange. <sup>1, 2, 3)</sup> However, the recent discovery that neutrinos are massive focuses the attention of the physicists on the mass mechanism rather than on these more exotic processes. The present brief review will therefore concentrate on the experimental search for  $0\nu$ -DBD and on its interpretation in terms of mass mechanism.

## 1.2 Experimental strategies

From the experimental point of view, the shape of the two electron sum energy spectrum enables to distinguish among the two discussed decay modes. In case of  $2\nu$ -DBD (process 1), this spectrum is expected to be a continuum between 0 and  $Q$  (the energy transition of the decay) with a maximum around  $1/3 \cdot Q$ . For  $0\nu$ -DBD (process 2), the spectrum is just a peak at the energy  $Q$ , enlarged only by the finite energy resolution of the detector. Additional signatures are the single electron energy distribution and the angular correlation between the two emitted electrons.  $Q$  ranges from 2 to 3 MeV for the most promising nuclides.

The experimental strategies pursued to investigate DBD can be divided into two main classes. The *indirect search* consists in looking for the daughter nuclei ( $A, Z + 2$ ) in a sample containing a large amount of candidate nuclei ( $A, Z$ ) and left undisturbed for a long time. Radiochemical and geochemical experiments belong to this class. This approach does not allow to distinguish among the two different channels (1) and (2). Important 20–30 years ago, it is no longer pursued nowadays. The *direct search* is based on the development and of the use of a proper nuclear detector, with the purpose to reveal the two emitted electrons in real time and to collect their sum energy spectrum as a minimal information. Additional pieces of information can be provided in some cases, like single electron energy and initial momentum. This nuclear detector must exhibit high energy resolution, since a peak must be identified over an almost flat background in case of  $0\nu$ -DBD, and low background, which requires

underground operation (to shield cosmic rays), very radiopure materials and well designed passive and/or active shielding against local environmental radioactivity. Large sources are of course necessary, in order to monitor many candidate nuclides. Present sources are of the order of 10–100 kg in the most sensitive searches, while the next generation experiments aim at sources in the ton scale. Event reconstruction method can be useful as well, in order to reject background and to provide additional kinematical information on the emitted electrons.

Normally, these features cannot be met simultaneously in a single detection method. It is up to the experimentalist to choose the philosophy of the experiment and to select consequently the detector characteristics, having in mind of course the final sensitivity of the set-up to half-life and to  $\langle m_\nu \rangle$ .

The direct searches can be further classified into two main categories: the so-called *calorimetric technique*, in which the source is embedded in the detector itself, and the *external-source approach*, in which source and detector are two separate systems. The calorimetric technique<sup>7)</sup> has been implemented with various types of detectors, such as scintillators, bolometers, solid-state devices and gaseous chambers. For the *external-source approach* many different detection techniques have been experimented as well: scintillation, gaseous TPCs, gaseous drift chambers, magnetic field for momentum and charge sign measurement, time-of-flight. With this option, it is possible in principle to get much information on the emitted electrons: not only sum energy, but also single electron energy distribution and angular distribution. On the other hand, it is difficult to achieve high energy resolution and high source mass, features which generally characterizes the calorimetric searches.

In order to compare different experiments, it is useful to give an expression providing the sensitivity of an experimental set-up to the  $0\nu$ -DBD lifetime of the investigated candidate, and hence to determine the sensitivity to  $\langle m_\nu \rangle$ . The first step involves only detector and set-up parameters, while for the second step one needs reliable calculations of the nuclear matrix elements. The sensitivity to lifetime  $F$  can be defined as the lifetime corresponding to the minimum detectable number of events over background at a  $1\sigma$  confidence level. For the case of source embedded in the detector and non-zero background, it holds:

$$F = \frac{N_A \cdot \varepsilon \cdot \eta}{A} \cdot \left( \frac{M \cdot T}{b \cdot \Delta E} \right)^{\frac{1}{2}} \quad (4)$$

where  $N_A$  is the Avogadro number,  $M$  the detector mass,  $\varepsilon$  the detector efficiency,  $\eta$  the ratio between the total mass of the candidate nuclides and the detector mass,  $\Delta E$  the energy resolution, and  $b$  the specific background, e.g. the number of spurious counts per mass, time and energy unit. From this formula one can see that, in order to improve the performance of a given set-up, one can use either brute force (e.g. increasing the exposition  $M \cdot T$ ) or better technology, improving detector performance ( $\Delta E$ ) and radio-cleanness ( $b$ ). Next generation experiments require to work on both fronts.

In order to derive the sensitivity to  $\langle m_\nu \rangle$ , indicated as  $F_{\langle m_\nu \rangle}$ , one must combine equations 4 with equation 3, obtaining

$$F_{\langle m_\nu \rangle} \propto \frac{1}{(G_{0\nu})^{\frac{1}{2}} |M^{0\nu}|} \cdot \left( \frac{b \cdot \Delta E}{M \cdot T} \right)^{\frac{1}{4}} \quad (5)$$

which shows how the nuclide choice is more relevant than the set-up parameters, on which the sensitivity depends quite weakly.

## 2 State of the art

Several experiments give limits on  $\langle m_\nu \rangle$  of about 1 eV, but now they are either stopped or close to their final sensitivity. Only a couple of projects (CUORICINO and NEMO3) have the potential to improve present limits. The main results obtained on the neutrinoless process are reported in table 1.

In the last ten years, the DBD scene was dominated by the Heidelberg-Moscow (HM) experiment <sup>8)</sup>. This search is based on a set of five Ge-diodes, enriched in the candidate isotope  $^{76}\text{Ge}$  at 86%, and operated underground (Laboratori Nazionali del Gran Sasso, Italy) with high energy resolution (typically, 3.5 keV FWHM). The total mass of the detectors is 10.9 kg, corresponding to a source strength of  $7.6 \times 10^{25}$   $^{76}\text{Ge}$  nuclei, the largest in DBD searches so far. The raw background, impressively low, is 0.11 counts/(keV kg y) around  $Q$  (2039 keV). It can be reduced further by using Pulse Shape Analysis to reject multi-site events. The limits on half-life and  $\langle m_\nu \rangle$  are respectively  $1.9 \times 10^{25}$  y and 0.3–2.5 eV (depending on the nuclear matrix elements chosen for the analysis). Similar results have been obtained by the IGEX collaboration, <sup>9)</sup> with an experiment based on the same approach.

A subset of the HM collaboration has however claimed the discovery of  $0\nu\text{-DBD}$  in 2001, with a half life best value of  $1.5 \times 10^{25}$  y (0.8–18.3  $\times 10^{25}$  y at

Table 1: *Summary of the most sensitive direct searches for  $0\nu$ -DBD. Limits are at 90% c.l.*

Experiment	Isotope	Half-life [y]	$\langle m_\nu \rangle$ [eV] *	Ref.
<i>Experiments with (almost) saturated sensitivity</i>				
Heidelberg-Moscow (2001)	$^{76}\text{Ge}$	$> 1.9 \times 10^{25}$	$< 0.35$	8)
IGEX (2002)	$^{76}\text{Ge}$	$> 1.6 \times 10^{25}$	$< 0.33 - 1.35$	9)
Mi DBD (2002)	$^{130}\text{Te}$	$> 2.1 \times 10^{23}$	$< 0.9 - 2.1$	10)
Bernabei et al. (2003)	$^{136}\text{Xe}$	$> 1.2 \times 10^{24}$	$< 1.1 - 2.9$	11)
Danevich et al. (2003)	$^{116}\text{Cd}$	$> 1.7 \times 10^{23}$	$< 1.7$	12)
Ejiri et al. (2001)	$^{100}\text{Mo}$	$> 5.5 \times 10^{22}$	$< 2.1$	13)
<i>New running experiments (preliminary results)</i>				
CUORICINO (2003)	$^{130}\text{Te}$	$> 7.5 \times 10^{23}$	$< 0.32 - 1.6$	14)
NEMO3 (2003)	$^{100}\text{Mo}$	$> 6.0 \times 10^{22}$	$< 1.2 - 2.7$	15)

\* As quoted by the authors.

95% c.l.), corresponding to a best value for  $\langle m_\nu \rangle$  of 0.39 eV (0.05–0.84 eV at 95% c.l. including nuclear matrix element uncertainty).<sup>16; 21)</sup> This claim is based on the identification of tiny peaks in the region of  $0\nu$ -DBD, one of which occurs at the  $^{76}\text{Ge}$  Q value. However, this announcement raised skepticism in the DBD community<sup>17)</sup>, including a part of the HM collaboration itself<sup>18)</sup>, due to the fact that not all the claimed peaks could be identified and that the statistical significance of the DBD peak looked weaker than the claimed  $2.2 \sigma$  and dependent on the spectral window chosen for the analysis.<sup>19; 20)</sup> A new paper<sup>21)</sup> published in 2004 however gives more convincing supports to the claim. The quality of the data treatment has improved and the exposure has also increased to 71.7 kg y. A  $4.2 \sigma$  effect is claimed. Unfortunately, the HM experiment is now over and the final word on this crucial result will be given by other searches.

The top level of the external-source technique was reached nowadays by the NEMO3 experiment.<sup>22)</sup> The NEMO3 detector, installed in the Modane underground laboratory (France), is based on well established technologies in experimental particle physics: the electrons emitted by the sources cross a magnetized tracking volume instrumented with Geiger cells and deliver their energy to a calorimeter based on plastic scintillators. Thanks to the division in 20 sectors of the set-up, many nuclides can be studied simultaneously, such as

$^{100}\text{Mo}$ ,  $^{82}\text{Se}$ ,  $^{150}\text{Nd}$ ,  $^{116}\text{Cd}$ ,  $^{130}\text{Te}$ ,  $^{96}\text{Zr}$ ,  $^{48}\text{Ca}$ . Presently, the strongest source is  $^{100}\text{Mo}$  with  $4.1 \times 10^{25}$  nuclei. A 2 kg  $^{82}\text{Se}$  source is planned for a second phase of the experiment. The energy resolution ranges from 11% to 14.5%. Preliminary results achieved with  $^{100}\text{Mo}$  fix the half-life limit to  $6 \times 10^{22}$  y, corresponding to limits of 1.2–2.7 eV on  $\langle m_\nu \rangle$ .<sup>15)</sup> The final sensitivity to this parameter is 0.1–0.3 eV.

Bolometric detection of particles is a calorimetric technique particularly suitable to  $0\nu$  DBD search, providing high energy resolution and large flexibility in the choice of the sensitive material.<sup>23)</sup> In bolometers, the energy deposited in the detector, kept at about 10 mK, by a nuclear event is measured by recording the temperature increase of the detector as a whole. The choice has fallen on natural  $\text{TeO}_2$  (tellurite) that has reasonable mechanical and thermal properties together with a very large (27% in mass) content of the  $2\beta$ -candidate  $^{130}\text{Te}$ . Moreover, the reasonably high transition energy (2528.8 keV) and the favorable nuclear matrix elements make this nuclide one of the best candidate for  $0\nu$  DBD search. A large international collaboration is presently running an experiment, named CUORICINO, based on this approach and installed in the Gran Sasso underground laboratory (Italy).<sup>14)</sup> CUORICINO consists of a tower of 13 modules, containing 62  $\text{TeO}_2$  crystals for a total mass of  $\sim 41$  kg, corresponding to a source strength of  $6.4 \times 10^{25}$   $^{130}\text{Te}$  nuclei. Preliminary results of CUORICINO are quite encouraging: a very low background (of 0.19 counts/(keV kg y)) was obtained in the DBD region, similar to the one achieved in the HM set-up. The energy resolution is about 8 keV FWHM, quite reproducible in all the crystals. The achieved limits on half-life and  $\langle m_\nu \rangle$  are respectively  $7.5 \times 10^{23}$  y and 0.32–1.6 eV.<sup>14)</sup> The latter is not far from that obtained with Ge-diodes in ten years. The sensitivity to  $\langle m_\nu \rangle$  for three years operation is 0.13–0.31 eV. Therefore, CUORICINO has a good chance to see a signal rather soon if the HM claim represents genuine observation of  $0\nu$ -DBD. However, it cannot disprove it due to the uncertainty on the nuclear matrix elements.

### 3 The future

DBD search is so a hot topic in today particle physics that a big number of projects have been proposed or are in the R&D phase, aiming at sensitivities in the range 10–50 meV on  $\langle m_\nu \rangle$ . For lacking of space, we refer to them in table

2, while we will give a short descriptions only of the most promising future experiments. For all of them, a realistic time scale is several years. More details can be found in recent reviews <sup>3)</sup> and in the references therein.

Table 2: *Summary of proposed future experiments for  $0\nu$ -DBD search*

Experiment	Isotope	Experimental approach
CAMEO	$^{116}\text{Cd}$	1 t $\text{CdWO}_4$ crystals
CANDLES	$^{48}\text{Ca}$	Tons of $\text{CaF}_2$ crystals in liq. scint.
COBRA	$^{130}\text{Te}$ , $^{116}\text{Cd}$	CdTe semiconductors
CUORE	$^{130}\text{Te}$	750 kg $\text{TeO}_2$ bolometers
DCBA	$^{150}\text{Nd}$	20 kg Nd layers in tracking chamb.
EXO	$^{136}\text{Xe}$	1 t Xe TPC (gas or liquid)
GEM	$^{76}\text{Ge}$	1 t Ge diodes in liquid $\text{N}_2$
GENTUS	$^{76}\text{Ge}$	1 t Ge diodes in liquid $\text{N}_2$
LNGS-LoI 35/04	$^{76}\text{Ge}$	1 t Ge diodes in liquid $\text{N}_2$ or Ar
GSO	$^{160}\text{Gd}$	2 t $\text{Gd}_2\text{SiO}_5\text{:Ce}$ in liquid scint.
MAJORANA	$^{76}\text{Ge}$	500 kg segmented Ge diodes
MOON	$^{100}\text{Mo}$	Mo sheets in plastic or liq. scint.
SUPER-NEMO	$^{82}\text{Se}$ , $^{100}\text{Mo}$	Ext. sources with composite detectors
XE	$^{136}\text{Xe}$	1.56 t of Xe as liquid scintillator
XMASS	$^{136}\text{Xe}$	10 t of liquid Xe

A very appealing approach remains the study of  $^{76}\text{Ge}$  with conventional Ge spectrometers, either in a traditional set-up (MAJORANA project <sup>24)</sup> or in a new configuration consisting of dipping Ge diodes in liquid nitrogen, acting both as cryogen for detector operation and as highly pure passive shield. <sup>25, 26)</sup> The main drawback of these experiments consist in the low isotopic abundance of  $^{76}\text{Ge}$  (7.8 %), which makes isotopic enrichment mandatory and economically prohibitive on such a large scale. Perhaps the best compromise between cost and sensitivity is represented by the CUORE project, <sup>27)</sup> a bolometric experiment which extends CUORICINO by a factor  $\sim 25$ . The high isotopic abundance of  $^{130}\text{Te}$  allows to approach a source strength of  $10^{27}$  nuclides without enrichment. Other competitive projects are based either on revolutionary techniques for background suppression (as for EXO, <sup>28)</sup> that aims at the coincident detection of the emitted electrons and of the  $^{136}\text{Ba}^{2+}$  ion) or on the use of existing facilities conceived for other searches to shield efficiently the detectors

(as for CAMEO <sup>29</sup>) and GEM, <sup>30</sup>) that could be housed in BOREXINO).

### References

1. Yu.G. Zdesenko, Rev. Mod. Phys. **74**, 683 (2002).
2. V.I. Tretyak and Yu.G. Zdesenko, At. Data Nucl. Data Tables, **80**, 83 (2002).
3. S.R. Elliot and P. Vogel, Ann. Rev. Nucl. Part. Sci. **52**, 115 (2002); S.R. Elliot and J. Engel, preprint hep-ph/0405078 (2004).
4. M. Göppert-Mayer, Phys. Rev. **48**, 512 (1935).
5. H.V. Klapdor-Kleingrothaus, H. Päs and A.Y. Smirnov, Phys.Rev. **D63**, 073005 (2001).
6. S. Pascoli, S.T. Petcov and W.Rodejohann, hep-ph/0212113 (2002).
7. G. F. Dell'Antonio and E. Fiorini, Suppl. Nuovo Cimento **17**, 132 (1960).
8. H.V. Klapdor-Kleingrothaus *et al*, Eur. Phys. J. A **12**, 147 (2001).
9. C.E. Aalseth *et al*, Phys. Rev. C **59**, 2108 (1999); hep-ex/0202026 (2002).
10. C. Arnaboldi *et al*, Phys. Lett. **B557**, 167 (2003).
11. R. Bernabei *et al*, INFN-LNGS internal report, INFN/EXP-08/03, October 2003.
12. F. Danevich *et al*, presented at NANP2003, Dubna, Russia, June 23–28, 2003.
13. H. Ejiri *et al*, Phys. Rev. C **63**, 065501 (2001).
14. C. Arnaboldi *et al*, Phys. Lett. **B584**, 260 (2004); private communication from the CUORICINO collaboration.
15. Barabash *et al*., “Nemo-3 Double Beta Decay Experiment: Present Status”, presented at TAUP2003, Seattle, USA, September 5–9, 2003.

16. H.V. Klapdor-Kleingrothaus *et al.*, Mod. Phys. Lett. A **16**, 2409 (2001);  
H.V. Klapdor-Kleingrothaus *et al.*, Nucl. Instrum. and Meth. A **510**, 281 (2003).
17. C.E.Aalseth *et al.*, Mod. Phys. Lett. A **17**, 1475 (2002).
18. S.T. Belyaev *et al.*, presented at NANP2003, Dubna, Russia, June 23–28, 2003.
19. F.Feruglio *et al.*, Nucl. Phys. B **637**, 345 (2002).
20. Yu.G. Zdesenko *et al.*, Phys. Lett. **B546**, 206 (2002).
21. H.V. Klapdor-Kleingrothaus *et al.*, Phys. Lett. **B586**, 198 (2004); H.V. Klapdor-Kleingrothaus *et al.*, Nucl. Instrum. Meth. A **522**, 371 (2004).
22. X. Sarazin *et al.*, preprint hep-ex/0006031A.
23. E. Fiorini and T. Niinikoski, Nucl. Instrum. and Meth. **224**, 83 (1984).
24. C. E. Aalseth *et al.*, preprint hep-ex/0201021 (2002).
25. H. V. Klapdor-Kleingrothaus *et al.*, Int. J. Mod. Phys. A **13**, 3953 (1998);  
J. Phys. G. **24**, 483 (1998); preprint hep-ph/0206249 and references therein.
26. S. Schoenert *et al.*, LNGS-LoI 35/04 “A new  $^{76}\text{Ge}$  Double Beta Decay Experiment at LNGS”.
27. C. Arnaboldi *et al.*, Astropart. Phys. **20**, 91 (2003); R. Ardito *et al.*, CUORE proposal, submitted to INFN, DOE, NSF.
28. M. Danilov *et al.*, Phys. Lett. **B480**, 12 (2000).
29. G. Bellini *et al.*, Eur. Phys. J. C **19**, 43 (2001).
30. Yu. G. Zdesenko *et al.*, J. Phys. G **27**, 2129 (2001) and preprint nucl-ex/0106021.

Frascati Physics Series Vol. XXXV (2004), p. 51  
HEAVY QUARKS AND LEPTONS - San Juan, Puerto Rico, June 1-5, 2004

## NEUTRINOS AND ASTROPHYSICS

P. Langacker  
*University of Pennsylvania, 3451 Walnut Street, Philadelphia,*  
PA 19104 215-898-5000

Written contribution not received



Frascati Physics Series Vol. XXXV (2004), pp. 53-62  
HEAVY QUARKS AND LEPTONS - San Juan, Puerto Rico, June 1-5, 2004

**ATMOSPHERIC NEUTRINOS:  
PAST, PRESENT AND FUTURE**

Takaaki Kajita  
*Research Center for Cosmic Neutrinos,  
Institute for Cosmic Ray Research, Univ. of Tokyo  
Kashiwa-no-ha 5-1-5, Kashiwa, Chiba 277-8582, Japan*

**ABSTRACT**

Neutrino oscillations was discovered by studying atmospheric neutrinos. The present data are consistent with pure 2 flavor  $\nu_\mu \rightarrow \nu_\tau$  oscillations. The allowed  $\nu_\mu \rightarrow \nu_\tau$  oscillation parameter region is  $\sin^2 2\theta_{23} > 0.92$  and  $1.5 < \Delta m_{23}^2 < 3.4 \times 10^{-3} \text{eV}^2$  at 90%C.L. Recent data from an  $L/E$  analysis found that the  $\nu_\mu$  disappearance probability obeys the sinusoidal function as predicted by neutrino oscillations. Future atmospheric neutrino experiments are also discussed emphasizing the measurement of  $\theta_{13}$  and the sign of  $\Delta m^2$ .

**1 Introduction**

Recently, neutrino oscillations have been studied extensively, since studies of neutrino masses and mixing angles are one of the few ways to explore physics beyond the standard model of particle physics.

Atmospheric neutrinos are produced by cosmic ray interactions in the atmosphere. The atmospheric  $(\nu_\mu + \bar{\nu}_\mu)/(\nu_e + \bar{\nu}_e)$  flux ratio is accurately predicted to be about 2 in the GeV energy region. Also, the atmospheric neutrino flux is predicted to be up-down symmetric for the neutrinos above a few GeV where the geomagnetic field effect on the incident primary cosmic ray particles can be neglected. Neutrino oscillations can be studied by comparing these predictions and the experimental data. Atmospheric neutrinos in the 1 GeV energy range are typically observed as fully-contained (FC) events, which are events occurring inside the fiducial volume of a detector and all the visible secondary particles stop inside the detector.  $\nu_\mu$  interactions in the 10 GeV energy range typically generate muons that pass through a detector. These events are identified as partially-contained (PC) events. High energy (typically between 10 and 1000 GeV)  $\nu'_\mu$ s that interact in the rock surrounding the detector are observed as upward going muons. Atmospheric neutrino experiments that observed these events have been contributing to the study of neutrino oscillations. This article describes the past, present and future studies of atmospheric neutrinos. Some results presented in this article have been updated after the conference.

## 2 Past

An initial, serious hint for the atmospheric neutrino oscillation was reported in 1988 when a smaller  $\nu_\mu/\nu_e$  flux ratio than expected in the 1 GeV energy region was observed in Kamiokande <sup>1)</sup>. This observation was confirmed by the IMB <sup>2)</sup> and Soudan-2 <sup>3)</sup> experiments. This result together with the size of the earth and the typical neutrino energy indicated the lower bound on  $\Delta m^2$ . In addition, these results indicated a large mixing angle. Subsequently, a zenith-angle dependent deficit of  $\nu_\mu$  events was observed <sup>4)</sup> for neutrinos in the multi-GeV energy range. The zenith angle dependence implied an upper limit on  $\Delta m^2$ . However, the data statistics was not high enough to be conclusive. Also, both  $\nu_\mu \rightarrow \nu_e$  and  $\nu_\mu \rightarrow \nu_\tau$  were allowed. Following these early studies, in 1998, neutrino oscillation ( $\nu_\mu \rightarrow \nu_\tau$ ) was discovered by Super-Kamiokande, which showed statistically significant zenith angle and energy dependent  $\nu_\mu$  deficit <sup>5)</sup>. Consistent results have been obtained from the other recent atmospheric neutrino experiments (see below).

### 3 Present

As of this writing, there are three major atmospheric neutrino experiments; Super-Kamiokande, Soudan-2 and MACRO. Two experiments have already stopped taking data. However the (near) final results have been published only recently. Thus results from these experiments are described.

Figure 1(top) shows the zenith angle distributions for various data samples from Super-Kamiokande (6). The zenith angle and energy dependent deficit of  $\mu$ -like (mostly charged current  $\nu_\mu$ ) events is clearly seen. Consistent results have been obtained from the analysis of the contained events in Soudan-2 (7) and the upward-going muons and PC events in MACRO (8), see Fig. 1.

Since there is no evidence for the oscillations involving  $\nu_e$  (see Fig. 1),  $\nu_\mu \rightarrow \nu_\tau$  oscillation is assumed to fit the data. The allowed regions for the  $\nu_\mu \rightarrow \nu_\tau$  oscillation parameters are estimated from these zenith angle distributions in Super-Kamiokande. In recent analyses in Soudan-2 (7) and MACRO (8), the data are plotted on the  $L/E$  axis and the oscillation analyses were carried out. (However, due to the limited event statistics and due to the resolution in  $L/E$ , the dip, which corresponds to the first maximum oscillation, in the  $L/E$  plots have not been observed in these experiments.) There are various sources of the systematic errors in the measurement. These errors are carefully evaluated and are taken into account in the fitting. The allowed regions of  $\nu_\mu \rightarrow \nu_\tau$  oscillation parameters from these experiments are shown in Figure 2. The allowed regions from various experiments are consistent. The 90% C.L. allowed region from Super-Kamiokande is  $1.5 \times 10^{-3} < \Delta m^2 < 3.4 \times 10^{-3} \text{eV}^2$  and  $\sin^2 2\theta > 0.92$ . Also shown is the allowed parameter region from the K2K long baseline experiment (9). The allowed regions from atmospheric and long baseline experiments are consistent.

In addition, atmospheric neutrino data have been used to constrain various alternative models such as  $\nu_\mu \rightarrow \nu_{sterile}$  oscillations (11) (12).

#### 3.1 $L/E$ analysis

Although Fig. 1 shows a clear zenith angle and energy dependent deficit of  $\nu_\mu$  events, these plots do not show any direct evidence for sinusoidal  $\nu_\mu$  survival probability as predicted by neutrino oscillations. Indeed, other models, such as

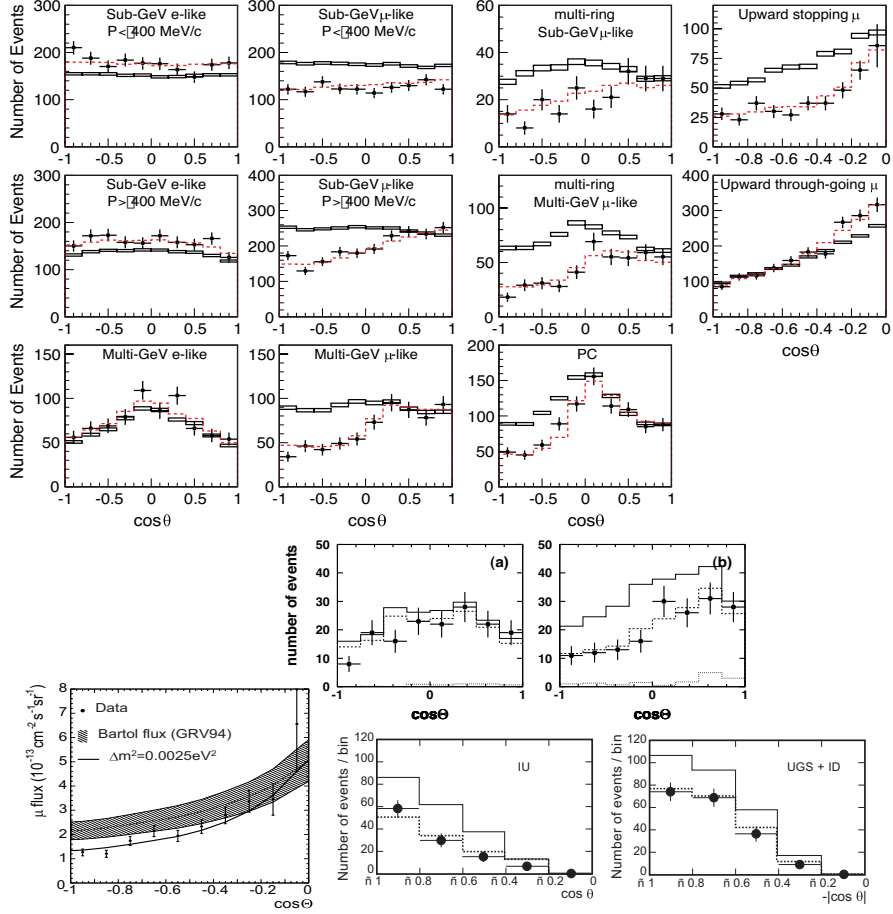


Figure 1: Zenith angle distributions for atmospheric neutrino events observed in Super-Kamiokande (top), Soudan-2 (middle, (a)e-like, (b) $\mu$ -like) and MACRO (bottom, left: through-going muon flux, middle: upward-going PC, right: upward-going stopping muons + downward-going PC).  $\cos\theta = 1(-1)$  means down-going (up-going). The histograms show the prediction with and without neutrino oscillations ( $\nu_\mu \rightarrow \nu_\tau$ ).

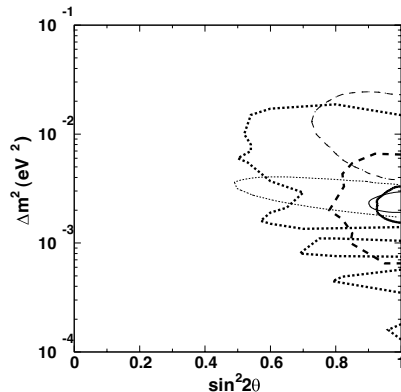


Figure 2: 90% C.L. allowed neutrino oscillation parameter regions for  $\nu_\mu \rightarrow \nu_\tau$  from atmospheric neutrino experiments <sup>10)</sup> (Kamiokande, thin dashed line) <sup>7)</sup> (Soudan-2, thick dotted line) <sup>8)</sup> (MACRO, thick dashed line) <sup>6)</sup> (Super-Kamiokande, thick line). The allowed region from the L/E analysis in Super-Kamiokande is shown by the thin line. The thin dotted line shows the allowed region from K2K <sup>9)</sup>.

the neutrino decay <sup>14)</sup> or the decoherence <sup>15)</sup> models, reasonably reproduce the observed atmospheric neutrino data. In order to really confirm neutrino "oscillation", it is important to demonstrate that the  $\nu_\mu$  survival probability obeys a sinusoidal function.

Recently Super-Kamiokande has shown evidence that the  $\nu_\mu$  survival probability obeys the sinusoidal function <sup>13)</sup>. They have selected events whose  $L/E$  resolution is better than 70%. Figure 3 (left) shows data/(non-oscillated MC) for  $\mu$ -like events as a function of  $L/E$  together with predictions by oscillation, decay and decoherence models. A dip was observed around  $L/E = 500\text{km/GeV}$  as predicted by Monte Carlo with neutrino oscillations. Clearly the oscillation prediction gives the best fit to the data. The  $\chi^2$  values for decay and decoherence models were 11.3 (3.4 standard deviations) and 14.5 (3.8 standard deviations) larger than that for oscillation, respectively. This is the first evidence that the neutrino survival probability obeys a sinusoidal function as predicted by neutrino oscillations. The neutrino oscillation parameters are determined by the  $L/E$  distribution. Figure 3 (right) shows the allowed parameter region from the  $L/E$  analysis. Since the dip is observed in

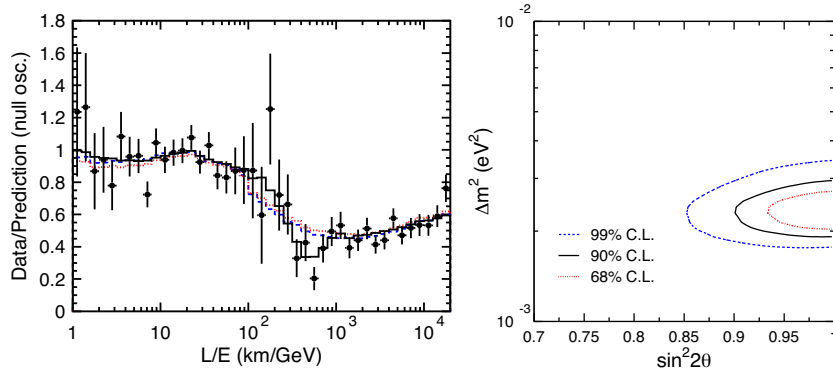


Figure 3: *Left: (Number of  $\mu$ -like events)/(predicted number of  $\mu$ -like events without oscillation) as a function of  $L/E$  from Super-Kamiokande. Only high  $L/E$  resolution FC+PC events were used. The solid, dashed and dotted histograms show the best-fit expectation for 2-flavor  $\nu_\mu \leftrightarrow \nu_\tau$  oscillations, neutrino decay and neutrino decoherence, respectively. Right: 68, 90 and 99% allowed  $\nu_\mu \rightarrow \nu_\tau$  oscillation parameter regions obtained by the  $L/E$  analysis.*

the distribution,  $\Delta m^2$  value is determined accurately.

#### 4 Future

The atmospheric neutrino experiments will continue to improve the determination of  $\theta_{23}$  and  $\Delta m_{23}^2$  parameters with the increasing data statistics. In addition, atmospheric neutrinos should be sensitive to other oscillation parameters. The sensitivities of future atmospheric neutrino detectors in the search for non-zero  $\theta_{13}$  and the determination of the sign of  $\Delta m_{23}^2$  are discussed.

##### 4.1 $\theta_{13}$

$\theta_{13}$  is a key parameter for the understanding of the neutrino mixing matrix. Therefore, various reactor and long-baseline accelerator experiments are designed to measure  $\theta_{13}$ . Atmospheric neutrino experiments have sensitivities in  $\theta_{13}$  as well. Assuming that the effect of  $\Delta m_{12}^2$  and  $\theta_{12}$  can be neglected (a reasonable assumption for multi-GeV atmospheric neutrinos), for example,  $\nu_\mu \rightarrow \nu_e$  oscillation probability is written as;

$$P(\nu_\mu \rightarrow \nu_e) = \sin^2 \theta_{23} \sin^2 2\theta_{13} \sin^2 \left( \frac{1.27 \Delta m_{23}^2 L}{E_\nu} \right), \quad (1)$$

Since  $\nu_e$  is involved in the oscillation, the matter effect (16)–(17) must be taken into account. The effect of a non-zero  $\theta_{13}$  could be observed as an excess of electron neutrinos in the upward-going direction through the matter resonance effect in the high energy range. For  $\Delta m^2 = 2$  to  $3 \times 10^{-3} \text{eV}^2$ , the resonance could occur for neutrinos with their energies between 5 and 10 GeV. Figure 4 (left) shows the  $\nu_e \leftrightarrow \nu_\mu$  oscillation probability as a function of the neutrino energy and zenith angle. A clear resonance effect is seen for upward-going neutrinos near 5 GeV. The present data, however, show no evidence for excess  $e$ -like events in the upward-going direction (see Fig. 1), and therefore set a limit on  $\sin^2 2\theta_{13}$  as shown in Fig. 4 (right).

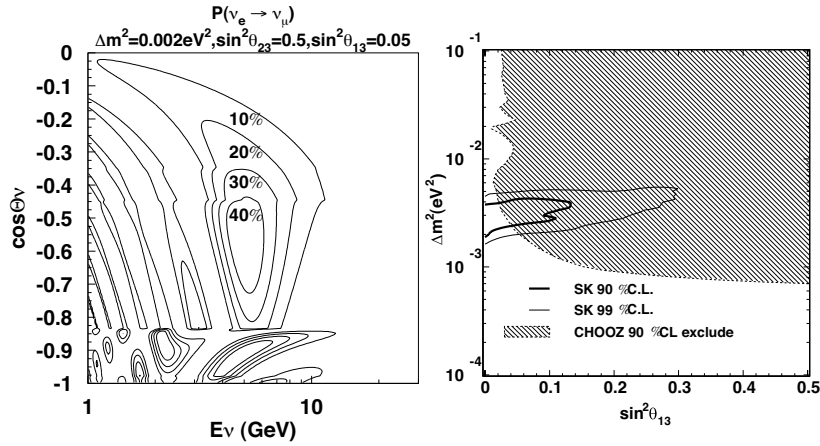


Figure 4: Left:  $\nu_e \leftrightarrow \nu_\mu$  oscillation probability for neutrinos passing through the earth as a function of the neutrino energy and zenith angle for  $\Delta m_{23}^2 = +2.0 \times 10^{-3} \text{eV}^2$  (positive  $\Delta m^2$ ),  $\sin^2 \theta_{23} = 0.50$  and  $\sin^2 \theta_{13} = 0.05$ . Right: 90 and 99% C.L. allowed regions on  $\sin^2 2\theta_{13}$  and  $\Delta m_{23}^2$  for positive  $\Delta m_{23}^2$  from Super-Kamiokande (1489 day data). Also shown is a 90% C.L. excluded region from the CHOOZ reactor experiment (18).

Figure 5 shows the expected  $\chi^2$  difference between the finite and null  $\sin^2 \theta_{13}$  assumptions for various  $\sin^2 \theta_{13}$ ,  $\sin^2 \theta_{23}$  and  $\Delta m_{23}^2$  values in a large water Cherenkov detector (23). It is evident that the chance of observing finite  $\theta_{13}$  increases for larger  $\sin^2 \theta_{23}$  (19). It is also found that the sensitivity does not depend strongly on  $\Delta m_{23}^2$ . Because of the matter effect, the sensitivity slowly changes above  $\sin^2 \theta_{13} = 0.01$ . It seems that the improvement of the data statistics by a factor of about 5 compared with the present statistics in

Super-Kamiokande is very important to observe a non-zero  $\theta_{13}$ .

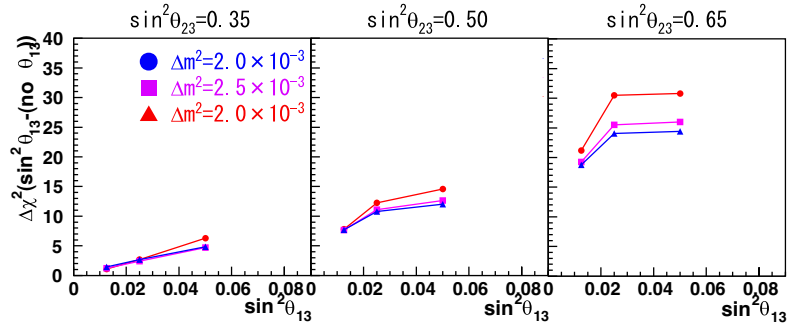


Figure 5: Expected  $\chi^2$  difference between the finite and null  $\sin^2 \theta_{13}$  for  $\Delta m^2_{23} = +2.0$  (circle),  $2.5$  (square) and  $3.0 \times 10^{-3} eV^2$  (triangle) (positive  $\Delta m^2_{23}$ ), and  $\sin^2 \theta_{23} = 0.35$  (left),  $0.5$  (center) and  $0.65$  (right). The detector exposure is assumed to be  $450$  kton-yr.

The resonance effect occurs only for neutrinos for positive  $\Delta m^2$ , and therefore only appears for the  $e^-$  and  $\mu^-$  spectrum. This, in turn, suggests that the sign of  $\Delta m^2_{23}$  could be measured by atmospheric neutrino experiments that are sensitive to the charge of the leptons. Large magnetized detectors (20) (21) could be sensitive to the sign of  $\Delta m^2_{23}$ . It is expected that these detectors can determine the sign of  $\Delta m^2_{23}$  if  $\sin^2 2\theta_{13}$  is larger than  $0.1$  ( $0.05$ ) for the detector exposure of  $200$  ( $400$ ) kton-yr (20).

Super-Kamiokande and other water Cherenkov detectors are unable to distinguish  $\nu_e$  and  $\bar{\nu}_e$  interactions event-by-event bases. However, the cross section and the  $y$  ( $= (E_\nu - E_{lepton})/E_\nu$ ) dependence of the cross section are different between  $\nu$  and  $\bar{\nu}$ , and therefore it may be possible to distinguish the positive and negative  $\Delta m^2_{23}$ . Since the neutrino interactions produce more high- $y$  events (i.e., more multi-hadron events) than the anti-neutrino interactions, a larger effect of the finite  $\theta_{13}$  can be seen in multi-ring  $e$ -like events for positive  $\Delta m^2_{23}$  than for negative  $\Delta m^2_{23}$ . It was concluded, based on a detailed MC study, that it is possible to measure the sign of  $\Delta m^2_{23}$  in water Cherenkov detectors, if the  $\sin^2 \theta_{13}$  and  $\sin^2 \theta_{23}$  values are near the present limit and  $\geq 0.5$ , respectively, provided that the detector exposure is about  $1$  Mton-yr or larger (23).

The present study does not include the oscillation terms that are related to solar neutrinos ( $\theta_{12}$  and  $\Delta m^2_{12}$ ). It has been pointed out that the  $\theta_{12}$  and  $\Delta m^2_{12}$

terms could play unique roles to the atmospheric neutrino oscillations, such as the possible measurement of  $\sin^2 \theta_{23}$ , (i.e., the discrimination of  $\theta_{23} > 45^\circ$  and  $< 45^\circ$ )<sup>22</sup>). These effects should be studied seriously taking various systematic errors into account.

## 5 Summary

Neutrino oscillation was discovered by studies of the atmospheric  $\nu_\mu/\nu_e$  flux ratio and the zenith angle dependence of the atmospheric neutrino flux. Atmospheric neutrinos are still playing a major role in the study of neutrino oscillations. The present data from various experiments are explained well by  $\nu_\mu \rightarrow \nu_\tau$  oscillations. The recent  $L/E$  analysis from Super-Kamiokande has shown that the  $\nu_\mu$  disappearance probability obeys the sinusoidal function as predicted by neutrino oscillations, excluding various other explanations of the data.

If the data statistics are high enough, future atmospheric neutrino experiments could measure  $\theta_{13}$  and the sign of  $\Delta m_{23}^2$ . It is likely that future atmospheric neutrino experiments will continue to make unique contributions to the study of neutrino oscillations.

## 6 Acknowledgements

This work has been supported by the Japanese Ministry of Education, Culture, Sports, Science and Technology.

## References

1. K.S. Hirata, *et al.*, Phys. Lett. B **205** 416 (1988).
2. D. Casper *et al.*, Phys. Rev. Lett. **66** 2561 (1991).
3. W.W.M. Allison *et al.*, Phys. Lett. B **391** 491 (1997).
4. Y. Fukuda *et al.*, Phys. Lett. B **335** 237 (1994).
5. Y. Fukuda *et al.*, Phys. Rev. Lett. **81** 1562 (1998).
6. Y. Ashie *et al.*, draft in preparation; also, E. Kearns, for the Super-Kamiokande collaboration, talk presented at the XXIth International

- conference on Neutrino Physics and Astrophysics (Neutrino2004), Paris, France, June 2004.
7. M. Sanchez *et al.*, Phys. Rev. D **68** 113004 (2003).
  8. M. Ambrosio *et al.*, Phys. Lett. B **566** 35 (2003).
  9. T. Nakaya, for the K2K collaboration, talk presented at the XXIth International conference on Neutrino Physics and Astrophysics (Neutrino2004), Paris, France, June 2004.
  10. S. Hatakeyama *et al.*, Phys. Rev. Lett. **81** 2016 (1998).
  11. S. Fukuda *et al.*, Phys. Rev. Lett. **85** 3999 (2000).
  12. M. Ambrosio *et al.*, Phys. Lett. B **517** 59 (2001).
  13. Y. Ashie *et al.*, Phys. Rev. Lett. in press, hep-ex/0404034.
  14. V.D. Barger *et al.*, Phys. Lett. B **462** 109 (1999).
  15. E. Lisi *et al.*, Phys. Rev. Lett. **85** 1166 (2000).
  16. S.P. Mikheyev and A.Yu. Smirnov, Sov. J. Nucl. Phys. **42**, 1441 (1985); Nuovo Cimento C **9**, 17 (1986).
  17. L. Wolfenstein, Phys. Rev. D. **17**, 2369 (1978).
  18. M. Apollonio, *et al.*, Phys. Lett. B **466**, 415 (1999).
  19. J. Bernabeu, S. Palomares-Ruiz and S.T. Petcov, Nucl. Phys. B **669**, 255 (2003).
  20. Tommaso Tabarelli de Fatis, Proc. of La Thuile 2001, Results and perspectives in particle physics, La Thuile, Italy (2001) p.677, hep-ph/0106252.
  21. G.Rajasekaran, hep-ph/0402246.
  22. O.L.G. Peres and Y.Au. Smirnov, Phys. Lett. B **456** 204 (1999); O.L.G. Peres and Y.Au. Smirnov, Nucl. Phys. B **680** 479 (2004).
  23. T. Kajita *et al.*, talk presented at the 5th International Workshop on Neutrino Oscillations and their Origin (NOON2004), Tokyo, Japan, Feb. 2004; to appear in the proceedings.

## THE LSND SIGNAL: PAST, PRESENT AND FUTURE

Ion Stancu – for the MiniBooNE collaboration <sup>1)</sup>  
*University of Alabama, Tuscaloosa, AL 35487, USA*

### ABSTRACT

The MiniBooNE experiment at Fermilab has been designed to confirm or dismiss the LSND observation by looking for  $\nu_e$  appearance in a  $\nu_\mu$  beam. The experiment began taking beam data in September 2002. Here we describe the experiment, the first neutrino candidate events, and our expected sensitivity to a neutrino oscillation signal.

### 1 Introduction

Neutrino oscillations appear to be a widely-accepted phenomenon which successfully explains the solar electron neutrino deficit, as well as the atmospheric muon neutrino deficit. Moreover, the same deficits have been observed in artificial neutrino sources, as reported by the KamLAND <sup>2)</sup> and K2K <sup>3)</sup> experiments, respectively. The mass squared differences involved in these phenomena

are  $\Delta m_{sol}^2 \approx 7 \times 10^{-5} \text{ eV}^2/c^4$  and  $\Delta m_{atm}^2 \approx 3 \times 10^{-3} \text{ eV}^2/c^4$ , while the corresponding mixing angles appear to be nearly maximal. In addition, the LSND experiment, which ran at the Los Alamos National Laboratory from August 1993 until December 1998, has also reported evidence for neutrino oscillations in two channels: the decay-at-rest channel  $\bar{\nu}_\mu \rightarrow \bar{\nu}_e$ , and the decay-in-flight channel  $\nu_\mu \rightarrow \nu_e$ . The LSND final result <sup>4)</sup>, combining all the data, yielded an excess of  $87.9 \pm 22.4 \pm 6.0$  events after background subtraction, which corresponds to an oscillation probability of  $(0.264 \pm 0.067 \pm 0.045)\%$ . The allowed values in the  $(\sin^2 2\theta, \Delta m^2)$  parameter space corresponding to this result are shown in Figure 1. Also shown are the 90% confidence level excluded regions

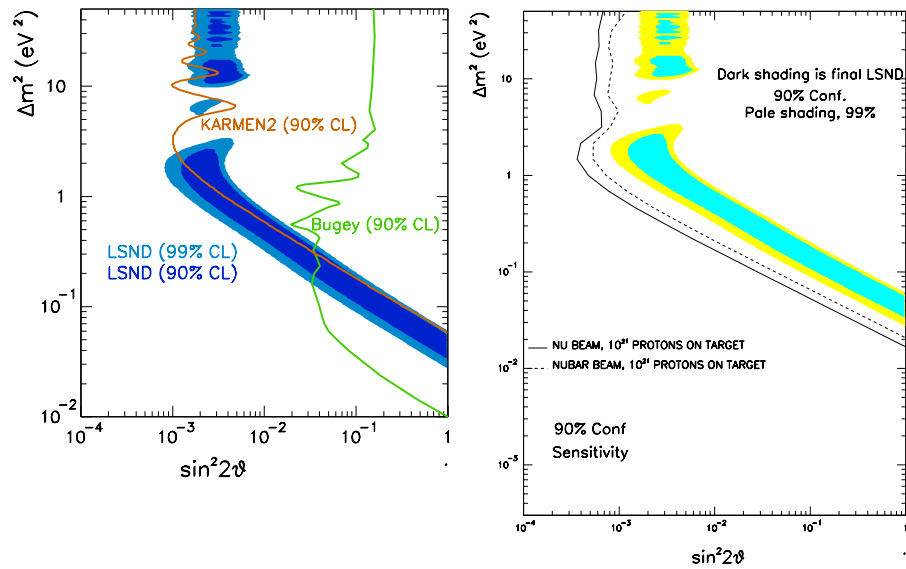


Figure 1: *LSND allowed regions in the  $(\sin^2 2\theta, \Delta m^2)$  parameter space and MiniBooNE expected oscillation sensitivity after 2 years of running.*

for the Bugey <sup>5)</sup> and KARMEN <sup>6)</sup> experiments. Despite the fact that the KARMEN data appears to exclude a significant fraction of the LSND-favoured region, a combined analysis of the two data sets showed that practically this entire region is compatible with both experiments at the 90% confidence level <sup>7)</sup>.

The Booster Neutrino Experiment (BooNE) at Fermilab is a natural follow-up to the LSND experiment, and has been designed to confirm or dismiss

the evidence for neutrino oscillations reported by the Los Alamos measurement. The first phase of the project, a single detector known as MiniBooNE (E-898), has become fully operational in September 2002. The experiment has two initial goals: (i) extend the sensitivity for  $\nu_\mu \rightarrow \nu_e$  oscillations by one order of magnitude in  $\Delta m^2$  over previous searches; (ii) obtain several hundreds of events per year if the LSND signals are indeed due to neutrino oscillations. Moreover, should neutrino oscillations be observed, MiniBooNE can test for CP violation in the lepton sector by switching to an antineutrino ( $\bar{\nu}_\mu$ ) beam, while the full BooNE project would add a second detector, at a distance dictated by the data themselves, and carefully parameterize the  $\nu_\mu \rightarrow \nu_e$  and  $\bar{\nu}_\mu \rightarrow \bar{\nu}_e$  mixings.

## 2 The Neutrino Beam

The MiniBooNE neutrino beam is initiated by a primary beam of 8 GeV protons from the Fermilab Booster accelerator incident on a 71-cm-long Be target within a magnetic horn focusing system, followed by a 50-m-long pion decay volume. The proton beam is delivered to the experiment at a rate of up to 5 Hz and an intensity of approximately  $5 \times 10^{12}$  per spill. Each spill is made up of 84 buckets of beam every 18.8 ns for a total duration of  $1.6 \mu\text{s}$  – which allows for a very low cosmic-ray background in the detector. The Booster can reliably deliver protons for about two thirds of a calendar year, which allows the experiment to receive up to  $5 \times 10^{20}$  protons on target (POT) per year.

The magnetic horn focuses secondary pions and kaons from the primary interactions. It operates at a current of 170 kA for a pulse duration of  $140 \mu\text{s}$ , producing a toroidal magnetic field that focuses  $\pi^+$  and defocuses  $\pi^-$  (or vice-versa). Therefore, a fairly pure  $\nu_\mu$  or  $\bar{\nu}_\mu$  beam can be produced, depending on the horn polarity. Figure 2 shows the shape of the expected neutrino fluxes at the location of the detector.

The neutrino flux at the detector will be determined using a variety of methods. Detailed simulations of the neutrino production processes have been performed and are ongoing. These simulations have been tuned using existing hadron production data, and will be complemented by data from the HARP experiment <sup>8)</sup> at CERN – which ran with the MiniBooNE Be target. A measurement of the  $\nu_\mu$  charged-current rate in the detector will check the  $\nu_\mu$  flux, as well as determine the energy distribution of the muons in the decay region – which contribute to the intrinsic  $\nu_e$  background via  $\mu^+ \rightarrow e^+ \nu_e \bar{\nu}_\mu$ . The  $\nu_e$

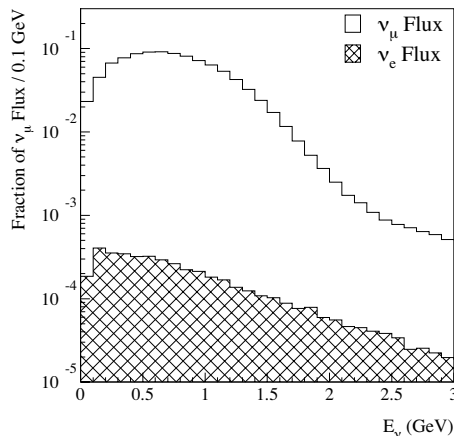


Figure 2: *Calculated MiniBooNE neutrino fluxes at the location of the detector.*

background from  $K^+ \rightarrow \pi^0 e^+ \nu_e$  decays will be determined by measuring the high-transverse-momentum muons from  $K^+ \rightarrow \mu^+ \nu_\mu$  decays.

### 3 The Detector

The MiniBooNE detector is located 500 meters from the neutrino source. It consists of a spherical tank of radius 6.1 m, lined with 1280 8-inch photomultiplier tubes (PMTs) supported on an inner structure of 5.75 m radius. These PMTs point inward and provide 10% photocathode surface coverage. The PMT support structure also provides an optical barrier to create an outer veto region, viewed by 240 8-inch PMTs. The tank is filled with 800 tons of mineral oil, which provides an inner fiducial region of about 500 tons.

The MiniBooNE mineral oil (Exxon/Mobil Marcol 7) has an attenuation length of approximately 26 meters at 450 nm, a density of  $0.836 \text{ g/cm}^3$  and an index of refraction of 1.46. This oil produces some scintillation light, so both prompt Čerenkov and delayed scintillation light will be produced for particles with  $\beta > 0.68$ . The total amount of light provides a good energy measurement for particles above and below the Čerenkov threshold.

A circular room located above the tank vault houses the electronics, data acquisition (DAQ), oil circulation, and calibration systems. The entire struc-

ture is covered with a mound of earth to provide some cosmic-ray shielding. Each PMT is attached to one Teflon-jacketed cable which provides the high voltage (HV) and returns the signal as well. The PMT cables are routed out of the tank into the DAQ system, where the signal is picked off the HV cable, amplified, and digitized. The DAQ hardware consists of custom-built cards in 13 VME crates which are read out via MVME2304 single-board computers (SBC). The data is zero suppressed by the SBCs and shipped via ethernet to a single Intel-based computer running Linux. This computer assembles the data and ships it to the Fermilab computer center where it is written to tape.

The trigger consists of an additional VME crate housing custom-built cards that collect PMT multiplicity and beam information to form event triggers. The primary trigger is a “beam-on-target” signal from the accelerator, which initiates a data readout in a  $20\ \mu\text{s}$  window around the  $1.6\ \mu\text{s}$  beam spill (regardless of PMT multiplicity). The DAQ hardware and software have sufficient data buffering capabilities to create a virtually dead-time-free system.

Calibration for the detector is obtained through three different systems. A pulsed laser provides light to four different light-scattering flasks hanging in the inner region of the tank. This light is used to determine the time and gain calibrations of each of the inner PMTs. An array of seven scintillator cubes hanging in the main region of the tank are used to tag a sample of stopping muons in the tank which allows energy calibration with muon tracks of known length. A muon tracker system consisting of 2 horizontal planes of scintillator is installed above the tank. The tracker allows muons of a well-known direction to be tagged and studied for direction calibration. In addition to these systems, the ubiquitous cosmic-ray muons provide a constant source of data with which to study and calibrate the detector. In particular, the stopped cosmic-ray muons provide, through their subsequent decays, an invaluable source of electrons as cross-checks of the Monte Carlo (MC) simulations, energy scale measure, and energy resolution. Preliminary studies indicate an electron energy resolution of 14% at the Michel electron endpoint energy (52.8 MeV).

#### 4 The MiniBooNE Neutrino Oscillations Search

The  $\nu_\mu \rightarrow \nu_e$  oscillation search will be conducted by measuring the event rate for the  $\nu_e$  induced reaction,  $\nu_e C \rightarrow e^- X$ , and comparing to the rate expected from background processes. If the LSND result is indeed due to neutrino os-

cillations, approximately 1000  $\nu_e$ -induced events are expected due to  $\nu_\mu \rightarrow \nu_e$  oscillations in two calendar years of running ( $10^{21}$  POT). The three main backgrounds to this search are: the intrinsic  $\nu_e$  background in the beam from  $\mu$  and  $K$  decay in the decay pipe, mis-identification of  $\mu$  events ( $\nu_\mu C \rightarrow \mu^- X$ ), and mis-identification of  $\pi^0$  events ( $\nu_\mu C \rightarrow \nu_\mu \pi^0 X$ ). The number of events for signal and backgrounds are listed in Table 1. These backgrounds will be

Table 1: *Estimated number of neutrino oscillation signal and background events after 2 years of data taking with neutrinos ( $10^{21}$  POT). Also shown are the number of events from other neutrino reactions in MiniBooNE.*

Process	Reaction	Number of events
LSND-based $\nu_\mu \rightarrow \nu_e$ signal	$\nu_e C \rightarrow e^- X$	1000
Intrinsic $\nu_e$ background	$\nu_e C \rightarrow e^- X$	1500
Mis-ID $\mu^-$ background	$\nu_\mu C \rightarrow \mu^- X$	500
Mis-ID $\pi^0$ background	$\nu_\mu C \rightarrow \nu_\mu \pi^0 X$	500
$\nu_\mu C$ charged-current scattering	$\nu_\mu C \rightarrow \mu^- X$	500,000
$\nu_\mu C$ neutral-current $\pi^0$ production	$\nu_\mu C \rightarrow \nu_\mu \pi^0 X$	50,000
$\nu_\mu e$ elastic scattering	$\nu_\mu e \rightarrow \nu_\mu e$	100

measured. As described in Section 2, the number of events from intrinsic  $\nu_e$  that are produced from  $\mu^+$  decays in the target region will be determined from  $\nu_\mu$  charged-current scattering in the detector. Also, the number of intrinsic  $\nu_e$  from  $K^+$  decays will be determined from the  $\mu$  detected with the off-axis LMC spectrometer. The number of  $\mu^-$  and  $\pi^0$  events mis-identified as  $e^-$  events will be measured via the large number of correctly identified  $\nu_\mu C \rightarrow \mu^- X$  and  $\nu_\mu C \rightarrow \nu_\mu \pi^0 X$  events, respectively.

## 5 Preliminary Data

The MiniBooNE detector and beam have been fully operational for over a year and a half now, and data taking has been proceeding very smoothly. The detector has been calibrated with laser calibration events, the energy scale and resolution have been determined from cosmic-ray muons and Michel electrons, and approximately 180,000 clean neutrino events have been recorded with  $2.7 \times 10^{20}$  POT. Figure 3 below illustrates the simple selection criteria which reduce the beam off backgrounds to a  $10^{-3}$  level: a veto shield multiplic-

ity cut  $N_{veto} < 6$  eliminates the cosmic-ray muons, while a tank multiplicity cut  $N_{tank} > 200$  eliminates the Michel electrons from the decay of the stopped cosmic-ray muons. The beam pulse width of about  $1.6 \mu\text{s}$  is in clearly seen.

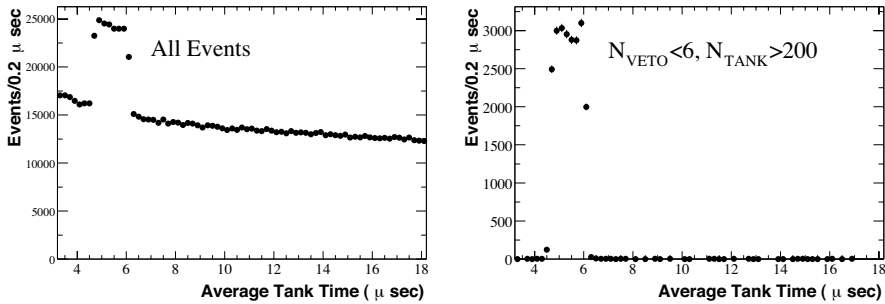


Figure 3: *MiniBooNE event distribution in and around the beam window before and after the simple selection criteria which reduce the beam off background.*

The  $\nu_e$  appearance search will be a blind analysis. Consequently, despite the fact that MiniBooNE can clearly identify the beam-induced events, one is allowed to either look at all information for some events or some information for all events, but not all information for all events. Meanwhile, in parallel to continuing understanding the detector response and tuning the MC simulations, the experiment is concentrating on other physics analyses which are not only interesting in their own right, but they are also necessary for the  $\nu_\mu \rightarrow \nu_e$  oscillations analysis: they will check the data/MC agreement, the reliability of the reconstruction and particle-identification algorithms, and provide understanding of the beam-induced backgrounds.

MiniBooNE is clearly identifying charged-current quasi-elastic  $\nu_\mu C \rightarrow \mu X$  events. These events have a relatively high abundance (about 40%), a simple topology, and can be identified with a relatively high efficiency and purity (of approximately 30% and 90%, respectively). The muons are forward peaked along the incident neutrino beam direction, as clearly seen in Fig. 4 below. The predicted MC distribution is shown superimposed in the same figure, with our current (conservative) estimates for the error bars; they include errors in the neutrino fluxes, cross sections and optical parameters of the detector medium. Both distributions have been normalized to unit area. The visible energy distribution is also in good agreement with the MC expectations, as

illustrated in the same figure.

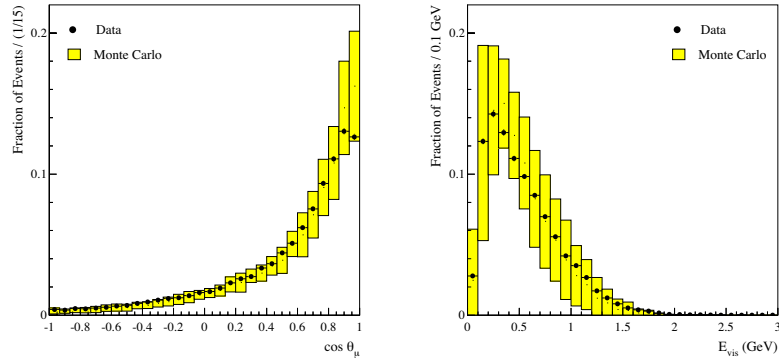


Figure 4: *MiniBooNE reconstructed event direction with respect to the incident neutrino beam and visible (electron-equivalent) energy distributions for  $\nu_\mu C$  charged-current quasi-elastic events.*

From a simple kinematic reconstruction one can use the reconstructed muon energy and direction to calculate the incident neutrino energy and also the momentum transfer. These quantities are shown in Fig. 5 below, along with the MC predictions with a relative normalization. The lower-than-predicted

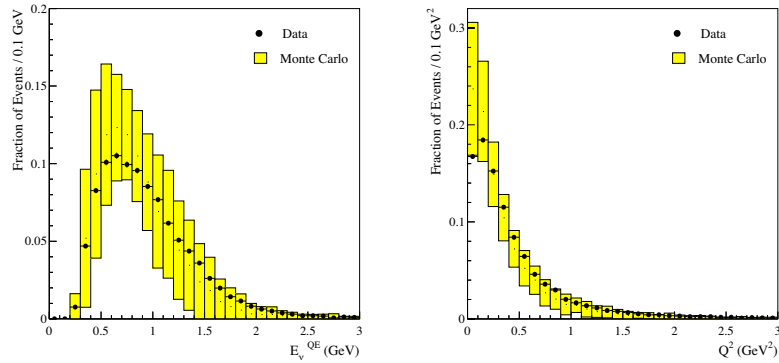


Figure 5: *MiniBooNE reconstructed incident neutrino energy and  $Q^2$  distributions for  $\nu_\mu C$  charged-current quasi-elastic events.*

data values at low  $Q^2$  are currently under investigation and can be influenced by a variety of factors, such as nuclear effects, nuclear form factors, etc. This

effect is also related to the lower-than-predicted number of events in the most forward direction (first bin in the  $\cos\theta_\mu$  distribution of Fig. 4).

MiniBooNE is also clearly identifying and reconstructing neutral current  $\pi^0$  events from either coherent production  $\nu_\mu C \rightarrow \nu_\mu \pi^0 X$ , or resonant production  $\nu_\mu(p/n) \rightarrow \nu_\mu \Delta$  and the subsequent  $\Delta$  decay. These events have a characteristic two ring topology (from the  $\pi^0 \rightarrow \gamma\gamma$  decay), and the invariant  $\pi^0$  is reconstructed from the reconstructed energies of the two photons,  $E_1$  and  $E_2$ , and their relative angle,  $\theta_{12}$ :  $m_\pi^2 = 2E_1E_2(1 - \cos\theta_{12})$ . The distribution of the reconstructed invariant mass is shown in Fig. 6 below, which yields a mass resolution of about 21 MeV. The events contributing to this sample have

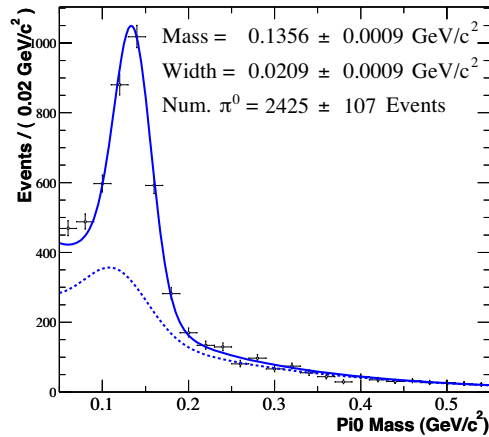


Figure 6: *MiniBooNE* reconstructed  $\pi^0$  mass distribution. The dashed curve denotes the expected background from MC simulations, which is also peaked.

the standard  $N_{veto} < 6$  and  $N_{tank} > 200$  selection criteria applied, the event vertex must reconstruct at least 50 cm away from the surface of the PMTs, and each ring must have at least an electron-equivalent energy of 40 MeV.

## 6 Conclusions

The MiniBooNE detector and beam line have been operating smoothly for over a year and a half now and we are in the process of analyzing different physics channels, while continuously improving our understanding of the detector response and MC simulations. Despite the fact that the total number of protons

on target is a factor of 2.5 below the original design intensity, we are convinced that continuing modifications and improvements to the Fermilab Booster will bring the neutrino beam to the required levels in the near future.

The current plan is to run in the  $\nu_\mu$  mode until MiniBooNE collects  $5 \times 10^{20}$  protons on target, with the possibility of changing to the  $\bar{\nu}_\mu$  mode afterwards and also 25 m absorber running. The future MiniBooNE schedule is dependent on the number of protons delivered per year to the experiment. First oscillations results are expected by 2005, and if the LSND signal is confirmed, an initial determination of the oscillation parameters can be made. A second detector (BooNE) will then be built at a different distance in order to obtain the highest precision measurement of the oscillation parameters. The neutrino flux goes as  $r^{-2}$  to very good approximation, so that a simple ratio of events in the two detectors as a function of energy will cancel most of the systematic uncertainties and will allow  $\Delta m^2$  to be measured to about  $\pm 0.02 \text{ eV}^2/c^4$ .

## References

1. The BooNE collaboration consists of the following institutions: University of Alabama, Bucknell University, University of Cincinnati, University of Colorado, Columbia University, Embry Riddle Aeronautical University, Fermi National Accelerator Laboratory, Indiana University, Los Alamos National Laboratory, Louisiana State University, University of Michigan and Princeton University.
2. K. Eguchi *et al.* (KamLAND Collab.), Phys. Rev. Lett. **90**, 021802 (2003).
3. M. H. Ahn *et al.* (K2K Collaboration), Phys. Rev. Lett. **90**, 041801 (2003).
4. A. Aguilar *et al.* (LSND Collaboration), Phys. Rev. **D64**, 112007 (2001).
5. B. Achkar *et al.*, Nucl. Phys. **B434**, 503 (1995).
6. B. Armbruster *et al.* (KARMEN Collab.), Phys. Rev. **D65**, 112001 (2002).
7. E. D. Church *et al.* (LSND Collaboration), Phys. Rev. **D66**, 013001 (2002).
8. "Proposal to study hadron production for the neutrino factory and for the atmospheric neutrino flux"; M. G. Catanesi *et al.*, CERN-SPSC/99-35 (1999).

Frascati Physics Series Vol. XXXV (2004), pp. 73-88  
HEAVY QUARKS AND LEPTONS - San Juan, Puerto Rico, June 1-5, 2004

## PRESENT STATUS AND PROSPECTS OF NEUTRINO OSCILLATION EXPERIMENTS

A. Ereditato  
*INFN Napoli, Italy*

### ABSTRACT

The solution of the long standing solar and atmospheric neutrino puzzles has led to the unambiguous confirmation that neutrinos oscillate and hence are massive. Several key experiments have contributed to clarify the experimental scenario. A wide programme is being executed and is planned for the next years, aimed at pinning down the oscillation parameters and at more sensitive measurements of the elements of the Pontecorvo, Maki, Nakagawa, Sakata (PMNS) mixing matrix. As far as accelerator neutrino experiments are concerned, further technological advances will be required for both beam facilities and detectors to realize the next generation of experiments that will address the issues of CP violation in the leptonic sector and of mass hierarchy. In this respect, we want to stress here the great potentialities of the LAr Time Projection Chamber (TPC) technology for future applications. The ICARUS R&D programme has demonstrated that the technology is mature and that one can build a large ( $\sim 1$  kton) LAr TPC with a fully industrial method. Nowadays one can conceive and design a very large mass LAr TPC with a mass of 100

kton by employing a monolithic technology based on the use of industrial, large volume cryogenic tankers. Such a detector would be an ideal match for a Super-Beam, a Beta-Beam or a Neutrino Factory, allowing to execute, in addition to a rich accelerator neutrino physics programme, experiments on atmospheric, solar and supernova neutrinos, as well as sensitive searches for nucleon decay.

## 1 Introduction

We can schematically summarize our present knowledge on (massive) neutrinos by stating that

- There is evidence for three light neutrinos in Nature, as an outcome of the LEP experiments <sup>1)</sup>.
- Direct neutrino mass measurements have so far only yielded limits in the range of 1 eV<sup>2</sup> or less. Very stringent limits have also recently come from cosmological measurements <sup>2)</sup>. This reinforces our common belief that the nature and the characteristics of the fascinating neutrino are closely linked to cosmological and astrophysical subjects.
- Neutrino oscillation experiment with solar and atmospheric neutrinos have contributed to build up a solid evidence for neutrino oscillations, hence confirming that neutrinos are massive: this must be considered as the first compelling evidence for physics beyond the Standard Model of particles and interactions.
- Neutrino mixing is described by the so called PMNS 3 x 3 matrix. Two of the mixing angles are rather large ( $\theta_{12}$  and  $\theta_{23}$ ) while the third is small or even null. The two  $\Delta m^2$  experimental values confirm the smallness of the neutrino masses (see *e.g.* <sup>3)</sup>.)

More interesting and stimulating is the list of the 'unknowns'. First is the actual neutrino mass scale and even more the explanation of why neutrino masses are small as compared to the masses of the other fermions. The second question is why (two of) the mixing angles are large (differently from what happens for the quark mixing) and why the third angle is apparently small or equal to zero. Another issue is the neutrino mass hierarchy: is the tau-neutrino the heaviest? Is  $\Delta m_{23}^2$  positive or negative? These important questions can

Table 1: *Global fit of oscillation data (from <sup>3)</sup>).*

Parameter	best fit value	$3\sigma$
$\Delta m_{21}^2$ ( $10^{-5}$ eV <sup>2</sup> )	7.9	7.2-9.1
$\Delta m_{31}^2$ ( $10^{-3}$ eV <sup>2</sup> )	2.3	1.4-3.3
$\sin^2\theta_{21}$	0.3	0.23-0.38
$\sin^2\theta_{23}$	0.5	0.34-0.68
$\sin^2\theta_{13}$	0.002	<0.047

be addressed by studying so called matter effects (MSW), namely the effects occurring to neutrinos oscillating through matter <sup>5)</sup>. Last but not least, there is the subject of CP violation in the neutrino sector. The PMNS matrix has a phase term that, if non zero, could cause CP violating effects, detectable *e.g.* by comparing oscillation results obtained with neutrinos and antineutrinos.

The answer to the above outstanding questions will likely keep neutrino physicists occupied for the next two decades, similarly to the time that has been required to go from the first signals of anomaly in the solar neutrino fluxes to the solid establishment of neutrino oscillations.

The present scenario is summarized in Table 1, where the results of a global fit of all oscillation data are presented <sup>3)</sup>. Needless to say, we assume that mixing occurs among three active neutrinos (two  $\Delta m^2$  and three mixing angles) and that, therefore, we do not take into account the so called LSND effect, that if real would naturally lead to the existence of a fourth (sterile) neutrino. The Fermilab MiniBoone experiment will soon clarify this issue <sup>4)</sup>.

From what we mentioned above, it is rather obvious what the tasks of future accelerator neutrino experiments will be, aimed at a deeper understanding of the physics of massive neutrinos:

- to observe  $\nu_\tau$  appearance: find the body after the murder;
- to know is there (some) room for a sterile neutrino: MiniBoone experiment and  $\nu_\mu$  disappearance;
- to measure the  $L/E$  dependence: atmospheric neutrinos and Wide Band Beam accelerator experiments (fixed  $L$ );
- to accurately measure the two  $\Delta m^2$ ,  $\theta_{12}$  and  $\theta_{23}$ : is  $\theta_{23}$  exactly  $\pi/4$ ?

- to find the value of  $\theta_{13}$  from  $P(\nu_\mu \rightarrow \nu_e)$ : benchmark measurement;
- to show MSW matter effects (without CP violation effects): mass hierarchy;
- to show CP violating effects (without matter effects): the ultimate goal?
- to be ready for the unexpected!: experiments may be running for long time.

In order to review the above experimental programme, we can start by briefly presenting the neutrino mixing matrix and some of its peculiar features.

The unitary mixing matrix, which can be parameterized as

$$U(\theta_{12}, \theta_{13}, \theta_{23}, \delta) = \begin{pmatrix} c_{12}c_{13} & s_{12}c_{13} & s_{13}e^{-i\delta} \\ -s_{12}c_{23} - c_{12}s_{13}s_{23}e^{i\delta} & c_{12}c_{23} - s_{12}s_{13}s_{23}e^{i\delta} & c_{13}s_{23} \\ s_{12}s_{23} - c_{12}s_{13}c_{23}e^{i\delta} & -c_{12}s_{23} - s_{12}s_{13}c_{23}e^{i\delta} & c_{13}c_{23} \end{pmatrix} \quad (1)$$

with  $s_{ij} = \sin\theta_{ij}$  and  $c_{ij} = \cos\theta_{ij}$ , we get the freedom of the complex phase (physical only if  $\theta_{13} \neq 0$ ).

For the interesting case of  $\nu_\mu \rightarrow \nu_e$  oscillations and under the empirical assumptions (justified by the experimental results) that

- $\Delta m_{atm}^2 \gg \Delta m_{sol}^2$ ;
- $L$  is comparable to the atmospheric oscillation length ( $\sim 1000$  km);
- the angle  $\theta_{13}$  is small,

the general three-neutrino oscillation formula can be developed as a sum of terms

$$\begin{aligned} P(\nu_\mu \rightarrow \nu_e) = & 4c_{13}^2 s_{13}^2 s_{23}^2 \sin^2 \Delta_{31} \\ & + 8c_{13}^2 s_{13} s_{23} c_{23} s_{12} c_{12} \sin \Delta_{31} [\cos \Delta_{32} \cos \delta - \sin \Delta_{32} \sin \delta] \sin \Delta_{21} \\ & - 8c_{13}^2 s_{13}^2 s_{23}^2 s_{12}^2 \cos \Delta_{32} \sin \Delta_{31} \sin \Delta_{21} \\ & + 4c_{13}^2 s_{12}^2 [c_{12}^2 c_{23}^2 + s_{12}^2 s_{23}^2 s_{13}^2 - 2c_{12}c_{23}s_{12}s_{23}s_{13} \cos \delta] \sin 2\Delta_{21} \\ & - 8c_{13}^2 s_{13}^2 s_{23}^2 (1 - 2s_{13}^2) \frac{aL}{4E_\nu} \sin \Delta_{31} \left[ \cos \Delta_{32} - \frac{\sin \Delta_{31}}{\Delta_{31}} \right] \end{aligned} \quad (2)$$

where  $s_{ij} = \sin\theta_{ij}$ ,  $c_{ij} = \cos\theta_{ij}$ ,  $\Delta_{jk} \equiv \Delta m_{jk}^2 L/4E_\nu$  and

$$a = 2\sqrt{2}G_F N_e E_\nu = 1.54 \times 10^{-4} Y_e \rho (g/cm^3) E_\nu (GeV) \quad (3)$$

with  $a$  is given in  $eV^2$ .

In the above formula the leading term is the first one. The third and fourth terms give CP conserving (small) contributions. The second term includes the CP violating effects due to  $\sin\delta$ . The last term includes matter effects, due to the passage of the oscillating neutrino through matter. One can notice that the  $\theta_{13}$  angle is the 'link' between the atmospheric and the solar term. As we will see later, this term has great importance for future studies: if it is exactly zero there will be no CP violating effects and the global oscillation phenomenology would certainly be poorer.

The above relation reduces to the following one if one restricts to vacuum oscillations computed to leading order

$$P(\nu_\mu \rightarrow \nu_e) = \sin^2 2\theta_{13} \times \sin^2 \theta_{23} \times \sin^2 \Delta_{23} \quad (4)$$

## 2 Present generation of accelerator-neutrino oscillation experiments

The K2K experiment in Japan can be considered as the 'mother' of all long baseline (LBL) experiments <sup>6)</sup>, designed to be tuned to the atmospheric neutrino oscillation parameters. The Super-Kamiokande <sup>7)</sup> detector is hit by the low energy neutrinos ( $\sim 1$  GeV) from KEK after a travel of about 250 km. The  $L/E$  of the experiment is such to provide sensitivity to the oscillation parameter of the atmospheric neutrino signal. Oscillation are searched for with a  $\nu_\mu$  disappearance experiment profiting of a series of near detectors used for flux normalization and background estimates. A comparison of near/far event rates and an analysis of the energy spectrum distortion are exploited to infer the oscillation signal. The latest results confirm the results obtained by Super-Kamiokande exposed to atmospheric neutrinos, indicating  $1.7 < \Delta m^2 < 3.5$   $eV^2$  and  $\sin^2 2\theta = 1$  at the 90% CL. The oscillation hypothesis is confirmed at nearly the  $4\sigma$  level.

The next LBL experiment to come on duty (2005) will be the MINOS detector <sup>8)</sup> in Minnesota in the NuMI neutrino beam from Fermilab, 730 km

away. Also in this case, a  $\nu_\mu$  disappearance search will be performed. The far detector is made of magnetized iron disks and scintillator strips, for a total mass of about 5400 ton. MINOS should collect 2500  $\nu_\mu$  charged current events per year. The main goal of the experiment will be the narrowing down of the errors on  $\sin^2\theta_{23}$  and  $\Delta_{23}$ , needed to determine  $\sin^2 2\theta_{13}$ , as shown in (4). Given its ability in discriminating electrons from muons, MINOS will also provide some sensitivity to  $\nu_\mu \rightarrow \nu_e$  oscillations, and hence directly on  $\sin^2 2\theta_{13}$ . In four years of running (by 2010) the existing limit of 0.14 from the CHOOZ reactor experiment <sup>9)</sup> should be improved to about 0.06 <sup>8)</sup>.

By 2006 the CERN-to-LNGS CNGS neutrino beam will be commissioned. In this case, we will deal with high energy neutrinos (10-20 GeV). This is needed to be well above threshold for  $\tau$  production, as required to allow for a  $\nu_\mu \rightarrow \nu_\tau$  appearance search, following the indications from the atmospheric neutrino measurements largely favoring this oscillation channel. Together with the ICARUS experiment <sup>10)</sup> that we will discuss later, the dedicated OPERA experiment <sup>11)</sup> is being built at LNGS, exploiting a novel application of nuclear emulsions for the direct detection of the short (less than 1 mm long)  $\tau$  track. Although with small statistics (less than 20 events in 5 years of running), thanks to the very low expected background ( $< 1$  event) OPERA should be capable to unambiguously confirm the  $\nu_\mu \rightarrow \nu_\tau$  oscillation hypothesis.

### 3 The next goal: the measurement of $\theta_{13}$

From what said in the Introduction, an important role in the neutrino oscillation framework is played by the  $\theta_{13}$  angle. On the one hand, it is the link between the atmospheric and the solar oscillation parameters, and on the other hand, only if it is non zero, one could expect a non vanishing CP violating phase in the mixing matrix.

A determination of  $\theta_{13}$  can be accomplished by measuring  $\nu_\mu \rightarrow \nu_e$  oscillations according to (4). This measurement can be well performed with accelerator neutrino experiments, although the present best limit has been set by the CHOOZ reactor experiment. The main experimental limitations are given by the prompt  $\nu_e$  contamination in the  $\nu_\mu$  beams, by the  $\pi_0$  background capable to fake the production of electrons, and by the additional background of low energy muons and pions that can be misidentified as electrons. Obviously, the relevance of the above backgrounds strongly depends upon the parameters

of the neutrino beam and on the adopted detection technique. It is worth to mention that the use of the future Beta-Beams providing pure  $\nu_e$  beams could allow to perform  $\nu_e \rightarrow \nu_\mu$  appearance experiments, by far less demanding from the detection point of view.

In any case, given the smallness of the effect ( $< 5\%$ ), the use of next generation high-intensity beam facilities is a must. In particular, one usually thinks of Super-Beams, namely conventional accelerator neutrino beams fed by high-intensity proton accelerators able to increase by factors 10-100 the presently achievable neutrino intensities.

Likely, the first Super-Beam to be operational by 2009 will be once more in Japan, for the T2K experiment<sup>12)</sup>. The far detector, at least in the first phase of operation, will still be Super-Kamiokande, placed about 300 km away from Tokay. A 0.8 MW, 50 GeV Proton Synchrotron will produce a high-intensity, low-energy neutrino beam. About 3000  $\nu_\mu$  charge current events per year will be produced in Super-Kamiokande, namely one order of magnitude increase with respect to K2K. The detector will be placed about 2 degrees off-axis with respect to the proton beam direction, to allow for an increase of the intensity around the neutrino energy optimizing the  $L/E$  ratio, and in parallel a suppression of the high energy tail of the spectrum, so that to reduce most of the backgrounds. Great care will have to be devoted to the near detectors and to the normalization procedure, since already in K2K the main systematic error is given by the differences in the near/far detector energy spectra. The experiment will perform both disappearance and appearance oscillation measurements. The expected sensitivity in the  $\nu_e$  appearance measurement of  $\sin^2 2\theta_{13}$  corresponds to a factor 20 improvement compared to the CHOOZ limit.

Other projects focusing on the key measurement of the  $\theta_{13}$  angle are planned of being discussed. We can mention, for example, the *Nova* experiment that has been proposed to run off-axis in the NuMI beam, starting around 2010<sup>13)</sup>. The experimental technique is based on a low-density (particle board and liquid scintillator), high-mass (50 kton) detector capable of a good electron identification. The rather long distance from the neutrino source (about 800 km) makes matter effect detectable. After its first phase of operation in the existing NuMI beam, the experiment would certainly benefit from the envisioned Fermilab Super-Beam, centered around a new proton driver. Under these cir-

cumstances the experiment would seriously compete with the T2K project, achieving a  $3\sigma$  sensitivity to  $\sin^2 2\theta_{13}$  around 0.006.

#### 4 More distant future: experiments on CP violation in the neutrino sector

After the next round of experiments aiming at the measurement of  $\sin^2 2\theta_{13}$ , in the fortunate hypothesis of success (non zero angle detected) the search for CP violating effects in the neutrino sector will be opened. A sensible method to pin down CP violating effects is the measurement of the so called asymmetry, shown below for vacuum oscillations

$$A_{CP} = \frac{P(\bar{\nu}_e \rightarrow \bar{\nu}_\mu) - P(\nu_e \rightarrow \nu_\mu)}{P(\bar{\nu}_e \rightarrow \bar{\nu}_\mu) + P(\nu_e \rightarrow \nu_\mu)} \sim \frac{\sin^2 \theta_{12}}{\sin \theta_{13}} \times \sin \delta \times \sin \frac{\Delta m_{12}^2 L}{4E} \quad (5)$$

From this relation it first turns out that larger effects are expected for larger values of  $\Delta m_{12}^2$  and  $\sin^2 \theta_{12}$ . That seems to be the case, being the LMA solution the preferred one for solar neutrino oscillations <sup>3)</sup>. One also sees that a small value of  $\sin \theta_{13}$  is preferable. However, this latter requirement is somehow in conflict with the fact that the oscillation probability increases with  $\sin^2 2\theta_{13}$ , as indicated by Equation (4). This 'conflict' has a clear impact on the detector design: if  $\theta_{13}$  is small one is confronted with low statistics and large asymmetry; if  $\theta_{13}$  is large one has the opposite.

The above described measurements will be likely accomplished with a further generation of beam facilities and detectors. As far as the beam are concerned, we already mentioned Super-Beams, Beta-Beams and (for a more distant future!) Neutrino Factories. Without entering in the details about these facilities, we insist once more on the fact that given the expected smallness of CP violating and matter effects high intensity facilities will be mandatory.

A global (physics driven) optimization of the neutrino beam parameters, of the detector technology and of its location will be required. As an example, we can mention two extreme approaches for the choice of  $L/E$  (Equation (6)): one could match this quantity to the first (or second) oscillation maximum with both a 'long  $L$ -high  $E$ ' or a 'short  $L$ -low  $E$ ' configuration.

The first case is well interpreted by the proposed projects at Fermilab and Brookhaven <sup>14)</sup>. In both cases, one envisages neutrino energies of a few GeV

matching baselines of 1000 km or more. CP violating effects would then increase with the long  $L$  ( $3/\pi/2$  vs  $\pi/2$ ) and a second maximum location would also increase the detectable asymmetry thanks to matter effects ( $E_{max2}/E_{max1}$ ). The second choice, *e.g.* as the one proposed for the discussed beam from CERN to Frejus, has the advantage of using neutrinos with energies below most of the competing background thresholds. However, for neutrino energies as low as a few hundreds of MeV one has to deal with backgrounds from atmospheric neutrinos and with the effect of Fermi momentum, limiting the resolution for muon events. Low energy has also a dramatic effect on the duration of the antineutrino runs (needed to assess the CP asymmetry), due to the smallness of the corresponding cross section.

On the other hand, matter effects can well induce degeneracies in the determination of the experimental results. For this reason one can anticipate that experiments with different baselines/energies/detection techniques might be required to fully exploit complementarity and disentangle the above degeneracies.

Concerning the apparatuses, a factor ten-twenty mass increase with respect to Super-Kamiokande is usually considered as a benchmark detector choice. Examples are given by the Hyper Kamiokande <sup>15)</sup> or UNO <sup>16)</sup> detectors. We believe that the main reason for this is the long series of outstanding results obtained with Super-Kamiokande, that successfully exploits the water Cerenkov detection technique. Moreover, one can extrapolate the cost to the larger mass detector with good confidence, that then appears to be a sufficiently cost effective solution. The detection method works rather well for low energy quasi-elastic (1-ring) neutrino events. The required electron/ $\pi_0$  rejection can be efficiently accomplished if the two gammas are well separated. However, some confusion may arise in the muon/pion separation at low energy and the detection threshold cannot be realistically reduced below 5 MeV for the 'working hypothesis' of a 40% PMT coverage. In addition, alternative photodetector devices might require quite a long R&D work. Last but not least, the relatively low-density and, hence, large-volume of a 500-1000 kton detector implies a huge cavern with a complex and costly excavation work.

For the above reasons, one is led to think about possible alternative or complementary approaches. Among these, the liquid Argon TPC technique is certainly a viable and realistic option for a next generation neutrino and

astroparticle physics experiments <sup>17)</sup>.

## 5 Liquid Argon TPC detectors: a technique for future neutrino experiments?

The technology of the Liquid Argon Time Projection Chamber (LAr TPC) was conceived and proposed by C. Rubbia in 1977 <sup>18)</sup> as a tool for high accuracy imaging of massive detector volumes. The operating principle of the LAr TPC is based on the fact that in highly purified LAr ionization tracks can be transported undistorted by a uniform electric field over distances of the order of meters. Imaging is provided by wire planes placed at the end of the drift path, continuously sensing and recording the signals induced by the drifting electrons. The main technological challenges of the detection technique are the liquid Argon purification, the operation of wire chambers in cryogenic liquid without charge amplification, the very low-noise analog electronics, and the continuous wave-form recording and digital signal processing.

The feasibility of the technology has been demonstrated by the extensive ICARUS R&D programme, culminated with the realization and the surface test with cosmic-rays of the 600 ton ICARUS T600 detector <sup>19)</sup>. The success of the fully industrial construction of the T600 module motivated and justified the idea of cloning the detector to reach the 3000 ton mass scale for experiments at LNGS. Here, the T3000 modularity was not imposed by the LAr TPC technique itself but it was an implementation choice motivated by the boundary conditions of the LNGS laboratory and by the requirement to build the detector outside of the underground hall.

Having at disposal the mature technique developed in the context of the ICARUS programme, physics is today calling for at least two applications at two different mass scales <sup>17)</sup> and with a high degree of interplay and synergy: on the one hand, future precision studies of neutrino interactions and near stations for long baseline beam experiments will need detectors in the range of  $\sim 100$  ton. On the other hand, ultimate nucleon decay searches and high statistics astrophysical and accelerator neutrino experiments will require very large masses, of the order of 100 kton, able to effectively compete with the large mass water Cerenkov detectors mentioned in the previous Section.

## 6 A 100 kton Liquid Argon TPC detector with charge imaging, scintillation and Cerenkov light readout

The possibility to construct and operate a very large LAr TPC can be considered a complex technical task. A single LAr volume is the most attractive solution from the point of view of construction, operation and cryogenics, and is to be favored over the modular approach. The basic design features of the detector can be summarized as follows<sup>17)</sup>

1. Single 100 kton boiling cryogenic tanker at atmospheric pressure for a stable and safe equilibrium condition (temperature is constant while Argon is boiling). The evaporation rate is small (less than  $10^{-3}$  of the total volume per day given by the favorable area-to-volume ratio) and is compensated by refilling of the evaporated Argon volume.
2. Charge imaging, scintillation and Cerenkov light readout for a redundant event reconstruction. This is a clear advantage over alternative detectors operating with only one of these readout modes.
3. Charge amplification to allow for very long drift paths. The detector runs in bi-phase mode. In order to allow for drift lengths as long as  $\sim 20$  m, which provides an economical way to increase the volume of the detector with a constant number of channels, charge attenuation will occur along the drift due to attachment to the remnant impurities present in the LAr. This effect is compensated with charge amplification near the anodes located in the gas phase.
4. Absence of magnetic field, although this possibility might be considered at a later stage, *e.g.* in conjunction with a future Neutrino Factory.

The cryogenic features of the above design are based on the industrial know-how in the storage of liquefied natural gases (LNG,  $T \simeq 110$  K at 1 bar), which developed in the last decades driven by the petrochemical industry. The technical problems associated to the design of large cryogenic tankers, their construction and safe operation have already been addressed and engineering problems have been solved by the petrochemical industry. The current state-of-the-art contemplates cryogenic tankers of  $200000$  m<sup>3</sup> and their number in the world is estimated to be  $\sim 300$  with volumes larger than  $30000$  m<sup>3</sup>. LNG

tankers are always of double-wall construction with efficient but non-vacuum insulation between the walls. Large tankers are of low aspect ratio (height to width) and cylindrical in design with a domed roof.

The detector discussed here is characterized by the large fiducial volume of LAr included in a tanker with external dimensions of 40 m in height and 70 m in diameter. A cathode located at the bottom of the inner tanker volume creates a drift electric field of the order of 1 kV/cm over a distance of about 20 m. In this field configuration ionization electrons are moving upwards while ions are going downward. The electric field is delimited on the sides of the tanker by a series of ring electrodes (race-tracks) placed at the appropriate potential by a voltage divider.

The tanker contains both liquid and gas Argon phases at equilibrium. Since purity is a concern for very long drifts, we assume that the inner detector could be operated in bi-phase mode: drift electrons produced in the liquid phase are extracted from the liquid into the gas phase with the help of a suitable electric field and then amplified near the anodes in proportional mode. In order to amplify the extracted charge one can consider various options: amplification near thin readout wires, GEM, or LEM<sup>17</sup>). Gain factors of 100-1000 are achievable in pure Argon.

After a drift of 20 m at 1 kV/cm the electron cloud diffusion reaches the size of 3 mm, corresponding to the envisaged wire readout pitch. If one assumes that the reachable electron lifetime is at least  $\tau \simeq 2$  ms, as obtained in ICARUS T600 detector, one then expects an attenuation of a factor  $\sim 150$  over the distance of 20 m. We remind that this attenuation (compensated by the amplification) will not introduce any detection inefficiency, given the value of  $\sim 6000$  ionization electrons/mm produced along a *m.i.p.* track in LAr.

In addition to charge readout, we envision to locate PMTs around the inner surface of the tanker. Scintillation and Cerenkov light can be readout independently. LAr is a very good scintillator with about 50000  $\gamma$ /MeV. However, this light is essentially distributed around a line at  $\lambda = 128$  nm and, therefore, a PMT wavelength shifter (WLS) is required. Cerenkov light from penetrating muon tracks has been successfully detected in a LAr TPC. Since water and liquid Argon have very similar Cerenkov light emission properties and also similar physical properties in terms of radiation length, interaction length, etc.

The potential of future LAr detectors anticipate a large physics programme ranging from neutrino physics with artificial beams or astrophysical neutrinos, to the search for nucleon decay. For more information we refer to <sup>17)</sup> and references therein.

The operation of a large 100 kton LAr apparatus in a neutrino Super-Beam advantageously profits from the very good granularity provided by the technique. In particular, the search for  $\nu_\mu \rightarrow \nu_e$  events is very clean owing to the excellent  $e/\pi^0$  separation. The imaging of the events and the high energy resolution in the LAr TPC make the study of Beta-Beams very attractive, in particular for the possibility to have separately pure  $\nu_e$  and  $\bar{\nu}_e$  beams. Good  $\mu/\pi^\pm$  discrimination is important in order to suppress the neutral current background with a charged leading  $\pi^\pm$ . The combination of the information from the imaging (tracking and energy) with the Cerenkov light could provide adequate particle muon/pion separation.

In order to fully address the oscillation processes at a Neutrino Factory, the ideal detector should be capable of identifying and measuring all three charged lepton flavors produced in charged current interactions and of measuring their charges to discriminate the incoming neutrino helicity. Embedding the volume of Argon into a magnetic field would not alter the imaging properties of the detector and the measurement of the bending of charged hadrons or penetrating muons would allow a precise determination of the momentum and a determination of their charge. A field of 0.1 T will allow to discriminate with  $> 3\sigma$  the charge for tracks longer than 4 m. The ability to measure electron and muon charges is the only way to address  $T$ -violation, since it implies the comparison between the appearance of  $\nu_\mu$  ( $\bar{\nu}_\mu$ ) and  $\bar{\nu}_e$  ( $\nu_e$ ) in a beam of stored  $\mu^+$  ( $\mu^-$ ) decays as a function of the neutrino energy.

The astrophysical neutrino physics programme is naturally very rich for a 100 kton LAr observatory. One expects about 10000 atmospheric neutrinos per year and about 100  $\nu_\tau$  charged current event per year from  $\nu_\mu$  oscillations. These events, given the excellent imaging capabilities of the LAr TPC, will provide an unbiased sample of atmospheric neutrinos with unprecedented resolution. Solar neutrinos provide 320000 events per year with electron recoil energy above  $\sim 5$  MeV. This will give the possibility to make precision measurements of the solar neutrino flux and to study possible short and long term variations. A galactic SN-II explosion at 10 kpc yields about 20000 events.

Sensitivity to extragalactic supernovae should also be possible as well as to relic SN neutrino fluxes. A unique feature of the LAr TPC is the accessibility to several independent detection channels which have different sensitivities to different neutrino flavors.

Last but not least, direct evidence for GUT and baryon number violation represents one of the outstanding goals of particle physics. Nucleon decay searches require a very good knowledge of the backgrounds induced by atmospheric neutrinos. A target of 100 kton =  $6 \times 10^{34}$  nucleons yields a sensitivity for protons of  $\tau_p/Br > 10^{34}$  years  $\times$  T(yr) $\times\epsilon$  at the 90% C.L. in the absence of background. This means that lifetimes in the range of  $10^{35}$  years can be reached within 10 years of operation. Channels like  $p \rightarrow \nu K$  have been shown to be indeed essentially background free.

## 7 Conclusions

The solution of the long standing solar and atmospheric neutrino problems has led to the unambiguous confirmation that neutrinos oscillate and hence are massive. Several key experiments have contributed so far to the building up of the oscillation scenario. A wide programme is being executed and is planned for the next years, aimed at more sensitive measurements of the elements of the PMNS mixing matrix.

As far as accelerator neutrino experiments are concerned, further technological advances will be required for both the beam facilities and the detectors to realize the next generation of experiments addressing the issues of CP violation in the leptonic sector and of mass hierarchy.

The LAr TPC technology, whose basic R&D work has been successfully conducted by the ICARUS Collaboration, has great potentials for new generation neutrino experiments. In particular, a large, 100 kton device could effectively compete with giant 500-1000 kton water Cerenkov detectors being proposed for future precision studies of the neutrino mixing matrix and for nucleon decay searches. This 100 kton LAr TPC would provide the widest output for accelerator and astroparticle physics. Coupled to future Super-Beams, Beta-Beams or Neutrino Factories it could greatly improve our understanding of the mixing matrix in the lepton sector with the goal of measuring the CP phase, and in parallel it would allow to conduct astroparticle experiments of unprecedented sensitivity.

## 8 Acknowledgments

I wish to warmly thank A. Rubbia with whom we have been developing ideas on future liquid Argon detectors.

## References

1. Particle Data Group, “Review of Particle Properties”, Phys. Rev. D66, 010001-381 (2002).
2. D.N. Spergel et al., Astrophys. J. Suppl. 148 (2003) 175.
3. M. Maltoni et al., “Status of global fits to neutrino oscillations”, arXiv:hep-ph/0405172.
4. <http://www-boone.fnal.gov/>
5. L. Wolfenstein, Phys. Rev. D 17, (1978) 2369;  
S.P. Mikheyev and A.Yu. Smirnov, Sov. J. Nucl. Phys. 42, (1986) 913.
6. M.H. Ahn et al., Phys. Rev. Lett. B90 041801 (2003).
7. <http://www-sk.icrr.w-tokyo.ac.jp/doc/sk/index.html>
8. <http://www-numi.fnal.gov/forscientists.html>
9. M. Apollonio et al., Phys. Lett. B466, (1999) 415.
10. <http://pcnometh4.cern.ch/>
11. <http://operaweb.web.cern.ch/operaweb/index.shtml>
12. T. Ishida, Contribed paper to the NuFact04 Conference, Osaka, July 2004.
13. D. Ayres et al., Fermilab LoI P929, 2002.
14. S. Holmes, Talk given at the Workshop on Physics with a Multi-MW Proton Driver, CERN, 25-27 May 2004;  
<http://physicsatmwatt.web.cern.ch/physicsatmwatt/>
15. Y. Itow et al., “The JHF-Kamioka neutrino project”, arXiv:hep-ex/0106019.

16. <http://ale.physics.sunysb.edu/uno/>
17. A. Rubbia, "Experiments for CP-violation: a giant liquid Argon scintillation, Cerenkov and charge imaging experiment?", Proc. of the II International Workshop on Neutrino Oscillations in Venice, December 2003, 321; A. Ereditato and A. Rubbia, "Next Generation Liquid Argon TPC Detectors", to appear on the Proceedings of NUINT04, LNGS, March 2004; A. Ereditato and A. Rubbia, "Ideas for a next generation liquid Argon TPC detector for neutrino physics and nucleon decay searches", Memorandum to the Special SPSC Session in Villars of September 2004, 27 April 2004; A. Ereditato and A. Rubbia, Talk given at the Workshop on Physics with a Multi-MW Proton Driver, CERN, 25-27 May 2004; <http://physicsatmwatt.web.cern.ch/physicsatmwatt/>
18. C. Rubbia, CERN-EP/77-08 (1977).
19. S. Amerio et al., "Design, construction and tests of the ICARUS T600 detector", Nucl. Instr.& Meth. A527 (2004) 329.

## THE CASE FOR A SUPER NEUTRINO BEAM

Milind V. Diwan  
*Brookhaven National Laboratory*

### ABSTRACT

In this paper I will discuss how an intense beam of high energy neutrinos produced with conventional technology could be used to further our understanding of neutrino masses and mixings. I will describe the possibility of building such a beam at existing U.S. laboratories. Such a project couples naturally to a large ( $> 100$  kT) multipurpose detector in a new deep underground laboratory. I will discuss the requirements for such a detector. Since the number of sites for both an accelerator laboratory and a deep laboratory are limited, I will discuss how the choice of baseline affects the physics sensitivities, the practical issues of beam construction, and event rates.

### 1 Introduction

In <sup>1)</sup> we argued that an intense broadband muon neutrino beam and a large detector located more than 2000 km away from the source could be used to

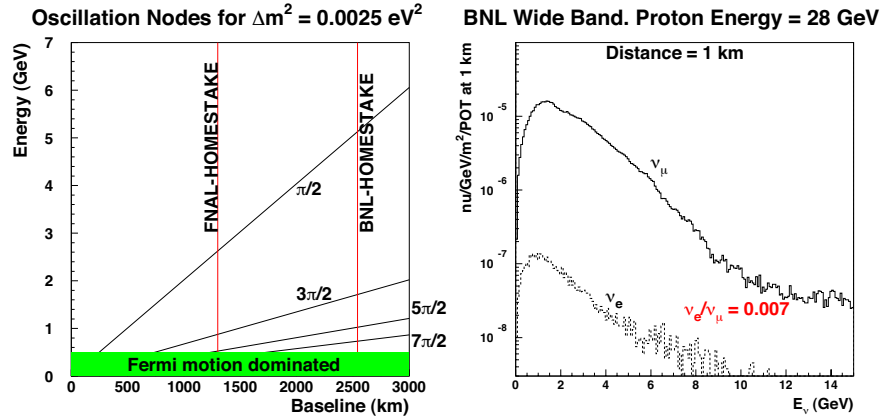


Figure 1: Nodes of oscillations for  $\Delta m_{32}^2 = 0.0025 \text{ eV}^2$  in neutrino energy versus baseline (left). Possible baselines from Brookhaven National Laboratory (BNL) and Fermi National Laboratory (FNAL) to the Homestake underground site are indicated. They correspond to distances of  $\sim 2540 \text{ km}$  and  $\sim 1290 \text{ km}$ , respectively. Right hand side shows the wide band neutrino spectrum from 28 GeV protons at a distance of 1 km from the target. The anti-neutrino spectrum looks similar, but has contamination from neutrinos.

perform precision measurements of neutrino properties such as the mass differences, the mass hierarchy, the mixing parameters, and CP violation in the neutrino sector. Using the currently deduced neutrino mass differences and mixing parameters <sup>2)</sup> and the same formalism as <sup>1)</sup> we formulated several simple rules for such an experiment:

For precise measurements of  $\Delta m_{32}^2$  and  $\sin^2 2\theta_{23}$ , it is desirable to observe a pattern of multiple nodes in the energy spectrum of muon neutrinos. Since the cross section, Fermi motion, and nuclear effects limit the resolution of muon neutrino interactions below  $\sim 1 \text{ GeV}$ , we need to utilize a wide band muon neutrino beam with energy range of 1-6 GeV and a distance of  $\sim 2000 \text{ km}$  to observe 3 or more oscillation nodes. See Fig. 1.

The appearance spectrum of electron neutrinos from the conversion  $\nu_\mu \rightarrow \nu_e$  contains information about  $\sin^2 2\theta_{13}$ ,  $\delta_{CP}$ ,  $\Delta m_{21}^2$  and the ordering of neutrino masses through the matter effect (i.e.  $(m_1 < m_2 < m_3)$  versus  $(m_3 < m_1 < m_2)$ ). We showed that the effects of the various parameters can be

separated using the broad-band 1-6 GeV beam and the  $\sim 2000$ km distance. The matter effect causes the conversion probability to rise with energy and is mostly confined to energies  $> 3$  GeV whereas the effects of  $\delta_{CP}$  fall as  $1/E$ . We showed that this energy dependence can be used to measure the value of  $\delta_{CP}$  and  $\sin^2 2\theta_{13}$  without taking data with anti-neutrinos.

The additional contribution to the appearance event rate due to 3-generation CP violation in the neutrino sector is approximately proportional to:  $\sin \delta_{CP} \sin 2\theta_{13} \times (\Delta m_{21}^2 L/4E_\nu)$ . This contribution increases linearly with distance while the total flux falls as  $1/L^2$  for a detector of a given size. The statistical sensitivity for the additional CP contribution, however, remains approximately independent of distance. It is therefore advantageous to perform the experiment with a very long ( $> 2000$  km) baseline because then we can relax the requirements on systematic errors on the flux, the cross sections, the other oscillation parameters, and the calculation of the matter effect.

Because of the electron neutrino contamination background in a conventional accelerator neutrino beam the sensitivity to  $\delta_{CP}$  will be limited to the parameter region  $\sin^2 2\theta_{13} > 0.01$ . The main CP-conserving contribution to the  $\nu_\mu \rightarrow \nu_e$  signal is proportional to  $\sin^2 2\theta_{13}$  in this region. The CP-violating term, on the other hand, is linear in  $\sin 2\theta_{13}$ . Therefore the fractional contribution due to the CP-violating term increases for small  $\sin 2\theta_{13}$ , although the total appearance signal decreases. The statistical sensitivity to the CP-violating term remains approximately independent of the value of  $\sin^2 2\theta_{13}$  as long as backgrounds do not dominate the observed spectrum<sup>3)</sup>. When  $\sin^2 2\theta_{13}$  is very small ( $< 0.002$ ) this rule no longer holds because the signal is no longer dominated by the  $\sin^2 2\theta_{13}$  term in the 3-generation formalism<sup>4)</sup>.

Current generation of accelerator experiments such as K2K<sup>5)</sup>, MINOS<sup>6)</sup>, or CNGS<sup>7)</sup> focus on obtaining a definitive signature of muon neutrino oscillations at the first node ( $\Delta m_{32}^2 L/4E \sim \pi/2$ ) for the atmospheric mass scale. Other recent proposed projects (JPARC-to-SK, NUMI-offaxis)<sup>8, 9)</sup> also focus mainly on the first node, but propose to use an off-axis narrow band beam to lower the background in the search of  $\nu_\mu \rightarrow \nu_e$  caused by a non-zero  $\theta_{13}$ . The narrow band beam and limited statistics, however, do not allow measurement of the parameters in a definitive way. Proposed reactor disappearance searches, also at the first node for the atmospheric mass scale, are only sensitive to  $\sin^2 2\theta_{13}$ <sup>4)</sup>.

Thus, current and near term accelerator based experiments are focussed on the atmospheric mass scale. Experiments using astrophysical sources such as solar neutrinos or atmospheric neutrinos are sensitive to either the solar or the atmospheric mass scale. The parameters are now known well enough ( $\Delta m_{32}^2 \sim 0.0025 eV^2$  and  $\Delta m_{21}^2 \sim 8 \times 10^{-5} eV^2$ )<sup>10, 11, 12)</sup> that it is possible to design a qualitatively different experiment that will have good sensitivity to both mass scales. The CP contribution is dependent on both atmospheric and solar  $\Delta m^2$ ; it is also likely that such an experiment is necessary to uncover any new physics in neutrino mixing or interactions with matter. A next generation accelerator experiment with well understood, pure beams, sufficiently long baseline, and low energy wide band beam (1-5 GeV) could fill this role.

In this paper we will discuss different options for the baseline. In<sup>1)</sup> we demonstrated that for 3-generation mixing the CP parameters could be measured using neutrino data alone. Any additional information from anti-neutrino running therefore could make the measurements more precise as well as constrain contributions from new physics, in particular, new interactions in matter or new sources of CP violation in the neutrino sector. We will calculate the significance with which the neutrino mass and mixing parameters can be measured using both neutrino and anti-neutrino data and the implications for the determination of the mass hierarchy and demonstration of CP violation.

## 2 Accelerator and Detector Requirements

Previously we described the BNL Alternating Gradient Synchrotron (AGS) operating at 28 GeV upgraded to provide total proton beam power of 1 MW<sup>13)</sup> and a 500 kTon detector placed at the proposed national underground laboratory (NUSEL)<sup>14)</sup> in the Homestake mine in South Dakota. The main components of the accelerator upgrade at BNL are a new 1.2 GeV Superconducting LINAC to provide protons to the existing AGS, and new magnet power supplies to increase the ramp rate of the AGS magnetic field from about 0.5 Hz of today to 2.5 Hz. For 1 MW operation the protons from the accelerator will be delivered in pulses of  $9 \times 10^{13}$  protons at 2.5 Hz. We have determined that 2 MW operation of the AGS is also possible by further upgrading the synchrotron to 5 Hz repetition rate and with further modifications to the LINAC and the RF systems. The neutrino beam will be built with conventional horn focussed technology and a 200 m long pion decay tunnel.

High energy multi-MW proton beams are also under consideration at FNAL. The most ambitious plans <sup>15)</sup> call for a 8 GeV superconducting LINAC that can provide  $1.5 \times 10^{14}$   $H^-$  ions at 10 Hz corresponding to 2 MW of total beam power. Some of these 8 GeV ions could be injected into the main injector (MI) to provide 2 MW proton beam power at any energy between 40 and 120 GeV; for example, 40 GeV at 2 Hz or 120 GeV at 0.67 Hz. Such a plan allows much flexibility in the choice of proton energy for neutrino production. As Figure 1 shows for observing multiple oscillation nodes in muon neutrino oscillations it is necessary to have a wide band beam with energies from 1 to 5 GeV. Protons above  $\sim 20$  GeV are needed to provide such a flux, clearly possible at either BNL or FNAL. For the purposes of the analysis in this paper we will assume that the spectrum from either the BNL or the FNAL beam will be the same. This will allow us a proper comparison of the physics issues regarding the baselines.

If a large detector facility (as a part of NUSEL) <sup>16, 17, 18)</sup> is located at Homestake (HS) the beam from BNL (FNAL) will have to traverse 2540km (1290km) through the earth. At BNL the beam would have to be built at an incline angle of about  $11.3^\circ$ . Current design for such a beam calls for the construction of a hill with a height of about 50 m <sup>13)</sup>. Such a hill will have the proton target at the top of the hill and a 200 m long decay tunnel on the downslope. At FNAL the inclination will be about  $5.7^\circ$ . There is already experience at FNAL in building the NUMI beam <sup>6)</sup>; this experience could be extended to build a new beam to HS. In either case, it is adequate to have a short decay tunnel (200 m) compared to the NUMI tunnel (750 m) to achieve the needed flux. The option of running with a narrow band beam using the off-axis technique <sup>19)</sup> could be preserved if the decay tunnel is made sufficiently wide. For example, a 4 m diameter tunnel could allow one to move and rotate the target and horn assembly so that a  $1^\circ$  off-axis beam could be sent to the far detector.

With 1 MW of beam, a baseline of 2540 km, and a 500kT detector we calculate that we would obtain  $\sim 60000$  muon charged current and  $\sim 20000$  neutral current events for  $5 \times 10^7$  sec of running in the neutrino mode in the absence of oscillations. For the same running conditions in the anti-neutrino mode (with the horn current reversed) we calculate a total of  $\sim 19000$  anti-muon charged current and  $\sim 7000$  neutral current events; approximately 20%

of the event rate in the anti-neutrino beam will be due to wrong-sign neutrino interactions. For the shorter baseline of 1290 km from FNAL to HS, the event rates will be higher by a factor of  $(2540/1290)^2$ . For both neutrino and anti-neutrino running approximately  $\sim 0.7\%$  of the charged current rate will be from electron charged current events which form a background to the  $\nu_\mu \rightarrow \nu_e$  search. It will be desirable to obtain similar numbers of events in the anti-neutrino and the neutrino beam. Therefore, for the calculations in this paper we assume 1 MW operation for  $5 \times 10^7 \text{ sec}$  in the neutrino mode and 2 MW operation for  $5 \times 10^7 \text{ sec}$  in the anti-neutrino mode.

A large detector facility at NUSEL will most likely be used for a broad range of physics goals. Important considerations for such a detector are the fiducial mass, energy threshold, energy resolution, muon/electron discrimination, pattern recognition capability, time resolution, depth of the location, and the cost. Two classes of detectors are under consideration: water Cherenkov detector instrumented with photo-multiplier tubes and a liquid Argon based time projection chamber.

A water Cherenkov detector built in the same manner as the super-Kamiokande experiment (with 20 inch photo-multipliers placed on the inside detector surface covering approximately 40% of the total area <sup>20</sup>) can achieve the 500 kT mass. This could be done by simply scaling the super-Kamiokande detector to larger size or by building several detector modules <sup>16, 17</sup>. Such a detector placed underground at NUSEL could have a low energy threshold ( $< 10 \text{ MeV}$ ), good energy resolution ( $< 10\%$ ) for single particles, good muon/electron separation ( $< 1\%$ ), and time resolution ( $< \text{few ns}$ ). For the experiment we propose here it is important to obtain good energy resolution on the neutrino energy. This can be achieved in a water Cherenkov detector by separating quasi-elastic scattering events with well identified leptons in the final state from the rest of the charged current events. The fraction of quasi-elastic events in the total charged current rate with the spectrum used in this paper is about 23% for the neutrino beam and 39% for the anti-neutrino beam. Separation of quasi-elastic events from the charged current background is being used by the K2K experiment <sup>5</sup>). Further work is needed to make this event reconstruction work at higher energies. The reconstruction algorithm could be enhanced by the addition of ring imaging techniques to the detector <sup>21</sup>).

A number of proponents have argued that a liquid Argon time projection

chamber (LARTPC) could be built with total mass approaching 100 kT<sup>18)</sup>. A fine grained detector such as this has much better resolution for separating tracks. It is possible therefore to use a large fraction of the charged current cross section (rather than only the quasi-elastic events) for determining the neutrino energy spectrum. The LARTPC will also have much better particle identification capability. Therefore, a LARTPC with a smaller total fiducial mass of  $\sim 100$  kT than the 500 kT assumed for the water Cherenkov tank is expected to have similar performance for the physics.

For the purposes of this paper we will assume the same detector performance as described in<sup>1)</sup>. For the physics sensitivity calculated in this paper we will assume 1 MW operation for  $5 \times 10^7$  sec in the neutrino mode and 2 MW operation for  $5 \times 10^7$  sec in the anti-neutrino mode. In both cases we will assume a detector fiducial mass of 500 kT. With the running times, the accelerator power level, and the detector mass fixed, we will consider two baselines: 1290 km (for FNAL to Homestake) and 2540 km (for BNL to Homestake) assuming that the detector is located at Homestake.

Lastly, we note that for this analysis the far detector could be at several comparable sites in the western US, notably WIPP or the Henderson mine in Colorado. While the detailed calculations change, the qualitative results are easily deduced from this work for other locations.

### 3 $\nu_\mu$ disappearance

We propose to use clean single muon events<sup>1)</sup> and calculate the neutrino energy from the energy and angle of these muons assuming they are all from quasi-elastic interactions. The expected spectrum is shown in Figure 2; the simulation includes effects of Fermi motion, detector resolution, and backgrounds from non-quasielastic events.

A great advantage of the very long baseline and multiple oscillation pattern in the spectrum is that the effect of systematic errors from flux normalization, background subtraction, and spectrum distortion due to nuclear effects or detector calibration can be small. Nevertheless, since the statistics and the size of the expected distortion of the spectrum are both large in the disappearance measurement, the final error on the precise determination of the parameters will most likely have significant contribution from systematic errors. In Figure 3 we show the 1 sigma resolutions that could be achieved on  $\Delta m_{32}^2$  and  $\sin^2 2\theta_{23}$ .

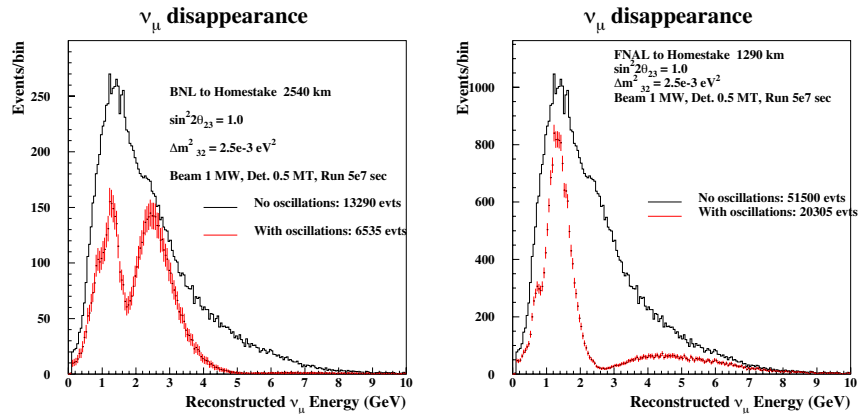


Figure 2: *Simulated spectrum of detected muon neutrinos for 1 MW beam and 500 kT detector exposed for  $5 \times 10^7$  sec. Left side is for baseline of 2540 km, right side for baseline of 1290 km. The oscillation parameters assumed are shown in the figure. Only clean single muon events are assumed to be used for this measurement (see text).*

The black lines (labeled (1)) show the resolutions for purely statistical errors. For the red lines (labeled (2)) we have included a 5% bin-to-bin systematic uncertainty in the spectrum shape and a 5% systematic uncertainty in the overall normalization. These uncertainties could include modeling of cross sections or knowledge of the background spectra. For the  $\Delta m_{32}^2$  resolutions we also show the expected resolution for an additional systematic error of 1% on the global energy scale (blue line labeled (3)). This uncertainty for the Super Kamioka water Cherenkov detector is estimated to be 2.5% in the multi-GeV region<sup>20</sup>).

Although the resolution on  $\Delta m_{32}^2$  will be dominated by systematic errors for the proposed experimental arrangement, a measurement approaching 1–2% precision can clearly be made. On the other hand, the resolution on  $\sin^2 2\theta_{23}$  is dominated by the statistical power at the first node. This results in a factor of  $\sim 2$  better resolution with 1290 km than with 2540 km using the same sized detector.

Running in the anti-neutrino mode with 2 MW of beam power will yield approximately the same spectra and resolutions on  $\Delta m_{32}^2$  and  $\sin^2 2\theta_{23}$ . By comparing the measurements with the results from neutrino running a test

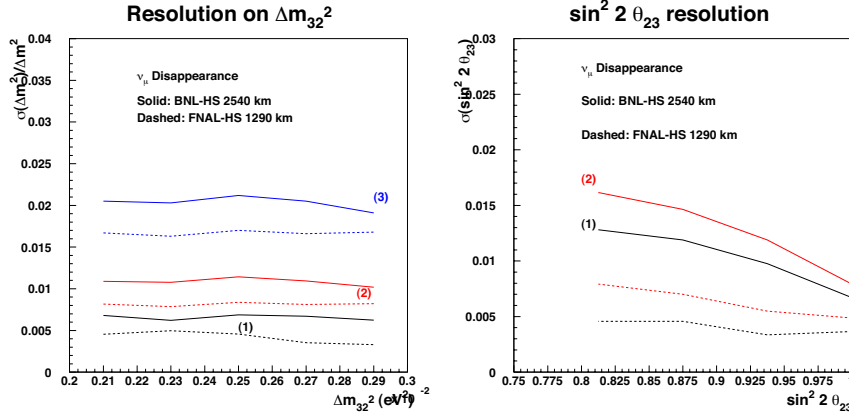


Figure 3:  $1\sigma$  resolutions on  $\Delta m_{32}^2$  (left) and  $\sin^2 2\theta_{23}$  (right) expected after analysis of the oscillation spectra from Figure 2. The solid curves are for BNL-HS 2540 km baseline, and the dashed are for FNAL-HS 1290 km baseline. The curves labeled 1 and 2 correspond to statistics only and statistics and systematics, respectively (similarly for dashed curves of the same color). The curve labeled (3) on the left has an additional contribution of 1% systematic error on the global energy scale.

of CPT is possible. In such a comparison many systematic errors, such as the global energy scale, common to the neutrino and anti-neutrino data sets should cancel yielding a comparison with errors less than 1%.

Finally, we remark that it is important to make precision measurements of both  $\Delta m_{32}^2$  and  $\sin^2 2\theta_{23}$  not only because they are fundamental parameters, but also because they are needed for interpreting the appearance ( $\nu_\mu \rightarrow \nu_e$ ) result. Knowledge of both  $\Delta m_{21}^2$  and  $\Delta m_{32}^2$  are essential in fitting the shape of the appearance signal to extract other parameters. In addition, it will be very important to definitively understand if  $\sin^2 2\theta_{23}$  is close to 1.0 or is  $< 1.0$ . If  $\sin^2 2\theta_{23} < 1.0$  then there will be an ambiguity in  $\theta_{23} \rightarrow \pi/2 - \theta_{23}$ . As we will describe below this ambiguity will affect the interpretation of the appearance spectrum.

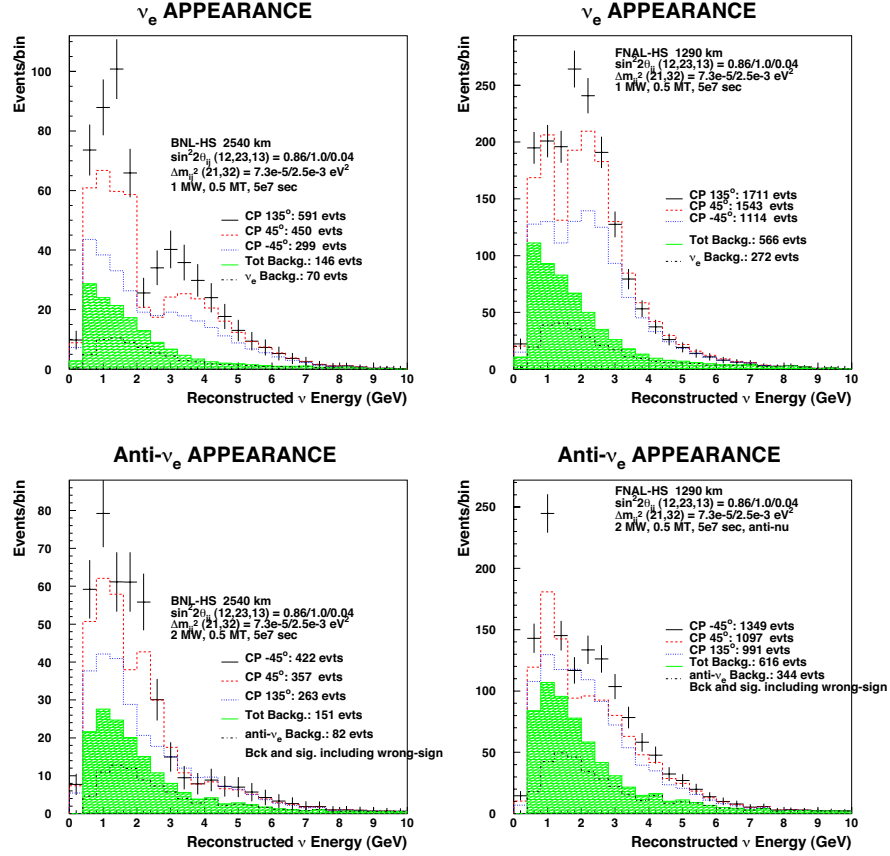


Figure 4: Simulation of detected electron neutrino (top plots) and anti-neutrino (bottom plots) spectrum (left for BNL-HS 2540km, right for FNAL-HS 1290 km) for 3 values of the CP parameter  $\delta_{CP}$ ,  $135^\circ$ ,  $45^\circ$ , and  $-45^\circ$ , including background contamination. Obviously, the dependence of event rate on the CP phase has the opposite order for neutrinos and anti-neutrinos. The hatched histogram shows the total background. The  $\nu_e$  beam background is also shown. The other assumed mixing parameters and running conditions are shown in the figure. These spectra are for the regular mass hierarchy (RO).

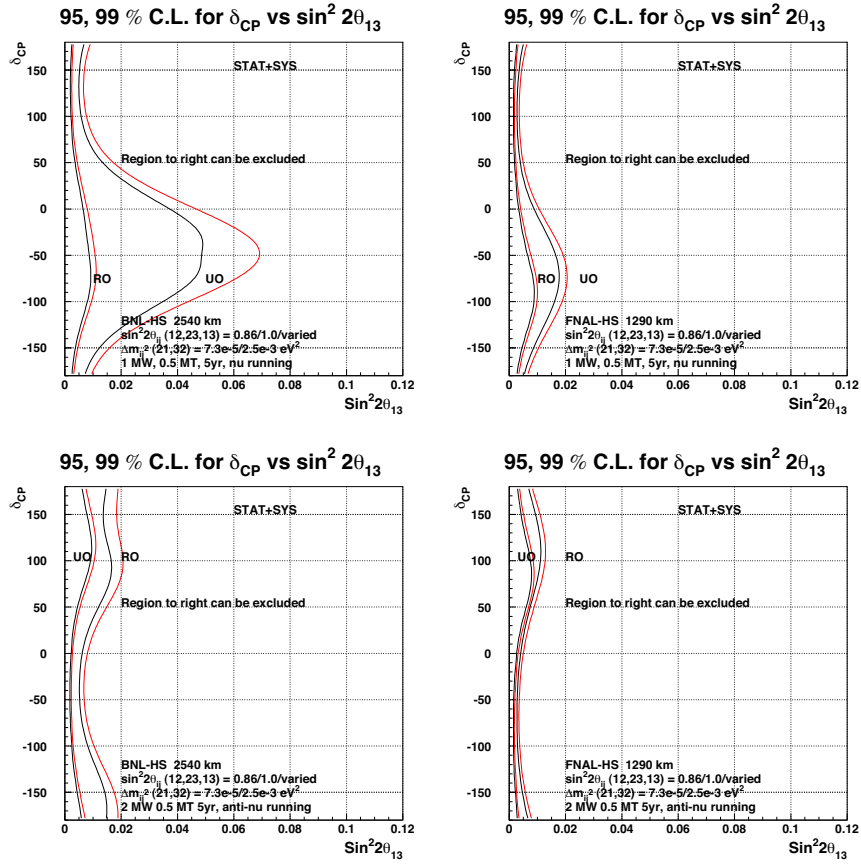


Figure 5: *Expected limit on  $\sin^2 2\theta_{13}$  as a function of  $\delta_{CP}$  for BNL-HS neutrino running only (top left), FNAL-HS neutrino running only (top right), BNL-HS anti-neutrino running only (bottom left), FNAL-HS anti-neutrino running only (bottom right).*

#### 4 $\nu_e$ appearance

Assuming a constant matter density, the oscillation of  $\nu_\mu \rightarrow \nu_e$  in the Earth for 3-generation mixing is described approximately by the following equation (22)

$$\begin{aligned}
P(\nu_\mu \rightarrow \nu_e) \approx & \sin^2 \theta_{23} \frac{\sin^2 2\theta_{13}}{(\hat{A} - 1)^2} \sin^2((\hat{A} - 1)\Delta) \\
& + \alpha \frac{\sin \delta_{CP} \cos \theta_{13} \sin 2\theta_{12} \sin 2\theta_{13} \sin 2\theta_{23}}{\hat{A}(1 - \hat{A})} \times \\
& \sin(\Delta) \sin(\hat{A}\Delta) \sin((1 - \hat{A})\Delta) \\
& + \alpha \frac{\cos \delta_{CP} \cos \theta_{13} \sin 2\theta_{12} \sin 2\theta_{13} \sin 2\theta_{23}}{\hat{A}(1 - \hat{A})} \times \\
& \cos(\Delta) \sin(\hat{A}\Delta) \sin((1 - \hat{A})\Delta) \\
& + \alpha^2 \frac{\cos^2 \theta_{23} \sin^2 2\theta_{12}}{\hat{A}^2} \sin^2(\hat{A}\Delta)
\end{aligned} \tag{1}$$

where  $\alpha = \Delta m_{21}^2 / \Delta m_{31}^2$ ,  $\Delta = \Delta m_{31}^2 L / 4E$ ,  $\hat{A} = 2VE / \Delta m_{31}^2$ ,  $V = \sqrt{2}G_F n_e$ .  $n_e$  is the density of electrons in the Earth. Recall that  $\Delta m_{31}^2 = \Delta m_{32}^2 + \Delta m_{21}^2$ . Also notice that  $\hat{A}\Delta = LG_F n_e / \sqrt{2}$  is sensitive to the sign of  $\Delta m_{31}^2$ . For anti-neutrinos, the second term in Equation 1 has the opposite sign. It is proportional to the following CP violating quantity.

$$J_{CP} \equiv \sin \theta_{12} \sin \theta_{23} \sin \theta_{13} \cos \theta_{12} \cos \theta_{23} \cos^2 \theta_{13} \sin \delta_{CP} \tag{2}$$

Equation 1 is an expansion in powers of  $\alpha$ . The approximation becomes inaccurate for  $\Delta m_{32}^2 L / 4E > \pi/2$  as well as  $\alpha \sim 1$ . For the actual results we have used the exact numerical calculation, accurate to all orders. Nevertheless, the approximate formula is useful for understanding important features of the appearance probability: 1) the first 3 terms in the equation control the matter induced enhancement for regular mass ordering (RO) ( $m_1 < m_2 < m_3$ ) or suppression for the unnatural or reversed mass ordering (UO) ( $m_3 < m_1 < m_2$ ) of the oscillation probability above 3 GeV; 2) the second and third terms control the sensitivity to CP in the intermediate 1 to 3 GeV range; and 3) the last term controls the sensitivity to  $\Delta m_{21}^2$  at low energies.

The  $\nu_e$  signal will consist of clean, single electron events (single showering rings in a water Cherenkov detector) that result mostly from the quasi-elastic

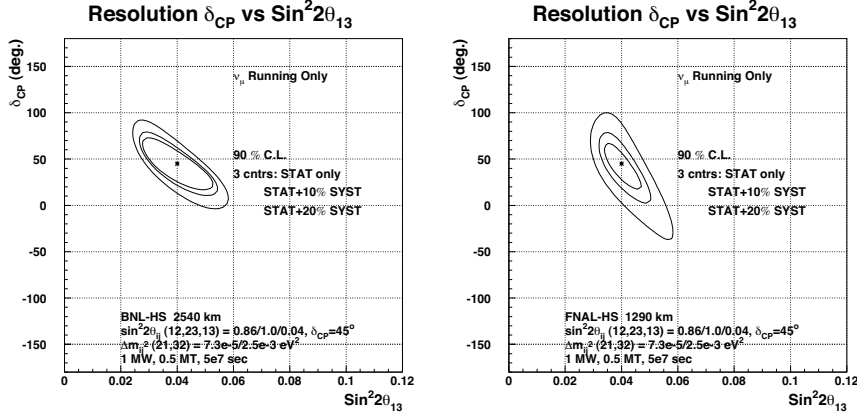


Figure 6: 90% confidence level error contours in  $\sin^2 2\theta_{13}$  versus  $\delta_{CP}$  for statistical and systematic errors with neutrino data alone. Left is for BNL-HS and right is for FNAL-HS. The test point used here is  $\sin^2 2\theta_{13} = 0.04$  and  $\delta_{CP} = 45^\circ$ .  $\Delta m_{32}^2 = 0.0025 eV^2$ , and  $\Delta m_{21}^2 = 7.3 \times 10^{-5} eV^2$ . The values of  $\sin^2 2\theta_{12}$  and  $\sin^2 2\theta_{23}$  are set to 0.86, 1.0, respectively.

reaction  $\nu_e + n \rightarrow e^- + p$ . The main backgrounds will be from the electron neutrino contamination in the beam and reactions that have a  $\pi^0$  in the final state. The  $\pi^0$  background will depend on how well the detector can distinguish events with single electron induced and two photon induced electromagnetic showers. Assuming the same detector performance as in <sup>1)</sup> we calculate the expected electron neutrino and anti-neutrino spectra shown in Figure 4. These spectra were calculated for the parameters indicated in the figures for the regular mass ordering (RO). For the reversed mass ordering (UO) the anti-neutrino (neutrino) spectrum will (not) have the large matter enhancement at higher energies. The dependence of the total event rate on the CP phase parameter is the same for RO and UO in either running mode.

#### 4.1 $\theta_{13}$ and $\delta_{CP}$ phase

If there is no excess of electron events observed then we can set a limit on the value of  $\sin^2 2\theta_{13}$  as a function of  $\delta_{CP}$ . Such 95 and 99% C.L. sensitivity limits are shown in Figure 5. These set of plots illustrate various considerations that must be evaluated for the very long baseline project. After running initially

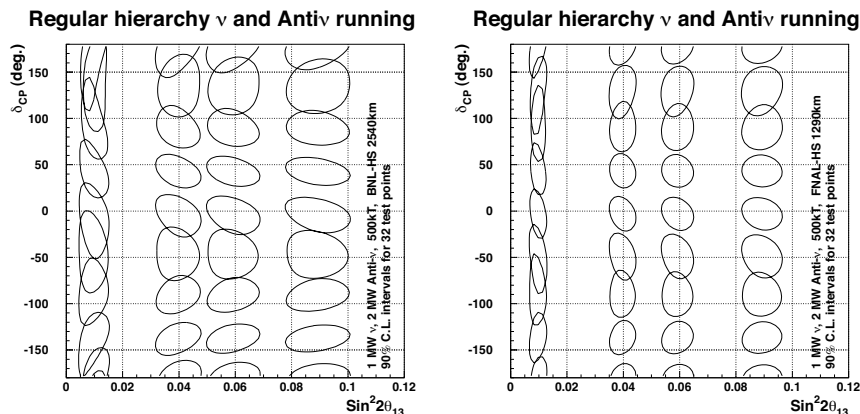


Figure 7: 90% confidence level error contours in  $\sin^2 2\theta_{13}$  versus  $\delta_{CP}$  for statistical and systematic errors for 32 test points. This simulation is for combining both neutrino and anti-neutrino data. Left is for BNL-HS and right is for FNAL-HS. We assume 10% systematic errors for this plot.

in the neutrino mode with 1 MW of beam power, if an excess signal is found then a measurement of  $\delta_{CP}$  versus  $\sin^2 2\theta_{13}$  can be made as shown in Figure 6, at the same time the mass hierarchy is determined from the strength of the signal in the higher energy region. If there is no signal in the neutrino mode then either  $\theta_{13}$  is too small for the regular mass hierarchy (RO) or the mass hierarchy is reversed (UO) and parameters are in the “unlucky” region ( $-140^\circ < \delta_{CP} < 30^\circ$ ). For the shorter baseline of 1290 km, the  $\theta_{13}$  sensitivity for the reversed hierarchy is not reduced as much as for 2540 km because both the CP-sensitivity and the matter effect are weaker. Although this yields a better limit for  $\sin^2 2\theta_{13}$  in the absence of signal, it affects the precision on  $\delta_{CP}$  and the determination of the mass hierarchy.

If there is no signal in the neutrino mode, we will run in the anti-neutrino mode to cover the “unlucky” parameter space for the appearance signal. A combination of neutrino and anti-neutrino running will yield a stringent limit approaching  $\sin^2 2\theta_{13} \sim 0.003$  independent of the value of  $\delta_{CP}$ . The simulation results shown here include wrong sign contamination in both the background and signal for anti-neutrinos. Interestingly, since more than 20% of the event rate in the anti-neutrino case actually arises from the neutrino contamination,

the  $\sin^2 2\theta_{13}$  limit in the anti-neutrino case exhibits less dependence on  $\delta_{CP}$  and the mass hierarchy. If there is a signal in the neutrino mode, we will get the first measurement of  $\delta_{CP}$  from neutrino data alone in the 3-generation model, but it will still be important to run in the anti-neutrino mode for better precision, over-constraints on the 3-generation model, and search for possible new physics either in the mixing or in the interactions of neutrinos.

In Figure 6 we show the 90% confidence level interval in the  $\delta_{CP}$  versus  $\sin^2 2\theta_{13}$  plane from neutrino running alone for the two baselines. We have chosen the point  $\delta_{CP} = 45^\circ$  and  $\sin^2 2\theta_{13} = 0.04$  as an example. At this test point for the regular mass hierarchy, the resolution on  $\delta_{CP}$  is  $\sim \pm 20^\circ$ . The mass hierarchy is also resolved at  $> 5$  sigma because of the large enhancement of the spectrum at higher energies. As we pointed out in the introduction, the resolution on the CP phase is approximately independent of the baseline. The major difference between the 1290 and 2540 km baselines is that the shorter baseline has higher correlation between the parameters,  $\delta_{CP}$  and  $\sin^2 2\theta_{13}$ , has better resolution on  $\sin^2 2\theta_{13}$ , and has worse sensitivity to systematic errors on the background and the spectrum shape. If the systematic errors exceed 10%, the shorter baseline will most likely have worse performance for measuring the CP parameter.

The sensitivity to systematic errors and the dependence on the mass hierarchy can be relieved by using data from both neutrino and anti-neutrino running. Figure 7 shows the 90% confidence level interval for 32 test points in the  $\delta_{CP}$  and  $\sin^2 2\theta_{13}$  plane after both neutrino and anti-neutrino data. A number of observations can be made: Figure 7 is for the regular mass hierarchy. The plot for the reversed mass hierarchy is similar. After both neutrino and anti-neutrino data the hierarchy will be resolved to more than 10 sigma (somewhat less significance for the shorter baseline) for  $\sin^2 2\theta_{13}$  as small as 0.01. The resolution on  $\delta_{CP}$  is seen to be approximately independent of  $\sin^2 2\theta_{13}$  for  $\sin^2 2\theta_{13} > 0.01$ . When  $\sin^2 2\theta_{13}$  is so small that the background becomes dominant, the  $\delta_{CP}$  resolution becomes poor. The resolution on  $\delta_{CP}$  is seen to be approximately the same for 2540 and 1290 km, except for small  $\sin^2 2\theta_{13}$  where large statistics at 1290 km are seen to overcome the background. The resolution on  $\sin^2 2\theta_{13}$  is, however, better for the shorter baseline because the sensitivity comes from the first node of oscillations which has much higher statistics at the shorter baseline.

#### 4.2 Correlations with other parameters

The measurement of  $\delta_{CP}$  using a wide band beam and multiple oscillation nodes is largely free of ambiguities and correlations<sup>23)</sup>. The  $\delta_{CP} \rightarrow \pi - \delta_{CP}$  ambiguity is resolved by the detection of multiple nodes including the effects of the  $\cos\delta_{CP}$  term. The mass hierarchy is resolved because it has a strong energy dependence obvious in the shape of the spectrum.

The remaining main sources of correlations are the uncertainty on  $\Delta m_{21}^2$  and  $\sin^2 2\theta_{23}$ . The CP terms in Equation 1 are linear in  $\Delta m_{21}^2$ , therefore the systematic uncertainty on the event rate at the second oscillation maximum will be  $< 10\%$ , which is the uncertainty on  $\Delta m_{21}^2$  from solar neutrino and KAMLAND experiments. As discussed above, this level of uncertainty will not affect the CP measurement for the longer baseline of 2540 km, but could be important for the shorter baseline of 1290 km.

An examination of Equation 1 shows that the knowledge of  $\theta_{23}$  affects the first ( $\Delta m_{31}^2$  dominated) and the last ( $\Delta m_{21}^2$  dominated) terms as  $\sin^2 \theta_{23}$  and  $\cos^2 \theta_{23}$ , respectively. The first term is responsible for the matter enhanced (or suppressed) appearance at high energies and the last term is responsible for appearance at low energies. Current knowledge of  $\theta_{23}$  from atmospheric neutrinos<sup>10)</sup> is rather poor:  $35 < \theta_{23} < 55^\circ$ . A precise determination of  $\sin^2 2\theta_{23}$  using the muon disappearance spectrum is, therefore, essential for proper interpretation of the appearance signal. A 1% determination of  $\sin^2 2\theta_{23}$  (Figure 3) leads to an uncertainty of  $\sim 10\%$  on the appearance event rates if  $\theta_{23} \sim 45^\circ$  and  $\sim 2\%$  if  $\theta_{23} \sim 35^\circ$ . If  $\theta_{23} \sim 35^\circ$  then there is also the additional ambiguity of  $\theta_{23} \rightarrow \pi/2 - \theta_{23}$ . Because of the strong energy dependence at low and high energies the ambiguity as well as the uncertainty should not affect the interpretation of the neutrino data in the case of the longer 2540km baseline. Uncertainties on both  $\Delta m_{21}^2$  and  $\theta_{23}$  affect the neutrino and anti-neutrino appearance spectra in the same manner, therefore after both data sets are acquired these systematic errors are expected to have little effect on establishing CP violation in neutrinos, but may affect the determination of parameters in the case of the shorter baseline.

It is important to understand the physics case for the super-beam if  $\sin^2 2\theta_{13}$  is so small that the background prevents us from detecting a signal. In this case, both the mass hierarchy through the matter effect and the CP phase measurement are not accessible for any baseline. However, the  $\nu_\mu \rightarrow \nu_e$  conver-

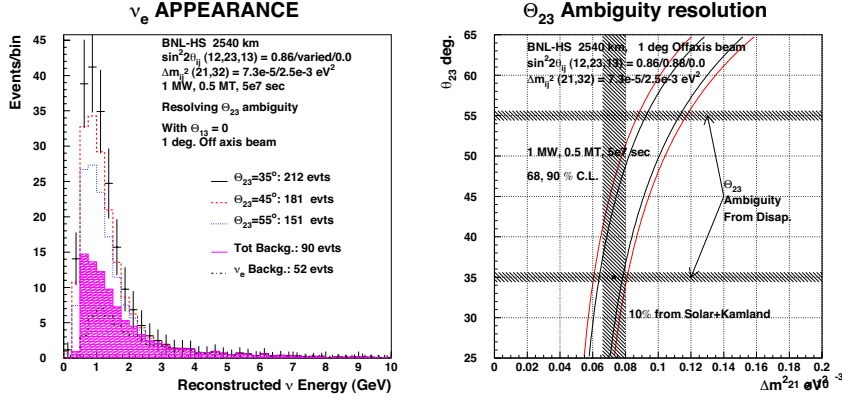


Figure 8: *Expected spectrum of electron neutrinos (left) for  $\theta_{13} = 0$  and other assumed parameters indicated in the figure. The right hand side shows the resolution of the  $\theta_{23} \rightarrow \pi/2 - \theta_{23}$  ambiguity using the measurement of  $\sin^2 2\theta_{23}$  from disappearance and assuming a 10% measurement of  $\Delta m_{21}^2$  from KAMLAND. The area between the curves is allowed by the appearance spectrum (left) for  $\theta_{23} = 35^\circ$ .*

sion signature still could be accessible for the longer baseline of 2540 km because of the last term in Equation 1. This term depends on the “solar”  $\Delta m_{21}^2$  as well as  $\sin^2 2\theta_{12}$  and  $\cos^2 \theta_{23}$ . For the current value of the solar parameters  $\sim 100$  events could be expected over a similar background. This is shown in Figure 8 where we have used a 1 degree off-axis neutrino spectrum to reduce the background level at low energies. For this calculation we have used  $\sin^2 2\theta_{23} = 1.0$  and  $\sin^2 2\theta_{23} = 0.88$  as test points. We assume that  $\sin^2 2\theta_{23}$  will be measured with  $\sim 1.5\%$  precision in disappearance. In the case of  $\sin^2 2\theta_{23} = 0.88$ , we are lead to an ambiguity in  $\theta_{23}$  of  $35^\circ \pm 0.6^\circ \rightarrow 55^\circ \pm 0.6^\circ$ . This ambiguity is clearly distinguished at several sigma in the case of the 2540 km baseline as shown in the right hand side of Figure 8. The ambiguity resolution is accomplished by comparing the result of appearance with the result of  $\bar{\nu}_e$  disappearance from solar and KAMLAND measurements. For Figure 8 we assume that  $\Delta m_{21}^2$  will be determined to  $\sim 10\%$ . This comparison of appearance and disappearance experiment could also be important for uncovering new physics in this sector.

## 5 Conclusion

We have studied various possible measurements using a powerful neutrino beam, using a MW-class proton source located either at BNL or FNAL, to a large capable detector with fiducial mass in excess of 100kT over a distance

$\sim 2000$ km. For our study here, we chose the distances of 1290 and 2540km because they correspond to the distances from FNAL and BNL to Homestake in South Dakota, one of the possible sites for a large detector. Nevertheless, our results are applicable to any other site in the U.S. at a comparable distance from an accelerator laboratory. Qualitatively, this project is motivated by the need to perform an experiment that is sensitive to both the atmospheric ( $\Delta m_{32}^2 \sim 0.0025 eV^2$ ) and the solar ( $\Delta m_{21}^2 \sim 8 \times 10^{-5} eV^2$ ) oscillation scales and to obtain an oscillatory pattern in the energy spectrum of muon neutrinos. The detector requirements for such an experiment – both in size and performance – are well-matched to other important goals in particles physics, such as detection of proton decay and astrophysical neutrinos. Therefore the potential physics impact is very broad for particle and astrophysics.

In this paper we have shown that very precise measurements of  $\Delta m_{32}^2$  and  $\sin^2 2\theta_{23}$  can be made using the observation of the oscillatory spectrum of muon neutrinos at either 1290 or 2540 km. For these precise measurements the shorter baseline has an advantage because of the increased statistical power, however it is very likely that the measurements will be systematics dominated to about 1% for either distance. We have also shown that very good bounds on  $\sin^2 2\theta_{13}$  can be obtained from both baselines using the appearance of electron neutrinos. The electron event rate at shorter baseline has smaller matter effect and smaller dependence on the CP phase. Therefore, the  $\theta_{13}$  bound using the neutrino data alone from the shorter baseline will have less dependence on the CP phase and the mass hierarchy. When both neutrino and anti-neutrino data are combined the  $\delta_{CP}$  and mass hierarchy dependence is eliminated for both baselines, and the  $\theta_{13}$  bound from either baseline will likely be dominated by the knowledge of backgrounds. The limit on  $\sin^2 2\theta_{13}$  could reach  $\sim 0.003$  if total number of background events can be controlled to about twice the expectation from the electron neutrino contamination in the beam ( $\sim 0.7\%$ ).

If a signal is found for electron appearance then the value of the CP phase can be determined from the shape of the spectrum using neutrino data alone for either baseline. A more precise measurement of the CP phase and further constraint on the 3-generation model can be made by additional running in the anti-neutrino mode. There are some advantages for having the longer 2540 km baseline for the CP measurement. The matter effect is much larger and therefore the mass hierarchy can be resolved with greater confidence. The effect of

$\delta_{CP}$  on the spectrum is also much larger for the longer baseline. This allows extraction of the parameter  $\delta_{CP}$  without relying on very precise determination of the spectrum shape. The systematics of the spectrum shape are dependent not only on the knowledge of the beam, but also on other neutrino parameters such as  $\Delta m_{31}^2$ ,  $\theta_{23}$ ,  $\Delta m_{21}^2$ , and  $\theta_{12}$ . These parameters must be obtained from solar and reactor experiments, and from the muon neutrino disappearance analysis. A 10% systematic uncertainty on the backgrounds and the shape of the spectrum is tolerable for the 2540 km baseline, whereas the uncertainty needs to be smaller for the shorter baseline experiment. In addition, the longer baseline allows detection of the appearance of electron neutrinos even if  $\theta_{13}$  is too small, through the effect of  $\Delta m_{21}^2$  alone. This observation can also help separate the  $\theta_{23} \rightarrow \pi/2 - \theta_{23}$  ambiguity if needed.

Despite the small, but significant differences between the two possible baselines, we conclude that an experiment using a beam from either FNAL or BNL to a large next generation multipurpose detector is very important for particle physics and could lead to major advances in our understanding of neutrino phenomena. It is important to recognize that the detector meant for such an experiment needs to be highly capable in terms of pattern recognition and energy resolution. If such a detector is located in a deep low background environment, it has broad applications in searching for nucleon decay and astrophysical neutrino sources. There are many advantages if both beams can be built and sent to the same detector. The correlation between parameters and the size of the matter effect are different for the two baselines. It is possible that by combining the results from the two baselines all dependence on external parameters could be eliminated, and the neutrino sector much better constrained. The requirement on total running time could also be reduced.

This work was supported by DOE grant DE-AC02-98CH10886. I also want to thank the Aspen Center for Physics where much of the writing of this paper took place.

## References

1. "Very Long Baseline Neutrino Oscillation Experiment for Precise Measurements of Mixing Parameters and CP Violating Effects", M. V. Diwan, *et al.*, PRD **68** (2003) 012002.

2. PDG, Phys. Rev. **D66**, 010001 (2002), p. 281.
3. W. Marciano, hep-ph/0108181, 22 Aug. 2001.
4. Stephen Parke, Talk in the HQL04 conference, Puerto Rico, June 1-June5, 2004.
5. S. H. Ahn et al., Phys. Lett. **B 511** 178 (2001).
6. Numi MINOS project at Fermi National Accelerator Laboratory, <http://www-numi.fnal.gov/>
7. The CERN Neutrino beam to Gran Sasso (Conceptual Technical Design), Ed. K. Elsener, CERN 98-02, INFN/AE-98/05, <http://proj-cngs.web.cern.ch/proj-cngs/>
8. The JHF-Kamioka neutrino project, Y. Itow et al., arXiv:hep-ex/0106019, June 2001.
9. Letter of Intent to build an Off-axis Detector to study numu to nue oscillations with the NuMI Neutrino Beam, D. Ayres *et al.*, hep-ex/0210005.
10. Y. Fukuda et al., Phys. Rev. Lett. **81**, 1562 (1998); S. Fukuda et al., Phys. Rev. Lett. **86** 5656, 2001; E.W. Beier, Phys. Lett. **B283**, 446 (1992); T. Kajita and Y. Totsuka, Rev. Mod. Phys. **73**, 85 (2001).
11. K. Eguchi, *et. al.*, Phys. Rev. Lett. **90**, 021802 (2003). hep-ex/0212021.
12. Q. R. Ahmad et al., Phys. Rev. Lett. **87** 071301 (2001). S. Fukuda et al., Phys. Rev. Lett., **86** 5651 (2001).
13. J. Alessi *et al.*, AGS Super Neutrino Beam Facility, Accelerator and Target system Design, BNL-71228-2003-IR. April 15, 2003. <http://nwg.phy.bnl.gov/>
14. Neutrinos and Beyond: New Windows on Nature, Neutrino Facilities Assessment Committee, National Research Council, (2003), ISBN-0-309-08716-3, <http://www.nap.edu/catalog/10583.html>.
15. R. Alber, et al., Accelerator Proton Driver Study Group FNAL-TM-2136, FNAL-TM-2169. <http://www-bd.fnal.gov/pdriver/>

16. Megaton Modular Multi-Purpose Neutrino detector, 3M collaboration, <http://www.hep.upenn.edu/Homestake>
17. Physics Potential and Feasibility of UNO, UNO collaboration, June 2001, Stony Brook University, SBHEP01-03.
18. D.B. Cline, F. Segiampietri, J.G. Learned, K.T. McDonald, *LANNDD, A Massive Liquid Argon Detector for Proton Decay, Supernova and Solar neutrino Studies, and a Neutrino Factory Detector* May 24, 2001, astro-ph/0105442; F. Arneodo et al., Nucl. Instrum. Meth. **A471** 272-275 (2000).
19. The “off-axis” neutrino beam was first proposed by the E889 Collaboration, Physics Design Report, BNL No. 52459, April, 1995. <http://minos.phy.bnl.gov/nwg/papers/E889>.
20. S. Fukuda et al., Nucl. Instrm. Meth. A **501**, (2003) 418-462.
21. P. Antonioli et al., Nuclear Instrm. Methods **A433** 104-120, (1999).
22. M. Freund, Phys.Rev. D64 (2001) 053003; M. Freund, P. Huber, M. Lindner, Nucl.Phys. B615 (2001) 331-357;
23. V.D. Barger, S. Geer, R. Raja, K. Whisnant, Phys. Rev. D63: 113011 (2001); V. Barger et al., hep-ph/0103052; P. Huber, M. Lindner, W. Winter, Nucl. Phys. B645, 3 (2002); V. Barger, D. Marfatia, K. Whisnant, Phys. Rev. D65: 073023 (2002).



***SESSION II – CP Violation I – B Decays***

- H. Yamamoto Search for new CP violating phases by Belle  
M. C. Simani Measurements Related to the CKM Angle  $\beta/\phi_1$  from BABAR  
K. E. Ford Measurement of the CKM Angles  $\alpha$  and  $\gamma$  at the BABAR Experiment  
R. Itoh Measurements of  $\phi_3/\gamma$  with  $B \rightarrow D^{(*)} K$  and  $B \rightarrow D^{(*)} \pi$  at Belle



Frascati Physics Series Vol. XXXV (2004), pp. 113  
HEAVY QUARKS AND LEPTONS - San Juan, Puerto Rico, June 1-5, 2004

**SEARCH FOR NEW CP VIOLATING PHASES BY BELLE**

H. Yamamoto  
*Tohoku University, Sendai, Japan*

Written contribution not received



## MEASUREMENTS RELATED TO THE CKM ANGLE $\beta/\phi_1$ FROM BABAR

Maria Chiara Simani, representing the BABAR Collaboration  
*Lawrence Livermore National Laboratory, 94550 Livermore, CA, USA*

### ABSTRACT

We present measurements related to the CKM angle  $\beta$  from the BABAR experiment based on 82 or 113  $\text{fb}^{-1}$  data samples collected at the PEP-II  $e^+e^-$  asymmetric  $B$  Factory collider. Updated CP measurements in the penguin dominated modes  $B^0 \rightarrow \phi K^0$ ,  $B^0 \rightarrow f_0(980)K_S^0$ ,  $B^0 \rightarrow \pi^0 K_S^0$ , and  $B^0 \rightarrow K^+K^-K_S^0$  are presented. In addition, a new method that allows to determine the *sign* of  $\cos 2\beta$  with the decay mode  $B^0 \rightarrow J/\psi K^{*0}$  is described.

### 1 Introduction

CP violation has been a primary objective of particle physics since its discovery in 1964 in the  $K^0$  mesons decay <sup>1)</sup>. In the three-generation Cabibbo-Kobayashi-Maskawa (CKM) quark mixing matrix <sup>2)</sup> the CP-violation effect is accounted for as a complex phase that breaks the CP symmetry of the flavor-changing transitions.

In general, CP-violating asymmetries arise from the interference between amplitudes with a weak phase difference. As an example, an initially produced state  $B^0$  ( $\overline{B}^0$ ) can decay to a final CP eigenstate  $f_{CP}$  either directly with amplitude  $A_{f_{CP}}$  ( $\overline{A}_{f_{CP}}$ ), or it can first oscillate into a  $\overline{B}^0$  ( $B^0$ ) state and then decay to  $f_{CP}$  with amplitude  $\overline{A}_{f_{CP}}$  ( $A_{f_{CP}}$ ). In the Standard Model (SM), the phase difference between the amplitudes  $\overline{A}_{f_{CP}}$  and  $A_{f_{CP}}$  is equal to twice the angle

$$\beta = \phi_1 = \arg(-V_{cd}V_{cb}^*/V_{td}V_{tb}^*) . \quad (1)$$

of the Unitarity Triangle <sup>3)</sup>. The measurement of the CP-violating asymmetry in theoretically and experimentally clean decays such as  $B^0 \rightarrow J/\psi K_S^0$  established the presence of CP violation in  $B$  meson decays from the direct determination of  $\sin 2\beta$ , and thus providing a crucial test for the SM <sup>4)</sup>.

The SM can be further challenged by measuring  $\sin 2\beta$  in penguin dominated channels, since new physics (NP) may enter the loop appearing in the diagram of these decays. A large departure from the  $\sin 2\beta$  value measured in the  $B^0 \rightarrow J/\psi K_S^0$  mode will be a clear signature of NP. Here, we present the recent results of BABAR CP measurements in the penguin dominated modes:  $B^0 \rightarrow \phi K^0$ ,  $B^0 \rightarrow f_0(980)K_S^0$ ,  $B^0 \rightarrow \pi^0 K_S^0$ , and  $B^0 \rightarrow K^+K^-K_S^0$ .

In addition, the high precision measurement of the CP violating parameter  $\sin 2\beta$  is determined up to a four-fold ambiguity on the angle  $\beta$  itself. This can be reduced to a two-fold ambiguity when measuring the sign of  $\cos 2\beta$ . In the SM  $\cos 2\beta$  is expected to be positive. The  $\cos 2\beta$  parameter can be measured with events  $B^0 \rightarrow J/\psi K^{*0}$ ;  $K^{*0} \rightarrow K_S\pi^0$ . However, also this decay contains a sign ambiguity, arising from a two-fold ambiguity in the determination of the strong phases involved in the decay. Here, we present a new method to break this strong phases ambiguity based on the analysis of the  $K\pi$  phase variation with mass. This will allow a first ambiguity-free measurement of  $\cos 2\beta$  and a direct test of the SM.

## 2 CP measurements with penguin dominated modes

The penguin dominated modes are considered “windows” to NP. In the SM, contributions beyond the leading penguin are affected by estimation uncertainty which depends on the channel. The “effective  $\sin 2\beta$ ” measured in each channel may then differ from  $\sin 2\beta$  by different amounts <sup>5)</sup>.

The proper-time distribution of a reconstructed  $B$  meson ( $B_{\text{rec}}$ ) which decays

to  $f_{CP}$ , can be expressed in terms of a complex parameter  $\lambda$  <sup>6)</sup>, which depends on both the  $B^0 - \overline{B}^0$  oscillation amplitude as well as the decay amplitudes  $A_{f_{CP}}$  and  $\overline{A}_{f_{CP}}$ . The decay rate  $f_+$  ( $f_-$ ) when the other  $B$  meson ( $B_{\text{tag}}$ ) decays as a  $B^0$  ( $\overline{B}^0$ ) is given by

$$\begin{aligned} f_{\pm}(\Delta t) &= \frac{e^{-|\Delta t|/\tau_{B^0}}}{4\tau_{B^0}} \left[ 1 \pm \frac{2\mathcal{I}m\lambda}{1+|\lambda|^2} \sin(\Delta m_d \Delta t) \mp \frac{1-|\lambda|^2}{1+|\lambda|^2} \cos(\Delta m_d \Delta t) \right], \\ &= \frac{e^{-|\Delta t|/\tau_{B^0}}}{4\tau_{B^0}} \left[ 1 \pm S \sin(\Delta m_d \Delta t) \mp C \cos(\Delta m_d \Delta t) \right], \end{aligned} \quad (2)$$

where  $\Delta t = t_{\text{rec}} - t_{\text{tag}}$  is the difference between the proper decay times of  $B_{\text{rec}}$  and  $B_{\text{tag}}$ ;  $\tau_{B^0}$  is the  $B^0$  lifetime, and  $\Delta m_d$  is the  $B^0 - \overline{B}^0$  oscillation frequency. The decay width difference  $\Delta\Gamma$  between the  $B^0$  mass eigenstates is assumed to be zero. The sine term is due to the interference between direct decay and decay after a net  $B^0 - \overline{B}^0$  oscillation. A non-zero cosine term arises from the interference between decay amplitudes with different weak and strong phases (direct CP violation) or CP violation in  $B^0 - \overline{B}^0$  mixing.

In the SM, CP violation in mixing is negligible, as is direct CP violation. With these assumptions,  $\lambda = \eta_f e^{-2i\beta}$ , where  $\eta_f$  is the CP eigenvalue of the final state  $f_{CP}$ . Thus, the measured time-dependent CP asymmetry is

$$A_{CP}(\Delta t) \equiv \frac{f_+ - f_-}{f_+ + f_-} = -\eta_f \cdot \sin 2\beta \cdot \sin(\Delta m_d \Delta t). \quad (3)$$

### 2.1 Decay modes $B^0 \rightarrow \phi K_S^0$ and $B^0 \rightarrow \phi K_L^0$

The decay  $B^0 \rightarrow \phi K^0$  is a  $b \rightarrow s\overline{s}s$  quark level decay. In the SM, the expected CP asymmetry is very close to  $\sim \sin 2\beta$ . The BABAR measurement is reported in Table 1 and decay rates are shown in Figure 1. The measurement is in agreement with the SM expectation.

### 2.2 Decay mode $B^0 \rightarrow f_0(980)K_S; f_0(980) \rightarrow \pi^+\pi^-$

The structure of the scalar meson  $f_0(980)$  is not well known, but recent studies favor an usual  $q\overline{q}$  interpretation <sup>11)</sup>, with  $f_0 = \cos \phi_s s\overline{s} + \sin \phi_s (u\overline{u} + d\overline{d})/\sqrt{2}$  and  $\phi_s = (-48 \pm 6)^\circ$ . The decay  $B^0 \rightarrow f_0(980)K_S$  should then be dominated by the  $b \rightarrow s\overline{s}s$  penguin, since the  $s\overline{s}$  component is sizeable and the  $b \rightarrow u\overline{u}s$  tree is doubly Cabbibo suppressed compared to the leading penguin. The

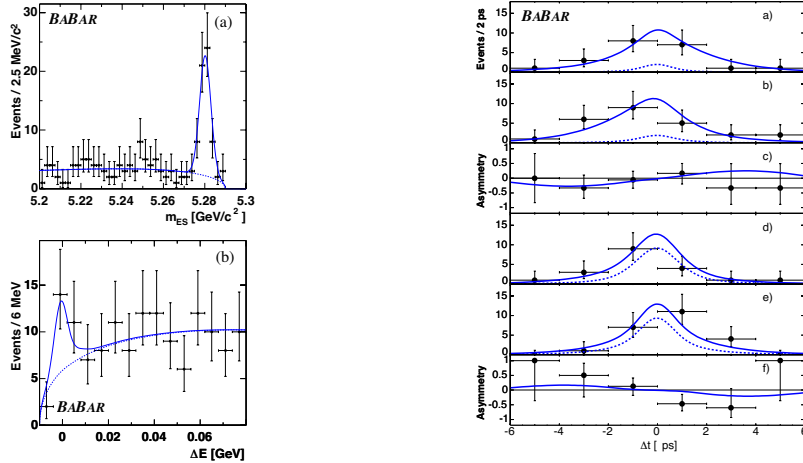


Figure 1: Top left: Mass distribution of  $B^0 \rightarrow \phi K_S^0$  events, with  $70 \pm 9$  candidates found out of a  $108\text{fb}^{-1}$  sample. Bottom left: Difference of measured and expected energy of  $B^0 \rightarrow \phi K_L^0$  candidates: only the  $K_L$  direction is known and the  $B$  mass constraint is used to estimate the  $B$  energy.  $52 \pm 16$  candidates are found. Right:  $\Delta t$  distributions and asymmetry for  $B^0 \rightarrow \phi K_S^0$  (a,b,c) and  $B^0 \rightarrow \phi K_L^0$  (d,e,f).

$B^0 \rightarrow f_0(980)K_S$  CP asymmetry expected in the SM is  $\sim -\sin 2\beta$ . A quasi two-body analysis is performed, and a cut in the  $\pi\pi K$  Dalitz plot is made to reduce the contributions from the  $\rho_0$  and the  $f_0(1370)$ . This is the first observation of the  $B^0 \rightarrow f_0(980)K_S$  decay (see Fig. 2). The signal is checked with a fit to the  $\pi^+\pi^-$  mass spectrum with a relativistic Breit-Wigner, leading to a mass and a width compatible with the PDG values for the  $f_0$ . The CP fit result is shown in Table 1, and the decay rates distributions are shown in Figure 2.

### 2.3 Decay mode $B^0 \rightarrow \pi^0 K_S$

This a  $b \rightarrow s\bar{d}d$  quark level decay. The SM expectation for this decay mode is  $\sim +\sin 2\beta$ . An experimental issue with this decay is the determination of the  $B^0$  vertex: no charged particles emerge from the  $B^0$  vertex. The reconstructed  $B$  direction is constrained to the beam spot in a plane transverse to the beam direction. This is used to estimate the  $B$  vertex position. The vertex deter-

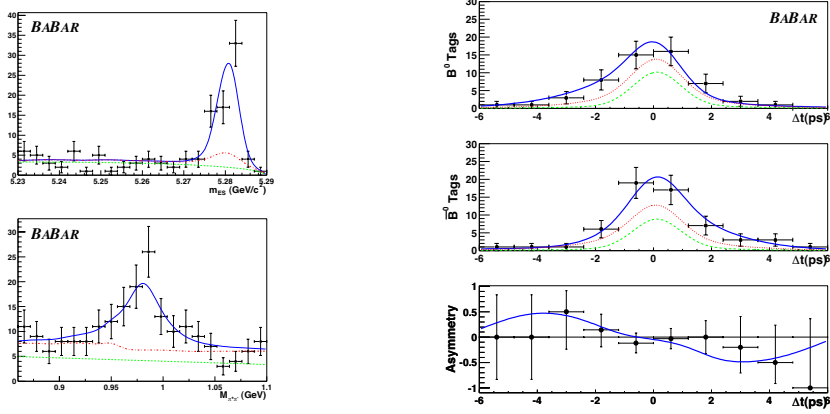


Figure 2: *Left: Top: Mass distribution of  $B^0 \rightarrow f_0(980)K_S$  candidates.  $94 \pm 14 \pm 6$  out of a  $111\text{fb}^{-1}$  sample are found. Bottom:  $\pi^+\pi^-$  invariant mass, fitted with a relativistic Breit-Wigner function. Right:  $\Delta t$  distributions and asymmetry.*

mination technique is checked with  $B^0 \rightarrow J/\psi K_S$  and  $B^+ \rightarrow \pi^+ K_S$  decays, ignoring the  $J/\psi$  or the  $\pi^+$ . An additional check makes use of the measured  $B^0$  lifetime. The CP asymmetry measurements are shown in Table 1 and decay rates plots are shown in Figure 3.

#### 2.4 Decay modes $B^0 \rightarrow K^+K^-K_S$ and $B^\pm \rightarrow K^\pm K_S K_S$

The CP asymmetry of the quark level decay  $b \rightarrow s\bar{s}s$  can also be measured with the inclusive  $B^0 \rightarrow K^+K^-K_S$  decay (excluding  $\phi \rightarrow K^+K^-$ ) and benefits from larger statistics than the  $B^0 \rightarrow \phi K_S^0$  mode. In contrast, the CP content is not known *a priori* and it can be determined from  $B \rightarrow KKK$  branching ratios of charged and neutral  $B$  mesons<sup>10</sup>):  $f_{\text{even}} = 2\Gamma(B^+ \rightarrow K^+K_S K_S)/\Gamma(B^0 \rightarrow K^+K^-K_S)$  BABAR measured the following branching ratios:

$$\text{Br}(B^+ \rightarrow K^+K_S K_S) = (10.7 \pm 1.2 \pm 1.0) \times 10^{-6}, \quad (4)$$

$$\text{Br}(B^0 \rightarrow K^+K^-K_S) = (23.8 \pm 2.0 \pm 1.6) \times 10^{-6}, \quad (5)$$

obtaining  $f_{\text{even}} = 0.98 \pm 0.15 \pm 0.04$ , which is compatible with a pure CP even state. In the SM the expected CP asymmetry for this channel is then  $\sim -\sin 2\beta$ . The measured CP asymmetry parameters  $S$  and  $C$  are shown in

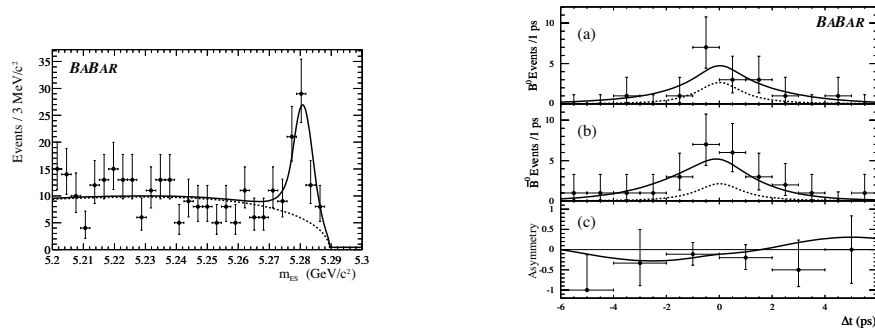


Figure 3: *Left: Mass distribution of  $B^0 \rightarrow \pi^0 K_S$  candidates, with  $122 \pm 16$  candidates found out of a  $113\text{fb}^{-1}$  sample. Right:  $\Delta t$  distributions and asymmetry.*

Table 1 and the decay rates are shown in Figure 4. The first measurement of the CP-violating charge asymmetry in the  $B^\pm \rightarrow K^\pm K_S K_S$  decay resulted in  $A_{CP}(B^\pm \rightarrow K^\pm K_S K_S) = -0.042 \pm 0.114(\text{stat}) \pm 0.02(\text{syst})$ .

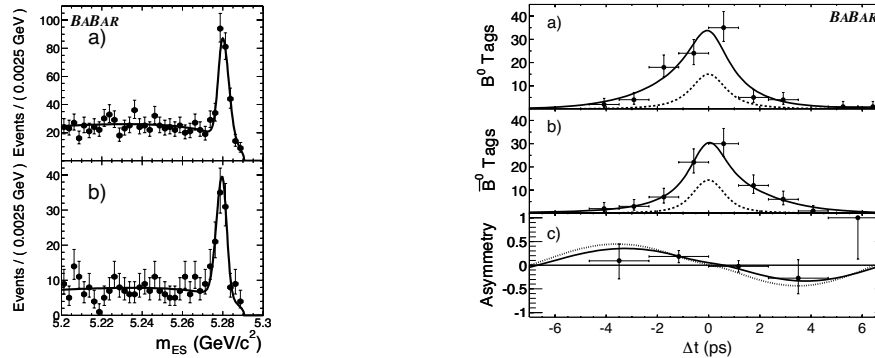


Figure 4: *Left: Mass distribution of a)  $B^0 \rightarrow K^+ K^- K_S$  and b)  $B^\pm \rightarrow K^\pm K_S K_S$  candidates.  $201 \pm 16$  and  $122 \pm 14$  candidates are found respectively out of a  $111\text{fb}^{-1}$  sample. Right:  $\Delta t$  distributions and asymmetry.*

Table 1:  $S$  and  $C$  CP parameters (Eq. 2) measured for various  $B$  decay modes. The (approximative) SM expectation for  $S$  is given in the second column. For  $S$  and  $C$ , the first uncertainty is statistical, the second one systematical. The “ $f_{\text{even}}$ ” uncertainty for  $S$  of  $K^+K^-K_S$  comes from the uncertainty on  $f_{\text{even}}$  itself. Details for each mode are given in the text.

$B$ decay	SM exp.	$S$	$C$
$\phi K^0$	$+\sin 2\beta$	$+0.47 \pm 0.34^{+0.08}_{-0.06}$	$+0.10 \pm 0.33 \pm 0.10$
$K^+K^-K_S$	$-\sin 2\beta$	$-0.56 \pm 0.25 \pm 0.04^{+0}_{-0.17}(f_{\text{even}})$	$-0.10 \pm 0.19 \pm 0.09$
$\pi^0 K_S$	$+\sin 2\beta$	$+0.48^{+0.38}_{-0.47} \pm 0.11$	$+0.40^{+0.27}_{-0.28} \pm 0.10$
$F(980)K_S$	$-\sin 2\beta$	$-1.62^{+0.56}_{-0.51} \pm 0.10$	$+0.27 \pm 0.36 \pm 0.15$

### 3 Measurement of the $\cos 2\beta$ sign with $B^0 \rightarrow J/\psi K^{*0}$ events

The CP content of the decay  $B^0 \rightarrow J/\psi K^{*0}(892); K^{*0}(892) \rightarrow K_S \pi^0$  is both even and odd. The  $\cos 2\beta$  parameter appears through CP-even and CP-odd interferences in the time and angular dependant distribution in the observables <sup>7)</sup>:

$$\cos(\delta_{\parallel} - \delta_{\perp}) \cdot \cos 2\beta, \quad \cos(\delta_{\perp} - \delta_0) \cdot \cos 2\beta, \quad (6)$$

where  $\delta_0, \delta_{\parallel}$  and  $\delta_{\perp}$  are the strong phases of the decay amplitudes  $A_0 = |A_0|e^{i\delta_0}, A_{\parallel} = |A_{\parallel}|e^{i\delta_{\parallel}}$ , which are CP-even, and  $A_{\perp} = |A_{\perp}|e^{i\delta_{\perp}}$ , which is CP-odd. These strong phases are measured on a large sample of neutral and charged  $B \rightarrow J/\psi K^*$  decays (see Table 2), up to the two-fold mathematical ambiguity:  $(\delta_{\parallel} - \delta_0, \delta_{\perp} - \delta_0) \leftrightarrow (-(\delta_{\parallel} - \delta_0), \pi - (\delta_{\perp} - \delta_0))$ . For the moduli of the decay amplitudes we obtain:

$$|A_0|^2 = 0.566 \pm 0.012 \pm 0.005 \quad (7)$$

$$|A_{\parallel}|^2 = 0.204 \pm 0.015 \pm 0.005 \quad (8)$$

$$|A_{\perp}|^2 = 0.230 \pm 0.015 \pm 0.004 \quad (9)$$

Under this transformation,  $\cos(\delta_{\parallel} - \delta_{\perp})$  and  $\cos(\delta_{\perp} - \delta_0)$  change of sign, implying that the two set of parameters  $(\delta_{\parallel} - \delta_0, \delta_{\perp} - \delta_0, \cos 2\beta) \leftrightarrow (-(\delta_{\parallel} - \delta_0), \pi - (\delta_{\perp} - \delta_0), -\cos 2\beta)$  are mathematically equivalent <sup>7)</sup>. Up to this point we considered the  $P$ -wave  $K^*(892)$  only. In fact, it is known that a  $K\pi$   $S$ -wave lies in the  $K^*(892)$  region <sup>8)</sup> and the resulting interference with the main  $K\pi$   $P$ -wave  $K^*(892)$  can be exploited to break the strong phases ambiguity. Taking into account a  $B \rightarrow J/\psi(K\pi)_{S\text{-wave}}$  amplitude, in addition to the three

Table 2: Values of the strong phases corresponding to the two possible solutions. The strong phases measured by an angular analysis on a sample of  $B^0 \rightarrow J/\psi(K^+\pi^-)^{*0}$ ,  $B^+ \rightarrow J/\psi(K_S\pi^+)^{*+}$ ,  $B^+ \rightarrow J/\psi(K^+\pi^0)^{*+}$ , and related charged conjugate decays. The integrated luminosity is  $82\text{fb}^{-1}$ . The yields corresponding to the three above channels are  $2376 \pm 51$ ,  $670 \pm 27$  and  $791 \pm 33$ , respectively. Note that we observe a  $7.6 \sigma$  significant strong phase:  $\delta_{\parallel} - \delta_{\perp} = 0.597 \pm 0.077 \pm 0.017$ .

	Solution I	Solution II
$\delta_{\parallel} - \delta_0$	$2.729 \pm 0.101 \pm 0.052$	$3.554 \pm 0.101 \pm 0.052$
$\delta_{\perp} - \delta_0$	$0.184 \pm 0.070 \pm 0.046$	$2.958 \pm 0.070 \pm 0.046$

$B \rightarrow J/\psi(K\pi)_{P\text{-wave}}$  ones ( $A_0, A_{\parallel}, A_{\perp}$ ); introduces the relative strength of the  $P$  and  $S$  contributions and a new relative phase  $\gamma = \delta_S - \delta_0$ . The ambiguity

$$(\delta_{\parallel} - \delta_0, \delta_{\perp} - \delta_0, \gamma) \leftrightarrow (-(\delta_{\parallel} - \delta_0), \pi - (\delta_{\perp} - \delta_0), -\gamma), \quad (10)$$

still remains, but the ambiguity on  $\gamma$  can be solved. According the Wigner’s causality principle <sup>9)</sup>, the phase of a resonance rotates counterclockwise with increasing mass. In the  $K^*(892)$  region, the  $(K\pi)_{S\text{-wave}}$  phase moves slow, while the  $(K\pi)_{P\text{-wave}}$  phase moves rapidly. The phase  $\gamma = \delta_S - \delta_0$  must then rotates clockwise in the  $K^*(892)$  region. Figure 5 shows the  $P$  and  $S$  wave intensities as function of the  $K\pi$  mass, as well as  $\gamma$  for both “Solution I” and “Solution II”. The physical variation of  $\gamma$  is observed for “Solution II”. As a cross-check of the phase evolution with mass, the  $\gamma$  phase evolution is compared in Figure 5 with the evolution observed in the  $Kp \rightarrow K\pi(n)$  high statistics LASS experiment <sup>8)</sup>. The agreement with the LASS experiment is remarkable. We perform a time and angular dependant analysis of the  $B^0 \rightarrow J/\psi(K_S\pi^0)^{*0}$  sample (104 events), fixing the angular structure of the decay using above amplitude moduli and strong phases “Solution II” (tab. 2). With  $\sin 2\beta$  and  $\cos 2\beta$  free in the fit, we obtain <sup>7)</sup>  $\sin 2\beta = -0.10 \pm 0.57(\text{stat}) \pm 0.14(\text{syst})$  and  $\cos 2\beta = +3.32_{-0.96}^{+0.76}(\text{stat}) \pm 0.27(\text{syst})$ . Using the world average  $\sin 2\beta = 0.731$  value, we obtain

$$\cos 2\beta = +2.72_{-0.79}^{+0.50}(\text{stat}) \pm 0.27(\text{syst}). \quad (11)$$

We thus measure a *positive*  $\cos 2\beta$  value, in agreement with the SM expectation. The fit result for  $\cos 2\beta$  can be illustrated by determining the moment of the

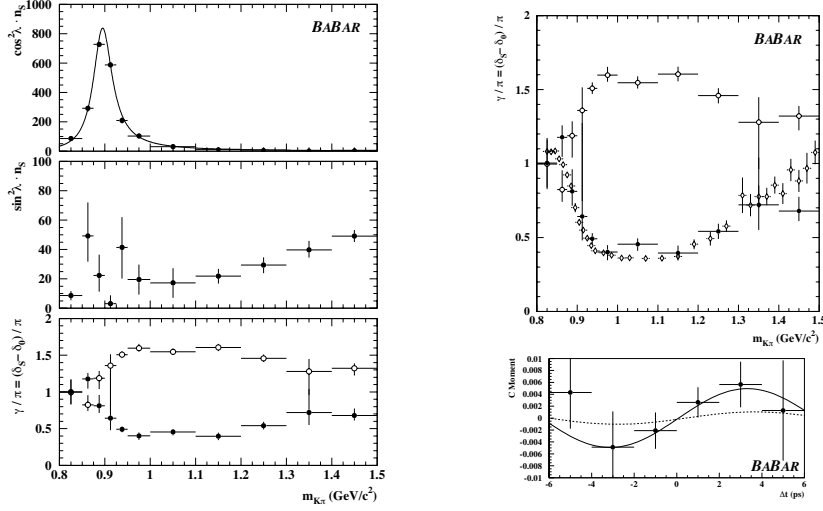


Figure 5: *Left plots: Top and middle panel are the P and S wave intensity as function of the  $K\pi$  mass ( $K^{\pm}\pi^{\mp}$  channel only). A fit with a Breit-Wigner lineshape including centrifugal effect is performed for the P wave intensity. Bottom:  $\gamma = \delta_S - \delta_0$  as function of the  $K\pi$  mass, where the open points are obtained with strong phases “Solution I” (Tab. 2) and the full points with “Solution II” (Tab. 2). Right plots: Top: Comparison of the  $\gamma = \delta_S - \delta_0$  phase with the  $K\pi$  mass with the LASS data (diamond markers). The LASS data correspond to the isospin 1/2 contribution, i.e., the one existing in the  $B \rightarrow J/\psi(K\pi)$  decay. A global  $\pi$  offset was added to the LASS data, which obviously does not change the slope. Bottom: Moment of the angular function weighting the  $\cos 2\beta$  contribution in the time and angular dependant distribution. The full line corresponds to  $\cos 2\beta = +3.32$ , the dashed line to  $\cos 2\beta = \sqrt{1 - 0.731^2} = +0.68$ .*

angular term weighting  $\cos 2\beta$  in the time and angular dependent distribution, as shown in Figure 5. Assuming  $\sin 2\beta$  and  $\cos 2\beta$  measure the same angle  $2\beta$ , we estimate on Monte Carlo that we exclude the negative  $\cos 2\beta$  solution at 89% CL. This is a preliminary estimate.

## 4 Conclusion

Measurements of CP asymmetries in the penguin dominated modes  $B^0 \rightarrow \phi K^0$ ,  $B^0 \rightarrow f_0(980)K_S^0$ ,  $B^0 \rightarrow \pi^0 K_S^0$ , and  $B^0 \rightarrow K^+ K^- K_S^0$  are all found compatible with SM expectations. A novel method to resolve the ambiguity of the strong phases in the  $B \rightarrow J/\psi K^*$  has been used to measure the sign of  $\cos 2\beta$  with  $B^0 \rightarrow J/\psi K^{*0}$ ;  $K^{*0} \rightarrow K_S \pi^0$  free from the strong phases ambiguity. This sign is found positive, in agreement with SM expectation.

## References

1. J.H. Christenson *et al.*, Phys. Rev. Lett. **13**, 138 (1964).
2. N.Cabibbo, Phys. Rev. Lett. **10**, 531 (1963); M.Kobayashi and T.Maskawa, Prog. Th. Phys. **49**, 652 (1973).
3. A.B.Carter and A.I.Sanda, Phys. Rev. D **23**, 1567 (1981); I.I Bigi and A.I.Sanda, Nucl. Phys. B **193**, 85 (1981).
4. BABAR Collaboration, Phys. Rev. Lett. **89**, 201802 (2002); BELLE Collaboration, Phys. Rev. D **66**, 071102 (2002).
5. D.London and A.Soni, Phys. Lett. B **407**,61-65 (1997); Y.Grossman, Z.Ligeti,Y.Nir, H.Quinn, Phys. Rev. D **68**,015004 (2003); M.Gronau, Y.Grossman, J.Rosner, Phys. Lett. B **579**,331-339 (2004).
6. See, for example, D. Kirkby and Y. Nir, Phys. Lett. **B592**, 1 (2004).
7. S. T'Jampens, Thesis (in French), Université Paris XI, 18 Dec. 2002.
8. D. Aston *et al.*, [LASS, aka E-135 Collaboration], Nucl. Phys. B **296**, 493 (1988).
9. E. P. Wigner, Phys. Rev. **98**, 145-147 (1955)
10. Belle Collaboration, Phys. Rev D **69**, 012001 (2004)
11. A. V. Anisovich *et al.*, hep-ph/0011191 (2000)

Frascati Physics Series Vol. XXXV (2004), pp. 125-134  
HEAVY QUARKS AND LEPTONS - San Juan, Puerto Rico, June 1-5, 2004

## MEASUREMENT OF THE CKM ANGLES $\alpha$ AND $\gamma$ AT THE *BABAR* EXPERIMENT

Kelly E. Ford  
*The University of Birmingham*  
*representing the BABAR Collaboration*

### ABSTRACT

The primary objective of the *BABAR* Experiment is to test the Standard Model explanation of *CP* violation in weak decays by over-constraining the CKM Unitarity Triangle. This includes the measurement of all three angles of the triangle. Although precise measurements of the angle  $\beta$  have been obtained using *B* decays to charmonium states, the remaining angles,  $\alpha$  and  $\gamma$ , pose greater experimental challenges. In this paper, the latest measurements of modes which will constrain  $\alpha$  and  $\gamma$  will be presented, including  $B^0 \rightarrow \rho^+ \rho^-$  for  $\alpha$  and a measurement of  $\sin(2\beta + \gamma)$  from the  $B^0 \rightarrow D^{(*)\pm} \pi^\mp$  system.

### 1 *CP* Violation

In the Standard Model, the imbalance between matter and anti-matter in the universe can be quantified by measuring the amount of *CP* Violation present in

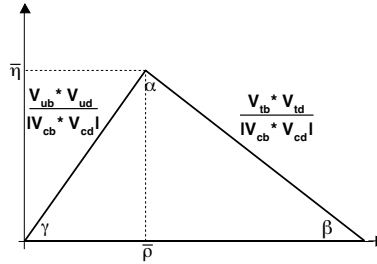


Figure 1: *The triangular representation of  $V_{ub}^* V_{ud} + V_{cb}^* V_{cd} + V_{tb}^* V_{td} = 0$ , which describes CP violation in the Standard Model for the B meson system.*

weak interactions.  $CP$  violation is described by a single phase ( $\eta$ ) in the quark mixing matrix for three generations, the Cabibbo-Kobayashi-Maskawa (CKM) matrix. The CKM matrix:

$$V_{CKM} = \begin{pmatrix} V_{ud} & V_{us} & V_{ub} \\ V_{cd} & V_{cs} & V_{cb} \\ V_{td} & V_{ts} & V_{tb} \end{pmatrix} \quad (1)$$

is the Standard Model description of  $CP$  violation, and can be rewritten in the Wolfenstein parameterization <sup>1)</sup>, as:

$$V_{CKM} = \begin{pmatrix} 1 - \lambda^2/2 & \lambda & A\lambda^3(\rho - i\eta) \\ -\lambda & 1 - \lambda^2/2 & A\lambda^2 \\ A\lambda^3(1 - \rho - i\eta) & -A\lambda^2 & 1 \end{pmatrix} + \mathcal{O}(\lambda^4) \quad (2)$$

The unitarity of the CKM matrix yields several interesting relationships for its components, including  $V_{ub}^* V_{ud} + V_{cb}^* V_{cd} + V_{tb}^* V_{td} = 0$  (Figure 1) which describes Standard Model  $CP$  violation in the  $B$  meson system. Measuring the two sides (the base is set to unit value) and all three angles of this triangle in many different processes tests whether this theory of  $CP$  violation is a full description of the processes which occur in the  $B$  meson system. The three angles ( $\alpha$ ,  $\beta$  and  $\gamma$ ) can be written in terms of the couplings between quarks:

$$\alpha \equiv \arg \left[ -\frac{V_{td} V_{tb}^*}{V_{ud} V_{ub}^*} \right] ; \quad \beta \equiv \arg \left[ -\frac{V_{cd} V_{cb}^*}{V_{td} V_{tb}^*} \right] ; \quad \gamma \equiv \arg \left[ -\frac{V_{ud} V_{ub}^*}{V_{cd} V_{cb}^*} \right] \quad (3)$$

The measurements of these angles can be made in the  $CP$  asymmetries of decay modes of the  $B$  meson. This paper describes recent analyses which aim to measure  $\alpha$  and  $\gamma$  from the  $BABAR$  experiment.

## 2 The $BABAR$ Experiment

The  $BABAR$  experiment is situated at the PEP-II <sup>2)</sup> asymmetric  $e^+e^-$  collider at the Stanford Linear Accelerator Center, U.S.A. As the  $BABAR$  detector is described completely elsewhere <sup>3)</sup>, only a brief description is included here. A Silicon Vertex Tracker (SVT) surrounds the beam-pipe, providing excellent tracking of charged particles close to interaction point. Surrounding the SVT is a drift chamber (DCH), which provides some particle identification (due to its measurements of the energy loss of charged particles) and precise measurements of track momenta inside the 1.5T magnetic field applied to the detector using a superconducting coil. The detector of internally reflected Cherenkov radiation (DIRC) provides charged hadron identification, whilst the CsI(Tl) electromagnetic calorimeter (EMC), is used to reconstruct neutral hadrons, detect photons and provide electron identification. Situated next is the magnet, followed by the instrumented flux return (IFR), which is used for the identification of muons and long-lived neutral hadrons.

## 3 Measurements of $\alpha$

Neutral  $B$  mesons decay to  $\pi^+\pi^-$  and  $\rho^+\rho^-$  primarily via a  $b \rightarrow u\bar{u}d$  tree diagram, with additional contributions from penguin diagrams. The amplitudes of the  $B^0$  ( $A$ ) and the  $\bar{B}^0$  ( $\bar{A}$ ) decay can be represented as a combination of the tree (T) and penguin (P) amplitudes:

$$A = e^{+i\gamma}T + e^{-i\beta}P \quad , \quad \bar{A} = e^{-i\gamma}T + e^{+i\beta}P \quad (4)$$

whose coefficients give the sensitivity to  $\alpha$ . The  $CP$  asymmetry between the  $B^0$  and the  $\bar{B}^0$  decays is given by the equation:

$$A_{CP}(t) = \frac{N(\bar{B}^0(t) \rightarrow h^+h^-) - N(B^0(t) \rightarrow h^+h^-)}{N(\bar{B}^0(t) \rightarrow h^+h^-) + N(B^0(t) \rightarrow h^+h^-)} \quad (5)$$

$$= S_{hh} \sin(\Delta m_d \Delta t) - C_{hh} \cos(\Delta m_d \Delta t) \quad (6)$$

where the measurable coefficients  $C_{hh}$  and  $S_{hh}$  are defined as:

$$C_{hh} = \frac{2\mathcal{I}m(\lambda_{hh})}{1 + |\lambda_{hh}|^2}, \quad S_{hh} = \frac{1 - |\lambda_{hh}|^2}{1 + |\lambda_{hh}|^2} \quad (7)$$

and  $\lambda_{hh}$  is given by:

$$\lambda_{hh} = \frac{q \bar{A}}{p A} = e^{2i\alpha} \frac{1 - \frac{P}{T} e^{-i\alpha}}{1 - \frac{P}{T} e^{+i\alpha}} = |\lambda| e^{2i\alpha_{\text{eff}}} \quad (8)$$

$q$  and  $p$  are the  $B$  mixing coefficients and  $h$  can be a  $\pi$  or a  $\rho$  meson.  $\alpha_{\text{eff}}$  is the experimentally measurable quantity, which is shifted from  $\alpha$  by an unknown amount due to penguin pollution.

### 3.1 $B \rightarrow \rho\rho$

Measurements of  $B \rightarrow \pi\pi$  <sup>4)</sup> and  $B \rightarrow \rho\pi$  <sup>5)</sup> have so far failed to yield a tight bound on the value of  $\alpha$ , but  $B \rightarrow \rho\rho$  provides an alternative.

On  $113 \text{ fb}^{-1}$  of data, a measurement of the longitudinal polarisation fraction,  $f_L = 1.00 \pm 0.02$ , confirmed that this decay is overwhelmingly dominated by the helicity zero state, making an angular analysis unnecessary. A fit to extract the time dependent  $CP$  parameters  $S$  and  $C$  for the longitudinal decay yields  $314 \pm 34$  signal events and:

$$C_{long} = -0.23 \pm 0.24 \pm 0.14 \quad ; \quad S_{long} = -0.19 \pm 0.33 \pm 0.11 \quad (9)$$

where the first error is statistical and the second is systematic in both cases, and  $C_{trans}$  and  $S_{trans}$  were fixed to zero in the fit.

A theoretical bound on the shift between  $\alpha$  and  $\alpha_{\text{eff}}$  is described by the Grossman-Quinn bound <sup>6)</sup>, which for  $B \rightarrow \rho\rho$  is written:

$$|\alpha - \alpha_{\text{eff}}| = \frac{\mathcal{B}(B^0 \rightarrow \rho^0 \rho^0)}{\mathcal{B}(B^0 \rightarrow \rho^+ \rho^-)} \quad (10)$$

It provides a reasonably tight theoretical constraint on the value of  $|\alpha - \alpha_{\text{eff}}|$  of  $15.9^\circ$  ( $13^\circ$ ) at 90% (68.3%) confidence level.

Measurements of  $C_{long}$  and  $S_{long}$  relate to  $\alpha$  up to a four-fold ambiguity <sup>7)</sup>, and the solution closest to the CKM best fit <sup>8)</sup> gives  $\alpha = (95 \pm 10 \pm 4)^\circ$ , where the first error is statistical and the second is systematic. There is an additional theoretical error from the Grossman-Quinn bound ( $< 13^\circ$ ) to account for the shift between  $\alpha$  and  $\alpha_{\text{eff}}$ .

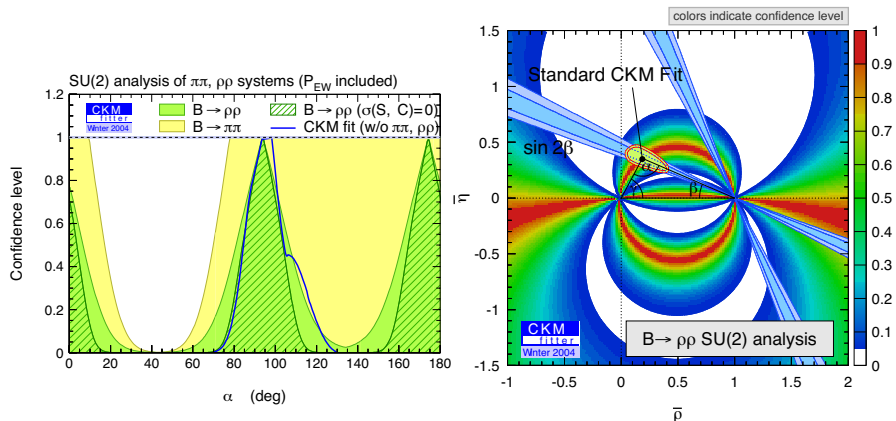


Figure 2: *The  $B \rightarrow \rho\rho$  analysis constrains the possible values of  $\alpha$ . The left-hand plot shows the  $\alpha$  plane constrained by the  $B \rightarrow \pi\pi$  and  $B \rightarrow \rho\rho$  (with and without experimental errors) analyses. These are overlaid with the global CKM fit without these two analyses included. The right-hand plot shows the constraint on the  $\rho - \eta$  plane due to the  $B \rightarrow \rho\rho$  analysis, which is shown overlaid by the Standard CKM fit<sup>9</sup>).*

An isospin analysis provides a complementary measurement of  $\alpha$ . Using  $C_{long}$  and  $S_{long}$ , together with the branching fractions and  $f_L$  measurements for  $B^+ \rightarrow \rho^+\rho^0$ ,  $B^0 \rightarrow \rho^0\rho^0$  (10) and  $B^0 \rightarrow \rho^+\rho^-$  (11) as inputs, and choosing the result nearest the CKM best fit<sup>8</sup>), gives  $\alpha = (96 \pm 10 \pm 4 \pm 13)^\circ$  which is consistent with the result from the time dependent fit and is shown in Figure 2.

#### 4 Measurements of $\gamma$

$\gamma$  measurements can be made in modes which have both  $b \rightarrow c$  and  $b \rightarrow u$  tree diagrams, which interfere. The magnitude of the interference is determined by the ratio of the two methods of decay.

##### 4.1 $B^0 \rightarrow D^{(*)+}\pi^-$

$B^0 \rightarrow D^{(*)+}\pi^-$  is sensitive to  $\sin(2\beta + \gamma + \delta)$ . The  $2\beta$  term is due to  $B^0 - \bar{B}^0$  mixing and the  $\delta$  represents the strong phase difference between the two decay

trees. The time-evolution of the decay is described by:

$$P_{B^0}(D^\mp\pi^\pm) \propto Ne^{-\Gamma|\Delta t|}(1 \pm C \cos(\Delta m_d \Delta t) + S^\mp \sin(\Delta m_d \Delta t)) \quad (11)$$

$$P_{\bar{B}^0}(D^\mp\pi^\pm) \propto Ne^{-\Gamma|\Delta t|}(1 \mp C \cos(\Delta m_d \Delta t) - S^\mp \sin(\Delta m_d \Delta t)) \quad (12)$$

and similar equations for  $D^*\pi$ , where

$$C = \frac{1-r^2}{1+r^2} \quad \text{and} \quad S^\mp = \frac{2r}{1+r^2} \sin(2\beta + \gamma \pm \delta) \quad (13)$$

and the ratio between the suppressed ( $b \rightarrow u$ ) and dominant ( $b \rightarrow c$ ) amplitudes is described as  $r = |V_{ub}^*V_{cd}/V_{cb}V_{ud}^*| \approx 0.02$ . As  $r$  is small,  $CP$  asymmetry is also expected to be small in this mode.

*BABAR* has undertaken two different analysis techniques for this mode, based on partial reconstruction and full reconstruction of the  $B$  meson.

The fully reconstructed method has the benefit of having an extremely pure sample, but has a very low efficiency. On  $82\text{fb}^{-1}$ ,  $5207 \pm 87$  events are fitted in the  $B^0 \rightarrow D^+\pi^-$  sample and  $4746 \pm 78$  events in the  $B^0 \rightarrow D^{*+}\pi^-$  sample. The results of the  $CP$  measurements were <sup>12)</sup>:

$$2r_{D^*\pi} \sin(2\beta + \gamma) \cos(\delta_{D^*\pi}) = -0.068 \pm 0.038 \pm 0.021 \quad (14)$$

$$2r_{D^*\pi} \sin(2\beta + \gamma) \sin(\delta_{D^*\pi}) = 0.031 \pm 0.070 \pm 0.035 \quad (15)$$

$$2r_{D\pi} \sin(2\beta + \gamma) \cos(\delta_{D\pi}) = -0.022 \pm 0.038 \pm 0.021 \quad (16)$$

$$2r_{D\pi} \sin(2\beta + \gamma) \sin(\delta_{D\pi}) = 0.025 \pm 0.068 \pm 0.035 \quad (17)$$

The partially reconstructed method is used only for the mode  $B^0 \rightarrow D^{*\pm}\pi^\mp$ . A useful feature of this decay is the presence of a ‘‘fast’’  $\pi$  from the  $B$  meson decay and a ‘‘slow’’  $\pi$  from the  $D^{*\pm}$  decay. These pions, together with beam constraints, allow the missing mass of the decay to be reconstructed. This mass distribution peaks at the  $D^0$  mass. This method finds  $6406 \pm 129$  events in the lepton tagged <sup>13)</sup> sample and  $25157 \pm 323$  in the kaon tagged <sup>13)</sup> sample in  $82\text{fb}^{-1}$  of data. When a time-dependent simultaneous fit is done to the kaon- and lepton-tagged events, the  $CP$  measurement is <sup>14)</sup>:

$$2r \sin(2\beta + \gamma) \cos(\delta) = -0.063 \pm 0.024 \pm 0.014 \quad (18)$$

The combined results for the two methods gives limits of:

$$|\sin(2\beta + \gamma)| > 0.58 \quad (95\% \text{ Confidence Level}) \quad (19)$$

$$|\sin(2\beta + \gamma)| > 0.87 \quad (68\% \text{ Confidence Level}) \quad (20)$$

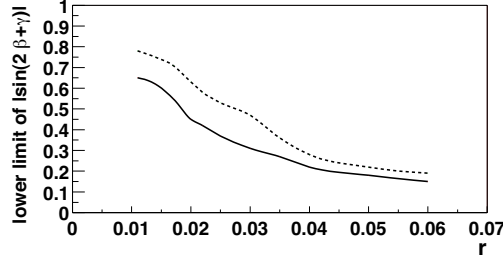


Figure 3: The comparison between the partially reconstructed limits (solid line) and the combined results of the partially and fully reconstructed fits (dashed line).

and the difference between the combined limit and the partial measurement can be seen in Figure 3.

#### 4.2 $B^\pm \rightarrow D^0 K^\pm$

One method of extracting  $\gamma$  from the mode  $B^\pm \rightarrow D^0 K^\pm$  is by studying the decay of the  $D^0$  to  $CP$  even eigenstates,  $K^+K^-$  and  $\pi^+\pi^-$ . These decays are described by  $R_{CP\pm}$  and can be compared to the flavor eigenstate decays ( $D^0 \rightarrow K^-\pi^+, K^-\pi^+\pi^0$  and  $K^-\pi^+\pi^-\pi^+$  and the charged conjugate decays) which are described by  $R$ :

$$R_{(CP\pm)} = \frac{\Sigma_{B^+,B^-} \Gamma(B \rightarrow D_{(CP\pm)}^0 K)}{\Sigma_{B^+,B^-} \Gamma(B \rightarrow D_{(CP\pm)}^0 \pi)} \quad (21)$$

$$\frac{R_{CP\pm}}{R} = 1 + r_{DK}^2 + 2r_{DK} \cos \gamma \cos \delta \quad (22)$$

where  $r_{DK}$  is the ratio of the suppressed amplitude to the dominant amplitude, which is expected to be of the order 0.1 - 0.2 for this mode. A charge asymmetry is also expected in this decay, which can be written as:

$$A_{CP\pm} = \frac{\Gamma(B^- \rightarrow D_{CP\pm}^0 K^-) - \Gamma(B^+ \rightarrow D_{CP\pm}^0 K^+)}{\Gamma(B^- \rightarrow D_{CP\pm}^0 K^-) + \Gamma(B^+ \rightarrow D_{CP\pm}^0 K^+)} \quad (23)$$

$$= \frac{\pm 2r_{DK} \sin \gamma \sin \delta}{R_{CP\pm}} \quad (24)$$

where  $\delta$  is the relative strong phase between  $B^- \rightarrow \overline{D^0}K^-$  and  $B^- \rightarrow D^0K^-$ . Measuring  $R$ ,  $R_{CP\pm}$  and  $A_{CP\pm}$  makes it possible to extract  $r_{DK}$ ,  $\delta$  and  $\gamma$ .

Using datasets of  $56\text{fb}^{-1}$  for the measurement of  $R$ , and  $82\text{fb}^{-1}$  for  $R_{CP\pm}$  and  $A_{CP\pm}$  BABAR finds <sup>15)</sup>:

$$R = (8.31 \pm 0.35 \pm 0.20)\% \quad (25)$$

$$R_{CP\pm} = (8.8 \pm 0.35 \pm 0.20)\% \quad (26)$$

$$A_{CP\pm} = 0.07 \pm 0.17 \pm 0.06 \quad (27)$$

which gives

$$R_{CP\pm}/R = 1.06 \pm 0.19 \pm 0.06. \quad (28)$$

No  $\gamma$  measurement is yet available.

## 5 $B^\mp \rightarrow [K^\mp\pi^\pm]_D K^\mp$

When combined with other modes in the Atwood, Dunietz and Soni method <sup>16)</sup>, it is possible to cleanly extract  $\gamma$  using this mode.  $CP$  violation could manifest itself as a large difference between the ratios of suppressed ( $b \rightarrow u$ ) to dominant tree ( $b \rightarrow c$ ) diagrams for  $B^+$  and  $B^- \rightarrow DK^\mp, D \rightarrow K^\mp\pi^\pm$ , where  $D$  is a  $D^0$  or a  $\overline{D^0}$ . When  $D$  mixing is ignored, the ratio can be expressed as:

$$R_{K\pi}^\pm = \frac{\Gamma([K^\mp\pi^\pm]_D K^\pm)}{\Gamma([K^\pm\pi^\mp]_D K^\mp)} = r_B^2 + r_D^2 + 2r_D r_B \cos(\pm\gamma + \delta) \quad (29)$$

$$r_B = \left| \frac{A(B^- \rightarrow \overline{D^0}K^-)}{A(B^- \rightarrow D^0K^-)} \right| \quad (30)$$

$$r_D = \left| \frac{A(D^0 \rightarrow K^+\pi^-)}{A(D^0 \rightarrow K^-\pi^+)} \right| = 0.060 \pm 0.003 \quad (31)$$

$$\delta \equiv \delta_B + \delta_D \quad (32)$$

where  $\delta$  is the strong phase difference between the  $B$  and  $D$  decay amplitudes,  $r_B$  is the ratio of the suppressed  $B$  decay to the dominant  $B$  decay (whose size determines the size of the interference), and  $r_D$  is the ratio of the suppressed  $D$  decay to the dominant  $D$  decay.

However, due to insufficient statistics at this time, the  $B^+$  and  $B^-$  samples are combined for this analysis ( $109\text{fb}^{-1}$ ), giving:

$$R_{K\pi} = \frac{\Gamma(B^- \rightarrow [K^+\pi^-]_D K^-) + \Gamma(B^+ \rightarrow [K^-\pi^+]_D K^+)}{\Gamma(B^- \rightarrow [K^-\pi^+]_D K^-) + \Gamma(B^+ \rightarrow [K^+\pi^-]_D K^+)} \quad (33)$$

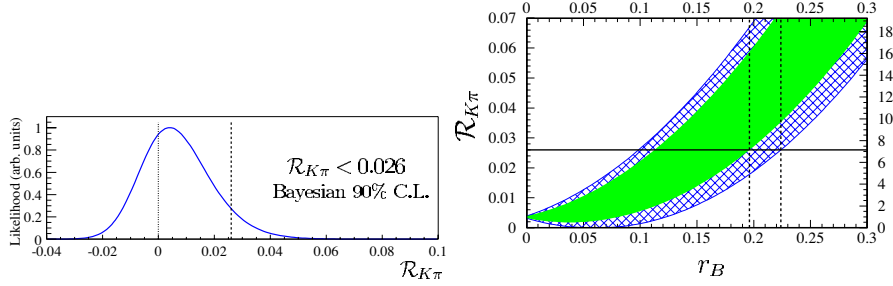


Figure 4: The left-hand plot shows the Bayesian model of the likelihood used to extract the Upper Limit for  $R_{K\pi}$  in  $B^\mp \rightarrow [K^\mp \pi^\pm]_D K^\mp$ . The right-hand plot describes the dependence of  $R_{K\pi}$  on  $r_B$  using  $0^\circ < \gamma, \delta < 180^\circ$  (hashed area) and the range of  $\gamma$  from CKM fits ( $48^\circ < \gamma < 73^\circ$ ).

$$= r_B^2 + r_D^2 + 2r_D r_B \cos \gamma \cos \delta \quad (34)$$

Using a Bayesian model to determine the Confidence Level, as shown in the left-hand plot of Figure 4, a value of  $R_{K\pi} < 0.026$  was found at 90% Confidence Level. Therefore, the  $b \rightarrow u$  contribution to the amplitude is very small, making it difficult to measure  $\gamma$  in this mode. To calculate  $r_B$ , the least restrictive limit is used, computed using maximal destructive interference (right-hand plot of Figure 4). The limit is:  $r_B < 0.22$  at a Confidence Level of 90%<sup>17</sup>.

## 6 Conclusion

The *BABAR* Experiment has conducted several analyses with the aim of extracting  $\alpha$  and  $\gamma$ . In the  $B^0 \rightarrow \rho^+ \rho^-$  system,  $\alpha = (96 \pm 10 \pm 4 \pm 13)^\circ$  has been measured using an isospin analysis. In  $B^0 \rightarrow D^{(*)+} \pi^-$ , a limit on  $\sin(2\beta + \gamma)$  from two different analysis methods was found to be  $|\sin(2\beta + \gamma)| > 0.58$  at 95% Confidence Level. Other methods of extracting both angles are under investigation, and tighter constraints on their values will be measured once larger data sets become available.

## References

1. L. Wolfenstein, Phys. Rev. Lett. **51** 1945 (1983).

2. PEP-II Conceptual Design Report, SLAC-0418 (1993).
3. B. Aubert *et al* [BABAR Collaboration], Nucl. Instr. and Methods **A479**, 117 (2002).
4. B. Aubert *et al* [BABAR Collaboration], Phys. Rev. Lett. **89** 281802 (2002),  
B. Aubert *et al* [BABAR Collaboration], Phys. Rev. Lett. **91** 021801 (2003),  
B. Aubert *et al*, BABAR Collaboration, Phys. Rev. Lett. **91** 241801 (2003).
5. B. Aubert *et al* [BABAR Collaboration], Phys. Rev. Lett. **91** 201802 (2003).
6. Y. Grossman *et al*, Phys. Rev. D **58** 017504 (1998).
7. A. Falk *et al*, Phys. Rev. D **69** 011502 (2004).
8. K. Hagiwara *et al*, Phys. Rev. D **66**, 010001 (2002).
9. Heavy Flavor Averaging Group, Results on Time-Dependent  $CP$  Measurements: Winter 2004, URL:  
<http://www.slac.stanford.edu/xorg/hfag/triangle/winter2004/index.shtml>  
(2004)
10. B. Aubert *et al* [BABAR Collaboration], Phys. Rev. Lett. **91** 171802 (2003).
11. Heavy Flavor Averaging Group, URL:  
<http://www.slac.stanford.edu/xorg/hfag/rare/index.html> (2003)
12. B. Aubert *et al* [BABAR Collaboration], "Measurement of Time-Dependent  $CP$  Asymmetry in  $B^0 \rightarrow D^{(*)\pm}\pi^\mp$  Decays and Constraints on  $\sin(2\beta+\gamma)$ ", hep-ex/0309017
13. B. Aubert *et al* [BABAR Collaboration], Phys. Rev. Lett. **89** 201802 (2002).
14. B. Aubert *et al* [BABAR Collaboration], "Measurement of Time-Dependent  $CP$  Asymmetries and Constraints on  $\sin(2\beta+\gamma)$  with Partial Reconstruction of  $B^0 \rightarrow D^{*+}\pi^-$  Decays", hep-ex/0310037.
15. B. Aubert *et al* [BABAR Collaboration], Phys. Rev. Lett. **92** 202002 (2004).
16. D. Atwood *et al*, Phys. Rev. D **63** 036005 (2001).
17. B. Aubert *et al* [BABAR Collaboration], "Search for  $B^\pm \rightarrow [K^\mp\pi^\pm]_D K^\pm$  and upper limit on the  $b \rightarrow u$  amplitude in  $B^\pm \rightarrow DK^\pm$ ", hep-ex/0402024.

Frascati Physics Series Vol. XXXV (2004), pp. 135  
HEAVY QUARKS AND LEPTONS - San Juan, Puerto Rico, June 1-5, 2004

**MEASUREMENTS OF  $\phi_3/\gamma$  WITH  $B \rightarrow D^{(*)}K$  AND  $B \rightarrow D^{(*)}\pi$  AT  
BELLE**

R. Itoh

*KEK - High Energy Accelerator Research Organization  
1-1 Oho, Tsukuba, Ibaraki 305-0801, Japan*

Written contribution not received



***SESSION III – CP Violation II – Strange and Charm Sectors***

- A. Maier      Charged Kaon Decays at NA48: Current Status and Future Plans  
A. Ledovskoy    KTeV Results on CP Violation in  $K_L \rightarrow \pi^+ \pi^- e^+ e^-$   
K. Nelson      Search for CP violation in Hyperon Decays and Measurement of  
                    Hyperon Decay Parameters  
D. Asner      CP Violation Results in Charm  
K. Flood      Review of Charm Mixing



Frascati Physics Series Vol. XXXV (2004), pp. 139  
HEAVY QUARKS AND LEPTONS - San Juan, Puerto Rico, June 1-5, 2004

**CHARGED KAON DECAYS AT NA48: CURRENT STATUS  
AND FUTURE PLANS**

A. Maier  
*CERN - Geneva, Switzerland*

Written contribution not received



**KTeV RESULTS ON CP VIOLATION IN  $K_L \rightarrow \pi^+\pi^-e^+e^-$**

A. Ledovskoy

*The Department of Physics and Institute of Nuclear and Particle Physics,  
University of Virginia, Charlottesville, VA 22901*

For KTeV Collaboration

**ABSTRACT**

The KTeV (E799-II) experiment at Fermilab analyzed the entire data set of  $K_L \rightarrow \pi^+\pi^-e^+e^-$  decays. Based on a sample of 5241 candidates with estimated background of  $185 \pm 14$  events we measured direct emission form factor parameters  $\tilde{g}_{M1} = (1.11 \pm 0.12_{stat} \pm 0.07_{syst})$  and  $a_1/a_2 = (-0.744 \pm 0.022_{stat} \pm 0.032_{syst})GeV^2$ , a “charge radius” amplitude  $|g_{CR}| = (0.163 \pm 0.017_{stat} \pm 0.023_{syst})$ , an upper limit on CP-violating E1 direct emission amplitude  $|g_{E1}|/|g_{M1}| \leq 0.04$  (90%CL), and CP-violating asymmetry in the distribution of an angle between  $\pi^+\pi^-$  and  $e^+e^-$  planes in kaon center of mass integrated over entire phase space  $A_\phi = (13.7 \pm 1.4_{stat} \pm 1.5_{syst})\%$ . Using measured  $|g_{CR}|$  value we obtained the  $K^0$  charge radius value of  $\langle R_K^2 \rangle = (-0.077 \pm 0.014)fm^2$

## 1 Introduction

Rare decay  $K_L \rightarrow \pi^+\pi^-e^+e^-$  presents an interesting opportunity for observation of CP violation. There are several contributions to this decay, both CP-violating and CP-conserving; all of them proceed through underlying  $K_L \rightarrow \pi^+\pi^-\gamma^*$  decay followed by internal conversion  $\gamma^* \rightarrow e^+e^-$ . First amplitude is an initial CP-violating decay of  $K_L$  into  $\pi^+\pi^-$  with one of the pions radiating a virtual bremsstrahlung photon. Another amplitude is an emission of a virtual photon directly from  $\pi^+\pi^-$  decay vertex. The most dominant direct emission process is associated with CP-conserving magnetic dipole transition (M1). A small contribution of CP-violating electric dipole (E1) direct emission also is possible.  $K_L \rightarrow \pi^+\pi^-e^+e^-$  decay can also proceed via initial  $K_L \rightarrow K_S\gamma^*$  transition with internal decay of  $K_S$  to  $\pi^+\pi^-$ . This CP-conserving amplitude is associated with  $K^0$  radius process.

The interference between CP-even and CP-odd amplitudes produces polarization of a virtual photon that results in asymmetry of the distribution of the angle  $\phi$  between the  $\pi^+\pi^-$  and the  $e^+e^-$  planes in the kaon center of mass. The CP-odd and T-odd variable  $\sin\phi\cos\phi$  is given by

$$\sin\phi\cos\phi = (\hat{n}_{ee} \times \hat{n}_{\pi\pi}) \cdot \hat{z}(\hat{n}_{ee} \cdot \hat{n}_{\pi\pi}) \quad (1)$$

where  $\hat{n}_{ee}$  and  $\hat{n}_{\pi\pi}$  are unit normals to  $e^+e^-$  and  $\pi^+\pi^-$  planes respectively and  $\hat{z}$  is the unit vector of  $\pi^+\pi^-$  direction in kaon center of mass. A CP-violating asymmetry in decay rate is defined as

$$A_\phi = \frac{\Gamma_{\sin\phi\cos\phi>0} - \Gamma_{\sin\phi\cos\phi<0}}{\Gamma_{tot}} \quad (2)$$

A non-zero value of  $A_\phi$  is a signature of CP-violation. The theoretical prediction for this asymmetry is about 14%<sup>1, 2)</sup>.

The KTeV E779-II experiment from FNAL reported the first observation of  $K_L \rightarrow \pi^+\pi^-e^+e^-$  decay<sup>3)</sup> and the first measurement of the CP-violating asymmetry  $A_\phi$ <sup>4)</sup> based on 1856 candidates, a fraction of the accumulated data. More recently, the NA48 experiment from CERN measured the value of  $A_\phi$  using their entire sample of 1162 candidates<sup>5)</sup>. The results from entire  $K_L \rightarrow \pi^+\pi^-e^+e^-$  data set accumulated by KTeV E799-II experiment are presented in this report.

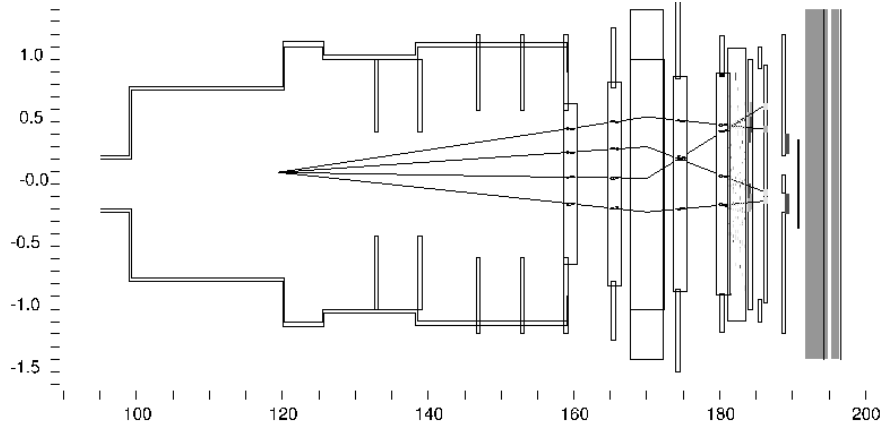
## 2 KTeV Experiment

KTeV is a fixed target experiment at Fermilab. It was designed to measure direct CP violation in neutral kaon decays (E832) and to study rare  $K_L$  decays (E799-II). It took data in 1997 and 1999. Figure 1 shows the schematics of the spectrometer. Neutral kaons were produced by  $800\text{GeV}$  protons from Tevatron in berillium oxide target at  $Z = 0m$  and entered decay region at  $Z = 90m - 160m$ . The decay volume was under vacuum and was separated from the rest of the spectrometer by a thin kevlar window positioned at  $Z = 160m$ . Decay products, in this case two pions and two electrons, entered the KTeV spectrometer that consisted of dipole magnet with horizontal  $p_t$ -kick and pair of drift chambers on both upstream and downstream sides of the magnet. An electromagnetic calorimeter was an array of 3100 pure CsI crystals. It was positioned at  $Z = 186m$  with a trigger hodoscope in front of it. Behind the calorimeter was muon detector consisted of three scintillator hodoscopes separated by muon filter walls. An array of photon veto detectors was positioned around the decay volume and the spectrometer to register particles escaping the fiducial volume of the KTeV detector. A special 4TRK on-line trigger selected events with a signature of three or more tracks in trigger hodoscope and drift chambers, with a good vertex in decay region, with a signature of two electrons in the calorimeter. The trigger also required no signals in muon detector and veto system. There were about 400 million 4TRK triggers recorded during 1997 and 1999 data taking for off-line analysis.

## 3 Analysis

During off-line analysis  $K_L \rightarrow \pi^+\pi^-e^+e^-$  candidates were selected as events with four tracks forming a vertex in the decay region. Tracks with  $E/p$  in  $0.95 - 1.05$  range were identified as  $e^\pm$  where  $E$  is energy deposited in EM calorimeter and  $p$  is momentum measured by the spectrometer. The major background was  $K_L \rightarrow \pi^+\pi^-\pi_D^0$  with  $\pi_D^0 \rightarrow e^+e^-\gamma$  where photon was not registered by the detector. It was significantly reduced by requiring variable  $P_{\pi^0}^2$  to be negative, where

$$P_{\pi^0}^2 = \frac{(M_K^2 - M_{\pi^0}^2 - M_{\pi\pi}^2)^2 - 4M_{\pi^0}^2M_{\pi\pi}^2 - 4(P_T^2)_{\pi\pi}M_K^2}{4(M_{\pi\pi}^2 + (P_T^2)_{\pi\pi})} \quad (3)$$

Figure 1: *KTeV Detector*.

Backgrounds from overlapping  $Ke3$  decays and  $\Xi^0 \rightarrow \Lambda\pi_D^0$  with  $\Lambda \rightarrow p\pi^-$  had much smaller rate and were reduced by requiring total transverse momentum of the decay products with respect to kaon line of flight to be small. Additionally, the overlapping decays were suppressed by vertex quality criteria.  $K_L \rightarrow \pi^+\pi^-\gamma$  decays with a photon conversions in the material of the detector were reduced by requiring invariant mass of  $e^+e^-$  pair to be greater than  $2MeV/c^2$ . Background from  $K_S \rightarrow \pi^+\pi^-e^+e^-$  was negligible after requiring the total energy of the decay product to be less than  $200GeV/c^2$

The distribution of  $M_{\pi\pi ee}$  for events that pass all selection criteria is shown in Figure 2. Events with opposite sign of  $\sin\phi\cos\phi$  are shown separately. There are 5241 events with  $M_{\pi\pi ee}$  in  $(0.492 - 0.504)GeV/c^2$  range with estimated background  $185 \pm 14$  events. This sample clearly exhibit CP violating asymmetry at kaon mass. The background events outside of the kaon mass window do not exhibit asymmetry. Corrections for detector acceptance are required to measure average CP-violating asymmetry over entire phase space and to compare this measurement with theoretical predictions.

Monte Carlo simulations used to study KTeV spectrometer acceptance has the following features. Neutral kaons are generated at the target and propagated along the beam line to the decay point. A kaon decays into appropriate final state inside the vacuum decay region according to chosen matrix ele-

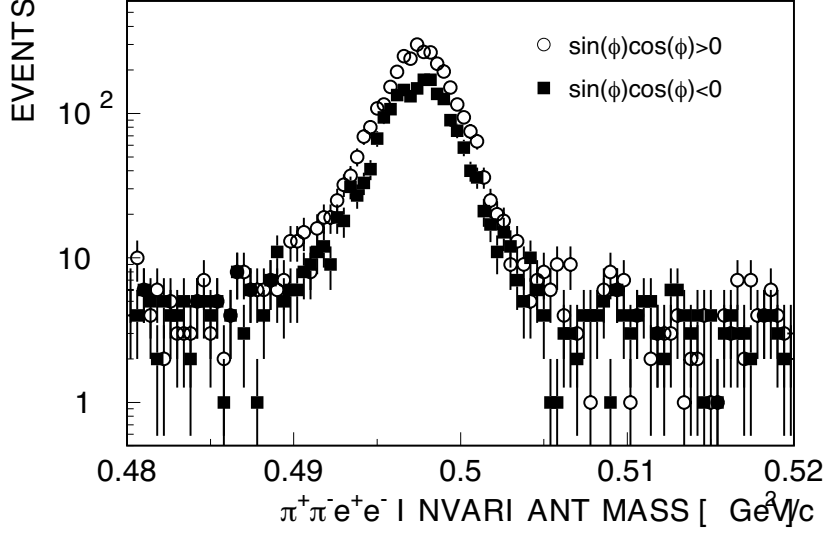


Figure 2:  $KTeV$  sample of  $K_L \rightarrow \pi^+\pi^-e^+e^-$  events.

ment. We used PHOTOS package to simulate radiative corrections. Decay products were traced through the detector using GEANT parameterization of scattering, secondary particle generation and showering. Detector response was simulated including digitization of the detector signals. To simulate accidental activity in the detector we overlayed MC event on top of the real random snapshots of the detector signals. We used a clean data sample of about 20 million  $K_L \rightarrow \pi^+\pi^-\pi_D^0$  decays to verify the accuracy of MC simulations of the detector acceptance.

The matrix element of  $K_L \rightarrow \pi^+\pi^-e^+e^-$  decay used in simulations included four amplitudes: the inner bremsstrahlung contribution, M1 and E1 direct emission amplitudes and “charge radius” amplitude with the following couplings respectively:

$$g_{BR} = |\eta_{+-}| e^{i(\delta_0(M_K) + \Phi_{+-})} \quad (4)$$

$$g_{M1} = i |g_{M1}| e^{i\delta_1(M_{\pi\pi})} \quad (5)$$

$$g_{E1} = -i \frac{|g_{E1}|}{|g_{M1}|} g_{M1} e^{i\Phi_{+-}} \quad (6)$$

$$g_{CR} = |g_{CR}|e^{i\delta_0(M_{\pi\pi})} \quad (7)$$

where  $\delta_0$  and  $\delta_1$  are phases of  $\pi\pi$  scattering in  $I = 0$  s-wave and  $I = 1$  p-wave states respectively. A form factor for direct emission coupling was introduced:

$$|g_{M1}| = \tilde{g}_{m1} \left[ 1 + \frac{a_1/a_2}{(M_\rho^2 + M_K^2) + 2M_KE_\gamma^*} \right] \quad (8)$$

where  $M_\rho = 770 \text{ MeV}/c^2$ .

Parameters  $\tilde{g}_{m1}$ ,  $a_1/a_2$ ,  $\frac{|g_{E1}|}{|g_{M1}|}$  and  $g_{CR}$  were measured by fitting our sample of 5241  $K_L \rightarrow \pi^+\pi^-e^+e^-$  candidates with a large sample of Monte Carlo events using likelihood function

$$\ln\mathcal{L}(\alpha) = \sum_{i=1}^{N_d} \ln \frac{d\Gamma(\beta_i, \alpha)}{d\beta} - N_d \ln \sum_{j=1}^{N_{mc}} \frac{d\Gamma(\beta_j, \alpha)/d\beta}{d\Gamma(\beta_j, \alpha_0)/d\beta} \quad (9)$$

where  $N_d$  and  $N_{mc}$  are the number of events in data and Monte Carlo samples respectively,  $d\Gamma(\beta, \alpha)/d\beta$  is differential decay rate at phase space location  $\beta$  which also depends on a set of parameters  $\alpha = \{\tilde{g}_{m1}, a_1/a_2, \frac{|g_{E1}|}{|g_{M1}|}, g_{CR}\}$ . The fit used Monte Carlo sample of 1.4 million events generated at  $\alpha_0 = \{1.2, -0.73, 0.0, 0.16\}$ .

Maximum of the likelihood function and its statistical uncertainty is found at  $\tilde{g}_{m1} = (1.11 \pm 0.12)$ ,  $a_1/a_2 = (-0.744 \pm 0.022) \text{ GeV}^2$ ,  $\frac{|g_{E1}|}{|g_{M1}|} \leq 0.028$ ,  $|g_{CR}| = (0.163 \pm 0.017)$ . With newly measured parameters of theoretical model for  $K_L \rightarrow \pi^+\pi^-e^+e^-$  decay we generated a Monte Carlo sample of signal events for acceptance calculations. Figure 3 shows a comparison of data and MC signal events in distribution of angle  $\phi$

The average asymmetry integrated over entire phase space is obtained by correcting the observed distribution of  $\phi$  angle with model dependent acceptance determined with Monte Carlo simulations. The asymmetry and its statistical uncertainty is  $A_\phi = (13.7 \pm 1.4)\%$

We evaluated the following sources of systematics for the fit results and asymmetry: various DATA/MC disagreements revealed during cut variations; effects of background presence; uncertainty on parameters used in our model. Additional sources of systematics to the fit results are the numerical error in likelihood function calculation due to limited statistics of Monte Carlo sample; the choice of parameter values for Monte Carlo sample used in likelihood function and implementation of radiative corrections. Table 1 summarises these

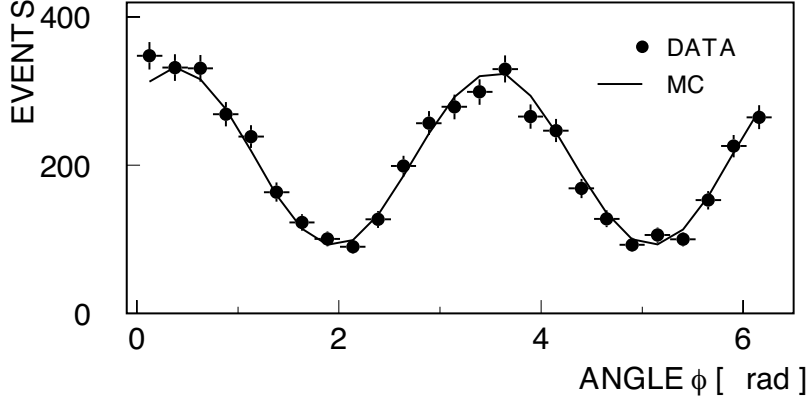


Figure 3: *Distribution of  $\phi$  angle for data and MC events.*

contributions to the systematics. The total systematic error was estimated to be 0.023 for  $|g_{CR}|$ , 0.02 for  $\frac{|g_{E1}|}{|g_{M1}|}$ , 0.032 for  $a_1/a_2$ , 0.07 for  $\tilde{g}_{m1}$ , and 1.46% for asymmetry.

#### 4 Conclusions

KTeV have analyzed its entire data sample of  $K_L \rightarrow \pi^+\pi^-e^+e^-$  decays. We have selected 5241 candidates with estimated background  $185 \pm 14$  events. It is the world's largest sample of  $K_L \rightarrow \pi^+\pi^-e^+e^-$  decays.

The measured parameters of form factor for direct emission amplitude are  $\tilde{g}_{m1} = (1.11 \pm 0.12_{stat} \pm 0.07_{syst})$  and  $a_1/a_2 = (-0.744 \pm 0.022_{stat} \pm 0.032_{syst})GeV^2$  and found to be highly correlated. These values are in good agreement with previously published results [4, 6, 5]

The first attempt to measure CP-violating E1 direct emission amplitude resulted in upper limit  $|g_{E1}|/|g_{M1}| \leq 0.04$  (90%CL)

The measured coupling for "charge radius" amplitude is  $|g_{CR}| = (0.163 \pm 0.017_{stat} \pm 0.023_{syst})$ . This parameter is proportional to  $K^0$  charge radius,  $|g_{CR}| = -\frac{1}{3}\langle R_K^2 \rangle M_K^2$  which is most sensitive to the difference of  $s$  and  $d$  quarks masses. The extracted value for  $K^0$  charge radius is  $\langle R_K^2 \rangle = (-0.077 \pm 0.014)fm^2$ . It is the most precise estimation of this parameter to date and it is in good agreement with previously published results [7, 5]

The model dependent acceptance was calculated and CP-violating asymmetry integrated over entire phase space is measured to be  $A_\phi = (13.7 \pm$

Table 1: *Systematic uncertainties of fit results and asymmetry*

Source	$ g_{CR} $	$ g_{E1} / g_{M1} $	$a_1/a_2$ [ $GeV^2$ ]	$\tilde{g}_{m1}$	$A_\phi$ [%]
Radiative Corr.	0.0	0.0	0.0	0.0	
Choice of $\alpha_0$	0.001	0.001	0.005	0.02	
MC statistics	0.001	0.001	0.002	0.001	
DATA/MC disagr.	0.021	0.018	0.022	0.041	0.71
Background	0.01	0.008	0.022	0.05	0.3
$ \eta_{+-} $ uncertainty	0.002	0.0002	0.0001	0.01	0.16
$\Phi_{+-}$ uncertainty	0.0002	0.0005	0.0003	0.002	0.11
$\delta_{0,1}$ uncertainty	0.001	0.0003	0.001	0.004	0.33
$ g_{E1} $ uncertainty					0.33
$ g_{CR} $ uncertainty					0.34
$\tilde{g}_{m1}, a_1/a_2$ errors					0.34
Total Syst. Error	0.023	0.020	0.032	0.07	1.46

$$1.4_{stat} \pm 1.5_{syst} \%$$

## 5 Acknowledgements

We thank Fermilab, the U.S. Department of Energy, the U.S. National Science Foundation, and the Ministry of Education and Science of Japan for their support.

## References

1. L.M. Sehgal and M. Wanninger, Phys. Rev. D **46**, 1035 (1992); Erratum: Phys. Rev.D **46**, 5209 (1992).
2. P. Heiliger and L.M. Sehgal, Phys. Rev. D **48**, 4146 (1993); Erratum: Phys. Rev.D **60**, 079902 (1999).
3. J. Adams *et al.*, Phys. Rev. Lett. **80**, 4123 (1998).
4. A. Alavi-Harati *et al.*, Phys. Rev. Lett. **84**, 408 (2000).
5. A. Lai *et al.*, Eur. Phys. J. C **30**, 33 (2003).
6. A. Alavi-Harati *et al.*, Phys. Rev. Lett. **86**, 761 (2001).
7. W.R. Molzon *et al.*, Phys. Rev. Lett. **41**, 1213 (1978).

Frascati Physics Series Vol. XXXV (2004), pp. 149  
HEAVY QUARKS AND LEPTONS - San Juan, Puerto Rico, June 1-5, 2004

**SEARCH FOR CP VIOLATION IN HYPERON DECAYS AND  
MEASUREMENT OF HYPERON DECAY PARAMETERS**

K. Nelson

*University of Virginia - CEBAF Newport News, Virginia, USA*

Written contribution not received



## CP VIOLATION RESULTS IN CHARM

David Asner - for the CLEO Collaboration  
*University of Pittsburgh, Department of Physics and Astronomy,  
3951 O'Hara St, Pittsburgh PA, 15260, USA*

### ABSTRACT

Searches for CP violation in the charm sector from the E791, FOCUS, CLEO, BABAR and BELLE experiments are presented. Most analyses consider CP violation in two-body or quasi-two-body decays. Preliminary results from CLEO and FOCUS using Dalitz-plot analyses are also presented.

### 1 Introduction

The violation of charge-parity (CP) in charm decay requires two amplitudes with different strong and weak phases that interfere to produce CP violating effects. There are three distinct types of CP violation. (1) CP violation from a non-vanishing relative phase between the mass and width components of the mixing matrix usually called “indirect”; (2) Direct CP violation due to the two decay amplitudes having different weak phases; (3) Interference between decays

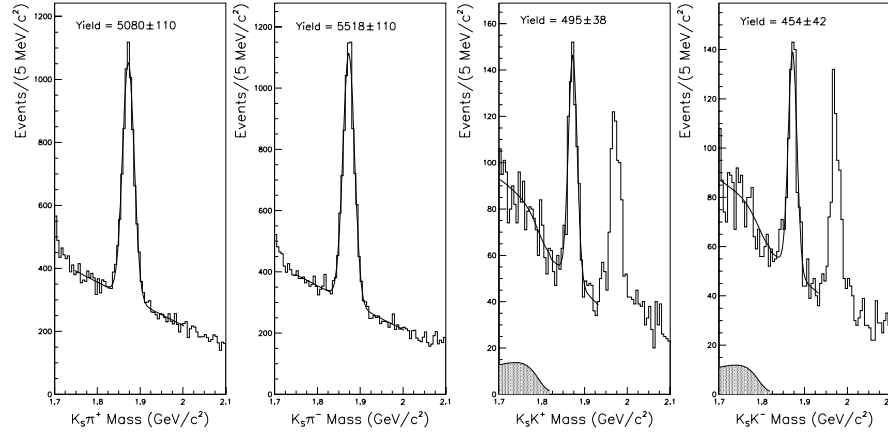


Figure 1:  $D^+ \rightarrow K_S^0 \pi^+, K_S^0 K^+$  mass plots.

with and without mixing. The CP conserving phase shift is usually generated by QCD final state interactions (FSI). In the Standard Model, the relative weak phase is typically between tree level and penguin amplitudes. Extensions to the Standard Model introduce additional amplitudes with weak phases that can contribute to CP violation. In the Standard Model, CP violation in the charm sector is small and  $D^0 - \bar{D}^0$  mixing is highly suppressed, so at current experimental sensitivities searches for CP violation in charm is for physics beyond the Standard Model. Most CP violation results are from the FNAL fixed target experiments E791 <sup>1)</sup> and FOCUS <sup>2)</sup>, and the CLEO <sup>3)</sup> experiment and search for direct CP violation. The CP violation asymmetry is defined as  $A_{CP} \equiv \frac{\Gamma(D \rightarrow f) - \Gamma(\bar{D} \rightarrow \bar{f})}{\Gamma(D \rightarrow f) + \Gamma(\bar{D} \rightarrow \bar{f})}$ . A few results from CLEO, BABAR <sup>4)</sup> and BELLE <sup>5)</sup> experiments consider CP violation in mixing.

## 2 Direct CP Violation

### 2.1 Two-body decays

FOCUS has published results <sup>6)</sup> using the two-body decay modes  $D^+ \rightarrow K_S^0 \pi^+$ , where Cabibbo favored and doubly-Cabibbo suppressed amplitudes can interfere, and  $D^+ \rightarrow K_S^0 K^+$  which is singly Cabibbo suppressed where interference

Table 1: *Branching ratios (BR) and  $A_{CP}$  of  $D^+ \rightarrow K_S^0 \pi^+, K_S^0 K^+$ .*

	FOCUS BR <sup>6)</sup>	PDG Average BR	$A_{CP}$ <sup>6)</sup>
$\frac{\Gamma(K^0 \pi^+)}{\Gamma(K^- \pi^+ \pi^+)}$	$(30.60 \pm 0.46 \pm 0.58)\%$	$(32.0 \pm 4.0)\%$	$(-1.6 \pm 1.5 \pm 0.9)\%$
$\frac{\Gamma(K^0 K^+)}{\Gamma(K^- \pi^+ \pi^+)}$	$(6.04 \pm 0.35 \pm 0.35)\%$	$(7.7 \pm 2.2)\%$	$(6.9 \pm 6.0 \pm 1.8)\%$
$\frac{\Gamma(K^0 K^+)}{\Gamma(K^0 \pi^+)}$	$(19.96 \pm 1.20 \pm 1.06)\%$	$(26.3 \pm 3.5)\%$	$(7.1 \pm 6.1 \pm 1.4)\%$

between tree and penguin may occur. The production mechanism in fixed target experiments yields different number of  $D$  and  $\bar{D}$  and so must normalize relative to another copious decay mode which is unlikely to exhibit CP violation, in this case  $D^+ \rightarrow K^- \pi^+ \pi^+$ . These decay modes will also manifest CP violation in  $K^0 - \bar{K}^0$  mixing. The results tabulated in Table 1 show no evidence for CP violation. This is consistent with Standard Model expectations  $O(\sim 10^{-3})$ .

## 2.2 Three-body decays

Direct CP violation searches in analyses of charm decays to three-body final states are more complicated than two-body decays. Three methods have been used to search for CP asymmetries. (1) Integrate over phase space and construct  $A_{CP}$  as in two-body decays; (2) Examine CP asymmetry in the quasi-two-body resonances; (3) Perform a full Dalitz-plot analysis for  $D$  and  $\bar{D}$  separately. The Dalitz-plot analysis procedure <sup>7; 8)</sup> allows increased sensitivity to CP violation by probing decay amplitudes rather than the decay rate. Both E791 <sup>9)</sup> and FOCUS have analyzed  $D^+ \rightarrow K^+ K^- \pi^+$  using method (1). E791 has also analyzed  $D^+ \rightarrow K^- K^+ \pi^+$  using method (2). These results

Table 2: *CP asymmetry in three-body decays.*

	E791 <sup>9)</sup>	FOCUS <sup>10)</sup>
$A_{CP}(K^- K^+ \pi^+)$	$(-1.4 \pm 2.9)\%$	$(0.6 \pm 1.1 \pm 0.5)\%$
$A_{CP}(\phi \pi^+)$	$(-2.8 \pm 3.6)\%$	Dalitz-plot analyses in progress
$A_{CP}(K^* K^+)$	$(-1.0 \pm 5.0)\%$	
$A_{CP}(\pi^+ \pi^- \pi^+)$	$(-1.7 \pm 4.2)\%$	

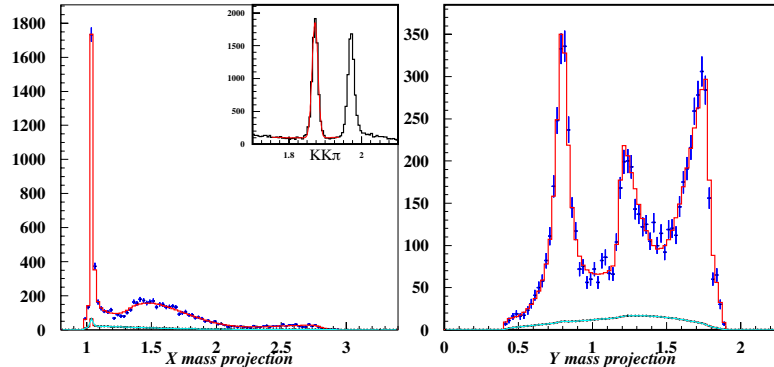


Figure 2: *FOCUS Dalitz-plot analysis of  $D^+ \rightarrow K^+K^-\pi^+$  <sup>10)</sup>*: Projection of data (points) and fit (contour) for left:  $m_{KK}^2$  and right:  $m_{K\pi}^2$ .

are shown in Table 2. FOCUS has a Dalitz-plot analysis in progress <sup>10)</sup>. The  $D^+ \rightarrow K^+K^-\pi^+$  Dalitz plot is well described by eight quasi-two-body decay channels. A signature of CP violation in charm Dalitz-plot analyses is different amplitudes and phases for  $D$  and  $\bar{D}$  samples. The amplitudes and phases for  $D^+ \rightarrow K^+K^-\pi^+$ ,  $D^- \rightarrow K^-K^+\pi^-$  and the combined sample are shown graphically in Fig. 2. No evidence for CP violation is observed.

The decay  $D^{*+} \rightarrow D^0\pi^+$  enables the discrimination between  $D^0$  and  $\bar{D}^0$ . The CLEO collaboration has searched for CP violation integrated across the Dalitz plot in  $D^0 \rightarrow K^\mp\pi^\pm\pi^0$ ,  $K_S^0\pi^+\pi^-$  and  $\pi^+\pi^-\pi^0$  decays. The integrated CP violation across the Dalitz plot is determined by

$$\mathcal{A}_{CP} = \int \frac{|\mathcal{M}_{D^0}|^2 - |\mathcal{M}_{\bar{D}^0}|^2}{|\mathcal{M}_{D^0}|^2 + |\mathcal{M}_{\bar{D}^0}|^2} dm_{ab}^2 dm_{bc}^2 / \int dm_{ab}^2 dm_{bc}^2. \quad (1)$$

The CLEO results for integrated CP asymmetry in  $D^0$  decays are reported in Table 3. No evidence of CP violation has been observed.

CLEO has considered CP violation more generally in a simultaneous fit to the  $D^0 \rightarrow K_S^0\pi^+\pi^-$  and  $\bar{D}^0 \rightarrow K_S^0\pi^+\pi^-$  Dalitz plots, shown in Fig. 4. In the isobar model <sup>7)</sup>, each resonance,  $j$ , has its own amplitude,  $a_j$ , and phase,  $\delta_j$ . A second process, not necessarily of Standard Model origin, is allowed to contribute to each  $j$ -th resonance. In general, the amplitudes to the  $j$ -th

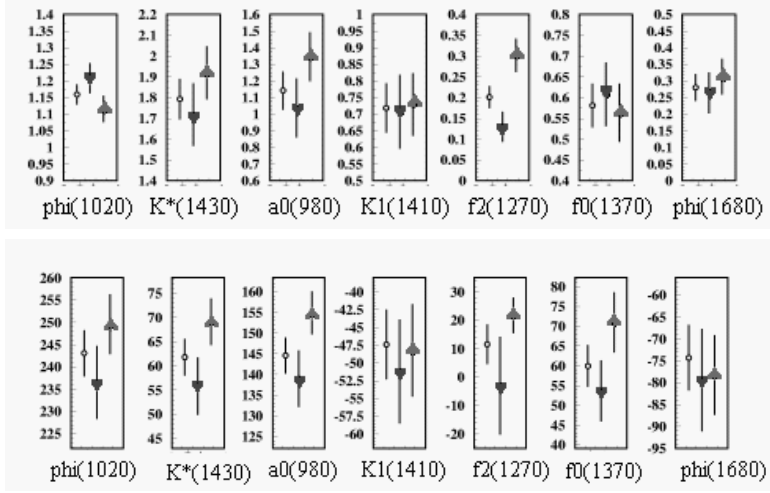


Figure 3: *FOCUS* results for  $D^+ \rightarrow K^+K^-\pi^+$  (10). Amplitudes(top) and phases(bottom) of resonant substructure for  $D^\pm$  (left),  $D^+$  (center),  $D^-$  (right).

quasi-two-body state can be expressed as

$$(a_j e^{i(\delta_j \pm \phi_j)} \pm b_j e^{i(\delta_j \pm \phi_j)}) A_j = a_j e^{i(\delta_j \pm \phi_j)} (1 \pm \frac{b_j}{a_j}) A_j, \quad (2)$$

with ‘+’ for  $D^0$  and ‘-’ for  $\bar{D}^0$  and  $A_j = A_j(m_{RS}^2, m_{\pi\pi}^2)$  is the spin-dependent Breit-Wigner amplitude for resonance  $j$  as described in Ref. (7). Thus  $a_j$  and  $\delta_j$  are explicitly CP conserving amplitude and phase,  $b_j$  is an explicit CP violating amplitude normalized by the CP conserving amplitude  $a_j$ , and  $\phi_j$  is an explicitly CP violating phase. In the absence of CP violation  $b_j$  and  $\phi_j$

Table 3: *Integrated CP asymmetry in Dalitz-plot analysis.*

	Decay Mode	$\mathcal{A}_{CP}(\%)$
CLEO (7)	$D^0 \rightarrow K^-\pi^+\pi^0$	$-3.1 \pm 8.6$
CLEO (11)	$D^0 \rightarrow K^+\pi^-\pi^0$	$9_{-25}^{+22}$
CLEO (8)	$D^0 \rightarrow K_S^0\pi^+\pi^-$	$-0.009 \pm 0.021_{-0.043-0.037}^{+0.010+0.013}$
CLEO (12)	$D^0 \rightarrow \pi^+\pi^-\pi^0$	$1_{-7}^{+9} \pm 9$

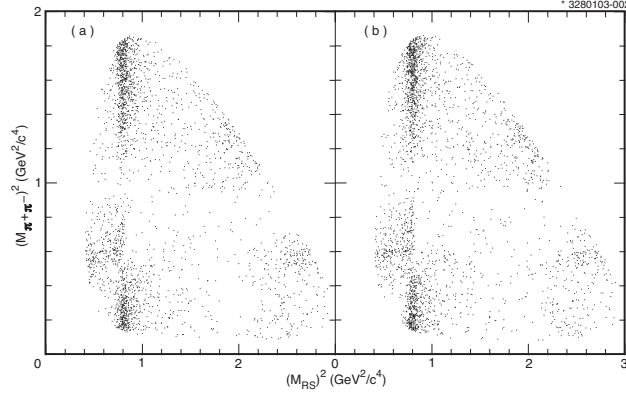


Figure 4: CLEO II.V:  $D^0 \rightarrow K_S^0 \pi^+ \pi^-$  and  $\bar{D}^0 \rightarrow K_S^0 \pi^+ \pi^-$  Dalitz plots  $\delta$ ).

Table 4: CLEO II.V: CP asymmetry in  $D^0 \rightarrow K_S^0 \pi^+ \pi^-$   $\delta$ ).

Component	Amplitude Ratio ( $b_j/a_j$ )
$K^*(892)^+ \pi^-, K^*(892)^+ \rightarrow K^0 \pi^+$	$-0.12^{+0.21}_{-0.22} \begin{matrix} +0.09 & +0.11 \\ -0.15 & -0.03 \end{matrix}$
$\bar{K}^0 \rho^0$	$0.001 \pm 0.022 \begin{matrix} +0.011 & +0.002 \\ -0.009 & -0.011 \end{matrix}$
$\bar{K}^0 \omega, \omega \rightarrow \pi^+ \pi^-$	$-0.14 \begin{matrix} +0.10 & +0.11 & +0.01 \\ -0.11 & -0.01 & -0.02 \end{matrix}$
$K^*(892)^- \pi^+, K^*(892)^- \rightarrow \bar{K}^0 \pi^-$	$-0.002 \pm 0.012 \begin{matrix} +0.008 & +0.002 \\ -0.003 & -0.002 \end{matrix}$
$\bar{K}^0 f_0(980), f_0(980) \rightarrow \pi^+ \pi^-$	$-0.04 \pm 0.06 \begin{matrix} +0.13 & +0.00 \\ -0.04 & -0.04 \end{matrix}$
$\bar{K}^0 f_2(1270), f_2(1270) \rightarrow \pi^+ \pi^-$	$0.16 \begin{matrix} +0.28 & +0.15 & +0.11 \\ -0.27 & -0.37 & -0.18 \end{matrix}$
$\bar{K}^0 f_0(1370), f_0(1370) \rightarrow \pi^+ \pi^-$	$0.08 \begin{matrix} +0.06 & +0.01 & +0.06 \\ -0.05 & -0.11 & -0.03 \end{matrix}$
$K_0^*(1430)^- \pi^+, K_0^*(1430)^- \rightarrow \bar{K}^0 \pi^-$	$-0.02 \pm 0.06 \begin{matrix} +0.04 & +0.00 \\ -0.02 & -0.01 \end{matrix}$
$K_2^*(1430)^- \pi^+, K_2^*(1430)^- \rightarrow \bar{K}^0 \pi^-$	$-0.05 \pm 0.12 \begin{matrix} +0.04 & +0.04 \\ -0.14 & -0.00 \end{matrix}$
$K^*(1680)^- \pi^+, K^*(1680)^- \rightarrow \bar{K}^0 \pi^-$	$-0.20 \begin{matrix} +0.28 & +0.05 & +0.02 \\ -0.27 & -0.22 & -0.01 \end{matrix}$

would be zero. The results of the fit to the  $D^0$  and  $\bar{D}^0 \rightarrow K_S^0 \pi^+ \pi^-$  Dalitz plots are consistent with each other and with no CP violation. The fractional CP violating amplitude and CP violating phase,  $b_j/a_j$  and  $\phi_j$  are given in Table 4 and 5.

Table 5: *CLEO II.V: CP asymmetry in  $D^0 \rightarrow K_s^0 \pi^+ \pi^-$   $\delta$* .

Component	Phase ( $\phi_i^c$ )
$K^*(892)^+ \pi^-, K^*(892)^+ \rightarrow K^0 \pi^+$	$6 \begin{smallmatrix} +21 & +13 & +18 \\ -22 & -35 & -4 \end{smallmatrix}$
$\bar{K}^0 \rho^0$	$-1 \begin{smallmatrix} +16 & +9 & +21 \\ -18 & -31 & -3 \end{smallmatrix}$
$\bar{K}^0 \omega, \omega \rightarrow \pi^+ \pi^-$	$-8 \begin{smallmatrix} +17 & +8 & +20 \\ -19 & -30 & -3 \end{smallmatrix}$
$K^*(892)^- \pi^+, K^*(892)^- \rightarrow \bar{K}^0 \pi^-$	$-3 \begin{smallmatrix} +16 & +9 & +21 \\ -18 & -30 & -3 \end{smallmatrix}$
$\bar{K}^0 f_0(980), f_0(980) \rightarrow \pi^+ \pi^-$	$9 \begin{smallmatrix} +16 & +10 & +20 \\ -17 & -29 & -3 \end{smallmatrix}$
$\bar{K}^0 f_2(1270), f_2(1270) \rightarrow \pi^+ \pi^-$	$22 \begin{smallmatrix} +19 & +12 & +20 \\ -20 & -32 & -2 \end{smallmatrix}$
$\bar{K}^0 f_0(1370), f_0(1370) \rightarrow \pi^+ \pi^-$	$8 \begin{smallmatrix} +15 & +10 & +20 \\ -17 & -28 & -4 \end{smallmatrix}$
$K_0^*(1430)^- \pi^+, K_0^*(1430)^- \rightarrow \bar{K}^0 \pi^-$	$-3 \begin{smallmatrix} +17 & +13 & +23 \\ -19 & -36 & -2 \end{smallmatrix}$
$K_2^*(1430)^- \pi^+, K_2^*(1430)^- \rightarrow \bar{K}^0 \pi^-$	$3 \begin{smallmatrix} +17 & +10 & +21 \\ -18 & -31 & -2 \end{smallmatrix}$
$K^*(1680)^- \pi^+, K^*(1680)^- \rightarrow \bar{K}^0 \pi^-$	$-3 \begin{smallmatrix} +19 & +20 & +27 \\ -20 & -25 & -2 \end{smallmatrix}$

### 2.3 Four-body decays

FOCUS has searched for T-violation using the four-body decay modes  $D^0 \rightarrow K^+ K^- \pi^+ \pi^-$  (22). A T-odd correlation can be formed with the momenta,  $C_T \equiv (\vec{p}_{K^+} \cdot (\vec{p}_{\pi^+} \times \vec{p}_{\pi^-}))$ . Under time-reversal,  $C_T \rightarrow -C_T$ , however  $C_T \neq 0$  does not establish T-violation. Since time reversal is implemented by an anti-unitary operator,  $C_T \neq 0$ , can be induced by FSI (23). This ambiguity can be resolved by measuring  $\bar{C}_T \equiv (\vec{p}_{K^+} \cdot (\vec{p}_{\pi^+} \times \vec{p}_{\pi^-}))$  in  $\bar{D}^0 \rightarrow K^+ K^- \pi^+ \pi^-$ ;  $C_T \neq \bar{C}_T$  establishes T violation. FOCUS reports a preliminary asymmetry  $A_T = 0.075 \pm 0.064$  from a sample of  $\sim 400$  decays. The mass distributions for  $D^0$  and  $\bar{D}^0$  for  $C_T$  and  $\bar{C}_T$  greater than and less than zero are shown in Fig. 5.

### 3 CP Violation in $D^0 - \bar{D}^0$ Mixing

E791, FOCUS and CLEO have all searched for CP violation in the Cabibbo suppressed decays to CP eigenstates,  $D^0 \rightarrow K^+ K^-$  and  $D^0 \rightarrow \pi^+ \pi^-$ . These measurements, tabulated in Table 6, are approaching the 1% level, where non-Standard Model physics may appear.

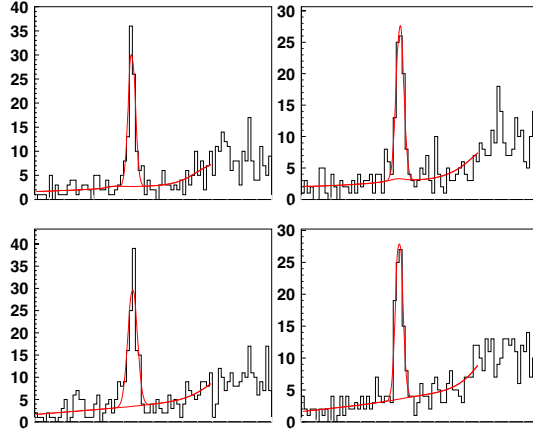


Figure 5: *Top (Bottom):*  $D^0 (\bar{D}^0)$   $m_{K^+K^-\pi^+\pi^-}$  for *Left (Right):*  $C_T < 0 (> 0)$ .

Table 6: *CP asymmetry in*  $D^0 \rightarrow K^+K^-, \pi^+\pi^-$ .

Expt	$A_{CP}(KK)$ (%)	$A_{CP}(\pi\pi)$ (%)
E791 <sup>13)</sup>	$-1.0 \pm 4.9 \pm 1.2$	$-4.9 \pm 7.8 \pm 3.0$
FOCUS <sup>14)</sup>	$-0.1 \pm 2.2 \pm 1.5$	$4.8 \pm 3.9 \pm 2.5$
CLEO <sup>16)</sup>	$0.0 \pm 2.2 \pm 0.8$	$1.9 \pm 3.2 \pm 0.8$
Expt	Mode(s)	$\Im(x)$ (%)
BELLE <sup>21)</sup>	$K^+K^-$	$-0.20 \pm 0.63 \pm 0.30$
BABAR <sup>20)</sup>	$K^+K^-, \pi^+\pi^-$	$-0.8 \pm 0.6 \pm 0.2$

Time dependent  $A_{CP}$  measurements performed by BABAR and BELLE can distinguish direct and indirect CP violation. Since mixing is small the decay time to CP eigenstates can be fit with a single exponential  $\exp[-\Gamma(1 + y \mp \Im(x))]$ . The signature of CP violation is  $D^0$  and  $\bar{D}^0$  having different decay rates,  $\Im(x) \neq 0$ , to CP eigenstates. The results are tabulated in Table 6 and are consistent with the absence of CP violation.

#### 4 Summary and Future Outlook

Searches for CP violation in charm decay at fixed target and  $e^+e^-$  facilities are summarized in Table 7 and 8, respectively, including additional results not discussed in the text.

Table 7: *Fixed target experiments: CP violation searches in charm.*

$A_{CP}$ mode	E791(%)	FOCUS(%)
$D^0 \rightarrow K^- K^+$	$-1.0 \pm 4.9 \pm 1.2$ <sup>13)</sup>	$-0.1 \pm 2.2 \pm 1.5$ <sup>14)</sup>
$D^0 \rightarrow \pi^- \pi^+$	$-4.9 \pm 7.8 \pm 3.0$ <sup>13)</sup>	$4.8 \pm 3.9 \pm 2.5$ <sup>14)</sup>
$D^+ \rightarrow K_S^0 \pi^+$		$-1.6 \pm 1.5 \pm 0.9$ <sup>6)</sup>
$D^+ \rightarrow K_S^0 K^+$		$6.9 \pm 6.0 \pm 1.8$ <sup>6)</sup>
$D^+ \rightarrow K^- K^+ \pi^+$	$-1.4 \pm 2.9$ <sup>9)</sup>	$0.6 \pm 1.1 \pm 0.5$ <sup>10)</sup>
$D^+ \rightarrow \phi \pi^+$	$-2.8 \pm 3.6$ <sup>9)</sup>	
$D^+ \rightarrow K^* K^+$	$-1.0 \pm 5.0$ <sup>9)</sup>	
$D^+ \rightarrow \pi^- \pi^+ \pi^+$	$-1.7 \pm 4.2$ <sup>9)</sup>	

Table 8:  $e^+e^-$  experiments: CP violation searches in charm.

$A_{CP}$ mode	CLEO	BABAR(%)	BELLE(%)
$D^0 \rightarrow K^+ \pi^-$	$2_{-20}^{+19}$ <sup>15)</sup>	$9.5 \pm 10.3$ <sup>19)</sup>	
$D^0 \rightarrow K^+ \pi^- \pi^0$	$9_{-22}^{+25}$ <sup>11)</sup>		
$D^0 \rightarrow K^- K^+$	$0.0 \pm 2.2 \pm 0.8$ <sup>16)</sup>	$-0.8 \pm 0.6$ <sup>20)</sup>	$0.2 \pm 0.7$ <sup>21)</sup>
$D^0 \rightarrow \pi^- \pi^+$	$1.9 \pm 3.2 \pm 0.8$ <sup>16)</sup>	$-0.8 \pm 0.6$ <sup>20)</sup>	
$D^0 \rightarrow \pi^0 \pi^0$	$0.1 \pm 4.8$ <sup>17)</sup>		
$D^0 \rightarrow K_S^0 K_S^0$	$-23 \pm 19$ <sup>17)</sup>		
$D^0 \rightarrow K_S^0 \pi^0$	$0.1 \pm 1.3$ <sup>17)</sup>		
$D^0 \rightarrow K_S^0 \pi^+ \pi^-$	$-3.9_{-4.9}^{+4.6}$ <sup>8)</sup>		
$D^0 \rightarrow K_S^0 \phi$	$2.8 \pm 9.4$ <sup>18)</sup>		
$D^0 \rightarrow K^- \pi^+ \pi^0$	$-3.1 \pm 8.6$ <sup>7)</sup>		
$D^0 \rightarrow \pi^+ \pi^- \pi^0$	$-1_{-11}^{+13}$ <sup>12)</sup>		

FOCUS and CLEO continue work on studying CP violation using Dalitz-plot analyses,  $D^+ \rightarrow K^+ K^- \pi^+, \pi^+ \pi^- \pi^+$  and  $D^0 \rightarrow K_S^0 \pi^0 \pi^0$ , respectively.

BABAR and BELLE have each accumulated twenty-five times the statistics of CLEO II.V, approaching sensitivity to CP violation in Kaon mixing, in modes like  $D \rightarrow K_S^0 \pi$ . Presently CLEO-c<sup>24)</sup> is taking data at the  $\psi(3770)$  with the goal of accumulating 18 million  $D\bar{D}$  events and attain sensitivity comparable to  $1 \text{ ab}^{-1}$  of B-factory data. In addition, CLEO-c will exploit the CP coherent  $D\bar{D}$  system to probe CP violation. Beginning in 2009 the BTeV experiment<sup>25)</sup> will start to accumulate  $\sim 1000\times$  the charm statistics of FOCUS opening up a new regime in charm CP and T violation studies.

### References

1. <http://ppd.fnal.gov/experiments/e791/detector/detector.html>
2. P. L. Frabetti *et al.* [E-687 Collaboration], Nucl. Instrum. Meth. A **320**, 519 (1992); P. Frabetti *et al.* FERMILAB-PROPOSAL-0831-1.
3. Y. Kubota *et al.* [CLEO Collaboration], Nucl. Instrum. Meth. A **320**, 66 (1992); T. S. Hill, Nucl. Instrum. Meth. A **418**, 32 (1998).
4. B. Aubert *et al.* [BABAR Collaboration], Nucl. Instrum. Meth. A **479**, 1 (2002).
5. [BELLE Collaboration], Nucl. Instrum. Meth. A **479**, 117 (2002).
6. J. M. Link *et al.* [FOCUS Collaboration], Phys. Rev. Lett. **88**, 041602 (2002) [Erratum-ibid. **88**, 159903 (2002)] [arXiv:hep-ex/0109022].
7. S. Kopp *et al.* [CLEO Collaboration], Phys. Rev. D **63**, 092001 (2001).
8. D. M. Asner *et al.* [CLEO Collaboration], arXiv:hep-ex/0311033.
9. E. M. Aitala *et al.* [E791 Collaboration], Phys. Lett. B **403**, 377 (1997).
10. S. Malvezzi, AIP Conf. Proc. **549** (2002) 569.
11. G. Brandenburg *et al.* [CLEO Collaboration], Phys. Rev. Lett. **87**, 071802 (2001).
12. V. V. Frolov *et al.* [CLEO Collaboration], arXiv:hep-ex/0306048.
13. E. M. Aitala *et al.* [E791 Collaboration], Phys. Lett. B **421**, 405 (1998).

14. J. M. Link *et al.* [FOCUS Collaboration], Phys. Lett. B **491**, 232 (2000) [Erratum-ibid. B **495**, 443 (2000)].
15. R. Godang *et al.* [CLEO Collaboration], Phys. Rev. Lett. **84**, 5038 (2000).
16. S. E. Csorna *et al.* [CLEO Collaboration], Phys. Rev. D **65**, 092001 (2002).
17. G. Bonvicini *et al.* [CLEO Collaboration], Phys. Rev. D **63**, 071101 (2001).
18. J. Bartelt *et al.* [CLEO Collaboration], Phys. Rev. D **52**, 4860 (1995).
19. B. Aubert *et al.* [BABAR Collaboration], Phys. Rev. Lett. **91**, 171801 (2003).
20. B. Aubert *et al.* [BABAR Collaboration], Phys. Rev. Lett. **91**, 121801 (2003).
21. K. Abe *et al.* [BELLE Collaboration], arXiv:hep-ex/0308034.
22. D. Pedrini, *Int. Conf on Frontier Science*, Frascati (Italy), October 2002.
23. I. I. Bigi, A. I. Sanda, *CP Violation*, Cambridge University Press, 2000.
24. R. A. Briere *et al.*, “CLEO-c and CESR-c”, CLNS-01-1742 (2001).
25. See proposal and TDR: <http://www-btev.fnal.gov/public/hep/general/prop>



## REVIEW OF CHARM MIXING

Kevin Flood  
*University of Wisconsin, Madison, WI 53706, USA*

### ABSTRACT

The current theoretical and experimental status of mixing in the neutral  $D$  meson system is reviewed.

### 1 Introduction

The study of mixing in the neutral  $K$ ,  $D$  and  $B$  meson systems allows sensitive searches to be made for possible new physics beyond the SM. In particular, because  $D^0$ - $\bar{D}^0$  mixing typically proceeds via loop diagrams involving intermediate down-type quarks, it can provide information inaccessible to analyses of  $K$  or  $B$  mixing, which are both mediated by up-type quarks with a strongly predominant contribution from the top quark. The current experimental limits on charm mixing are already at a level that can provide useful constraints on new physics models. However, since Standard Model (SM) predictions for charm mixing run over several orders of magnitude, only the observation of

a CP-violating mixing signal would indicate the presence of new physics — CP violation in charm decays is discussed by David Asner elsewhere in these Proceedings. Recent experimental results and theoretical predictions of charm mixing are discussed below.

## 2 Charm Mixing Formalism

The time evolution of the neutral  $D$  meson system <sup>1) 2)</sup> is given by the solutions to the time-dependent Schrodinger equation,

$$\frac{\partial}{\partial t} \begin{pmatrix} D^0 \\ \bar{D}^0 \end{pmatrix} = -i \left( \mathbf{M} - i \frac{\mathbf{\Gamma}}{2} \right) \begin{pmatrix} D^0 \\ \bar{D}^0 \end{pmatrix}, \quad (1)$$

where  $\mathbf{M}$  and  $\mathbf{\Gamma}$  are Hermitian matrices representing the observable masses and decay widths, and  $M_{11} = M_{22} \equiv M$  and  $\Gamma_{11} = \Gamma_{22} \equiv \Gamma$  from CPT invariance. The mass eigenstates of the neutral  $D$  system can be written,

$$|D_1\rangle = p |D^0\rangle + q |\bar{D}^0\rangle, \quad |D_2\rangle = p |D^0\rangle - q |\bar{D}^0\rangle; \quad |p|^2 + |q|^2 = 1, \quad (2)$$

where  $p$  and  $q$  are complex mixing parameters which represent the flavor eigenstate components in the mass eigenstates. Solving Eq. 1 gives the time evolution of the physical states,

$$|D_i(t)\rangle = e^{-iM_i t - \frac{1}{2}\Gamma_i t} |D_i(t=0)\rangle, \quad (3)$$

where,

$$\Gamma_{1,2} = \Gamma \pm 2\Im \left[ \left( M_{12} - i \frac{\Gamma_{12}}{2} \right) \left( M_{12}^* - i \frac{\Gamma_{12}^*}{2} \right) \right]^{\frac{1}{2}}, \quad (4)$$

$$M_{1,2} = M \mp \Re \left[ \left( M_{12} - i \frac{\Gamma_{12}}{2} \right) \left( M_{12}^* - i \frac{\Gamma_{12}^*}{2} \right) \right]^{\frac{1}{2}}. \quad (5)$$

The proper time dependence of a pure  $D^0$  or  $\bar{D}^0$  that results from a strong interaction at time  $t=0$  is thus,

$$\begin{aligned} |D^0(t)\rangle &= g_+(t) |D^0\rangle + \frac{q}{p} g_-(t) |\bar{D}^0\rangle, \\ |\bar{D}^0(t)\rangle &= \frac{p}{q} g_-(t) |D^0\rangle + g_+(t) |\bar{D}^0\rangle, \end{aligned} \quad (6)$$

where,

$$\begin{aligned} g_-(t) &= \exp\left(-t\left[iM + \frac{\Gamma}{2}\right]\right) i \sin\left(\frac{t}{2}\left[\Delta M - \frac{i\Delta\Gamma}{2}\right]\right), \\ g_+(t) &= \exp\left(-t\left[iM + \frac{\Gamma}{2}\right]\right) \cos\left(\frac{t}{2}\left[\Delta M - \frac{i\Delta\Gamma}{2}\right]\right), \\ \Delta M &\equiv M_2 - M_1, \quad \Delta\Gamma \equiv \Gamma_2 - \Gamma_1. \end{aligned} \quad (7)$$

The amplitudes for  $D^0$  or  $\bar{D}^0$  decays to a final state  $f$ , or its CP-conjugate state  $\bar{f}$ , where  $f$  ( $\bar{f}$ ) is intended to represent a mixed final state which can be reached by a process other than mixing, can be defined as

$$A \equiv \langle f | H | D^0 \rangle, \quad \bar{A} \equiv \langle \bar{f} | H | \bar{D}^0 \rangle. \quad (8)$$

The amplitudes for Cabbibo-favored (CF) decays can also be similarly defined,

$$B \equiv \langle f | H | \bar{D}^0 \rangle, \quad \bar{B} \equiv \langle \bar{f} | H | D^0 \rangle, \quad (9)$$

and the mixed amplitudes can then be expressed as

$$\langle f | H | D^0 \rangle = B \frac{q}{p} (\lambda g_+(t) + g_-(t)), \quad \langle \bar{f} | H | \bar{D}^0 \rangle = \bar{B} \frac{p}{q} (\bar{\lambda} g_+(t) + g_-(t)), \quad (10)$$

$$\lambda \equiv \frac{p A}{q B}, \quad \bar{\lambda} \equiv \frac{q \bar{A}}{p \bar{B}}. \quad (11)$$

It is experimentally known that  $\Delta M \ll \Gamma$ ,  $\Delta\Gamma \ll \Gamma$  and  $|\lambda| \ll 1$ , and so the expression for the decay rates of mixed decays can be approximated by

$$\begin{aligned} \Gamma(D^0(t) \rightarrow f) &= \frac{e^{-\Gamma t}}{4} |B|^2 \left| \frac{q}{p} \right|^2 \times \\ &\left[ 4|\lambda|^2 + \left( \Delta M^2 + \frac{\Delta\Gamma^2}{4} \right) t^2 + 2\Re(\lambda) \Delta\Gamma t + 4\Im(\lambda) \Delta M t \right], \end{aligned} \quad (12)$$

and,

$$\begin{aligned} \Gamma(\bar{D}^0(t) \rightarrow \bar{f}) &= \frac{e^{-\Gamma t}}{4} |\bar{B}|^2 \left| \frac{q}{p} \right|^2 \times \\ &\left[ 4|\bar{\lambda}|^2 + \left( \Delta M^2 + \frac{\Delta\Gamma^2}{4} \right) t^2 + 2\Re(\bar{\lambda}) \Delta\Gamma t + 4\Im(\bar{\lambda}) \Delta M t \right]. \end{aligned} \quad (13)$$

### 3 Experimental Results

Three different mixed decay time distributions can be distinguished depending on the type of neutral  $D$  final state: (a) semileptonic final states, (b) non-CP hadronic final states, and (c) CP-even/odd hadronic final states. Regardless of which final states are used, the kinematically self-tagging decay  $D^{*+} \rightarrow \pi^+ D^0 (\rightarrow X)$  (+c.c., +h.c.) is generally used to reconstruct neutral  $D$  decays in mixing analyses. The correlation of the charge sign of the  $D^{*+}$  pion daughter with the neutral  $D$  decay products provides a production flavor tag with very low mistag rates. It is common in the charm mixing literature to scale  $\Delta M$  and  $\Delta\Gamma$  into two dimensionless mixing parameters,

$$x \equiv \frac{\Delta M}{\Gamma}, \quad y \equiv \frac{\Delta\Gamma}{2\Gamma}, \quad (14)$$

and these reduced mixing parameters will be used hereinafter. Also, as noted above, CP violation in charm decays is discussed elsewhere in these Proceedings and is, with one exception, not considered further in this article.

#### 3.1 Semileptonic Final States

Because only one SM neutral  $D$  decay channel can produce semileptonic final states consistent with a mixed event, there are no amplitudes present of the type represented by Eq. 8 and the decay time distribution of mixed events going to semileptonic final states is particularly simple. Integrating over all times and normalizing to the unmixed rate, the rate of mixed events going to semileptonic final states is

$$r_{mix} = \frac{x^2 + y^2}{2}. \quad (15)$$

The use of semileptonic final states provides no sensitivity to the individual mixing parameters because Eq. 15 contains only their sum in quadrature. The only published semileptonic charm mixing analysis is from E791 and sets an upper limit of  $r_{mix} < 0.005$  (90% CL) using both semi-electronic and semi-muonic decays.<sup>3)</sup> Two other results have been shown at conference during the past two years but have not been published to date — a CLEO analysis sets an upper limit of  $r_{mix} < 0.0086$  (95% CL) using the  $K^{*+} e^- \bar{\nu}_e$  mode,<sup>4)</sup> while a FOCUS analysis using semi-muonic decays sets a much more stringent limit of  $r_{mix} < 0.0013$  (95% CL).<sup>5)</sup>

Year	Experiment	$y'$ (95% CL)	$x'/2$ (95% CL)
2003	Babar <sup>6)</sup>	$-5.6 < y' < 3.9\%$	$< 0.11\%$
2001	FOCUS <sup>7)</sup>	$-12.4 < y' < -0.5\%$	$< 0.076\%$
2000	CLEO <sup>8)</sup>	$-5.8 < y' < 1.0\%$	$< 0.041\%$

Table 1: Charm mixing results from non-CP hadronic decays.

### 3.2 Non-CP Hadronic Final States

Unlike their semileptonic counterparts, mixed neutral  $D$  decays to non-CP hadronic final states (e.g.,  $K^+\pi^-$ ) have Doubly Cabibbo Suppressed (DCS) final-state contributions of the type represented by Eq. 8. In addition, these decays also contain an unknown strong phase  $\delta$  between the DCS and CF amplitudes. Ignoring the possibility of CP violation, the mixed decay time distribution is

$$r_{mix}(t) = e^{-\Gamma t} \left( r_{DCS} + y't\sqrt{r_{DCS}} + \frac{x'^2 + y'^2}{2}t^2 \right), \quad (16)$$

$$x' \equiv x \cos \delta + y \sin \delta, \quad y' \equiv y \cos \delta - x \sin \delta. \quad (17)$$

Although hadronic analyses incorporating time-dependence are sensitive to both  $y'$  and  $x'^2$ , the presence of the strong phase represents an unknown rotation in the  $x, y$ -plane and an independent determination of the strong phase must be made to obtain the individual contributions to mixing. CLEO-C should be able to make this determination by exploiting the coherent nature of their charmed hadron production.

Several time-dependent analyses using the  $K^+\pi^-$  final state have been performed over the past few years and the resulting upper limits on the individual charm mixing components are shown in Table 1.

### 3.3 CP Eigenstate Final States

There is no distinction between the final states,  $f$  and  $\bar{f}$ , when a neutral  $D$  meson decays to a CP-even or CP-odd eigenstate, and the two amplitudes shown in Eq. 8 are identical, with  $A = \bar{A}$ . Explicitly incorporating CP violation in this instance, the time-dependence of CP-even final states, such as  $K^+K^-$  and  $\pi^+\pi^-$ , can be written,

Year	Experiment	$y$ (%)
2003	Babar <sup>9)</sup>	$0.8 \pm 0.4^{+0.5}_{-0.4}$
2003	Belle <sup>10)</sup>	$1.15 \pm 0.69 \pm 0.38$
2001	CLEO <sup>11)</sup>	$-1.1 \pm 2.5 \pm 1.4$
2001	Belle <sup>12)</sup>	$0.5 \pm 1.0^{+0.7}_{-0.8}$
2000	FOCUS <sup>13)</sup>	$3.4 \pm 1.4 \pm 0.7$
1999	E791 <sup>14)</sup>	$0.8 \pm 2.9 \pm 1.0$

Table 2: Lifetime ratio charm mixing results.

$$\Gamma(\overline{D}^0 \rightarrow K^+K^-) \approx e^{-\Gamma t} [1 - r_{mix}^{-1} (y \cos \phi + x \sin \phi) \Gamma t], \quad (19)$$

$$\phi \equiv \frac{q \langle f|H|D^0 \rangle}{p \langle f|H|\overline{D}^0 \rangle}. \quad (20)$$

In the limit of no CP violation, the ratio of non-CP (e.g.,  $K^-\pi^+$ ) to CP-even rates becomes

$$\frac{\Gamma(D^0 \rightarrow K^-\pi^+)}{\Gamma(D^0 \rightarrow K^-K^+)} = \frac{\Gamma(D^0 \rightarrow K^-\pi^+)}{\Gamma(\overline{D}^0 \rightarrow K^-K^+)} \approx 1 + y \quad (21)$$

The same relationship holds for  $\pi^+\pi^-$  and other CP-even final states. A similar relation can be derived for CP-odd final states, in which case the ratio is equal to  $1 - y$ . Several recent charm mixing results using the lifetime ratio method are shown in Table 2. The Babar and CLEO results used both  $K^+K^-$  and  $\pi^+\pi^-$  modes — all other results are for  $K^+K^-$  only.

### 3.4 Summary of Experimental Results

Figure 1 graphically summarizes the above discussion of recent experimental results in charm mixing.

## 4 Charm Mixing Predictions

Charm mixing in the SM is expected to proceed through short-distance  $\Delta C = 2$  box diagrams <sup>16)</sup> with potential enhancements from long-distance  $\Delta C = 1$  effects. Some recent papers examining the magnitude of possible SM contributions have concluded that the SM can naturally accommodate rates near

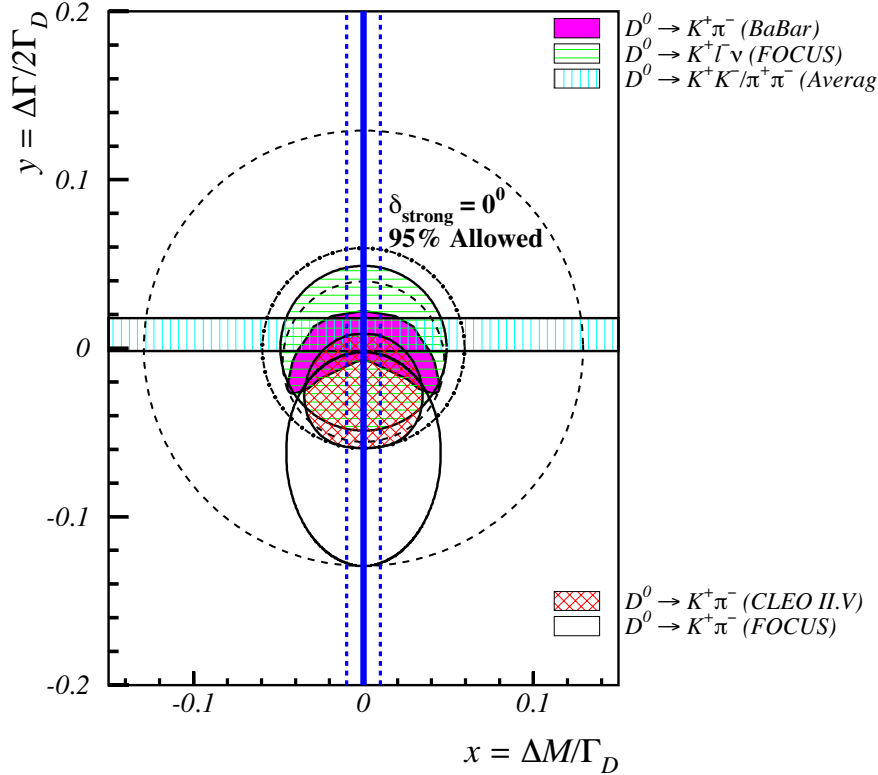


Figure 1: Current experimental limits on charm mixing shown in the  $x, y$ -plane. <sup>15)</sup> The solid vertical lines indicate a “typical” standard-model prediction for  $x$ . The dashed vertical lines indicate the upper range of non-standard-model predictions for  $x$ . The horizontal band is the world average 95% CL limit in  $y$ . The circle with horizontal shading is the 95% CL limit in  $(x, y)$ . The strong-phase shift  $\delta_{K\pi}$  between the Cabibbo-favored and doubly Cabibbo-suppressed decays is assumed to be zero in plotting the  $D^0 \rightarrow K^+\pi^-$  results, where in each case  $CP$  conservation is assumed. For the CLEO and FOCUS measurements, the statistical error is included; for the BaBar measurement, both the statistical and systematic errors are included. The strong phase shift is expected to be close to zero, but until it is actually measured, the allowed region from the  $D^0 \rightarrow K^+\pi^-$  measurements must be expanded to include the area swept out by rotating these regions about the origin. The three circles (small radius dashed, dot-dashed, and large radius dashed) are  $2\pi$  rotations of the BABAR, CLEO, and FOCUS regions, respectively. This figure and the caption text are reproduced from reference <sup>15)</sup>.

the current experimental limits. In addition, new physics contributions to the mixing rate can arise from a variety of sources — however, because of the possibly large SM contributions, the presence of new physics in charm mixing will necessarily involve searches for CP-violating effects, which are not expected at all in the SM. Various SM and new physics mixing predictions are discussed below.

#### 4.1 Standard Model Contributions

In the SM, short-distance  $\Delta C = 2$  transitions occur through box diagrams with an amplitude that can be written 16)

$$A = V_{cd}^* V_{cs}^* V_{ud} V_{us} [A(d, s) + A(s, d) - A(d, d) - A(s, s)] + (d \rightarrow b) + (s \rightarrow b) \quad (22)$$

where the  $A(i, j)$  represent amplitudes for the internal quarks  $i$  and  $j$  apart from the CKM matrix elements,  $V_{mn}$ . It can be seen that the b-quark contribution to mixing is suppressed by the small  $V_{ub}$  CKM matrix element,  $|V_{ub} V_{cb}^*|^2 / |V_{us} V_{cs}^*|^2 \sim \mathcal{O}(10^{-6})$ , and that mixing in the  $D^0\text{-}\bar{D}^0$  system therefore substantially involves only the first two quark generations. This implies that CP violation, which arises from the addition of a third quark generation to the CKM matrix, is a feature not expected in SM charm mixing.

The leading contribution to charm mixing is from the strange quark and the effective  $\Delta C = 2$  Hamiltonian governing mixing can be written 15) 16)

$$\mathcal{H}_{eff}^{\Delta C=2} = \frac{G_F^2}{4\pi^2} |V_{cd} V_{cs}^*|^2 \frac{(m_s^2 - m_d^2)}{m_c^2} \frac{(m_s^2 - m_d^2)}{m_W^2} (\mathcal{O} + 2\mathcal{O}') \quad (23)$$

where,

$$\begin{aligned} \mathcal{O} &\equiv \bar{u} \gamma_\mu (1 - \gamma_5) c \bar{u} \gamma^\mu (1 - \gamma_5) c \\ \mathcal{O}' &\equiv \bar{u} (1 + \gamma_5) c \bar{u} (1 + \gamma_5) c \end{aligned}$$

and the matrix elements due to these operators can be parameterized as

$$\langle D^0 | \mathcal{O} | \bar{D}^0 \rangle = \frac{8}{3} m_D^2 f_D^2 B_D \quad \langle D^0 | \mathcal{O}' | \bar{D}^0 \rangle = -\frac{5}{3} \left( \frac{m_D}{m_c} \right) m_D^2 f_D^2 B'_D \quad (24)$$

It is clear from Equation 23 that mixing disappears in the limit that flavor is a good symmetry and that, in any event, there are substantial heavy quark and GIM suppressions in the mixing rate.

Taking typical values for  $f_D$  and  $m_s$ ,<sup>2)</sup> and noting that  $B_D = B'_D \sim 1$  in the vacuum-insertion approximation, the box diagrams' contribution to  $\Delta M$  is  $x_{box} \sim \mathcal{O}(10^{-5} - 10^{-6})$ . There are additional contributions from  $y$ <sup>15)</sup> and dipenguin diagrams<sup>17)</sup> roughly at or slightly below this rate, and the total mixing rate due to SM diagrams is quite small,  $r_{mix} \sim 10^{-10}$ .

As shown above, charm mixing manifestly involves the breaking of flavor symmetry and can be shown to occur only as a second-order effect<sup>18)</sup>

$$x, y \sim \sin^2 \theta_C \times [SU(3) \text{ breaking}]^2 \quad (25)$$

There are a number of possible sources for this  $SU(3)$  violation and two general methods are used to estimate possible contributions: heavy quark effective theory<sup>19)</sup> and approaches involving summations over families of two-, three- and higher multi-body decays. Long-distance contributions to charm mixing cannot be precisely characterized in the SM at present as these types of transitions involve inherently non-perturbative calculations. Two recent papers by Falk *et al.* use HQET to estimate the level of  $SU(3)$ -breaking involving phase-space effects only and find natural possible enhancements of both  $x$ <sup>20)</sup> and  $y$ <sup>18)</sup> to  $\sim 1\%$ , near the current experimental limits.

A large number of theoretical predictions of  $x$  and  $y$ , ranging over several orders of magnitude and based on a variety of SM mechanisms, have recently been compiled by Petrov<sup>21)</sup> and are shown in Figure 2 — the current experimental limits are beginning to exclude the upper region of this figure.

#### 4.2 New Physics Predictions

There have been numerous charm mixing predictions based on a variety of models made over the last two decades and Figure 3 shows some of the predictions for  $x$ .<sup>21)</sup> As with Figure 2, the current experimental limits are beginning to exclude the upper region of Figure 3. Predictions using new physics models generally proceed by calculating the possible contributions of new particles running through the box diagram loop or by positing new tree-level  $\Delta C = 2$  decays (such as might be mediated by a neutral Higgs). If massive particles, such as Higgs candidates, fourth generation down-type quarks, leptoquarks or supersymmetric partners, are allowed in the box diagram loop, then the rate reductions due to light flavor symmetry, GIM mechanism and small CKM matrix elements are no longer pertinent, and enhancements to the charm mixing

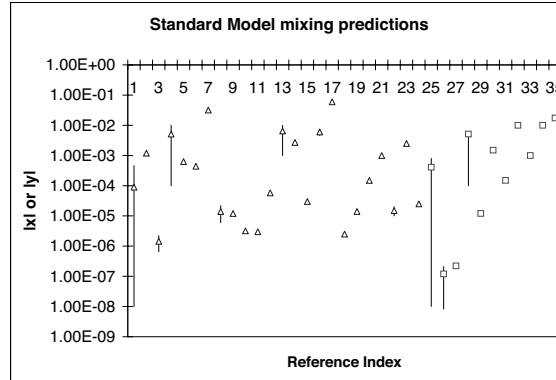


Figure 2: SM predictions for  $|x|$  (triangles) and  $|y|$  (squares) — the horizontal axis is roughly ordered in chronological order from left (earliest) to right (most recent) for each of the  $|x|$  and  $|y|$  figure regions. This plot is taken from reference <sup>21)</sup> — the reference index numbers along the horizontal axis refer to the table in this source in which citations for particular SM predictions are listed.

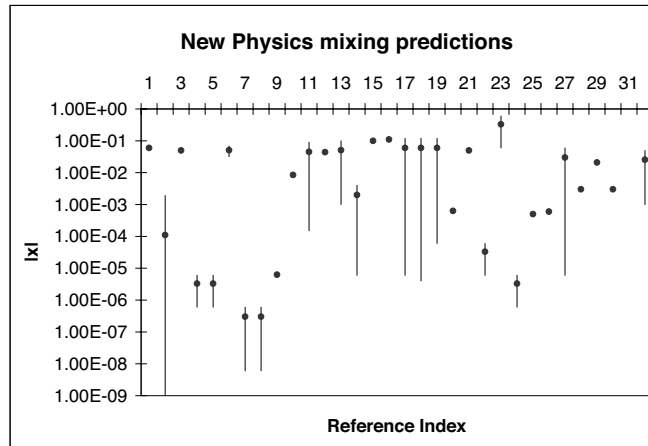


Figure 3: New physics predictions for  $|x|$  — the horizontal axis is roughly ordered in chronological order from left (earliest) to right (most recent). This plot is taken from reference <sup>21)</sup> — the reference index numbers along the horizontal axis refer to the table in this source in which citations for particular new physics predictions are listed.

rate may occur.

As in the SM, the range of predictions for new physics charm mixing runs over several orders of magnitude and, therefore, it will be difficult for an observation of charm mixing alone to signal the presence of new physics. However, continuing to reduce the upper limit will provide a useful constraint for new theoretical models and, perhaps, eliminate some already existing new physics scenarios.

### References

1. G. Blaylock, A. Seiden and Y. Nir, Phys. Lett. B **355**, 555 (1995) [arXiv:hep-ph/9504306].
2. S. Eidelman *et al.* [Particle Data Group Collaboration], Phys. Lett. B **592**, 1 (2004).
3. E. M. Aitala *et al.* [E791 Collaboration], Phys. Rev. Lett. **77**, 2384 (1996) [arXiv:hep-ex/9606016].
4. S. McGee, UMI-30-71810.
5. M. G. Hosack, UMI-30-71944.
6. B. Aubert *et al.* [BABAR Collaboration], Phys. Rev. Lett. **91**, 171801 (2003) [arXiv:hep-ex/0304007].
7. J. M. Link *et al.* [FOCUS Collaboration], Phys. Rev. Lett. **86**, 2955 (2001) [arXiv:hep-ex/0012048].
8. R. Godang *et al.* [CLEO Collaboration], Phys. Rev. Lett. **84**, 5038 (2000) [arXiv:hep-ex/0001060].
9. B. Aubert *et al.* [BABAR Collaboration], Phys. Rev. Lett. **91**, 121801 (2003) [arXiv:hep-ex/0306003].
10. K. Abe *et al.* [BELLE Collaboration], arXiv:hep-ex/0308034.
11. S. E. Csorna *et al.* [CLEO Collaboration], Phys. Rev. D **65**, 092001 (2002) [arXiv:hep-ex/0111024].

12. K. Abe *et al.* [Belle Collaboration], Phys. Rev. Lett. **88**, 162001 (2002) [arXiv:hep-ex/0111026].
13. J. M. Link *et al.* [FOCUS Collaboration], Phys. Lett. B **485**, 62 (2000) [arXiv:hep-ex/0004034].
14. E. M. Aitala *et al.* [E791 Collaboration], Phys. Rev. Lett. **83**, 32 (1999) [arXiv:hep-ex/9903012].
15. G. Burdman and I. Shipsey, Ann. Rev. Nucl. Part. Sci. **53**, 431 (2003) [arXiv:hep-ph/0310076].
16. A. Datta and D. Kumbhakar, Z. Phys. C **27**, 515 (1985).
17. A. A. Petrov, Phys. Rev. D **56**, 1685 (1997) [arXiv:hep-ph/9703335].
18. A. F. Falk, Y. Grossman, Z. Ligeti and A. A. Petrov, Phys. Rev. D **65**, 054034 (2002) [arXiv:hep-ph/0110317].
19. H. Georgi, Phys. Lett. B **297**, 353 (1992) [arXiv:hep-ph/9209291].
20. A. F. Falk, Y. Grossman, Z. Ligeti, Y. Nir and A. A. Petrov, Phys. Rev. D **69**, 114021 (2004) [arXiv:hep-ph/0402204].
21. A. A. Petrov, arXiv:hep-ph/0311371.

***SESSION IV – Searches for Pentaquarks***

H. J. Lipkin    The Theory of Pentaquarks  
L. Stanco      Pentaquark Searches at HERA  
D. J. Tedeschi   Pentaquark Searches with Intermediate Energy Probes



## THE THEORY OF PENTAQUARKS

Harry J. Lipkin

*Department of Particle Physics, Weizmann Institute of Science,  
Rehovot, Israel*

and

*School of Physics and Astronomy  
Raymond and Beverly Sackler Faculty of Exact Sciences  
Tel Aviv University, Tel Aviv, Israel*

and

*High Energy Physics Division, Argonne National Laboratory  
Argonne, IL 60439-4815, USA*

### ABSTRACT

Is there a theory or good experimental evidence? Bj's question: Pentaquark is created by  $e^+e^-$ .  $2q + q \rightarrow$  Baryon ;  $2q + \bar{q} \rightarrow$  Triquark;  $2q + \text{Triquark} \rightarrow$  Pentaquark Does it live long enough to be observable? Basic physics of constituent quarks and flavor antisymmetry. Report of  $\Theta^+$  violating flavor antisymmetry indicates need for two-cluster model.. Ball in Experimental Court - Some experiments see  $\Theta^+$ ; others don't. Possible production mechanisms present in some experiments, absent in others; e.g. via  $N^*(2.3 \text{ GeV}) \rightarrow \Theta^+ + \bar{K}$ ?

## 1 QCD Guide to the search for exotics

### 1.1 Words of Guidance from Eugene Wigner's Wisdom

With a few free parameters I can fit an elephant.

With a few more I can make him wiggle his trunk

Wigner's response to questions about a particular theory he did not like was:

"I think this theory is wrong. But the old Bohr - Sommerfeld quantum theory was also wrong.. Could we have reached the right theory without it?"

### 1.2 BJ's question in 1986

In  $e^+e^-$  annihilation a created  $q\bar{q}$  fragments into hadrons.  $q + \bar{q} \rightarrow$  meson;  $2q + q \rightarrow$  baryon. But  $2q + \bar{q} \rightarrow$  Triquark and  $2q + \text{Triquark} \rightarrow$  Pentaquark..

BJ asked whether quark model says such state is bound or lives long enough to be observable as hadron resonance. Listening to BJ usually pays off.

### 1.3 Crucial role of color-magnetic interaction

1. QCD motivated models <sup>1)</sup> show same color-electric interaction for large multiquark states and separated hadrons and no binding. Only short-range color-magnetic interaction produces binding.
2. Jaffe <sup>2)</sup> extended DGG model <sup>1)</sup> with one-gluon-exchange color factor to multiquark sector in a single cluster or bag model, defined  $(\bar{q}q)_8$  and  $(qq)_6$  interactions and explained why lowlying exotics not observed
3. Hyperfine interaction suggested search for  $H$  dibaryon <sup>2)</sup>  $uuddss$  and anticharmed strange pentaquark <sup>3)</sup>  $(\bar{c}uuds)$  (1987)

### 1.4 Flavor antisymmetry principle - removes leading exotics

The Pauli principle requires flavor-symmetric quark pairs to be antisymmetric in color and spin at short distances. Thus the short-range color-magnetic interaction is always repulsive between flavor-symmetric pairs. Best candidates for multiquark binding have minimum number of same-flavor pairs

1. Nucleon has only one same-flavor pair;  $\Delta^{++}(uuu)$  has three.
2. Extra two same-flavor pairs costs 300 Mev .
3. Deuteron separates six same-flavor pairs into two nucleons  
Only two same-flavor pairs feel short range repulsion.
4.  $H(uuddss)$  has three same-flavor pairs. Optimum for light quark dibaryon

5. The  $(uuds\bar{c})$  pentaquark has only one same-flavor pair
6.  $\Theta^+$  ( $uudd\bar{s}$ ) has two same-flavor pairs, more than  $(uuds\bar{c})$ .

Quark model calculations told experimenters "Look for  $\bar{c}(uuds)$  not  $\Theta^+$ .

Ashery's E791 search for  $\bar{c}uuds$  found events <sup>4)</sup>; not convincing enough.

Better searches for this pentaquark are needed; e.g. searches with good vertex detectors and good particle ID <sup>3)</sup>...

Any proton emitted from secondary vertex is interesting. One gold-plated event not a known baryon is enough; No statistical analysis needed.

## 2 The 1966 basic physics of hadron spectroscopy - Sakharov-Zeldovich, Nambu and beyond

### 2.1 Sakharov-Zeldovich (1966)

Sakharov and Zeldovich noted that the  $\Lambda$  and  $\Sigma$  are made of same quarks and asked why their masses are different. Their answer was that a unified two-body hyperfine interaction not only answers this question but led to a unified mass formula for both meson and baryon ground states mesons and baryon masses and showed that all are made of same quarks <sup>5)</sup>

$$M = \sum_i m_i + \sum_{i>j} \frac{\vec{\sigma}_i \cdot \vec{\sigma}_j}{m_i \cdot m_j} \cdot v_{ij}^{hyp} \quad (1)$$

Using (1) Sakharov and Zeldovich noted that both the mass difference  $m_s - m_u$  between strange and nonstrange quarks and the flavor dependence of their hyperfine splittings (later related <sup>1)</sup> to the mass ratio  $m_s/m_u$ ) have the same values when calculated from baryon masses and meson masses <sup>5)</sup>, along with the comment that the masses are of course effective masses <sup>6)</sup>:

$$\begin{aligned} \langle m_s - m_u \rangle_{Bar} &= M_\Lambda - M_N = 177 \text{ MeV} \\ \langle m_s - m_u \rangle_{mes} &= \frac{3(M_{K^*} - M_\rho) + M_K - M_\pi}{4} = 180 \text{ MeV} \end{aligned} \quad (2)$$

$$\begin{aligned} \langle m_s - m_u \rangle_{Bar} &= \frac{M_N + M_\Delta}{6} \cdot \left( \frac{M_\Delta - M_N}{M_{\Sigma^*} - M_\Sigma} - 1 \right) = 190 \text{ MeV} \\ \langle m_s - m_u \rangle_{mes} &= \frac{3M_\rho + M_\pi}{8} \cdot \left( \frac{M_\rho - M_\pi}{M_{K^*} - M_K} - 1 \right) = 178 \text{ MeV}, \end{aligned} \quad (3)$$

The same value  $\pm 3\%$  for  $m_s - m_u$  is obtained from four independent calculations. The same approach for  $m_b - m_c$  gives

$$\begin{aligned}\langle m_b - m_c \rangle_{Bar} &= M(\Lambda_b) - M(\Lambda_c) = 3341 \text{ MeV} \\ \langle m_b - m_c \rangle_{mes} &= \frac{3(M_{B^*} - M_{D^*}) + M_B - M_D}{4} = 3339 \text{ MeV}\end{aligned}\quad (4)$$

The same value  $\pm 2.5\%$  for the ratio  $\frac{m_s}{m_u}$  is obtained from meson and baryon masses.

$$\left(\frac{m_s}{m_u}\right) = \frac{M_\Delta - M_N}{M_{\Sigma^*} - M_\Sigma} = 1.53 = \frac{M_\rho - M_\pi}{M_{K^*} - M_K} = 1.61 \quad (5)$$

DeRujula, Georgi and Glashow <sup>1)</sup> in 1975 used QCD arguments to relate hyperfine splittings to quark masses and baryon magnetic moments. This led to remarkable agreement with experiment including three magnetic moment predictions with no free parameters

$$\begin{aligned}\mu_\Lambda &= -0.61 \text{ n.m.} = -\frac{\mu_p}{3} \cdot \frac{m_u}{m_s} = -\frac{\mu_p}{3} \frac{M_{\Sigma^*} - M_\Sigma}{M_\Delta - M_N} = -0.61 \text{ n.m.} \\ \mu_p + \mu_n &= 0.88 \text{ n.m.} = \frac{M_p}{3m_u} = \frac{2M_p}{M_N + M_\Delta} = 0.865 \text{ n.m.} \\ -1.46 &= \frac{\mu_p}{\mu_n} = -\frac{3}{2},\end{aligned}\quad (6)$$

## 2.2 Two Hadron Spectrum puzzles -Why $qqq$ and $q\bar{q}$ ?

1. The Meson-Baryon Puzzle - The  $qq$  and  $\bar{q}q$  forces must be peculiarly related to bind both mesons and baryons. It cannot be a vector interaction giving equal and opposite forces, nor a scalar or tensor giving equal attractions for both.
2. Exotics Puzzle - No low-lying hadrons with exotic quantum numbers have been observed; e.g. no  $\pi^+\pi^+$  or  $K^+N$  bound states.

Nambu solved both puzzles <sup>7)</sup> in 1966 by introducing the color degree of freedom and a two-body interaction from a non-abelian gauge theory with the color-factor of one-gluon exchange. This both related mesons and baryons and eliminated exotics.

A unified treatment of  $qq$  and  $\bar{q}q$  interactions binds both mesons and baryons with the same forces. Only  $qqq$  and  $q\bar{q}$  are stable in any single-cluster model with color space factorization. Any color singlet cluster that can break up into two color singlet clusters loses no color electric energy and gains kinetic energy. The Nambu color factor does not imply dynamics of one-gluon exchange. Higher order diagrams can have same color factor

Looking beyond bag or single-cluster models for possible molecular bound states Lipkin(1972) showed that the color-electric potential energy could be lowered in potential models by introducing color-space correlations; e.g,  $q\bar{q}q\bar{q}$  at corners of a square, but not enough to compensate for the kinetic energy <sup>8)</sup>

### 2.3 Important systematics in the experimental spectrum

A large spin-dependent interaction  $\approx 300$  MeV but a very weak interaction  $\approx 2$  MeV binding normal hadrons.

$$M(\Delta) - M(N) \approx 300MeV \gg M(n) + M(p) - M(d) \approx 2MeV \quad (7)$$

### 2.4 Conclusions from basics

The low-lying hadron spectrum is described by a linear effective mass term and a hyperfine interaction with a one-gluon exchange color factor.

The  $(\bar{q}q)$  and  $(qqq)$  states behave like neutral atoms with a strong color electric field inside hadrons and none outside. No molecular bound states arise in the simplest cases. A strong spin-dependent interaction is crucial to understanding the spectrum

Only color singlet and  $3^*$  color factors arise in  $(\bar{q}q)$  and  $(qqq)$ . The low-lying hadron spectrum provides no direct experimental information on  $(\bar{q}q)_8$  and  $(qq)_6$  interactions needed for multi-quark exotic configurations.

### 2.5 What can QED teach us about QCD?

QCD is a Great Theory, but nobody knows how to connect it with experiment or which approximations are good. We need to construct instructive simplified models. I often recall the response by Yoshio Yamaguchi at a seminar at the Weizmann Institute in 1960 when asked if there had been any thought at CERN about a possible breakdown of QED at small distances: “No. . . Many calculations. No thought.”

What can we learn from QED; a Great Theory that everyone knows how to connect with experiment? We know how isolated free electrons behave and carry currents. But nobody could explain the fractional Hall effect until Robert Laughlin told us the Hall Current is not carried by single electrons! It is carried by quasiparticles related to electrons by a complicated transformation.

Nobody has ever seen an isolated free quark. Current quark fields appear in the Standard Model Lagrangian. But experiments tell us that baryons are  $qqq$  and mesons are  $q\bar{q}$  and these are not the quarks that appear in the QCD Lagrangian.

Nobody knows what these quarks are. Are they complicated quasiparticles related to current quarks by a complicated transformation?. Is Hadron Spectroscopy Waiting for Laughlin? Does QCD need another Laughlin to tell us what constituent quarks are?

### 3 The $\Theta^+$ was reported! A Two-cluster Model?

#### 3.1 Following Wigner's Guidance to Understand QCD and the Pentaquark

One good wrong model that stays away from free parameters and may teach us something: a two-cluster  $P$ -wave ( $ud$ ) diquark-( $ud\bar{s}$ ) triquark model <sup>9, 10</sup>) for the  $\Theta^+$  that separates  $uu$  and  $dd$  pairs and eliminates their short range repulsive interaction... Its hidden-strangeness  $N^*$  partner keeps the same triquark with the ( $us$ ) and ( $ds$ )  $SU(3)$  partners of the ( $ud$ ) diquark. Its mass is roughly <sup>11</sup>)

$$M[N^*(1775)] \approx M(\Theta^+) + M(\Lambda) - M(N) + \frac{3}{4} \cdot [M(\Sigma) - M(\Lambda)] \approx 1775 \text{ MeV} \quad (8)$$

#### 3.2 The skyrmion model

Experimental search motivated by another wrong model. Skyrmion model has no simple connection with quarks except by another wrong model. The  $1/N_c$  expansion invented <sup>12</sup>) pre-QCD to explain absence of free quarks.

The binding Energy of  $q\bar{q}$  pairs into mesons  $E_M \approx g^2 N_c$ .

At large  $N_c$  the cross section for meson-meson scattering breaking up a meson into its constituent quarks is

$$\sigma[MM \rightarrow M + q + \bar{q}] \approx g^2 \frac{E_M}{N_c} \approx 0 \quad (9)$$

But  $\frac{1}{N_c} = \frac{1}{3}$ ;  $\frac{\pi}{N_c} \approx 1$  This is NOT A SMALL PARAMETER!

#### 4 Experimental contradictions about the $\Theta^+$

Some experiments (13, 14, 15, 16) see the  $\Theta^+$ ; others (17, 18) definitely do not. Further analysis is needed to check presence of specific production mechanisms in experiments that see it and their absence in those that do not (19). No theoretical model addresses this question. Comprehensive review (20) analyzes different models..

##### 4.1 Production via decay of a cryptoexotic $N^*(2400)$

The reported (14, 21, 22, 23)  $N^*(2400)$  can be the  $D$ -wave excitation of the  $N^*(1775)$ .with a  $(ds)$  diquark in a  $D$ -wave with the same  $ud\bar{s}$  triquark. Its dominant decays would be  $N^*(2400) \rightarrow K^-\Theta^+$  via the diquark transition  $ds \rightarrow ud + K^-$ .and  $N^*(2400) \rightarrow \pi^- N^*(1775)^+ \rightarrow \pi^- \Lambda K^+$  via  $ds \rightarrow us + \pi^-$ .

Decays like  $\Lambda K$  and  $\Sigma K$  would be suppressed by the centrifugal barrier forbidding a quark in the triquark from joining the diquark.

Some experimental checks of this mechanism are:

1. Experiments which see the  $\Theta^+$  and have sufficient energy for producing the  $N^*(2400)$  should look for an accompanying  $K^-$  or  $K_s$  and examine the mass spectrum of the  $K^-\Theta^+$  and  $K_s\Theta^+$  systems.
2. Experiments should look for  $N^*(2400) \rightarrow \pi^- N^*(1775)^+ \rightarrow \pi^- \Lambda K^+$  .
3. Experiments searching for the  $\Theta^+$  should check possible production of a  $K^-\Theta^+$  or  $K_s\Theta^+$  resonance in the 2.4 GeV region.  $B$ -decay modes suggested for pentaquark searches (24, 25) would not produce this 2.4 GeV  $N^*$ . Similar considerations should be applied to searches in  $e^+e^-$  and  $\gamma\gamma$  like those proposed in Ref. (26).
4. The other  $N^*(2400)$  decay modes.; e.g.  $K\Lambda$ ,  $K\Sigma$ ,  $K\Sigma^*$ ,  $\phi N$ , are suppressed by the centrifugal barrier in the D-wave diquark-triquark mode but may be appreciable.. Finding them would give further evidence for this model for pentaquark production. The relative branching ratios would also provide information about the structure of th  $N^*(2400)$ .

#### 4.2 Angular distribution tests for production mechanisms

1. The angular distribution of the kaon emitted with the  $\Theta^+$  in  $\gamma p \rightarrow \bar{K}^0 \Theta^+$  (27) carries interesting information. Production from a cryptoexotic  $N^*$ , gives no forward-backward kaon asymmetry. Meson exchange gives forward peaking. Baryon exchange gives backward peaking, produces the  $\Theta^+$  equally by photons on protons and neutrons. and the same baryon exchange should be seen (28) in  $\gamma n \rightarrow K^- \Theta^+$ ..
2. The more complicated angular distributions in  $\gamma p \rightarrow \pi^+ K^- K^+ n$  (14) may still carry interesting information.

All the above discussion for  $\gamma p \rightarrow \bar{K}^0 \Theta^+$  applies to the angular distribution of a  $\bar{K}^*$ . in  $\gamma p \rightarrow \bar{K}^{*0} \Theta^+ \rightarrow \pi^+ K^- \Theta^+$ . Models (28) with a suppressed  $NK\Theta^+$  coupling relative to  $NK^*\Theta^+$  predict stronger  $\Theta^+$  production with a backward  $K^*$  than with a backward kaon.. In  $\gamma p \rightarrow \pi^+ N^* \rightarrow \pi^+ \Theta^+ K^-$  (14), the pion goes forward and everything else is in the target fragmentation region. (21) ..

#### 4.3 Other experimental considerations

1. Search for exotic positive-strangeness baryon exchange in normal nonexotic reactions. The baryon exchange diagram (27) for  $\Theta^+$  photoproduction with an outgoing kaon is simply related to backward  $K^-p$  charge-exchange (28). The lower  $KN\Theta^+$  vertices are the same; the upper vertex is also  $KN\Theta^+$  for  $K^-p$  charge-exchange but  $\gamma\Theta^+\Theta^+$  for  $\Theta^+$  photoproduction. If this diagram contributes appreciably to  $\Theta^+$  photoproduction, the contribution of the  $KN\Theta^+$  vertex is appreciable and should also contribute appreciably to backward  $K^-p$  charge-exchange. Some previously ignored backward  $K^-p$  charge-exchange data may be available.
2. The baryon and  $\bar{s}$  constituents of the  $\Theta^+$  are already initially present in low-energy photoproduction experiments in the target baryon and the  $\bar{s}$  component of the photon. In experiments where baryon number and strangeness must be created from gluons, the cost of baryon antibaryon and  $s\bar{s}$  production by gluons must be used to normalize the production cross section in comparison with the photoproduction cross sections; e.g. from baryon-antibaryon production and  $s\bar{s}$  production data in the same experiment that does not see the  $\Theta^+$ .

## 5 Acknowledgements

The original work reported in this talk was in collaboration with Marek Karliner. This work was partially supported by the U.S. Department of Energy, Division of High Energy Physics, Contract W-31-109-ENG-38

## References

1. A. De Rujula, H. Georgi and S.L. Glashow, *Phys. Rev. D* **12** (1975) 147
2. R. L. Jaffe, *Phys. Rev. Lett.* **38**, 195 (1977)
3. Harry J. Lipkin, *Nucl. Phys.* **A625**, 207 (1997)
4. E.M. Aitala et al., FERMILAB-Pub-97/118-E, *Phys. Lett.* **B448**, 303 (1996).
5. Ya.B. Zeldovich and A.D. Sakharov, *Yad. Fiz* **4**(1966)395; *Sov. J. Nucl. Phys.* **4**(1967)283.
6. A. D. Sakharov, private communication; H.J. Lipkin, *Annals NY Academy of Sci.* **452**(1985)79, and *London Times Higher Education Supplement*, Jan. 20,1984, p. 17.
7. Y. Nambu, in *Preludes in Theoretical Physics*, edited by A. de Shalit, H. Feshbach and L. Van Hove, (North-Holland Publishing Company, Amsterdam, 1966), p. 133
8. H.J. Lipkin, *Phys. Lett.* **45B** (1973) 267
9. M. Karliner and H. J. Lipkin, hep-ph/0307243.
10. M. Karliner and H.J. Lipkin, *Phys. Lett. B* **575** (2003) 249.
11. Marek Karliner and Harry J. Lipkin. hep-ph/0402008
12. Harry J. Lipkin, in: "Physique Nucleaire, Les Houches 1968," edited by C. de Witt and V. Gillet, Gordon and Breach, New York (1969). p. 585
13. T. Nakano *et al.* [LEPS Coll.], *Phys. Rev. Lett.* **91**, 012002 (2003), hep-ex/0301020.

14. V. Kubarovsky *et al.* [CLAS Coll.], [Phys. Rev. Lett. **92**, 032001 (2004)]  
Erratum – *ibid.* **92**, 049902 (2004), hep-ex/0311046.
15. T. Nakano, talk at NSTAR 2004, March 24-27, Grenoble, France,  
<http://lpsc.in2p3.fr/congres/nstar2004/talks/nakano.pdf> .
16. Y. A. Troyan *et al.*, hep-ex/0404003.
17. J. Z. Bai *et al.* [BES Collaboration], hep-ex/0402012.
18. Throsten Wengler [reporting DELPHI Coll. results], talk at Moriond '04  
QCD,  
<http://moriond.in2p3.fr/QCD/2004/WednesdayAfternoon/Wengler.pdf>
19. Marek Karliner and Harry J. Lipkin. hep-ph/0405002
20. For a review of the considerable theoretical literature on pentaquark models  
and an in-depth discussion, see Byron K. Jennings and Kim Maltman, hep-  
ph/0308286.
21. V. Burkert, talk at NSTAR 2004, March 24-27, Grenoble, France,  
[http://lpsc.in2p3.fr/congres/nstar2004/talks/burkert\\_2.pdf](http://lpsc.in2p3.fr/congres/nstar2004/talks/burkert_2.pdf) .
22. L. G. Landsberg, Phys.Rept.320(1999) 223; hep-ex/9910048.
23. D. Barna [presenting NA49 Coll. data], lecture at 3rd Budapest Winter  
School on Heavy Ion Physics, Dec. 8-11,  
[http://www.hef.kun.nl/  
URLtildenovakt/school03/agenda/Barnatalk.pdf](http://www.hef.kun.nl/URLtildenovakt/school03/agenda/Barnatalk.pdf)
24. Jonathan L. Rosner, hep-ph/0312269.
25. T. E. Browder, I. R. Klebanov and D. R. Marlow, hep-ph/0401115.
26. S. Armstrong, B. Mellado and S. L. Wu, hep-ph/0312344.
27. M. Battaglieri [presenting CLAS Coll. data], talk at Pentaquark Workshop,  
Feb. 10-12, 2004, Trento, Italy,
28. M. Karliner and H. J. Lipkin, Phys. Lett. B **586**, 303 (2004) hep-  
ph/0401072.

Frascati Physics Series Vol. XXXV (2004), pp. 187  
HEAVY QUARKS AND LEPTONS - San Juan, Puerto Rico, June 1-5, 2004

**PENTAQUARK SEARCHES AT HERA**

L. Stanco  
*INFN Padova, Via Marzolo 8, 35131 Padova, Italy*

Written contribution not received



Frascati Physics Series Vol. XXXV (2004), pp. 189-196  
HEAVY QUARKS AND LEPTONS - San Juan, Puerto Rico, June 1-5, 2004

## PENTAQUARK SEARCHES WITH INTERMEDIATE ENERGY PROBES

David J. Tedeschi  
*University of South Carolina, Columbia, SC*  
CLAS Collaboration  
*Thomas Jefferson National Accelerator Facility, Newport News, VA*

### ABSTRACT

Recent experimental results suggesting exotic 5-quark baryons (pentaquarks) have been presented at international conferences and published in refereed scientific journals. These data are claimed to herald a new chapter in hadron spectroscopy. Taken collectively, the data paint a compelling picture; however, valid criticism regarding the analysis methods and the statistical significance of individual experiments cannot be ignored. The experimental evidence from searches at intermediate energies for pentaquark states is reviewed.

### 1 Introduction

Since the 1960's when Gell-Mann introduced quarks and Nambu introduced color, baryons and mesons have been considered as three quark and quark-antiquark color singlets. This classification of known particles is largely unchanged today as searches for particles consisting of more than three quarks

have not been successful. <sup>1)</sup> Nevertheless, recent theoretical predictions for new baryon states - based on the chiral soliton and quark cluster models - have reinvigorated the search for exotic hadrons. <sup>2, 3, 4)</sup> One member of a new anti-decuplet, the  $\Theta^+$ , is an  $S=1$  baryon composed of  $uudd\bar{s}$  and is predicted to have a mass of 1540 MeV and a width of 15 MeV. <sup>2)</sup> The state is exotic due to its strangeness and enigmatic due to its predicted narrow width.

An early discussion by Gao and Ma of pentaquark search possibilities at Jefferson Lab generated little activity. <sup>5)</sup> However, since the announcement at PANIC 2002 by the LEPS group for a pentaquark signal in photoproduction data <sup>6)</sup>, there has been a renewed effort by the medium energy community to analyze existing data for signals of exotic baryons. Understanding the properties of the putative pentaquark has become a focus of the hadron spectroscopy community. This paper will discuss pentaquark searches at intermediate energies and summarize the status as of this conference.

## 2 Experimental Data

There are now more than a dozen reports of possible pentaquark signals (see Figure 1) with reported masses clustering around 1530 and 1540 MeV. These claims for a new  $S=1$  state come from a structure in the invariant mass distributions that are constructed from the detected particles of the decay  $\Theta^+ \rightarrow n + K^+$  or  $\Theta^+ \rightarrow p + K^0$ . This amount of evidence would seem enough to ensure the discovery is accepted by the scientific community. However, in addition to these positive results, there are an almost equal number of null results that have been reported at various conferences, though only a few are posted on the pre-print archive. <sup>8)</sup> Moreover the reported structure in the  $S=1$  channel is argued to come from reflections of normal meson production. <sup>7)</sup> Thus, given the marginal statistical significance of all the positive results, the experimental situation regarding the existence of pentaquark baryons is open to interpretation.

The first publication of a pentaquark signal came from the LEPS collaboration. <sup>9)</sup> Using a photon beam ( $1.8 < E_\gamma < 2.4$  GeV) the group analyzed  $K^+K^-$  pairs created in a scintillator start counter. After accounting for Fermi motion, the missing mass spectrum from the  $K^-$  shows an excess of counts at the mass of 1540 MeV. The width is consistent with the detector resolution. The comparison with  $\Lambda^*(1520)$  production from hydrogen (dotted line) demon-

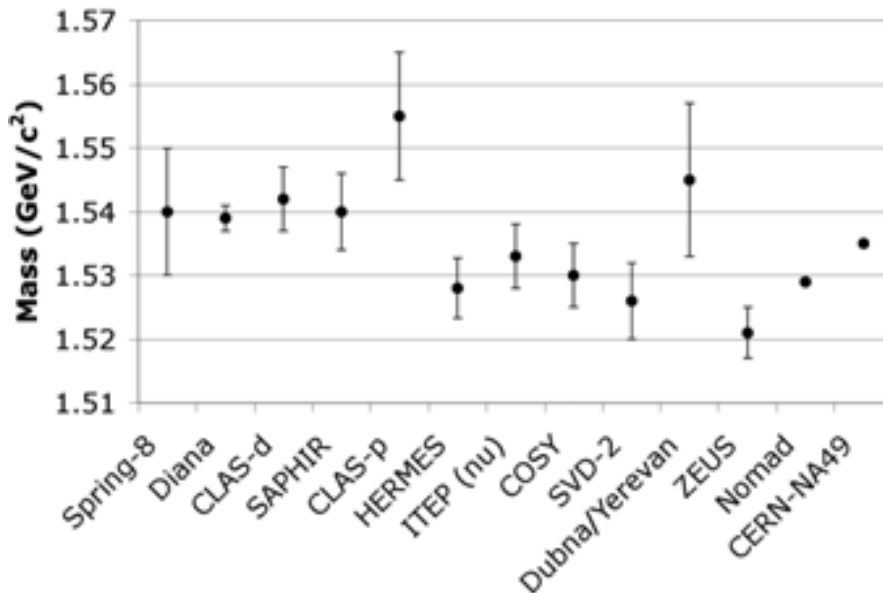


Figure 1: *Mass of the  $\Theta^+$  as seen by different experiments.*

states the experimental technique and gives a good account of the background, but there are only 19 events in the peak above the background.

Following the LEPS publication came results from DIANA <sup>10</sup>), CLAS <sup>11</sup>), and SAPHIR <sup>12</sup>). The DIANA data is from a 750 MeV/c  $K^+$  beam incident on a Xe bubble chamber. Events with a proton and two charged pions that reconstruct to a neutral kaon are analyzed. An excess of events at  $m(pK^0) = 1.54 \text{ GeV}/c^2$  is attributed to the  $\Theta^+$ . The result relies on kinematic cuts to suppress final state interactions.

The CLAS result is the first exclusive result from photoproduction on deuterium. The  $pK^+K^-$  final state was detected and the neutron was identified via missing mass. With the final state completely determined, Fermi motion corrections were not necessary; and a peak in the  $m(nK^+)$  spectrum at 1540 MeV was published. But detecting an energetic proton required a complicated production mechanism including FSI and questions remain as to the

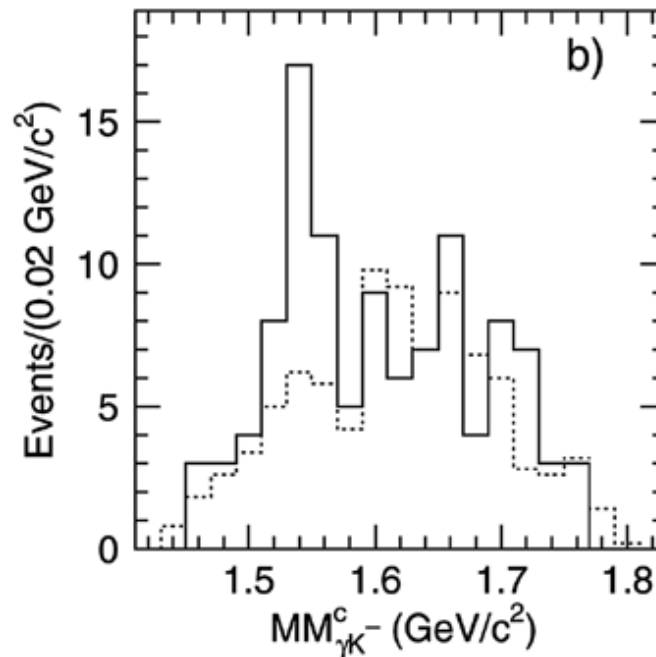


Figure 2: *Missing mass of LEPS event sample (solid line). The dotted line is from LH2 target.* <sup>9)</sup>

significance of the published peak. Similar problems plague the SAPHIR result. Initially the group predicted a very large cross section for  $\Theta^+$  production. A reanalysis of the data suggest a much smaller cross section and is still under study. <sup>13)</sup>

In 2004, the publication of data mining efforts continues. The efforts include data from a variety of probes. The CLAS <sup>14)</sup> and HERMES <sup>15)</sup> groups use photo- and electro-production. The ZEUS <sup>20)</sup>, COSY-TOF <sup>17)</sup>, SVD-2 <sup>18)</sup>, and Dubna <sup>19)</sup> groups analyzed data from hadronic beams, and the ITEP <sup>16)</sup> and Nomad <sup>21)</sup> results are from neutrino beam experiments. The appearance of a structure in results with different probes rules out any systematic effect from choice of beam. Of these experiments, though, only the CLAS and COSY results detected two strange particles to ensure  $S=1$  for the mass spectrum analyzed for pentaquark evidence.

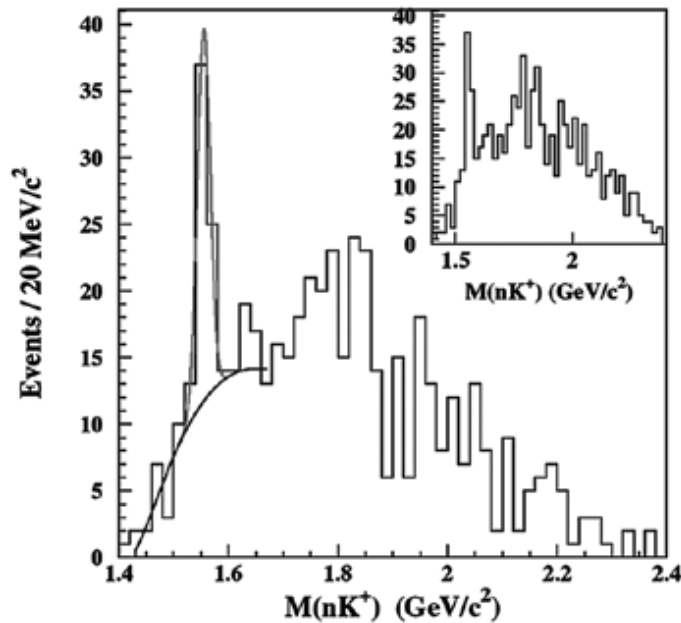


Figure 3: The  $nK^+$  invariant mass spectrum (left) with  $\cos(\theta_{K^+}^*) < 0.6$  and  $\cos(\theta_{\pi^+}^*) > 0.8$  where the angles are with respect to the photon beam in the center of mass system. <sup>14)</sup>

The second CLAS data set was acquired using a proton beam of energy  $3.0 < E_\gamma < 5.5 \text{ GeV}$  incident on a liquid hydrogen target, with a  $K^+, K^-$ , and  $\pi^+$  detected while the neutron was reconstructed via missing mass. <sup>14)</sup> The results are shown in Figure 3. The  $m(nK^+)$  invariant mass distribution is shown with the cuts:  $\cos(\theta_{K^+}^*) < 0.6$  and  $\cos(\theta_{\pi^+}^*) > 0.8$  where the angles are with respect to the photon beam in the center of mass system. A peak at 1555 MeV is observed. The solid line is a background shape derived from Monte Carlo simulation. The inset shows the same distribution but only requires  $\cos(\theta_{\pi^+}^*) > 0.8$ . While the signal is strong, the peak position is much higher than all other signals and has a large error ( $\pm 10 \text{ MeV}$ ).

Figure 4 is the  $m(nK^+K^-)$  invariant mass for events that are in the  $\Theta^+$  peak. While the statistics are quite low, there seems to be an excess of events at

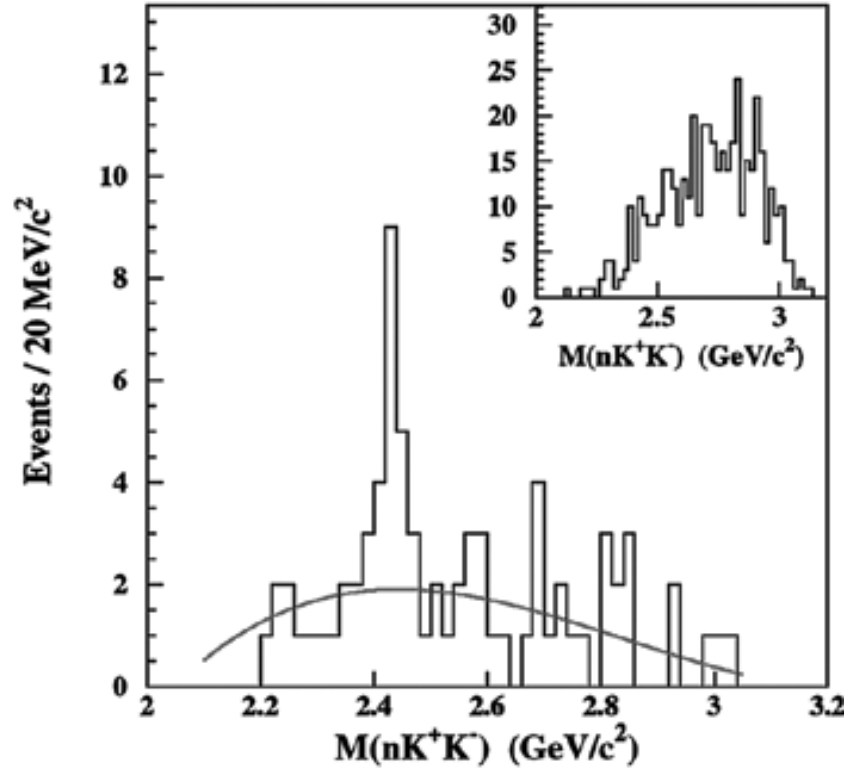


Figure 4: The  $nK^+K^-$  invariant mass spectrum (right) for events in the  $\Theta^+$  peak. Inset is for all other events. <sup>14)</sup>

2.4 GeV compared to the simulation (solid line). The inset shows the  $nK^+K^-$  invariant mass for all other events. This may be the first clue for a production mechanism thus it is critical for other experiments to reproduce or refute this result.

In addition to the analyses of existing individual data sets, cross section databases have been examined for evidence of a  $K^+N$  resonance. From arguments based on experimental cross sections, Nussinov established an upper bound for the  $\Theta^+$  width of 6 MeV. <sup>22)</sup> This finding was reinforced and lowered to about 1 MeV by a reanalysis of the SAID database <sup>23)</sup> and a comparison of the DIANA result with  $K^+d$  and  $K^+Xe$  scattering cross sections. <sup>24)</sup> A further analysis of  $K^+d$  scattering data that includes  $K^+$  double scattering and neutron Fermi motion corrections claims a measurable effect of the  $\Theta^+$ . <sup>25)</sup> A slight enhancement of the cross section at beam momenta between 0.450 and

0.500 GeV/c is attributed to a narrow  $S=1$  resonance with a mass of 1.55 GeV.

### 3 Conclusion

At the present time the existence of the  $\Theta^+$  is still a matter of debate. Positive signals from the analysis of individual data sets are marginal, and while there are null results reported, they do not completely rule the possibility of an  $S=1$  resonance. Moreover, the re-examination of existing KN data is similarly inconclusive. The effect on the total cross section is slight, leading to a very narrow width (1MeV), yet at least one analysis claims a positive signal. While 5 quark states can be accommodated by the existing models, the narrow width is difficult to explain theoretically.

Two years ago, pentaquark search were rather obscure. Now many groups around the world are performing dedicated searches. Two new experiments at CLAS, one on deuterium and the other on hydrogen are expected to improve statistics by an order of magnitude over previously published data. The LEPS group is analyzing a new data set using a deuterium target. HERMES has a dedicated pentaquark trigger and the COSY-TOF group has a new run beginning in the fall of 2004. These experiments will hopefully provide quality data sets that can be used to address the question of the existence of the exotic  $\Theta^+$  pentaquark and its production mechanism. Additionally, if these experiments provide positive results, to put the pentaquark on solid ground, an effort must be made to understand the lack of a signal from the searches reporting null results.

### 4 Acknowledgements

This material is based upon work supported by the National Science Foundation under Grant No. 0244982.

### References

1. S. Eidelman *et al.*, Phys. Lett. B **592**, 1 (2004).
2. D. Diakonov, V. Petrov, and M. Polyakov, Z. Phys. A **359**, 305 (1997).
3. M. Karliner and H.J. Lipkin, Phys. Lett. B **575**, 249 (2003).

4. R. Jaffe and F. Wilczek, Phys. Rev. Lett. **91**, 232003 (2003).
5. H. Gao and B.-Q. Ma, Mod. Phys. Lett. A **14**, 2313 (1999).
6. T. Nakano *et al.*, Nucl. Phys. A **721**, C112 (2003).
7. A. Dzierba *et al.*, Phys. Rev. D **69**, 051901 (2004).
8. J.Z. Bai *et al.*, hep-ex/0402012; K.T. Knopfle *et al.*, hep-ex/0403020; C. Pinkenburg *et al.*, nucl-ex/0404001.
9. T. Nakano *et al.*, Phys. Rev. Lett. **91**, 012002 (2003).
10. V.V. Barmin *et al.*, Yad. Phys. **66**, 1763 (2003).
11. S. Stepanyan *et al.*, Phys. Rev. Lett. **91**, 252001 (2003).
12. J. Barth *et al.*, Phys. Lett. B **572**, 127 (2003).
13. M. Ostrick *et al.*, Pentaquark03 Workshop, Jefferson Lab, Nov. 6-8, 2003.
14. V. Kubarovsky *et al.*, Phys. Rev. Lett. **92**, 032001 (2004).
15. A. Airapetian *et al.*, Phys. Lett. B **585**, 312 (2004).
16. A.E. Astrayan *et al.*, Phys. Atom. Nucl. **67**, 682 (2004), Yad. Fiz. **67**, 704 (2004).
17. M. Abdel-Bary *et al.*, hep-ex/0403011 Accepted by Phys. Lett. B.
18. A. Aleev *et al.*, NPI-MSU-2004-4-743, Submitted to Yad. Fiz.
19. P.Zh. Aslanyan *et al.*, hep-ex/0403044.
20. S. Chekanov *et al.*, hep-ex/0405013.
21. L. Camilleri *et al.*, Talk at Neutrino 2004, July 13-19 (2004).
22. S. Nussinov, hep-ph/0307357.
23. R.A. Arndt *et al.*, Phys. Rev. C **68**, 042201 (R) (2003), Phys. Rev. C **69**, 019901 (E) (2004).
24. R.N. Cahn and G.H. Trilling, Phys. Rev. D **69**, 011501 (R) (2004).
25. W. R. Gibbs, nucl-th/0405024.

***SESSION V – CKM Matrix Elements from D and B Decays***

- A. Gray      Unquenched Lattice Gauge Theory Calculations for Semileptonic  $B$ ,  
 $D$  Decays
- J. Wiss      Review of Charm Semileptonic Decays
- C.W. Bauer    Inclusive Determinations of  $|V_{ub}|$  and  $|V_{cb}|$
- D. Fortin      Measurement of  $|V_{cb}|$  and HQE Parameters from Semileptonic  
B Decays
- C. Schwanda    New Methods for  $|V_{ub}|$  Determination
- C. Stepaniak    Spectral moments from B Decays at CLEO



Frascati Physics Series Vol. XXXV (2004), pp. 199-208  
HEAVY QUARKS AND LEPTONS - San Juan, Puerto Rico, June 1-5, 2004

**UNQUENCHED LATTICE GAUGE THEORY  
CALCULATIONS FOR SEMILEPTONIC  $B$ ,  $D$  DECAYS**

Alan Gray

*Department of Physics, The Ohio State University, OH 43210, USA*

**ABSTRACT**

This paper reviews recent progress of lattice gauge theory determinations of semileptonic B and D decay form factors. These determinations are important in extracting the remaining CKM matrix elements.

**1 Introduction**

A large scale experimental and theoretical effort is underway to overconstrain the CKM matrix and uncover any internal inconsistencies revealing new physics. Uncertainties in determinations of the CKM elements arise not only from experiment but also, in no small part, from the theoretical calculations needed to account for hadronic QCD effects. Within the next few years the theoretical uncertainties must be reduced to the few percent level in order not to dominate uncertainties from experiment.

$B$  decay and mixing processes are most suitable for extracting  $|V_{ub}|$ ,  $|V_{cb}|$ ,  $|V_{td}|$ , and  $|V_{ts}|$ ; a large fraction of the CKM matrix. The QCD coupling at the relevant hadronic scales is large and thus a non perturbative method is needed. Lattice QCD holds the most promise in being able to provide the required hadronic factors with the required accuracy. Recent lattice QCD results give confidence that the required precision calculations are now possible.

This paper reviews the current status of lattice QCD calculations for the semileptonic decays of the  $B$  mesons needed to determine  $V_{ub}$  and  $V_{cb}$ . Additionally, semileptonic  $D$  meson decay calculations, suitable as rigorous checks of lattice methods, are discussed.

## 2 Lattice QCD

Lattice QCD (see, e.g. <sup>1</sup>) involves the use of a mathematical ‘trick’ where spacetime is discretized into a finite lattice. Quarks live on the lattice points and gluons live on the links between the points. This formalism regularizes QCD by providing a momentum cut-off: no momenta greater than  $\pi/a$  can propagate where  $a$ , typically  $\sim 0.1\text{fm}$ , is the lattice spacing. The Feynman path integral becomes an ordinary integral over a finite number of degrees of freedom, and can be computed numerically on a computer. Continuum QCD results can be obtained by taking the lattice spacing to zero, provided that the *matching factors*, or differences between the continuum and lattice renormalization schemes, have been taken into account. In heavy-light physics these matching factors are usually determined by comparing a perturbative continuum calculation with the corresponding perturbative calculation on the lattice.

Unfortunately, the numerical integrations corresponding to the Feynman path integral are extremely computationally expensive. Even with the use of efficient Monte Carlo methods approximations must be done in order to obtain results with the computational technology of today. A dramatic saving can be made by ignoring closed quark loops in the vacuum, and the vast majority of lattice calculations have been done in this so called *quenched approximation*. The use of this incorrect theory, however, leads to systematic errors at the 10-20% level. Unquenched calculations must be done in order to achieve the above precision results.

In quenched calculations, when vacuum or *dynamical* quarks are in-

cluded, the expense of the simulation increases dramatically with decreasing dynamical quark mass, meaning that in practice the light dynamical quarks are included with masses greater than their physical masses. If light enough, however, extrapolations can be done to the correct physical masses with the help of ‘chiral perturbation theory’ (see, e.g. <sup>2</sup>): an effective theory involving expansions around the massless limit. Up until recently, unquenched simulations have not been able to reach this ‘chiral regime’.

Now for the first time, simulations have been done with dynamical quarks light enough to allow the agreement at the 3% level of theory with experiment for a variety of (simply calculable) quantities <sup>3</sup>). These simulations have been possible due to the combination of ever increasing computing power and the emergence of a better understanding about the properties of quarks on the lattice, which has led to the use of the so called *improved staggered* formulation. This was used by the MILC collaboration (see <sup>4, 5</sup>) and references therein) to create ensembles of ‘configurations’ (snapshots of the QCD vacuum on the lattice) which are then used to ‘measure’ required physical quantities such as those above.

### 3 Heavy Quarks on the Lattice

Naive discretization of heavy quark fields leads to large  $\mathcal{O}(am_Q)$  discretization errors due to large heavy quark mass  $m_Q$ . However, one can use effective theories which take advantage of the fact that the heavy quarks typically have low velocities within the hadron, and are therefore somewhat non-relativistic. This also often results in simplifications reducing simulation time and allowing high statistics. The calculations reviewed in this paper incorporate two alternative heavy quark methods.

Non Relativistic QCD (NRQCD) <sup>6</sup>) involves an expansion of the QCD Lagrangian in powers of  $1/m_Q$ . This is very useful for  $b$  quarks but not so appropriate for  $c$  quarks.

The Fermilab method <sup>7</sup>) (although more complicated than NRQCD) is very appropriate for  $c$  quarks as it incorporates smooth transitions from relativistic light quarks to non relativistic heavy quarks.

#### 4 Semileptonic Decays

Recently the first fully unquenched results for the semileptonic decay form factors have appeared and, although preliminary, are very promising.

The matrix element for the decay of a heavy  $B$  or  $D$  meson to a pion is given by

$$\begin{aligned} \langle \pi(p_\pi) | V^\mu | H(p_H) \rangle &= f_+(q^2) \left[ p_H^\mu + p_\pi^\mu - \frac{M_H^2 - m_\pi^2}{q^2} q^\mu \right] \\ &\quad + f_0(q^2) \frac{M_H^2 - m_\pi^2}{q^2} q^\mu \\ &\equiv \sqrt{2m_H} (f_{\parallel}(E_\pi) v^\mu + f_{\perp}(E_\pi) p_{\perp}^\mu) \end{aligned} \quad (1)$$

where  $v^\mu = p_H^\mu/M_H$  and  $p_{\perp}^\mu = p_\pi^\mu - E_\pi v^\mu$  become  $(1, \vec{0})$  and  $(0, \vec{p}_\pi)$  respectively in the heavy meson rest frame.

The alternative  $f_{\parallel}(E_\pi)$  and  $f_{\perp}(E_\pi)$  form factors have been introduced because they are more appropriate for lattice calculations and the associated chiral perturbation theory formulae are usually given in terms of  $E_\pi$ , the pion energy in the heavy meson rest frame. It is straightforward to interchange between these two conventions.

Unfortunately, experimental results are limited to the small  $q^2$  region whereas, for  $B$  mesons, lattice calculations are most reliable for small recoil (large  $q^2$ ). This is because lattice calculations currently work in the  $B$  meson rest frame and large recoil would give the pion large momenta introducing large  $\mathcal{O}(a^2 p_\pi^2)$  discretization errors and large statistical errors. However, the lattice community is excited about the development of Moving NRQCD <sup>8)</sup> which allows the momentum to be shared between the  $B$  and the  $\pi$ . This will allow calculations over the full  $q^2$  range providing excellent overlap with experiment and should be ready to implement within the next year.

In the mean time it is necessary to use a model in order to extrapolate the lattice results to the low  $q^2$  region. It will, however, be seen that results using the Becirevic Kaidalov (BK) parameterization <sup>9)</sup> are encouraging. The BK parameterization satisfies Heavy Quark Effective Theory scaling laws, the fact that  $f_+$  must have a pole at  $q^2 = M_{B^*}^2$  and the necessary condition  $f_+(0) = f_0(0)$ .

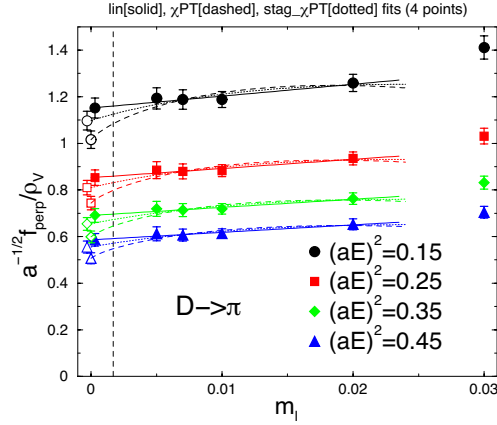


Figure 1: *Chiral extrapolations for  $f_{\perp}^{D \rightarrow \pi}$  with Fermilab heavy quarks <sup>10)</sup>. Solid: linear; dashed: chiral perturbation theory without staggered effects; dotted: full staggered chiral perturbation theory.*

## 5 Semileptonic $D$ Decay Results

The CKM elements  $|V_{cs}|$  and  $|V_{cd}|$  are known more accurately than  $|V_{ub}|$  and the CLEO-c program aims to further improve this accuracy <sup>11)</sup>. Semileptonic  $D$  decays are thus very suitable processes for testing lattice calculations.

Using the MILC ensembles and Fermilab heavy quarks, Okamoto *et al* <sup>10)</sup> have calculated the  $D \rightarrow \pi$  (and similarly  $D \rightarrow K$ ) form factors. Lattice determinations of the matrix element Eq. 1 were done for several  $q^2$  and light quark mass  $m_q$ . For each  $m_q$ , the BK parameterization was used to interpolate to common  $E_{\pi}$  values. Then, for each  $E_{\pi}$ , chiral extrapolations were done to obtain results at the physical light quark masses. Chiral perturbation theory is used to give the appropriate extrapolation function, dependent on the lattice action used. Figure 1 shows chiral extrapolations for  $f_{\perp}$ . The correct (full staggered) chiral extrapolation is shown along with linear and non-staggered functions.  $\rho_v$  is a matching factor between the lattice and continuum renormalization schemes which is 1 at tree-level.

Figure 2 shows results for linearly<sup>1</sup> chirally extrapolated form factors as

<sup>1</sup>The analysis for the full staggered chirally extrapolated form factors is underway.

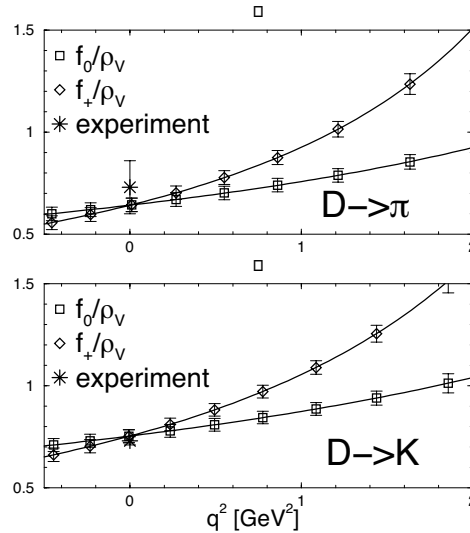


Figure 2:  $D \rightarrow \pi$  and  $D \rightarrow K$  form factors with Fermilab heavy quarks <sup>10)</sup>.

a function of  $q^2$  for both  $D \rightarrow \pi$  and  $D \rightarrow K$ . In both cases good agreement with experiment at  $q^2 = 0$  is seen, although the CLEO-c results will provide a more stringent test over the full  $q^2$  range.

There exists one set of MILC ensembles with a relatively large lattice spacing (the ‘coarse’ set) and there similarly exists a ‘fine’ set. This work has so far only been done on the coarse ensembles and must be repeated on the fine ensembles to check for lattice spacing dependence.

## 6 $B \rightarrow \pi l \nu$ Results

The MILC coarse ensembles were again used for  $B \rightarrow \pi l \nu$  calculations. Both NRQCD and Fermilab heavy quarks have been used.

In similar fashion to the  $D$  decay analysis, the form factor results were interpolated to common  $E_\pi$  values and chiral extrapolations were performed, but only linearly so far. Figure 3 shows these extrapolations for  $f_{\parallel}$  and  $f_{\perp}$  for the NRQCD case <sup>12)</sup>. The full staggered chiral function has recently been determined and must now be incorporated into this analysis. The BK parameterization was then used to extrapolate to the low  $q^2$  region, as can be seen

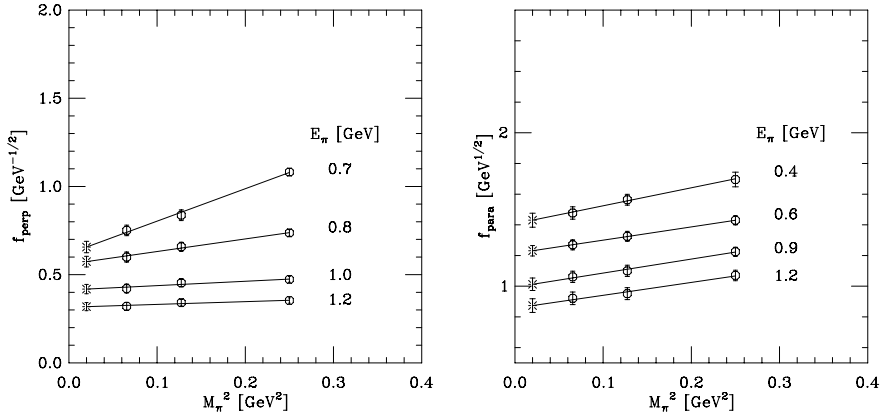


Figure 3: Linear chiral extrapolations for  $f_{\parallel}^{B \rightarrow \pi}$  and  $f_{\perp}^{B \rightarrow \pi}$  with NRQCD heavy quarks <sup>12)</sup>.

on the left hand side of figure 4. The data fits the model excellently with  $f_+$  exhibiting the expected pole at  $q^2 = M_{B^*}^2$  and with  $f_0$  consistent with the soft pion relation  $f_0(M_B^2) = f_B/f_\pi$ . Although  $f_0$  is not needed for the decay rate, it has relatively small statistical errors and its inclusion in the fit is very useful in constraining  $f_+$ . These results include one-loop matching but  $\mathcal{O}(1/am_b)$  currents have still to be included, and again this work must be repeated on the fine ensembles. This plot includes old quenched results for comparison, some of which have had their errors removed for clarity.

An equivalent plot of results with Fermilab quarks <sup>10)</sup> is shown on the right hand side of figure 4, again comparing with old quenched results. In this case again only the coarse ensembles have been used, only tree level matching has been done, and  $m_b$  is not tuned well. These issues are being addressed.

From their NRQCD form factor results, Shigemitsu *et al.* <sup>12)</sup> have estimated a result for  $|V_{ub}|$  by integrating

$$\frac{1}{|V_{ub}|^2} \frac{d\Gamma}{dq^2} = \frac{G_F^2}{24\pi^3} p_\pi^3 |f_+(q^2)|^2 \quad (2)$$

where the CLEO branching fraction <sup>13)</sup> was used to get  $\Gamma$ . The preliminary

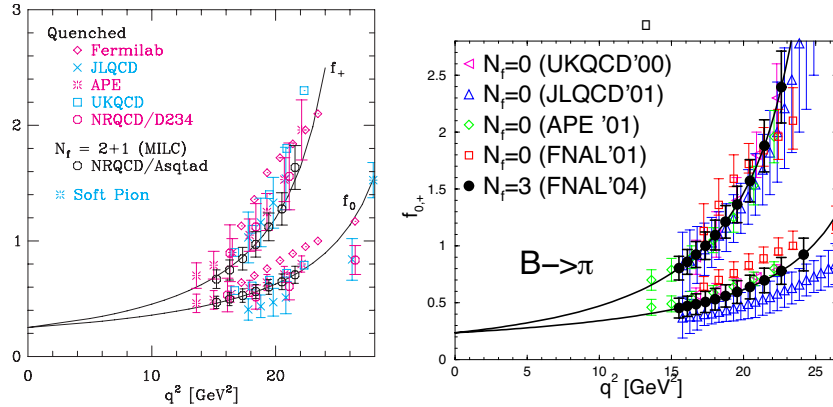


Figure 4:  $BK$  parameterization fits to  $f_+^{B \rightarrow \pi}$  and  $f_0^{B \rightarrow \pi}$  with NRQCD heavy quarks <sup>12)</sup> (left), where the burst shows the soft pion result, and with Fermilab heavy quarks <sup>10)</sup> (right). Both plots include old quenched results.

results from both the full and high  $q^2$  ranges are

$$|V_{ub}| = \begin{cases} 3.86(35)(62) \times 10^{-3} & 0 \leq q^2 \leq q_{max}^2 \\ 3.52(70)(42) \times 10^{-3} & 16 \text{GeV}^2 \leq q^2 \end{cases} \quad (3)$$

where the errors are experimental and lattice respectively, and are both tentative. It is encouraging that these results agree with each other, and are consistent with the current inclusive  $B$  decay determinations <sup>14)</sup>.

It is hoped that the lattice errors for this quantity will be at around the 10-13% level when this analysis is complete. The main sources of error are uncertainties in chiral extrapolations, continuum extrapolations and matching. Estimates have been made as to how the magnitude of the overall error will reduce with future calculations <sup>15)</sup>. The next generation of machines, being built just now, should allow simulations where  $a^2$  or  $m_l$  is halved, shrinking the error to the 5.5-6.5% level, assuming that 2-loop matching has been performed. Looking further ahead, if both  $a^2$  and  $m_l$  could be halved it is hoped that 4-5% precision will be possible, again assuming 2-loop matching. The timescale for this, however, is not known.

## 7 $B \rightarrow D^* l \nu$ Results

The differential  $B \rightarrow D^* l \nu$  decay width is given by

$$\frac{d\Gamma}{d\omega} \propto |V_{cb}| \mathcal{F}_{B \rightarrow D^*}(\omega) \quad (4)$$

where  $\omega = v' \cdot v$  and  $v$  and  $v'$  are the  $B$  and  $D$  four-velocities respectively. In order to extract  $|V_{cb}|$ , the form factor at zero recoil  $\mathcal{F}(1)$  must be determined. Since  $B$  and  $D$  mesons can both be considered heavy, heavy quark symmetry can be exploited. The errors then scale with  $1 - \mathcal{F}(1)$  instead of  $\mathcal{F}(1)$  because in the infinitely heavy quark limit  $\mathcal{F}(1) = 1$  <sup>16)</sup>.

The best lattice determination thus far, which is in the quenched approximation and uses Fermilab heavy quarks, is given by <sup>17)</sup>

$$\mathcal{F}_{B \rightarrow D^*}(1) = 0.913_{-0.017}^{+0.024} \pm 0.016_{-0.014-0.016-0.014}^{+0.003+0.000+0.006} \quad (5)$$

where the errors are from statistics, matching, lattice spacing dependence, chiral extrapolation, and quenching respectively.

With reference to the previous section, it is hoped that this total error will be reduced from 4% to around the 2% level with the next generation of machines and then to as low as 1% with the next again generation. At this level, it will be important to compute the slope and curvature of  $\mathcal{F}(\omega)$ , and Moving NRQCD will again be of great help in achieving this.

## 8 Conclusions

Unquenched lattice gauge theory calculations are appearing, and have already made an impact. The lattice community is confident that such calculations can now be done to obtain the quantities important for extracting the CKM elements, including the semileptonic  $B$  decay form factors. Comparison of  $D$  semileptonic decay lattice results with precise CLEO-c data should enhance this confidence.

The calculations are still at a preliminary stage, but good understanding exists on, and plans are in place to address, all sources of error. Precision results are likely to appear within the next few years.

## References

1. R. Gupta, hep-lat/9807028.

2. D. Arndt, hep-lat/0406011.
3. HPQCD, C. T. H. Davies *et al.*, Phys. Rev. Lett. **92**, 022001 (2004), [hep-lat/0304004].
4. C. W. Bernard *et al.*, Phys. Rev. **D64**, 054506 (2001), [hep-lat/0104002].
5. C. Aubin *et al.*, hep-lat/0402030.
6. G. P. Lepage, L. Magnea, C. Nakhleh, U. Magnea and K. Hornbostel, Phys. Rev. **D46**, 4052 (1992), [hep-lat/9205007].
7. A. X. El-Khadra, A. S. Kronfeld and P. B. Mackenzie, Phys. Rev. **D55**, 3933 (1997), [hep-lat/9604004].
8. K. M. Foley and G. P. Lepage, Nucl. Phys. Proc. Suppl. **119**, 635 (2003), [hep-lat/0209135]; K. M. Foley *et al.*, Lattice 2004 proceedings in preparation.
9. D. Becirevic and A. B. Kaidalov, Phys. Lett. **B478**, 417 (2000), [hep-ph/9904490].
10. M. Okamoto *et al.*, Nucl. Phys. Proc. Suppl. **129**, 334 (2004), [hep-lat/0309107]; M. Okamoto *et al.*, Lattice 2004 proceedings in preparation.
11. CLEO-c,  
<http://www.lns.cornell.edu/public/CLEO/spoke/CLEOc/ProjDesc.html>  
(2001).
12. J. Shigemitsu, Lattice 2004 proceedings in preparation.
13. CLEO, S. B. Athar *et al.*, Phys. Rev. **D68**, 072003 (2003), [hep-ex/0304019].
14. A. Ali, hep-ph/0312303.
15. C. Bernard, private communication.
16. N. Isgur and M. B. Wise, Phys. Lett. **B237**, 527 (1990).
17. S. Hashimoto, A. S. Kronfeld, P. B. Mackenzie, S. M. Ryan and J. N. Simone, Phys. Rev. **D66**, 014503 (2002), [hep-ph/0110253].

Frascati Physics Series Vol. XXXV (2004), pp. 209-219  
HEAVY QUARKS AND LEPTONS - San Juan, Puerto Rico, June 1-5, 2004

## REVIEW OF CHARM SEMILEPTONIC DECAYS

Jim Wiss  
*University of Illinois, Urbana-Champaign*

### ABSTRACT

I will review some recent results on charm semileptonic decays. Because of time constraints I will concentrate on the exclusive decays of charmed mesons. I begin with a discussion to motivate the importance of this physics before turning to a discussion of the pseudoscalar  $\ell\nu$  decays and vector  $\ell\nu$  decays.

### 1 Motivation

The semileptonic decay processes considered here can be computed by tree level diagrams apart from  $q^2$  dependent form factors that describe the coupling of various helicity states of the virtual  $W^\pm$  state to the current carried by the charm parent and daughter meson. Measurements of the form factors can potentially provide unique, incisive tests of non-perturbative QCD. The decay rate is proportional to the squared modulus of the CKM

element factor ( $|V_{cq}|^2$ ) describing the coupling of virtual  $W^\pm$  to the charm and light quark current. In the future, when the semileptonic form factors can be reliably computed to great accuracy, charm semileptonic decays can supply additional information on the CKM matrix that can be used to refine tests of CKM matrix unitarity. Perhaps a stronger motivation concerns the role of charm semileptonic processes in "calibrating" the techniques used to compute hadronic corrections to many of the critical CKM measurement processes accessible through beauty decay. Such "calibrations" are particularly timely in light of the ability of LQCD (lattice QCD) to make *unquenched* and  $q^2$  dependent form factor calculations thus reducing the present substantial ( $\approx 15\%$ ) systematic errors.

## 2 $D \rightarrow$ pseudoscalar $\ell\nu$ decay

Eq. 1 gives the expression for the decay rate differential in  $q^2$  – the square of the neutrino and charged lepton invariant mass up to the corrections proportional the square of the charged lepton mass.

$$\frac{d\Gamma}{dq^2} = \frac{G_F^2 |V_{cq}|^2 P_P^3}{24\pi^2} \{ |f_+(q^2) + m_\ell^2 ( \quad ) \} \quad (1)$$

The rate is proportional to the square of the relevant CKM matrix element, the cube of the pseudoscalar daughter momentum as measured in the charm parent rest frame, and the squared modulus of the  $f_+(q^2)$  form factor.<sup>1</sup> Eq. 1 implies that measurement of  $d\Gamma/dq^2$  in  $D \rightarrow$  pseudoscalar  $\ell\nu$  decay provides information on the product  $V_{cq} \times f_+(q^2)$  that can be viewed as either a measurement of CKM matrix elements or a test of LQCD predictions for the scale of the form factor and its  $q^2$  dependence. The  $P_P^3$  factor plays a critical determining the decay kinematics. The daughter momentum ( $P_P$ ) depends on the rest masses of the parent and daughter hadron and  $q^2$ . As  $q^2$  increases, the daughter momentum decreases implying that the maximum rate is zero at the maximum  $q^2$  and grows dramatically as  $q^2 \rightarrow 0$ . Older experimental results were plagued by both a lack of statistics and the inability to accurately measure  $q^2$  due to the missing neutrino. As a result, experimentalists in the past needed to rely on one of two common  $f(q^2)$  parameterizations reported and

<sup>1</sup>An additional form factor ( $f_-(q^2)$ ) is present as well but its square as well as its interference with the  $f_+(q^2)$  piece are multiplied by  $m_\ell^2$  in Eq. 1.

their results at the point of maximum rate or  $f_+(q^2 = 0)$ . The older LQCD predictions computed  $f_+(q^2)$  at one point – the maximum  $q^2$ . This led to an important disconnect between theory and experiment.

### 2.1 CLEO measurements of $D^0 \rightarrow K^- \ell^+ \nu$ and $D^0 \rightarrow \pi^- \ell^+ \nu$

This analysis<sup>1)</sup> concentrates on both a measurement of the  $\Gamma(D^0 \rightarrow \pi^- \ell^+ \nu)/\Gamma(D^0 \rightarrow K^- \ell^+ \nu)$  as well as a study of  $f_+(q^2)$  for both of these processes. The neutral D mesons used in this analysis were from electron-positron annihilation running near the  $\Upsilon(4S)$  resonance. The charged lepton was primarily an electron rather than a muon. The neutrino was reconstructed using energy-momentum balance along with the constraint that the mass of hadron-lepton-neutrino formed the mass of a  $D^0$ . The reconstructed neutrino was combined with the well-measured lepton and hadron momentum to form the 4-vector of the  $D$  and combined with an appropriate charged pion to reconstruct the decay  $D^{*+} \rightarrow D^0 \pi^+$ . The  $D^0 \rightarrow K^- \ell^+ \nu$  and  $D^0 \rightarrow \pi^- \ell^+ \nu$  yields are estimated by fitting the  $D^+ - D^0$  mass difference to a combination of the expected signal line shape, a peaking background due to  $D^0 \pi^+$  where the  $D^0$  does not decay according to the targeted modes, and a non-peaking background. CLEO obtains the branching ratio  $\Gamma(D^0 \rightarrow \pi^- \ell^+ \nu)/\Gamma(D^0 \rightarrow K^- \ell^+ \nu) = 0.082 \pm 0.006 \pm 0.005$ . Using Eq. 1, this branching ratio implies:

$|f_+^\pi(0)|^2 |V_{cd}|^2 / |f_+^K(0)|^2 |V_{cs}|^2 = 0.038_{-0.007}^{+0.006+0.005}$  or using the known values for the CKM elements:  $|f_+^\pi(0)|^2 / |f_+^K(0)|^2 = 0.86 \pm 0.07_{-0.04}^{+0.06} \pm 0.01$  where the third error is from the CKM matrix elements. This value is consistent with the expected degree of SU(3) symmetry breaking in the form factors and is compared to previous measurements in Table 1. All three values are consistent (CL = 68 %) with my weighted average of  $\Gamma(D^0 \rightarrow \pi^- \ell^+ \nu)/\Gamma(D^0 \rightarrow K^- \ell^+ \nu) = 0.085 \pm 0.007$ . The new CLEO number represents a significant improvement over previous measurements.

CLEO<sup>1)</sup> also reports new information on the  $q^2$  dependence of the  $f_+$  form factor for  $D^0 \rightarrow K^- \ell^+ \nu$  and  $D^0 \rightarrow \pi^- \ell^+ \nu$ . Separate  $D^+ - D^0$  mass difference plots were made in three  $q^2$  bins, and deconvolved to take into account the  $q^2$  smearing due to the missing neutrino. The resulting corrected  $q^2$  distributions were then fit to both the ISGW2 (2) form as well as the pole form ( $f_+(q^2) \propto 1/(1 - q^2/m_{\text{pole}}^2)$ ). The higher statistics  $D^0 \rightarrow K^- \ell^+ \nu$

Table 1: *Measurements of  $\Gamma(D^0 \rightarrow \pi^- \ell^+ \nu)/\Gamma(D^0 \rightarrow K^- \ell^+ \nu)$ . The older values of the pole mass are referenced in Reference <sup>3)</sup>.*

group	value
CLEO (95)	$0.103 \pm 0.039 \pm 0.013$
E687 (96)	$0.101 \pm 0.02 \pm 0.003$
<b>CLEO (04)</b> <sup>1)</sup>	$0.082 \pm 0.006 \pm 0.005$
<b>Average</b>	$0.085 \pm 0.007$

Table 2: *Measurements of the pole mass. The older values of the pole mass are referenced in Reference <sup>3)</sup>.*

group	value ( $GeV/c^2$ )
MK3	$1.8_{-0.2}^{+0.5} \pm 0.25$
E691	$2.1_{-0.2}^{+0.4} \pm 0.2$
CLEO 91	$2.100_{-0.200}^{+0.400} \pm 0.250$
CLEO 93	$2.000_{-0.12}^{+0.12} \pm 0.18$
E687 tag	$1.97_{-0.22}^{+0.43} \pm 0.07$
E687 inc	$1.87_{-0.08}^{+0.11} \pm 0.07$
<b>CLEO 04</b> <sup>1)</sup>	$1.89 \pm 0.005 \pm 0.035$
<b>Average</b>	$1.901 \pm 0.051$

sample was inconsistent with the ISGW2 form by about  $4.2 \sigma$ . The pole mass they obtained is compared to previous measurements in Table 2 along with my weighted average. The new CLEO measurement is a significant advance over previous values and all the measurements are very consistent with a pole mass of  $1.9 \pm 0.051$ , which is  $\approx 4.2 \sigma$  below the  $D^*$  spectroscopic pole mass.

### 3 Vector $\ell^+ \nu$ charm meson decays

In this section we describe several new results on  $D^0$ ,  $D^+$  and  $D_s^+$  semileptonic decays into a vector meson featuring recent results from Focus and CLEO. We begin with several new results on  $D^+ \rightarrow K^- \pi^+ \mu^+ \nu$  from Focus. Five kinematic variables describe this four-body decay process. These are the  $K^- \pi^+$  invariant mass ( $m_{K\pi}$ ), the square of the  $\mu\nu$  mass ( $q^2$ ), and the three decay angles illustrated in Figure 1: the angle between the  $\pi$  and the  $D$  direction in the

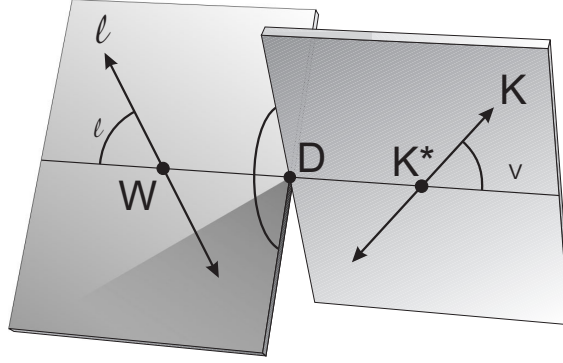


Figure 1: Definition of kinematic variables.

$K^-\pi^+$  rest frame ( $\theta_V$ ), the angle between the  $\nu$  and the  $D$  direction in the  $\mu\nu$  rest frame ( $\theta_\ell$ ), and the acoplanarity angle between the two decay planes ( $\chi$ ).

### 3.1 s-wave interference

$D^+ \rightarrow K^-\pi^+\mu^+\nu$  decay is known to be strongly dominated by the  $D^+ \rightarrow \bar{K}^{*0}\mu^+\nu$  process, but in 2002 Focus <sup>4)</sup> obtained evidence for a small, s-wave, interfering amplitude that creates an  $\approx -15\%$  forward-backward asymmetry in the  $\cos\theta_V$  projection. The pure  $D^+ \rightarrow \bar{K}^{*0}\mu^+\nu$  process has an angular distribution proportional to  $1 + \alpha \cos^2 \theta_V$ . The interference of the s-wave  $K^-\pi^+$  and p-wave  $K^-\pi^+$  from the  $\bar{K}^{*0}$  produces a term proportional to  $\cos\theta_V$ . The product of a nearly constant s-wave amplitude and the more rapidly varying Breit-Wigner p-wave amplitude of the  $K^{*0}$  produces a  $\cos\theta_V$  asymmetry with a characteristic dependence on  $m_{K\pi}$  that can be used to accurately determine both the phase and amplitude of the s-wave piece relative to the  $\bar{K}^{*0}$  amplitude. The Focus data had a s-wave amplitude that was about 7% of the  $\bar{K}^{*0}$  Breit-Wigner amplitude<sup>2</sup> with the same phase relative to the  $\bar{K}^{*0}$  that was obtained by the LASS Collaboration <sup>5)</sup> for the isodoublet, p-wave  $K\pi$  phase shift relative to the s-wave  $K\pi$  phase shift near  $m_{K\pi} = 0.896 \text{ GeV}/c^2$ . The latter observation suggests that there is no re-phasing of the s-wave amplitude

<sup>2</sup>The s-wave amplitude only interferes with the  $D^+ \rightarrow \bar{K}^{*0}\mu^+\nu$  piece where the virtual  $W^+$  has zero helicity. The 7% is relative to the zero helicity piece evaluated at the  $\bar{K}^{*0}$  pole mass.

relative to p-wave due to final state interactions as expected for a semileptonic decay process. Given the strength of the s-wave contribution, one sees at most a very mild distortion of the overall  $m_{K\pi}$  line-shape from that expected for pure  $D^+ \rightarrow \bar{K}^{*0} \mu^+ \nu$ .

### 3.2 $D^+ \rightarrow \bar{K}^{*0} \ell^+ \nu_\ell$ form factors

The Focus s-wave amplitude was discovered during their measurement of the  $D^+ \rightarrow \bar{K}^{*0} \ell^+ \nu_\ell$  form factors. In the zero mass charged lepton limit, the  $D^+ \rightarrow \bar{K}^{*0} \ell^+ \nu_\ell$  amplitude is described by three form factors that essentially describe the amplitude for finding the virtual  $W^+$  to exist in each of its three allowed helicity states. The three helicity basis form factors, are generally written as combinations of two axial form factors ( $A_1(q^2)$ ,  $A_2(q^2)$ ) and one vector form factor ( $V(q^2)$ ) that are parameterized in terms of spectroscopic pole forms.<sup>3</sup>

Given their large ( $\approx 30,000$  events) and relatively clean  $D^+ \rightarrow K^- \pi^+ \mu^+ \nu$  sample they were unable to get a satisfactory fit to the expected joint angular distribution for  $D^+ \rightarrow \bar{K}^{*0} \mu^+ \nu$  decay. Prior discovering the s-wave amplitude, typical fits had a  $\chi^2$  of 325 for 79 degrees of freedom. Ultimately Focus was able to obtain a good quality (CL = 11%) fit with a  $\chi^2$  of 95 for 79 degrees of freedom by including the s-wave amplitude, correcting for the influence of charm backgrounds, and eliminating events with  $q^2 < 0.2 \text{ GeV}^2/c^2$ .

Figure 2 compares the  $\cos\theta_\ell$  projection for events with  $q^2 < 0.2 \text{ GeV}^2/c^2$  to those with  $q^2 > 0.2 \text{ GeV}^2/c^2$ . The pronounced deviation from the expected  $\cos\theta_\ell$  distribution in the low  $q^2$  sample might imply a problem with the vector form factor  $V(q^2)$  at low  $q^2$  since this form factor controls the level of forward-backward asymmetry in  $\cos\theta_\ell$  although Focus cannot rule out alternative explanations for this interesting discrepancy.

Table 3 gives a summary of measured and predicted  $r_v$  and  $r_2$  values for  $D^+ \rightarrow \bar{K}^{*0} \ell^+ \nu_\ell$ . I have divided rows into experimental measurements, followed by quark model estimates, and finally followed by LQCD estimates. My weighted average of all experimental values is  $r_v = 1.618 \pm 0.055$  and

<sup>3</sup>The vector and axial pole masses are generally taken to be  $2.1 \text{ GeV}/c^2$  and  $2.5 \text{ GeV}/c^2$  corresponding to the  $D_s^{*+}$  and the  $D_s^{**}$  respectively. The role of the two axial form factors is distinguished since they are multiplied by different  $q^2$  dependent kinematic factors in the linear combinations that form the helicity basis form factors.

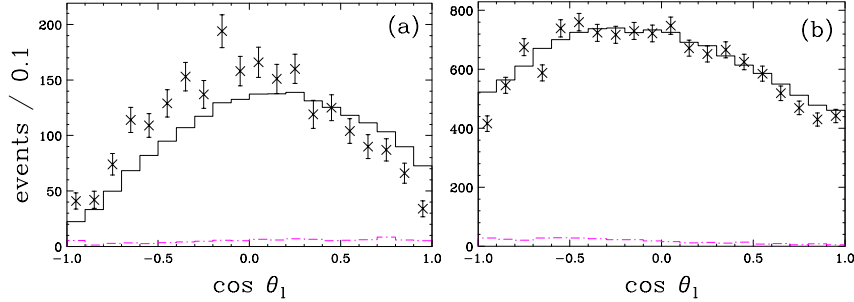


Figure 2:  $\cos\theta_\ell$  distributions obtained by Focus in their study of  $D^+ \rightarrow \bar{K}^{*0} \mu^+ \nu$  form factors. The points with error bars are the data. The upper histogram is expected "best fit" distribution. The lower (dashed) histogram is the expected  $\cos\theta_\ell$  distribution for charm backgrounds. (a)  $\cos\theta_\ell$  distribution for  $q^2 < 0.2 \text{ GeV}^2/c^2$ . (b)  $\cos\theta_\ell$  distribution for  $q^2 > 0.2 \text{ GeV}^2/c^2$

$r_2 = 0.830 \pm 0.054$ . The experimental data and LQCD predictions are fairly consistent in both  $r_v$  and  $r_2$ . The quark model predictions seem to be somewhat higher than the experimental average for  $r_2$ . The latest experimental numbers from Focus and  $r_v$  LQCD prediction from SPQR represent a significant improvement in experimental and theoretical precision. The Focus  $r_v$  number is about  $2\sigma$  lower in  $r_v$  to the next highest statistics number from E791.

### 3.3 Anomalies in $D_s^+ \rightarrow \phi \ell^+ \nu_\ell$ form factor ratios.

There is new data on a long standing anomaly between the  $D_s^+ \rightarrow \phi \ell^+ \nu_\ell$  form factor ratios and those measured for  $D^+ \rightarrow \bar{K}^{*0} \ell^+ \nu_\ell$ . By SU(3) symmetry and explicit calculation, the  $r_v$  and  $r_2$  form factor ratios for these two decays are expected to lie within  $\approx 10\%$  of each other. But previous to the very recent measurement by the Focus experiment <sup>6)</sup>, the  $r_2$  cross section measured for  $D_s^+ \rightarrow \phi \mu^+ \nu$  was roughly twice as high as that measured for  $D^+ \rightarrow \bar{K}^{*0} \ell^+ \nu_\ell$ , although the  $r_v$  form factors were consistent. The most precise of these previous measurements from the E791 Collaboration <sup>7)</sup>, quoted the significance of this discrepancy at about the  $3\sigma$  level. The latest number from Focus <sup>6)</sup> has  $r_v = 1.549 \pm 0.250 \pm 0.145$  and  $r_2 = 0.713 \pm 0.202 \pm 0.266$  for  $D_s^+ \rightarrow \phi \ell^+ \nu_\ell$  which is in excellent agreement with their own as well the present world average values for  $D^+ \rightarrow \bar{K}^{*0} \ell^+ \nu_\ell$  quoted in Table 3. Perhaps this surprising anomaly

Table 3: Measurements and predictions of  $D^+ \rightarrow \bar{K}^{*0} \ell^+ \nu_\ell$  form factors. Other references appear in Reference 9)

group	$r_1$	$r_2$
<b>Focus</b> 9)	$1.504 \pm 0.057 \pm 0.039$	$0.875 \pm 0.049 \pm 0.064$
BEAT	$1.45 \pm 0.23 \pm 0.07$	$1 \pm 0.15 \pm 0.03$
E791	$1.87 \pm 0.08 \pm 0.07$	$0.73 \pm 0.06 \pm 0.08$
E687	$1.74 \pm 0.27 \pm 0.28$	$0.78 \pm 0.18 \pm 0.1$
E653	$2 \pm 0.33 \pm 0.16$	$0.82 \pm 0.22 \pm 0.11$
E691	$2 \pm 0.6 \pm 0.3$	$0 \pm 0.5 \pm 0.2$
<b>Ave</b>	$1.618 \pm 0.055$	$0.830 \pm 0.054$
ISGW2	2	1.3
ISGW	1.4	1
WSB	1.4	1.3
KS	1	1
AW/GS	2	0.8
Stech	1.55	1.06
BKS	$1.99 \pm 0.22 \pm 0.33$	$0.7 \pm 0.16 \pm 0.17$
LMMS	$1.6 \pm 0.2$	$0.4 \pm 0.4$
LANL	$1.75 \pm 0.09$	$0.87 \pm 0.21$
ECL	$1.3 \pm 0.2$	$0.6 \pm 0.3$
APE	$1.6 \pm 0.3$	$0.7 \pm 0.4$
UKQCD	$1.4 \pm 0.35$	$0.9 \pm 0.2$
BBD	$2.2 \pm 0.2$	$1.2 \pm 0.2$
<b>SPQR</b> 10)	$1.48 \pm 0.12$	$0.6 \pm 0.3$

values for  $D^+ \rightarrow \bar{K}^{*0} \ell^+ \nu_\ell$  quoted in Table 3. Perhaps this surprising anomaly is starting to fade away with better data.

#### 3.4 The semileptonic vector to pseudoscalar ratio

An old problem in semileptonic charm decay concerns the ratio of  $\mathcal{R} \equiv \Gamma(D^+ \rightarrow \bar{K}^{*0} \ell^+ \nu_\ell) / \Gamma(D^+ \rightarrow \bar{K}^0 \ell^+ \nu_\ell)$ . The early quark models predicted  $\mathcal{R}$  to be approximately unity, whereas experimentally the ratio was roughly 1/2. Three relatively new results from Focus and CLEO bear on this problem. In 2002, CLEO 8) published a new measurement of  $\Gamma(D^+ \rightarrow \bar{K}^{*0} \ell^+ \nu_\ell) / \Gamma(D^0 \rightarrow K^- \pi^+ \pi^+) = 0.74 \pm 0.04 \pm 0.05$  that was somewhat higher than the previous world average of about 0.6 thus

Table 4: Measurements and predictions of  $D_s^+ \rightarrow \phi \ell^+ \nu_\ell$  form factors. (Full references appear in Reference 6)

group	$r_v$	$r_2$
Focus	$1.549 \pm 0.250 \pm 0.145$	$0.713 \pm 0.202 \pm 0.266$
791	$2.27 \pm 0.35 \pm 0.22$	$1.570 \pm 0.250 \pm 0.190$
CLEO	$0.9 \pm 0.6 \pm 0.3$	$1.400 \pm 0.500 \pm 0.300$
E653	$1.3 \pm 1 \pm 0.4$	$2.100 \pm 0.550 \pm 0.200$
E687	$1.8 \pm 0.9 \pm 0.2$	$1.100 \pm 0.800 \pm 0.100$
Ave	$1.679 \pm 0.213$	$1.310 \pm 0.197$
BKS	$2 \pm 0.19 \pm 0.22$	$0.780 \pm 0.080 \pm 0.150$
LMMS	$1.65 \pm 0.21$	$0.330 \pm 0.330$
ISGW2	2.1	1.300

obtaining a value of  $\mathcal{R}$  more in line with the old quark model predictions. Shortly thereafter, Focus <sup>11)</sup> published a new value for  $\Gamma(D^+ \rightarrow \bar{K}^{*0} \ell^+ \nu_\ell) / \Gamma(D^0 \rightarrow K^- \pi^+ \pi^+) = 0.602 \pm .01 \pm 0.021$  that was very consistent with the previous world average.

Recently Focus <sup>12)</sup> produced a direct measurement of the ratio  $\mathcal{R} = \Gamma(D^+ \rightarrow \bar{K}^{*0} \mu^+ \nu) / \Gamma(D^+ \rightarrow \bar{K}^0 \mu^+ \nu)$  using a technique designed to significantly reduce systematic errors. In this analysis the  $\bar{K}^{*0} \rightarrow K^- \pi^+$  and  $\bar{K}^0 \rightarrow K_s^0 \rightarrow \pi^+ \pi^-$  resulting in a final state consisting of three charged particles (a muon and two hadrons) for the numerator and denominator sample of  $\mathcal{R}$ . In order that vertex characteristics of the three charged particle final state are very similar, only upstream  $K_s^0 \rightarrow \pi^+ \pi^-$  decays are used which decay prior to the end of the Focus microstrip system. The upstream requirement reduces the denominator sample by about a factor of 10 but dramatically reduces potential systematic error. Table 5 summarizes measurements of  $\mathcal{R}$ . The Focus measurement represents a significant improvement over existing measurements and is a direct measurement that is not inferred from separate measurement of the numerator and denominator. This newest result is very consistent with the older values of  $\mathcal{R} \approx 0.6$ , which, as discussed in Reference <sup>12)</sup>, is also very consistent with the more recent theoretical estimates. The recent CLEO(02) measurement in Table 5 is large  $\mathcal{R} = 0.99 \pm 0.06 \pm 0.07 \pm 0.06^4$  compared to most of the data and the new Focus result. This partially re-

<sup>4</sup>An additional uncertainty of  $\pm 0.12$  should be included in addition to the

flects the fact that CLEO measured a somewhat higher than average value for  $\Gamma(D^+ \rightarrow \bar{K}^{*0} \ell^+ \nu_\ell) / \Gamma(D^0 \rightarrow K^- \pi^+ \pi^+)$  and normalized to their value for  $\mathcal{B}(D^+ \rightarrow \bar{K}^0 e^+ \nu)$ . As discussed in Reference <sup>12)</sup>,  $\mathcal{B}(D^+ \rightarrow \bar{K}^0 e^+ \nu)$  is probably anomalously low. Had CLEO(02) used  $\mathcal{B}(D^0 \rightarrow K^- \mu^+ \nu)$  and isospin symmetry for their quoted  $\mathcal{R}$  value, this value for  $\mathcal{R}$  would be much more in line with the weighted average value in Table 5.

Table 5: Measurements  $\mathcal{R} = \Gamma(D^+ \rightarrow \bar{K}^{*0} \mu^+ \nu) / \Gamma(D^+ \rightarrow \bar{K}^0 \mu^+ \nu)$  (Full references appear in <sup>12)</sup>)

Experiment	Quantity	Result
CLEO(91)	$\frac{\Gamma(D^0 \rightarrow K^{*-} e^+ \nu)}{\Gamma(D^0 \rightarrow K^- e^+ \nu)}$	$0.51 \pm 0.18 \pm 0.06$
CLEO(93)	$\frac{\Gamma(D^0 \rightarrow K^{*-} e^+ \nu)}{\Gamma(D^0 \rightarrow K^- e^+ \nu)}$	$0.60 \pm 0.09 \pm 0.07$
CLEO(93)	$\frac{\Gamma(D^+ \rightarrow \bar{K}^{*0} e^+ \nu)}{\Gamma(D^+ \rightarrow \bar{K}^0 e^+ \nu)}$	$0.65 \pm 0.09 \pm 0.10$
E691(89)	$\frac{\Gamma(D^+ \rightarrow \bar{K}^{*0} e^+ \nu)}{\Gamma(D^0 \rightarrow K^- e^+ \nu)}$	$0.55 \pm 0.14$
E687(93)	$\frac{\Gamma(D^+ \rightarrow \bar{K}^{*0} \mu^+ \nu)}{\Gamma(D^0 \rightarrow K^- \mu^+ \nu)}$	$0.59 \pm 0.10 \pm 0.13$
E687(95)	$\frac{\Gamma(D^+ \rightarrow \bar{K}^{*0} \mu^+ \nu)}{\Gamma(D^0 \rightarrow K^- \mu^+ \nu)}$	$0.62 \pm 0.07 \pm 0.09$
CLEO(02) <sup>8)</sup>	$\frac{\Gamma(D^+ \rightarrow \bar{K}^{*0} e^+ \nu)}{\Gamma(D^+ \rightarrow \bar{K}^0 e^+ \nu)}$	$0.99 \pm 0.06 \pm 0.07 \pm 0.06$
FOCUS(04) <sup>12)</sup>	$\frac{\Gamma(D^+ \rightarrow \bar{K}^{*0} \mu^+ \nu)}{\Gamma(D^+ \rightarrow \bar{K}^0 \mu^+ \nu)}$	$0.594 \pm 0.043 \pm 0.030$

#### 4 Acknowledgments

It is my pleasure to acknowledge my old colleagues in FOCUS, new colleagues in CLEO, and the organizers of this terrific conference in beautiful Puerto Rico.

#### References

1. The CLEO Collaboration, hep-ex/0407035.
2. D. Scora and N. Isgur, Phys. Rev. D **52**, 2783 (1995).

errors quoted in CLEO(02) due to uncertainties in  $\mathcal{B}(D^+ \rightarrow \bar{K}^0 e^+ \nu)$ .

3. CHARM AT FIXED TARGET. By J. Wiss (Illinois U., Urbana),. Jul 1997. Prepared for International School of Physics, 'Enrico Fermi': Heavy Flavor Physics - A Probe of Nature's Grand Design, Varenna, Italy, 8-18 Jul 1997. In \*Varenna 1997, Heavy flavour physics\* 39-93.
4. J. M. Link *et al.* [FOCUS Collaboration], Phys. Lett. B **535**, 43 (2002).
5. D. Aston *et al.*, Nucl. Physics B **296** 491 (1988).
6. J. M. Link *et al.* [FOCUS Collaboration], Phys. Lett. B **586**, 21 (2004).
7. E791 Collab. E.M. Aitala *et al.*, , Phys. Lett. B **450** 294 (1999).
8. G. Brandenburg *et al.* [CLEO Collaboration], Phys. Rev. Lett. **89**, 222 (2002).
9. J. M. Link *et al.* [FOCUS Collaboration], Phys. Lett. B **544**, 89 (2002).
10. A. Abada, *et al.* [SPQcdR Collaboration], hep-lat/0209116 (2002).
11. J. M. Link *et al.* [Focus Collaboration], Phys. Lett. B **541**, 243 (2002).
12. J. M. Link *et al.* [FOCUS Collaboration], Submitted to Physics Letters hep-ex/0406060



Frascati Physics Series Vol. XXXV (2004), pp. 221-230  
HEAVY QUARKS AND LEPTONS - San Juan, Puerto Rico, June 1-5, 2004

## INCLUSIVE DETERMINATIONS OF $|V_{ub}|$ AND $|V_{cb}|$

Christian W. Bauer  
*California Institute of Technology*

### ABSTRACT

In this talk I review the status of our ability to extract the CKM matrix elements  $|V_{ub}|$  and  $|V_{cb}|$  from inclusive semileptonic decays. I focus on model independent determinations of these parameters and discuss the expected theoretical uncertainties.

### 1 Introduction

The magnitudes of the Cabbibo, Kobayashi, Maskawa (CKM) matrix elements  $V_{ub}$  and  $V_{cb}$  are two of the parameters of the standard model which can be determined at current experimental facilities producing  $B$  mesons. Semileptonic decays of  $B$  mesons mediated by the weak decay of a  $b$  quark to either an up or a charm quark are an ideal way to perform these measurements, since the part

of the process involving the leptonic final states can be calculated perturbatively. The theoretical calculations required can be split into two parts. First, the decay rate of the  $b$  quark to either an up or a charm quark is required, and second the hadronic effects which bind these quarks into the observed hadrons in the experiment have to be dealt with.

The perturbative expressions for the  $b \rightarrow u\ell\bar{\nu}$  decay is known to order  $\alpha_s^2$  <sup>1)</sup>, while the  $b \rightarrow c\ell\bar{\nu}$  decay rate is currently known to order  $\alpha_s^2\beta_0$  <sup>2)</sup>, where  $\beta_0$  is the one loop coefficient of the QCD beta function. The hadronization effects can not be calculated perturbatively and is governed by long distance physics. There are two distinct ways to extract the CKM from decays of  $B$  mesons. One can use exclusive decays to a well defined hadronic final state, such as  $D$  or  $D^*$  mesons for  $b \rightarrow c$  transitions, or  $\pi$  or  $\rho$  mesons for the measurement of  $|V_{ub}|$ . All non-perturbative physics is then encoded in the hadronic form factors. For  $D$  and  $D^*$  mesons heavy quark effective theory (HQET) <sup>3)</sup> can be used to obtain the form factor at leading order in an expansion in  $1/m_{b,c}$  at the zero recoil point <sup>4)</sup>, and because of Luke's theorem <sup>5)</sup> corrections are absent at order  $1/m_{b,c}$ . For the decay to an up quark HQET is not applicable, and the relevant form factors have to be determined using other non-perturbative methods, such as lattice QCD <sup>6)</sup> or QCD sumrules <sup>7)</sup>. Recently there has also been progress using the soft collinear effective theory <sup>8)</sup> to determine the required form factors from experiment.

An alternative approach is to use decays to inclusive final states, which include all final states containing either an up or a charm quark. Decays to such inclusive final states can be calculated using the operator product expansion (OPE), which states that at leading order in  $1/m_b$  the inclusive decay is identical to the perturbatively calculable parton level decay. Corrections are given by matrix elements of local operators, which are suppressed by powers in  $1/m_b$ . By determining enough of these matrix elements the CKM parameters  $V_{ub}$  and  $V_{cb}$  can be determined with high accuracy. I review the recent progress on inclusive determinations of  $V_{ub}$  and  $V_{cb}$  in this talk.

## 2 Inclusive determination of $V_{ub}$

The inclusive decay rate  $B \rightarrow X_u\ell\bar{\nu}$  is directly proportional to  $|V_{ub}|^2$  and can be calculated reliably and with small uncertainties using the operator product expansion (OPE). Unfortunately, the  $\sim 100$  times background from  $B \rightarrow X_c\ell\bar{\nu}$

makes the measurement of the totally inclusive rate an almost impossible task. Several cuts have been proposed in order to reject the  $b \rightarrow c$  background, however care has to be taken to ensure that the decay rate in the restricted region of phase space can still be predicted reliably theoretically. The proposed cuts are

1. Cut on the lepton energy  $E_\ell > (m_B^2 - m_D^2)/(2m_B)$
2. Cut on the hadronic invariant mass  $m_X < m_D$  <sup>9)</sup>
3. Cut on the leptonic invariant mass  $q^2 > (m_B - m_D)^2$  <sup>10)</sup>
4. Cut on light cone component of the hadronic momentum  $P_+ < m_D^2/m_B$  <sup>11)</sup>
5. Combined lepton-hadron invariant mass cut <sup>12)</sup>

While the cut on the energy of the charged lepton is easiest to implement experimentally, it has the largest theoretical uncertainties. This is due to the fact that only  $\sim 10\%$  of the  $b \rightarrow u$  events survive this cut, amplifying any higher order, uncalculated terms drastically. Thus, it is not useful for a precision determination of  $|V_{ub}|$ , although it can be used as a check for consistency.

The remaining four cuts each have their advantages and disadvantages, and it remains to be seen which will yield the individually smallest uncertainty on  $|V_{ub}|$  ultimately. To illustrate the effect of these four phase space cuts, we show the allowed phase space of the  $B \rightarrow X_u \ell \bar{\nu}$  transition, in terms of two light cone projections of the hadronic four-momentum,

$$\begin{aligned} P_+ &= n \cdot P = E - |\vec{P}| \\ P_- &= n \cdot P = E + |\vec{P}|. \end{aligned} \quad (1)$$

The projections satisfy  $P_+ P_- = P^2$  and thus it is obvious that the boundaries of phase space are

$$m_\pi^2/P_- < P_+ < P_- < m_B \quad (2)$$

The resulting phase space diagram is shown in Fig. 1. Also displayed in a rough distribution of the events obtained from a toy Monte Carlo simulation. While this distribution should not be viewed as a sound theoretical prediction, it qualitatively helps to understand the phase space better. The region of

phase space occupied by the  $b \rightarrow c$  background is given by  $P_+ P_- > m_D^2$  and is indicated by the gray area.

The region satisfying  $P_+ \ll P_-$ , denoted by the ellipse in Fig. 1, is called the shape function region. The decay rate in the presence of cuts which include this region contain higher dimensional operators contributing at order  $(P_+ \Lambda_{\text{QCD}}/P_-^2)^n$ . This fraction becomes order unity and all these terms have to be resummed to all orders into an unknown function, called the shape function [13]. This function is a universal property of the  $B$  meson, and can be measured in other  $B$  decays, such as the radiative decay  $B \rightarrow X_s \gamma$ . Note that it is not simply related to the  $b$  quark mass and the kinetic energy of the  $b$  quark as is often assumed [14]. In fact, at leading order in both  $\alpha_s$  and  $\Lambda_{\text{QCD}}/m_b$ , the shape of the photon energy spectrum is precisely given by this light cone distribution function. At order  $1/m_b$  several new subleading shape functions enter [15], which are at present completely unknown. Thus, even with perfect knowledge of the photon energy spectrum in  $B \rightarrow X_s \gamma$  the uncertainties in regions of phase space which include the shape function region of order  $\Lambda_{\text{QCD}}/m_b$ .

The regions of phase space surviving the four cuts are also illustrated in Fig. 1. On the left we show the  $m_X < m_D$  and  $P_+ < m_D^2/m_B$  cuts, which both include the shape function region, while on the right we show the  $q^2 > (m_B - m_D)^2$  and the combined hadron-lepton invariant mass cut, which do not include the shape function region. It is clear that the cut on the hadronic invariant mass  $m_X < m_D$  [9] is optimal in the sense that it keeps all events which are not accessible by  $b \rightarrow c \ell \bar{\nu}$  transitions. It has been estimated that  $\sim 80\%$  of the  $b \rightarrow u$  events survive this cut. Uncertainties from subleading shape functions are of order  $\Lambda_{\text{QCD}}/m_b$ , however they have recently been estimated to be at the few percent level [16]. Precise knowledge of the shape function is however still required to achieve an uncertainty on  $|V_{ub}|$  below the 10% level.

The situation is similar for the cut on the light cone momentum  $P_+$ , which also includes the shape function region. While this cut includes slightly less phase space, it has been argued that the relationship between the shape function and the differential rate of  $B \rightarrow X_s \gamma$  is slightly simpler for this cut than for the  $m_X$  cut described above [11]. The resulting uncertainties on  $|V_{ub}|$  are expected to be at the same order as for the  $m_X$  cut.

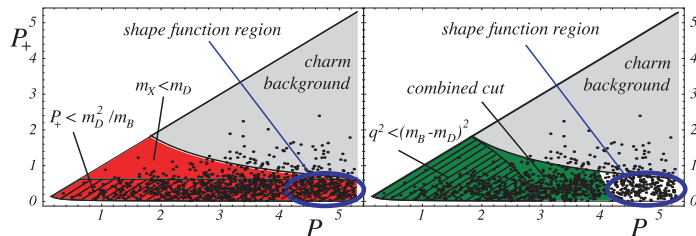


Figure 1: *The dalitz plot in the  $q^2/s_H$  and  $q^2/E_\ell$  plane. In both plots the gray area denotes the area contaminated by  $b \rightarrow c$  events. The left plot shows the  $m_X < m_D$  and  $P_+ < M_D^2/m_B$  cuts, while the right hand plot shows the  $q^2 > (m_B - m_D)^2$  and the combined  $q^2 - m_X$  cut. Also shown in both plots is the shape function region.*

The situation is qualitatively different for the remaining two cuts, which involve a cut on the leptonic invariant mass. Since a lepton invariant mass cut removes the shape function region, the decay rate in the presence of these cuts can be calculated using the standard OPE in an expansion in local operators, but the expansion is in powers of  $1/m_c$  rather than  $1/m_b$  <sup>17</sup>). For the pure  $q^2$  cut, where  $q^2 > (m_B - m_D)^2$ , the fraction of events surviving the cut is estimated to be about  $(17 \pm 3)\%$  <sup>10</sup>). This gives an uncertainty on  $|V_{ub}|$  at the 10% level.

The final cut discussed here is a combined cut on both the hadronic and the leptonic invariant mass. The idea here is to use the cut on  $m_X$  to remove the charm background, and the cut on  $q^2$  to keep the sensitivity on the shape small. The ideal combination of cuts remains to be determined in a detailed experimental study, but using the combined cuts  $m_X < m_D$  GeV,  $q^2 > 6$  GeV<sup>2</sup> one finds the fraction of surviving events to be  $(45 \pm 5)\%$  <sup>12</sup>). Since the decay rate is proportional to  $|V_{ub}|^2$ , this allows for a determination of  $|V_{ub}|$  with uncertainties well below the 10% level.

To summarize, there are currently five types of cuts to eliminate the charm background proposed in the literature. While a cut on the lepton energy is easiest to measure, it has by far the largest theoretical problems. A cut on the leptonic invariant mass alone also leads to relatively large theoretical uncertainties and will probably not yield a measurement of  $|V_{ub}|$  with uncertainties below the 10% level. The remaining three cuts all can yield a determination of this CKM matrix element with uncertainties considerably below the 10% level,

and all of them should be used together for a precision measurement of  $|V_{ub}|$ .

### 3 Inclusive determination of $V_{cb}$

Inclusive semileptonic  $B$  decays can be calculated using an operator product expansion (OPE). This leads to a simultaneous expansion in powers of the strong coupling constant  $\alpha_s(m_b)$  and inverse powers of the heavy  $b$  quark mass. At leading order in this expansion this reproduces the parton model result

$$\Gamma_0 = \frac{G_F^2 |V_{cb}|^2 m_b^5}{192\pi^3} (1 - 8\rho + 8\rho^3 - \rho^4 - 12\rho^2 \log \rho), \quad (3)$$

where  $\rho = m_c^2/m_b^2$ , and nonperturbative corrections are suppressed by at least two powers of  $m_b$ . The state of the art is to use theoretical predictions to order  $\alpha_s^2 \beta_0^{-2}$  in the perturbative expansion, to order  $\Lambda_{\text{QCD}}^3/m_b^3$  (18) in the non-perturbative power expansion and to order  $\alpha_s \Lambda_{\text{QCD}}/m_b$  in the mixed terms. Here  $\beta_0$  is the one loop coefficient of the QCD beta function  $\beta_0 = 25/3$  for  $n_f = 4$  light quark flavors. There are no non-perturbative contributions at order  $1/m_b$  and thus the inclusive rate can be written schematically as

$$\begin{aligned} \Gamma^{b \rightarrow c} = \Gamma_0 & \left\{ 1 + A \left[ \frac{\alpha_s}{\pi} \right] + B \left[ \left( \frac{\alpha_s}{\pi} \right)^2 \beta_0 \right] + 0 \left[ \frac{\Lambda}{m_b} \right] + C \left[ \frac{\Lambda^2}{m_b^2} \right] \right. \\ & \left. + D \left[ \frac{\Lambda^3}{m_b^3} \right] + E \left[ \frac{\alpha_s}{\pi} \frac{\Lambda}{m_b} \right] + \mathcal{O} \left( \alpha_s^2, \frac{\Lambda^4}{m_b^4}, \alpha_s \frac{\Lambda^2}{m_b^2} \right) \right\}, \quad (4) \end{aligned}$$

The coefficients  $A - E$  depend on the quark masses  $m_{(c,b)}$ . At order  $\Lambda_{\text{QCD}}^2/m_b^2$  there are two matrix elements ( $\lambda_{1,2}$ ) parametrizing the non-perturbative physics, while at order  $\Lambda_{\text{QCD}}^3/m_b^3$  there are six additional matrix elements ( $\rho_{1,2}, \mathcal{T}_{1-4}$ ).

The total inclusive branching fraction for  $B$  decays is currently measured with uncertainties around 2%. To predict this branching ratio with comparable precision requires detailed knowledge of the value of the matrix elements  $\lambda_{1,2}$  and even some rough knowledge of the matrix elements at order  $\Lambda_{\text{QCD}}^3/m_b^3$ . The best way to determine these parameters is to use the semileptonic data itself. Many differential decay spectra have been measured, and moments of these spectra have been calculated to the same accuracy as the total branching ratio itself (19). A global fit to all experimental data is able to test how well the OPE is able to describe the inclusive observables (20).

The mass of the  $b$ -quark which naturally appears in the OPE calculations is the pole mass. It has been long known that using these pole masses gives rise to a poorly behaved perturbative expansion, due to the presence of a renormalon. There are several threshold mass definitions, which do not contain a renormalon, called  $1S$  mass <sup>21)</sup> PS mass <sup>22)</sup>, and kinetic mass <sup>23)</sup>.

The  $c$  quark can be treated as a heavy quark. This allows one to compute the  $D^{(*)}$  meson masses as an expansion in powers of  $\Lambda_{\text{QCD}}/m_c$ . The observed  $B-D$  mass splitting can be used to determine  $m_b - m_c$ . Since the computations are performed to  $\Lambda_{\text{QCD}}^3/m_c^3$ , this introduces errors of fractional order  $\Lambda_{\text{QCD}}^4/m_c^4$  in  $m_c$ , which gives fractional errors of order  $\Lambda_{\text{QCD}}^4/(m_b^2 m_c^2)$  in the inclusive  $B$  decay rates, since charm mass effects first enter at order  $m_c^2/m_b^2$ . This is the procedure used in Ref. <sup>20)</sup>. An alternative approach is to avoid using the  $1/m_c$  expansion for the charm quark <sup>24)</sup>. In this case heavy quark effective theory (HQET) can no longer be used for the  $c$  quark system, and there are no constraints on  $m_c$  from the  $D$  and  $D^*$  meson masses. At the same time, it is not necessary to expand heavy meson states in an expansion in  $1/m_{b,c}$ , so that the time-ordered products  $\mathcal{T}_{1-4}$  can be dropped. The number of parameters is the same whether or not one expands in  $1/m_c$ .

Currently, there are 75 pieces of data available combining moments of the hadronic invariant mass spectrum and the lepton energy spectrum of inclusive measured of semileptonic decays and the photon energy spectrum in  $B \rightarrow X_s \gamma$  by BABAR <sup>26)</sup>, BELLE <sup>27)</sup>, CDF <sup>28)</sup>, CLEO <sup>29)</sup> and DELPHI <sup>30)</sup> together with moments of the photon energy spectrum in  $B \rightarrow X_s \gamma$  measured by BABAR, BELLE and CLEO. These observables can all be predicted using the same OPE and have been calculated in all of the mass schemes discussed above and depend on 7 parameters. A global fit to all these 75 observables was performed in <sup>25)</sup>. This allowed to extract the value of  $|V_{cb}|$  simultaneously with the non-perturbative parameters of the OPE. It was shown that all schemes give consistent values for  $|V_{cb}|$ ,  $m_b$  and the matrix elements appearing at order  $1/m_b^2$ . In Table 1 we show the results of the fits in the  $1S$  and the kinetic scheme. One can see that the two schemes give consistent results, with the uncertainties in the  $1S$  scheme being slightly smaller than the ones in the kinetic scheme.

Table 1: *Fit results for  $|V_{cb}|$ ,  $m_b$  and  $\lambda_1$  in the  $1S$  and  $kin$  schemes, where  $m_c$  is obtained from the  $B - D$  mass splitting.*

Scheme	$ V_{cb}  \times 10^3$	$m_b^{1S}$ [GeV]	$\lambda_1$ [GeV <sup>2</sup> ]
$1S_{\text{exp}}$	$42.1 \pm 0.6$	$4.68 \pm 0.04$	$-0.23 \pm 0.06$
$kin_{\text{exp}}$	$42.2 \pm 0.4 \pm 0.4$	$4.67 \pm 0.04 \pm 0.02$	$-0.17 \pm 0.06 \pm 0.06$

#### 4 Conclusions

In this talk I reviewed the current status of determining the magnitude of the CKM matrix elements  $|V_{ub}|$  and  $|V_{cb}|$  from inclusive semileptonic  $B$  meson decays. For  $B \rightarrow X_c \ell \bar{\nu}$ , the operator product expansion has been calculated to order  $1/m_b^3$ , with a total of 6 parameters in addition to  $|V_{cb}|$  appearing at that order. These 6 parameters can be determined in a fit to precision measurements of inclusive decay spectra and one finds  $|V_{cb}| = (42.1 \pm 0.6) \times 10^{-3}$ . Also obtained in the fit is the value of the  $b$ -quark mass and the parameter  $\lambda_1$ , which are shown in Table 1.

To measure  $|V_{ub}|$  from the inclusive decay  $B \rightarrow X_u \ell \bar{\nu}$  one has to deal with the large background from  $b \rightarrow c$  transitions. Imposing kinematic cuts to suppress this background tends to destroy the convergence of the OPE. Several cuts have been presented which allow to suppress this background experimentally, and in the future it should be possible to determine the value of  $|V_{ub}|$  with uncertainties well below the 10% level.

#### 5 Acknowledgements

I would like to thank the organizers for organizing such a wonderful meeting in such a wonderful location. This work was supported by the Department of Energy under grant DE-FG03-92-ER-40701.

#### References

1. Y. Nir, Phys. Lett. B **221**, 184 (1989). T. van Ritbergen, Phys. Lett. B **454**, 353 (1999)
2. M. Jezabek and J. H. Kuhn, Nucl. Phys. B **314**, 1 (1989); M. E. Luke, M. J. Savage and M. B. Wise, Phys. Lett. B **345**, 301 (1995).

3. A. V. Manohar and M. B. Wise, Cambridge Monogr. Part. Phys. Nucl. Phys. Cosmol. **10**, 1 (2000).
4. N. Isgur and M. B. Wise, Phys. Lett. B **232**, 113 (1989); Phys. Lett. B **237**, 527 (1990); E. Eichten and B. Hill, Phys. Lett. B **234**, 511 (1990). H. Georgi, Phys. Lett. B **240**, 447 (1990).
5. M. E. Luke, Phys. Lett. B **252**, 447 (1990).
6. For a recent review of heavy quarks on the lattice see: S. Hashimoto and T. Onogi, arXiv:hep-ph/0407221.
7. P. Ball, JHEP **9809**, 005 (1998); P. Ball and R. Zwicky, arXiv:hep-ph/0406232.
8. C. W. Bauer, S. Fleming and M. E. Luke, Phys. Rev. D **63**, 014006 (2001); C. W. Bauer, S. Fleming, D. Pirjol and I. W. Stewart, Phys. Rev. D **63**, 114020 (2001); C. W. Bauer and I. W. Stewart, Phys. Lett. B **516**, 134 (2001); Phys. Rev. D **65**, 054022 (2002).
9. Phys. Lett. B **406**, 225 (1997); I. I. Y. Bigi, R. D. Dikeman and N. Uraltsev, Eur. Phys. J. C **4**, 453 (1998).
10. C. W. Bauer, Z. Ligeti and M. E. Luke, Phys. Lett. B **479**, 395 (2000).
11. S. W. Bosch, B. O. Lange, M. Neubert and G. Paz, arXiv:hep-ph/0403223.
12. C. W. Bauer, Z. Ligeti and M. E. Luke, Phys. Rev. D **64**, 113004 (2001).
13. M. Neubert, Phys. Rev. D **49**, 3392 (1994); Phys. Rev. D **49**, 4623 (1994).
14. C. W. Bauer and A. V. Manohar, arXiv:hep-ph/0312109.
15. C. W. Bauer, M. E. Luke and T. Mannel, Phys. Rev. D **68**, 094001 (2003); Phys. Lett. B **543**, 261 (2002); A. K. Leibovich, Z. Ligeti and M. B. Wise, Phys. Lett. B **539**, 242 (2002).
16. C. N. Burrell, M. E. Luke and A. R. Williamson, Phys. Rev. D **69**, 074015 (2004).
17. M. Neubert and T. Becher, Phys. Lett. B **535**, 127 (2002).

18. M. Gremm and A. Kapustin, Phys. Rev. D **55**, 6924 (1997) [arXiv:hep-ph/9603448].
19. A. F. Falk, M. E. Luke and M. J. Savage, Phys. Rev. D **53**, 2491 (1996); M. Gremm, A. Kapustin, Z. Ligeti and M. B. Wise, Phys. Rev. Lett. **77**, 20 (1996); A. F. Falk and M. E. Luke, Phys. Rev. D **57**, 424 (1998); M. Gremm and A. Kapustin, Phys. Rev. D **55** (1997) 6924. C. Bauer, Phys. Rev. D **57**, 5611 (1998) [Erratum-ibid. D **60**, 099907 (1998)]; C. W. Bauer and C. N. Burrell, Phys. Lett. B **469**, 248 (1999). Phys. Rev. D **62** (2000) 114028;
20. C. W. Bauer, Z. Ligeti, M. Luke and A. V. Manohar, Phys. Rev. D **67**, 054012 (2003).
21. A. H. Hoang, Z. Ligeti and A. V. Manohar, Phys. Rev. Lett. **82**, 277 (1999); Phys. Rev. D **59**, 074017 (1999).
22. M. Beneke, Phys. Lett. B **434**, 115 (1998).
23. I. I. Y. Bigi *et al.*, Phys. Rev. D **52**, 196 (1995).
24. P. Gambino and N. Uraltsev, Eur. Phys. J. C **34**, 181 (2004) [arXiv:hep-ph/0401063].
25. C. W. Bauer, Z. Ligeti, M. Luke, A. V. Manohar and M. Trott, arXiv:hep-ph/0408002.
26. B. Aubert *et al.* [BABAR Collaboration], Phys. Rev. D **69**, 111103 (2004); 111104 (2004); arXiv:hep-ex/0207074.
27. P. Koppenburg *et al.* [Belle Collaboration], arXiv:hep-ex/0403004.
28. CDF Collaboration, CDF note 6973, available at:  
<http://www-cdf.fnal.gov/physics/new/bottom/040428.blessed-bhad>
29. S. Chen *et al.*, Phys. Rev. Lett. **87**, 251807 (2001); S. E. Csorna *et al.*, arXiv:hep-ex/0403052; A. H. Mahmood *et al.*, arXiv:hep-ex/0403053.
30. DELPHI Collaboration, DELPHI note: 2003-028-CONF-648,  
<http://delphiwww.cern.ch/pubxx/conferences/summer03/PapNo046.ht>

Frascati Physics Series Vol. XXXV (2004), pp. 231-239  
HEAVY QUARKS AND LEPTONS - San Juan, Puerto Rico, June 1-5, 2004

## MEASUREMENT OF $|V_{cb}|$ AND HQE PARAMETERS FROM SEMILEPTONIC B DECAYS

Dominique Fortin

*Department of Physics and Astronomy, University of Victoria, BC, Canada.*

### ABSTRACT

Measurements of the CKM matrix element  $|V_{cb}|$  are performed using semileptonic B decays recorded with the BaBar detector. These decays are primarily identified by the presence of a high momentum lepton. Several measurements of the hadronic mass and lepton energy moments are then performed as a function of the minimum allowed lepton energy  $E_{\text{cut}}$ . Combining these measurements into the HQE kinetic-mass scheme allows for the simultaneous determination of the inclusive semileptonic branching ratio  $\mathcal{B}(B \rightarrow X_c \ell \nu)$ ,  $|V_{cb}|$ , the b- and c-quark masses, and the HQE parameters.

### 1 Introduction

The element  $|V_{cb}|$  of the CKM matrix is a fundamental parameter of the Standard Model and, as such, a precise measurement of  $|V_{cb}|$  is important. The

weak decay rate for  $B \rightarrow X_c \ell \nu$  may be calculated accurately at the parton level; it is proportional to  $|V_{cb}|^2$  and also depends on the charm and bottom quark masses. In order to extract  $|V_{cb}|$  from the measurements of the semileptonic  $B$ -meson decay rate, corrections to the parton-level calculations must be applied to encompass the effects of strong interactions. Heavy-Quark Expansions (HQEs) <sup>1)</sup> have become a useful tool for calculating perturbative and non-perturbative QCD corrections <sup>2)</sup>, and for estimating their uncertainties. For instance, in the kinetic-mass scheme <sup>3)</sup>, expansions in terms of  $1/m_b$  and  $\alpha_s(m_b)$  to order  $\mathcal{O}(1/m_b^3)$  contain six parameters: the running kinetic masses of the b- and c-quarks,  $m_b(\mu)$  and  $m_c(\mu)$ , and four non-perturbative parameters. These parameters may be determined simultaneously from a fit to the moments of the hadronic-mass and electron-energy distributions from semileptonic  $B$  decays to charm particles. This fit yields significantly improved measurements of the inclusive branching fraction  $B \rightarrow X_c \ell \nu$  and of  $|V_{cb}|$  <sup>4)</sup>. It also allows to test the consistency of the data with the HQEs employed and to check for the possible impact of higher-order contributions. In my presentation, I limited myself to the results obtained by the BaBar experiment <sup>5)</sup>, and summarize these below. New models <sup>6; 7; 8)</sup> have recently become available and are currently under study.

## 2 Moments and fitting technique

The results I presented were based on moment measurements described in <sup>9; 10)</sup> These moments were derived from the inclusive hadronic-mass ( $M_X$ ) and electron energy ( $E_\ell$ ) distributions in  $B \rightarrow X_c \ell \nu$  decays produced at the  $\Upsilon(4S)$  resonance, and averaged over charged and neutral  $B$ . In the case of energy moments, only electrons were used, whereas muons were also used for the mass moments.

The electron-energy distribution was measured in events tagged by a high-momentum electron from the second  $B$  meson. To differentiate between primary and secondary decay electrons, the data were divided into unlike- and like-sign samples,  $Q(e_{\text{tag}}) = \mp Q(e_{\text{sig}})$ , respectively. Primary signal electrons made up most of the unlike-sign sample. Background electrons originating from the same  $B$  meson as the tagged electron usually have opposite charge and direction; they were suppressed by applying a cut on the opening angle between the two electrons. Further backgrounds from  $J/\Psi \rightarrow e^+e^-$  were re-

moved by applying a veto on the invariant mass  $M_{e\bar{e}}$  of the tagged electron for the interval  $2.9 < M_{e\bar{e}} < 3.15 \text{ GeV}/c^2$ . Like-sign electrons are mostly produced in secondary decays. Energy spectra for electrons produced via photon conversion and Dalitz decays were extracted from data studies, whereas spectra for cascade  $b \rightarrow c\tau\nu$  and  $b \rightarrow c\bar{c}s$  electrons were estimated from Monte Carlo simulations. Continuum backgrounds, which contribute to both like- and unlike-sign samples, were subtracted out by scaling the off-resonance yields to on-resonance luminosity and energy.

The hadronic-mass distribution was measured in events tagged by the fully reconstructed hadronic decay of the second  $B$  meson, which allowed for a knowledge of the  $B$  flavour and momentum  $\mathbf{p}_B$ . The kinematic consistency of the  $B_{\text{reco}}$  candidates was checked by computing the beam-energy-substituted mass  $m_{ES} = \sqrt{s/4 - \mathbf{p}_B^2}$ . Combinatorial backgrounds were subtracted out from a fit to the  $m_{ES}$  distribution using an empirical function <sup>11)</sup> describing the combinatorial background from both continuum and  $B\bar{B}$  events and a narrow signal function <sup>12)</sup> peaked at the  $B$ -meson mass. Further requirements were applied on the recoil  $B$ : the lepton charge needed to be consistent with the  $B_{\text{recoil}}$  flavour, and the measured missing energy and momentum had to be consistent with a neutrino. The extracted hadronic mass of the meson was then corrected for detector resolution and efficiency losses on an event-by-event basis using the linear relationships observed between the measured and generated  $M_X$  values in Monte Carlo simulations. To verify this procedure, the calibration was applied to measured masses for exclusive final states in simulated  $\bar{B} \rightarrow X_c \ell \bar{\nu}$  decays and the resulting calibrated mass was compared to the true one. No significant mass bias was observed after calibration for the full mass range. The procedure was also validated on a data sample of partially reconstructed  $D^{*+} \rightarrow D^0 \pi^+$  decays.

All moments were measured as functions of  $E_{\text{cut}}$ , a lower limit on the lepton energy, and were corrected for detector effects and QED radiation <sup>13)</sup>. Charmless contributions were subtracted out based on the branching fraction  $B \rightarrow X_u \ell \nu = (0.22 \pm 0.05)\%$  <sup>14)</sup>. The first electron energy moment, defined as  $M_1^\ell(E_{\text{cut}}) = \langle E_\ell \rangle_{E_\ell > E_{\text{cut}}}$ , and the second and third moments, defined as  $M_n^\ell(E_{\text{cut}}) = \langle (E_\ell - M_1^\ell(E_{\text{cut}}))^n \rangle_{E_\ell > E_{\text{cut}}}$  with  $n=2,3$ , were measured. In addition, the partial branching fraction  $M_0^\ell(E_{\text{cut}}) = \int_{E_{\text{cut}}}^{E_{\text{max}}} (d\mathcal{B}_{c\ell\nu}/dE_\ell) dE_\ell$  was also obtained. The hadronic-mass moments  $M_n^X(E_{\text{cut}}) = \langle m_X^n \rangle_{E_\ell > E_{\text{cut}}}$  were

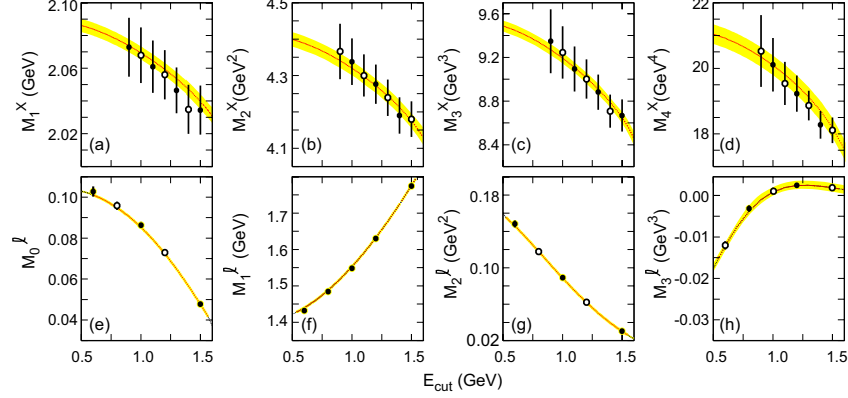


Figure 1: The measured hadronic-mass (a-d) and electron-energy (e-h) moments as a function of the cut-off energy,  $E_{cut}$ , compared with the result of the simultaneous fit (line), with the theoretical uncertainties<sup>16)</sup> indicated as shaded bands. The solid data points mark the measurements included in the fit. The vertical bars indicate the experimental errors. Moment measurements for different  $E_{cut}$  are highly correlated.

measured for  $n = 1, 2, 3, 4$ . The measured electron-energy and hadronic-mass moments as a function of  $E_{cut}$  are shown in Fig. 1.

In the kinetic-mass scheme the HQE to  $\mathcal{O}(1/m_b^3)$  for the rate of  $B \rightarrow X_c \ell \nu$  decays can be expressed as<sup>15)</sup>

$$\Gamma_{c\ell\nu} = \frac{G_F^2 m_b^5}{192\pi^3} |V_{cb}|^2 (1 + A_{ew}) A_{pert}(r, \mu) \times \left[ z_0(r) \left( 1 - \frac{\mu_\pi^2 - \mu_G^2 + \frac{\rho_D^3 + \rho_{LS}^3}{m_b}}{2m_b^2} \right) - 2(1-r)^4 \frac{\mu_G^2 + \frac{\rho_D^3 + \rho_{LS}^3}{m_b}}{m_b^2} + d(r) \frac{\rho_D^3}{m_b^3} + \mathcal{O}(1/m_b^4) \right]. \quad (1)$$

The leading non-perturbative effects arise at  $\mathcal{O}(1/m_b^2)$  and are parameterized by  $\mu_\pi^2(\mu)$  and  $\mu_G^2(\mu)$ , the expectation values of the kinetic and chromomagnetic dimension-five operators. At  $\mathcal{O}(1/m_b^3)$ , two additional parameters enter,  $\rho_D^3(\mu)$  and  $\rho_{LS}^3(\mu)$ , the expectation values of the Darwin ( $D$ ) and spin-orbit

( $LS$ ) dimension-six operators. These parameters depend on the scale  $\mu^1$  that separates short-distance from long-distance QCD effects. Electroweak corrections are  $1 + A_{ew} \approx 1.014$ , and perturbative QCD corrections are estimated to be  $A_{pert}(r, \mu) \cong 0.91 \pm 0.01$  <sup>15)</sup>. Linearized expressions for the HQEs <sup>16)</sup> were then substituted into equation 1.

HQEs in terms of the same heavy-quark parameters are available for the hadronic-mass and electron-energy moments. The dependence on the heavy-quark parameters was again linearized using the same *a priori* estimates of the parameters <sup>15, 16)</sup>. The differences between the linearized expressions and the full theoretical calculation were shown to be small in all cases. These linear equations allowed for the determination of the unknown heavy-quark parameters, the total branching fraction  $\mathcal{B}(B \rightarrow X_c \ell \nu)$ , and  $|V_{cb}|$  from a simultaneous  $\chi^2$  fit to the measured moments and the partial branching fraction, all as a function of the cut-off lepton energy,  $E_{cut}$ .

In total, four hadronic-mass moments for each of seven different values of  $E_{cut}$ , ranging from 0.9 to 1.5 GeV, and three electron-energy moments plus the partial branching fraction at five values of  $E_{cut}$ , ranging from 0.6 to 1.5 GeV, were available <sup>9, 10)</sup>. Many of these individual moments were highly correlated such that a set of moments for which the correlation coefficients do not exceed 95% was chosen. As a result, only half of the 28 mass moments and 13 of the 20 energy moments were kept for the fit.

### 3 Results

The global fit took into account the statistical and systematic errors and correlations of the individual measurements, as well as the uncertainties of the expressions for the individual moments. As suggested in <sup>16)</sup>, the uncertainty of the calculated moments was assessed by varying in the linearized expressions the *a priori* estimates for  $\mu_\pi^2$  and  $\mu_G^2$  by  $\pm 20\%$  and for  $\rho_{LS}^3$  and  $\rho_D^3$  by  $\pm 30\%$ . For a given moment, these changes were assumed to be fully correlated for all values of  $E_{cut}$ , but uncorrelated for different moments. The resulting fit, shown in fig. 1, describes the data well with  $\chi^2 = 15.0$  for 20 degrees of freedom. Table 1 lists the fitted parameters and their errors. Note that for the mass difference, BaBar obtained  $m_b - m_c = (3.436 \pm 0.025_{exp} \pm 0.018_{HQE} \pm 0.010_{\alpha_s})$  GeV.

<sup>1</sup>Calculations are performed for  $\mu = 1$  GeV <sup>3)</sup>.

Table 1: *Fit results and error contributions from the moment measurements, approximations to the HQEs, and additional theoretical uncertainties from  $\alpha_s$  terms and other perturbative and non-perturbative terms contributing to  $\Gamma_{c\ell\nu}$ .*

Parameter	Result	$\delta_{exp}$	$\delta_{HQE}$	$\delta_{\alpha_s}$	$\delta_{\Gamma}$
$ V_{cb} $ ( $10^{-3}$ )	41.390	0.437	0.398	0.150	0.620
$m_b$ (GeV)	4.611	0.052	0.041	0.015	
$m_c$ (GeV)	1.175	0.072	0.056	0.015	
$\mu_\pi^2$ ( $\text{GeV}^2$ )	0.447	0.035	0.038	0.010	
$\rho_D^3$ ( $\text{GeV}^3$ )	0.195	0.023	0.018	0.004	
$\mu_G^2$ ( $\text{GeV}^2$ )	0.267	0.055	0.033	0.018	
$\rho_{LS}^3$ ( $\text{GeV}^3$ )	-0.085	0.038	0.072	0.010	
$\mathcal{B}(B \rightarrow X_c \ell \nu)$ (%)	10.611	0.163	0.063	0.000	

Beyond the uncertainties that are included in the fit, the limited knowledge of the expression for the decay rate, including various perturbative corrections and higher-order non-perturbative corrections, introduces an error in  $|V_{cb}|$ , assessed to be 1.5%<sup>15)</sup>. On the other hand, the uncertainty in  $\alpha_s$  is estimated to have a relatively small effect.

The fit results are fully compatible with independent estimates<sup>16)</sup> of  $\mu_G^2 = (0.35 \pm 0.07) \text{ GeV}^2$ , based on the  $B^* - B$  mass splitting, and of  $\rho_{LS}^3 = (-0.15 \pm 0.10) \text{ GeV}^3$ , from heavy-quark sum rules<sup>17)</sup>. Figure 2 shows the  $\Delta\chi^2 = 1$  ellipses for  $|V_{cb}|$  versus  $m_b$  and  $\mu_\pi^2$ ; for a fit to all moments and separate fits to the electron-energy moments and the hadronic-mass moments, but including the partial branching fractions in both. The lepton-energy and hadronic-mass moments have slightly different sensitivity to the fit parameters, but the results for the separate fits are fully compatible with each other and with the global fit to all moments. Since the expansions for the two sets of moments are sensitive to different theoretical uncertainties and assumptions, in particular the differences in the treatment of the perturbative corrections, the observed consistency of the separate fits indicates that such differences are small compared with the experimental and assumed theoretical uncertainties.

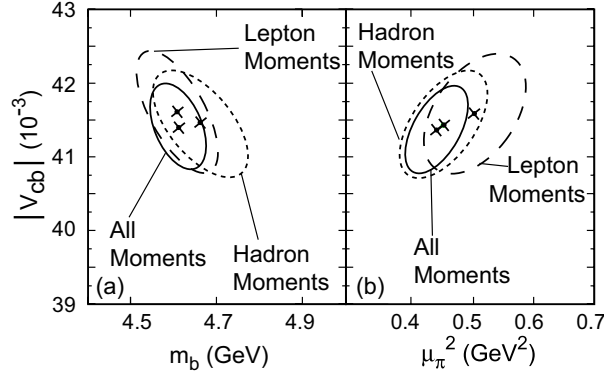


Figure 2: Fit results (crosses) with contours corresponding to  $\Delta\chi^2 = 1$  for two pairs of the eight free parameters a)  $m_b$  and b)  $\mu_\pi^2$  versus  $|V_{cb}|$ , separately for fits using the hadronic-mass, the electron-energy, and all moments.

#### 4 Conclusion

BaBar extracted  $|V_{cb}|$ , the semileptonic branching fraction, and the heavy-quark masses,

$$\begin{aligned}
 |V_{cb}| &= (41.4 \pm 0.4_{exp} \pm 0.4_{HQE} \pm 0.6_{th}) \times 10^{-3}, \\
 \mathcal{B}_{ce\nu} &= (10.61 \pm 0.16_{exp} \pm 0.06_{HQE})\%, \\
 m_b(1 \text{ GeV}) &= (4.61 \pm 0.05_{exp} \pm 0.04_{HQE} \pm 0.02_{th}) \text{ GeV}, \\
 m_c(1 \text{ GeV}) &= (1.18 \pm 0.07_{exp} \pm 0.06_{HQE} \pm 0.02_{th}) \text{ GeV},
 \end{aligned}$$

as well as the non-perturbative parameters in the kinetic-mass scheme up to order  $(1/m_b^3)$ .

Based on a large set of hadronic-mass and electron-energy moments and a consistent set of HQE calculations, uncertainties in the  $\mathcal{O}(1/m_b^3)$  terms were determined from the data without constraints to any *a priori* values. The fitted values of the parameters appear to be consistent with theoretical estimates (3, 15), and the uncertainties on the quark masses are much smaller than those of previous measurements (18). Finally, the result on  $|V_{cb}|$  is in agreement with previous measurements using HQEs, either for a different mass scheme and with fixed terms of  $\mathcal{O}(1/m_b^3)$  (7), or for the kinetic-mass scheme,

but with external constraints on almost all HQE parameters <sup>8)</sup>, as well as with an analysis combining both of these measurements <sup>6)</sup>.

### References

1. M. Voloshin and M. Shifman, *Sov. J. Nucl. Phys.* **41**, 120 (1985); J. Chay, H. Georgi, and B. Grinstein, *Phys. Lett.* **B247**, 399 (1990); I. I. Bigi, and N. Uraltsev, *Phys. Lett.* **B280**, 271 (1992).
2. I. I. Bigi, N. Uraltsev, and A. I. Vainshtein, *Phys. Lett.* **B293**, 430 (1992); I. I. Bigi, M. Shifman, N. Uraltsev, and A. Vainshtein, *Phys. Rev. Lett.* **71**, 496 (1993); B. Blok, L. Koyrakh, M. Shifman, and A. Vainshtein, *Phys. Rev.* **D49**, 3356 (1994); A. V. Manohar and M. B. Wise, *Phys. Rev.* **D49**, 1310 (1994); M. Gremm and A. Kapustin, *Phys. Rev.* **D55**, 6924 (1997).
3. I. I. Bigi, M. Shifman, N. Uraltsev, and A. Vainshtein, *Phys. Rev.* **D56**, 4017 (1997).
4. B. Aubert *et al.* [BaBar Collaboration], *Phys. Rev.* **D67**, 031101 (2003).
5. B. Aubert *et al.* [BaBar Collaboration], *Phys. Rev. Lett.* **93**, 011803 (2004).
6. C. W. Bauer, Z. Ligeti, M. Luke and A. V. Manohar *Phys. Rev.* **D67**, 054012 (2003).
7. A. H. Mahmood *et al.* [CLEO Collaboration], *Phys. Rev.* **D67**, 072001 (2003) .
8. M. Battaglia *et al.* [DELPHI Collaboration], *Phys. Lett.* **B556**, 41 (2003).
9. B. Aubert *et al.* [BaBar Collaboration], *Phys. Rev. D* **69**, 111104 (2004).
10. B. Aubert *et al.* [BaBar Collaboration], *Phys. Rev. D* **69**, 111103 (2004).
11. H. Albrecht *et al.* [ARGUS Collaboration], *Phys. Lett.* **B185**, 218 (1987).
12. T. Skwatnicki *et al.* [Crystal Ball Collaboration], DESY F31-86-02 (1986).
13. E. Barbiero and Z. Was, *Comput. Phys. Comm.* **79**, 291 (1994).
14. B. Aubert *et al.* [BaBar Collaboration], *Phys. Rev. Lett.* **92**, 071802 (2004).

- 
15. D. Benson, I. I. Bigi, T. Mannel, and N. Uraltsev, Nucl. Phys. **B665**, 367 (2003).
  16. P. Gambino and N. Uraltsev, *Moments of Semileptonic B Decay Distributions in the  $1/m_b$  Expansion*, hep-ph/0401063, to be published in Eur. Phys. J. C (2004).
  17. I. I. Bigi, M. A. Shifman, and N. G. Uraltsev, Ann. Rev. Nucl. Part. Sci., **47**, 591 (1997).
  18. K. Hagiwara *et al.* Phys. Rev. **D66**, 010001 (2002).



Frascati Physics Series Vol. XXXV (2004), pp. 241  
HEAVY QUARKS AND LEPTONS - San Juan, Puerto Rico, June 1-5, 2004

**NEW METHODS FOR  $|V_{ub}|$  DETERMINATION**

C. Schwanda  
*University of Vienna, Vienna, Austria*

Written contribution not received



Frascati Physics Series Vol. XXXV (2004), pp.243  
HEAVY QUARKS AND LEPTONS - San Juan, Puerto Rico, June 1-5, 2004

**SPECTRAL MOMENTS FROM B DECAYS AT CLEO**

C. Stepaniak

*University of Minnesota, 16 Church Street S.E., Minneapolis, Minnesota 55455, USA*

Written contribution not received



## ***SESSION VI – CKM Matrix Elements from K Decays***

P. Talavera	Extraction of CKM Parameters - K Decays
A. Antonelli	$V_{us}$ From $K_0$ Semileptonic Decays at KLOE
K. Kleinknecht	Mesurement of the Branching Ratio of the Decay $K_L \rightarrow \pi^\pm e^\mp$ and the Coupling Constant $V_{us}$
A. Sher	Mesurement of the $K^+ \rightarrow \pi^0 e^+ \nu (K_{e3}^+)$ Branching Ratio by E865 at Brookhaven National Laboratory
R. Kessler	KTeV Determination of the CKM Parameter $ V_{us} $



Frascati Physics Series Vol. XXXV (2004), pp. 247  
HEAVY QUARKS AND LEPTONS - San Juan, Puerto Rico, June 1-5, 2004

## **EXTRACTION OF CKM PARAMETERS - K DECAYS**

P. Talavera

*Universitat Politècnica de Catalunya, C/Jordi Girona, 31, 08034 Barcelona*

Written contribution not received



## $V_{us}$ FROM $K^0$ SEMILEPTONIC DECAYS AT KLOE

The KLOE Collaboration \*  
presented by A. Antonelli

*Laboratori Nazionali di Frascati dell'INFN, Frascati (Italy)*

---

\*The KLOE collaboration: A. Aloisio, F. Ambrosino, A. Antonelli, M. Antonelli, C. Bacci, G. Bencivenni, S. Bertolucci, C. Bini, C. Bloise, V. Bocci, F. Bossi, P. Branchini, S. A. Bulychjov, R. Caloi, P. Campana, G. Capon, T. Capussela, G. Carboni, F. Ceradini, F. Cervelli, F. Cevenini, G. Chiefari, P. Ciambrone, S. Conetti, E. De Lucia, A. De Santis, P. De Simone, G. De Zorzi, S. Dell'Agello, A. Denig, A. Di Domenico, C. Di Donato, S. Di Falco, B. Di Micco, A. Doria, M. Dreucci, O. Erriquez, A. Farilla, G. Felici, A. Ferrari, M. L. Ferrer, G. Finocchiaro, C. Forti, P. Franzini, C. Gatti, P. Gauzzi, S. Giovannella, E. Gorini, E. Graziani, M. Incagli, W. Kluge, V. Kulikov, F. Lacava, G. Lanfranchi, J. Lee-Franzini, D. Leone, F. Lu, M. Martemianov, M. Martini, M. Matsyuk, W. Mei, L. Merola, R. Messi, S. Miscetti, M. Moulson, S. Müller, F. Murtas, M. Napolitano, F. Nguyen, M. Palutan, E. Pasqualucci, L. Passalacqua, A. Passeri, V. Patera, F. Perfetto, E. Petrolo, L. Pontecorvo, M. Primavera, P. Santangelo, E. Santovetti, G. Saracino, R. D. Schamberger, B. Sciascia, A. Sciubba, F. Scuri, I. Sfiligoi, A. Sibidanov, T. Spadaro, E. Spiriti, M. Tabidze, M. Testa, L. Tortora, P. Valente, B. Valeriani, G. Venanzoni,

## ABSTRACT

We present a preliminary measurement of the branching ratios for the two charge modes of the decay  $K_S \rightarrow \pi e \nu$  performed using the KLOE detector.  $K_S$ -mesons are produced in the reaction  $e^+e^- \rightarrow \phi \rightarrow K_S K_L$  at the DAΦNE collider. In a sample of  $\sim 1.5 \times 10^8$   $K_S$ -tagged events we find  $22700 \pm 200$  semileptonic  $K_S$  decays. Normalizing to the  $K_S \rightarrow \pi^+ \pi^-$  count in the same data sample, we obtain  $\text{BR}(K_S \rightarrow \pi^- e^+ \nu) = (3.54 \pm 0.05_{\text{stat}} \pm 0.05_{\text{syst}}) \times 10^{-4}$  and  $\text{BR}(K_S \rightarrow \pi^+ e^- \bar{\nu}) = (3.54 \pm 0.05_{\text{stat}} \pm 0.04_{\text{syst}}) \times 10^{-4}$ . The total branching ratio is  $\text{BR}(K_S \rightarrow \pi e \nu) = (7.09 \pm 0.07_{\text{stat}} \pm 0.08_{\text{syst}}) \times 10^{-4}$ . Each BR is inclusive of radiative photons in the final state. The  $V_{\text{us}}$  value extracted from the measurement of the  $K_S \rightarrow \pi e \nu$  branching ratio and lifetime is  $V_{\text{us}} = 0.2245 \pm 0.0026$ . We measure for the first time the charge asymmetry  $A_S = (-2 \pm 9_{\text{stat}} \pm 6_{\text{syst}}) \times 10^{-3}$ .

## 1 Introduction

The measurement of the kaon semileptonic decay widths allow us to test many fundamental aspects of the Standard Model.

The most precise test of unitarity of the CKM matrix comes from its first row:  $1 - \Delta \simeq |V_{\text{ud}}|^2 + |V_{\text{us}}|^2$ . Using  $|V_{\text{ud}}|$  as extracted from nuclear beta decays, and  $|V_{\text{us}}|$  as extracted from the semileptonic decay width of the  $K_L$ , a precision test on  $\Delta$  with a precision of few parts per mil can be performed. We are able to test if  $\Delta$  is zero with a comparable precision, extracting  $V_{\text{us}}$  from the measurement of  $K_S$  semileptonic decay width. Finally, discrete symmetries are tested through the measurement of the charge asymmetries for  $K_L$  and  $K_S$  decays,  $A_{L,S}$ , defined as

$$A_{L,S} = \frac{\Gamma(K_{L,S} \rightarrow \pi^- e^+ \nu) - \Gamma(K_{L,S} \rightarrow \pi^+ e^- \bar{\nu})}{\Gamma(K_{L,S} \rightarrow \pi^- e^+ \nu) + \Gamma(K_{L,S} \rightarrow \pi^+ e^- \bar{\nu})}$$

If  $CPT$  symmetry is assumed, each of the two charge asymmetries are expected to be equal to  $2 \times \text{Re}(\epsilon) \simeq 3 \times 10^{-3}$ , where  $\epsilon$  is the parameter describing  $CP$  violation in the  $K^0 - \bar{K}^0$  mass matrix. A difference between  $A_S$  and  $A_L$  signals  $CPT$  violation either in the mass matrix, or in the decay amplitudes. The value of  $A_L$  is known at present with a precision of  $10^{-4}$  <sup>1, 2)</sup>, while  $A_S$  has never yet been measured. At present, the most precise test of  $CPT$  conservation in

---

S. Veneziano, A. Ventura, R. Versaci, I. Vilella, G. Xu.

the mixing has been performed using interferometry technique at the CPLEAR experiment <sup>3)</sup> and has a precision of  $3 \times 10^{-4}$ .

## 2 Measurement method

We measure  $K_S$  branching ratios using kaons from  $\phi \rightarrow K_S K_L$  decays, collected at the KLOE experiment operating at the DAΦNE  $e^+e^-$  collider <sup>4)</sup>.  $\phi$ -mesons are produced in small angle (25 mrad) collisions of equal energy electrons and positrons, giving the  $\phi$  a small transverse momentum component in the horizontal plane,  $p_\phi \sim 13 \text{ MeV}/c$ .  $\phi$ -mesons decay  $\sim 34\%$  of the time into neutral kaons. Produced  $K_L$ 's and  $K_S$ 's decay with mean paths  $\lambda_L \sim 340 \text{ cm}$  and  $\lambda_S \sim 0.6 \text{ cm}$ , respectively.

The main advantage of studying kaons at a  $\phi$ -factory is that  $K_L$ 's and  $K_S$ 's are produced nearly back-to-back in the laboratory so that detection of a long-lived kaon tags the production of a  $K_S$ -meson and gives its direction and momentum. The contamination from  $K_L K_L \gamma$  and  $K_S K_S \gamma$  final states is negligible for our measurement <sup>5, 6)</sup>. Since the branching ratio for  $K_S \rightarrow \pi^+ \pi^-$  is known with an accuracy of  $\sim 0.4\%$  <sup>7)</sup>, the  $K_S \rightarrow \pi e \nu$  branching ratio is evaluated by normalizing the number of signal events, separately for each charge state, to the number of  $K_S \rightarrow \pi^+ \pi^-$  events in the same data set. This allows cancellation of the uncertainties arising from the integrated luminosity, the  $\phi$  production cross section, and the tagging efficiency. The measurement is based on an integrated luminosity of  $410 \text{ pb}^{-1}$  at the  $\phi$  peak collected during two distinct data-taking periods in the years 2001 and 2002, corresponding to  $\sim 1.2 \times 10^9$   $\phi$ -mesons produced. Since the machine conditions were different during the two periods, we have measured the branching ratios separately for each data set. Our final results are based on the averages of these measurements.

## 3 Selection criteria

About half of the  $K_L$ -mesons reach the calorimeter, where most interact. A  $K_L$  interaction is called a  $K_L$ -crash in the following. A  $K_L$ -crash is identified as a local energy deposit with energy above 100 MeV and a time of flight indicating low velocity:  $\beta \sim 0.218$ . The coordinates of the energy deposit determine the  $K_L$ 's direction to  $\sim 20 \text{ mrad}$  and its momentum  $\mathbf{p}_L$ , which is weakly dependent

on the  $K_L$  direction because of the motion of the  $\phi$ -meson. A  $K_L$ -crash thus tags the production of a  $K_S$  of momentum  $\mathbf{p}_S = \mathbf{p}_\phi - \mathbf{p}_L$ .  $K_S$ -mesons are tagged with an overall efficiency of  $\sim 30\%$ . Both  $K_S \rightarrow \pi e \nu$  and  $K_S \rightarrow \pi^+ \pi^-$  decays are selected from this tagged sample. Event selection consists of fiducial cuts, particle identification by time of flight, and kinematic closure.

Identification of  $K_S \rightarrow \pi^+ \pi^-$  decays requires two tracks of opposite curvature. Tracks must extrapolate to the interaction point (IP) within few centimeters. The reconstructed momenta and polar angles must lie in the intervals  $120 \text{ MeV}/c < p < 300 \text{ MeV}/c$  and  $30^\circ < \theta < 150^\circ$ . A cut in  $(p_\perp, p_\parallel)$  selects non-spiralling tracks. The numbers of  $K_S \rightarrow \pi^+ \pi^-$  events found in each data set are shown in table 3. Contamination due to  $K_S$  decays other than  $K_S \rightarrow \pi^+ \pi^-$  is well below the per-mil level and is ignored.

Identification of  $K_S \rightarrow \pi e \nu$  events also begins with the requirement of two tracks of opposite curvature. Tracks must extrapolate *and form a vertex* close to the IP. The invariant mass  $M_{\pi\pi}$  of the pair calculated assuming both tracks are pions must be smaller than 490 MeV. This rejects  $\sim 95\%$  of the  $\pi^+ \pi^-$  decays.

Electrons and pions are discriminated by time of flight (TOF). Tracks are therefore required to be associated with calorimeter energy clusters. For each track, we compute the difference  $\delta_t(m) = t_{cl} - L/c\beta(m)$  using the cluster time  $t_{cl}$  and the track length  $L$ . The velocity  $\beta$  is computed from the track momentum for each mass hypothesis,  $m = m_e$  and  $m = m_\pi$ . In order to avoid uncertainties due to the determination of  $T_0$  (the time of the bunch crossing producing the event), we make cuts on the two-track difference

$$d\delta_{t,ab} = \delta_t(m_a)_1 - \delta_t(m_b)_2,$$

where the mass hypothesis  $m_{a(b)}$  is used for the track 1(2). This difference is zero for the correct mass assignments. An additional fraction of  $K_S \rightarrow \pi^+ \pi^-$  events is rejected by requiring  $|d\delta_{t,\pi\pi}| > 1.7 \text{ ns}$ . The differences  $d\delta_{t,\pi e}$  and  $d\delta_{t,e\pi}$  are calculated for events surviving the previous cut. The scatter plot of the two variables is shown in Fig. 1 for Monte Carlo events. The cuts applied on these time differences for the selection of  $K_S \rightarrow \pi e \nu$  events are illustrated in the figure:  $|d\delta_{t,\pi e}| < 1.4 \text{ ns}$ ,  $d\delta_{t,e\pi} > 3.2 \text{ ns}$ ; or  $|d\delta_{t,e\pi}| < 1.4 \text{ ns}$ ,  $d\delta_{t,\pi e} > 3.2 \text{ ns}$ . After the TOF requirements, particle types and charges for signal events can be assigned very precisely: the probability of misidentifying a  $\pi^+ e^- \bar{\nu}$  ( $\pi^- e^+ \nu$ ) event as a  $\pi^- e^+ \nu$  ( $\pi^+ e^- \bar{\nu}$ ) is negligible.

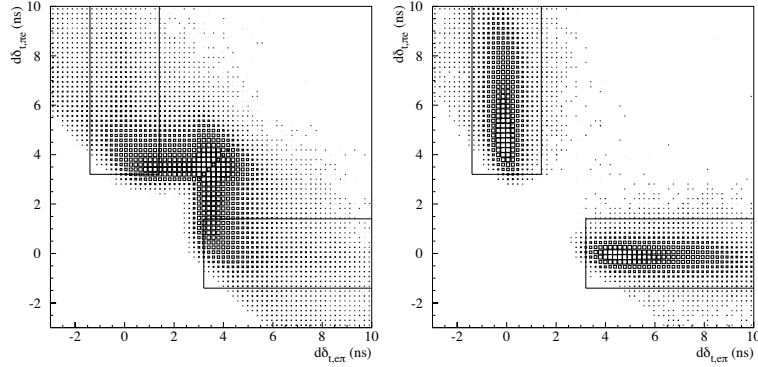


Figure 1: Scatter plot of the time differences  $d\delta_{t,\pi e}$  vs  $d\delta_{t,e\pi}$  for  $e\pi$  and  $\pi e$  mass assignments for Monte Carlo events, from all  $K_S$  decays (left) and from  $K_S \rightarrow \pi e \nu$  decays (right).

Finally, for events passing all of the above criteria, we compute the missing energy and momentum  $E_{\text{miss}}, p_{\text{miss}}$ . For  $\pi^\pm e^\mp \bar{\nu}(\nu)$  decays, these variables are the neutrino energy and momentum, and satisfy  $E_{\text{miss}} = cp_{\text{miss}}$ . The distribution of  $E_{\text{miss}} - cp_{\text{miss}}$  is shown in Fig. 2 after the time-of-flight cuts are imposed for  $\pi^+ e^- \bar{\nu}$  (left panel) and for  $\pi^- e^+ \nu$  (right panel) candidate events. A clear peak at  $E_{\text{miss}} - cp_{\text{miss}} = 0$  is evident and corresponds to a clean signal for  $K_S \rightarrow \pi e \nu$ . Events with  $E_{\text{miss}} - cp_{\text{miss}} > 10 \text{ MeV}$  are mostly due to  $K_S \rightarrow \pi^+ \pi^-$  decays in which a pion decays to a muon before reaching the tracking volume or in which one of the two pion tracks is badly reconstructed.

The solid line in the graph on the right is a fit of the data to the sum of the signal and background spectra simulated using the Monte Carlo (MC). The MC simulation of  $K_S \rightarrow \pi e \nu$  decays includes an infra-red-finite treatment of radiative corrections. The kinematics of the decay  $K_S \rightarrow \pi e \nu$  has been sampled from a four-body differential decay width which includes a photon in the final state <sup>8)</sup>.

The free fit parameters are the signal and background normalizations. Three independent fits are performed: one for each charge state and one in which we do not distinguish by charge. The estimated numbers of signal events are shown in table 3. The quoted errors includes the contributions from fluctuations in the signal statistics, from the background subtraction, and from the

Channel	Number of selected events	
	Year 2001	Year 2002
$K_S \rightarrow \pi^+\pi^-$	20903541	37313575
$K_S \rightarrow \pi^+e^-\bar{\nu}$	$4082 \pm 83$	$7176 \pm 117$
$K_S \rightarrow \pi^-e^+\nu$	$4155 \pm 81$	$7282 \pm 112$
$K_S \rightarrow \pi e \nu$	$8236 \pm 116$	$14458 \pm 162$

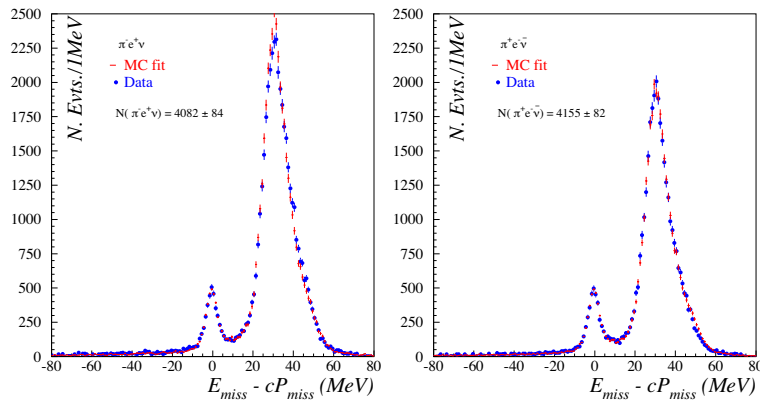


Figure 2:  $E_{\text{miss}} - cP_{\text{miss}}$  spectrum for  $\pi^-e^+\nu$  (left panel) and for  $\pi^+e^-\bar{\nu}$  (right panel) candidate events. Filled dots represent data from year-2001 data set; the solid line is the result of a fit varying the normalization of MC distributions for signal and background.

finite statistics of the MC spectra, which amount to  $\sim 74\%$ ,  $\sim 24\%$ , and  $\sim 59\%$ , respectively.

#### 4 Efficiency estimates

For both  $K_S \rightarrow \pi^+\pi^-$  (normalization) and  $K_S \rightarrow \pi e \nu$  (signal) events, contributions to the tagging and selection inefficiencies due to purely geometrical effects have been estimated using MC simulation, while data have been used to estimate the corrections for tracking and trigger inefficiencies. For  $K_S \rightarrow \pi e \nu$  events, the corrections for vertex reconstruction and time-of-flight  $\pi$ - $e$  identification inefficiencies have also been evaluated using a data control sample of  $K_L \rightarrow \pi e \nu$  prompt decays.

The methods used for estimating selection efficiency are described in detail

$K_S$ decay mode	Selection efficiency	
	Year 2001	Year 2002
$\pi^+\pi^-(\gamma)$	$0.6123 \pm 0.0006_{\text{stat}} \pm 0.0025_{\text{svst}}$	$0.6273 \pm 0.0002_{\text{stat}} \pm 0.0025_{\text{svst}}$
$\pi^-e^+\nu$	$0.2277 \pm 0.0013_{\text{stat}} \pm 0.0017_{\text{svst}}$	$0.2358 \pm 0.0010_{\text{stat}} \pm 0.0024_{\text{svst}}$
$\pi^+e^-\bar{\nu}$	$0.2324 \pm 0.0013_{\text{stat}} \pm 0.0012_{\text{svst}}$	$0.2378 \pm 0.0012_{\text{stat}} \pm 0.0015_{\text{svst}}$
$\pi e \nu$	$0.2297 \pm 0.0009_{\text{stat}} \pm 0.0016_{\text{svst}}$	$0.2361 \pm 0.0008_{\text{stat}} \pm 0.0018_{\text{svst}}$
$K_S$ decay mode	Ratio of tagging efficiencies	
$\pi^-e^+\nu$	$0.9924 \pm 0.0020_{\text{stat}} \pm 0.0020_{\text{svst}}$	
$\pi^+e^-\bar{\nu}$	$0.9912 \pm 0.0020_{\text{stat}} \pm 0.0020_{\text{svst}}$	
$\pi e \nu$	$0.9918 \pm 0.0015_{\text{stat}} \pm 0.0015_{\text{svst}}$	

Table 1: *Selection efficiencies.*

elsewhere <sup>9, 10, 11</sup>). For  $K_S \rightarrow \pi e \nu$  decays, three efficiencies are estimated: one for each charge state and one for events in which we do not distinguish by charge. We summarize the results for the total efficiencies, given the tag requirement, in Tab. 1. The uncertainty in the trigger efficiency is the dominant contribution to systematic errors. The difference between efficiencies for the two semileptonic charge states arises from the different response of the calorimeter to  $\pi^+$  and  $\pi^-$ , influencing both the trigger and the TOF efficiencies.

In principle, the  $K_L$ -crash identification efficiency cancels out in the ratio of the number of selected  $K_S \rightarrow \pi e \nu$  and  $K_S \rightarrow \pi^+\pi^-$  events. In practice, since the event  $T_0$  is obtained from the  $K_S$  and the  $K_L$  is recognized by its time of flight, there is a small dependence of the  $K_L$ -crash identification efficiency on the  $K_S$  decay mode. A correction for this effect is obtained by studying the accuracy of the  $T_0$  determination in each case <sup>9, 10, 11</sup>). The ratio  $R_{\text{tag}}$  of the tagging efficiencies for  $K_S \rightarrow \pi e \nu$  and  $K_S \rightarrow \pi^+\pi^-$  is found to differ from unity by  $\sim 1\%$  (see Tab. 1).

## 5 Preliminary results

The value for  $\text{BR}(K_S \rightarrow \pi e \nu)$  is obtained by normalizing the number of signal events to the number of  $K_S \rightarrow \pi^+\pi^-$  events in the same data set, correcting for the total selection efficiencies and the ratio  $R_{\text{tag}}$  of tagging efficiencies, and using the present experimental value for  $\text{BR}(K_S \rightarrow \pi^+\pi^-)$  <sup>7</sup>):

$$\text{BR}(K_S \rightarrow \pi e \nu) = \frac{N(\pi e \nu)}{N(\pi \pi)} \times \frac{\varepsilon_{\text{tot}}^{\pi \pi}}{\varepsilon_{\text{tot}}^{\pi e \nu}} \times R_{\text{tag}} \times \text{BR}(K_S \rightarrow \pi^+\pi^-).$$

Averaging the results obtained for each data set, we obtain the following branching ratios:

$$\begin{aligned}\text{BR}(K_S \rightarrow \pi^- e^+ \nu) &= (3.54 \pm 0.05_{\text{stat}} \pm 0.05_{\text{syst}}) \times 10^{-4}, \\ \text{BR}(K_S \rightarrow \pi^+ e^- \bar{\nu}) &= (3.54 \pm 0.05_{\text{stat}} \pm 0.04_{\text{syst}}) \times 10^{-4}, \\ \text{BR}(K_S \rightarrow \pi^\pm e^\mp \bar{\nu}(\nu)) &= (7.09 \pm 0.07_{\text{stat}} \pm 0.08_{\text{syst}}) \times 10^{-4}.\end{aligned}$$

The charge asymmetry is also obtained as follows

$$\begin{aligned}A_S &= \frac{N(\pi^- e^+ \nu)/\varepsilon^+ - N(\pi^+ e^- \bar{\nu})/\varepsilon^-}{N(\pi^- e^+ \nu)/\varepsilon^+ + N(\pi^+ e^- \bar{\nu})/\varepsilon^-}, \\ A_S &= (-2 \pm 9_{\text{stat}} \pm 6_{\text{syst}}) \times 10^{-3}\end{aligned}$$

This result is compatible with that for  $K_L$  semileptonic decays and with the expectation obtained assuming CPT symmetry,  $A_S = 2\text{Re}(\epsilon)$ .

### 5.0.1 $V_{us}$ determination

The most precise constraints on the size of CKM matrix elements is provided by the determinations of  $|V_{us}|$  and  $|V_{ud}|$ . The  $V_{us}$  value can be extracted from the measurement of the  $K_S \rightarrow \pi e \nu$  branching ratio and lifetime measurements using <sup>12)</sup>:

$$V_{us} \cdot f_+^{K^0 \pi^-}(0) = \left[ \frac{\Gamma}{\mathcal{N} S_{\text{ew}} I_i(\lambda_+, \lambda_0; 0)} \right]^{1/2} \frac{1}{1 + \delta_{e^2 p^2}^i + \frac{1}{2} \Delta I_i(\lambda_+, \lambda_0)}$$

with

$$\mathcal{N} = \frac{G_\mu^2 M_{K_i}^5}{192 \pi^3}$$

where  $f_+^{K^0 \pi^-}$  is the vector form factor at zero momentum transfer,  $I_i(\lambda_+, \lambda_0; 0)$  is the result of the phase space integration after factoring out  $f_+^{K^0 \pi^-}$ , both are evaluated in absence of radiative corrections. The radiative corrections for the form factor and the phase space integral are included by  $\delta_{e^2 p^2}^i$  and  $\Delta I_i(\lambda_+, \lambda_0)$  respectively.  $\lambda_+$  and  $\lambda_0$  are the parameters that describe the transfer momentum dependence of the vector and scalar form factor.

Using  $\lambda_+ = 0.0291 \pm 0.0018$  from PDG we obtain:

$$f_+^{K^0 \pi^-} \cdot V_{us} = 0.2157 \pm 0.0018 \quad \text{from } K_S \rightarrow \pi e \nu$$

In Fig. 3 our value of  $f_+^{K^0\pi^-} \cdot V_{\text{us}}$  is shown and compared with the one obtained using PDG averages for kaon branching ratios and with the most recent result from E865<sup>13)</sup> experiment. Our preliminary result agrees better with the latest  $K^+$  data, while showing a deviation from the old  $K^0 \rightarrow \pi e \nu$  data.

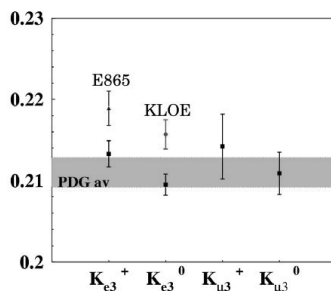


Figure 3:  $f_+^{K^0\pi^-} \cdot V_{\text{us}}$  obtained by KLOE compared with the ones obtained using PDG averages for kaon branching ratios and with the most recent result from E865 experiment.

Several theoretical calculations have been performed to evaluate  $f_+^{K^0\pi^-}$ . Using  $f_+^{K^0\pi^-} = 0.961 \pm 0.008$  from<sup>14)</sup>, that is in agreement with a recent lattice calculation<sup>15)</sup> we obtain  $V_{\text{us}} = 0.2245 \pm 0.0026$ .

## References

1. A. Alavi-Harati *et al.*, Phys. Rev. Lett. **88**, 181601 (2002), **hep-ex/0202016**.
2. R. Wanke, New Results on Kaon Decays from NA48, in: Proc. 38th Rencontres de Moriond on Electroweak Interactions and Unified Theories, Les Arcs, Savoie, France March 15-22, 2003, p. 6, **hep-ex/0305059**.
3. A. Angelopoulos *et al.*, Phys. Lett. B **444**, 52 (1998).
4. S. Guiducci, Status of DAΦNE, in: Proc. 2001 Particle Accelerator Conference, Chicago, IL, U.S.A., 2001, p. 353.

5. I. Dunietz, J. Hauser, J. Rosner, Phys. Rev. D **35**, 2166 (1987).
6. N. Brown, F. E. Close, Scalar mesons and kaons in  $\phi$  radiative decay & their implications for studies of CP violation at DAΦNE, in: The DAΦNE Physics Handbook (ed.L. Maiani, G. Pancheri, N. Paver), **2**, 447 (1992).
7. S. Eidelman *et al.*, Review of Particle Physics, Phys. Lett. B 592, 1 (2004).  
<http://pdg.lbl.gov>
8. C. Gatti, MC generators for radiative kaon decays, KLOE memo 290 (2004).  
<http://www.lnf.infn.it/kloe/private/memos/km290.ps>
9. C. Gatti, T. Spadaro, Measurement of  $\text{BR}(K \rightarrow \pi^\pm e^\mp \bar{\nu}(\nu))$ , KLOE note 176 (2002).  
<http://www.lnf.infn.it/kloe/pub/knote/kn176.ps.gz>
10. T. Spadaro, Studies of  $K_S$  decays at the Kloe Experiment, Ph.D. thesis, Università degli Studi di Roma "La Sapienza" (2001).  
<http://www.infn.it/thesis/PDF/187-Spadaro-dottorato.pdf>
11. C. Gatti, Measurement of the branching fraction for the decay  $K_S \rightarrow \pi^\pm e^\mp \bar{\nu}(\nu)$  with the KLOE detector, Ph.D. thesis, Università degli Studi di Pisa (2002).  
<http://www.infn.it/thesis/PDF/253-Gatti-dottorato.ps>
12. M. Battaglia *et al.*, The ckm matrix and the unitarity triangle (2003), **hep-ph/0304132**.
13. A. Sher *et al.*, Phys. Rev. Lett. **91**, 291802 (2002), **hep-ex/0305042**.
14. H. Leutwyler, M. Roos, Determination of the elements  $v(us)$  and  $v(ud)$  of the Kobayashi-Maskawa matrix, Z. Phys. C25, 91 (1984).
15. D. Becirevic *et al.*, The  $K \rightarrow \pi$  vector form factor at zero momentum transfer on the lattice (2004), **hep-ph/0403217**.

**MEASUREMENT OF THE BRANCHING RATIO OF THE  
DECAY  $K_L \rightarrow \pi^\pm e^\mp \nu$  AND THE COUPLING CONSTANT  $V_{us}$**

Konrad Kleinknecht  
*Institut fuer Physik*  
*Johannes Gutenberg-Universität Mainz*

**ABSTRACT**

We present a new measurement of the branching ratio of the decay  $K_L \rightarrow \pi^\pm e^\mp \nu$  relative to all charged  $K_L$  decays based on data taken with the NA48 detector at the CERN SPS. We measure  $R = 0.4981 \pm 0.0035$ . From this we derive the  $K_{e3}$  branching fraction and the weak coupling parameter  $V_{us}$  in the CKM matrix. We obtain  $|V_{us}|f_+(0) = 0.2148 \pm 0.0016$ , where  $f_+(0)$  is the vector form factor in the  $K_{e3}$  decay.

**1 Introduction**

The unitary condition for the first row of the CKM quark mixing matrix is at present fulfilled only at the 10% C. L. <sup>1)</sup>. This has renewed interest in the measurement of the coupling constant  $V_{us}$  for strangeness-changing weak transitions. The most precise information on  $V_{us}$  comes from the decay  $K_L \rightarrow$

$\pi e\nu$ , which is a vector transition, and therefore is protected from SU(3) breaking effects by the Ademollo-Gatto theorem. We present here a new measurement with improved experimental precision.

## 2 Apparatus

The experiment was performed using the NA48 detector in a beam of long-lived neutral kaons derived from the 450 GeV proton synchrotron SPS at CERN. This experiment was originally designed and used for the precision measurement of direct CP violation in Kaon decays <sup>2)</sup>. The main elements of the detector relevant for this exposure are the following:

The magnetic spectrometer is designed to measure the momentum of the charged particles with a high precision - the momentum resolution is given by

$$\sigma(p)/p = 0.48\% \oplus 0.009 \cdot p\% \quad (1)$$

where  $p$  is in GeV/c.

The hodoscope is placed downstream of the last drift chamber. It consists of two planes of scintillators segmented in horizontal and vertical strips and arranged in four quadrants. The signals are used for a fast coincidence of two charged particles in the trigger. The time resolution from the hodoscope is 200 ps per track.

The electromagnetic calorimeter (Lkr) is a quasi-homogeneous calorimeter based on liquid krypton, with tower read out. The 13248 read-out cells have cross sections of  $2 \times 2$  cm<sup>2</sup>. The energy resolution is:

$$\sigma(E)/E = 3.2\%/\sqrt{E} \oplus 9.0\%/E \oplus 0.42\% \quad (2)$$

where  $E$  is in GeV, and the time resolution for one shower with energy between 3 GeV and 100 GeV is 500 ps.

A more detailed description of the NA48 setup can be found elsewhere [2].

### 3 Data taking and data processing

#### 3.1 Trigger and data taking

The experiment was performed in a  $K_L$  beam in september 1999. Charged decays were triggered with a two-level trigger system. The trigger requirements were two charged particles in the scintillator hodoscope or in the drift chambers, coming from a vertex in the decay region.

The data volume consists of about 1.6 TB of data from 80 million triggers.

#### 3.2 Analysis strategy and event selection

The basic quantity measured in this experiment is the ratio  $R$  of decay rates of  $K_{e3}$  decays relative to all decays with two charged particles in the final state, mainly  $\pi e \nu$ ,  $\pi \mu \nu$ ,  $\pi^+ \pi^- \pi^0$ ,  $\pi^+ \pi^-$  and  $\pi^0 \pi^0 e e \gamma$ . Since the neutral decay modes to  $3\pi^0$ ,  $2\pi^0$  and  $\gamma\gamma$  are well measured, the sum of branching ratios of all charged modes  $B(2T)$  is experimentally known

$$B(2T) = 1 - \frac{\Gamma(K_L \rightarrow \text{all neutral})}{\Gamma(K_L \rightarrow \text{all})} \quad (3)$$

$$= 1 - B(3\pi^0) - B(2\pi^0) - B(\gamma\gamma) + B(3\pi_D^0) = 1.0061 - B(3\pi^0). \quad (4)$$

Using this number, the branching ratio of  $K_{e3}$  can be obtained:

$$B(e3) = \frac{\Gamma(K_{e3})}{\Gamma(K_L \rightarrow \text{all})} = \frac{\Gamma(K_{e3})}{\Gamma(K_L \rightarrow \text{all charged})} \times B(2T). \quad (5)$$

In this experiment, we therefore measure the ratio of  $K_{e3}$  events to all 2-track events  $N_{2T}$  both divided by their acceptances  $a_e$  or  $a_{2T}$  respectively:

$$R = \frac{N_e/a_e}{N_{2T}/a_{2T}}. \quad (6)$$

Both numbers,  $N_e$  and  $N_{2T}$  are extracted from the same sample of about 80 million recorded two-track events. These were reconstructed and subjected to off-line filtering.

The basic selection criteria were the following: Two tracks belonging to particles with opposite charges and one vertex in the decay region were required. The closest distance of approach between these tracks had to be less than 3 cm to form a vertex. The decay region was defined by requirements that the vertex had to be between 8 m and 33 m from the last collimator and that the distance between the vertex and the beam axis had to be less than 3 cm.

Events in which the time difference between the tracks was more than 6 ns were rejected. Only events with both tracks inside the detector acceptance were used. Particles with a momentum of less than 10 GeV/c ( $P_{min}$ ) or above 120 GeV/c ( $P_{max}$ ) were rejected. In order to allow a clear separation of pion and electron showers, we required the distance between the entry points of the two tracks at the front face of the electromagnetic calorimeter to be larger than 25 cm.

For the denominator  $N_{2T}$  in the R ratio, no identification of the individual decay mode is done but all two track events are treated in the same way. As an incomplete but well-defined measure of the kaon momentum, the sum of the two moduli of the two momenta  $P = P_1 + P_2$  is used. As a result 12.592 million events with  $P > 60$  GeV/c remained.

For the numerator  $N_e$  in the ratio R, however, the  $K_{e3}$  signal is selected by identification of electrons. We use the ratio of the measured cluster energy,  $E$ , in the calorimeter associated to a track, to the momentum  $p$  of this track as measured in the magnetic spectrometer. For the selection of  $K_{e3}$  events we solely require at least one track to have  $E/p > 0.93$  to be compatible with an electron. 6.759 million events were accepted.

### 3.3 Event number corrections

The number of  $K_{e3}$  events was corrected for the inefficiency of the electron identification (electrons with  $E/p < 0.93$ ) and background coming from  $K_{\mu 3}$  and  $K_{3\pi}$  decays (pion with  $E/p > 0.93$ ). Both inefficiency and background were measured in data.

For the background determination a sample of events having one track

with  $E/p > 1.0$  was selected. The background probability for pions  $W(\pi \rightarrow e)$  is then determined from the  $E/p$  spectrum of the pion tracks (see fig. 1) to be

$$W(\pi \rightarrow e) = (0.576 \pm 0.005)\%.$$

As a cross check the probability was also derived from the  $E/p$  spectrum of  $K_{3\pi}$  events, giving the same number within its error.

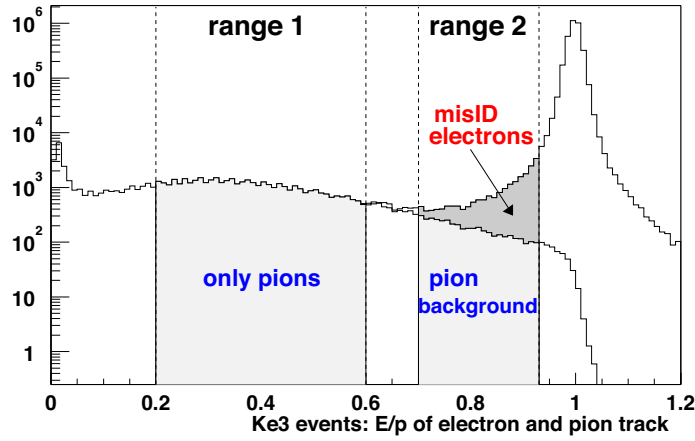


Figure 1: *The ratio of calorimetric energy  $E$  and the momentum  $p$  for electron and pion tracks*

The electron ID inefficiency  $W(e \rightarrow \pi)$  is determined in a similar way: requiring  $E/p < 0.7$  for one track we assign it to a pion. We use the  $E/p$  distribution for the other track, which consists mainly of electrons but also of a small part of pions, especially in the range below 0.7. We subtract this pion component by taking the known pion distribution, normalized in the range  $0.2 < E/p < 0.6$ . From this we then obtain the probability for losing an electron by the condition  $E/p > 0.93$ , and the result is

$$W(e \rightarrow \pi) = (0.487 \pm 0.004)\%.$$

### 3.4 Monte Carlo Simulation

To reproduce the detector response, a GEANT-based simulation of the NA48 apparatus was employed [2] for the five decay modes  $e3$ ,  $\mu3$ ,  $\pi^+\pi^-\pi^0$ ,  $\pi^+\pi^-$  and  $\pi^0\pi^0\pi_D^0$ . Radiative corrections were included for the  $K_{e3}$  mode. We used the PHOTOS program package <sup>4)</sup> to simulate external bremsstrahlung, and added the calculations from <sup>3)</sup> on virtual photons and electrons. Some comparisons between data and MC for identified  $K_{e3}$  events are shown in (z-vertex).

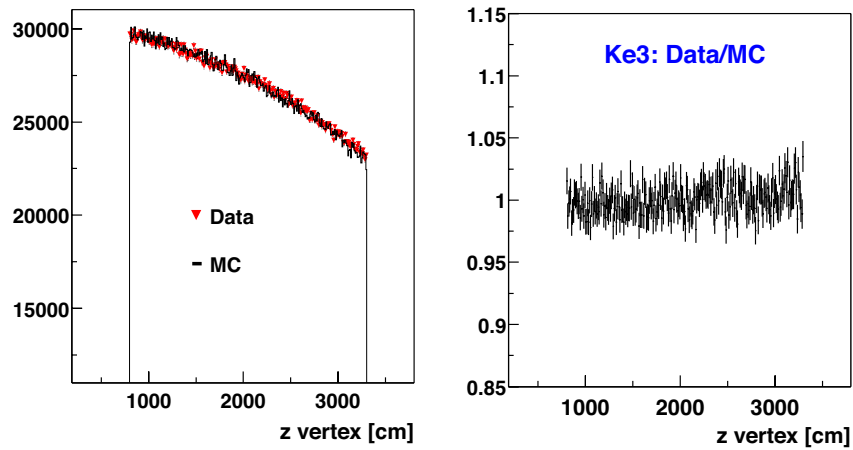


Figure 2: Longitudinal vertex distribution for  $Ke3$  events, data (left) and ratio of data over Monte Carlo simulation (right)

We obtain the individual acceptances  $a_i$  as shown in table 1.

The average two-track acceptance was obtained from a weighted mean of the individual acceptances which only depends on ratios of decay rates measured in other experiments:

$$a_{2T} = \frac{B_e a_e + B_\mu a_\mu + B_\pi a_\pi + B_{2\pi} a_{2\pi} + B_D a_D}{B_e + B_\mu + B_\pi + B_{2\pi} + B_D} \quad (7)$$

$$= \frac{a_e \left( 1 + \frac{B_\mu}{B_e} \frac{a_\mu}{a_e} + \frac{B_\pi}{B_e} \frac{a_\pi}{a_e} + \frac{B_{2\pi}}{B_e} \frac{a_{2\pi}}{a_e} + \frac{B_D}{B_e} \frac{a_D}{a_e} \right)}{\left( 1 + \frac{B_\mu}{B_e} + \frac{B_\pi}{B_e} + \frac{B_{2\pi}}{B_e} + \frac{B_D}{B_e} \right)}. \quad (8)$$

Table 1: *Detector acceptances for the charged decay modes*

decay mode	acceptance
$K_{e3}$	0.2599
$K_{\mu3}$	0.2849
$K_{3\pi}$	0.0975
$K_{2\pi}$	0.5229
$K_{3\pi_D^0}$	0.0001

Here  $B_i$  are the branching ratios for the decay channels ( $i = e : K_{e3}$ ;  $i = \mu : K_{\mu3}$ ;  $i = \pi : \pi^+\pi^-\pi^0$ ;  $i = 2\pi : \pi^+\pi^-$ ;  $i = D : \pi^0\pi^0\pi_D^0$ ). The acceptance for channel  $i$  is  $a_i$ . We use as effective branching ratios a weighted average of the 2002 PDG values <sup>1)</sup> and the new KTeV data <sup>10)</sup>. The uncertainty is evaluated according to PDG rules for averaging inconsistent data. The values are  $B_\mu/B_e = 0.666 \pm 0.011$ ,  $B_\pi/B_e = 0.309 \pm 0.004$ ,  $B_{2\pi}/B_e = (4.90 \pm 0.14)10^{-3}$ ,  $B_D/B_e = (1.85 \pm 0.05)10^{-2}$

In fig. 3 we show a comparison of the energy spectra for identified  $K_{3\pi}$  and  $K_{2\pi}$  events, where we can fully reconstruct the energy, between data and MC simulation. Fig. 4 shows the comparison between data and the Monte Carlo simulation for the sum of track momenta in identified  $Ke3$  events in the range between 60 GeV/c and 130 GeV/c, which contains 95% of the data. The agreement between data and MC is better with radiative corrections switched on.

Radiative corrections mainly reduce the electron momentum, so residual uncertainties here also affect  $P$  in a different way for  $Ke3$  than for the other charged modes. To get the worst case uncertainty of this dependence, we varied the lower cut on the value of  $P$  from 50 GeV/c to 80 GeV/c, rejecting 70% of the events. The resulting relative uncertainty of the acceptance is 0.67%.

The two track acceptance defined in eq. (8) depends only on ratios of branching ratios as weight factors. The two track acceptance  $a_{2T}$  is very similar to the  $Ke3$  acceptance  $a_e$ , making this measurement very insensitive to whatever previous measurements of the  $Ke3$  branching fraction. Varying the

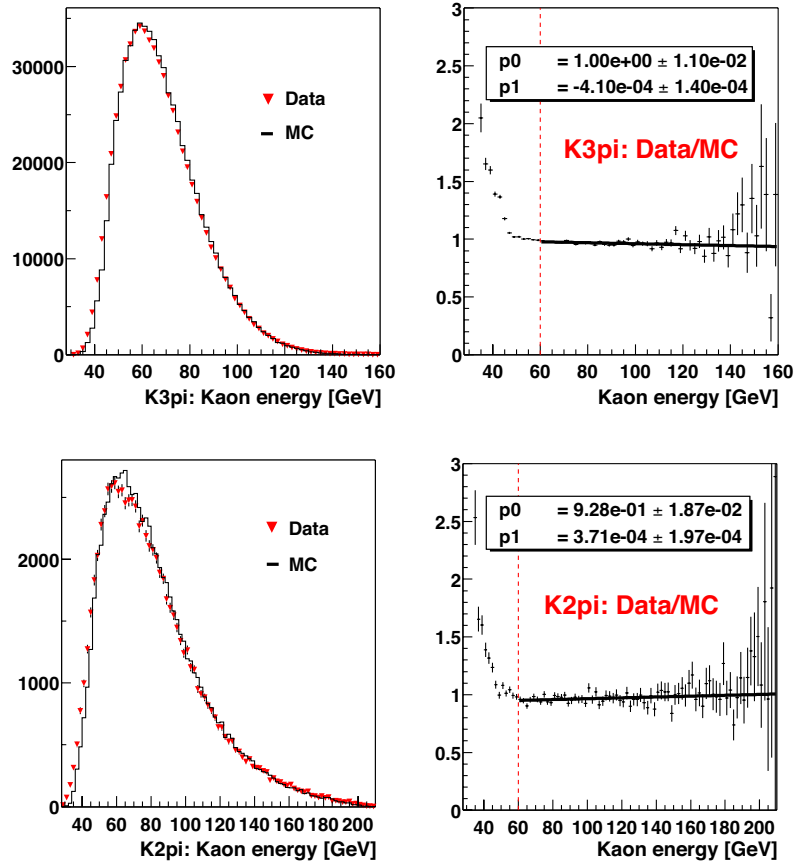


Figure 3: Reconstructed kaon energy from  $K_{3\pi}$  and  $K_{2\pi}$  decays - comparison between data and MC

constraints given by the effective branching ratios within their errors we get a relative variation of the acceptance of 0.25%.

To estimate the uncertainty coming from the  $E/p$  cut to select  $K_{e3}$  events, we varied the cut value between  $E/p > 0.90$  and  $E/p > 0.96$ . As a result, inefficiency and background due to this criteria vary significantly, leading to very different net corrections of  $K_{e3}$  event numbers (table 2). Applying these correc-

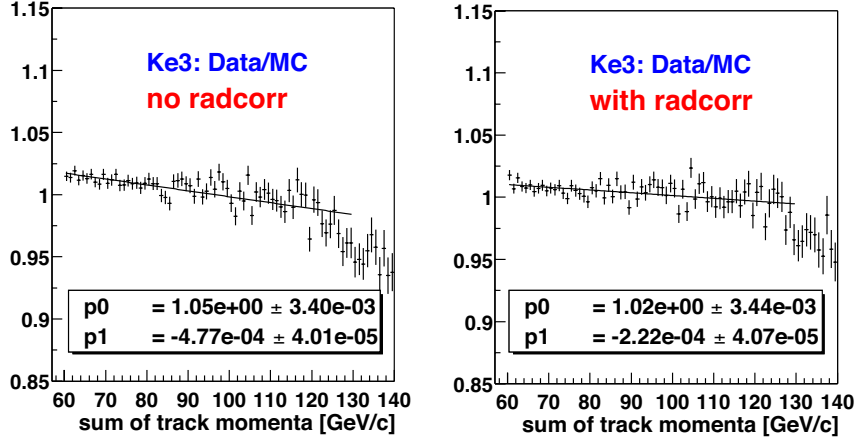


Figure 4: Ratio of data and simulation as a function of the sum of track momenta

tions, however, we get almost the same number of events, thus demonstrating the correctness of this selection principle. Obviously,  $E/p > 0.93$  is the best cut value as both inefficiency and background are very small and nearly cancel. The resulting relative uncertainty on R is  $\Delta R = 0.05\%$ .

Table 2: Variation of the  $E/p$  cut to select  $K_{e3}$  events

	$E/p > 0.90$	$E/p > 0.93$	$E/p > 0.96$
inefficiency [%]	0.275	0.487	1.424
background [%]	0.914	0.576	0.266
$K_{e3}$ event number after $E/p$ cut	6796461	6759184	6673114
net $K_{e3}$ correction	-42624	-5705	77182
corrected $K_{e3}$ event number	6753836	6753478	6750296

The data used in this analysis origin from two different triggers ( $Q2 + 2trk * Q1/20$ ), where  $Q2$  requires two or more planes of the hodoscope counter to be hit, while  $Q1 * 2trk$  requires one or more hodoscope planes plus two tracks

from the drift chamber trigger system. Selecting one trigger allows to measure the efficiency of the other, taking into account the different downscaling. The trigger efficiencies for 2-track and  $K_{e3}$  events differ slightly for the Q2 trigger bit (  $(97.38 \pm 0.02)\%$  for 2-track events,  $(97.49 \pm 0.03)\%$  for  $K_{e3}$  events). As a check, the analysis was done accepting only events with the 2trk trigger word set, which was measured to be equally efficient for all events. The relative uncertainty due to different trigger efficiencies is very small:  $\Delta R = 0.05\%$ .

In rare cases the drift chambers see multiple hits in one wire which lead to an overflow condition. This can be expected to be more likely for electrons than for minimal ionizing pions or muons. Comparing the results with or without cutting on the overflow condition accounts for a possibly different behaviour of electrons over the other particle, and turned out to be almost negligible:  $\Delta R = 0.05\%$ .

In order to be independent from potential asymmetries in the setup, about half of the data were recorded with positive polarity and half with negative polarity. We analyzed the data separately for both polarities, but found no relevant dependence:  $\Delta R = 0.05\%$ .

We summarize the systematic uncertainties in table 3:

Table 3: *Systematic uncertainties*

	relative uncertainty [%]
experimental normalization (energy spectrum)	0.67
normalization error from input ratios	0.25
E/p cut	0.05
trigger efficiency	0.05
DCH overflows	0.05
magnet polarity	0.05

Using the acceptances given in table 1, the effective ratios of branching fractions from Sect. 3.4 and the above evaluation of the systematic uncertainties, we obtain as average two track acceptance  $a_{2T} = (0.2414 \pm 0.0017)$ .

#### 4 Results

From the event numbers and acceptances the following corrections have to be applied:

Correction for the inefficiency of the electron identification increases the number of  $K_{e3}$  decays by 0.49%. Background from misidentified  $K_{\mu3}$  and  $K_{3\pi}$  decays reduce the number by 0.58%, leading to a net correction of -5705 events.

$$R = \frac{B(K_L \rightarrow \pi e \nu)}{B(K_L \rightarrow \text{all charged})} = \frac{6753478/0.2599}{12592096/0.2414} = 0.4981 \pm 0.0036. \quad (9)$$

For the branching ratio of the  $3\pi^0$  decay, the current experimental situation is unsatisfactory. We use a weighted mean of the PDG2002 value  $(21.05 \pm 0.28)\%$  and the recent value of the KTeV collaboration,  $(19.45 \pm 0.18)\%$ , and obtain  $(19.92 \pm 0.70)\%$ , where the error is enlarged because of the bad agreement. Therefore the branching ratio for all 2 track events is  $B(2T) = (80.69 \pm 0.72)\%$  and

$$B(e3) = \frac{\Gamma(K_L \rightarrow \pi e \nu)}{\Gamma(K_L \rightarrow \text{all})} = R * B(2T) = 0.4019 \pm 0.0028 \pm 0.0035, \quad (10)$$

with the first error being the complete experimental error and the second the external error from the normalization, to be combined to

$$B(e3) = 0.4019 \pm 0.0044. \quad (11)$$

As explained above, this measurement depends on three other measurements of ratios of partial  $Ke3$  decay widths. This dependence is given by:

$$\begin{aligned} \Delta B(e3) = & \left( \frac{\Gamma(\mu3)}{\Gamma(e3)} - 0.666 \right) * 0.077 - \left( \frac{\Gamma(3\pi)}{\Gamma(e3)} - 0.309 \right) * 0.075 \\ & - \left( \frac{\Gamma(3\pi^0)}{\Gamma(e3)} - 0.515 \right) * 0.151 \end{aligned} \quad (12)$$

The decay rate of  $K_L \rightarrow \pi e \nu$  is obtained by using the  $K_L$  lifetime  $\tau(K_L) = (5.15 \pm 0.04) \cdot 10^{-8} s$

$$\Gamma(K_{e3}) = B(e3) / \tau(K_L) = (7.80 \pm 0.10) \cdot 10^6 s^{-1}. \quad (13)$$

## 5 Value of $V_{us}$

The CKM matrix element  $|V_{us}|$  can be extracted from the  $K_{e3}^0$  decay parameters by

$$|V_{us}| = \sqrt{\frac{128\pi^3\Gamma(K_{e3}^0)}{G_F^2 M_{K^0}^5 S_{EW} I_{K^0}} \frac{1}{f_+^{K^0\pi^-}}} \quad (14)$$

Three quantities in this equation have to be given from theory.  $S_{EW}$  is the short distance enhancement factor,  $I_{K^0}$  is the phase space integral and  $f_+^{K^0\pi^-}$  is the form factor.

To determine  $V_{us}$  we follow the prescription and use the numerical results from <sup>6)</sup>. This paper presents a detailed numerical study of the  $K_{e3}$  decays to  $\mathcal{O}(p^6)$  in chiral perturbation theory with virtual photons and leptons. The integrals given there correspond to the specific prescription of radiative events to accept only those events which have pion and electron energies within the whole  $K_{e3}$  Dalitz plot. From a Monte Carlo simulation we obtain this correction to be small

$$\frac{\text{Number of } K_{e3(\gamma)} \text{ events inside Dalitz plot}}{\text{Number of all } K_{e3(\gamma)} \text{ events}} = 0.99423. \quad (15)$$

Using equations (13) and (15),  $S_{EW} = 1.0232$ ,  $I_{K^0} = 0.10339 \pm 0.00063$  we obtain a value for the product of the CKM matrix element  $V_{us}$  and the vector form factor  $f_+^{K^0\pi^-}$ ,

$$|V_{us}|f_+(0) = 0.2148 \pm 0.0016. \quad (16)$$

For the vector form factor, different theoretical calculations have been published recently. Chiral models including the corrections to the order  $p^6$  obtain  $f_+(0) = 0.981 \pm 0.010$  <sup>6)</sup>,  $f_+(0) = 0.976 \pm 0.010$  <sup>7)</sup> and  $f_+(0) = 0.974 \pm 0.011$  <sup>8)</sup>, to be compared with the older value  $f_+(0) = 0.961 \pm 0.010$  <sup>5)</sup>. Lattice calculations have also put forward results in the quenched fermion approximation,  $f_+(0) = 0.961 \pm 0.009$  <sup>9)</sup>, but the uncertainty of the quenched approximation is not included in the error. Therefore the most probable value is the average of the chiral calculations, which is  $0.973 \pm 0.010$ . With this value, we obtain the CKM element to be

$$|V_{us}| = 0.2207 \pm 0.0028. \quad (17)$$

The error on  $|V_{us}|$  is dominated by the theoretical uncertainties, the error on  $f_+^{K^0\pi^-}$  alone contributes with  $\pm 0.0022$ .

## 6 Conclusions

We presented a direct measurement of the ratio of  $K_{e3}^0$  to all  $K^0$  decays with charged tracks,

$$R = \frac{B(K_L \rightarrow \pi e \nu)}{B(K_L \rightarrow \text{all charged})} = 0.4981 \pm 0.0036. \quad (18)$$

Using the unsatisfactory current experimental knowledge of the  $3\pi^0$  branching ratio, this leads to a branching ratio  $B(e3) = 0.4019 \pm 0.0044$ . From the measured branching ratios, we extract a value of the CKM matrix element  $|V_{us}| = 0.2207 \pm 0.0028$ , in fair agreement with unitarity of the first row of the matrix.

## 7 Acknowledgements

I would like to thank the organizers of HQL04, in particular Angel Lopez, for their hospitality at Puerto Rico.

## References

1. K. Hagiwara et al., Phys. Rev. D 66, 010001 (2002) and 2003 off-year partial update for the 2004 edition available on the PDG WWW pages
2. A. Lai et al., NA 48 Collaboration, Eur. Physics J. C 22 (2001) 231
3. E. S. Ginsberg, Phys.Rev.171:1675,1968, Erratum-ibid.174:2169,1968
4. Photos program package, by E. Barberio, B. Van Eijk and Z. Was
5. H. Leutwyler and M. Roos, Z.Phys. C25, 91 (1984)
6. V.Cirigliano, H. Neufeld and H. Pichl, hep-ph / 0401173v1 23. Jan 2004

7. J. Bijmans and P. Talavera, Nucl.Phys. B669, 341 (2003)
8. M. Jamin., J. A. Oller and A. Pich, JHEP02,047(2004), hep-ph/0401080
9. D.Becirevic et al., hep-ph / 04003217v1 19. Mar 2004
10. T. Alexopoulos et al., hep-ex / 04006002v1 1. Jun 2004, and talk by R. Kessler at HQL04

Frascati Physics Series Vol. XXXV (2004), pp. 273-280  
HEAVY QUARKS AND LEPTONS - San Juan, Puerto Rico, June 1-5, 2004

**MEASUREMENT OF THE  $K^+ \rightarrow \pi^0 e^+ \nu$  ( $K_{e3}^+$ )  
BRANCHING RATIO BY E865 AT BROOKHAVEN NATIONAL  
LABORATORY**

A. Sher for the E865 collaboration  
*University of Pittsburgh, Pittsburgh, PA 15260, USA*  
*Present address: SCIPP UC Santa Cruz, Santa Cruz, CA 95064*

**ABSTRACT**

E865 at the Brookhaven National Laboratory AGS collected about 70,000  $K_{e3}^+$  events to measure the  $K_{e3}^+$  branching ratio relative to the observed  $K^+ \rightarrow \pi^+ \pi^0$ ,  $K^+ \rightarrow \pi^0 \mu^+ \nu$ , and  $K^+ \rightarrow \pi^+ \pi^0 \pi^0$  decays. The  $\pi^0$  in all the decays was detected using the  $e^+ e^-$  pair from  $\pi^0 \rightarrow e^+ e^- \gamma$  decay and no photons were required. Using the Particle Data Group branching ratios <sup>1)</sup> for the normalization decays we obtain  $BR(K_{e3(\gamma)}^+) = (5.13 \pm 0.02_{stat} \pm 0.09_{sys} \pm 0.04_{norm})\%$ , where  $K_{e3(\gamma)}^+$  includes the effect of virtual and real photons. This result <sup>2)</sup> is  $\approx 2.3\sigma$  higher than the current Particle Data Group value. Implications for the  $V_{us}$  element of the CKM matrix, and the matrix's unitarity are discussed.

The experimentally determined Cabibbo-Kobayashi-Maskawa (CKM) matrix describes quark mixing in the Standard Model framework. Any deviation from the matrix's unitarity would undermine the validity of the Standard

Model. One unitarity condition involves the first row elements:

$$|V_{ud}|^2 + |V_{us}|^2 + |V_{ub}|^2 = 1 - \delta \quad (1)$$

where a non-zero value of  $\delta$  indicates a deviation from unitarity. The  $V_{ud}$  element is obtained from nuclear and neutron decays.  $V_{ub}$ , from the semileptonic decays of B mesons<sup>1)</sup>, is too small to affect Eq. 1. The  $V_{us}$  element can be determined either from hyperon,  $K \rightarrow \pi\mu\nu(K_{\mu 3})$  or from  $K \rightarrow \pi e\nu(K_{e 3})$  decays. However,  $K_{e 3}$  decays provide a smaller theoretical uncertainty<sup>1, 3)</sup>. The most precise value of  $V_{ud}$  obtained from the nuclear superallowed Fermi beta decays leads to  $\delta = (3.2 \pm 1.4) \cdot 10^{-3}$ <sup>4)</sup>, a  $2.3\sigma$  deviation from unitarity.

Both experimental and theoretical efforts to improve the determination of  $V_{ud}$  continue. Theoretical contributions to  $V_{us}$  were reevaluated recently<sup>5, 6, 7, 8)</sup>, but there has been little new experimental input on the  $K_{e 3}^+$  branching ratio. Since the  $V_{ud}^2$  and  $V_{us}^2$  uncertainties are comparable, a high statistics measurement of the  $K_{e 3}^+$  branching ratio (B.R.) with good control of systematic errors is useful.

The bare (without QED corrections)  $K_{e 3}^+$  decay rate<sup>3, 5, 6, 9)</sup> is:

$$d\Gamma(K_{e 3}^+) = C(t)|V_{us}|^2|f_+(0)|^2\left[1 + \lambda_+ \frac{t}{M_\pi^2}\right]^2 dt \quad (2)$$

where  $t = (P_K - P_\pi)^2$ ,  $C(t)$  is a known kinematic function, and  $f_+(0)$  is the vector form factor value at  $t = 0$ , determined theoretically<sup>3, 5)</sup>. Two recent experiments<sup>10, 11)</sup> give  $\lambda_+$  (the form factor slope) measurements consistent with each other and with previous measurements. An omitted negligible term contributing to Eq. 2 contains the form factor  $f_-$ , and is proportional to  $M_e^2/M_\pi^2$ .

E865<sup>12)</sup> searched for the lepton flavor violating decay  $K^+ \rightarrow \pi^+\mu^+e^-$ . The detector resided in a 6 GeV/c positive beam<sup>12)</sup>. For the  $K_{e 3}^+$  running, the intensity was reduced by a factor of 10, to  $10^7$  kaons,  $2 \times 10^8$  protons, and  $2 \times 10^8\pi$  per 2.8 second spill. The beam was intentionally debunched at extraction to remove rf structure at the experiment. The first dipole magnet separated particles by charge, while the second magnet together with four multiwire proportional chambers (MWPCs: P1-P4) formed the spectrometer. The particle identification used the threshold multichannel Čerenkov detectors (C1 and C2, each separated into left and right volumes, for four independent counters) filled with gaseous methane (Čerenkov threshold  $\gamma_t \approx 30$  and electron

detection efficiency  $\epsilon_e \approx 0.98$  <sup>13)</sup>), an electromagnetic calorimeter <sup>12)</sup>, and a muon detector (not used for the  $K_{e3}^+$  measurement). The D and A scintillator hodoscopes gave left/right and crude vertical position.

The  $\pi^0$  from the kaon decays was detected through the  $e^+e^-$  from the  $\pi^0 \rightarrow e^+e^-\gamma$  decay, with the  $\gamma$  detected in some cases. To eliminate the uncertainty (2.7%) of the  $\pi^0 \rightarrow e^+e^-\gamma$  B.R., and to reduce systematic uncertainty we used the other three major decay modes with a  $\pi^0$  in the final state ( $K^+ \rightarrow \pi^+\pi^0(K_{\pi 2}^+)$ ,  $K_{\mu 3}^+$ ,  $K^+ \rightarrow \pi^+\pi^0\pi^0(K_{\pi 3}^+)$ ) for the normalization sample (“Kdal”).

The  $K_{e3}^+$  data was collected in a one-week dedicated run in 1998, with special on-line trigger logic.

The Kdal and  $K_{e3}^+$  data were collected by the “ $e^+e^-$ ” trigger, which was designed to detect  $e^+e^-$  pairs and required at least one D-counter scintillator slat on each (left and right) side of the detector and signals from each of the four Čerenkov counters. The Čerenkov efficiency trigger required only 3 out of 4 Čerenkov counters (no D-counter requirement). The “TAU” trigger, requiring only two D-counter scintillator hits (one left, and one right), collected events for the  $K^+ \rightarrow \pi^+\pi^+\pi^-$  ( $K_\tau$ ) sample, to study the detector unbiased by Čerenkov requirements. About 50 million triggers were accumulated,  $\approx 37$  million in the “ $e^+e^-$ ” trigger. About 75% of “ $e^+e^-$ ” triggers included accidental tracks, often a  $\mu$  from high momentum  $K \rightarrow \mu\nu$  or  $\pi \rightarrow \mu\nu$  decays partially satisfying the Čerenkov requirement.

Off-line reconstruction used the spectrometer only. The Čerenkov and D counter efficiencies were obtained from the Čerenkov efficiency triggers. The redundancy of the MWPCs (4 planes/chamber) and track reconstruction was used to extract MWPC efficiencies. The absence of the electromagnetic calorimeter from the trigger allowed its efficiency determination. Each efficiency was measured over its relevant phase space.

Relevant kaon decay chains <sup>13)</sup> were simulated with GEANT <sup>14)</sup> (including decays of secondary pions and muons). For  $K_{e3}^+$ ,  $\lambda^+ = 0.0278 \pm 0.0019$  <sup>1)</sup> was used. The radiative corrections to the  $K_{e3}^+$  decay phase-space density <sup>5)</sup> were used. The  $K_{e3\gamma}^+$  (inner bremsstrahlung) decays outside the  $K_{e3}^+$  Dalitz plot boundary were explicitly simulated <sup>9)</sup>. For  $\pi^0 \rightarrow e^+e^-\gamma$  decay, radiative corrections were taken into account according to Ref. <sup>15)</sup>. Measured efficiencies were applied <sup>13)</sup>, and accidental detector hits (from reconstructed  $K_\tau$

events) were added. About 10% of both the  $K_{e3}^+$  and Kdal samples had extra reconstructed tracks.

Selection criteria <sup>13)</sup>, common to  $K_{e3}^+$  and Kdal, required good quality three track events with the low ( $M_{ee} < 0.05$  GeV) mass  $e^+e^-$  pair identified in the Čerenkov counters. All tracks were required to have less than 3.4 GeV/c momentum corresponding to the muon Čerenkov threshold. A geometric Čerenkov ambiguity cut rejected events where the Čerenkov counter response could not be unambiguously assigned to separate tracks <sup>13)</sup>. The  $K_{e3}^+$  sample was then selected by requiring the second positive track to be identified as  $e^+$  in 2 of the 3 electron detectors: C1, C2, or the calorimeter, each with efficiency  $\epsilon_e \approx 98\%$ . Events entering the Kdal sample had no response in at least one of the two Čerenkov counters. The  $K_{\pi 2}$  acceptance is  $\approx 1.2\%$ . The  $K_{e3}^+$  acceptance  $\approx 0.7\%$  <sup>13)</sup>, somewhat lower because of the lower average  $e^+$  momentum in the  $K_{e3}^+$  decay. The final  $K_{e3}$  and Kdal samples were 71,204 and 558,186, respectively.

Contamination of the  $K_{e3}^+$  sample by other  $K^+$  decays occurred when  $\pi^+$  or  $\mu^+$  from Kdal decays were misidentified as  $e^+$ , or as a result of  $\pi^0 \rightarrow e^+e^-e^+e^-$ . Contamination due to secondary particle decays was estimated to be at the level of 0.1%. About 8% of final state pions decayed into muons inside the spectrometer. The careful MWPC simulation gave good agreement of reconstructed track  $\chi^2$  and vertex distributions between data and Monte Carlo. No tight track  $\chi^2$  cuts were applied, and the systematic uncertainties estimated by variation of the vertex cuts were included in the final result. The check of B.R.(  $K_{\tau}$ /Kdal), described below, also tests the final state  $\pi$  and  $\mu$  decays.

Total contamination of the Ke3 sample was estimated to be  $(2.49 \pm 0.05_{stat} \pm 0.32_{sys})\%$ , with the systematic uncertainty caused by the simulation accuracy of the C1 and C2 response to  $\pi^+$  and  $\mu^+$ . Contamination due to overlapping events was  $(0.25 \pm 0.07)\%$  and  $(0.12 \pm 0.05)\%$  of the Kdal and  $K_{e3}^+$  respectively. Figure 1 shows the energy distribution in the calorimeter from the  $e^+$  in the  $K_{e3}^+$  sample. The contamination is manifest in the minimum ionization spike at 250 MeV. The small excess of data in the spike agrees with our contamination uncertainty estimate.

The final  $K_{e3}^+$  sample included  $\approx 30\%$  of events with a fully reconstructed  $\pi^0$ s. We used the  $\pi^0$  information as a consistency check. Not requiring  $\pi^0$ s in

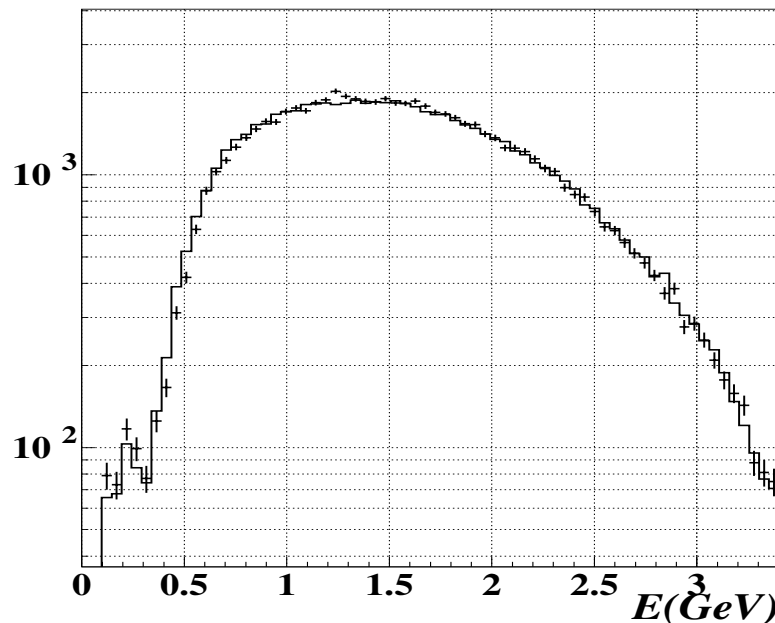


Figure 1: Energy deposited in the calorimeter by the second positive track from the selected  $K_{e3}^+$  sample ( $e^+$  which is not from the low mass  $e^+e^-$  pair). No calorimeter information was used for the  $e^+$  identification. Markers with errors represent data; the histogram is simulation.

our main analysis minimized the uncertainty arising from photon detection and reconstruction in the calorimeter, but increased vulnerability to contamination from upstream decays and photon conversion. Upstream decays whose photon produced pairs before the decay volume (evacuated to about  $10^{-8}$  nuclear interaction length) were suppressed by requiring the three track vertex to be more than two meters downstream of the decay volume entrance. In addition, the results obtained from the two independent samples, one with and one without the  $\pi^0$  reconstructed, did not show a statistically significant discrepancy.

The  $K_{e3}^+$  statistical precision is 0.4%. The systematic error estimate was determined from the B.R. stability under variation of reconstruction procedure, selection criteria, assumed detector efficiencies, and subdivision of both  $K_{e3}^+$  and  $K_{\text{dal}}$  samples<sup>13)</sup>. No significant correlations between any of the different systematic uncertainties were observed. The total systematic error was estimated to be 1.8%. Individual contributions to it are discussed in detail in

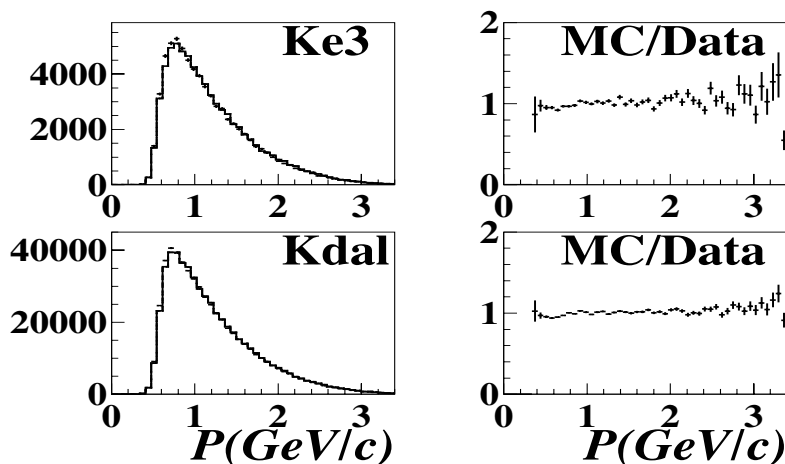


Figure 2: Reconstructed momentum of the  $e^+$  from the low mass  $e^+e^-$  pair from the selected  $K_{e3}^+$  and  $K_{dal}$  samples. Histograms represent Monte Carlo; points with errors represent data. Plots on the right show the bin by bin Monte Carlo to data ratio.

13).

The two largest contributions to the systematic error come from the discrepancies<sup>13)</sup> between data and Monte Carlo in the momentum (Figure 2) and spatial distributions. These errors were determined by dividing the  $K_{e3}^+$  and  $K_{dal}$  events into two roughly equal subsamples, using the relevant parameters, and observing the variation of the result<sup>13)</sup>. The errors were found to be uncorrelated. The sensitivity of the vertical spatial discrepancy to the MWPC alignment and of the momentum discrepancy to the spectrometer parameters is indicative of their possible origins<sup>13)</sup>. The Z-vertex position is also sensitive to the magnetic field, but has a smaller systematic error contribution as determined from both upstream and downstream cuts in Z.

As an additional consistency check, we estimated the  $K_\tau/K_{dal}$  B.R.. The result was  $(1.01 \pm 0.02) \times$  the PDG ratio<sup>1)</sup>, (the theoretical prediction<sup>16)</sup> was used for the  $\pi^0 \rightarrow e^+e^-\gamma$  decay rate). The 2% error was dominated by the uncertainty in the prescale factor of the TAU trigger. A second consistency check compared the  $K_{e3}^+$  B.R. from 1998 and 1997 data. The 1997  $K_{e3}^+$  data used a trigger that required calorimeter hits, and A and D-counters. That trigger neither allowed measurement of these detector efficiencies nor of the

trigger efficiency. While we did not use the 1997 data for our final result, the 1997  $K_{e3}^+$  branching ratio was statistically consistent (within one sigma) with that from 1998. We estimated the form factor slope  $\lambda_+$  from both 1998 and 1997  $K_{e3}^+$  data <sup>13)</sup>. We obtained:  $\lambda_+ = 0.0324 \pm 0.0044_{stat}$  for 1998, and  $\lambda_+ = 0.0290 \pm 0.0044_{stat}$  for the 1997 data, both consistent with the current PDG fit.

After contamination subtraction <sup>13)</sup>, our result is  $BR(K_{e3(\gamma)}^+)/ (BR(K_{\pi 2}^+) + BR(K_{\mu 3}^+) + BR(K_{\pi 3}^+)) = 0.1962 \pm 0.0008_{stat} \pm 0.0035_{sys}$ , where  $K_{e3(\gamma)}^+$  includes all QED contributions (loops and inner bremsstrahlung).

Using current <sup>1)</sup> Kdal B.R.'s we infer  $BR(K_{e3(\gamma)}^+) = (5.13 \pm 0.02_{stat} \pm 0.09_{sys} \pm 0.04_{norm})\%$ , where the normalization error was determined by the PDG estimate of the Kdal B.R. uncertainties. This result does not include the correction due to the correlation of the PDG kaon decay ratios, since it was estimated to be small compared to the systematic error. The PDG fit to the previous  $K^+$  decay experiments yields  $BR(K^+ \rightarrow \pi^0 e^+ \nu) = (4.87 \pm 0.06)\%$  <sup>1)</sup>,  $\approx 2.3\sigma$  lower than our result.

Radiative corrections for decays inside the  $K_{e3}^+$  Dalitz plot boundary were estimated to be  $-1.3\%$  using the procedure of Ref. <sup>5)</sup>;  $K_{e3\gamma}^+$  decays outside the Dalitz plot boundary gave  $+0.5\%$ . Thus the total radiative correction was  $-0.8\%$  resulting in the bare  $BR(K_{e3}^+) = (5.17 \pm 0.02_{stat} \pm 0.09_{sys} \pm 0.04_{norm})\%$ .

Using the PDG value for  $G_F$ , the short-distance enhancement factor  $S_{EW}(M_\rho, M_Z) = 1.0232$  <sup>5), 17)</sup>, and our result for the bare  $K_{e3}^+$  rate we obtain  $|V_{us} f_+(0)| = 0.2243 \pm 0.0022_{rate} \pm 0.0007_{\lambda_+}$ , which gives  $|V_{us}| = 0.2272 \pm 0.0023_{rate} \pm 0.0007_{\lambda_+} \pm 0.0018_{f_+(0)}$  if  $f_+(0) = 0.9874 \pm 0.0084$  <sup>3), 5)</sup>. With this value of  $V_{us}$  and  $V_{ud}$  from superallowed nuclear Fermi beta decays <sup>4)</sup>,  $\delta = 0.0003 \pm 0.0016$ .

This result is consistent with CKM unitarity, and shows reasonable agreement with the recent measurements of  $V_{us}$  from neutral  $K_{e3}$  decays (KLOE, NA48, KTeV) <sup>18)</sup>. Charged  $K_{e3}$  measurements in progress (NA48, KLOE) <sup>18)</sup> should help to clarify the experimental situation.

We thank V. Cirigliano for the  $K_{e3}^+$  radiative corrections code. We gratefully acknowledge the contributions by the staffs of the AGS, and participating institutions. This work was supported in part by the U.S. Department of Energy under contract DE-AC02-98CH10886, the National Science Foundations of the USA, Russia and Switzerland, and the Research Corporation. I would

also like to thank the organizers of HQL2004 for their hospitality in Puerto Rico.

### References

1. K. Hagiwara *et al.*, Phys. Rev. D **66**, 010001 (2002).
2. A. Sher *et al.*, Phys. Rev. Lett. **91**, 261802 (2003).
3. H. Leutwyler, M. Roos, Z. Phys. C **25**, 91 (1984).
4. J.C. Hardy and I.S. Towner, J. Phys. G **29**, 197 (2003).
5. V. Cirigliano *et al.*, Eur. Phys. J. C **23**, 121 (2002).
6. A. Bytnev *et al.*, Eur. Phys. J. C **27**, 57 (2003).
7. G. Calderon and G. Lopez Castro, Phys. Rev. D **65**, 073032 (2002).
8. J. Bijnens and P. Talavera, e-Print Archive: hep-ph/0303103.
9. J. Bijnens *et al.*, Nucl. Phys. **B396**, 81 (1993).
10. S. Shimizu *et al.*, Phys. Lett. **B495**, 33 (2000).
11. I.V. Ajinenko *et al.*, Phys. Atom. Nucl. **66**, 105 (2003).
12. R. Appel *et al.*, Nucl. Instr. and Meth. A **479**, 349 (2002).
13. A. Sher, Ph.D. thesis, University of Pittsburgh (2002)  
<http://scipp.ucsc.edu/~sasha/thesis/th.ke3.ps>.
14. R. Brun *et al.*, "GEANT, Detector Description and Simulation Tool", CERN, Geneva (1994).
15. K.O. Mikaelian, J. Smith, Phys. Rev. **D5**, 1763 (1972).
16. B.E. Lautrup, J. Smith, Phys. Rev. **D3**, 1122 (1971).
17. W.J. Marciano, A. Sirlin, Phys. Rev. Lett. **71**, 3629 (1993).
18. Heavy Quarks and Leptons Workshop. San Juan, Puerto Rico, June 1-5, 2004.

## KTeV DETERMINATION OF THE CKM PARAMETER $|V_{us}|$

R.Kessler

(for the KTeV collaboration)

*Enrico Fermi Institute, University of Chicago, Chicago, Illinois 60637*

### ABSTRACT

KTeV has recently reported results for the six largest  $K_L$  branching fractions, and also for the form factors in  $K_L \rightarrow \pi^\pm e^\mp \nu$  and  $K_L \rightarrow \pi^\pm \mu^\mp \nu$  decays. Using these results, we present a new determination of the CKM parameter  $|V_{us}|$ .

### 1 Introduction

For more than two decades, the first row of the Cabibbo-Kobayashi-Maskawa (CKM) matrix has indicated a  $2\sigma$  discrepancy in the unitarity condition. The first hint of resolving this discrepancy came last year when Brookhaven Experiment E865 reported a new measurement of  $B(K^+ \rightarrow \pi^0 e^+ \nu)$  <sup>1)</sup> that is 6% higher than the PDG evaluation; <sup>6)</sup> the resulting  $|V_{us}|$  value is consistent with unitarity. To address the situation in which  $|V_{us}|$  is extracted from  $K_L$  decays, KTeV has recently measured the  $K_L$  semileptonic branching fractions <sup>3)</sup> and

form factors<sup>4</sup>). An overview of the  $|V_{us}|$  extraction from our results has been reported in<sup>2</sup>). Here we give a brief description of the technique and results.

The  $K_L \rightarrow \pi^\pm \ell^\mp \nu$  ( $K_{\ell 3}$ ) decay rate is related to  $|V_{us}|$  by

$$\Gamma_{K_{\ell 3}} = \frac{G_F^2 M_K^5}{192\pi^3} S_{EW} (1 + \delta_K^\ell) |V_{us}|^2 f_+^2(0) I_K^\ell, \quad (1)$$

where  $\ell = e$  or  $\mu$ ,  $M_K$  is the kaon mass,  $S_{EW}$  is the short-distance radiative correction,  $\delta_K^\ell$  is the mode-dependent long-distance radiative correction,  $f_+(0)$  is the calculated form factor at zero momentum transfer for the  $\ell\nu$  system, and  $I_K^\ell$  is the phase-space integral, which depends on measured semileptonic form factors. Note that the experimental input includes the semileptonic branching fractions, form factors, and  $K_L$  lifetime; the theoretical input includes radiative corrections and  $f_+(0)$ .

To improve the  $|V_{us}|$  determination with  $K_L$  decays, the KTeV experiment at Fermilab has measured the six largest  $K_L$  branching fractions, which account for more than 99.9% of the decay rate, and we have also measured the semileptonic form factors. In our  $|V_{us}|$  determination, the  $K_L$  lifetime is the only experimental input that we take from the PDG. The KTeV measurements are based on high statistics samples ( $10^5$ - $10^6$ ), and we take advantage of the precise calibrations and Monte Carlo simulation used in our  $e'/\epsilon$  analysis.

## 2 KTeV Measurements

The KTeV analysis and Monte Carlo simulation of the  $K_L$  decay modes are described elsewhere<sup>3, 4</sup>). A significant improvement in the  $|V_{us}|$  analysis is the use of KLOR<sup>5</sup>) to generate  $K_L \rightarrow \pi^\pm \ell^\mp \nu(\gamma)$  decays in the MC; KLOR includes virtual photon exchange and inner Bremsstrahlung (IB). The effects of IB are most important in the  $K_{e3}$  decay mode in which IB modifies the acceptance by  $\sim 3\%$ . Radiative effects are also important in the form factor measurements (Sec. 2.2).

### 2.1 $K_L$ Branching Fractions

To determine the  $K_L$  branching fractions, we have measured the following five partial width ratios:

$$\Gamma_{K_{\mu 3}}/\Gamma_{K_{e 3}} \equiv \Gamma(K_L \rightarrow \pi^\pm \mu^\mp \nu)/\Gamma(K_L \rightarrow \pi^\pm e^\mp \nu) \quad (2)$$

$$\Gamma_{+-0}/\Gamma_{Ke3} \equiv \Gamma(K_L \rightarrow \pi^+\pi^-\pi^0)/\Gamma(K_L \rightarrow \pi^\pm e^\mp \nu) \quad (3)$$

$$\Gamma_{000}/\Gamma_{Ke3} \equiv \Gamma(K_L \rightarrow \pi^0\pi^0\pi^0)/\Gamma(K_L \rightarrow \pi^\pm e^\mp \nu) \quad (4)$$

$$\Gamma_{+-}/\Gamma_{Ke3} \equiv \Gamma(K_L \rightarrow \pi^+\pi^-)/\Gamma(K_L \rightarrow \pi^\pm e^\mp \nu) \quad (5)$$

$$\Gamma_{00}/\Gamma_{000} \equiv \Gamma(K_L \rightarrow \pi^0\pi^0)/\Gamma(K_L \rightarrow \pi^0\pi^0\pi^0), \quad (6)$$

Each ratio uses a statistically independent sample, and each pair of decay modes is recorded in the same trigger to avoid uncertainties in the trigger efficiency. To further reduce systematic uncertainties, (i) the  $K_L \rightarrow \pi^\pm \mu^\mp \nu$  decay mode is identified *without* using the muon system to avoid uncertainties in modeling the effect of muon scattering through steel, and (ii) the  $K_L \rightarrow \pi^+\pi^-\pi^0$  decay mode is identified only by the  $\pi^+\pi^-$  tracks, and the  $\pi^0$  is ignored.

The partial width ratio results are given in [3, 2](#)). The largest uncertainty is 1.2% on  $\Gamma_{000}/\Gamma_{Ke3}$  because this ratio does not benefit from detector efficiency cancellations; the uncertainties on the other partial width ratios are between 0.4% and 0.6%. The ratios with  $\Gamma_{Ke3}$  in the denominator show significant disagreement compared with the PDG evaluation [6](#)); only  $\Gamma_{00}/\Gamma_{000}$  is consistent with PDG. Assuming that these six branching fractions sum to 0.9993<sup>1</sup>, the resulting branching fractions are plotted in Fig. 1, and compared with the PDG fit values. The KTeV/PDG ratio for the six branching fractions are shown in Fig. 2. Four of the six branching fractions show a large deviation from PDG fit value; only  $B(K_L \rightarrow \pi^\pm \mu^\mp \nu)$  and  $B(K_L \rightarrow \pi^+\pi^-\pi^0)$  are consistent with PDG.

## 2.2 Semileptonic Form Factors

To determine the phase space integrals,  $I_K^\xi$  and  $I_K^\mu$ , we have measured the semileptonic form factors with the following parametrization:

$$f_+(t) = f_+(0) \left[ 1 + \lambda'_+ \frac{t}{m_\pi^2} + \frac{1}{2} \lambda''_+ \frac{t^2}{m_\pi^4} \right], \quad f_0(t) = f_+(0) \left[ 1 + \lambda_0 \frac{t}{m_\pi^2} \right], \quad (7)$$

where  $t$  is the square of the four-momentum of the lepton-neutrino system, and  $\lambda'_+$ ,  $\lambda''_+$ ,  $\lambda_0$  are the form factor parameters that are measured experimentally. Compared to PDG,  $f_+(t)$  is measured with three times better precision, and

<sup>1</sup>The missing  $K_L$  decay channels (from PDG) are  $B(K_L \rightarrow \gamma\gamma) = 0.060\%$ ,  $B(K_L \rightarrow \pi^0\pi^\pm e^\mp \nu) = 0.005\%$ , and the direct emission  $B(K_L \rightarrow \pi^+\pi^-\gamma) = 0.002\%$

$f_0(t)$  is measured with five times better precision. For  $f_+(t)$ , we find the first evidence ( $4\sigma$ ) of a second order term in  $K_L$  decays.<sup>2</sup> Although the KTeV form factors have much improved precision, leading to 0.3% statistical uncertainty in the  $I_K^\ell$  integrals, the model dependence in the form factor parametrization limits the systematic precision on  $I_K^\ell$ . Specifically, we find that a pole model gives a very good fit to our data, but results in a 0.7% shift in the  $I_K^\ell$  integrals compared to the nominal parametrization in Eq. 7. This 0.7% shift is included as a systematic uncertainty in our extraction of  $|V_{us}|$ .

The quality of the Monte Carlo simulation and the KLOR generator is shown by a data-MC comparison of the reconstructed pion-lepton invariant mass,  $m_{\pi\ell}$ . In Fig. 3, data and MC show excellent agreement in the  $m_{\pi\ell}$  distributions, with  $\chi^2/dof = 35/32$  for  $K_{e3}$  and  $23/25$  for  $K_{\mu3}$ . To illustrate our sensitivity to the precise modeling of radiative corrections, consider a test case in which we use the approximate radiative generator PHOTOS<sup>8)</sup> (instead of KLOR), and repeat the form factor analysis. In this test scenario,  $\lambda_+$  increases by  $2\sigma_{\text{stat}}$  and  $\lambda_0$  increases by  $8\sigma_{\text{stat}}$ ; however, the corresponding  $\chi^2/dof$  in the  $m_{\pi\ell}$  distributions increases to  $57/32$  and  $39/25$  for  $K_{e3}$  and  $K_{\mu3}$ , respectively, showing the limitation of radiative corrections from PHOTOS. In addition to the  $m_{\pi\ell}$  distributions, several other crosschecks on radiative effects are given in 4).

### 2.3 Summary of Changes

Here is a summary of changes in the experimental input that is used to extract  $|V_{us}|$  from Eq. 1:

- KTeV  $B(K_{e3})$  is 5% higher compared to PDG (Fig. 1).
- KTeV  $B(K_{\mu3})$  is consistent with PDG.
- KTeV  $I_K^e$  is 1.7% lower than PDG.
- KTeV  $I_K^\mu$  is 4.2% lower than PDG.

Note that both  $I_K^\ell$  integrals include a  $-1\%$  shift due to the second order term in the form factor ( $\chi_+^\ell$  in Eq. 7). The impact of these measurements will clearly

<sup>2</sup>In  $K^- \rightarrow \pi^0 e^- \nu$  decays, ISTRA+ has recently reported a second order term with  $2\sigma$  significance.<sup>7)</sup>

increase  $|V_{us}|$  by a few percent. A new feature in this analysis is that we can also use  $K_{\mu 3}$  to determine  $|V_{us}|$  because  $\lambda_0$  is sufficiently well measured such that both  $I_K^e$  and  $I_K^\mu$  have comparable precision.

An important test of the new KTeV results compares  $G_F$  for the two decay modes by taking the ratio of Eq. 1 for  $K_L \rightarrow \pi^\pm \mu^\mp \nu$  and  $K_L \rightarrow \pi^\pm e^\mp \nu$ :

$$\left(\frac{G_F^\mu}{G_F^e}\right)^2 = \left[\frac{\Gamma(K_L \rightarrow \pi^\pm \mu^\mp \nu)}{\Gamma(K_L \rightarrow \pi^\pm e^\mp \nu)}\right] / \left(\frac{1 + \delta_K^\mu}{1 + \delta_K^e} \cdot \frac{I_K^\mu}{I_K^e}\right). \quad (8)$$

The ratio of radiative corrections is calculated to be  $(1 + \delta_K^\mu)/(1 + \delta_K^e) = 1.0058 \pm 0.0010$  <sup>5)</sup>, the ratio of the phase space integrals is  $I_K^\mu/I_K^e = 0.6622 \pm 0.0018$  <sup>4)</sup>, and  $\Gamma_{K\mu 3}/\Gamma_{Ke 3} = 0.6640 \pm 0.0026$  <sup>3)</sup>. The resulting ratio of couplings squared is  $(G_F^\mu/G_F^e)^2 = 0.9969 \pm 0.0048$ , consistent with lepton universality. The same ratio calculated from PDG widths and form factors is  $(G_F^\mu/G_F^e)^2 = 1.0270 \pm 0.0182$ . Note that the 0.5% uncertainty in our universality test is much smaller than the differences between the KTeV and PDG partial width ratios and phase space integrals.

### 3 Determination of $|V_{us}|$

The theoretical inputs to Eq. 1 are:

- $S_{EW} = 1.022$  from <sup>9)</sup> (cutoff at the proton mass)
- $\delta_K^e = 0.013(3)$  and  $\delta_K^\mu = 0.019(3)$  from <sup>5)</sup>
- $f_+(0) = 0.961 \pm 0.008$  from <sup>10)</sup>.

As described in <sup>2)</sup>, we average the  $|V_{us}|$  values from  $K_L \rightarrow \pi^\pm e^\mp \nu$  and  $K_L \rightarrow \pi^\pm \mu^\mp \nu$  decays and find

$$|V_{us}|f_+(0) = 0.2165 \pm 0.0012 \quad (9)$$

$$|V_{us}| = 0.2252 \pm 0.0008_{\text{KTeV}} \pm 0.0021_{\text{ext}} \quad (10)$$

where the external error is from  $f_+(0)$ ,  $\tau_L$ , and radiative corrections. Using  $|V_{ud}|$  and  $|V_{ub}|$  from PDG <sup>6)</sup>, and  $|V_{us}|$  from Eq. 10,

$$1 - |V_{ud}|^2 - |V_{us}|^2 - |V_{ub}|^2 = 0.0018 \pm 0.0019, \quad (11)$$

consistent with unitarity.

### 3.1 Comparison with Other Measurements and with Theory

A comparison of  $|V_{us}|f_+(0)$  determinations is shown in Fig. 4. Note that the uncertainty in the experimental quantity  $|V_{us}|f_+(0)$  (circles) does not include the  $\sim 1\%$  theoretical uncertainty from  $f_+(0)$ , but does include the 0.4% uncertainty from the external measurement of the kaon lifetime, and the 0.15% uncertainty from radiative corrections.  $|V_{us}|f_+(0)$  based on the KTeV  $K_L$  measurements is 3% ( $5\sigma$ !) higher compared with PDG. There is a similar discrepancy between E865 and PDG in the  $K^+$  sector; however, the KTeV result cannot distinguish between these two evaluations based on  $K^+$  decays. The corresponding prediction based on unitarity,  $f_+(0)\sqrt{1 - |V_{ud}|^2 - |V_{ub}|^2}$  (open squares in Fig 4), includes uncertainties from both  $f_+(0)$  and  $|V_{ud}|$ .

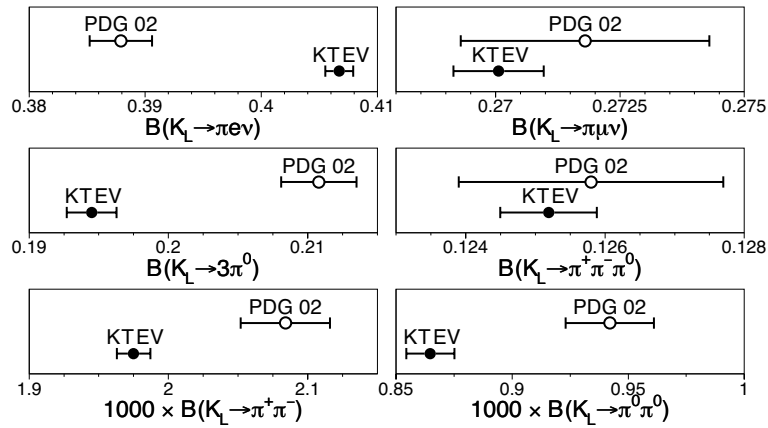


Figure 1: The six largest  $K_L$  branching fractions measured by KTeV (solid dots) and from the PDG 02 evaluation (open circles).

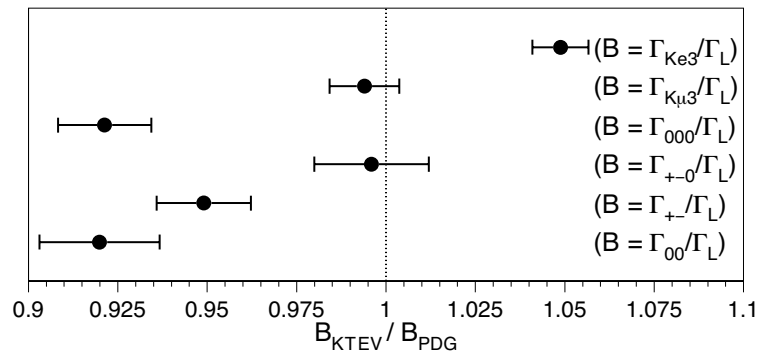


Figure 2: The  $KTeV/$ PDG02 ratio for the six branching fractions shown in Fig. 1.

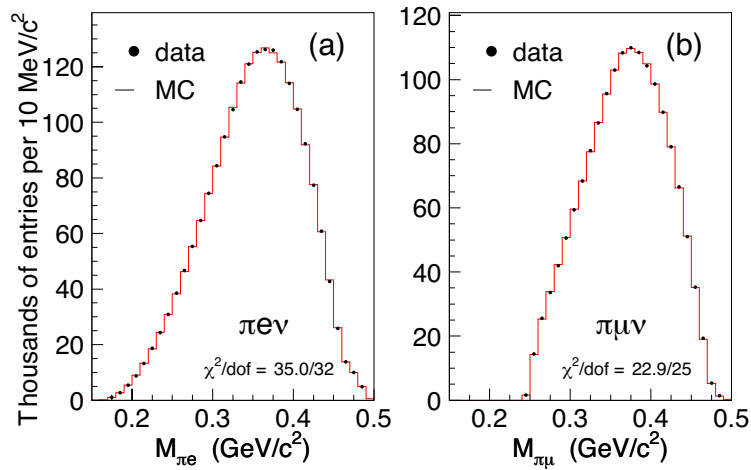


Figure 3: In the  $KTeV$  form factor analysis, distribution of (a) pion-electron mass for  $K_L \rightarrow \pi^\pm e^\mp \nu$ , and (b) pion-muon mass for  $K_L \rightarrow \pi^\pm \mu^\mp \nu$ . Data are shown as dots; MC as histogram.

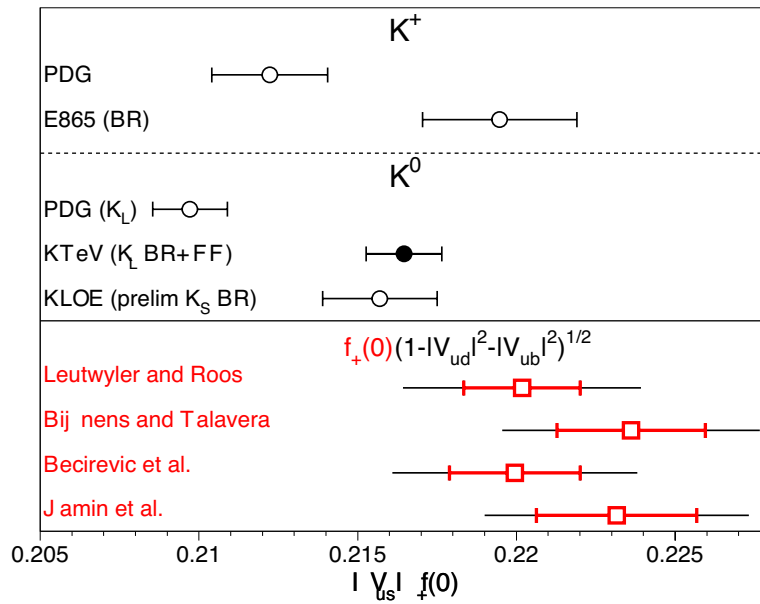


Figure 4: Comparison of  $|V_{us}|f_+(0)$  determined with  $K^+$  and  $K^0$  decays. The solid dot is based on the KTeV branching fractions and form factors <sup>2)</sup>. The E865 result is from <sup>1)</sup>, and the preliminary result from KLOE is based on  $K_S$  decays <sup>11)</sup>. The PDG values are evaluated by KTeV using the PDG branching fractions, lifetimes, and form factors. The open squares show different theoretical values of  $f_+(0)$  <sup>10, 12, 13, 14)</sup> multiplied by  $\sqrt{1 - |V_{ud}|^2 - |V_{ub}|^2}$ ; the inner error bar shows the theory uncertainty on  $f_+(0)$  and the total error includes the uncertainty on  $|V_{ud}|$ .

---

**References**

1. A. Sher *et al* (BNL E865), Phys. Rev. Lett. **91**, 261802 (2003)
2. T. Alexopoulos *et al* (KTeV), submitted to Phys. Rev. Lett, hep-ex/0406001.
3. T. Alexopoulos *et al* (KTeV), submitted to Phys. Rev. D, hep-ex/0406002.
4. T. Alexopoulos *et al* (KTeV), submitted to Phys. Rev. D, hep-ex/0406003.
5. T. Andre., submitted to Phys. Rev. D, hep-ph/0406006.
6. Particle Data Group, Phys. Rev. **D66**, 1 (2002)
7. O.P.Yushchenko *et al* (ISTRA+), Phys. Lett. **B589**, 111 (2004)
8. E.Barberio and Z.Was, Comput. Phys. Commun. **79**, 291 (1994)
9. A.Sirlin, Nucl. Phys. **B196**, 83 (1982)
10. H.Leutwyler and M.Roos, Z.Phys. **C25**, 91 (1984)
11. See talk by A. Antonelli in these proceedings.
12. J.Bijnens and P.Talvera, Nucl. Phys. **B669**, 341 (2003)
13. D.Becirevic *et al*, hep-ph **0403217** (2004)
14. M.Jamin *et al*, JHEP **02**, 047 (2004)



***SESSION VII – Heavy Quark Decays***

G. Boca Beauty and Charm Lifetimes. An Experimental Review  
L. Moroni Dalitz Plot Analysis of D Decays



## BEAUTY AND CHARM LIFETIMES. AN EXPERIMENTAL REVIEW

Gianluigi Boca

*Dipartimento di Fisica Nucleare e Teorica and INFN, via Bassi 6, 27100 Pav*

### ABSTRACT

A summary of the current status of the experimental measurements of the beauty and singly charmed hadron lifetime is given. The comparison with theoretical predictions mainly based on a HQE expansion in terms of  $\frac{1}{m_Q}$  shows a general agreement except for few cases. Nowadays the precision of experiment often reaches the percent level or better for many hadrons. Heavy Quark Expansion can give calculable answers up to order  $\mathcal{O}(\frac{1}{m_Q^3})$  of the expansion, and almost always the theoretical uncertainties are larger than the experimental errors. This will be even more true in the near future, when the B factories are expected to substantially improve the present errors on those lifetimes.

### 1 Theory

The total decay width of a weakly decaying hadron (like most of the beauty and singly charmed hadrons) can be written as the sum of three contributions,

the hadronic decay width, the semileptonic and the fully leptonic (if it exists) decay width :

$$\Gamma_{tot}(H_Q) = \Gamma_{hadro}(H_Q) + \Gamma_{semilept.}(H_Q) + \Gamma_{lept.}(H_Q)$$

Usually the fully lepton width is a very small fraction of the total width or it is absent. The semileptonic widths typically range from  $\sim 6\%$  to  $\sim 10\%$  of the total decay width, consequently most of the differences among the various lifetimes of the heavy quark mesons and baryons are due to  $\Gamma_{hadro}(H_Q)$ .

Nowadays theoretical predictions of weak decay lifetime are based on a Heavy Quark Expansion <sup>1)</sup> in terms of  $\frac{1}{m_Q}$ , where  $m_Q \equiv$  mass of the heavy quark. This expansion leads to the following formula :

$$\Gamma_{hadro}(H_Q) = \frac{G_F m_Q^5}{192\pi^3} |V_{CKM}|^2 [A_0 + \frac{A_2}{m_Q^2} + \frac{A_3}{m_Q^3} + \mathcal{O}(\frac{1}{m_Q^4})] \quad (1)$$

where  $G_F \equiv$  Fermi constant;

$V_{CKM} \equiv$  the relevant CKM matrix element;

$A_0 =$  constant derived from the matrix element of the spectator diagram; this is the leading term and it is the same for all hadrons with a given flavor;

$A_2 =$  constant corresponding to the leading nonperturbative correction term; it reflects the motion of the heavy quark inside the hadron and its spin interaction with the light degrees of freedom;

$A_3 =$  constant derived from the matrix element of Weak Annihilation and Weak eXchange diagrams; also the Pauli Interference effect is taken into account by this constant.

Two general remarks can be made :

a) the lifetime differences for beauty hadrons are smaller (and theoretical calculations more reliable) compared with those of the charmed hadrons because the mass of the beauty quark is larger than the mass of the charm quark and the series (1) converges more rapidly;

b) HQE is better equipped to predict the ratios of lifetimes, rather than the lifetimes themselves.

One of the latest theory prediction about the lifetime ratios of the beauty hadrons are contained in reference <sup>2)</sup> :  $\frac{\tau(B_u^+)}{\tau(B_d^+)} = 1.06 \pm 0.02$ ;  $\frac{\tau(B_s^+)}{\tau(B_d^+)} = 1.00 \pm 0.01$ ;  $\frac{\tau(\Lambda_b)}{\tau(B_d)} = 0.90 \pm 0.05$ . In agreement with what was stated above, it can be noted that these ratios are very close to 1. References <sup>1) 3)</sup> predict ratios about

the charm hadron lifetimes :  $\frac{\tau(D^+)}{\tau(D^0)} \simeq 1 + (\frac{f_D}{200\text{MeV}}) \simeq 2.4$ ;  $\frac{\tau(D_s^+)}{\tau(D^0)} \simeq 1.0 - 1.07$  without WA and  $\simeq 0.9 - 1.3$  with WA;  $\frac{\tau(\Lambda_c^+)}{\tau(D^0)} \simeq 0.5$ ;  $\frac{\tau(\Xi_c^+)}{\tau(\Lambda_c^+)} \simeq 1.3 - 1.7$ ;  $\frac{\tau(\Lambda_c^+)}{\tau(\Xi_c^0)} \simeq 1.6 - 2.2$ ;  $\frac{\tau(\Xi_c^+)}{\tau(\Xi_c^0)} \simeq 2.8$ ;  $\frac{\tau(\Xi_c^+)}{\tau(\Omega_c^0)} \simeq 4$ ;  $\frac{\tau(\Xi_c^0)}{\tau(\Omega_c^0)} \simeq 1.4$  One notices that these ratios can be considerably different from 1 and with large theoretical errors; sometimes the theoretical errors are not even quoted.

## 2 Experimental situation for the beauty hadrons

The beauty hadrons were or are studied only in collider experiments and in three types of reactions : 1)  $p\bar{p} \rightarrow b\bar{b} + X$  at  $\sqrt{s} = 1.8$  TeV at Fermilab; 2)  $e^+e^- \rightarrow Z^0 \rightarrow b\bar{b} + X$  at LEP at Cern or SLD at SLAC; 3)  $e^+e^- \rightarrow \Upsilon(4S)(10580) \rightarrow b\bar{b}$  at the present B-factories BaBar (SLAC) and Belle (KEK, Japan).

Fixed target experiments using reactions like  $p\bar{p} \rightarrow b\bar{b} + X$  are instead are not favoured because the production cross section decreases at small  $\sqrt{s}$ .

Historically the first measures on beauty hadron lifetimes were performed by the LEP experiments Aleph, Delphi, L3, Opal, and the SLD experiment. More recently, CDF and D0 started showing results both on the meson and the baryon lifetimes. Lately BaBar and Belle are performing the most precise measurements, even if limited to the B mesons. Presumably in the near future the increasing integrated luminosity of BaBar, Belle and CDF Run II will improve more and more the statistical precision (which is now generally at the few percent level) of the measures until the second generation B-factories BTev at Fermilab and LHCb at Cern will take over with orders of magnitude larger experimental samples.

### 2.1 B mesons

Many experiments measured the B meson lifetimes. Here all results since 1995 are taken into account <sup>4)</sup>. Two of them (Belle 2001 and D0 2003) are still preliminary. The weighted average of these results is  $\tau_{B_u} = 1.651 \pm 0.013$  ps. As far as the  $B_d^0$  is concerned here the last thirteen <sup>5)</sup> independent results<sup>1</sup>

<sup>1</sup>for all neutral states like this for which mixing is possible -  $B_s$ ,  $D_0$  etc. - by lifetime I mean  $\tau = \frac{1}{\Gamma}$ , with  $\Gamma = \frac{\Gamma_1 + \Gamma_2}{2}$ , where  $\Gamma_1$  and  $\Gamma_2$  are the total decay widths of the two weak Hamiltonian eigenstates.

Table 1: *Theoretical predictions <sup>2)</sup> of lifetime ratios and comparison with the experimental result averages for the beauty hadrons.*

lifetime ratio for beauty hadrons	HQE expectations	experimental results (using averages)
$\frac{\tau(B_u)}{\tau(B_d)}$	$1.06 \pm 0.02$	$1.077 \pm 0.012$
$\frac{\tau(B_s)}{\tau(B_d)}$	$1.00 \pm 0.01$	$0.926 \pm 0.033$
$\frac{\tau(\Lambda_b)}{\tau(B_d)}$	$0.90 \pm 0.05$	$0.776 \pm 0.040$

since 1997 are considered. Their weighted average is  $\tau_{B_d} = 1.533 \pm 0.012$  ps. Concerning the  $B_s$  there have been ten results from different experiment <sup>6)</sup> in the last twelve years; two of them are still preliminary (CDF 2003 and D0 2003). Their weighted average is  $\tau_{B_s} = 1.42 \pm 0.05$  ps. Finally, only one measurement exists on the  $B_c$  lifetime by CDF in 1998 <sup>7)</sup>, that gave as a result  $\tau_{B_c} = 0.46^{+0.18}_{-0.16} \pm 0.03$  ps.

As said earlier, it is preferable to compare ratios of the lifetimes, for instance  $\frac{\tau_{B_u}}{\tau_{B_d}}$  and  $\frac{\tau_{B_s}}{\tau_{B_d}}$ , with theory. In Table 1, first two rows, such comparison is shown. The weighted averages of  $\tau_{B_u}$ ,  $\tau_{B_d}$  and  $\tau_{B_s}$  mentioned before are used in these ratios. The agreement between theory and experiment is excellent for  $\frac{\tau(B_u)}{\tau(B_d)}$  (agreement within  $0.73 \sigma$ 's) while it is less good for  $\frac{\tau(B_s)}{\tau(B_d)}$  (the theoretical and experimental results are  $2.1 \sigma$ 's away). One may notice that nowadays the experimental errors are smaller than the theoretical uncertainties. Moreover most probably BaBar and Belle will statistically improve such measurements further in the future. We hope that theory can keep up with this trend reducing the uncertainty on the predictions soon.

## 2.2 Beauty baryons

$\tau(\Lambda_b)$  has also been measured by several experiments (six experiments since 1998 <sup>8)</sup>). Two of the results are still preliminary (CDF 2003 and D0 2003). The weighted average of all results is  $\tau(\Lambda_b) = 1.19 \pm 0.06$  ps. Consequently the ratio  $\frac{\tau(\Lambda_b)}{\tau(B_d)}$  is  $0.776 \pm 0.040$ . In Table 1 you can see the comparison with the theoretical prediction. There is agreement within  $1.9 \sigma$ 's.

The experimental situation for  $\Xi_b^0$  and  $\Xi_b^-$  is less clear, in the sense that only the 'global' lifetime of a mixture of these two baryons was measured in the

past by Delphi in 1995 and Aleph in 1996 <sup>9)</sup>. The weighted average of these measurements is  $\tau(\Xi_b) = 1.4 \pm 0.3$  ps, in agreement with the general expectation that all hadrons composed by a beauty quark and a light quark should have similar lifetime.

### 3 Experimental situation for the charm hadrons

As explained above, theoretical predictions for charm hadrons are more uncertain than those for beauty hadron, because the charm quark is lighter and so the convergence of the Heavy Quark Expansion is slower. On the opposite, experimentally it is relatively easier to detect charm hadrons than beauty hadrons and consequently historically larger statistics of charm hadrons have been collected by experiments. Since the production cross section is relatively large even at lower  $\sqrt{s}$ , it is possible to produce charm also in fixed target experiments at the Tevatron, in reactions like  $pN \rightarrow c\bar{c} + X$  and  $\gamma N \rightarrow c\bar{c} + X$  where  $N$  means target proton or neutron. The short lifetime of the charmed hadrons (always  $\leq 0.5$  ps except for the  $D^\pm$ ), favours the fixed target experiments over the collider experiments since the former can exploit the Lorentz boost to better measure the proper decay time of the charmed particles. That's one of the reasons why presently the fixed target Focus at Fermilab (that ran in 1996/97) is still dominating all the lifetime measurements of charm particles. The near future results for the lifetime measurements of the  $D$  mesons will come from the B-factories BaBar and Belle that so far have mostly presented preliminary results. Since they are still running, eventually they should be able to collect samples large enough to reduce the statistical errors below the percent level. On the opposite for the charm baryons no new results are expected from these experiments simply because they cannot produce charm baryons copiously. Although the question of the charm baryons hierarchy was essentially settled about ten years ago after the first measurement of the  $(\Omega_c)$  lifetime, more results are desirable in the charm baryon sector in order to bring the precision of the measurements down to the percentage level for the less studied baryons. A contribution in this sense will come very soon from the fixed target experiment Selex, at Fermilab, since they are publishing a new measurement of  $\tau(\Omega_c)$ , the most imprecisely known charm baryon lifetime.

In the far future, the second generation B-factories BTeV and LHCb will also collect enormously large samples of charm hadrons and they will be able to

Table 2: Theoretical predictions <sup>1) 3)</sup> of lifetime ratios and comparison with the experimental result averages for the charm hadrons.

lifetime ratio for charm hadrons	HQE expectations	experimental results (using averages)
$\frac{\tau(D^+)}{\tau(D^0)}$	$\simeq 1 + (\frac{f_D}{200\text{MeV}}) \simeq 2.4$	$2.52 \pm 0.02$
$\frac{\tau(D_s^+)}{\tau(D^0)}$	1.0 – 1.07 without WA 0.9 – 1.3 with WA	$1.21 \pm 0.01$
$\frac{\tau(\Lambda_c^+)}{\tau(D^0)}$	$\simeq 0.5$	$0.485 \pm 0.007$
$\frac{\tau(\Xi_c^+)}{\tau(\Lambda_c^+)}$	$\simeq 1.3 - 1.7$	$2.2 \pm 0.1$
$\frac{\tau(\Lambda_c^+)}{\tau(\Xi_c^0)}$	$\simeq 1.6 - 2.2$	$1.80 \pm 0.18$
$\frac{\tau(\Xi_c^+)}{\tau(\Xi_c^0)}$	$\simeq 2.8$	$4.0 \pm 0.4$
$\frac{\tau(\Xi_c^+)}{\tau(\Omega_c^0)}$	$\simeq 4$	$5.39 \pm 1.05$
$\frac{\tau(\Xi_c^0)}{\tau(\Omega_c^0)}$	$\simeq 1.4$	$1.5 \pm 0.32$

supersede the current results.

As far as the theoretical calculations is concerned, for the charm hadrons even more than for the beauty hadrons, the present precision of the theoretical predictions is in general much worse than the experimental precision. We should hope that further developments in the calculation technique will be possible soon.

### 3.1 *D mesons*

As far as the  $\tau(D^+)$  is concerned, even though there are only four results since 1994, two fixed target, two at  $e^+e^-$  collider machines <sup>10)</sup> (of which the Belle result in 2001 is still preliminary) the error on the weighted average is half of a percentage especially thanks to the high statistics of the latest samples :  $\tau(D^+) = 1.039 \pm 0.006$  ps, which is a remarkable 0.6% level of accuracy.

For the lifetime of the  $D^0$  there are eight experimental results <sup>11)</sup> since 1994 (the Belle 2001 and 2003 and BaBar 2001 results are still preliminary). The weighted average is  $\tau(D^0) = 412.1 \pm 0.8$  fs, with again a rather remarkable 0.5% accuracy.

With these world averages, the ratio  $\frac{\tau(D^+)}{\tau(D^0)}$  is  $2.52 \pm 0.02$  which is only 5%

different from the theoretical prediction of Table 2; it is impossible to estimate the statistical agreement since the theoretical error on this prediction is not quoted in <sup>1)</sup>.

The lifetime of the  $D_s$  <sup>12)</sup> has been measured by six different experiments since 1993 (the Focus and Belle results are still preliminary). The weighted average is  $\tau(D^0) = 500 \pm 4$  fs. The internal consistency of these results, assessed calculating the  $\chi^2$  of all results, is 73.3% confidence level. The ratio  $\frac{\tau(D_s)}{\tau(D^0)}$  is  $1.21 \pm 0.01$  in agreement with the theoretical prediction with W Annihilation contribution (see Table 2).

### 3.1.1 Charm baryons

As far as the charmed baryons are concerned, the  $\Lambda_c$  lifetime is the most easily measured, typically in the  $\Lambda_c \rightarrow pK\pi$  decay channel. In fact there are four results <sup>13)</sup> since 1993 and their weighted average is  $\tau(\Lambda_c) = 200 \pm 3$  fs, achieving a precision at the level of 1%. The ratio  $\frac{\tau(\Lambda_c)}{\tau(D^0)}$  is  $0.485 \pm 0.007$  (see Table 2). The theoretical calculation is  $\simeq 0.5$  but again no theoretical uncertainty estimation is given in <sup>1)</sup> on that number. Therefore I cannot tell whether or not theory and experiment agree in this case.

The next most precise measurement for the baryons is the lifetime of the  $\Xi_c^+$ , for which three results <sup>14)</sup> are available since 1998. Their weighted average is  $\tau(\Xi_c^+) = 439 \pm 20$  fs, which means a 2% precision level. The ratio  $\frac{\tau(\Xi_c^+)}{\tau(\Lambda_c)}$  is  $2.2 \pm 0.1$  whereas theory predicts  $1.3 - 1.7$  (Table 2). Disagreement here is evident.

The next remaining singly charmed baryon lifetimes are more poorly known, due to increased experimental difficulties in producing and detecting them. As far as the  $\Xi_c^0$  is concerned, there are only three results <sup>15)</sup> so far since 1990. The weighted average of them is  $\tau(\Xi_c^0) = 111 \pm 11$  fs, a 10% precision level result. The ratio  $\frac{\tau(\Lambda_c)}{\tau(\Xi_c^0)} = 1.80 \pm 0.18$  in agreement with the also rather imprecise theoretical prediction of  $1.6 - 2.22$ , while  $\frac{\tau(\Xi_c^+)}{\tau(\Xi_c^0)} = 4.0 \pm 0.4$  which is apparently far away from the theoretical 2.8 in Table 2.

Finally for the  $\Omega_c$  lifetime up to now there are only two measurements <sup>16)</sup> since this is the most difficult charmed baryon to detect. The first is an article from the Fermilab experiment E687 (1995) and the second is an analysis from its continuation Focus (2003) (a third result from experiment WA89 at Cern hasn't been considered here because they could never resolve the problem of

an inconsistent  $\Omega_c$  mass in the different decay channels they used in their analysis). The weighted average of the two results is  $\tau(\Omega_c) = 74 \pm 14$  fs. The ratio  $\frac{\tau(\Xi_c^+)}{\tau(\Omega_c)} = 5.39 \pm 1.05$  while theory predicts  $\simeq 4$ , and  $\frac{\tau(\Xi_c^0)}{\tau(\Omega_c)} = 1.5 \pm 0.3$  when theory predicts  $\simeq 1.4$ ; in both cases there is agreement within errors between theory and experiments.

### References

1. see for instance D.Benson, S.Bianco, I.Bigi,F.L.Fabbri, 'A Cicerone for the physics of charm', *Il Nuovo Cimento* (2003) and also hep-ex/0309021, (2003).
2. 'The CKM Matrix and the Unitarity triangle', workshop held at Cern, 13-16 February 2002; hep-ph/0304132, (13 Oct 2003).
3. Bellini, Bigi, Dorman; *Phys. Rep.* **289**, 1 (1997)
4. Delphi coll., *Eur.Phys.J.* **C33**, 307 (2004); CDF coll. and D0 coll., L.Vacavant, proceedings of the 38<sup>th</sup> Rencontres de Moriond on QCD and High-Energy Hadronic Interactions, Les Arcs, Savoie, France, 22-29 Mar 2003; Belle coll., *PRL* **88**, 171801 (2002); CDF coll., *PR D* **65**, 92009 (2002); Belle coll., A.Tajima proceedings of the 36<sup>th</sup> Rencontres de Moriond on QCD and High-Energy Hadronic Interactions, Les Arcs, Savoie, France, 22-29 Mar 2001; BaBar coll., *PRL* **87**, 201803 (2001); Aleph coll., *PL B492*, 275 (2000); Opal coll., *Eur.Phys.J.* **C12**, 609 (2000); L3 coll., *PL B438* 417 (1998); SLD coll., *PRL* **79** 590 (1997); Aleph coll., *Z.Phys. C* **71** 31 (1996); Delphi coll., *Z.Phys. C* **68** 13 (1995); Opal coll., *Z.Phys. C* **67** 379 (1995).
5. Delphi coll., *Eur.Phys.J.* **C33**, 307 (2004); BaBar coll., *PR D* **67**, 91101 (2003); BaBar coll., *PR D* **67**, 72002 (2003); CDF coll., *PR D* **65**, 92009 (2002); Belle coll., *PRL* **88**, 171801 (2002); BaBar coll., *PRL* **89**, 11802 (2002); BaBar coll., *PRL* **87**, 201803 (2001); Opal coll., *Eur.Phys.J.* **C12**, 609 (2000); Opal coll., *PLB* **493**, 266 (2000); Aleph coll., *PL B492*, 275 (2000); L3 coll., *PL B438* 417 (1998); CDF coll., *PR D* **58**, 92002 (1998); SLD coll., *PRL* **79** 590 (1997).
6. CDF coll. and D0 coll., L.Vacavant, proceedings of the 38<sup>th</sup> Rencontres de Moriond on QCD and High-Energy Hadronic Interactions, Les Arcs,

- Savoie, France, 22-29 Mar 2003; D0 coll., Wine&Cheese talk at Fermilab on August 8<sup>th</sup>, 2003; Delphi coll., Eur.Phys.J. **C18** (2000); Delphi coll., Eur.Phys.J. **C16** 555 (2000); CDF coll., PR **D 59**, 32004 (1999); CDF coll., PR **D 57**, 5382 (1998); Opal coll., PL **B426**, 161 (1998); Opal coll., Eur.Phys.J. **C2**, 407 (1998); Aleph coll., Eur.Phys.J. **C4**, 367 (1998); Aleph coll., PL **B377**, 205 (1996).
7. CDF coll., PRL **81** 2432 (1998).
  8. D0 coll., Wine&Cheese talk at Fermilab on August 8<sup>th</sup>, 2003; CDF coll., PRL **77**, 1439 (1996); Delphi coll., Eur.Phys.J. **C10** 185 (1999); Opal coll., PL **B426**, 161 (1998); Aleph coll., Eur.Phys.J. **C2**, 197 (1998).
  9. Aleph coll., PL **B384**, 449 (1996); Delphi coll., Z.Phys. **C 68** 541 (1995).
  10. Focus coll., PL **B537**, 192 (2002); Belle coll., proceedings of the XX Internationale Symposium on Lepton and Photon Interactions at High Energies, Rome, Italy, July 23-28, 2001; Cleo II coll., PRL **82**, (1999); E687 coll., PL **B323**, 459 (1994).
  11. Belle coll., proceedings of the International Conference Lepton Photon 2003, also in hep-ex/0308034; Focus coll., PL **B537**, 192 (2002); Selex coll., PRL **86**, 5243 (2001); Belle coll., proceedings of the XX Internationale Symposium on Lepton and Photon Interactions at High Energies, Rome, Italy, July 23-28, 2001; BaBar coll., proceedings of the 9<sup>th</sup> International Symposium on Heavy Flavours, Pasadena, CA, USA, 10-13 Sep. 2001; E791 coll., PRL **83**, 82 (1999); Cleo coll., PRL **82**, 4586 (1999); E687 coll., PL **B323**, 459 (1994).
  12. Belle coll., proceedings of the XX Internationale Symposium on Lepton and Photon Interactions at High Energies, Rome, Italy, July 23-28, 2001; Selex coll., PL **B523**, 22 (2001); H.Cheung 'review of charm Lifetimes', proceedings of the 8<sup>th</sup> International Symposium on Heavy Flavour Physics, Southampton, England, 25-29 July, 1999; E791 coll., PL **B445** (1999); Cleo coll., PRL **82** (1999); E687 coll., PRL **71** (1993).
  13. Focus coll., PRL **88** 161801 (2002); Selex coll., PRL **86**, 5243 (2001); Cleo coll., PRL **86**, 2232 (2001); E687 coll., PRL **70** 1755 (1993).

14. Cleo coll., PL **D65** 31102 (2002); Focus coll., PL **B523**, 53 (2001); E687 coll., PL **B427** 211 (1998).
15. Focus coll., PL **B541**, 211 (2002); E687 coll., PRL **70** 2058 (1993). ACC-MOR coll., PL **B326**, (1990).
16. Focus coll., PL **B561**, 41 (2003); E687 coll., PL **B357** (1995).

## DALITZ PLOT ANALYSIS OF D DECAYS

Luigi Moroni  
*INFN Milano Via Celoria 16, 20133 Milano-Italy*

### ABSTRACT

In this paper I will address the key issues of the Heavy Flavour Dalitz analysis. I will discuss the formalization problems, the failure of the traditional 'isobar model' and the need for the K-matrix approach. I will conclude with the implications for the future Dalitz analyses in the B-sector. I will address these issues in the context of the recent  $D^+$ ,  $D_s^+ \rightarrow \pi^+\pi^-\pi^+$  Dalitz analysis we performed in FOCUS.

### 1 Unexpected complications in hadronic decay dynamics: $D^+$ and $D_s^+ \rightarrow \pi^+\pi^-\pi^+$

Charm-meson decay dynamics has been extensively studied in the last decade. The analysis of the three-body final state by fitting Dalitz plots has proved to be a powerful tool for investigating effects of resonant substructure, interference

patterns, and final state interactions in the charm sector. The isobar formalism, which has traditionally been applied to charm amplitude analyses, represents the decay amplitude as a sum of relativistic Breit–Wigner propagators multiplied by form factors plus a term describing the angular distribution of the two body decay of each intermediate state of a given spin. Many amplitude analyses require detailed knowledge of the light-meson sector. In particular, the need to model intermediate scalar particles contributing to the charm meson decays into three-body hadronic channels has caused experimentalists of the field to question the validity of the Breit–Wigner approximation for the description of the relevant scalar resonances <sup>1; 2)</sup>. Resonances are associated with poles of the *S-matrix* in the complex energy plane. The position of the pole in the complex energy plane provides the fundamental, model-independent, process-independent resonance description. A simple Breit–Wigner amplitude corresponds to the most elementary type of extrapolation from the physical region to an unphysical-sheet pole. In the case of a narrow, isolated resonance, there is a close connection between the position of the pole on the unphysical sheet and the peak we observe in experiments at real values of the energy. However, when a resonance is broad and overlaps with other resonances, then this connection is lost. The Breit–Wigner parameters measured on the real axis (mass and width) can be connected to the pole-positions in the complex energy plane only through models of analytic continuation. A formalism for studying overlapping and many channel resonances has been proposed long ago and is based on the *K-matrix* <sup>3; 4)</sup> parametrization. This formalism, originating in the context of two-body scattering, can be generalized to cover the case of production of resonances in more complex reactions <sup>5)</sup>, with the assumption that the two-body system in the final state is an isolated one and that the two particles do not simultaneously interact with the rest of the final state in the production process <sup>4)</sup>. The *K-matrix* approach allows for including the positions of the poles in the complex plane directly in the analysis, incorporating in the charm analysis the results from light spectroscopy experiments <sup>6; 7)</sup>. In addition, the *K-matrix* formalism provides a direct way of imposing the two-body unitarity constraint which is not explicitly guaranteed in the simple isobar model. Minor unitarity violations are expected for narrow, isolated resonances but more severe ones exist for broad, overlapping states. The validity of the assumed quasi two-body nature of the process of the *K-matrix* approach

can only be verified by a direct comparison of the model predictions with data. In particular, the failure to reproduce three-body-decay features would be a strong indication of the presence of neglected three-body effects.

### 1.1 The isobar formalism

The formalism traditionally applied to three-body charm decays relies on the so-called isobar model. A resonant amplitude for a quasi-two-body channel, of the type

$$D \rightarrow \begin{cases} r + c \\ \hookrightarrow a + b, \end{cases} \quad (1)$$

is interpreted *à la* Feynman. For the decay  $D \rightarrow \pi\pi\pi$  of Fig. 1, a  $D \rightarrow \pi$

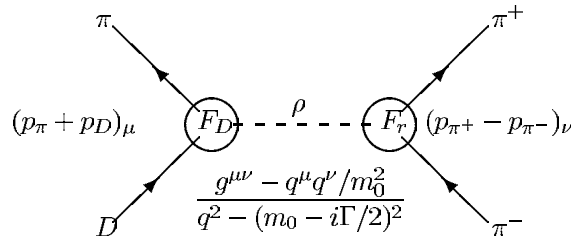


Figure 1: The  $D^+ \rightarrow \pi\pi\pi$  decay diagram.

current with form factor  $F_D$  interacts with a di-pion current with form factor  $F_r$  through an unstable propagator with an imaginary width contribution in the propagator mass. Each resonant decay function is thus,

$$A = F_D F_r \times |\bar{c}|^J |\bar{a}|^J P_J(\cos \Theta_{ac}^r) \times BW(m_{ab}) \quad (2)$$

i.e., the product of two vertex form factors (Blatt–Weisskopf momentum-depend factors), a Legendre polynomial of order  $J$  representing the angular decay wave function, and a relativistic Breit–Wigner (BW). In this approach, already applied in the previous analyses of the same channels<sup>8)</sup>, the total amplitude (Eq. 3) is assumed to consist of a constant term describing the direct non-resonant three-body decay and a sum of functions (Eq. 2) representing intermediate two-body resonances.

$$A(D) = a_0 e^{i\delta_0} + \sum_i a_i e^{i\delta_i} A_i, \quad (3)$$

### 1.2 The $K$ -matrix formalism

For a well-defined wave of specific isospin and spin  $IJ$ , characterized by narrow and isolated resonances the propagator is, as anticipated, of the simple BW form. In contrast, when the specific wave  $IJ$  is characterized by large and heavily overlapping resonances, just as the scalars, the propagation is no longer dominated by a single resonance, but is the result of complicated interplay among the various resonances. In this case, it can be demonstrated on very general grounds that the propagator may be written in the context of the  $K$ -matrix approach as

$$(I - iK \cdot \rho)^{-1} \quad (4)$$

where  $K$  is the matrix for the scattering of particle  $a$  and  $b$  ( Eq. 1) and  $\rho$  is the phase-space matrix. In this picture, the production process is viewed as consisting of an initial preparation of several states, which then propagate via the term  $(I - iK\rho)^{-1}$  into the final state. In particular, the three-pion final state can be fed by an initial formation of  $(\pi\pi)\pi$ ,  $(K\bar{K})\pi$ ,  $(\eta\eta)\pi$ ,  $(\eta\eta')\pi$  and multi-meson states (mainly four-pion states at  $\sqrt{s} < 1.6$  GeV). While the need for a  $K$ -matrix parametrization, or in general for a more accurate description than the isobar model, might be questionable for the vector and tensor amplitudes, since the resonances are relatively narrow and well isolated, this parametrization is needed for the correct treatment of scalar amplitudes. Indeed the  $\pi\pi$  scalar resonances are large and overlap each other in such a way that it is impossible to single out the effect of any one of them on the real axis. In order to write down the propagator, we need the scattering matrix. To perform a meaningful fit to  $D$  mesons to three-pion data, a full description of the scalar resonances in the relevant energy range, updated to the most recent measurements in this sector is needed. At the present time the only self-consistent description of  $S$ -wave isoscalar scattering is that given in the  $K$ -matrix representation by Anisovich and Sarantsev in <sup>7)</sup> through a global fit of the available scattering data from the  $\pi\pi$  threshold up to 1900 MeV.

FOCUS has performed the first fit to charm data with the  $K$ -matrix formalism <sup>9)</sup> in the  $D^+$  and  $D_s^+ \rightarrow \pi^+\pi^-\pi^+$  channels. The  $K$ -matrix used is that of <sup>7)</sup>:

$$K_{ij}^{00}(s) = \left\{ \sum_{\alpha} \frac{g_i^{(\alpha)} g_j^{(\alpha)}}{m_{\alpha}^2 - s} + f_{ij}^{\text{scatt}} \frac{1 \text{ GeV}^2 - s_0^{\text{scatt}}}{s - s_0^{\text{scatt}}} \right\} \times \frac{s - s_{A0} m_{\pi}^2 / 2}{(s - s_{A0})(1 - s_{A0})}. \quad (5)$$

The factor  $g_i^{(\alpha)}$  is the coupling constant of the  $K$ -matrix pole  $\alpha$  to meson channel  $i$ ; the parameters  $f_{ij}^{\text{scatt}}$  and  $s_0^{\text{scatt}}$  describe a smooth part of the  $K$ -matrix elements; the factor  $\frac{s-s_A m_\pi^2/2}{(s-s_{A0})(1-s_{A0})}$  suppresses a false kinematical singularity in the physical region near the  $\pi\pi$  threshold (Adler zero). The  $K$ -matrix values of <sup>7)</sup> generate a physical  $T$ -matrix;  $T = (I - i\rho \cdot K)^{-1}K$ , which describes the scattering in the  $(00)^{++}$ -wave with five poles, whose masses, half-widths, in GeV are (1.019, 0.038), (1.306, 0.167), (1.470, 0.960), (1.489, 0.058) and (1.749, 0.165). The  $K$ -matrix formalism, originated in the context of the two-body scattering, can be generalized to deal with formation of resonances in more complex reactions, through the  $P$ -vector <sup>5)</sup> approach. The decay amplitude for the  $D$  meson into three-pion final state, where  $\pi^+\pi^-$  are in a  $(IJ^{PC} = 00^{++})$ -wave, can thus written as

$$A(D \rightarrow (\pi^+\pi^-)_{00^{++}}\pi^+) = F_1 = (I - iK\rho)_{1j}^{-1} \times \left\{ \sum_{\alpha} \frac{\beta_{\alpha} g_j^{(\alpha)}}{m_{\alpha}^2 - m^2} + f_{1j}^{\text{prod}} \frac{1 \text{ GeV}^2 - s_0^{\text{prod}}}{s - s_0^{\text{prod}}} \right\} \times \frac{s - s_A m_\pi^2/2}{(s - s_{A0})(1 - s_{A0})}. \quad (6)$$

where  $\beta_{\alpha}$  is the coupling to the pole  $\alpha$  in the ‘initial’ production process;  $f_{1j}^{\text{prod}}$  and  $s_0^{\text{prod}}$  are the  $P$ -vector slowly varying (SVP) parameters. In the end, the complete decay amplitude of the  $D$  meson into three-pion final state is <sup>9)</sup>:

$$A(D) = a_0 e^{i\delta_0} + \sum_i a_i e^{i\delta_i} A_i + F_1 \quad (7)$$

where the index  $i$  now runs only over the vector and tensor resonances, which can be safely treated as simple Breit–Wigner’s (see Eq. 2). In the fit to the data, the  $K$ -matrix parameters are fixed to the values of <sup>7)</sup>, which consistently reproduce measured  $S$ -wave isoscalar scattering. The free parameters are those peculiar to the  $P$ -vector, i.e.,  $\beta_{\alpha}$ ,  $f_{1j}^{\text{prod}}$  and  $s_0^{\text{prod}}$ , and those in the remaining isobar part of the amplitude,  $a_i$  and  $\delta_i$ .

The three-pion samples selected in FOCUS (Fig. 2) consist of  $1527 \pm 51$  and  $1475 \pm 50$  events for the  $D^+$  and  $D_s$  respectively. The Dalitz-plot (Fig. 3) analyses are performed on yields within  $\pm 2\sigma$  of the fitted mass value.

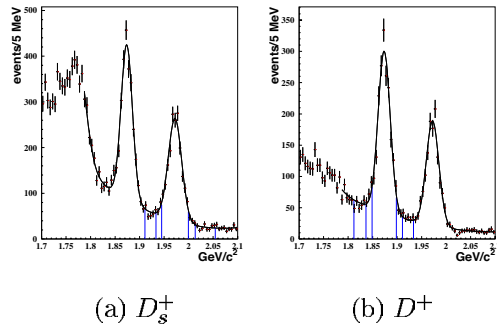


Figure 2: Signal and side-band regions of the three-pion invariant-mass distribution for a)  $D_s^+$  and b)  $D^+$  Dalitz-plot analysis respectively from FOCUS.

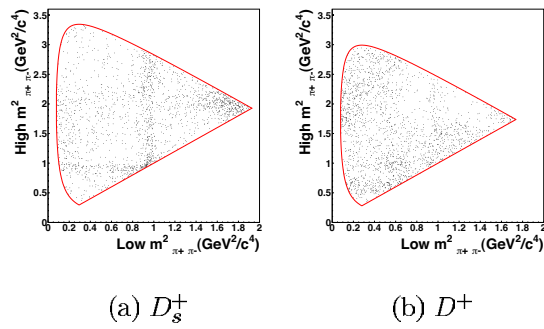


Figure 3: a)  $D_s^+$  and b)  $D^+$  Dalitz plots from FOCUS.

### 1.2.1 FOCUS results for the $D_s^+ \rightarrow \pi^+\pi^-\pi^+$ decay

The general procedure adopted for the fits consists of several successive steps in order to eliminate contributions whose effects on fits are marginal. Initially all the well established, non-scalar resonances decaying to  $\pi^+\pi^-$  with a sizeable branching ratio are considered. Contributions are removed if their amplitude coefficients,  $a_i$  of Eq. 7, are less than  $2\sigma$  significant *and* the fit confidence level increases due to the decreased number of degrees of freedom in the fit. The *P-vector* initial form includes the complete set of *K-matrix* poles and slowly varying function (SVP) as given in reference <sup>(7)</sup>;  $\beta_\alpha$  as well as the  $f_{1j}^{\text{prod}}$  terms of Eq. 6 are removed with the same criteria. The fit confidence levels (C.L.) are evaluated with a  $\chi^2$  estimator over a Dalitz plot with bin size adaptively chosen to maintain a minimum number of events in each bin. Once the minimal set of parameters is reached, addition of each single contribution previously eliminated is reinstated to verify that the C.L. does not improve. The resulting fit fractions <sup>1</sup>, phases and amplitude coefficients are quoted in Table 1. Both the three-body non-resonant and  $\rho^0(770)\pi^+$  components are not required by the fit. This result is to be compared with that obtained with the simple isobar model, which requires a non-resonant component of about 25% to get a decent fit to the data <sup>(10)</sup>. This component, which crosses the Dalitz plot uniformly, seems to compensate, with its interference with the other contributions, for the inability of the model to properly describe some non-trivial resonant features not properly accounted for in the model. In this way the potentiality of the Dalitz-plot analysis to gauge the level of the annihilation contribution in the charm hadronic decays is limited. An additional difficulty with the isobar model is the general poor knowledge of scalar resonances: the measurements reported in the PDG are dispersed over a wide range of values and can not be used as input parameters of charm decay amplitudes. Masses and widths of the corresponding Breit-Wigner forms have to be let free in the fit: the isobar model can thus be viewed as an effective model able to reproduce the data with a sum of effective resonances but its phenomenological interpretation has to be considered with caution. The entire *S-wave* contribution obtained with the *K-matrix* formalism is represented by a single fit fraction since, as

<sup>1</sup>The quoted fit fractions are defined as the ratio between the intensity for a single amplitude integrated over the Dalitz plot and that of the total amplitude with all the modes and interferences present.

previously discussed, one cannot distinguish the different resonance or SVP  $S$ -wave contributions on the real axis. The  $D_s^+$  Dalitz projections of FOCUS data are shown in Fig. 4 superimposed with final fit projections. The fit C.L. is 3%.

Table 1: FOCUS fit results from the  $K$ -matrix model for  $D_s^+$ .

decay channel	fit fraction (%)	phase (deg)	amplitude coefficient
( $S$ -wave) $\pi^+$	$87.04 \pm 5.60 \pm 4.17$	0 (fixed)	1 (fixed)
$f_2(1270) \pi^+$	$9.74 \pm 4.49 \pm 2.63$	$168.0 \pm 18.7 \pm 2.5$	$0.165 \pm 0.033 \pm 0.032$
$\rho^0(1450) \pi^+$	$6.56 \pm 3.43 \pm 3.31$	$234.9 \pm 19.5 \pm 13.3$	$0.136 \pm 0.030 \pm 0.035$
Fit C.L.	3.0%		

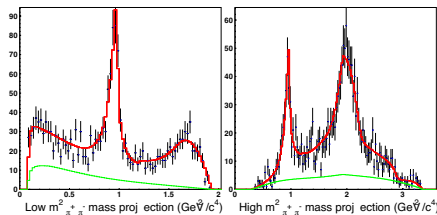


Figure 4:  $D_s^+$  Dalitz-plot projections with the  $K$ -matrix fit superimposed from FOCUS. The background shape under the signal is also shown.

### 1.2.2 FOCUS results for the $D^+ \rightarrow \pi^+\pi^-\pi^+$ decay

The  $D^+ \rightarrow \pi^+\pi^-\pi^+$  Dalitz plot shows an excess of events at low  $\pi^+\pi^-$  mass, which cannot be explained in the context of the simple isobar model with the usual mixture of well established resonances along with a constant, non-resonant amplitude. A new scalar resonance, the  $\sigma(600)$ , has been previously proposed (11) to describe this excess. However we know that complex structure can be generated by the interplay among the  $S$ -wave resonances and the underlying non-resonant  $S$ -wave component that cannot be properly described in the context of a simple isobar model. It is therefore interesting to study this channel with the present formalism, which embeds all the experimental knowledge about the  $S$ -wave  $\pi^+\pi^-$  scattering dynamics. With the same procedure

based on statistical significance and fit confidence level used in the  $D_s^+$  analysis, the final set of contributions is reached. Beside the  $S$ -wave component, the decay appears to be dominated by the  $\rho^0(770)$  plus a  $f_2(1270)$  component. The  $\rho^0(1450)$  was always found to have less than  $2\sigma$  significance and was therefore dropped from the final fit. In analogy with the  $D_s^+$ , the direct three-body non-resonant component was not necessary since the SVP of the  $S$ -wave could reproduce the entire non-resonant portion of the Dalitz plot. The complete fit results are reported in Table 2. The  $D^+$  Dalitz projections are shown in Fig. 5.

Table 2: FOCUS fit results from the  $K$ -matrix model fit for  $D^+$ .

decay channel	fit fraction (%)	phase (deg)	amplitude coefficient
( $S$ -wave) $\pi^+$	$56.00 \pm 3.24 \pm 2.08$	0 (fixed)	1 (fixed)
$f_2(1270) \pi^+$	$11.74 \pm 1.90 \pm 0.23$	$-47.5 \pm 18.7 \pm 11.7$	$1.147 \pm 0.291 \pm 0.047$
$\rho^0(770) \pi^+$	$30.82 \pm 3.14 \pm 2.29$	$-139.4 \pm 16.5 \pm 9.9$	$1.858 \pm 0.505 \pm 0.033$
Fit C.L.	7.7%		

The fit C.L. is 7.7%.

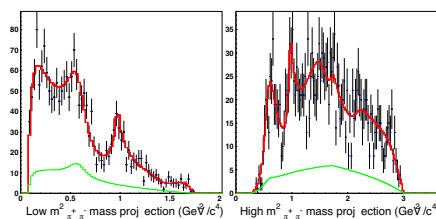


Figure 5:  $D^+$  Dalitz-plot projections with the final fit superimposed from FOCUS. The background shape under the signal is also shown.

The most interesting feature of these results is the fact that the better treatment of the  $S$ -wave contribution provided by the  $K$ -matrix model can reproduce the low-mass  $\pi^+\pi^-$  structure of the  $D^+$  Dalitz plot. This suggests that any  $\sigma$ -like object in the  $D$  decay should be consistent with the same  $\sigma$ -like object measured in the  $\pi^+\pi^-$  scattering. Additional studies with higher statistics will be required to completely understand the  $\sigma$  puzzle. It is interesting to recall the close analogy between the  $D \rightarrow \pi\pi\pi$  channel and the  $B \rightarrow \rho\pi$  one, which is a good candidate to measure the angle  $\alpha$  of the Standard Model Unitarity Triangle; the analysis of  $B \rightarrow \rho\pi$  will proceed through a time-dependent

Dalitz-plot analysis of the three-pion final state and will likely present similar parametrization complications.

### 1.3 Interpretation of the $D_s^+$ and $D^+ \rightarrow \pi^+\pi^-\pi^+$ results of FOCUS

The *K-matrix* formalism has been applied for the first time to the charm sector in the FOCUS Dalitz-plot analyses of the  $D_s^+$  and  $D^+ \rightarrow \pi^+\pi^-\pi^+$  final states. The results are extremely encouraging since the same *K-matrix* description gives a coherent picture of both two-body scattering measurements in light-quark experiments *as well as* charm meson decay. This result was not obvious beforehand. Furthermore, the same model is able to reproduce features of the  $D^+ \rightarrow \pi^+\pi^-\pi^+$  Dalitz plot that otherwise would require an *ad hoc*  $\sigma$  resonance. In addition, the non-resonant component of each decay seems to be described by known two-body *S*-wave dynamics without the need to include constant amplitude contributions. The *K-matrix* treatment of the *S*-wave component of the decay amplitude allows for a direct interpretation of the decay mechanism in terms of the five virtual channels considered:  $\pi\pi$ ,  $K\bar{K}$ ,  $\eta\eta$ ,  $\eta\eta'$  and  $4\pi$ . By inserting  $KK^{-1}$  in the decay amplitude,  $F$ ,

$$F = (I - iK\rho)^{-1}P = (I - iK\rho)^{-1}KK^{-1}P = TK^{-1}P = TQ \quad (8)$$

we can view the decay as consisting of an initial production of the five virtual states which then scatter via the physical  $T$  into the final state. The *Q-vector* contains the production amplitude of each virtual channel in the decay. The resulting picture, for both  $D_s^+$  and  $D^+$  decay, is that the *S*-wave decay is dominated by an initial production of  $\eta\eta$ ,  $\eta\eta'$  and  $K\bar{K}$  states. Dipion production is always much smaller. This suggests that in both cases the *S*-wave decay amplitude primarily arises from a  $s\bar{s}$  contribution such as that produced by the Cabibbo-favored weak diagram for the  $D_s^+$  and one of the two possible singly Cabibbo-suppressed diagrams for the  $D^+$ . For the  $D^+$ , the  $s\bar{s}$  contribution competes with a  $d\bar{d}$  contribution. That the  $f_0(980)$  appears as a peak in the  $\pi\pi$  mass distribution in  $D^+$  decay, as it does in  $D_s$  decay, shows that for the *S*-wave component the  $s\bar{s}$  contribution dominates<sup>2)</sup>. Comparing the relative *S*-wave fit fractions that we observe for  $D_s^+$  and  $D^+$  reinforces this picture. The *S*-wave decay fraction for the  $D_s^+$  (87%) is larger than that for the  $D^+$  (56%). Rather than coupling to an *S*-wave dipion, the  $d\bar{d}$  piece prefers to couple to a vector state like  $\rho^0(770)$  that alone accounts for  $\sim 30\%$  of  $D^+$

decay. This interpretation also bears on the role of the annihilation diagram in the  $D_s^+ \rightarrow \pi^+\pi^-\pi^+$  decay. This study suggests that the  $S$ -wave annihilation contribution is negligible over much of the dipion mass spectrum. It might be interesting to search for annihilation contributions in higher spin channels, such as  $\rho^0(1450)\pi$  and  $f_2(1270)\pi$ .

## 2 Conclusions

Dalitz plot analysis is and will be a crucial tool to extract physics from the Heavy Flavour decays. To fully exploit this unlimited potential a systematic revision of the amplitude formalization on the Dalitz plot is required. Thanks to FOCUS, the K-matrix approach has been shown to be the real breakthrough to resolve the formalization issues and to gain a deep insight in the hadronic decays. Its application to  $D^+$ ,  $D_s^+ \rightarrow \pi^+\pi^-\pi^+$  has been decisive in clearing up a situation that recently became quite fuzzy and confusing. It is worth noting that new 'ad hoc' resonances were required to explain the data in the traditional isobar-model context, e.g. the  $\sigma(600)$  and the  $\kappa(900)$ . Now, strong dynamic effects in D-decays seem under control and fully consistent with those measured in the light-quark scattering experiments, without requiring any new resonance. The new scenario is very promising for the future measurements in the B-sector and, in particular, for the extraction of the  $CP$ -violating phases from the Dalitz analysis of the B hadronic decays, where a proper description of the different amplitudes is essential.

## References

1. S. Spanier and N. A. Törnqvist, Scalar Mesons (rev.), Particle Data Group, Phys. Rev. **D66** (2002) 010001-450.
2. M. R. Pennington, *Proc. of Oxford Conf. in honour of R. H. Dalitz*, Oxford, July, 1990, Ed. by I. J. R. Aitchison, *et al.*, (World Scientific) pp. 66–107; *Proc. of Workshop on Hadron Spectroscopy (WHS 99)*, Rome, March 1999, Ed. by T. Bressani *et al.*, (INFN, Frascati).
3. E. P. Wigner, Phys. Rev. **70** (1946) 15.
4. S. U. Chung *et al.*, Ann. Physik **4** (1995) 404.

5. I. J. R. Aitchison, Nucl. Phys. **A189** (1972) 417.
6. K. L. Au, D. Morgan, and M. R. Pennington, Phys. Rev. **D35** (1987) 1633.
7. V. V. Anisovich and A. V. Sarantsev, Eur. Phys. J. **A16** (2003) 229.
8. P. L. Frabetti *et al.*, Phys. Lett. **B407** (1997) 79.
9. J. Link *et al.*, Phys. Lett. **B585** (2004) 200.
10. S. Malvezzi *Proc. of the Workshop on Scalar Mesons*, Utica, May, 2003, Ed. by A. H. Fariborz, AIP Conf. Proc. **688**, 276, Nucl. Phys. Proc. Suppl. **126**, (2004) 220 also hep-ex/0307055 .
11. E. M. Aitala *et al.*, Phys. Rev. Lett. **86** (2001) 770.

***SESSION VIII – Heavy Quark Production***

G. Gómez-Ceballos	Heavy Quark Production at the Tevatron
F. Di Capua	Study of Neutrino Induced Charm-Production with the Chorus Experiment
F. Sefkow	Heavy Quark Production in Electron-Proton Collisions at HERA



Frascati Physics Series Vol. XXXV (2004), pp. 317-326  
HEAVY QUARKS AND LEPTONS - San Juan, Puerto Rico, June 1-5, 2004

## HEAVY QUARK PRODUCTION AT THE TEVATRON

Guillermo Gómez-Ceballos  
*Massachusetts Institute of Technology, Cambridge, MA 02139, USA*

### ABSTRACT

The Tevatron, operating at  $\sqrt{s} = 1.96 \text{ TeV}$ , provides a very rich environment for the study of charm and bottom hadrons. In this paper we will show measurements from the CDF and DØ collaborations on heavy flavor production, together with a couple of selected topics on exclusive analyses.

### 1 Introduction

Measurements of the production cross-section of heavy flavor quarks in the Tevatron provide us tests on the Quantum Chromodynamics (QCD) predictions. The bottom quark cross-section was measured by both CDF and DØ experiments in the Run I <sup>1)</sup>, and found initially to be about three times larger than the next-to-leading (NLO) QCD computations <sup>2)</sup>. Nevertheless,

the discrepancy has recently been reduced, after more precise theoretical computations have been performed <sup>3)</sup>.

## 2 The Tevatron: CDF and DØ experiments

The Fermilab accelerator complex has undergone a major upgrade for the Run II era, where the centre-of-mass energy has been increased to 1.96 TeV in comparison with 1.80 TeV in the Run I. By the beginning of the summer 2004 the peak of instantaneous luminosity reached by the Tevatron was  $\sim 9 \times 10^{31} \text{ cm}^{-2}\text{sec}^{-1}$ , and the total integrated luminosity of both CDF and DØ experiments was above  $300 \text{ pb}^{-1}$ . The average data taking efficiency is about 85-90% per experiment.

Both CDF and DØ experiments were also dramatically upgraded for Run II. A detailed description of the upgraded detectors can be found elsewhere <sup>4, 5)</sup>. The most important new features in the CDF experiment for heavy flavor physics are: a Silicon Vertex Trigger (SVT), which allows to select long lived heavy flavor particles by requiring to be displaced from the primary vertex interaction point, with a precision similar to that achieved by the offline full reconstruction; an excellent tracking resolution coming from the combination of the silicon and Central Outer Tracker (COT) detectors; and an improved particle identification based on the  $dE/dx$  information of the COT and the Time-of-Flight system (TOF), with a resolution of about  $100 \text{ ps}$ . The Run II DØ detector has excellent tracking and lepton acceptance, being possible to reconstruct tracks with momentum as low as  $180 \text{ MeV}/c$  and pseudo-rapidity as large as 2.5-3.0. A silicon based hardware trigger is being commissioned to trigger on long lived particles. Impact parameter requirements are already applied at the Level 3, which is based on a software filter.

## 3 Cross-section measurements

CDF has performed a measurement of prompt charm meson production cross-section <sup>6)</sup> using only about  $6 \text{ pb}^{-1}$  of Run II data. The implementation of the SVT plays a crucial role, because tracks coming from either charm or bottom quarks can be directly triggered. The charm mesons are reconstructed in the following four modes:  $D^0 \rightarrow K^-\pi^+$ ,  $D^{*+} \rightarrow D^0\pi^+$  with  $D^0 \rightarrow K^-\pi^+$ ,

$D^+ \rightarrow K^- \pi^+ \pi^+$  and  $D_s^+ \rightarrow \phi \pi^+$  with  $\phi \rightarrow K^+ K^-$ <sup>1</sup>.

The direct prompt contribution and the charm decays from a  $B$  meson are statistically separated using the impact parameter of the charm candidate with respect to the primary vertex point. A prompt charm meson usually points to the beam line, while a secondary charm coming from a  $B$  decay does not necessarily point back to the primary vertex, and therefore the impact parameter distribution is much wider. The prompt charm contribution is measured as a function of its  $p_T$ , and it is found on average over all  $p_T$  bins to be:  $(86.5 \pm 0.4(\text{stat.}) \pm 3.5(\text{syst.}))\%$  for  $D^0$ ,  $(88.1 \pm 1.1(\text{stat.}) \pm 3.9(\text{syst.}))\%$  for  $D^{*+}$ ,  $(89.1 \pm 0.4(\text{stat.}) \pm 2.8(\text{syst.}))\%$  for  $D^+$  and  $(77.3 \pm 4.0(\text{stat.}) \pm 3.4(\text{syst.}))\%$  for  $D_s^+$ . The measured prompt charm meson cross-sections are found to be:  $\sigma(D^0, p_T > 5.5 \text{ GeV}/c, |y| < 1) = (13.3 \pm 0.2(\text{stat.}) \pm 1.5(\text{syst.}))\mu\text{b}$ ,  $\sigma(D^{*+}, p_T > 6.0 \text{ GeV}/c, |y| < 1) = (5.2 \pm 0.1(\text{stat.}) \pm 0.8(\text{syst.}))\mu\text{b}$ ,  $\sigma(D^+, p_T > 6.0 \text{ GeV}/c, |y| < 1) = (4.3 \pm 0.1(\text{stat.}) \pm 0.7(\text{syst.}))\mu\text{b}$ ,  $\sigma(D_s^+, p_T > 8.0 \text{ GeV}/c, |y| < 1) = (0.75 \pm 0.05(\text{stat.}) \pm 0.22(\text{syst.}))\mu\text{b}$ . Figure 1 shows the comparison between the data and two QCD calculations<sup>7)</sup> for the differential cross-sections. The observed data values are higher than the QCD predictions, but however they are compatible within the errors.

The CDF II detector has improved the dimuon trigger system with a lower threshold in the transverse momentum of both muons of  $1.5 \text{ GeV}/c^2$ , and then it is possible to collect dimuons with transverse momentum as low as  $0 \text{ GeV}/c$ . CDF has measured the total inclusive  $J/\psi \rightarrow \mu^+ \mu^-$  cross-section in the central rapidity region,  $|y(J/\psi)| < 0.6$ , using  $39.7 \text{ pb}^{-1}$  data<sup>8)</sup>. The total integrated cross-section is measured to be  $\sigma(p\bar{p} \rightarrow J/\psi X, |y(J/\psi)| < 0.6) = (240 \pm 1(\text{stat.}) \pm 28(\text{syst.}))\text{nb}$ . The differential cross-section results are displayed in Figure 2.

The DØ collaboration has verified, using a sample of  $4.7 \text{ pb}^{-1}$  Run II data, that the  $J/\psi$  cross-section is independent of the rapidity range of the  $J/\psi$  for  $0 < |y(J/\psi)| < 2$ <sup>9)</sup>. This study has been performed for  $p_T > 5 \text{ GeV}/c$  and  $p_T > 8 \text{ GeV}/c$ .

CDF has also performed a measurement of the  $p_T$  differential and integrated inclusive b-hadron production cross-section using  $H_b \rightarrow J/\psi X$  decays<sup>8)</sup>, where  $H_b$  include any type of b-hadron with  $J/\psi$  decays. The contribution from b-hadron decays is extracted from the inclusive  $J/\psi$  cross-section

<sup>1</sup>Charge conjugate states are implied throughout the text.

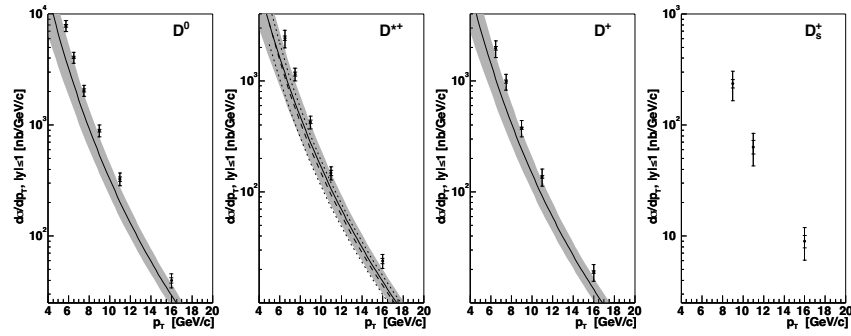


Figure 1: The measured differential cross-section for  $|y(D)| < 1$  from the CDF experiment, shown by the dots. The inner bars correspond to the statistical uncertainties; the outer bars are the quadratic sum of the statistical and the systematic uncertainties. The solid curves are the theoretical predictions from Cacciari and Nason, with the uncertainties indicated by the shaded bands. The dashed curve shown with the  $D^{*+}$  cross-section is the theoretical prediction from Kniehl; the dotted lines indicate the uncertainty. No prediction is available yet for  $D_s^+$  production.

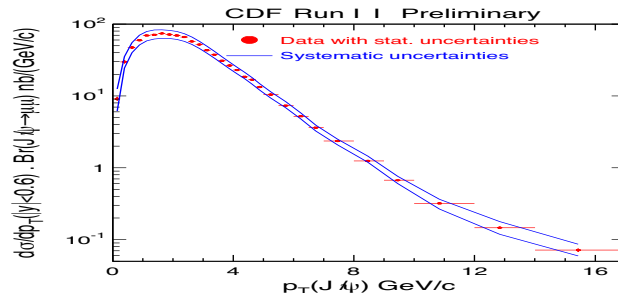


Figure 2: The differential cross-section for  $p\bar{p} \rightarrow J/\psi X$  as a function of  $p_T(J/\psi)$  from the CDF experiment.

measurement. The vertex of the  $J/\psi$  decayed from a  $b$ -hadron is usually displaced from the primary vertex due to the long lifetime of the  $b$ -hadrons, while the vertex is close to interaction point for the prompt  $J/\psi$  contribution or decayed from higher charmonium states. Therefore, it is possible to separate these two components by applying an unbinned maximum likelihood fit to the flight path of the  $J/\psi$  in the  $r - \phi$  plane. The first measurement of the total  $b$ -hadron cross-section at a hadron collider machine has been extracted and was found to be  $\sigma(p\bar{p} \rightarrow H_b X, |y(J/\psi)| < 0.6) BR(H_b \rightarrow J/\psi X) BR(J/\psi \rightarrow \mu\mu) = (24.5 \pm 0.5(\text{stat.}) \pm 4.7(\text{syst.})) \text{nb}$ , and the total single  $b$  quark cross-section was found to be  $\sigma(p\bar{p} \rightarrow bX, |y(b)| < 1.0) = (29.4 \pm 0.6(\text{stat.}) \pm 6.2(\text{syst.})) \mu\text{b}$ . Figure 3 shows the  $b$ -hadron differential cross-section as a function of  $p_T(H_b)$ .

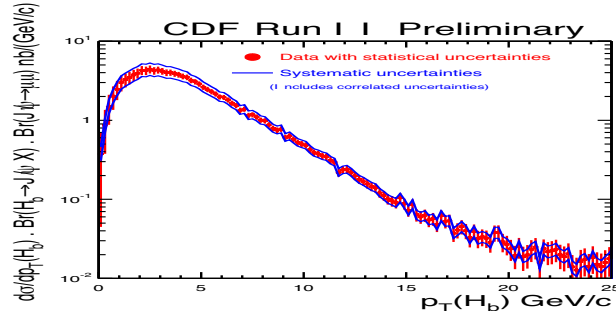


Figure 3: The  $b$ -hadron differential cross-section as a function of  $p_T(H_b)$  from the CDF experiment.

A  $b$ -jet production cross-section measurement has been performed by DØ using  $3.4 \text{ pb}^{-1}$  Run II data in a muon plus jet sample<sup>9)</sup>, where the muon had to be inside a  $\Delta R$  cone<sup>2)</sup> around the jet of 0.7. The signal and QCD background templates were extracted from Monte Carlo simulation, and the  $b$ -jet cross-section measurement was extracted, after applying muon and jet reconstruction efficiencies, and jet calorimeter corrections. The comparison between the data and the theoretical prediction as a function of the  $p_T$  of the jet is shown in Figure 4.

$$^2\Delta R = \sqrt{\Delta\eta^2 + \Delta\phi^2}$$

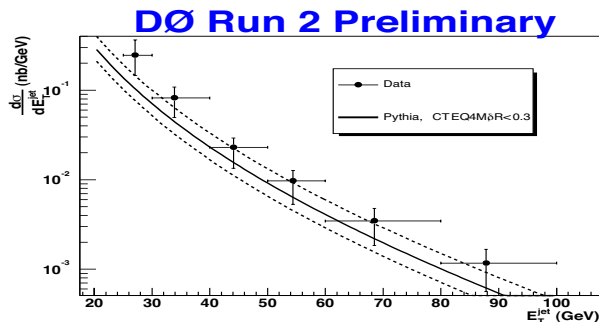


Figure 4: Measured  $b$ -jet cross-section compared to the theoretical prediction from the  $DØ$  experiment.

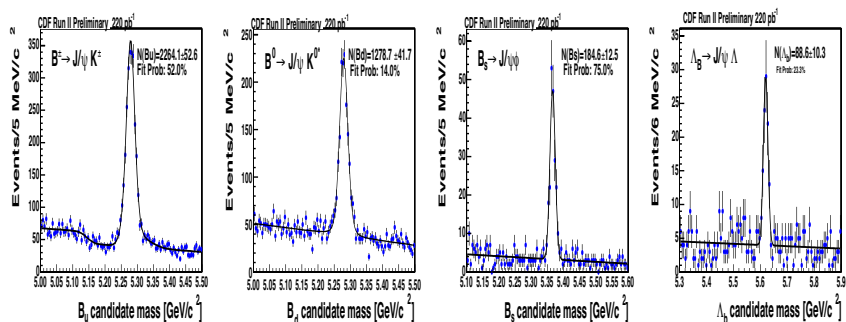
#### 4 Exclusive measurements

Once the global picture looks like rather good, we can move to exclusive measurements. Here, we will just show two specific selected topics, but there are many analyses where the Tevatron is making an important contribution.

Measurements of  $B$  hadron masses are basic to demonstrate the understanding of the detector, and in addition all these measurements can already be competitive with the PDG results. CDF has measurements on  $B$  hadron masses using four fully reconstructed  $J/\psi$  modes:  $B^+ \rightarrow J/\psi K^+$ ,  $B^0 \rightarrow J/\psi K^*$ ,  $B_s \rightarrow J/\psi \phi$ ,  $\Lambda_b \rightarrow J/\psi \Lambda$  <sup>8)</sup>. Figure 5 shows the mass distributions on all these channels. A very small systematic uncertainty, at the level of  $0.5 \text{ MeV}/c^2$ , can be achieved with very precise calibration studies using the big  $J/\psi \rightarrow \mu\mu$  inclusive sample.

Table 1 shows the results, together a comparison with the PDG value. It is important to notice that the  $B^+$  and  $B^0$  are the world best single mass measurements, and the  $B_s$  and  $\Lambda_b$  mass measurements are better than the combined PDG result <sup>10)</sup>. The  $DØ$  experiment expects to have new results soon with a improved yield after a new reprocessing.

$B_d^0$  mixing frequency  $\Delta m_d$  has already been measured with a high precision at the  $B$  factories <sup>10)</sup>. Nevertheless, it is a very important analysis for both CDF and  $DØ$  experiments. It is a benchmark of the initial state flavor tagging and it is a mandatory step toward the  $B_s$  mixing anal-

Figure 5:  $B$  hadron mass distributions from the CDF experiment.

$B$ hadron	CDF measurement	PDG value
$B^+$	$5279.10 \pm 0.41 \pm 0.34$	$5279.0 \pm 0.5$
$B^0$	$5279.57 \pm 0.53 \pm 0.30$	$5279.4 \pm 0.5$
$B_s$	$5366.01 \pm 0.73 \pm 0.30$	$5369.6 \pm 2.4$
$\Lambda_b$	$5619.7 \pm 1.2 \pm 1.2$	$5624 \pm 9$

Table 1:  $B$  hadron mass measurements from the CDF experiment in comparison with the PDG value (units in  $\text{MeV}/c^2$ ). CDF results are shown with the statistical (first) and systematic (second) uncertainties. PDG values are shown with the total combined uncertainty.

ysis, which is one of the main goals of the Run II Tevatron Physics program.  $B_d^0 - \bar{B}_d^0$  oscillations have been studied by the DØ experiment with a large sample of semileptonic  $B$  decays corresponding to a integrated luminosity of about  $250 \text{ pb}^{-1}$  <sup>9</sup>). The flavor of the final state of  $B_d^0$  meson was determined using the muon charge from the partially reconstructed decay  $B_d^0 \rightarrow \mu^+ D^{*-} X$ ;  $D^{*-} \rightarrow \bar{D}^0 \pi^-$ ;  $\bar{D}^0 \rightarrow K^- \pi^+$ . Figure 6 shows the mass difference  $M(D^0 \pi) - M(D^0)$  distribution for  $B \rightarrow \mu D^* X$  candidates. The opposite-side muon tagging was used for the initial state flavor determination. The asymmetry for the tagging candidates versus the visible proper decay length <sup>3</sup> is shown in Figure 7. This distribution is fitted in order to compute  $\Delta m_d$ , which is found to be  $\Delta m_d = (0.506 \pm 0.055(\text{stat.}) \pm 0.049(\text{syst.})) \text{ps}^{-1}$ .

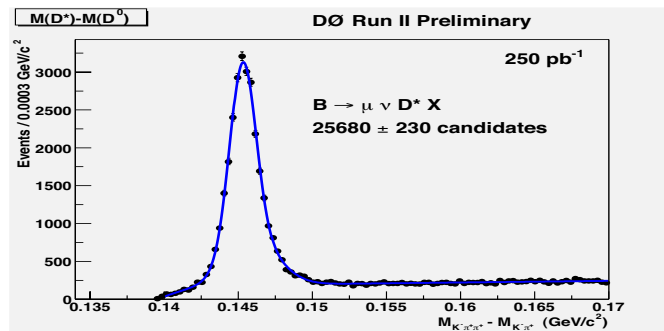


Figure 6: The mass difference  $M(D^0 \pi) - M(D^0)$  distribution for  $B \rightarrow \mu D^* X$  candidates from the DØ experiment.

CDF has performed a  $B^0$  frequency analysis using a sample corresponding to a total integrated luminosity of about  $245 \text{ pb}^{-1}$  on the exclusive decay modes  $B^0 \rightarrow J/\psi$  and  $B^0 \rightarrow D^- \pi^+$  <sup>8</sup>). The flavor of the  $B$  meson at the production time was inferred using the Same Side Tagging (SST) algorithm <sup>11</sup>). This algorithm relies on the existing charge correlation between the  $b$ -quark and the closest particle in the fragmentation string. Figure 8 shows the measured time dependent asymmetries for those two modes. The combined analysis gives a value of  $\Delta m_d = (0.55 \pm 0.09(\text{stat.}) \pm 0.01(\text{syst.})) \text{ps}^{-1}$ . Both experiments get results compatible with the PDG value and further improvements are expected

$${}^3V PDL = L_{xy} M_B / P_T^{\mu D^0}$$

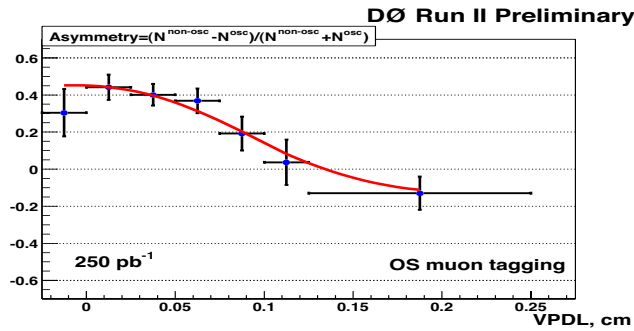


Figure 7: The asymmetry in the  $B_d^0 \rightarrow \mu^+ D^{*-} X, D^{*-} \rightarrow \bar{D}^0 \pi^-, \bar{D}^0 \rightarrow K^- \pi^+$  sample as a function of the visible proper decay length from the DØ experiment. The overlaid curve comes from the asymmetry fit.

very soon.

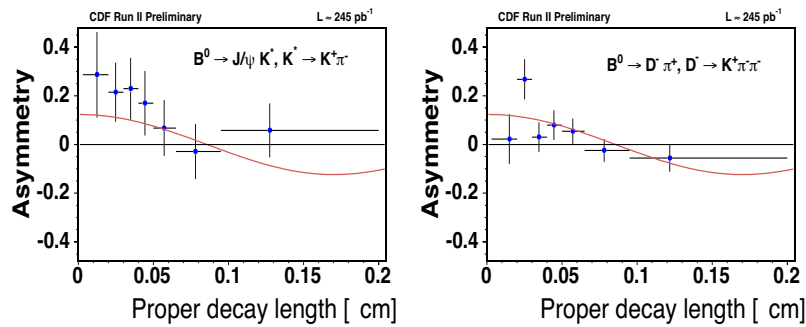


Figure 8: Time dependent asymmetries in the  $B^0$  mixing analysis from the CDF experiment. In both plots, the overlaid curve comes from the simultaneous asymmetry fit for both  $B^0$  modes.

### 5 Conclusions

The large amount of data collected by the CDF and DØ experiments are improving our knowledge about Heavy Flavor Physics. The inclusive cross-section

measurements agree, within the errors, with the theoretical expectations. Nevertheless, further improvements from both experimental and theoretical points of view are expected in next years. The Run II data can already make high precision measurements, and an example has been shown with the measurement of the  $B$  hadron masses at the level of  $0.5 \text{ MeV}/c^2$ . In addition  $B_d^0$  mixing is well established in both CDF and DØ experiments, which is a crucial step toward a  $B_s$  mixing measurement.

### References

1. B. Abbott *et al.*, *Phys. Lett.*, **B 487**, 264-272 (2000);  
D. Acosta, *et al.*, *Phys. Rev.*, bf D65, 052005 (2005).
2. P. Nason, S. Dawson and R. K. Ellis, *Nucl. Phys.*, **327**, 49-92 (1989);  
C. Albajar *et al.*, *Phys. Lett.*, **B186** 237 (1987).
3. M. Cacciari and P. Nason, *Phys. Rev. Lett.*, **89**, 122003 (2002).
4. R. Blair *et al.*, *The CDF-II detector: Technical Design report*, FERMILAB-PUB-96-390-E (1996).
5. A. Abachi *et al.*, *The D0 upgrade: The detector and its physics*, FERMILAB-PUB-96-357-E (1996).
6. D. Acosta *et al.*, *Phys. Rev. Lett.*, **91**, 241804 (2003).
7. M. Cacciari and P. Nason, *JHEP*, **0309**, 006 (2003);  
B. Kniehl (private communication). His calculation employs the method describes in B. Kniehl, G. Kramer, B. Potter, *Nucl. Phys.*, **B597**, 337-369 (2001).
8. CDF public web pages.
9. DØ public web pages.
10. K. Hagiwara *et al.*, *Phys. Rev.*, **D66**, 010001 (2002).
11. F. Abe *et al.*, *Phys. Rev.*, **D59**, 032001 (1999).

Frascati Physics Series Vol. XXXV (2004), pp. 327-340  
HEAVY QUARKS AND LEPTONS - San Juan, Puerto Rico, June 1-5, 2004

## STUDY OF NEUTRINO INDUCED CHARM-PRODUCTION WITH THE CHORUS EXPERIMENT

Francesco Di Capua  
*Università Federico II and INFN, Napoli, Italy*

### ABSTRACT

The CHORUS experiment was designed to search for  $\nu_\mu \rightarrow \nu_\tau$  oscillation by detecting the decay topology of the  $\tau$  in charged-current (CC)  $\nu_\tau$  events. The CHORUS hybrid apparatus consists of active nuclear emulsion targets and electronic detectors. It was exposed to the CERN/SPS Wide Band Neutrino Beam in the years 1994/1997. With the recent improved performance of the automated emulsion scanning systems, it has become possible to perform large volume scanning around the located interaction vertex. All tracks belonging to it can thus be recognized and precisely measured. This technique has been applied to search for  $\nu_\mu - \nu_\tau$  oscillation as well as for the recognition of events where charmed particles are produced. By using this technique, 2059 charm hadrons have been found on 95450 CC events. We report on new measurements based on a sub-sample of data. Finally, we give the prospects for the study of charm-production induced by neutrinos within the CHORUS experiment.

## 1 Introduction

About thirty year after the discovery of the charm quark at SLAC and BNL, the study of the charmed particles is still a challenging field of particle physics. In particular, the neutrino induced charm-production offers the possibility to study the strange-quark content of the nucleon, to measure “directly” the CKM matrix element  $V_{cd}$  and to test models for charm-production and subsequent hadronization. Moreover, unlike colliding beams, neutrinos produce charmed hadrons also via specific processes like quasi-elastic and diffractive scattering which provide an unique tool for exclusive charm studies. Furthermore, charm-quark pairs can also be produced, although with considerably lower cross-sections, allowing for the investigation of higher order mechanism.

Several experiments studied charm-production induced by neutrinos through the detection of dimuon events (CDHS <sup>1</sup>), CCFR <sup>2</sup>), CHARM, CHARM II <sup>3</sup>), NOMAD <sup>4</sup>) and NuTeV <sup>5</sup>). In these events, the leading muon is interpreted as originating from the neutrino interaction vertex and the other as the product of the charmed particle semileptonic decay. These experiments do not identify the decay topology of the short-lived charmed hadrons. Hence they suffer from background in which the second muon originates from an undetected decay in flight of a pion or a kaon rather than from a charmed particle decay. In order to keep this background as low as possible only high energy neutrinos are considered. Consequently the threshold effect of the charm-production cannot be studied.

Conversely CHORUS, as well as the former E531 experiment, by exploiting the high spatial resolution of nuclear emulsion is able to detect the short-lived charmed hadrons directly through their peculiar decay topology. This allow for a smaller background and the investigation of charm-production at low neutrino energies hence, of the threshold effect.

The paper is organized as follow. In Section 2 we describe the technique of nuclear emulsions used in CHORUS and, in Section 3 we report the achieved results. Finally, we give the prospects for the study of charm-production induced by neutrinos and our conclusions.

## 2 The CHORUS experiment

The CHORUS experiment <sup>6)</sup> was designed to search for  $\nu_\mu \rightarrow \nu_\tau$  oscillations in the SPS Wide Band Neutrino Beam at CERN through the direct observation of the  $\tau$  lepton decay. The detector is a hybrid setup that combines a nuclear emulsion target of 770 Kg with various electronic detectors. Neutrino interactions are reconstructed by a scintillating fiber tracker situated immediately downstream of the emulsion target. The reconstructed tracks are followed back in the emulsion plates, starting from the most downstream plate. A reconstructed track which is missed in two consecutive plates constitutes a vertex candidate and the first plate where the track is missed is called the vertex plate. The emulsion scanning has been performed by fully automatic microscopes equipped with CCD cameras and a read out system, evolved from the so-called *Track Selector* <sup>7)</sup>.

Once the vertex plate has been identified, additional scanning is performed for the detection of short-lived particles, which are interesting for the oscillation search as well as for studies of charmed particles produced in neutrino interactions. The improvements in the automatic emulsion scanning systems allowed for large volume data-taking around located neutrino interactions through a procedure called Netscan. Within a volume of  $1.5 \times 1.5 \times 6.3 \text{ mm}^3$  all track segments whose angle with the neutrino beam direction is less than 0.4 rad are scanned. On average 800 tracks are found in each plate, most of them are muons from other beam lines or from neutrino interactions in material upstream of the CHORUS detector. These tracks are used for an alignment procedure and enable a resolution of  $0.3 \mu\text{m}$  in position and 2 mrad in angle to be achieved. Thanks to this resolution it is possible to perform a topological identification of charmed hadrons decays (Fig. 1), which brings a very low level of background contamination. The CHORUS experiment collected a statistics of 2059 charmed particle decay candidate out of 95450 CC events.

## 3 Charm analysis

### 3.1 Measurement of $\Lambda_c^+$ production rate <sup>8)</sup>

Charged charmed particles produced by  $\nu_\mu CC$  interactions are mainly  $D^+$ ,  $D_s^+$  and  $\Lambda_c^+$ . The  $\Lambda_c^+$  production rate has been evaluated by a statistical method which makes use of the flight length distribution. Since the lifetime of the  $\Lambda_c^+$

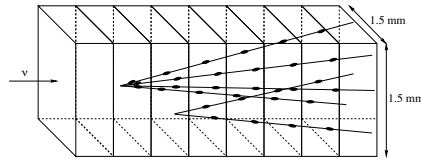


Figure 1: Schematic view of reconstructed neutrino interaction vertex and charmed hadron decay.

Table 1: Number of candidates after the selection on flight length

	Selection A $40 \mu\text{m} < FL < 400 \mu\text{m}$	Selection B $400 \mu\text{m} < FL < 2400 \mu\text{m}$
C1	62	133
C3	66	77
Total	128	210

is smaller than that of other charged charm particles, the sample of charged charm with a short flight decay forms a sample enriched in  $\Lambda_c^+$ ; while long flight decay events are dominated by  $D^+$  and  $D_s^+$ . Therefore, the analysis is performed applying two different selections:

- **Selection A:** short flight decay. A daughter track must have a minimum distance of  $5 \mu\text{m}$  to  $30 \mu\text{m}$  with respect to a track which is identified as a muon. This selection has been applied to 50414 events.
- **Selection B:** long flight decay. Both the parent track and the daughter track are reconstructed. The parent track must have a minimum distance smaller than  $5 \mu\text{m}$  with respect to the reconstructed muon. The daughter track must have a minimum distance of  $5 \mu\text{m}$  to  $30 \mu\text{m}$  with respect to the parent track. This selection has been applied to 56761 events.

The selected candidates, 1614 for the selection 'A' and 586 events for 'B', were visually inspected to identify their decay topology and to reject background. To ensure a high efficiency of the visual inspection, a cut on the charm flight length has been applied. The results are summarized in Table 1.

Combining 'A' and 'B', and taking into account the detection efficiency and background estimation, the number of  $\Lambda_c^+$  candidates was found to be

$861 \pm 198(stat) \pm 98(syst)_{-54}^{+140}(QE)$ . At an average neutrino energy of 27 GeV, the  $\Lambda_c^+$  production cross section in  $\nu_\mu CC$  interactions was measured to be:

$$\frac{\sigma(\Lambda_c^+)}{\sigma(CC)} = (1.54 \pm 0.35(stat) \pm 0.18(syst)) \times 10^{-2}.$$

### 3.2 Quasi-elastic charmed baryon production <sup>9)</sup>

For a particular class of events, at low  $Q^2$ , the quark  $c$  produced in the neutrino interaction does not fragment, but dresses himself with the spectator quarks. Therefore, the final hadronic state contains only the charmed particle. The simplest exclusive charm-production reactions are:

$$\nu_\mu n \rightarrow \mu^- \Lambda_c^+ \quad (1)$$

$$\nu_\mu n \rightarrow \mu^- \Sigma_c^+ (\Sigma_c^{*+}) \quad (2)$$

$$\nu_\mu p \rightarrow \mu^- \Sigma_c^{++} (\Sigma_c^{*++}). \quad (3)$$

Since in the final state we have always a  $\Lambda_c^+$ , a selection aimed to the construction of a sample enriched in  $\Lambda_c^+$  decays showing the peculiar quasi-elastic topology and kinematics has been developed. This selection acts on the following variables:

1. flight length ( $< 200 \mu m$ );
2. track multiplicity at primary vertex ( $\leq 3$ );
3. hadronic energy ( $E_{EM} < 2 \text{ GeV}^2$ );
4. angle  $\Phi$  between the primary muon and the charmed particle trajectory in the plane transverse to the incident neutrino direction ( $> 165^\circ$ ).

The selection criteria were applied to 46,105  $\nu_\mu CC$  interactions. Figure 2 shows the distribution of the angle  $\Phi$  after the cuts 1-3,  $\Phi > 165^\circ$  will be required to isolate the signal. The final sample contain 13 events with an

<sup>1</sup>In the processes (2)-(3) the production of a charmed baryon is always followed by a strong decay in the channel  $\Lambda_c^+ \pi$ .

<sup>2</sup> $E_{EM}$  is the energy measured in the first sector of the calorimeter (EM).

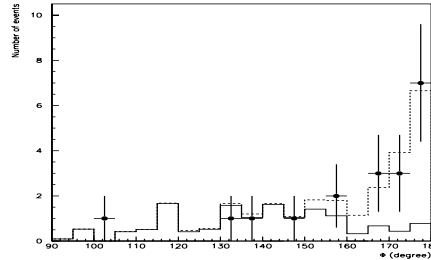


Figure 2: *Azimuthal angle between the primary muon and the charmed particle trajectory in the transverse plane, for events after cuts 1-3. The solid and dashed lines are the expectations from deep inelastic scattering and deep inelastic scattering and quasi-elastic simulation, respectively.*

estimated background of 1.7 events, mainly due to DIS  $\Lambda_c^+$  production. Normalizing to the number of CC events in the sample, a value of

$$\frac{\sigma(QE)}{\sigma(CC)} = (0.23^{+0.12}_{-0.06}(\text{stat})^{+0.02}_{-0.03}(\text{syst})) \times 10^{-2}$$

is obtained for the ratio of the cross-sections for quasi-elastic production of charmed baryons and for  $\nu N$  CC interactions.

### 3.3 Measurement of $D^0$ production rate

A measurement of the production rate of  $D^0$  mesons is performed based on full CHORUS statistics. The following criteria were applied to select  $D^0$  candidates. A muon track at the primary vertex and at least one daughter track were reconstructed in the emulsion and matched with tracks in the detector. The daughter track was required to have a impact parameter with respect to the primary vertex in the range  $3 - 15 \mu m < I.P. < 400 \mu m$ . After performing visual inspection, we confirmed that 841 events show a 2-prong decay topology (V2) and 230 events show a 4-prong decay topology (V4). The average efficiency of the  $D^0$  decay search is  $(56.3 \pm 0.5)\%$  for V2 and  $(74.2 \pm 0.9)\%$  for V4. Subtracting the background and correcting for the efficiencies, the measured ratio is

$$\frac{V4}{V2} = (22.9 \pm 1.8)\%$$

Using the  $BR(D^0 \rightarrow V4) = (13.3 \pm 0.7) \times 10^{-2}$  from the PDG <sup>11)</sup> tables, we obtain the branching ratio of  $D^0$  decaying into neutral particles by using the simple expression:

$$BR(D^0 \rightarrow neutrals) = 1 - BR(D^0 \rightarrow V4) \times \left(1 + \left(\frac{V4}{V2}\right)^{-1}\right).$$

A preliminary result gives

$$BR(D^0 \rightarrow neutrals) = (28.7 \pm 5.2)\%.$$

Taking into account this result, the total  $D^0$  cross-section rate is measured to be

$$\frac{\sigma(D^0)}{\sigma(CC)} = (3.0 \pm 0.1(stat) \pm 0.2(syst)) \times 10^{-2}.$$

#### 3.4 Semi-leptonic branching fraction of charm hadrons <sup>12)</sup>

This is the only direct measurement of the semi-muonic branching ratio of charm hadrons. For this search, 1055 candidates were selected from a sample of 56172 events analyzed. To evaluate the purity of the selection, a sub sample of 244 events was visually inspected. Out of 244 events, 11 do not have a secondary vertex related to the event and 12 were identified as secondary hadronic interactions. This results in a selection purity of  $0.91 \pm 0.02$ , which brings the corrected number of selected charm events to

$$N^{selected} = 956 \pm 35.$$

Muons are identified in the calorimeter and the muon spectrometer. For muon momenta above 4 GeV, the identification efficiency is of the order of 95%. The secondary muon identification has an average efficiency of about 55%. Out of the  $956 \pm 35$  selected charm events, the number of events with a secondary muon is

$$N_{2\mu}^{selected} = 88 \pm 10(stat) \pm 8(syst).$$

corrected for the efficiency of the muon identification. For the determination of the semi-leptonic branching fraction we used the correction factor (R) defined as

$$R = \frac{\sum_{D_i} \epsilon_{D_i} f_{D_i}}{\sum_{D_i} \epsilon_{D_i}^{\mu} f_{D_i}}$$

where  $\epsilon_{D_i}$  is the selection efficiency for charm species  $D_i$ ;  $\epsilon_{D_i^\mu}$  the selection efficiency for semi-leptonic decays of  $D_i$ ; and  $f_{D_i}$  the production fraction of each charm hadron. The measurement of  $BR(D^0 \rightarrow \text{neutrals})$ , for which a preliminary result is given in the previous subsection, strongly affects the value of the factor  $R$ . In fact, an increase of the invisible  $D^0$  decays determine a decrease of the factor  $R$ . Taking into account of this result, the measurement<sup>3</sup> given in Ref. 12), for the semi-muonic branching ratio of charm hadrons has been revised to be

$$B_\mu = (8.1 \pm 0.8(\text{stat}) \pm 0.8(\text{syst}))\%.$$

A new analysis based on full statistics is in progress, its result, combined with the measurement of  $B_\mu |V_{cd}|^2$  obtained from the fit of dimuon data, can be used to extract  $V_{cd}$ .

### 3.5 Associated charm production

Associated charm production in neutrino interactions is a very rare process, difficult to detect. Associated charm-production in CC originates from a gluon emitted by bremsstrahlung from a light quark. In the past, indirect evidence for this process was obtained by studying trimuon and same-sign dimuon events<sup>13)</sup>. Recently a direct search for this process has started in the emulsions of the CHORUS experiment: in a sample of in 95540 CC events, 5 candidates for associated charm-production have been found.

Associated charm-production in NC interactions proceeds through both gluon bremsstrahlung and gluon-boson fusion process. So far one event has been “directly” observed by the E531 experiment<sup>14)</sup>, while an indirect observation has been recently published by the NuTeV experiment<sup>15)</sup>. Both experiments measured a rate of the order of  $10^{-3}$ , normalized to CC events. In the CHORUS experiment, 3 candidates have been found in a sample of 26568 NC events. The analysis of these data and the cross-section measurements will be completed by the end of this year.

---

<sup>3</sup>The number quoted in Ref. 12) for the muonic branching ratio of the charm hadrons is  $B_\mu = (9.3 \pm 0.9(\text{stat}) \pm 0.9(\text{syst}))\%$ .

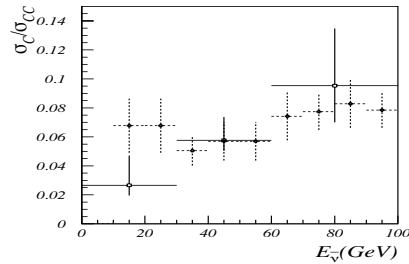


Figure 3: Charm production rate in  $\bar{\nu}_\mu$  events as a function of antineutrino energy as measured in CHORUS (empty box) compared with those derived from di-lepton data (dashed lines) <sup>16)</sup> scaled with the  $B_\mu$  as given by <sup>12)</sup>.

### 3.6 Measurement of charm production in antineutrino charged-current interactions

A measurement of antineutrino induced charm production is performed by using the presence of a 5% antineutrino component in the neutrino beam. The number of antineutrino CC interactions corrected for the contamination and for the efficiencies is evaluated to be  $4975 \pm 187(stat) \pm 53(syst)$ . In these events 32 decay topologies were observed in emulsion with an estimated background of 2.7 events. At an average antineutrino energy of 18 GeV, the charm production rate induced by antineutrinos is measured to be

$$\frac{\sigma(\bar{\nu}_\mu N \rightarrow \mu^+ \bar{c} X)}{\sigma(\bar{\nu}_\mu N \rightarrow \mu^+ X)} = (5.0^{+1.4}_{-1.0}) \times 10^{-2}.$$

This is the first direct measurement of the antineutrino induced charm production. The cross-section as a function of antineutrino energy has been compared with theoretical prediction showing a reasonable agreement (Fig. 3).

## 4 Future prospects

### 4.1 Inclusive charm cross-section

From the analysis of the CHORUS full charm sample a direct measurement of the inclusive charm cross-section is possible. So far only E531 <sup>14)</sup> performed this measurement with a statistics of 122 events. Using a statistics about 20 times larger than E531, CHORUS should be able to make a much more precise

measurement and an accurate study of the threshold behavior of the cross-section.

#### 4.2 Hadronization of charm-quarks to charmed hadrons

In near future, from the analysis of CHORUS data, a better understanding of the process which drives from charm-quark to charm hadrons will be possible. The hadronization mechanism involves relatively low energies, of the order of the hadron mass so that is described by non-perturbative models. All fragmentation models define a fragmentation parameter  $z$  such that the observed hadrons have a longitudinal momentum  $zp_h^{max}$  with respect to quark's momentum, where  $p_h^{max}$  is the momentum of the quark, namely the maximum momentum the hadron can have. The connection between the quarks, the gluons and the physically observed hadrons is established by using the factorization theorem of QCD <sup>17)</sup> in which the cross-section for the production of a charmed hadron  $C$  can be connected to the charm quark cross-section via fragmentation functions:

$$\frac{d\sigma(\nu N \rightarrow \mu^- CX)}{dx dy dz dp_T^2} = \frac{d\sigma(\nu N \rightarrow \mu^- cX)}{dx dy} \times \sum_h f_h \times D_c^h(z, p_T^2) \quad (4)$$

Here,  $D_c^h(z, p_T^2)$  is the probability distribution for the charm-quark to fragment into a charmed hadron of type  $h(= D^0, D^+, D_s^+, \Lambda_c^+)$  carrying a fraction  $z$  of the quark longitudinal momentum and transverse momentum  $p_T$  with respect to the quark direction. The number  $f_h$  is the mean multiplicity of the hadron  $h$  in neutrino charm-production. A similar expression holds for  $\bar{\nu}$ . The analytical form of the fragmentation function usually depends on the quark mass. For heavy quarks two parameterizations are usually used, the Peterson function <sup>18)</sup>

$$D(z) \propto \frac{1}{z \left(1 - \frac{1}{z} - \frac{\epsilon_P}{1-z}\right)} \quad (5)$$

and the Collins-Spiller function <sup>19)</sup>

$$D(z) \propto \frac{\frac{1-z}{z} + \frac{\epsilon_C(2-z)}{1-z}}{1 - \frac{1}{z} - \frac{\epsilon_C}{1-z}} \times (1 + z^2) \quad (6)$$

where  $\epsilon_{CS}$ ,  $\epsilon_P$  and  $b$  are free parameters.

The parameter  $\epsilon$  which characterizes the fragmentation functions of heavy quarks can be determined by using two different approaches:

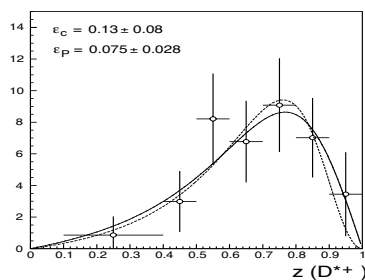


Figure 4: *NOMAD* results for  $D^*$  mesons:  $z$  distribution the results of fits with the functions 5 and 6 are shown.

Table 2: *Summary of all available determinations of  $\varepsilon$ .*

Collaboration	$\varepsilon_P$	$\varepsilon_C$	Comments
E531 <sup>20)</sup>	$0.076 \pm 0.014$	—	All charmed hadrons are used
NOMAD <sup>21)</sup>	$0.075 \pm 0.046$	$0.13 \pm 0.14$	Only $D^{*+}$ are used
CDHS <sup>22)</sup>	$[0.02 \div 0.14]$	—	
CCFR (LO) <sup>23)</sup>	$0.22 \pm 0.05$	$0.88 \pm 0.12$	All charmed hadrons are used
CHARM II <sup>24)</sup>	$0.072 \pm 0.017$	—	All charmed hadrons are used
NuTeV	—	$2.07 \pm 0.31$	All charmed hadrons are used

- Indirect measurements:  $\varepsilon$  is left as one of the free parameters of the fit to the dimuon data. Dimuon analysis has been performed by CDHS, CCFR, CHARM II and NuTeV.
- Direct measurements: the  $z$  distribution is reconstructed and fitted in order to extract the parameter  $\varepsilon$ . Such analysis has been performed by E531, NOMAD (see Fig. 4) and is currently in progress in CHORUS;

The available results from both approaches are summarized in Table 4.2.

### 4.3 Charmed fractions determination

The charmed fractions  $f_h$  have been measured directly only by the E531 experiment <sup>20)</sup>. In checking over the E531 results, a bias was detected in the extraction of the charmed fractions. Therefore, the data was refit with the bias removed <sup>25)</sup>. The analysis of CHORUS data is in progress and its result will

constitutes the more precise determination of the charmed fractions in neutrino experiments.

## 5 Conclusions

Nuclear emulsions with their sub-micrometric resolution allow a direct identification of the charmed hadrons. Thanks to the higher speed of the scanning systems, it has been possible to analyze large amount of data. With its final statistics the CHORUS experiment has found more than 2000 charm decays out of 95450 CC events. From a subsample of collected data  $\Lambda_c^+$ , quasi-elastic charmed baryons and  $D^0$  cross-section rates have been measured. A direct measurement of the semi-leptonic branching ratio is also reported. Future results from CHORUS experiment are expected to include:

- a study of the threshold behavior of the charm-production cross-section;
- the determination of charm-quark hadronization parameters;
- the determination of the charm hadrons production fractions;
- a determination of  $V_{cd}$ ;
- the cross-section measurement of associated charm-production both in neutral- and charged-current interactions.

## References

1. H. Abramowicz *et al.*, Z. Phys., C **15** (1982) 19.
2. CCFR Collaboration, S.A. Rabinowitz *et al.*, Phys. Rev. Lett. **70** (1993) 134.
3. CHARM II Collaboration, P. Vilain *et al.*, Eur. Phys. Journal C **11** (1999), 19.
4. Nomad Collaboration, P. Astier *et al.*, Phys. Lett. B **486** (2000) 35.
5. M. Goncharov *et al.*, NuTeV Collaboration, Phys. Rev. D **64** (2001) 112006.
6. E.Eskut *et al.*, Nuclear Instruments and Methods A **401** (1997) 7.

7. S.Aoki *et al.* Nuclear Instruments and Methods B **51** (1990) 466.
8. A.Kaysis-Topaksu *et al.*, CHORUS Collaboration, Phys. Lett. B **555** (2003) 156.
9. A.Kaysis-Topaksu *et al.*, CHORUS Collaboration, Phys. Lett. B **575** (2003) 198.
10. A. Kayis-Topaksu *et al.* [CHORUS Collaboration], Phys. Lett. B **527** (2002) 173.
11. Particle Data Group, K.Hagiwara *et al.*, Phys. Rev. D **66** (2002) 010001.
12. A.Kaysis-Topaksu *et al.*, CHORUS Collaboration, Phys. Lett. B **549** (2002) 48.
13. P. H. Sandler *et al.*, Z. Phys. C **57** (1993) 1.
14. N. Ushida *et al.* [Fermilab E531 Collaboration], Phys. Lett. B **206** (1988) 375.
15. A. Alton *et al.* [NuTeV Collaboration], Phys. Rev. D **64** (2001) 012002 [Int. J. Mod. Phys. A **16S1B** (2001) 764] [arXiv:hep-ex/0008068].
16. G. De Lellis *et al.*, J. Phys. G **28** (2002) 1515
17. D.E. Soper, J.C. Collins and G. Sterman, World Scientific, Singapore (1989).
18. C. Peterson, D. Schlatter, I. Schmitt and P. M. Zerwas, Phys. Rev. D **27** (1983) 105.
19. P. D. Collins and T. P. Spiller, J. Phys. G **11** (1985) 1289.
20. N. Ushida *et al.* [Fermilab E531 Collaboration], Phys. Lett. B **206** (1988) 380.
21. P. Astier *et al.* [NOMAD Collaboration], Phys. Lett. B **526** (2002) 278.
22. H. Abramowicz *et al.*, Z. Phys. C **15** (1982) 19.
23. S. A. Rabinowitz *et al.*, Phys. Rev. Lett. **70** (1993) 134.

24. P. Vilain *et al.* [CHARM II Collaboration], *Eur. Phys. J. C* **11** (1999) 19.
25. T. Bolton, arXiv:hep-ex/9708014.

Frascati Physics Series Vol. XXXV (2004), pp. 341  
HEAVY QUARKS AND LEPTONS - San Juan, Puerto Rico, June 1-5, 2004

**HEAVY QUARK PRODUCTION IN ELECTRON-PROTON  
COLLISIONS AT HERA**

F. Sefkow  
*DESY, Hamburg, Germany*

Written contribution not received



***SESSION IX – Onia States***

J. M. Yelton First Results from CLEO-c  
Z. Metreveli Heavy Quarkonia



Frascati Physics Series Vol. XXXV (2004), pp. 345-354  
HEAVY QUARKS AND LEPTONS - San Juan, Puerto Rico, June 1-5, 2004

## FIRST RESULTS FROM CLEO-c

John M Yelton  
Phys. Dept, U.of Florida, Gainesville, FL 32611-8440  
On Behalf of the CLEO Collaboration

### ABSTRACT

We present the first results from the CLEO-c experiment. CLEO-c is a new detector configuration running at the charmonium and charm meson threshold energies at the Cornell Electron Storage Ring. Here, we show the first results on data taken at the  $\psi(3770)$  resonance. In particular, we present the first significant signal of the decay  $D^+ \rightarrow \mu\nu$  which leads to a measure of the  $D$  meson decay constant  $f_D$ .

### 1 Introduction

The summer of 2004 is an exciting time for the CLEO collaboration. For some years, we have been showing Monte Carlo simulations of the data we will be able to present using the CLEO-c detector. Now, for the first time, we can show results that in many aspects match the simulations. In particular, we

see that the background estimates were reasonable, and will not preclude the measurements we hope to make. I stress that all the data and results presented here are preliminary, and are taken using a fraction of the luminosity we intend to accumulate.

## 2 The CLEO-c Detector and the CESR-c Accelerator

The CLEO collaboration has been taking data at the Cornell Electron Storage Ring since 1980. The latest detector configuration is known as CLEO-c, where the “c” denotes charm, as it incorporates changes to make it more suitable for taking data at around the charm threshold energies. CLEO-c retains the CLEO III main drift chamber and particle ID system (Ring Imaging Cherenkov counters (RICH) <sup>1</sup>) and energy loss ( $dE/dx$ ) measurements), and the CsI crystal calorimeter for photon and electron detection that was built for CLEO II <sup>2</sup>). The main change from CLEO III is the replacement of the silicon vertex detector with a six-layer, all-stereo, inner drift chamber <sup>3</sup>). This is known as the “ZD”, as its primary role is the measurement of the tracks in the “Z” (along the beam) direction. The ensemble is centered in the CLEO solenoidal magnet, which is run at 1.0 Tesla, rather than 1.5T which was used for CLEO III. The lower magnetic field reduces the fraction of curling tracks.

The CESR accelerator has been modified to enable the changing physics plans. Superconducting wiggler magnets are being added to the machine lattice to help damp the synchrotron radiation. Six such wigglers were already operational for the data run discussed here; the rest have just been installed and will be operational in Fall 2004.

## 3 The CLEO-c Data Set

We have collected  $3 \text{ pb}^{-1}$  of  $\psi(2S)$  data in CLEO-c. Together with some earlier exploratory running (before the new inner drift chamber was installed), we have a total of  $5.5 \text{ pb}^{-1}$  of  $\psi(2S)$  data which include about 3 million  $\psi(2S)$  decays. We also have  $20 \text{ pb}^{-1}$  of continuum data taken at  $\sqrt{s} \simeq 3.67 \text{ GeV}$ , just below the  $\psi(2S)$ . Perhaps the most exciting new data sample is  $\approx 57 \text{ pb}^{-1}$  taken on the  $\psi(3770)$  resonance which yields  $D\bar{D}$  pairs, and this talk will concentrate on this last sample. The  $\psi(2S)$  results are being presented in another talk.

These datasets are only the start of the CLEO-c program. The run-plan

presently calls for a massive  $3 \text{ fb}^{-1}$  of  $\psi(3770)$  running, a factor of around 60 greater than presented here. We stress that this goal is contingent on CESR being able to quickly reach its design luminosity of  $\approx 3 \times 10^{32} \text{ cm}^{-2} \text{ s}^{-1}$ , which is a factor of six higher than has been achieved so far. The physics run-plan is deliberately flexible so that it can change in reaction to the results obtained. The planned final dataset would correspond to around 18,000,000  $D\bar{D}$  decays, and around 3,600,000 *tagged*  $D$  decays which is 310 times larger than the MARKIII collaboration and around 170 times larger than that obtained by BES.

After the  $\psi(3770)$  data, the plan calls for  $3 \text{ fb}^{-1}$  running at the  $D_s^+ D_s^-$  threshold, giving maybe 300,000 *tagged*  $D_s$  decays (130 times the BES sample). Fall 2006 will give the opportunity of running at the  $J/\psi$  with maybe a billion events collected! Details of the CLEO-c program may be found elsewhere <sup>4)</sup>.

#### 4 The Physics at the $\psi(3770)$

The main decay of the  $\psi(3770)$  is into  $D\bar{D}$  mesons. However, the total cross-section also includes a large (and not well understood) continuum component, the radiative tail of the  $\psi(2S)$ , and maybe some other processes as yet unexplored. Using the data taken at, and below, the  $\psi(2S)$  we are studying the first two of these. To know how many  $D$  mesons we will eventually be able to reconstruct, we need to know the cross-section into  $D$  pairs, that is ( $\sigma \rightarrow D\bar{D}$ ) at  $E=3.77 \text{ GeV}$ . MARKIII <sup>5)</sup> measured the observed cross section to be  $(5.0 \pm 0.5) \text{ nb}$ . Recently BES II <sup>6)</sup>, using  $17 \text{ pb}^{-1}$  measured  $(5.78 \pm 0.11 \pm 0.38) \text{ nb}$ . In the BES method, the cross-section depended upon the value for the branching fraction in the final state under study. Here, we present a double-tag method (along the lines of that used by MARK III) to find a value of  $\sigma(e^+e^- \rightarrow D\bar{D})$  independent of any branching fraction measurement.

##### 4.1 General Analysis Techniques

Good  $K - \pi$  separation is obtained by  $dE/dx$  up to momenta of around 600 MeV/c. For higher momentum particles we combine RICH information with the  $dE/dx$ . In several analyses, we find  $K_s^0$  candidates from their displaced vertices, and reconstruct  $\pi^0$  mesons from two  $\gamma$  signatures in the CsI calorimeter.

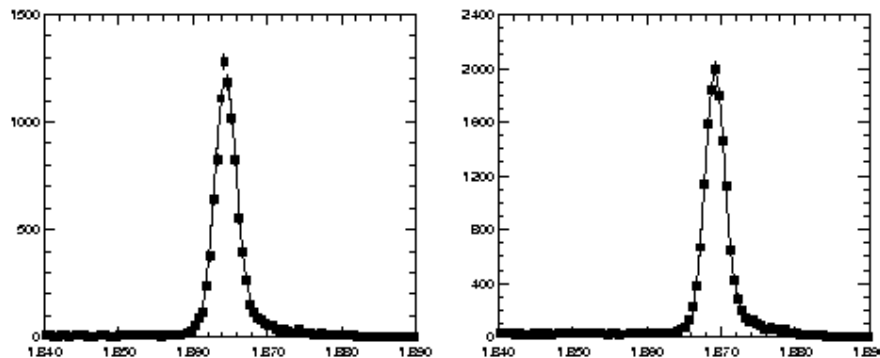


Figure 1: *Beam-constrained mass distributions for a)  $D^0 \rightarrow K^-\pi^+$ , and b)  $D^+ \rightarrow K^-\pi^+\pi^+$*

To find  $D$  mesons from the  $\psi(3770)$ , we first calculate the energy of the  $D$  and compare with the beam energy. If the two values are consistent, we calculate the beam-constrained mass  $M_{BC} = \sqrt{(E_{BEAM}^2 - p(D)^2)}$ . The resolution of this quantity is in many cases limited only by the energy spread in the beam. The signal to noise ratio in such a plot is very good, especially in the golden decay modes  $D^0 \rightarrow K^-\pi^+$  and  $D^+ \rightarrow K^-\pi^+\pi^+$  (Fig. 1) which show spectacularly clean signals.

#### 4.2 Double-tag Method to Measure $\sigma(e^+e^- \rightarrow D\bar{D})$

Comparing single and double tag yields allows one to easily extract the total  $D\bar{D}$  cross-section independently of branching ratios. The number of single  $D$  tags,  $S$ , in a given mode is  $S = 2N_{D\bar{D}}B\epsilon_1$ , where the variables denote the number of  $D\bar{D}$  pairs produced, the branching fraction of the mode, and the efficiency, respectively. The number of double tags,  $D$ , in a given mode is  $D = 2N_{D\bar{D}}B^2\epsilon_2$ , where  $\epsilon_2 \simeq \epsilon_1^2$  is the efficiency for finding both tags. One can then determine the cross section as  $\sigma_{D\bar{D}} = S^2/(4DL)$ , where  $L$  is the integrated luminosity. The branching ratio cancels, as does most of the efficiency (with  $\epsilon_2 \neq \epsilon_1^2$  treated as a systematic error).

Table 1 shows the preliminary results from this analysis. We note that our results are consistent with, but a little higher than, previous results on this subject. This is good news for CLEO-c because it implies a larger number of

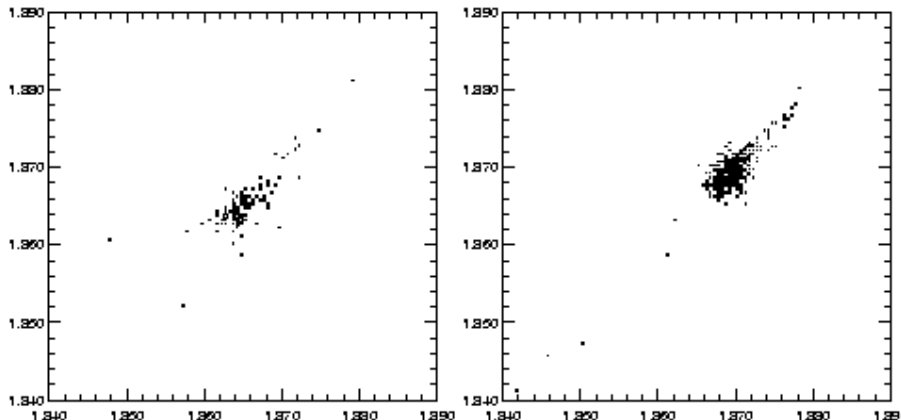


Figure 2: *Beam-constrained mass plots for double tags from  $D^0 \rightarrow K^- \pi^+, \bar{D}^0 \rightarrow K^+ \pi^-$  (left) and  $D^+ \rightarrow K^- \pi^+ \pi^+, D^- \rightarrow K^+ \pi^- \pi^-$  (right).*

Table 1: *Cross sections of the  $\psi(3770) \rightarrow D\bar{D}$ .*

	$\sigma(D^+D^-)$	$\sigma(D^0\bar{D}^0)$	$\sigma(DD)$
CLEO-c	$2.58 \pm 0.15 \pm 0.16$	$3.93 \pm 0.42 \pm 0.23$	$6.51 \pm 0.44 \pm 0.39$
BES <sup>6)</sup>	$2.52 \pm 0.07 \pm 0.23$	$3.26 \pm 0.09 \pm 0.26$	$5.78 \pm 0.11 \pm 0.38$
MARK III <sup>5)</sup>	$2.1 \pm 0.3$	$2.9 \pm 0.4$	$5.0 \pm 0.5$

$D$  mesons will be produced. The largest systematic uncertainty is due to the luminosity measurement.

### 5 Results Using D-Tagging

The remainder of the analyses we will present here, depend on the technique of “ $D$ -tagging”. That is, by reconstructing one  $D$  in the event, we know that another  $D$  of a particular charge and flavor, must exist in the remainder of the event. The net-tagging efficiency from a combination of  $D$  modes is of the order of 20%, and the expectation is that from the full dataset we will be able to tag several million events in this way.

Tagging can be used to find absolute branching fractions not only of hadronic decays, but semi-leptonic and even purely leptonic decays that cannot be fully reconstructed.

### 5.1 Determination of $f_D$ from $D^+ \rightarrow \mu^+ \nu_\mu$ Decay

The leptonic decay width of a pseudoscalar meson, such as the  $D^+$ , is proportional constant:  $\Gamma_{\ell\nu} \propto f_D^2$ . The decay constant  $f_D$  is related to the quarks annihilation rate via the short-distance weak interaction. The same parameter enters the box diagram of neutral meson mixing (e.g.,  $f_D$  for  $D^0 \leftrightarrow \bar{D}^0$ , or  $f_B$  for  $B^0 \leftrightarrow \bar{B}^0$ ). In particular,  $f_B$  is needed to extract the CKM matrix element information from the already precise  $B$  mixing data;  $f_{B_s}$  will be needed once  $B_s$  mixing is observed. Lattice gauge theories connect the decay constants in the  $D$  and  $B$  regimes.

We search for  $D^+ \rightarrow \mu^+ \nu_\mu$  decays in events where a  $D$  tag is present. For this analysis we augment the  $K^- \pi^+ \pi^+$  events with four other decay modes,  $K_s^0 \pi^+$ ,  $K_s^0 \pi^+ \pi^0$ ,  $K_s^0 \pi^+ \pi^+ \pi^0$ , and  $K^0 \pi^+ \pi^- \pi^+$ . We then require that the rest of the event have exactly one charged track consistent with a muon hypothesis (based on energy deposit in the CsI calorimeter) and relatively little extra energy in unmatched (to tracks) calorimeter showers. We calculate for the candidate muon the *missing mass* squared  $MM^2 = (E_{bm} - E_\mu)^2 - (-\vec{P}_{tag} - \vec{p}_\mu)^2$  which will peak at zero for signal.

Backgrounds include  $\pi^+ \pi^0$  events which peak nearby in  $MM^2$  and sometimes survive the calorimeter activity veto, combinatorics from continuum,  $K^0 \pi^+$  events, and  $D^0 \bar{D}^0$  events.

We find 9 events within a  $2\sigma$  window in  $MM^2$  (see Fig. 3), with a predicted background of  $0.67 \pm 0.24$  events. This has a high significance and gives  $\mathcal{B}(D^+ \rightarrow \mu^+ \nu_\mu) = (4.57 \pm 1.66 \pm 0.41) \times 10^{-4}$ , which can be combined with the known  $D^+$  lifetime to extract  $f_D = (230 \pm 42 \pm 10)$  MeV. This is consistent with the theoretical expectations, for instance the UKQCD lattice result <sup>7)</sup> of  $210 \pm 10_{-16}^{+17}$  MeV. The most significant systematics include the muon efficiency (5%) and background level (7.4%). This result is clearly statistics limited; more data will also assist some systematic studies.

## 6 Inclusive $D \rightarrow X e \nu_e$ Decays

Improved measurements of inclusive lepton spectra from charm mesons are of considerable interest. The integrated spectra providing the inclusive branching fraction, and the shape is also of interest. We concentrate on electrons due to the difficulties of soft muon identification.

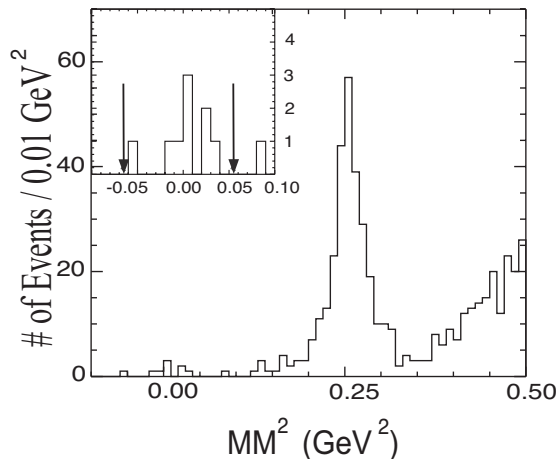


Figure 3: *Missing-mass-squared spectra of  $D^+ \rightarrow \mu^+ \nu_\mu$  candidates.*

Electron identification was optimized using radiative Bhabha events; key variables include  $E/p$  from the CsI and tracking along with  $dE/dx$  and RICH information. The preliminary results shown here use only one mode for each type of  $D$  meson ( $K^-\pi^+$  and  $K^-\pi^+\pi^+$ ). Even with this limitation and the modest data sample, the statistical uncertainties on the branching fraction are  $\approx 0.6\%$  which can be compared with the current PDG world average of  $(17.2 \pm 1.9\%)$ . For the neutral case the CLEO-c has a similar statistical uncertainty, but here the PDG precision ( $6.75 \pm 0.29\%$ ) has not yet been reached. We hope to be able to reveal numbers for the actual branching fraction some time in Summer 2004. We must remember that this constitutes a small fraction of the data to be taken at this energy.

## 7 Exclusive Semileptonic $D$ Decays

Exclusive semileptonic modes are also easily studied with the  $D$  tag technique. Here, we display signals using the variable  $U \equiv E_{miss} - |p_{miss}|$ , where  $E_{miss}$  ( $p_{miss}$ ) denote the missing energy (momentum). This is computed by comparing the known beam energies to the sum of the  $D$  tag plus the observed particles in the semileptonic candidates. Clearly,  $U$  will peak at 0 if only a neutrino is missing.

Fig. 5 shows the  $U$  distributions for the Cabibbo-allowed  $K^- e^+ \nu_e$  fi-

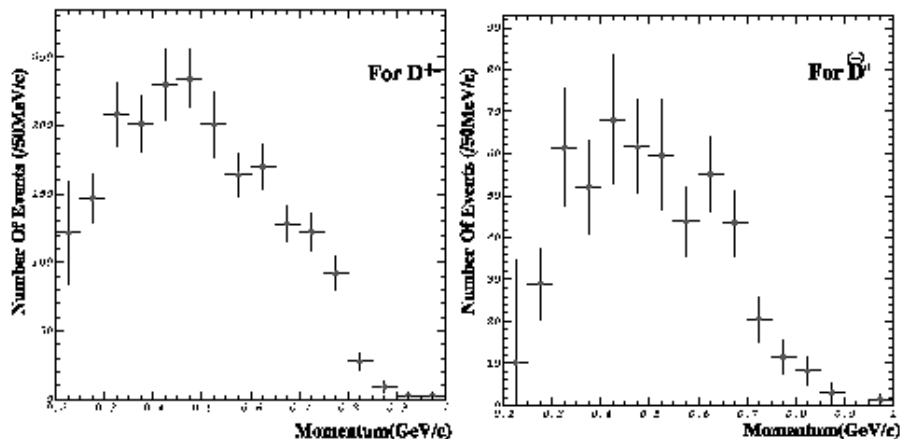


Figure 4: *Inclusive electron spectra extracted from charged (left) and neutral (right) D meson decays.*

nal state, as well as the Cabibbo-suppressed  $\pi^- e^+ \nu_e$ . Tagging allows one to separate the rarer  $\pi$  mode kinematically, rather than relying on particle identification alone. In Fig. 6, we display two other Cabibbo-suppressed modes,  $\rho^0 e^+ \nu_e$  and  $\rho^- e^+ \nu_e$ . The first of these has previously been seen, though not well-measured, whereas for the second this represents a first observation. Many other semileptonic modes are also accessible, and with the expected data set taken in the next year, CLEO-c can expect to produce the definitive results on 8 semi-leptonic  $D$  decays, with more to come later after the running at the  $D_s$  threshold.

## 8 Conclusion

We have shown the first results from the CLEO-c detector running at the  $\psi(3770)$ . The  $D$  mesons found from using the beam energy constraint are specularly clean, and can give large samples of *tagged D* events. One notable preliminary result is that of the  $D$  meson decay constant of  $f_D = (230 \pm 42 \pm 10)$  MeV.

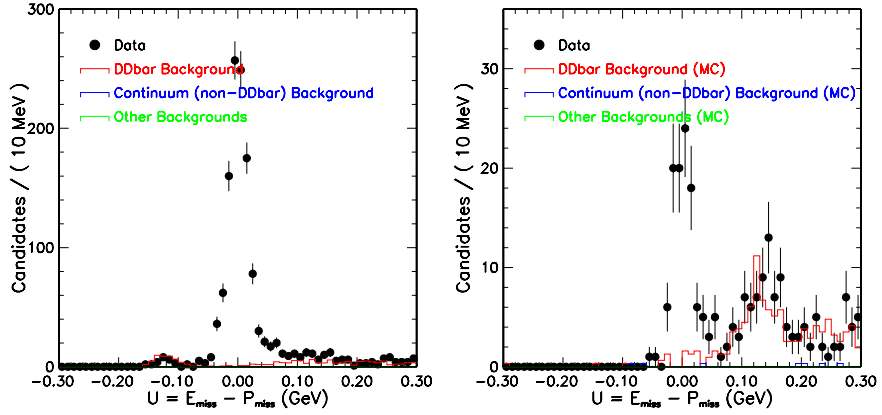


Figure 5: Distributions of  $U \equiv E_{miss} - |p_{miss}|$  for the Cabibo-allowed final state of  $K^- e^+ \nu_e$  (left) and the Cabibo-suppressed final state  $\pi^- e^+ \nu_e$  (right).

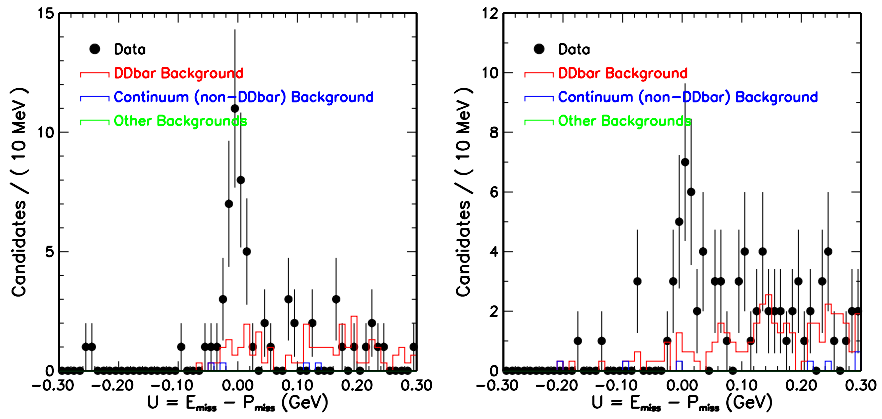


Figure 6: Distributions of  $U \equiv E_{miss} - |p_{miss}|$  for the Cabibo-suppressed states  $\rho^0 e^+ \nu_e$  (left), and  $\rho^- e^+ \nu_e$  (right).

## 9 Acknowledgements

I would like to thank all my CLEO colleagues, but in particular Victor Pavluvin, Batbold Sanghi, Nabil Mena, Laria Redjimi, Roy Briere and Basit Athar.

## References

1. M. Artuso *et al*, Nucl. Instrum. Methods A **502**, 91 (2003).
2. Y. Kubota *et al*, Nucl. Instrum. Methods A **320**, 66 (1992).
3. D. Peterson *et al*, Nucl. Instrum. Methods A **478**, 142 (2002).
4. R.A. Briere *et al*, CLNS 01/1742, 2001.
5. J. Adler *et al*, PRL **60**, 89 (1988).
6. G. Rong, on behalf of BES collaboration, hep-ex/0406027.
7. L.Lellouch and C.J.Lin, Phys Rev **D64**, 094501 (2001).

Frascati Physics Series Vol. XXXV (2004), pp. 355-364  
HEAVY QUARKS AND LEPTONS - San Juan, Puerto Rico, June 1-5, 2004

## HEAVY QUARKONIA

Zaza Metreveli

*Department of Physics, Northwestern University, Evanston, IL 60208, USA*

### ABSTRACT

Recent experimental results on heavy quarkonia spectroscopy and decays are reviewed. In particular, new results are discussed on charmonium spin singlet states, bottomonium D-states, photon and hadronic transitions from heavy quarkonium states, and the unexplained narrow X(3872) state.

### 1 Introduction

Heavy quarkonia are the bound states of charm and bottom quarks. They are strong interaction analogs of positronium. Because charm and bottom quarks have large masses ( $\sim 1.5$  and  $\sim 4.5$  GeV), velocities of quarks in hadrons are nonrelativistic. The strong coupling constant  $\alpha_s$  is small ( $\sim 0.3$  for  $c\bar{c}$  and  $\sim 0.2$  for  $b\bar{b}$ ). Therefore heavy quarkonia spectroscopy is a good testing ground for theories of strong interactions: QCD in both perturbative and non-perturbative

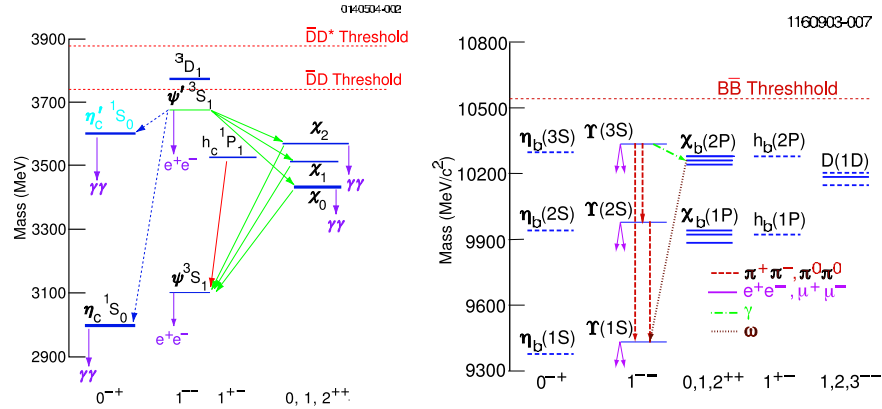


Figure 1: The spectra for charmonia (left) and bottomonia (right) below and near the open flavor threshold. Some typical transitions are indicated. None of the singlet  $\eta_b$  or  $h_b$  bottomonium states or  $h_c$  charmonium state have been observed yet.

regimes, QCD inspired purely phenomenological potential models, NRQCD and Lattice QCD.

Quarkonium states can be produced (fig.1) in  $e^+e^- \rightarrow \gamma^* \rightarrow q\bar{q}$  processes (direct production of  $n^3S_1$ :  $J^{PC} = 1^{--}$  vector states), two photon fusion processes at the  $e^+e^-$  colliders (production of  $\eta_c$ ,  $\eta_c'$ ,  $\chi_{0,2}$ :  $J^{PC} = 0^{-+}, 0^{++}, 2^{++}$  states),  $p\bar{p}$  annihilation via two or three gluons (production of  $q\bar{q}$  mesons with any quantum numbers), B meson decays (production of states with any quantum numbers with associated particles), radiative or hadronic transitions from higher states of quarkonia.

## 2 New in Charmonium Spectroscopy

In this section new experimental results on charmonium states produced below the open flavor production threshold are reviewed, obtained from the large data samples collected with the BaBar, Belle, BES and CLEO detectors.

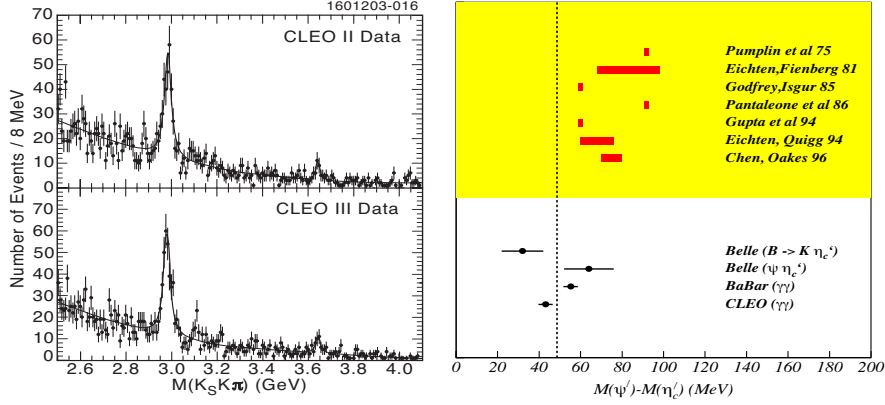


Figure 2:  $K_s K^\pm \pi^\mp$  invariant mass distributions for events in two photon fusion processes from the CLEO data, indicating  $\eta_c$  and  $\eta_c'$  resonances (left). A summary of the theoretical predictions and new experimental measurements of  $\Delta M_{hf}(2S)$  (right).

## 2.1 Spin Singlet States

These states are generally the most difficult states to access and study because they are not directly formed in  $e^+e^-$  annihilation and the radiative decays of spin triplet states  $^3S_1(J/\psi, \psi', \Upsilon, \dots)$  to spin singlet states  $^1S_0(\eta_c, \eta_b)$  are M1 transitions and therefore are highly suppressed. In  $^1P_1(h_c, h_b)$  cases, the radiative decays are entirely forbidden by C-conservation. As a result, no singlet states have ever been identified in bottomonium and only the  $\eta_c$  singlet state was identified in charmonium until recently.

The radial excitation of the charmonium spin singlet ground state,  $\eta_c'(2^1S_0)$  is known to be bound. It is important to identify it because it can shed light on the nature of the spin-spin hyperfine interaction between a quark and antiquark. The hyperfine interaction produces the splitting between the spin-singlet and spin-triplet states. For the charmonium 1S states splitting ( $M(J/\psi) - M(\eta_c)$ ) is known to be  $\Delta M_{hf}(1S) = 117 \pm 2 \text{ MeV}^{-1}$ . It is important to know hyperfine splitting for the 2S states, because these states increasingly sample the confinement part of the  $q\bar{q}$  potential.

Crystal Ball has claimed observation of  $\eta_c'$  in an earlier measurement

with  $M(\eta'_c) = 3594 \pm 5$  MeV in the  $\psi'$  inclusive photon spectrum <sup>2)</sup>. CLEO, with similar sensitivity, does not confirm the Crystal Ball observation <sup>3)</sup>. In 2002 Belle announced the evidence for  $\eta'_c$  in two different measurements: in  $B \rightarrow (\eta'_c)K \rightarrow (K_s K^\pm \pi^\mp)K$  channel with  $M(\eta'_c) = 3654 \pm 6 \pm 8$  MeV <sup>4)</sup> and in double charmonium production  $e^+e^- \rightarrow J/\psi \eta'_c$  with  $M(\eta'_c) = 3622 \pm 12$  MeV <sup>5)</sup>. This was followed by CLEO <sup>6)</sup> (fig.2) and BaBar <sup>7)</sup> observations of  $\eta'_c$  in two-photon fusion processes with the results:

CLEO	BaBar
$M(\eta'_c) = 3642.9 \pm 3.1 \pm 1.5$ (MeV),	$M(\eta'_c) = 3630.8 \pm 3.4 \pm 1.0$ (MeV),
$\Gamma(\eta'_c) < 31$ MeV (90% CL),	$\Gamma(\eta'_c) = 17.0 \pm 8.3 \pm 2.5$ (MeV).
$\Gamma_{\gamma\gamma}(\eta'_c) = 1.3 \pm 0.6$ (keV) <sup>1</sup> .	

The world average of the  $\eta'_c$  mass value (fig.2) is  $M(\eta'_c) = 3637.4 \pm 4.4$  (MeV) and corresponds to hyperfine mass splitting  $\Delta M_{hf}(2S) = M(\psi') - M(\eta'_c) = 48.6 \pm 4.4$  (MeV). This is a factor 2.4 smaller than  $\Delta M_{hf}(1S)$  and is not predicted by the potential model calculations (fig.2). This result should lead to a new insight into coupled channel effects and the spin-spin contribution of the confinement part of  $q\bar{q}$  potential.

## 2.2 Two Body Hadronic $\psi(2S)$ Decays

According to pQCD, because both  $^3S_1 \rightarrow \gamma \rightarrow e^+e^-$  and  $^3S_1 \rightarrow ggg \rightarrow hadrons$  decays are proportional to  $|\psi(0)|^2$ , the ratio

$$Q_h \approx \frac{\mathcal{B}(\psi(2S) \rightarrow h)}{\mathcal{B}(J/\psi \rightarrow h)} \approx \frac{\mathcal{B}(\psi(2S) \rightarrow e^+e^-)}{\mathcal{B}(J/\psi \rightarrow e^+e^-)} \approx (13 \pm 1)\%. \quad (1)$$

It was noted many years ago that the vector-pseudoscalar (VP) decay to  $\rho\pi$  strongly violates the expectation of equation 1. This problem is known as the “ $\rho - \pi$ ” puzzle and has received great theoretical attention. BES has recently measured vector-tensor (VT) ( $\omega f_2, \rho a_2, K^* \bar{K}_2^*, \phi f_2'$ ) decays of  $\psi'$  with a data sample of  $14 \times 10^6$   $\psi'$  events <sup>8)</sup>. CLEO has measured  $\psi'$  decays to VP final states ( $\rho\pi, \omega\pi, \rho\eta, K^{*0} \bar{K}^0$ ) and to  $\pi^+\pi^-\pi^0$  with a data sample of  $3 \times 10^6$   $\psi'$  events. <sup>9)</sup>. The results are summarized in fig.3.

The experimental status of the “ $\rho - \pi$ ” puzzle, based on the new measurements, can be summarized as follows:

<sup>1</sup>Assuming that the branching fractions for  $\eta_c$  and  $\eta'_c$  decays to  $K_s K \pi$  are equal and using  $\Gamma_{\gamma\gamma}(\eta_c) = 7.4 \pm 0.4 \pm 0.5 \pm 2.3(br)$  (keV) <sup>6)</sup>.

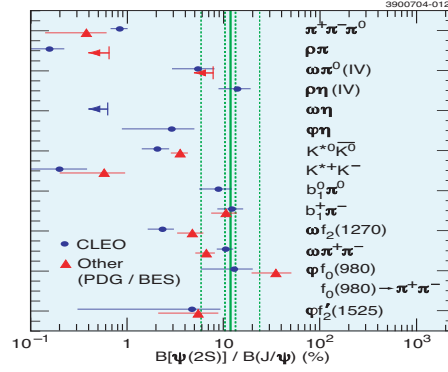


Figure 3: The ratio of branching fractions of  $\psi'$  and  $J/\psi$  decays to different final hadronic states. Vertical solid line indicates the pQCD expectation.

- For VP final states, decays through three gluons are severely suppressed with respect to the 13% rule and the corresponding isospin violating channels ( $\omega\pi$ ,  $\rho\eta$ ) are not;
- VT decay modes are suppressed by a factor of 3-5 compared to the 13% rule;
- Axial-pseudoscalar decay modes do not appear to be suppressed.

### 2.3 Radiative Transitions from $\psi(2S)$

The measurements of radiative E1 electric dipole transitions ( $\Delta L = 1$ ,  $\Delta S = 0$ ) from  $\psi(2S)$  were mainly done in 1980s by the Crystal Ball <sup>10</sup>. The latest improvements of these transition measurements come from CLEO with a  $\psi(2S)$  data sample comparable to the Crystal Ball sample. The preliminary CLEO results from the  $\psi(2S)$  inclusive photon spectrum are <sup>3</sup>):  $\mathcal{B}(\psi(2S) \rightarrow \gamma\chi_{cJ}) = [9.75 \pm 0.14 \pm 1.17, 9.64 \pm 0.11 \pm 0.69, 9.83 \pm 0.13 \pm 0.87]\%$  for  $J = [2, 1, 0]$ , respectively and for the “hindered” M1 transition:  $\mathcal{B}(\psi(2S) \rightarrow \gamma\eta_c) = (0.278 \pm 0.033 \pm 0.049)\%$ .

BES has measured the following branching fractions, using  $\gamma\gamma J/\psi$  events, from a sample of  $14 \times 10^6$   $\psi(2S)$  decays:  $\mathcal{B}(\psi(2S) \rightarrow \gamma\chi_{c1} \rightarrow \gamma\gamma J/\psi) = (2.81 \pm 0.05 \pm 0.23)\%$ ,  $\mathcal{B}(\psi(2S) \rightarrow \gamma\chi_{c2} \rightarrow \gamma\gamma J/\psi) = (1.62 \pm 0.04 \pm 0.12)\%$ ,  $\mathcal{B}(\psi(2S) \rightarrow \pi^0 J/\psi) = (1.43 \pm 0.14 \pm 0.12) \times 10^{-3}$ ,  $\mathcal{B}(\psi(2S) \rightarrow \eta J/\psi) = (2.98 \pm 0.09 \pm 0.23)\%$  <sup>11</sup>. A two photon cascade measurements from the CLEO data should be forthcoming soon.

### 3 New in Upsilon Spectroscopy

In this section new results are reviewed from the large data samples collected with the CLEO detector running at and in the vicinity of the  $\Upsilon(1S)$ ,  $\Upsilon(2S)$  and  $\Upsilon(3S)$  resonances (about 20, 10 and 5 million events, respectively).

#### 3.1 First Observation of a $\Upsilon(1D)$ State

$D$ -wave states in charmonium are expected to be unbound and none, except the vector state at 3770 MeV, have ever been firmly identified. In bottomonium the  $1D$  and  $2D$  states are all expected to be bound but, until now, none had been identified. The  $1^3D_2$  state has been identified with a significance of  $10.2\sigma$  at CLEO in the four photon cascade (fig.1)<sup>12</sup>:  $\Upsilon(3S) \rightarrow \gamma\chi_b(2P)$ ,  $\chi_b(2P) \rightarrow \gamma\Upsilon(1D)$ ,  $\Upsilon(1D) \rightarrow \gamma\chi_b(1P)$ ,  $\chi_b(1P) \rightarrow \gamma\Upsilon(1S)$ , followed by the  $\Upsilon(1S)$  annihilation into  $e^+e^-$  or  $\mu^+\mu^-$ . The measured mass  $M(1^3D_2) = 10161.1 \pm 0.6 \pm 1.6$  (MeV) is in agreement with both lattice and potential model calculations. The measured product branching ratio of the five decays is  $(2.5 \pm 0.5 \pm 0.5) \times 10^{-5}$  and is also in agreement with theoretical estimates.

#### 3.2 $\mathcal{B}_{\mu\mu}$ of the $\Upsilon$ States

The total width ( $\Gamma$ ) of the narrow  $\Upsilon(1S, 2S, 3S)$  resonances produced in  $e^+e^-$  interactions can not be measured directly because their natural width (25-50 keV) is much smaller than the energy resolution of an  $e^+e^-$  collider (4-5 MeV). An indirect method of determining  $\Gamma(\Upsilon(nS))$  is to combine the leptonic branching fraction ( $\mathcal{B}_l$ ) with the leptonic decay width ( $\Gamma_l$ ), i.e.,  $\Gamma = \Gamma_l/\mathcal{B}_l$ . Assuming lepton universality,  $\Gamma_l$  can be replaced with  $\Gamma_{ee}$  (CLEO plans to measure  $\Gamma_{ee}$  with a few percent precision from scans of the resonant line shapes) and  $\mathcal{B}_l$  replaced with  $\mathcal{B}_{\mu\mu}$ . Therefore the precise measurement of  $\mathcal{B}_{\mu\mu}$  leads to a precise determination of  $\Gamma(\Upsilon(nS))$ .

CLEO has measured  $\mathcal{B}_{\mu\mu}$  for the  $\Upsilon(1S)$ ,  $\Upsilon(2S)$  and  $\Upsilon(3S)$  resonances by comparing muon and hadron yields at the peaks of resonances and the preliminary results are:  $\mathcal{B}_{\mu\mu}(\Upsilon(1S)) = (2.53 \pm 0.02 \pm 0.05)\%$ ,  $\mathcal{B}_{\mu\mu}(\Upsilon(2S)) = (2.11 \pm 0.03 \pm 0.05)\%$  and  $\mathcal{B}_{\mu\mu}(\Upsilon(3S)) = (2.44 \pm 0.07 \pm 0.05)\%$ . The  $\Upsilon(1S)$  result agrees with the PDG average<sup>1</sup>) but the  $\Upsilon(2S, 3S)$  results are significantly higher. They also imply narrower  $\Gamma(\Upsilon(2S, 3S))$ . Results are shown in fig.4.

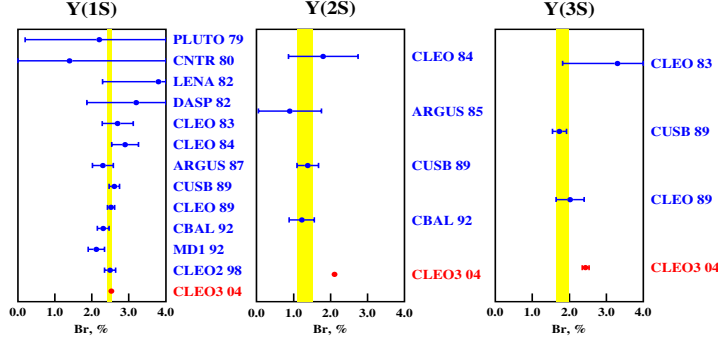


Figure 4: Comparison of the new preliminary CLEO results of  $\mathcal{B}(\Upsilon \rightarrow \mu^+\mu^-)$  to other available measurements and the PDG average.

### 3.3 $\Upsilon(1S)$ Decays to Charmonium Final States

An explanation for the unexpected large charmonium production rates in  $p\bar{p}$  collisions at the Tevatron was given by *color octet* models, where a single gluon fragments into a color octet  $^3S_1 c\bar{c}$  pair which then evolves non-perturbatively into a color-singlet by emission of a soft gluon. *Color singlet* models produce final state  $c\bar{c}$  mesons with two gluons.  $\Upsilon(1S)$  decays are a good testing ground for the color octet and color singlet model predictions.

CLEO has measured <sup>13)</sup> the branching ratio  $\mathcal{B}(\Upsilon(1S) \rightarrow J/\psi + X) = (6.4 \pm 0.4 \pm 0.6) \times 10^{-4}$  using  $J/\psi \rightarrow \mu^+\mu^-$  and  $J/\psi \rightarrow e^+e^-$  decays. Feed-down to  $J/\psi$  from other charmonium states, e.g.,  $\psi'$ ,  $\chi_{cJ}$ , is included. The color octet <sup>14)</sup> and color singlet <sup>15)</sup> model predictions of the branching fraction ( $6.2 \times 10^{-4}$  and  $5.9 \times 10^{-4}$ , respectively) are both in agreement with the above result. However, the continuum subtracted  $J/\psi$  momentum spectrum (fig.5) is in contradiction with the present color octet model prediction.

### 3.4 Neutral Dipion Transitions of $\Upsilon(3S)$ to $\Upsilon(1S)$ and $\Upsilon(2S)$

Precise measurements of the dipion transition branching ratios for  $\Upsilon(3S) \rightarrow \Upsilon(2S, 1S)$  and dipion invariant mass spectra provide an experimental testing ground for many theoretical calculations <sup>16)</sup>, isospin conservation validation in charged and neutral dipion transition modes, and the deviation of dipion invariant mass from the phase space description.

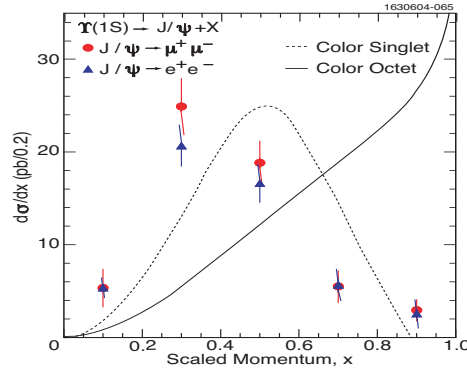


Figure 5:  $J/\psi$  momentum spectrum in  $\Upsilon(1S) \rightarrow J/\psi X$  from the CLEO data. Theoretical expectations based on the color-octet and color-singlet models are shown with lines.

CLEO has measured the following preliminary branching ratios:

$$\mathcal{B}(\Upsilon(3S) \rightarrow \pi^0 \pi^0 \Upsilon(2S)) = 2.02 \pm 0.18 \pm 0.38 (\%),$$

$$\mathcal{B}(\Upsilon(3S) \rightarrow \pi^0 \pi^0 \Upsilon(1S)) = 1.88 \pm 0.08 \pm 0.31 (\%).$$

The  $\pi^0 \pi^0$  effective mass spectrum from  $\Upsilon(3S) \rightarrow \pi^0 \pi^0 \Upsilon(2S)$  has the shape consistent with several theoretical predictions.  $\Upsilon(3S) \rightarrow \pi^0 \pi^0 \Upsilon(1S)$  was found to have a double peaked shape, also observed in the charged pion transitions <sup>16)</sup>.

#### 4 New Narrow State $X(3872)$

Belle recently observed a narrow state,  $X(3872)$ , in  $B^\pm \rightarrow K^\pm X$ ,  $X \rightarrow \pi^+ \pi^- J/\psi$ ,  $J/\psi \rightarrow l^+ l^-$ , measuring  $M(X) = 3872.0 \pm 0.6 \pm 0.5$  (MeV) and  $\Gamma < 2.3$  MeV (90% CL) <sup>17)</sup>. CDF <sup>18)</sup> and D0 <sup>19)</sup> in  $p\bar{p} \rightarrow X(3872) + \dots$ ,  $X \rightarrow \pi^+ \pi^- J/\psi$  and BaBar <sup>20)</sup>, in the same channel as Belle, confirmed this observation with  $M(X) = [3871.3 \pm 0.7 \pm 0.4, 3871.8 \pm 3.1 \pm 3.0, 3873.4 \pm 1.4]$  MeV, respectively.

Many theoretical papers exist interpreting the  $X(3872)$  state as: - a conventional charmonium state; - a  $D\bar{D}^*$  molecule; - an exotic state. Identification of the quantum numbers is important to understand the structure of the state.

CLEO has searched for  $X(3872)$  with  $\sim 15 fb^{-1}$  of CLEO III data in untagged  $\gamma\gamma$  fusion production, where the state can be produced if it has  $J^{PC} = 0^{\pm+}, 2^{\pm+}, \dots$ , and initial state radiation (ISR) production, where the state can

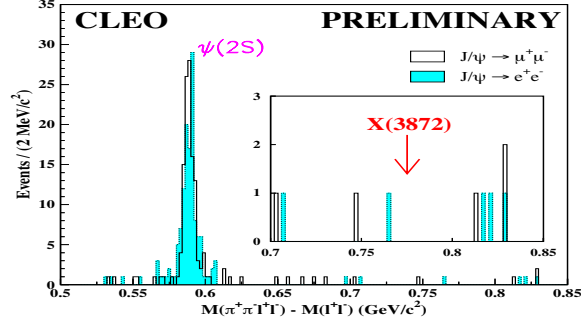


Figure 6: Observed distribution of counts as a function of the effective mass difference  $M(\pi^+\pi^-l^+l^-) - M(l^+l^-)$  from the CLEO data. The arrow indicates the expected location of the  $X(3872)$  signal.

be produced if it has  $J^{PC} = 1^{--}$ . The exclusive channels  $X \rightarrow \pi^+\pi^-J/\psi$ ,  $J/\psi \rightarrow l^+l^-$  were analyzed. No signals were found and the following preliminary upper limits were set (fig.6):

$$(2J+1)\Gamma_{\gamma\gamma}\mathcal{B}(X \rightarrow \pi^+\pi^-J/\psi) < 16.7 \text{ eV (90\% CL) in } \gamma\gamma \text{ fusion,}$$

$$\Gamma_{ee}\mathcal{B}(X \rightarrow \pi^+\pi^-J/\psi) < 6.8 \text{ eV (90\% CL) in ISR.}$$

Systematic errors are included in the upper limits.

## 5 Summary

Heavy quarkonium physics is an active field. Large data samples are being collected and analyzed for quarkonia in  $e^+e^-$  annihilation by BES-II ( $c\bar{c}$ ), CLEO III ( $b\bar{b}$ ), CLEOc ( $c\bar{c}$ ).

Many new important experimental observations and measurements are available and many others are expected.

Progress is being made in NRQCD and Lattice QCD calculations. Hopefully many unresolved puzzles will be resolved soon.

## 6 Acknowledgements

I would like to thank the many collaborators on CLEO for providing analysis results and discussions and also colleagues from BaBar, Belle and BES.

## 9 Acknowledgements

I would like to thank all my CLEO colleagues, but in particular Victor Pavluvin, Batbold Sanghi, Nabil Mena, Laria Redjimi, Roy Briere and Basit Athar.

## References

1. M. Artuso *et al*, Nucl. Instrum. Methods A **502**, 91 (2003).
2. Y. Kubota *et al*, Nucl. Instrum. Methods A **320**, 66 (1992).
3. D. Peterson *et al*, Nucl. Instrum. Methods A **478**, 142 (2002).
4. R.A. Briere *et al*, CLNS 01/1742, 2001.
5. J. Adler *et al*, PRL **60**, 89 (1988).
6. G. Rong, on behalf of BES collaboration, hep-ex/0406027.
7. L.Lellouch and C.J.Lin, Phys Rev **D64**, 094501 (2001).

## ***SESSION X – Rare Decays***

- M. M. Velasco Latest Results from NA48 on  $K_L$  &  $K_s$  CP Violating Related  
Rare Decays
- E. Cheu KTeV Results on Rare Kaon Decays
- D. E. Jaffe E949  $K^+ \rightarrow \pi^+ \nu \bar{\nu}$  Results
- D. Nicolò Status and Perspectives in  $\mu \rightarrow e\gamma$  Decay Search
- M.-C. Chuan New Results on  $B \rightarrow VV$  and  $PV$  Modes
- P. D. Jackson Rare B Decays



Frascati Physics Series Vol. XXXV (2004), pp. 367-376  
HEAVY QUARKS AND LEPTONS - San Juan, Puerto Rico, June 1-5, 2004

## LATEST RESULTS FROM NA48 ON $K_L$ & $K_S$ CP VIOLATING RELATED RARE DECAYS

Mayda M. Velasco  
*Northwestern University*  
*Department of Physics & Astronomy,*  
*2145 Sheridan Rd, Evanston IL 60208, USA*

### ABSTRACT

We present the results of a search for  $K_S \rightarrow \pi^0 e^+ e^-$  and  $K_S \rightarrow \pi^0 \mu^+ \mu^-$ , from the NA48 high intensity 2002  $K_S$  run. These channels are needed to fully understand their CP-violating contributions in the corresponding  $K_L$  decays. In addition, we show the collected data sample of  $K^\pm \rightarrow \pi^\pm e^+ e^-$  and  $K^\pm \rightarrow \pi^\pm \mu^+ \mu^-$  from the 2003  $K^\pm$  run. That data sample will help determine whether the resulting interference between the direct and indirect CP-violating amplitudes in  $K_L \rightarrow \pi^0 \ell^+ \ell^-$  are constructive or destructive.

### 1 Introduction

Physics beyond the standard model could be accessed from  $K \rightarrow \pi \ell \ell$  from existing machines! New physics could manifest itself through loops for  $K_L, K_S$ , and  $K^\pm$  in these channels. In this talk, we focus on recent NA48 results

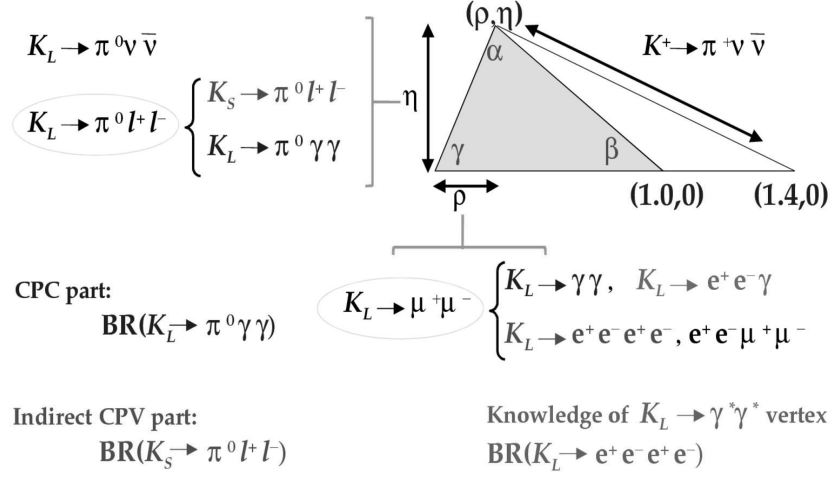


Figure 1: Unitary triangle in the Kaon system, and contribution from various rare decays.

on  $K_L, K_S$ , and  $K^\pm$  rare decays that will allow us to predict the CP conserving(CPC), CP-violating(CPV) and interference components of  $K_L \rightarrow \pi \ell \ell$ , where  $\ell = e, \mu$ . These processes will allow us to perform high-precision tests of Standard Model (SM) flavor physics, including the CKM mechanism for CP violation (Fig. 1), and define very sensitive probes of new physics.

The CKM matrix has the explicit form

$$V = \begin{pmatrix} V_{ud} & V_{us} & V_{ub} \\ V_{cd} & V_{cs} & V_{cb} \\ V_{td} & V_{ts} & V_{tb} \end{pmatrix} \simeq \quad (1)$$

$$\begin{pmatrix} 1 - \lambda^2/2 & \lambda & A\lambda^3(\varrho - i\eta) \\ -\lambda & 1 - \lambda^2/2 & A\lambda^2 \\ A\lambda^3(1 - \varrho - i\eta) & -A\lambda^2 & 1 \end{pmatrix} \quad (2)$$

where the second expression is the useful approximate representation due to Wolfenstein with the parameters  $\lambda, A, \varrho$  and the complex phase  $\eta$ . The absolute values of the elements of the CKM matrix show a hierarchical pattern with the diagonal elements being close to unity, the elements  $|V_{us}| = \lambda$  and  $|V_{cd}|$  being of order 0.2, the elements  $|V_{cb}| = A\lambda^2$  and  $|V_{ts}|$  of order  $4 \cdot 10^{-2}$  whereas  $|V_{ub}|$  and

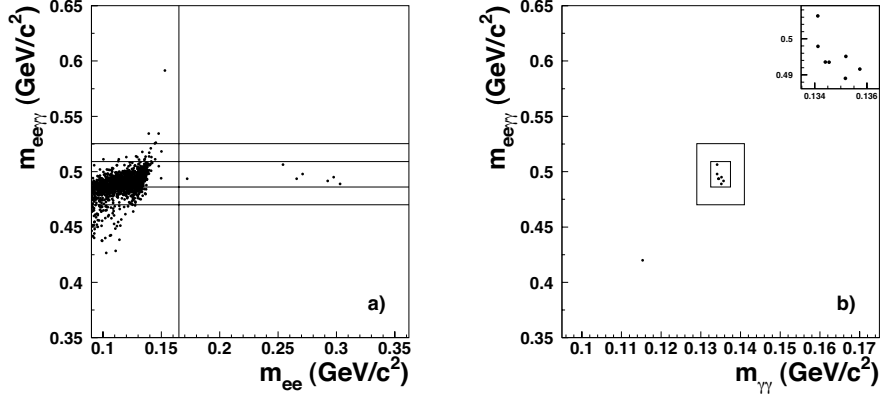


Figure 2: Scatter plot of  $m_{ee\gamma\gamma}$  versus  $m_{ee}$  (a) and  $m_{ee\gamma\gamma}$  versus  $m_{\gamma\gamma}$  (b) for events passing all the cuts described in Ref. <sup>1</sup>). The regions of  $3\sigma$  and  $6\sigma$  are shown.

$|V_{td}|$  are of order  $5 \cdot 10^{-3}$ . Recent results on  $\lambda$  based on kaon semileptonic decays were discussed at this conference, but in this talk we will focus on channels that provide the  $\varrho$  and  $\eta$  parameters like  $K_L \rightarrow \pi^0 e^+ e^-$  and  $K_L \rightarrow \pi^0 \mu^+ \mu^-$ . As shown in Fig. 1, this requires the measurement of several rare kaon decays, like  $K_S \rightarrow \pi^0 \ell^+ \ell^-$  to determine the indirect CPV component and the interference term,  $K_L \rightarrow \pi^0 \gamma \gamma$  to determine the CPC component, and  $K^\pm \rightarrow \pi^\pm \ell^+ \ell^-$  as extra information to determine the sign of the interference term.

## 2 Results and Discussion for the $K_S \rightarrow \pi^0 \ell^+ \ell^-$ ( $\ell = e, \mu$ )

The  $K_S$  run used in these analyses took place in 2002 and it had a total of  $(2 - 4) \times 10^{10}$   $K_S$  decays. As shown in Fig. 2, seven events were found in the  $K_S \rightarrow \pi^0 e^+ e^-$  signal region, with a background estimate of  $0.15^{+0.10}_{-0.04}$  events (Fig. 3), while six events were found in the signal region for  $K_S \rightarrow \pi^0 \mu^+ \mu^-$  (Fig. 4), with a background estimate of  $0.22^{+0.18}_{-0.11}$  events (Fig. 5). These are the first observations for  $K_S \rightarrow \pi^0 e^+ e^-$  and  $K_S \rightarrow \pi^0 \mu^+ \mu^-$  decays.

The kinematic properties of the  $K_S \rightarrow \pi^0 e^+ e^-$  and  $K_S \rightarrow \pi^0 \mu^+ \mu^-$  candidates were consistent with those expected based on Monte Carlo simulation of the signal.

Taking into account the trigger efficiency, the acceptance and the flux,

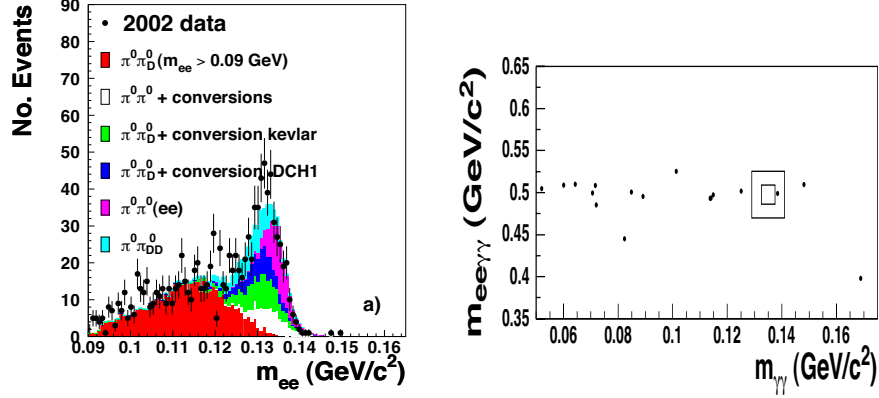


Figure 3: (a) Distributions of  $m_{ee}$  after all the cuts have been applied. Superimposed we show the Monte Carlo predictions from all important sources. Figure (a) shows the components with opposite-sign tracks. (b) Scatter plot of  $m_{ee\gamma\gamma}$  versus  $m_{\gamma\gamma}$  for events selected as  $K_L \rightarrow e^+e^-\gamma\gamma$  in the 2001 data used to estimate the background. The boxes represent the  $3\sigma$  and  $6\sigma$  regions.

the  $K_S \rightarrow \pi^0 e^+ e^-$  branching ratio was measured to be <sup>1)</sup>:

$$B(K_S \rightarrow \pi^0 e^+ e^-) = [5.8_{-2.3}^{+2.8}(\text{stat}) \pm 0.8(\text{syst})] \times 10^{-9}, \quad (3)$$

and the  $K_S \rightarrow \pi^0 \mu^+ \mu^-$  <sup>2)</sup>:

$$B(K_S \rightarrow \pi^0 \mu^+ \mu^-) = [2.9_{-1.2}^{+1.5}(\text{stat}) \pm 0.2(\text{syst})] \times 10^{-9}. \quad (4)$$

The results for  $K_S \rightarrow \pi^0 e^+ e^-$  includes the extrapolation to the low  $m_{e^+e^-}$ -region excluded from the analysis in order to avoid backgrounds. These results are consistent within errors with the recent predictions based on Chiral Perturbation Theory <sup>4, 5)</sup>.

## 2.1 Test of Chiral Perturbation Theory

Chiral Perturbation Theory (ChPT) can be used to predict the branching ratio for  $K_S \rightarrow \pi^0 \ell^+ \ell^-$  and the corresponding dilepton mass spectrum,  $m_{\ell\ell}$ . The measurement presented here tests these predictions and constrains the parameters of the model.

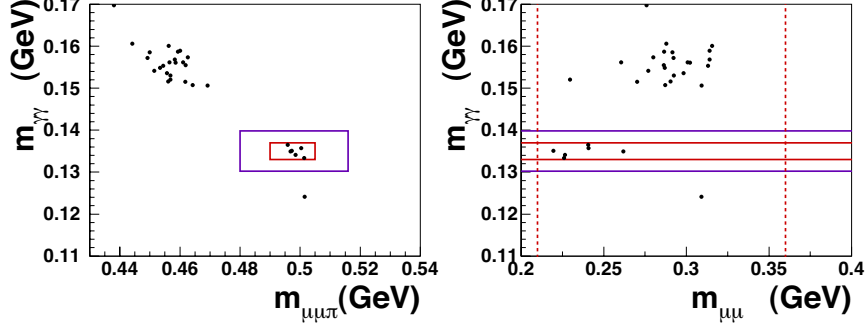


Figure 4: Scatter plot for the events passing all the cuts described in <sup>2)</sup>: (a) for the  $m_{\gamma\gamma}$  versus  $m_{\mu\mu\pi}$  plane and (b) for the  $m_{\gamma\gamma}$  versus  $m_{\mu\mu}$  plane. The  $2.5\sigma$  and the  $6\sigma$  signal and control regions and the  $m_{\mu\mu}$  kinematic limits are also shown.

The  $K_S \rightarrow \pi^0 \ell^+ \ell^-$  branching ratios can be expressed as a function of two parameters,  $a_S$  and  $b_S$  <sup>4)</sup>:

$$B(K_S \rightarrow \pi^0 e^+ e^-) = [0.01 - 0.76a_S - 0.21b_S + 46.5a_S^2 + 12.9a_S b_S + 1.44b_S^2] \times 10^{-10} \quad (5)$$

$$B(K_S \rightarrow \pi^0 \mu^+ \mu^-) = [0.07 - 4.52a_S - 1.50b_S + 98.7a_S^2 + 57.7a_S b_S + 8.95b_S^2] \times 10^{-11} \quad (6)$$

where the total form factor is  $W_S(z) = G_F m_K^2 (a_S + b_S z) + W_S^{\pi\pi}(z)$ ,  $z = m_{\ell\ell}^2/m_K^2$ ,  $m_K$  is the kaon mass,  $m_{\ell\ell}$  is the invariant mass of the two leptons, and  $W_S^{\pi\pi}(z)$  is expected to be small. Assuming VMD, which predicts  $b_S = 0.4a_S$  <sup>4)</sup>, the value of the parameter  $|a_S|$  can be obtained from the measurement of the individual  $K_S \rightarrow \pi^0 \ell^+ \ell^-$  branching ratios via the relations <sup>6)</sup>

$$B(K_S \rightarrow \pi^0 e^+ e^-) \simeq 5.2 \times 10^{-9} a_S^2, \quad (7)$$

$$B(K_S \rightarrow \pi^0 \mu^+ \mu^-) \simeq 1.2 \times 10^{-9} a_S^2. \quad (8)$$

Using our new results for these branching ratios, the value of the parameter  $|a_S|$  is found to be:

$$|a_S|_{ee} = 1.06^{+0.26}_{-0.21} \pm 0.07,$$

$$|a_S|_{\mu\mu} = 1.54^{+0.40}_{-0.32} \pm 0.06.$$

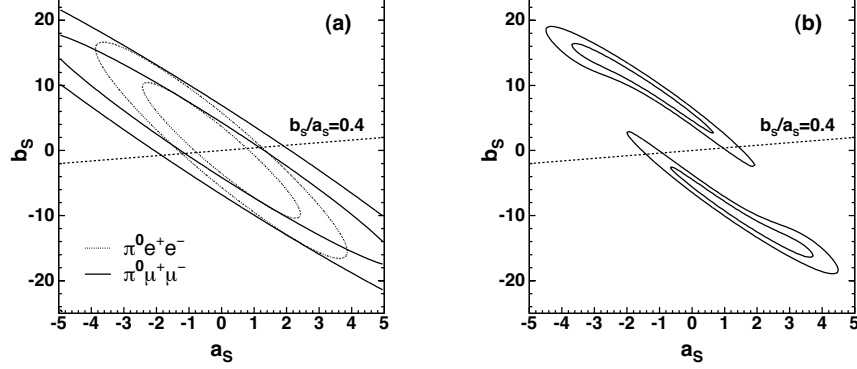


Figure 6: (a) Allowed regions of  $a_S$  and  $b_S$  determined from the observed number of  $K_S \rightarrow \pi^0 \mu^+ \mu^-$  and  $K_S \rightarrow \pi^0 e^+ e^-$  events separately. The region between the inner and outer solid (dashed) elliptical contours is the allowed region for  $K_S \rightarrow \pi^0 \mu^+ \mu^-$  ( $K_S \rightarrow \pi^0 e^+ e^-$ ) at 68% CL. (b) Allowed regions of  $a_S$  and  $b_S$  for the  $K_S \rightarrow \pi^0 \mu^+ \mu^-$  and  $K_S \rightarrow \pi^0 e^+ e^-$  channels combined. The inner (outer) contour of each pair delimits the  $1\sigma$  ( $2\sigma$ ) allowed region from the combined log-likelihood. The dashed straight line in both plots corresponds to  $b_S = 0.4a_S$ , as predicted by the VMD model.

assessment of the linear dependence of the form factor on  $z$ .

## 2.2 CPV component of $K_L \rightarrow \pi^0 \ell^+ \ell^-$

The branching ratios for the decay  $K_S \rightarrow \pi^0 \ell^+ \ell^-$  ( $\ell = e, \mu$ ) measured by NA48 allows us to predict the CPV contribution to the branching ratio of the corresponding  $K_L$  decay,  $K_L \rightarrow \pi^0 \ell^+ \ell^-$ , as a function of  $\text{Im}(\lambda_t)$  to within a sign ambiguity [8]):

$$B(K_L \rightarrow \pi^0 \ell^+ \ell^-)_{\text{CPV}} \times 10^{12} = C_{\text{MIX}} \pm C_{\text{INT}} \left( \frac{\text{Im}(\lambda_t)}{10^{-4}} \right) + C_{\text{DIR}} \left( \frac{\text{Im}(\lambda_t)}{10^{-4}} \right)^2, \quad (11)$$

where

$$\begin{aligned} C_{\text{MIX}}^{ee} &= 3.0 \times 10^9 B(K_S \rightarrow \pi^0 e^+ e^-), & C_{\text{MIX}}^{\mu\mu} &= 3.1 \times 10^9 B(K_S \rightarrow \pi^0 \mu^+ \mu^-), \\ C_{\text{INT}}^{ee} &= 8.6 \times 10^4 \sqrt{B(K_S \rightarrow \pi^0 e^+ e^-)}, & C_{\text{INT}}^{\mu\mu} &= 4.6 \times 10^4 \sqrt{B(K_S \rightarrow \pi^0 \mu^+ \mu^-)}, \\ C_{\text{DIR}}^{ee} &= 2.4 & C_{\text{DIR}}^{\mu\mu} &= 1.0. \end{aligned}$$

$C_{\text{INT}}$  is the coefficient for the term due to the interference between the direct ( $C_{\text{DIR}}$ ) and indirect ( $C_{\text{MIX}}$ ) CPV components, and  $\lambda_t = V_{td} V_{ts}^*$ .

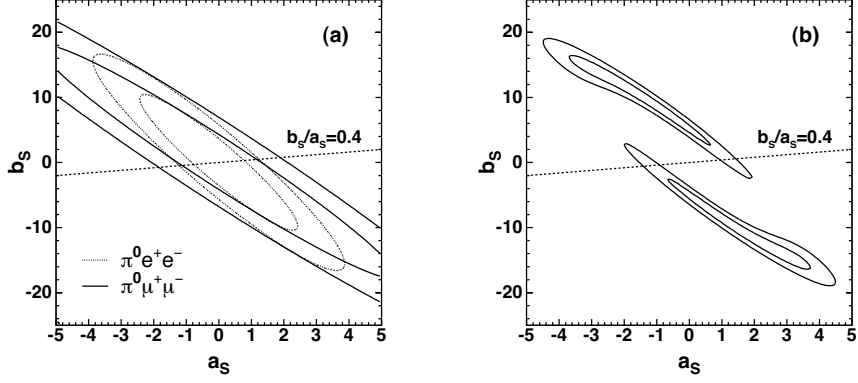


Figure 6: (a) Allowed regions of  $a_S$  and  $b_S$  determined from the observed number of  $K_S \rightarrow \pi^0 \mu^+ \mu^-$  and  $K_S \rightarrow \pi^0 e^+ e^-$  events separately. The region between the inner and outer solid (dashed) elliptical contours is the allowed region for  $K_S \rightarrow \pi^0 \mu^+ \mu^-$  ( $K_S \rightarrow \pi^0 e^+ e^-$ ) at 68% CL. (b) Allowed regions of  $a_S$  and  $b_S$  for the  $K_S \rightarrow \pi^0 \mu^+ \mu^-$  and  $K_S \rightarrow \pi^0 e^+ e^-$  channels combined. The inner (outer) contour of each pair delimits the  $1\sigma$  ( $2\sigma$ ) allowed region from the combined log-likelihood. The dashed straight line in both plots corresponds to  $b_S = 0.4a_S$ , as predicted by the VMD model.

assessment of the linear dependence of the form factor on  $z$ .

## 2.2 CPV component of $K_L \rightarrow \pi^0 \ell^+ \ell^-$

The branching ratios for the decay  $K_S \rightarrow \pi^0 \ell^+ \ell^-$  ( $\ell = e, \mu$ ) measured by NA48 allows us to predict the CPV contribution to the branching ratio of the corresponding  $K_L$  decay,  $K_L \rightarrow \pi^0 \ell^+ \ell^-$ , as a function of  $\text{Im}(\lambda_\ell)$  to within a sign ambiguity <sup>8)</sup>:

$$B(K_L \rightarrow \pi^0 \ell^+ \ell^-)_{\text{CPV}} \times 10^{12} = C_{\text{MIX}} \pm C_{\text{INT}} \left( \frac{\text{Im}(\lambda_\ell)}{10^{-4}} \right) + C_{\text{DIR}} \left( \frac{\text{Im}(\lambda_\ell)}{10^{-4}} \right)^2, \quad (11)$$

where

$$\begin{aligned} C_{\text{MIX}}^{ee} &= 3.0 \times 10^9 B(K_S \rightarrow \pi^0 e^+ e^-), & C_{\text{MIX}}^{\mu\mu} &= 3.1 \times 10^9 B(K_S \rightarrow \pi^0 \mu^+ \mu^-), \\ C_{\text{INT}}^{ee} &= 8.6 \times 10^4 \sqrt{B(K_S \rightarrow \pi^0 e^+ e^-)}, & C_{\text{INT}}^{\mu\mu} &= 4.6 \times 10^4 \sqrt{B(K_S \rightarrow \pi^0 \mu^+ \mu^-)}, \\ C_{\text{DIR}}^{ee} &= 2.4 & C_{\text{DIR}}^{\mu\mu} &= 1.0. \end{aligned}$$

$C_{\text{INT}}$  is the coefficient for the term due to the interference between the direct ( $C_{\text{DIR}}$ ) and indirect ( $C_{\text{MIX}}$ ) CPV components, and  $\lambda_\ell = V_{td} V_{ts}^*$ .

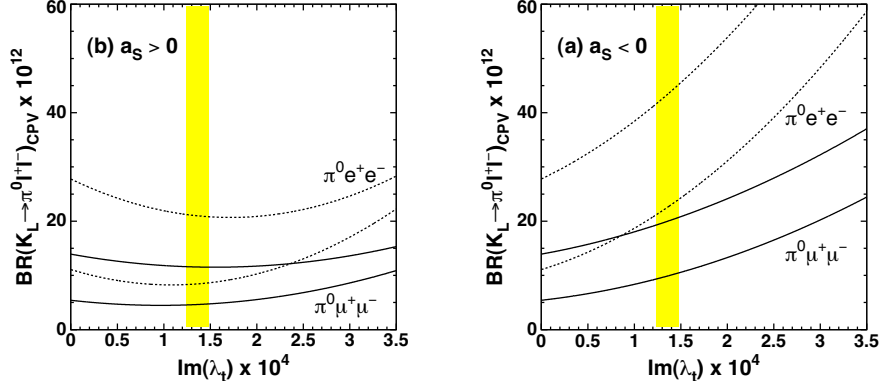


Figure 7: Predicted CPV component of the  $K_L \rightarrow \pi^0 \mu^+ \mu^-$  (solid curves) and  $K_L \rightarrow \pi^0 e^+ e^-$  (dashed curves) branching ratios as a function of  $\text{Im}(\lambda_t)$  assuming (a)  $a_S < 0$  and (b)  $a_S > 0$ . Each pair of curves delimits the allowed range derived from the  $\pm 1\sigma$  measured values of  $|a_S|$ . The vertical shaded band corresponds to the world average value of  $\text{Im}(\lambda_t)$ .

Taking the central value of the measured branching ratio  $B(K_S \rightarrow \pi^0 \ell^+ \ell^-)$  and  $\text{Im}(\lambda_t) = 1.36 \times 10^{-4}$  <sup>9)</sup> gives:

$$B(K_L \rightarrow \pi^0 e^+ e^-)_{CPV} \times 10^{12} \approx 17.2_{\text{mixing}} \pm 9.4_{\text{interference}} + 4.7_{\text{direct}}, \quad (12)$$

$$B(K_L \rightarrow \pi^0 \mu^+ \mu^-)_{CPV} \times 10^{12} \approx 8.8_{\text{mixing}} \pm 3.3_{\text{interference}} + 1.8_{\text{direct}}. \quad (13)$$

The predicted dependence of  $B(K_L \rightarrow \pi^0 \ell^+ \ell^-)_{CPV}$  on  $\text{Im}(\lambda_t)$  is shown in Fig. 7 assuming VMD.

### 2.3 SM prediction for $K_L \rightarrow \pi^0 \ell^+ \ell^-$

The CPC component of  $K_L \rightarrow \pi^0 \ell^+ \ell^-$  decays can be constrained using NA48 and KTeV measurements of the decay  $K_L \rightarrow \pi^0 \gamma \gamma$  <sup>10, 11)</sup>. A recent analysis based on ChPT obtained the prediction  $(5.2 \pm 1.6) \times 10^{-12}$  <sup>8)</sup> for the muon channel, while it is negligible for the electron.

Combining the CPV and the CPC components, the central value for the total  $K_L \rightarrow \pi^0 e^+ e^-$  ( $K_L \rightarrow \pi^0 \mu^+ \mu^-$ ) branching ratio is estimated to be  $32(19) \times 10^{-12}$  or  $13(12) \times 10^{-12}$ , depending on the sign of the interference term between the direct and the indirect (mixing) amplitudes. This estimate is consistent with the present experimental upper limit presented by KTeV

in this conference, that is  $B(K_L \rightarrow \pi^0 e^+ e^-)$  of  $2.8 \times 10^{-10}$  (90% CL) and  $B(K_L \rightarrow \pi^0 \mu^+ \mu^-)$  of  $3.8 \times 10^{-10}$  (90% CL).

### 3 Results and Discussion for the $K^\pm \rightarrow \pi^\pm \ell^+ \ell^-$

In principle,  $\chi$ PT theory can predict whether the resulting interference between the direct and indirect CP-violating amplitudes in  $K_L \rightarrow \pi^0 \ell^+ \ell^-$  are constructive or destructive. To gain confidence in this model, we must compare its predictions for the decay rate and the invariant  $\ell^+ \ell^-$  mass spectrum. There are not enough events in the NA48  $K_S \rightarrow \pi^0 e^+ e^-$  and  $K_S \rightarrow \pi^0 \mu^+ \mu^-$  data sample. Therefore, analyses of mass spectrum for  $K^\pm \rightarrow \pi^\pm e^+ e^-$  and  $K^\pm \rightarrow \pi^\pm \mu^+ \mu^-$  will be studied instead.

After combining the data from the 2003 and 2004  $K^\pm$  run, we will have a  $K^\pm \rightarrow \pi^\pm e^+ e^-$  that will be as large as the world data sample, that is, we will have more than 10,000 events. The current world data on  $K^\pm \rightarrow \pi^\pm \mu^+ \mu^-$  consist of only 800 events. The NA48 sample will be at least three times larger. In both channels the background levels will be low, see Fig. 8.

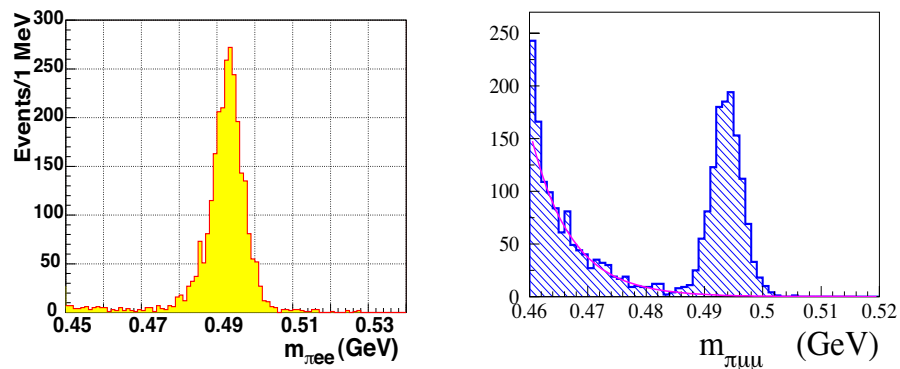


Figure 8: NA48 reconstructed  $K^\pm \rightarrow \pi^\pm e^+ e^-$  and  $K^\pm \rightarrow \pi^\pm \mu^+ \mu^-$  events for a fraction of the available data sample.

### References

1. J.R. Batley *et al.*, Physics Letters B576 (2003) 43.

2. J.R. Batley *et al.*, CERN-PH-EP Preprint 2004-025, Accepted for publication by Physics Letters.
3. J.R. Batley *et al.*, Physics Letters B544 (2002) 97.
4. G. D'Ambrosio, G. Ecker, G. Isidori and J. Portoles, Journal of High Energy Physics 08 (1998) 004.
5. S. Friot, D. Greynat, and E. de Rafael, "Rare Kaon Decays Revisited," hep-ph/0404136.
6. G. Buchalla, G. D'Ambrosio and G. Isidori, Nuclear Physics B672 (2003) 387.
7. G. Ecker, A. Pich, and E. de Rafael, Nuclear Physics B291 (1987) 692.
8. G. Isidori, C. Smith and R. Unterdorfer, "The rare decay  $K_L \rightarrow \pi^0 \mu \mu$  within the SM," hep-ph/0404127.
9. M. Battaglia *et al.*, "The CKM matrix and the unitarity triangle," hep-ph/0304132.
10. A. Lai *et al.*, Physics Letters B536 (2002) 229.
11. A. Alavi-Harati *et al.*, Physical Review Letters 83 (1999) 917.

## KTeV RESULTS ON RARE KAON DECAYS

Elliott Cheu  
*University of Arizona*

### ABSTRACT

The KTeV experiment has carried out a broad program of studies of rare kaon decays. In this paper we present results on  $K_L \rightarrow \pi^0 \ell \bar{\ell}$  decay modes. These decays offer a possible window for observing direct CP violation in a decay. We do not observe any signals in these decays and present 90% upper limits for each of the modes. Our analyses represent the most sensitive searches to date.

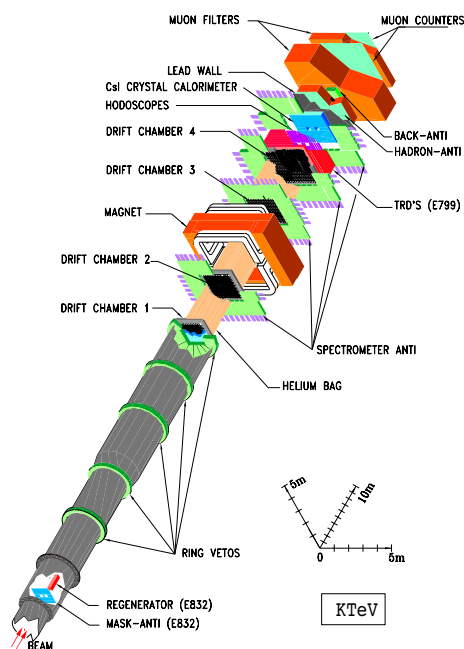
### 1 Introduction

The decays  $K_L \rightarrow \pi^0 \ell \bar{\ell}$ , where  $\ell \bar{\ell}$  represents  $\nu \bar{\nu}$ ,  $e^+ e^-$  or  $\mu^+ \mu^-$ , are interesting because they can be used to observe direct CP violation in a decay. In addition, mechanisms for new physics beyond the Standard Model suggest that the branching ratios for these decays can be significantly enhanced relative to their

Standard Model values. <sup>1)</sup> Three components contribute to the  $K_L \rightarrow \pi^0 \bar{l}l$  amplitude: direct CP violation, indirect CP violation (and an interference term), and a CP conserving term. Recent measurements of the decay  $K_S \rightarrow \pi^0 e^+ e^-$  <sup>2)</sup> and  $K_S \rightarrow \pi^0 \mu^+ \mu^-$  <sup>3)</sup> have helped to determine the indirect CP violating contributions to  $K_L \rightarrow \pi^0 e^+ e^-$  and  $K_L \rightarrow \pi^0 \mu^+ \mu^-$ . The magnitude of the CP conserving contributions to  $K_L \rightarrow \pi^0 \bar{l}l$  can be determined by measurements of the decay  $K_L \rightarrow \pi^0 \gamma \gamma$ . <sup>4, 5)</sup> Therefore, measuring the branching ratio of any of the  $K_L \rightarrow \pi^0 \bar{l}l$  decays allows one to extract the direct CP violating component. In the mode  $K_L \rightarrow \pi^0 \mu^+ \mu^-$ , the three amplitudes are predicted <sup>7)</sup> to be roughly of the same size. In the electron final state, the CP conserving term is estimated to be small <sup>8)</sup>. And, in the neutrino mode, the direct CP violating terms are expected to dominate, with the indirect and CP conserving amplitudes negligible. <sup>9)</sup>

The KTeV experiment is a fixed target experiment located at Fermilab, and is shown in Figure 1. The detector contains a charged spectrometer with four drift chambers, two on either side of a large dipole magnet. At the downstream end of the detector is a two-meter square calorimeter consisting of 3100 pure CsI blocks. Just upstream of the CsI calorimeter is a transition radiation detector capable of  $e/\pi$  separation of 200:1 with a 90% efficiency. Following the calorimeter are 10 cm of lead and 5 meters of steel which act as a muon filter. Two planes of scintillator, used for muon detection, are located just downstream of the steel. Photon vetoes to detect the the presence of particles that would otherwise escape detection surround the spectrometer. The charged spectrometer achieves a hit resolution of better than 100  $\mu\text{m}$ , while the CsI calorimeter obtains better than 1% energy resolution over the range of energies of interest.

The KTeV experiment took data during two runs in 1997 and 1999. Between the 1997 and 1999 runs, a number of upgrades were made to the detector to increase its reliability and to improve its live time. In addition, the transverse kick from the magnet was reduced from 205 MeV/c to 150 MeV/c, enabling a larger acceptance for high multiplicity decay modes. In the first period, nearly  $3 \times 10^{11}$   $K_L$  decayed in the detector, while in 1999 a flux of  $3.6 \times 10^{11}$   $K_L$  decays was recorded. This large kaon flux allows us to have an unprecedented sensitivity to a number of rare kaon decays with large multiplicity final states.

Figure 1: *The KTeV detector.*

## 2 $K_L \rightarrow \pi^0 \nu \bar{\nu}$

In the decay  $K_L \rightarrow \pi^0 \nu \bar{\nu}$  the final state consists of a single  $\pi^0$  with nothing else detected in the experiment. In our experiment, the calorimeter cannot determine a photon's angle of incidence. So, we cannot reconstruct the mass of a  $\pi^0$  from its daughter photons without first determining the decay vertex. To circumvent this problem, we use the Dalitz decay ( $\pi^0 \rightarrow e^+ e^- \gamma$ ) to reconstruct the  $\pi^0$  vertex and mass. This requirement reduces our sensitivity by about two orders of magnitude because of the small Dalitz decay branching ratio.

Our analysis utilizes only the 1997 data set. We proceed by first selecting events with two electrons and a photon in the final state. Electrons are determined by using the ratio of the energy in the calorimeter to the momentum measured in the charged spectrometer ( $E/p$ ). Events with a good  $\pi^0$  mass are selected and the transverse momentum  $p_T$  of the  $\pi^0$  is plotted. Because of the

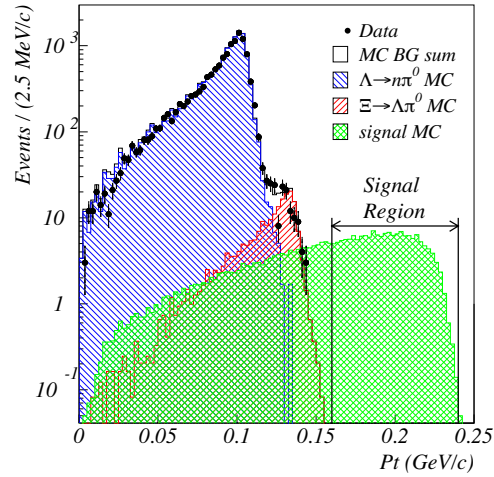


Figure 2: The reconstructed transverse momentum for  $K_L \rightarrow \pi^0 \nu \bar{\nu}$  candidates. The solid histogram represents the sum of our Monte Carlo background estimate. No candidates are found in the signal region indicated in the figure.

two missing neutrinos, the  $p_T$  for  $K_L \rightarrow \pi^0 \nu \bar{\nu}$  events should be relatively large.

Backgrounds to this measurement come from both kaon and hyperon decays. In particular, the largest sources of background result from  $\Lambda \rightarrow n\pi^0$  and  $\Xi \rightarrow \Lambda\pi^0$  where the neutron and the  $\Lambda$  daughters are not reconstructed.

As shown in Figure 2, we find no events in the signal region. We determine the kaon flux by reconstructing the decay  $K_L \rightarrow e^+e^-\gamma$ , and set an upper limit of  $\text{BR}(K_L \rightarrow \pi^0 e^+e^-) < 5.9 \times 10^{-7}$ .<sup>10)</sup> Note that this limit is significantly higher than the Standard Model prediction. Clearly, using the  $\pi^0 \rightarrow \gamma\gamma$  decay rather than the  $\pi^0 \rightarrow e^+e^-\gamma$  decay mode would significantly help to improve the limit. Two experiments KOPIO and E391A propose to use the  $\pi^0 \rightarrow \gamma\gamma$  decay to reach the Standard Model prediction for  $K_L \rightarrow \pi^0 \nu \bar{\nu}$ .

### 3 $K_L \rightarrow \pi^0 e^+ e^-$

As opposed to the  $K_L \rightarrow \pi^0 \nu \bar{\nu}$  decay, all final state particles in the mode  $K_L \rightarrow \pi^0 e^+ e^-$  can be reconstructed in our detector. Since the decay position can be determined from the  $e^+ e^-$  vertex, we do not need to rely on the  $\pi^0$  Dalitz decay, but instead use the  $\pi^0 \rightarrow \gamma\gamma$  final state. Again, we look for events with two oppositely charged electrons. In this analysis the TRDs are also used to help improve the electron purity.

The most serious background in this analysis comes from the decay  $K_L \rightarrow e^+ e^- \gamma\gamma$ . Since this decay is produced through inner and outer bremsstrahlung, there are strong kinematic constraints that can distinguish this decay from that of  $K_L \rightarrow \pi^0 e^+ e^-$ . In particular, we rely on  $\cos \Theta_\pi$ , where  $\Theta_\pi$  is the angle between the momentum of the  $e^+ e^-$  system and the  $\gamma$  in the  $\gamma\gamma$  center-of-mass. This variable is uniform for signal events because of the  $\pi^0$  spin but peaks near  $\pm 1$  for background events. We also cut on the variable  $\Theta_{min}$  which is the smallest angle between the photon and the  $e^\pm$  in the  $K_L$  center-of-mass. For signal events, this variable is uniformly distributed, while it is peaked at small angles for background because of radiation.

This analysis uses data collected in both 1997 and 1999. We expect  $0.87 \pm 0.15$  events from background. We find two events in the signal region as shown in Figure 3. Using the decay  $K_L \rightarrow \pi^0 \pi^0$ ,  $\pi^0 \rightarrow e^+ e^- \gamma$ , we determine  $\text{BR}(K_L \rightarrow \pi^0 e^+ e^-) < 2.8 \times 10^{-10}$ . 11)

### 4 $K_L \rightarrow \pi^0 \mu^+ \mu^-$

Like the previous search, in the  $K_L \rightarrow \pi^0 \mu^+ \mu^-$  decay, all of the final state particles can be reconstructed in the KTeV detector. We search for two oppositely charged muons, and two neutral clusters in the calorimeter. The two photons are required to have a mass consistent with a  $\pi^0$ .

The most serious background to this decay comes from  $K_L \rightarrow \mu^+ \mu^- \gamma\gamma$  decays, which has a branching ratio of  $2.62 \pm 0.40 \pm 0.17) \times 10^{-9}$ . Like the  $K_L \rightarrow \pi^0 e^+ e^-$  search, we can utilize two kinematic variables  $\cos \Theta_\pi$  and  $\Theta_{min}$ . However, the  $\Theta_{min}$  cut is less effective than in the  $K_L \rightarrow \pi^0 e^+ e^-$  search because there is less bremsstrahlung radiation. So, while the branching ratio for the background decays is much smaller, there are fewer kinematic constraints in this decay.

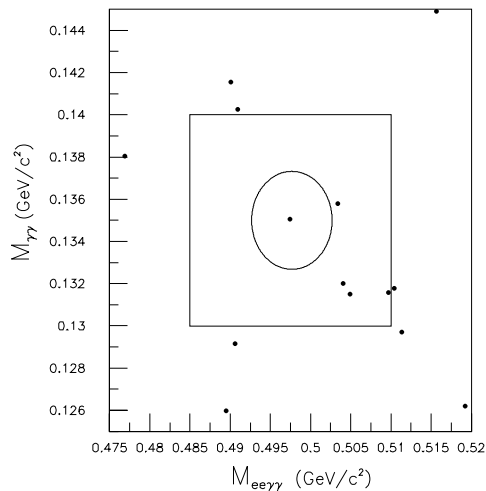


Figure 3: Reconstructed  $\gamma\gamma$  mass versus  $e^+e^-\gamma\gamma$  mass for  $K_L \rightarrow \pi^0 e^+ e^-$  candidates. The square region represents the area masked off while the selection criteria were determined. The ellipse represents the signal region. One candidate event is present in the signal region.

As shown in Figure 4, we expect  $0.99 \pm 0.35$  background events in our signal region. We find one event, and determine a 90% upper limit of  $\text{BR}(K_L \rightarrow \pi^0 \mu^+ \mu^-) < 3.8 \times 10^{-10}$  (90% C.L.).<sup>12)</sup> This result is based upon our 1997 data. A combined result using both our 1997 and 1999 data should be forthcoming shortly. As of this time, there are no other planned experiments to measure this decay mode.

## 5 Summary and Conclusions

The KTeV experiment has made the best measurements to date on the decays  $K_L \rightarrow \pi^0 \nu \bar{\nu}$ ,  $K_L \rightarrow \pi^0 e^+ e^-$  and  $K_L \rightarrow \pi^0 \mu^+ \mu^-$ . These results are approaching the Standard Model limits, leaving little room for new physics. We expect to make further improvements to the  $K_L \rightarrow \pi^0 \mu^+ \mu^-$  search, and future experiments have been designed to push the limits on  $K_L \rightarrow \pi^0 \nu \bar{\nu}$ . Figure 5 shows the current status on the  $K_L \rightarrow \pi^0 l \bar{l}$  decays.

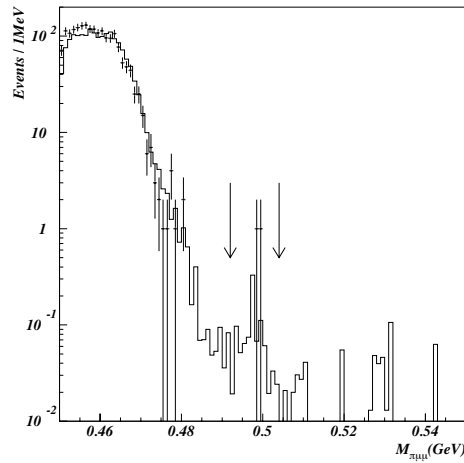


Figure 4: The reconstructed  $\mu^+\mu^-\gamma\gamma$  mass for  $K_L \rightarrow \pi^0\mu^+\mu^-$  candidates. The solid histogram represents a Monte Carlo prediction of our estimated background. Two events were found in the signal region indicated by the arrows.

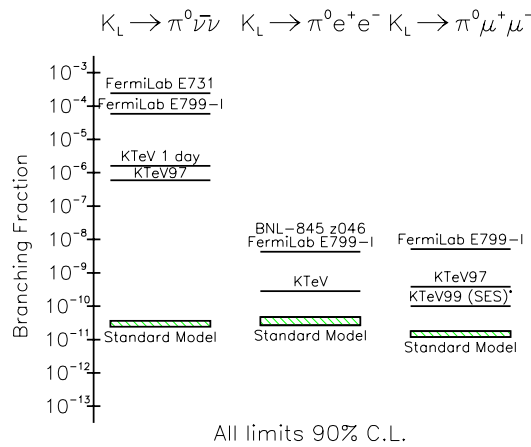


Figure 5: Current status of  $K_L \rightarrow \pi^0 l \bar{l}$  searches.

---

**References**

1. A.J. Buras, G. Colangelo, G. Isidori, A Romanino, and L. Silvestrini, Nucl. Phys **B566** 3 (2000).
2. J.R. Batley *et al.*, Phys. Lett. **B576**, 43 (2003).
3. J.R. Batley *et al.*, CERN PH-EP Preprint 2004-025.
4. A. Lai *et al.*, Phys. Lett. **B536**, 229 (2002).
5. A. Alavi-Harati *et al.*, Phys. Rev. Lett. **83**, 917 (1999).
6. A.J. Buras, F. Schwab, S. Uhlig, hep-ph/0405132.
7. G. Isidori, C. Smith, R. Unterdorfer, hep-ph/0404127.
8. G. D'Ambrosio, G. Ecker, G. Isidori and J. Portoles, J. High Energy Physics, **08**, 004 (1998).
9. L.S. Littenberg, Phys. Rev **D39** 3322 (1989).
10. A. Alavi-Harati *et al.*, Phys. Rev. **D61** 072006 (2000).
11. A. Alavi-Harati *et al.*, Phys. Rev. Lett. **93** 021805 (2004).
12. A. Alavi-Harati *et al.*, Phys. Rev. Lett. **84** 5279 (2000).

### E949 $K^+ \rightarrow \pi^+ \nu \bar{\nu}$ RESULTS

David E. Jaffe  
*Brookhaven National Laboratory, Upton, NY, USA*

#### ABSTRACT

The recent results on  $K^+ \rightarrow \pi^+ \nu \bar{\nu}$  from Brookhaven experiment E949 are presented.

The decay  $K^+ \rightarrow \pi^+ \nu \bar{\nu}$  is one of a handful of processes that offer clear and unambiguous information on the CKM unitarity triangle <sup>1)</sup>. Specifically, the rate of charged kaon decay to the  $\pi \nu \bar{\nu}$  final state is governed by flavor-changing neutral currents in the standard model (SM) and is proportional to the squared of the CKM matrix element  $V_{td}$  with an uncertainty of  $\sim 5\%$  due to a mild dependence on the charm quark mass <sup>2)</sup>. Precision measurement of  $\mathcal{B}(K^+ \rightarrow \pi^+ \nu \bar{\nu})$  along with the corresponding neutral kaon decay  $\mathcal{B}(K_L^0 \rightarrow \pi^0 \nu \bar{\nu})$  suffice to determine the apex of the CKM unitarity triangle. Indeed, a comparison of  $\mathcal{B}(K^+ \rightarrow \pi^+ \nu \bar{\nu})/\mathcal{B}(K_L^0 \rightarrow \pi^0 \nu \bar{\nu})$  with the time-dependent asymmetry of  $B^0 \rightarrow J/\psi K_S^0$  decays is perhaps the definitive test of the SM description of CP violation <sup>1)</sup>.

Given the current knowledge of the CKM matrix elements and their uncertainties,  $\mathcal{B}(K^+ \rightarrow \pi^+ \nu \bar{\nu})$  is expected to be  $(0.78 \pm 0.12) \times 10^{-10}$ . This extremely low rate, coupled with the lack of a distinctive kinematic signature, makes observation of  $K^+ \rightarrow \pi^+ \nu \bar{\nu}$  an experimental challenge. Experiment E787 at Brookhaven National Laboratory (BNL) has observed two candidates for the decay  $K^+ \rightarrow \pi^+ \nu \bar{\nu}$  upon an estimated background of  $0.15 \pm 0.04$  events in the kinematic region between the copious two-body decays  $K^+ \rightarrow \pi^+ \pi^0$  and  $K^+ \rightarrow \mu^+ \nu$  dubbed “pnn1”. If these candidates are interpreted as  $K^+ \rightarrow \pi^+ \nu \bar{\nu}$  decays, the corresponding branching fraction is  $(1.57_{-0.82}^{+1.75}) \times 10^{-10}$  and is statistically consistent with the SM expectation but with a central value that two times higher than expected<sup>3)</sup>.

Experiment E949 was approved in 1999 as an extensive upgrade of E787 with the goal of observing 5-10  $K^+ \rightarrow \pi^+ \nu \bar{\nu}$  events. E949 accumulated  $1.8 \times 10^{12}$  stopped  $K^+$  in the spring of 2002 before high energy physics running at the BNL Alternating Gradient Synchrotron (AGS) was halted. The 12 weeks corresponds to approximately one-fifth of the approved running and E949 is seeking additional funding to complete the experiment. The results of the 2002 run in the pnn1 kinematic region are the subject of this report.

As alluded to earlier,  $K^+ \rightarrow \pi^+ \nu \bar{\nu}$  is an experimental challenge because of its low rate and kinematic signature. It is a three-body final state with only one observable particle. Table 1 contrasts the expected rate of this decay with known processes quantitatively illustrating the need of enormous background suppression. The backgrounds can be classified into four groups:

1.  $K^+ \rightarrow \pi^+ \pi^0$  ( $K_{\pi 2}$ );
2.  $K^+$  decays with a muon in the final state including  $K^+ \rightarrow \mu^+ \nu$  ( $K_{\mu 2}$ ),  $K^+ \rightarrow \mu^+ \nu \gamma$ ,  $K^+ \rightarrow \mu^+ \nu \pi^0$  and  $K^+ \rightarrow \pi^+ \pi^0$  with  $\pi^+$  decay-in-flight, (the latter three components are referred to as  $K_{\mu m}$ );
3. beam backgrounds when a  $\pi^+$  from the beam scatters in the target into the detector and
4. the charge-exchange (CEX) process  $K^+ n \rightarrow K^0 X$ ,  $K^0 \rightarrow K_L^0$ ,  $K_L^0 \rightarrow \pi^+ \ell^- \nu$  with  $\ell = \mu$  or  $e$ .

E949, like its predecessor E787, operates in a low-energy separated beam with a nominal  $K^+/\pi^+$  rate of 4 at a momentum of  $\sim 700$  MeV/c<sup>4)</sup>. The

Table 1: *The rates of background processes to  $K^+ \rightarrow \pi^+ \nu \bar{\nu}$ . CEX  $\equiv (K^+ n \rightarrow K^0 X) \times (K^0 \rightarrow K_L^0) \times (K_L^0 \rightarrow \pi^+ \ell^- \nu)$ .  $\ell^-$  is  $\mu^-$  or  $e^-$ . The  $K^+ n \rightarrow K^0 X$  rate is empirically determined.*

Process	Rate
$K^+ \rightarrow \pi^+ \nu \bar{\nu}$	$0.78 \times 10^{-10}$
$K^+ \rightarrow \pi^+ \pi^0$	$2113000000.00 \times 10^{-10}$
$K^+ \rightarrow \mu^+ \nu$	$6343000000.00 \times 10^{-10}$
$K^+ \rightarrow \mu^+ \nu \gamma$	$55000000.00 \times 10^{-10}$
$K^+ \rightarrow \pi^0 \mu^+ \nu$	$327000000.00 \times 10^{-10}$
CEX	$\sim 46000.00 \times 10^{-10}$
Scattered $\pi^+$ beam	$\sim 25000000.00 \times 10^{-10}$

charged beam is directed along the axis of a 1T solenoid and through Cherenkov detectors and wire chambers, slowed in BeO and an active degrader and stopped in a scintillating fiber target. The trigger accepts  $K^+$  decays after a delay of  $\sim 2$  ns with an outgoing charged particle that traverses a low-mass drift chamber and stops in a cylindrical range stack (RS) of 2 cm thick layers of plastic scintillator. The RS is instrumented with 500 MHz transient digitizers that permit observation of the  $\pi \rightarrow \mu \rightarrow e$  decay chain for positive  $\pi^+$  identification. The RS is surrounded by lead/scintillator sandwich-style detectors for photon detection. Endcaps of pure CsI crystals and other lead/scintillator detectors in the beam region comprise the remainder of the photon detectors.

E949 relies on two independent methods of rejection of each of the four background processes in order to measure the level of suppression with the data as well as achieve the necessary level of background. As an example,  $K^+ \rightarrow \pi^+ \pi^0$  decays are suppressed by measurement of the  $\pi^+$  kinematic quantities energy (E), momentum (P) and range (R) in plastic scintillator and by detection of photons from  $\pi^0$  decay. Inversion of the criteria (“cuts”) of each method enhances the background and permits a measurement of the background rejection of the complementary cut with the data. To confirm the background estimate with this method, the rate of events outside the pre-determined signal region is compared with the prediction as the two complementary cuts are loosened simultaneously to accept background rates hundreds of times that expected in the signal region. The results of this procedure for the  $K^+ \rightarrow \pi^+ \pi^0$  and  $K^+ \rightarrow \mu^+ X$  backgrounds show good agreement between

Table 2: The fitted constants  $c$  of the ratios of the observed to the predicted numbers of background events and the probability of  $\chi^2$  of the fits for the two-body backgrounds,  $K_{\pi 2}$ ,  $K_{\mu 2}$  and multi-body  $K_{\mu m}$  backgrounds near but outside the signal region. The first uncertainty in  $c$  was due to the statistics of the observed events and the second was due to the uncertainty in the predicted rate. The predicted numbers of background events within the signal region and their statistical uncertainties are also tabulated in the fourth column. Other backgrounds contributed an additional  $0.014 \pm 0.003$  events resulting in a total number of background events expected in the signal region of  $0.30 \pm 0.03$ .

Background	$c$		$\chi^2$ Probability	Events
$K_{\pi 2}$	0.85	$+0.12$ $-0.11$	0.17	$0.216 \pm 0.023$
$K_{\mu 2}$	1.15	$+0.25$ $-0.21$	0.67	$0.044 \pm 0.005$
$K_{\mu m}$	1.06	$+0.35$ $-0.29$	0.40	$0.024 \pm 0.010$

the prediction and expectation (Table 2) and show no indication of correlation between the cuts. The total predicted background is  $0.30 \pm 0.03$  events and is dominated by  $K^+ \rightarrow \pi^+ \pi^0$ . This background rate for  $1.8 \times 10^{12}$  stopped  $K^+$  was intentionally selected to be higher than the  $0.15 \pm 0.04$  background events expected for the entire E787 exposure of  $5.9 \times 10^{12}$  stopped  $K^+$ .

E949 elected to allow a higher total background in order to increase the signal acceptance. The E787 experience provides E949 with confidence in estimating the background rates and to more fully exploit the available data. By tightening the cuts, the background rate from each contributing processes can be reduced in a portion of the signal region. This knowledge, along with the acceptance in the same region, allows the signal region to be subdivided into 3781 cells with a predicted rate of background and signal acceptance in each cell. The  $K^+ \rightarrow \pi^+ \nu \bar{\nu}$  branching fraction corresponding to an observation of candidates in such cells can then be evaluated using a likelihood ratio technique [5]).

A single candidate was observed in the pre-determined signal region. Events passing all cuts except those on range and energy are shown in Figure 1. The observed candidate has all the characteristics of a  $K^+ \rightarrow \pi^+ \nu \bar{\nu}$  decay but its high values of P, R, and E as well as its low apparent pion decay time of 6.2 ns indicate a significant probability that it is due to  $K^+ \rightarrow \mu^+ X$ . The probability that the background alone could give rise to this event or any more signal-like event is 7% which is higher than the corresponding probabili-

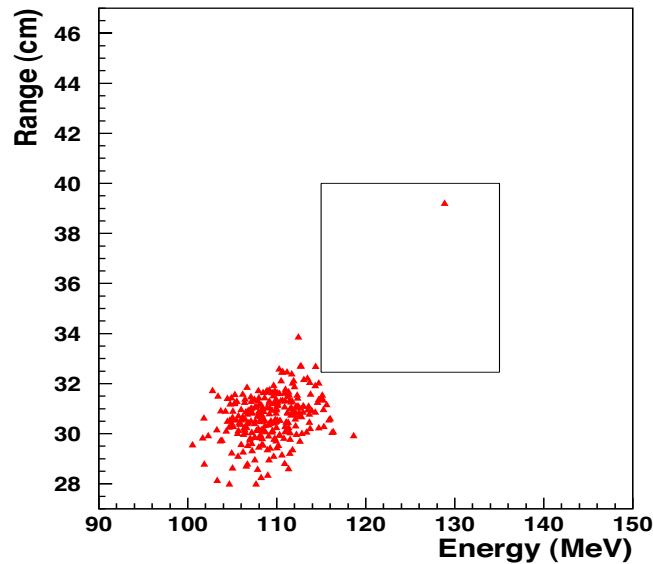


Figure 1: *Range (cm) vs Energy (MeV) for E949 data after all other cuts applied. The solid line shows signal region. The cluster of events near 110 MeV is unvetoes  $K^+ \rightarrow \pi^+\pi^0$ .*

ties of 0.7% and 2% of the candidates observed in E787. The probability that background alone could produce a more signal-like configuration than the three observed candidates is 0.1%. The  $K^+ \rightarrow \pi^+\nu\bar{\nu}$  branching fraction evaluated for all three candidates is  $(1.47^{+1.30}_{-0.89}) \times 10^{-10}$  [6].

The upgrades to E787 resulted in improved photon veto rejection of  $K^+ \rightarrow \pi^+\pi^0$  for the pnn1 region as well as the ability to accept higher instantaneous rates. The upgrades should permit comparable sensitivity in the kinematic region below the  $K^+ \rightarrow \pi^+\pi^0$  peak (“pnn2”). Previous analyses of the pnn2 region by E787 have demonstrated that this region is dominated by background from  $K^+ \rightarrow \pi^+\pi^0$  in which the kinematics of the charged pion are degraded by nuclear scattering in the target. The photon veto detector in the beam region is particularly important for suppression of this background process. Work is currently in progress to assess the impact of the upgrades to the photon veto detectors in the beam region and improvements to the algorithms that aid in

the detection of the scattered pion.

E949 has observed an additional candidate for  $K^+ \rightarrow \pi^+ \nu \bar{\nu}$  decay in the kinematic region above  $K^+ \rightarrow \pi^+ \pi^0$ . Combined with the E787 results,  $\mathcal{B}(K^+ \rightarrow \pi^+ \nu \bar{\nu}) = (1.47_{-0.89}^{+1.30}) \times 10^{-10}$ . Analysis of the kinematic region below  $K^+ \rightarrow \pi^+ \pi^0$  is in progress. Additional sources of funding are being sought to complete the E949 experiment. Given the importance of this mode to the understanding of the SM picture of CP violation, various programs to measure the  $K^+ \rightarrow \pi^+ \nu \bar{\nu}$  branching fraction at KEK, FNAL and CERN are under consideration <sup>7)</sup>.

I wish to thank the organizers for an interesting and informative conference in beautiful San Juan. I also wish to thank Steve Kettell for helpful comments and suggestions to this document.

## References

1. G. Buchalla and A. J. Buras, Nucl. Phys. **B548** 309 (1999).
2. A. J. Buras, R. Fleischer, S. Recksiegel, F. Schwab, arXiv:hep-ph/0402112 (2004).
3. S. Adler *et al.*, Phys. Rev. Lett. **88**, 041803 (2002).
4. Due to a failure of the primary AGS power supply, the AGS primary proton beam energy was lowered to 22 GeV from 24 GeV to attain a duty factor of 41%. Reduced operating voltage of one of the electro-magnetostatic separators in the kaon beam line resulted in increased pion contamination. The  $K^+$  to  $\pi^+$  ratio of the beam was 3 (4) for E949 (E787). The resultant instantaneous rates in the E949 detector were roughly twice those in typical E787 operations.
5. T. Junk, Nucl. Instr. Meth. **A434**, 435 (1999).
6. V.V. Anisimovsky *et al.*, Phys. Rev. Lett. **93**, 31801 (2004).
7. Workshop on Future Kaon Experiments at the AGS, 13 May 2004, <http://www3.bnl.gov/FutureK/>.

## STATUS AND PERSPECTIVES IN $\mu \rightarrow e\gamma$ DECAY SEARCH

Donato Nicolò

*Dipartimento di Fisica dell' Università di Pisa and I.N.F.N.*

### ABSTRACT

The  $\mu \rightarrow e\gamma$  decay, as well as other related Lepton Flavour Violation processes, is foreseen by a wide class of Supersymmetric Grand-Unified theories, with a branching ratio ranging between  $10^{-14}$  and  $10^{-12}$ . So it is considered as one of the most sensitive probe for the existence of Physics beyond the Standard Model. Past and present experiments will be reviewed on the light of current theoretical models. Particular emphasis will be laid on the MEG experiment, to be operated at PSI, which will be able to improve the current sensitivity ( $10^{-11}$ ) by two orders of magnitude so as to address the range of predictions.

### 1 Physics motivation

$\mu \rightarrow e\gamma$  decay, like other Lepton Flavour Violation (LFV) processes, is considered as one of the most interesting probe of Physics beyond the Standard

Model (SM). In the SM, Lepton Flavour is conserved as long as neutrino fields are massless. Also, LFV is allowed in extensions of the SM to include massive Dirac neutrinos, so as to give rise to neutrino oscillations, but the resulting branching ratios are so tiny ( $10^{-45} \div 10^{-50}$ ) to be ever observed.

On the other hand, LFV is predicted with much higher branching ratios by a wide class of Grand-Unified, Supersymmetric theories (often referred to as Gravitation-mediated SUSY), as a result of a finite mixing in the slepton sector. LFV mainly arises through radiative corrections due the heavy top quark mass<sup>1)</sup> and these predictions depend on the symmetry group and on the parameters of the theory. However, according to evaluations based on minimal SUSY SU(5),  $\mu \rightarrow e\gamma$  decay should occur, apart from accidental cancellations, with a branching ratio (BR) above  $10^{-14}$ , as shown in Fig. 1<sup>1</sup>.

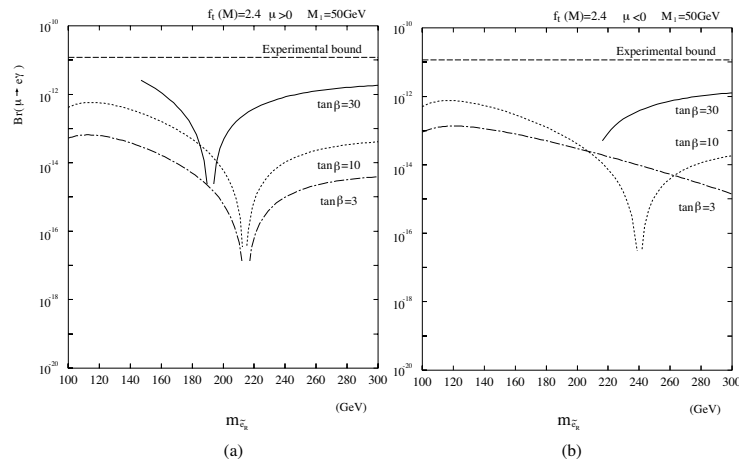


Figure 1: Predictions for  $BR(\mu \rightarrow e\gamma)$  in the minimal SU(5) SUSY model<sup>1)</sup>. Also shown is the current experimental limit set by the MEGA experiment<sup>2)</sup>. Values of  $\tan\beta < 3$  have been recently excluded at 95% C.L. by recent analyses of LEP data<sup>3)</sup>.

It has been pointed out that an additional contribution to LFV is associated with neutrino oscillations via the see-saw mechanism induced by heavy

<sup>1</sup>Even larger rates are predicted by theories based on symmetry groups other than SU(5); in SO(10), for instance,  $BR(\mu \rightarrow e\gamma)$  is enhanced by two orders of magnitude about, induced by loop diagrams whose amplitude is proportional to the  $\tau$  mass.

right-handed Majorana neutrinos, which is invoked to explain the extremely small neutrino masses<sup>4)</sup>. A possible contribution to the slepton mixing between  $\tilde{\mu}$  and  $\tilde{e}$  comes from  $V_{21}$ , the neutrino mixing matrix element to account for solar neutrino deficit. With this mixing parameter confined to the MSW large mixing angle (LMA) solution and right-handed neutrino mass scale above  $10^{12}$  GeV, the BR for  $\mu \rightarrow e\gamma$  is predicted to be larger than  $10^{-13}$ .

## 2 Experimental status

### 2.1 Event signature and background

The signature of  $\mu^+ \rightarrow e^+\gamma$  at rest is a coincidence of a  $e^+$  and a  $\gamma$ , moving back-to-back and both with energy equal to 52.8 MeV, *i.e.* half the mass of muon. Past searches were carried out by using  $\mu^+$ -decay at rest to benefit from the simple kinematics of two-body decays. Nuclear capture on materials prevents from using negative muons.

This signature can be mimicked by radiative muon decays,  $\mu^+ \rightarrow e^+\gamma\nu_e\bar{\nu}_\mu$ , with  $e^+$  and  $\gamma$  emitted back-to-back and the two neutrinos sharing almost no energy (“correlated” background), or by accidental coincidences of a  $e^+$  from “normal” Michel decays and a high-energy  $\gamma$  due to positron interaction (annihilation or brehmsstrahlung) with surrounding materials (“accidental” background). The background rate crucially depends on detector performances; in particular, the accidental component, which is the most dangerous, approximately depends on the detector resolution on positron and photon energy, on the relative timing and on the angle between them according to the expression

$$\delta E_e \cdot (\delta E_\gamma)^2 \cdot \delta t_{e\gamma} \cdot (\delta\theta_{e\gamma})^2 \quad (1)$$

### 2.2 The first attempt

Searches for  $\mu \rightarrow e\gamma$  have a long history reaching back 1947, when a first attempt was operated by Pontecorvo without a muon beam available yet<sup>5)</sup>. So he was forced to use cosmic rays as a muon source, lead blocks as muon moderator and  $\gamma$ -converter at the same time, and Geiger-Muller counters to detect both  $\gamma$  and  $e$  tracks. The number of events collected turned out to be compatible with the background; the resulting upper limit ( $BR < 10\%$ ) was too loose if compared with more recent searches, but it used to be low enough

to safely exclude  $\mu \rightarrow e\gamma$  as the dominant branch in muon decay<sup>2</sup>.

### 2.3 Last results

During the last 25 years, the sensitivity to was raised by two order of magnitudes about. This was possible thanks to improved detection resolution of the four variables appearing on the right side of Eq.1. In tab.1, the 90% C.L. upper limits of  $\mu^+ \rightarrow e^+\gamma$  decay in past experiments are listed along with their detector performances.

Table 1: *Progress of  $\mu \rightarrow e\gamma$  search during the era of meson factories. The upper limits are at 90% C.L., while the resolution is quoted as full width at half maximum (FWHM).*

Place	Year	$\Delta E_e/E_e$	$\Delta E_\gamma/E_\gamma$	$\Delta t_{e\gamma}$	$\Delta\theta_{e\gamma}$	Upper limit
TRIUMF <sup>7)</sup>	1977	10%	8.7%	6.7 ns	—	$< 3.6 \times 10^{-9}$
SIN <sup>8)</sup>	1980	8.7%	9.3%	1.4 ns	—	$< 1.0 \times 10^{-9}$
LANL <sup>9)</sup>	1982	8.8%	8%	1.9 ns	37 mrad	$< 1.7 \times 10^{-10}$
LANL <sup>10)</sup>	1988	8%	8%	1.8 ns	87 mrad	$< 4.9 \times 10^{-11}$
LANL <sup>2)</sup>	1999	1.2%	4.5%	1.6 ns	17 mrad	$< 1.2 \times 10^{-11}$
MEG	2005	0.8%	4%	0.15 ns	19 mrad	$10^{-13}$

### 3 The future: the MEG experiment

The MEG experiment will be conducted at PSI, where the most intense DC muon beam in the world is currently available, by a joint italian-japanese-russian-swiss collaboration <sup>11)</sup>. This search for  $\mu^+ \rightarrow e^+\gamma$  aims at reaching a sensitivity of  $5 \times 10^{-14}$ , an improvement of about to orders of magnitude with respect to the current limit set by the MEGA experiment <sup>2)</sup>. This is possible thanks to unprecedented detector performances at these energies (see last row in tab.1); in particular, the resolution on photon energy and direction plays a key role in background suppression (see eq.1) and requires research and

<sup>2</sup>Just one year after, Steinberger <sup>6)</sup> measured the continuous electron spectrum, which lead to formulate the hypothesis of two neutrinos in the final state.

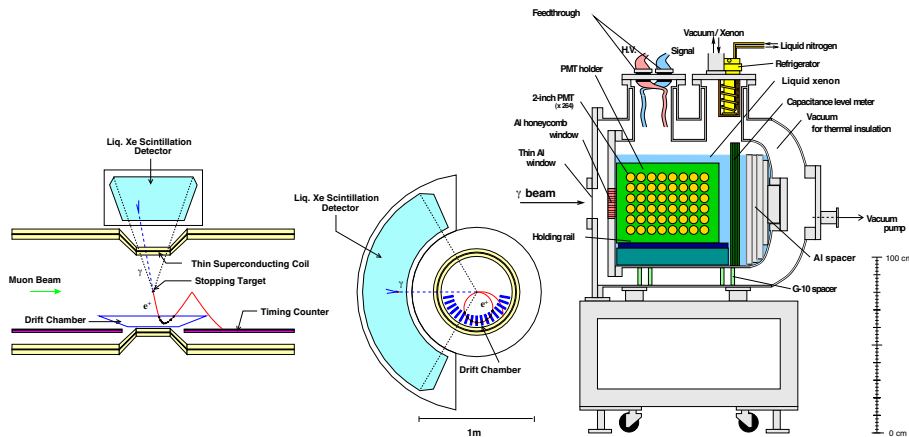


Figure 2: Left: the MEG detector layout (front and side views). Right: the liquid Xenon calorimeter prototype.

development of a new challenging detection technique, based on liquid Xenon calorimetry.

### 3.1 Detector layout

The detector set-up is shown in fig.2. The design obeys the need of minimizing the amount of material being traversed by the positron and the photon, so as to reduce their interaction with matter which might deteriorate both resolution and detection efficiencies.

#### *Beam and target*

The beam mainly consists of 28 MeV muons (“surface” muons) coming from decays at rest of charged pions produced by 590 MeV protons colliding on a Be target. The beam can reach an intensity up to  $10^{-8} \mu^+ \text{ s}^{-1}$  and is focussed on a  $\sim 5 \text{ mm}$ -wide spot and stopped on 150  $\mu\text{m}$ -thick polyethylene target. The positron contamination of the beam is of the order of 1% about.

#### *The spectrometer*

Positrons are detected by a spectrometer, combining position measurements of 17 drift chambers (DC) and timing information provided by scintillation

timing counters (TC). The magnet of the spectrometer (named COBRA, from COnstant Bending RAdius) provides a quasi-solenoidal field, with a gradient in the target region such that the bending radius is almost independent of the emission angle over a wide angular range. That gradient is also needed to sweep out high- $p_{\perp}$  positrons, which else might turn and hit the DCs many times, thereby increasing their occupancy.

The positron momentum resolution is 0.8% FWHM, provided that DC hits are reconstructed with a precision of 200  $\mu\text{m}$  for the radial coordinate and 300  $\mu\text{m}$  for the axial one. The timing resolution of TCs is  $\sim 100$  ps.

#### *The Liquid Xenon calorimeter*

A 800 l liquid Xenon calorimeter (LXe) is used to detect photons and provide precise energy, direction and timing information. The main properties of liquid Xenon are listed in tab.2. LXe has a high light yield (comparable to

Table 2: *Properties of liquid Xenon.*

Density	2.95 g/cm <sup>3</sup>
Energy deposition per scintillation photon	24 eV
Radiation length	2.77 cm
Decay-time	4.2 ns, 22 ns, 45 ns
Peak emission wavelength	175 nm
Scintillation absorption length	> 100 cm
Attenuation length (Rayleigh scattering)	$\sim 40$ cm
Refractive index	1.56

a NaI) and a fast decay time (one order of magnitude shorter than inorganic crystals), which are necessary ingredients for energy and timing resolution as tiny as required for this experiment. Moreover, LXe is transparent to its own scintillation light, which makes detector response more homogeneous than in scintillating crystals. However, the optical properties might be affected by contaminants, mostly water, able to absorb UV light in the Xe emission band. Therefore, the liquid Xenon batch needs to be purified by circulation through molecular sieves and water content must be continuously monitored during detector operation. The scintillation is collected by about 800 photomultipliers (PMT coverage  $\sim 35\%$ ), whose output provides a detailed image of the scintillation light needed to reconstruct the vertex of photon interaction as well as

to identify pile-up  $\gamma$ -rays.

### Trigger and electronics

The trigger scheme utilizes the fast signals provided by LXe and TC. These are sampled by 100 Mhz FADC and processed by FPGAs to obtain a fast event reconstruction. The expected acquisition rate is expected to be  $\sim 20 \text{ s}^{-1}$  for a nominal muon stop rate of  $10^{-8} \text{ s}^{-1}$ . Every photomultiplier in both LXe and TC and each DC cell is readout by a fast (2 Ghz sampling speed) waveform digitizer based on a custom-made chip (DOMINO), which is needed to achieve excellent timing, energy and position resolutions.

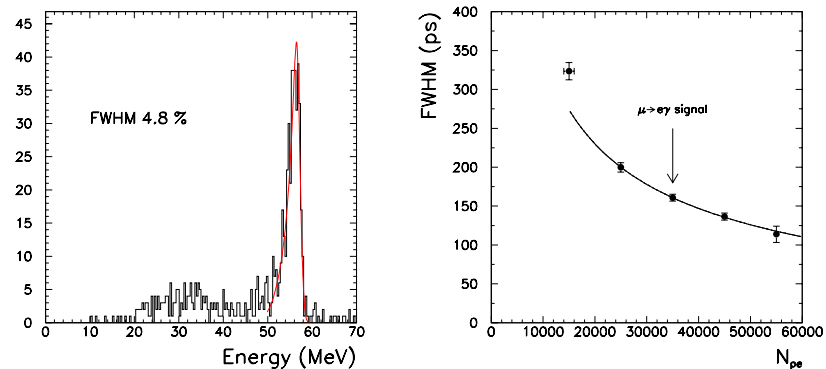


Figure 3: Performance of LXe. Left: energy resolution for 55 MeV  $\gamma$  from  $\pi^0$ -decay. Right: intrinsic timing resolution as a function of the number of collected photoelectrons. The arrow in the plot points towards the bin corresponding to the 52.8 MeV energy window.

### 3.2 The e.m. calorimeter prototype

R&D work on the photon detector has been accomplished by using a 100 l prototype, deep enough ( $\sim 18X_0$ ) to fully contain the photon e.m. shower (see fig.2). It was first used for PMT calibration and to study the main optical properties of LXe. More recently (fall 2003) it was exposed to a 55 MeV  $\gamma$ s, from decays of  $\pi^0$  from charge exchange reaction ( $\pi^-p \rightarrow \pi^0n$ ) on a liquid Hydrogen target, to test the detector behaviour under conditions similar to

$\mu \rightarrow e\gamma$  decay. The photon tagging was performed by using a NaI detector on the opposite side with respect to the  $\pi^-$  target.

The results obtained for energy and timing resolution are shown in fig.3. The energy distribution was obtained by applying simple topological cuts (distance from the photon spot centre  $< 1.5$  cm and depth  $> 3$  cm) to exclude photons interacting respectively with the sidewalls of a Lead collimator and with the front wall of the LXe prototype. The resolution turned out to 4.8% FWHM, dominated by escape effects on the low-energy tail (the right edge, which does not depend on these effects, is 1.8% wide), which is close to the experimental goal. The timing resolution was studied as a function of the energy deposit in the calorimeter and found to improve with photostatistics, as expected. The value obtained for 55 MeV photons is 160 ps, which is still higher than needed. However, the use of PMTs with higher quantum efficiency (from current 5% to 20%) will improve the timing resolution by a factor two, so as to match the experimental goal.

### References

1. R. Barbieri and J. L. Hall, Phys. Lett. **B338** (1994) 212,
2. MEGA collaboration, M.Ahmed *et al.* Phys. Rev. **D65** (2002) 112002.
3. ALEPH, DELPHI, L3 and OPAL collaboration, hep-ex/0107030.
4. J. Hisano and N. Nomura, Phys. Rev. **D59** (1999) 116005.
5. E. P. Hincks and B. Pontecorvo, Phys. Rev. **73** (1948) 246.
6. J. Steinberger, Phys. Rev. **74** (1948) 500.
7. P. Depommier *et al.*, Phys. Rev. Lett. **39** (1977) 1113.
8. A. Van der Schaaf *et al.*, Nucl. Phys. **A340** (1980) 249.
9. W.W. Kinnison *et al.*, Phys. Rev. **D25** (1982) 2846.
10. R.D. Bolton *et al.*, Phys. Rev. **D38** (1988) 2077.
11. L. M. Barkov *et al.*, "Search for  $\mu^+ \rightarrow e^+\gamma$  down to  $10^{-14}$  branching ratio" (1999);  
A. Baldini *et al.* (MEG collaboration), "The MEG experiment: search for the  $\mu^+ \rightarrow e^+\gamma$  decay at PSI" (2002).

## NEW RESULTS ON $B \rightarrow VV$ AND $PV$ MODES

M.-C. Chang \*

*Department of Physics, National Taiwan University*  
Taipei 106, Taiwan, R.O.C.

### ABSTRACT

We review the results from the  $B$  factory experiments on  $B \rightarrow VV$  and  $B \rightarrow PV$  decays. The possible CKM constraints and new physics probed by these decays will be also discussed.

### 1 Introduction

The study of charmless  $B$  decays is sensitive to the weak phases  $\alpha = \phi_2 \equiv \arg[-V_{td}V_{tb}^*/V_{ud}V_{ub}^*]$  and  $\gamma = \phi_3 \equiv \arg[-V_{ud}V_{ub}^*/V_{cd}V_{cb}^*]$  arising from the elements of the Cabibbo-Kobayashi-Maskawa (CKM) mixing matrix <sup>1)</sup>, and enables searches for phenomena beyond the standard model <sup>2)</sup>. It also plays

---

\* On behalf of Belle Collaboration

an important role in the understanding of direct  $CP$  violation in the  $B$  system by comparing the decay probabilities of two  $CP$ -conjugate processes:

$$A_{CP} \equiv \frac{\Gamma(\bar{B} \rightarrow \bar{f}) - \Gamma(B \rightarrow f)}{\Gamma(\bar{B} \rightarrow \bar{f}) + \Gamma(B \rightarrow f)}. \quad (1)$$

The charmless vector-vector ( $VV$ ) and pseudoscalar-vector ( $PV$ )  $B$  meson decays involving the vector particles -  $\phi$ ,  $\rho$ ,  $\omega$ , and  $K^*(892)$  resonances - have recently been studied at the two  $B$  factories: by the BaBar and Belle experiments. In this paper, only the new observed or measured modes are discussed.

The  $VV$  charmless  $B$  decays have very rich structure because of the presence of both  $CP$  even and  $CP$  odd final states which can provide additional information about the decay dynamics and strong phases. The strong phases could be obtained from the analysis of angular distributions <sup>3)</sup>. The decays  $B \rightarrow \phi K^*$  are expected to proceed through pure penguin diagrams ( $b \rightarrow s$  loops). The decays  $B \rightarrow \rho K^*$  are expected to be dominated by  $b \rightarrow s$  penguin transitions with additional contributions from Cabibbo-suppressed tree-level  $b \rightarrow u$  transitions, while the decays  $B \rightarrow \rho\rho$  proceed primarily through Cabibbo-favored tree-level  $b \rightarrow u$  transitions and CKM-suppressed  $b \rightarrow d$  penguins.

The decay  $B \rightarrow \phi K^*$  is sensitive to non-standard model predictions <sup>4)</sup>. In the standard model, direct  $CP$  violation could arise due to the difference between the  $b \rightarrow u$  tree and  $b \rightarrow s$  ( $b \rightarrow d$ ) penguin amplitude weak phases <sup>5)</sup>, which is  $\gamma$  ( $\alpha$ ) in the case of the decays  $B \rightarrow \rho K^*$  ( $B \rightarrow \rho\rho$ ). However, direct  $CP$  violation is difficult to observe because the strong phases are expected to be small.

The time-dependent asymmetries in  $B$  decays to  $CP$  eigenstates would provide important tests of the standard model <sup>6)</sup>. Time-dependent measurements in  $B \rightarrow \rho\rho$  modes combined with isospin relations among the decay amplitudes for these modes would provide a measurement of  $\alpha$  ( $\phi_2$ ). Angular analysis is important for time-dependent asymmetries because of the mixture of  $CP$ -odd and  $CP$ -even components, and for the isospin analysis of the decay  $B \rightarrow \rho\rho$ .

The  $PV$  charmless  $B$  decays proceed primarily through interfering  $b \rightarrow s$  penguin and  $b \rightarrow u$  tree transitions. The recent study on these decays provide the information on the understanding of direct  $CP$  violation and the interfer-

ence of decay amplitudes with differing weak and strong phases. The decays  $B \rightarrow \rho\pi$  can be used to measure  $\alpha(\phi_2)$ . However, a model independent extraction of  $\alpha(\phi_2)$  from time-dependent  $CP$ -asymmetry measurements requires an isospin analysis of the decay rates of all the  $\rho\pi$  decay modes<sup>7)</sup>. The decays  $B^+ \rightarrow \rho^0\pi^+$  and  $B^0 \rightarrow \rho^\pm\pi^\mp$  have already been measured<sup>8)</sup>, motivating the study of the remaining two decays  $B^0 \rightarrow \rho^0\pi^0$  and  $B^+ \rightarrow \rho^+\pi^0$ .

For the decays  $B \rightarrow \pi^\mp\pi^0h^\pm$  ( $h = K$  or  $\pi$ ), a large fraction of the decays proceed through intermediate two-body decay processes, such as  $B^+ \rightarrow K^*(892)^0\pi^+$ ,  $K^*(892)^0 \rightarrow K^+\pi^-$ . However, higher mass  $K^+\pi^-$  and  $\pi^+\pi^-$  states may contribute but are not clearly identified due to limited statistics. The quasi-two-body decays in the  $K^+\pi^-\pi^0$  final state are considered to include three  $PV$  modes:  $K^*(892)^0\pi^0$ ,  $K^*(892)^+\pi^-$ , and  $\rho(770)^-K^+$ . It is important to uncover the quasi-two-body decay  $K^*(892)\pi$  and  $\rho(770)^-K^+$  which are sensitive to  $\gamma(\phi_3)$ .

## 2 The BaBar and Belle Experiments

Both BaBar and Belle experiments are based on  $\Upsilon(4S) \rightarrow B\bar{B}$  decays. The data samples are collected with the detector at the asymmetric-energy  $e^+e^-$  collider. The detector and the collider located at SLAC are BaBar<sup>9)</sup> and PEP-II<sup>10)</sup>; located at KEK are Belle<sup>11)</sup> and KEKB<sup>12)</sup>.

## 3 Event Selection

The data used in these analyses were accumulated with the BaBar and Belle detector. The corresponding dataset will be included in the result table. The event selection is summarized in Table 1. The charged tracks are required to come from the collision point. Looser criteria are applied to tracks belonging to  $K_S^0 \rightarrow \pi^+\pi^-$ .

$B$  candidates are selected using two kinematic variables. The used name in BaBar and Belle may different, but the meaning is the same. They are beam-energy-substituted mass  $m_{ES} = \sqrt{s/4 - \mathbf{p}_B^{*2}}$  (BaBar) which is equal to the  $M_{bc} = \sqrt{E_{\text{beam}}^{*2} - \mathbf{p}_B^{*2}}$  (Belle) and the energy difference  $\Delta E = E_B^* - \sqrt{s}/2$  (BaBar) which is equal to  $\Delta E = E_B^* - E_{\text{beam}}^*$  (Belle). The  $s$  is the square of the invariant mass of the electron-positron system,  $E_{\text{beam}}^*$  is the beam energy in the center-of-mass frame, and  $\mathbf{p}_B^*$  and  $E_B^*$  are the momentum and energy of the

Table 1: *Hadronic events are selected based on track multiplicity and event topology. We fully reconstruct  $B$  meson candidates from their charged and neutral decay products including the intermediate states, where inclusion of the charge conjugate states is implied.*

Reconstructed decay	with
$\phi \rightarrow K^+K^-$	$\pi^0 \rightarrow \gamma\gamma$
$K^{*0} \rightarrow K^+\pi^-$	$K^0 \rightarrow K_S^0 \rightarrow \pi^+\pi^-$
$K^{*0} \rightarrow K^0\pi^0$	
$K^{*+} \rightarrow K^+\pi^0$	
$K^{*+} \rightarrow K^0\pi^+$	
$\rho^0 \rightarrow \pi^+\pi^-$	
$\rho^+ \rightarrow \pi^+\pi^0$	
$\omega \rightarrow \pi^+\pi^-\pi^0$	

reconstructed  $B$  candidate in the  $\Upsilon(4S)$  frame. For signal events  $m_{\text{ES}}(M_{bc})$  peaks at the  $B$  mass and  $\Delta E$  at zero. In most of the case, our initial selection requires  $m_{\text{ES}}(M_{bc}) > 5.2 \text{ GeV}/c^2$  and  $|\Delta E| < 0.2 \text{ GeV}$ .

## 4 Source of Background and Suppression Techniques

### 4.1 QCD Continuum Background

Charmless hadronic modes suffer from a large background due to random combinations of tracks produced in quark-antiquark continuum events ( $e^+e^- \rightarrow q\bar{q}, q = u, d, s, c$ ). Background events from the continuum are distinguished by a jet-like structure as opposed to the more spherical topology of  $B\bar{B}$  pairs produced in  $\Upsilon(4S)$  events.

Several event-shape variables are designed to take advantage of this difference. Usually, we use the Fisher discriminant  $\mathcal{F}$ , which is subsequently used as a discriminating variable. The variables entering the Fisher discriminant vary in different studies (13, 14, 15, 16, 17). In Belle, we usually use a likelihood ratio method to reduce the continuum background. In BaBar, a neural network (NN) method is used. The final sample of signal candidates are selected with a cut on the Likelihood ratio or NN optimized output.

## 4.2 $B\bar{B}$ Backgrounds

Most charmless hadronic  $B$  decay analysis do not have much background from other  $B$  decays. We have found, however, that some of the signal modes do suffer from backgrounds from charmless hadronic decay modes. When we find an indication of a high selection rate for a particular background decay mode (by MC), we use the experimentally measured (when available) or theoretically predicted branching fraction of that mode to determine its expected contribution. Fits to simulated experiments are used to evaluate whether such events cause a significant bias to the measured signal yield.

## 5 Physics Results

We use a maximum-likelihood (ML) fit <sup>17)</sup> to extract signal yields, asymmetries, and angular polarizations simultaneously. In BaBar, the signal yields are from the ML fit. In Belle, the signal yields are mainly from the 1D fit on  $\Delta E$  and sometimes from the 2D fit on  $M_{bc}-\Delta E$  scatter plot.

### 5.1 $B \rightarrow VV$ modes

- Updated Measurement of polarization and  $CP$ -violating terms in a full angular analysis of  $B \rightarrow \phi K^{*0}$  at BaBar: The branching fractions ( $\mathcal{B}$ ),  $CP$  asymmetries ( $A_{CP}$ ), and polarization of  $B \rightarrow \phi K^*$  decay modes have been measured <sup>18)</sup>. New released result from BaBar is a preliminary updated polarization study (full polarization study) <sup>19)</sup>. The longitudinal polarization in this decay is found to be surprising for which confirms earlier measurements and is still not understood theoretically.
- Updated Measurement of the polarization for the decay  $B \rightarrow \rho^+\rho^-$  at BaBar: Based on the recently observed <sup>20)</sup> decay  $B^0 \rightarrow \rho^+\rho^-$ , we continue to measure the longitudinal polarization <sup>21)</sup>. The result shows the longitudinal polarization very close to 1 which is the same as the previous observed <sup>22, 23)</sup> in the decays  $B^0 \rightarrow \rho^+\rho^0$  and  $B \rightarrow \rho^0 K^{*+}$ .

### 5.2 $B \rightarrow PV$ modes

- Updated Measurement of branching fraction and  $CP$ -violating asymmetry of the decay  $B \rightarrow \rho^+\pi^0$  at Belle: The branching fractions and  $CP$

Table 2: Updated  $B \rightarrow VV$  modes

BaBar Experiment				
Mode	$\mathcal{B} (\times 10^{-6})$	$f_L$	$A_{CP}$	$\mathcal{L} (\text{fb}^{-1})$
$\phi K^{*+}$	$12.7^{+2.2}_{-2.0} \pm 1.1$	$0.46 \pm 0.12 \pm 0.03$	$+0.16 \pm 0.17 \pm 0.03$	82
$\phi K^{*0}$	$11.2 \pm 1.3 \pm 0.8$	$0.65 \pm 0.07 \pm 0.02$	$+0.04 \pm 0.12 \pm 0.02$	82
$\phi K^0$	-	$0.52 \pm 0.07 \pm 0.02$	$-0.12 \pm 0.10 \pm 0.03$	110
$\rho^0 K^{*+}$	$10.6^{+3.0}_{-2.6} \pm 2.4$	$0.96^{+0.04}_{-0.15} \pm 0.04$	$+0.20^{+0.32}_{-0.29} \pm 0.04$	82
$\rho^0 \rho^+$	$22.5^{+5.7}_{-5.4} \pm 5.8$	$0.97^{+0.03}_{-0.07} \pm 0.04$	$-0.19 \pm 0.23 \pm 0.03$	82
$\rho^+ \rho^-$	$33 \pm 4 \pm 5$	$0.99 \pm 0.03^{+0.04}_{-0.03}$	-	82
$\rho^0 \rho^0$	$< 2.1$	-	-	82
Belle Experiment				
Mode	$\mathcal{B} (\times 10^{-6})$	$f_L$	$A_{CP}$	$\mathcal{L} (\text{fb}^{-1})$
$\phi K^{*+}$	$6.7^{+2.1+0.7}_{-1.9-1.0}$	-	$-0.13 \pm 0.29^{+0.08}_{-0.11}$	78
$\phi K^{*0}$	$10.0^{+1.6+0.7}_{-1.5-0.8}$	$0.43 \pm 0.09 \pm 0.04$	$+0.07 \pm 0.15^{+0.05}_{-0.03}$	78
$\rho^0 \rho^+$	$31.7 \pm 7.1^{+3.8}_{-6.7}$	$0.95 \pm 0.11 \pm 0.02$	$+0.00 \pm 0.22 \pm 0.03$	78

Table 3: Updated  $B \rightarrow PV$  modes

BaBar Experiment			
Mode	$\mathcal{B} (\times 10^{-6})$	$A_{CP}$	$\mathcal{L} (\text{fb}^{-1})$
$\phi K^+$	$10.0^{+0.9}_{-0.8} \pm 0.5$	$0.04 \pm 0.09 \pm 0.01$	82
$\phi K^0$	$8.4^{+1.5}_{-1.3} \pm 0.5$	-	82
$\phi \pi^+$	$< 0.4$	-	82
$\phi \pi^0$	$< 1.0$	-	82
$\omega K^+$	$4.8 \pm 0.8 \pm 0.4$	$-0.09 \pm 0.17 \pm 0.01$	82
$\omega K^0$	$5.9^{+1.6}_{-1.3} \pm 0.5$	-	82
$\omega \pi^+$	$5.5 \pm 0.9 \pm 0.5$	$+0.03 \pm 0.16 \pm 0.01$	82
$\omega \pi^0$	$< 1.2$	-	82
$\rho^+ \pi^-$	$22.6 \pm 1.8 \pm 2.2$	$-0.18 \pm 0.08 \pm 0.03$	82
$\rho^+ \pi^0$	$10.9 \pm 1.9 \pm 1.9$	$+0.24 \pm 0.16 \pm 0.06$	82
$\rho^0 \pi^+$	$9.5 \pm 1.1 \pm 0.8$	$-0.19 \pm 0.11 \pm 0.02$	82
$\rho^0 \pi^0$	$< 2.9$	-	82
$\rho^+ K^-$	$7.3^{+1.3}_{-1.2} \pm 1.3$	$0.28 \pm 0.17 \pm 0.08$	82
Belle Experiment			
Mode	$\mathcal{B} (\times 10^{-6})$	$A_{CP}$	$\mathcal{L} (\text{fb}^{-1})$
$\phi K^+$	$9.4 \pm 1.1 \pm 0.7$	$0.01 \pm 0.12 \pm 0.05$	78
$\phi K^0$	$9.0^{+2.2}_{-1.8} \pm 0.7$	-	78
$\omega K^+$	$6.5^{+1.3}_{-1.2} \pm 0.6$	$+0.06^{+0.21}_{-0.18} \pm 0.01$	78
$\omega K^0$	$4.0^{+1.9}_{-1.6} \pm 0.5(\text{evidence})$	-	78
$\omega \pi^+$	$5.7^{+1.4}_{-1.3} \pm 0.6$	$+0.50^{+0.23}_{-0.20} \pm 0.02$	78
$\omega \pi^0$	$< 1.9$	-	78
$\rho^+ \pi^0$	$13.2 \pm 2.3^{+1.4}_{-1.9}$	$+0.06 \pm 0.19^{+0.04}_{-0.06}$	140
$\rho^0 \pi^0$	$5.1 \pm 1.6 \pm 0.9(\text{evidence})$	-	140
$\rho^+ K^-$	$15.1^{+3.4+2.4}_{-3.3-2.6}$	$0.22^{+0.22+0.06}_{-0.23-0.02}$	78
$K^{*+} \pi^-$	$14.8^{+4.6+2.8}_{-4.4-1.3}$	-	78
$K^{*0} \pi^0$	$< 3.5$	-	78

timing counters (TC). The magnet of the spectrometer (named COBRA, from COnstant Bending RAdius) provides a quasi-solenoidal field, with a gradient in the target region such that the bending radius is almost independent of the emission angle over a wide angular range. That gradient is also needed to sweep out high- $p_{\perp}$  positrons, which else might turn and hit the DCs many times, thereby increasing their occupancy.

The positron momentum resolution is 0.8% FWHM, provided that DC hits are reconstructed with a precision of 200  $\mu\text{m}$  for the radial coordinate and 300  $\mu\text{m}$  for the axial one. The timing resolution of *TCs* is  $\sim 100$  ps.

#### *The Liquid Xenon calorimeter*

A 800 l liquid Xenon calorimeter (LXe) is used to detect photons and provide precise energy, direction and timing information. The main properties of liquid Xenon are listed in tab.2. LXe has a high light yield (comparable to

Table 2: *Properties of liquid Xenon.*

Density	2.95 g/cm <sup>3</sup>
Energy deposition per scintillation photon	24 eV
Radiation length	2.77 cm
Decay-time	4.2 ns, 22 ns, 45 ns
Peak emission wavelength	175 nm
Scintillation absorption length	> 100 cm
Attenuation length (Rayleigh scattering)	$\sim 40$ cm
Refractive index	1.56

a NaI) and a fast decay time (one order of magnitude shorter than inorganic crystals), which are necessary ingredients for energy and timing resolution as tiny as required for this experiment. Moreover, LXe is transparent to its own scintillation light, which makes detector response more homogeneous than in scintillating crystals. However, the optical properties might be affected by contaminants, mostly water, able to absorb UV light in the Xe emission band. Therefore, the liquid Xenon batch needs to be purified by circulation through molecular sieves and water content must be continuously monitored during detector operation. The scintillation is collected by about 800 photomultipliers (PMT coverage  $\sim 35\%$ ), whose output provides a detailed image of the scintillation light needed to reconstruct the vertex of photon interaction as well as

This is another question to the theoretical predictions. The inconsistent results of the  $B^0 \rightarrow \rho^+ K^-$  indicate the difficult part on the Dalitz analysis.

### References

1. M. Kobayashi and T. Maskawa, *Prog. Theor. Phys.* **49**, 652 (1973).
2. Y. Grossman, M.P. Worah, *Phys. Lett. B* **395**, 241 (1997); D. London, A. Soni, *Phys. Lett. B* **407**, 61 (1997).
3. G. Kramer, W.F. Palmer, *Phys. Rev. D* **45**, 193 (1992); R. Aleksan *et al.*, *Phys. Lett. B* **356**, 95 (1995); C.-H. Chen, Y.-Y. Keum, H.-N. Li, *Phys. Rev. D* **66**, 054013 (2002).
4. I. Hinchliffe, N. Kersting, *Phys. Rev. D* **63**, 015003 (2001).
5. M. Bander, D. Silverman, and A. Soni, *Phys. Rev. Lett.* **43**, 242 (1979).
6. A.B. Carter and A.I. Sanda, *Phys. Rev. D* **23**, 1567 (1981); I.I. Bigi and A.I. Sanda, *Nucl. Phys. B* **193**, 85 (1981).
7. H. J. Lipkin, Y. Nir, H. R. Quinn, A. Snyder, *Phys. Rev. D* **44**, 1454 (1991); A. E. Snyder, H. R. Quinn, *Phys. Rev. D* **48**, 2139 (1993).
8. A. Gordon, Y. Chao *et al.* (Belle Collaboration), *Phys. Lett. B* **542**, 183 (2002).
9. B. Aubert *et al.* (BaBar Collaboration), *Nucl. Instrum. and Meth. A* **479**, 1 (2002).
10. PEP-II Conceptual Design Report, SLAC-R-418 (1993).
11. A. Abashian *et al.* (Belle Collaboration), *Nucl. Instrum. and Meth. A* **479**, 117 (2002).
12. S. Kurokawa and E. Kikutani, *Nucl. Instrum. and Meth. A* **499**, 1 (2003), and other papers included in this Volume.
13. The Fox-Wolfram moments were introduced in G. Fox and S. Wolfram, *Phys. Rev. Lett.* **41**, 1581 (1978). The modified Fox-Wolfram moments were described in K. Abe *et al.* (Belle Collaboration), *Phys. Lett. B* **511**, 151 (2001).

14. R. Ammar *et al.* (CLEO Collaboration), Phys. Rev. Lett. **71**, 674 (1993).
15. K. Abe *et al.* (Belle Collaboration), Phys. Rev., Lett. **87** 091802 (2001);  
K. Abe *et al.* (Belle Collaboration), Phys. Rev., D **66** 071102 (2002);  
H. Kakuno *et al.* (Belle Collaboration), hep-ex/0403022, submitted to Nucl.  
Instr. Meth. A.
16. D.M. Asner *et al.* (CLEO Collaboration), Phys. Rev. D **53**, 1039 (1996).
17. B. Aubert *et al.* (BaBar Collaboration), Phys. Rev., Lett. **87** 151801 (2001);  
B. Aubert *et al.* (BaBar Collaboration), Phys. Rev., D **65** 051101 (2002).
18. K.-F. Chen, A. Bozek, *et al.* (Belle Collaboration), Phys. Rev., Lett. **91**  
201801 (2003); B. Aubert *et al.* (BaBar Collaboration), Phys. Rev., Lett.  
**91** 171802 (2003).
19. J.G. Smith (representing the BaBar Collaboration), Moriond QCD pro-  
ceedings, hep-ex/0406063.
20. B. Aubert *et al.* (BaBar Collaboration), Phys. Rev., D **69** 031102 (2004).
21. B. Aubert *et al.* (BaBar Collaboration), hep-ex/0404029.
22. J. Zhang, M. Nakao, *et al.* (Belle Collaboration), Phys. Rev. Lett. **91**,  
221801 (2003); B. Aubert *et al.* (BaBar Collaboration), Phys. Rev., Lett.  
**91** 171802 (2003).
23. B. Aubert *et al.* (BaBar Collaboration), Phys. Rev., Lett. **91** 171802 (2003).
24. J. Zhang *et al.* (Belle Collaboration), hep-ex/0406006, submitted to Phys.  
Rev. Lett.
25. B. Aubert *et al.* (BaBar Collaboration), hep-ex/0311049, submitted to  
Phys. Rev. Lett.
26. J. Dragic *et al.* (Belle Collaboration), hep-ex/0405068, submitted to Phys.  
Rev. Lett.
27. C.-W. Chiang, M. Gronau, Z. Luo, J.L. Rosner and D.A. Suprun, Phys.  
Rev. D **69**, 034001 (2004); M. Beneke and M. Neubert, Nucl. Phys. B **675**,  
333 (2003).

- 
28. B. Aubert *et al.* (BaBar Collaboration), hep-ex/0311049, submitted to Phys. Rev. Lett.
  29. B. Aubert *et al.* (BaBar Collaboration), hep-ex/0403025.
  30. C.-H. Wang *et al.* (Belle Collaboration), hep-ex/0403033, submitted to Phys. Rev. D.
  31. B. Aubert *et al.* (BaBar Collaboration), Phys. Rev. Lett. **92**, 061801 (2004);  
B. Aubert *et al.* (BaBar Collaboration), hep-ex/0403025.
  32. P. Chang *et al.* (Belle Collaboration), hep-ex/0406075, submitted to Phys. Lett. B.
  33. E. Eckhart *et al.* (CLEO Collaboration), Phys. Rev. Lett. **89**, 251801 (2002).
  34. B. Aubert *et al.* (BaBar Collaboration), Phys. Rev. Lett. **91**, 201802 (2003).



## RARE B DECAYS

Paul D. Jackson

*Department of Physics and Astronomy, University of Victoria, BC, Canada.*

### ABSTRACT

Recent results from Belle and BaBar on rare  $B$  decays involving flavour-changing neutral currents or purely leptonic final states are presented. Measurements of the CP asymmetries in  $B \rightarrow K^* \gamma$  and  $b \rightarrow s \gamma$  are reported. Also reported are updated limits on  $B^+ \rightarrow K^+ \nu \bar{\nu}$ ,  $B^+ \rightarrow \tau^+ \nu$ ,  $B^+ \rightarrow \mu^+ \nu$  and the recent measurement of  $B \rightarrow X_s \ell^+ \ell^-$ .

### 1 Introduction

The study of radiative and leptonic rare  $B$  decays represents a very attractive field in the search for discrepancies with respect to the theoretical predictions of the Standard Model (SM). Many extensions to the Standard Model predict visible effects in these decays whose measurements allow constraints to be placed on new physics, or indeed, the potential to discover such phenomena. The BaBar <sup>1)</sup> and Belle <sup>2)</sup> collaborations are exploiting the unprecedented

luminosities provided by the PEP-II and KEK-B facilities to perform an extensive and detailed series of studies of these decay channels. Samples on the order of  $200 \times 10^6$   $\Upsilon(4S) \rightarrow B\bar{B}$  decays have been recorded by the two collaborations. The paper will summarise experimental results based on a subset of these datasets.

## 2 Electroweak penguin decays

In the SM, the amplitudes which contribute to the  $b \rightarrow s\ell^+\ell^-$  and the  $b \rightarrow s\nu\bar{\nu}$  decays at leading order are the  $W^+W^-$  box diagram, the  $Z^0$  penguin diagram and, for the charged lepton decay, the photonic penguin diagram. An important consequence of the loop structure of these decays is that their branching fractions and their kinematic variables, such as the transferred momentum squared or the virtual  $\gamma$  or  $Z$  ( $q^2 = M(\ell^+\ell^-)^2$ ) and the forward-backward asymmetry of the lepton decay angle ( $A_{FB}$ ) in the  $b \rightarrow s\ell^+\ell^-$  decays, can be significantly affected by the presence of new particles or couplings predicted in non-standard scenarios.

### 2.1 $B \rightarrow X_s\ell^+\ell^-$

The BaBar collaboration finalised measurements of branching fractions of the exclusive processes  $B \rightarrow K\ell^+\ell^-$  and  $B \rightarrow K^*\ell^+\ell^-$  <sup>3)</sup> using  $113\text{fb}^{-1}$  of data. A preliminary measurement of the inclusive branching fraction  $B \rightarrow X_s\ell^+\ell^-$  using a sum over exclusive modes in which  $X_s$  system is composed of one charged kaon and one or more charged and/or neutral pions <sup>4)</sup> yielding:

$$B(B \rightarrow X_s\ell^+\ell^-) = (6.3 \pm 1.6_{-2.5}^{+1.8}) \times 10^{-6}. \quad (1)$$

All of these results are consistent with the SM theoretical predictions.

### 2.2 $B^+ \rightarrow K^+\nu\bar{\nu}$

The  $B^+ \rightarrow K^+\nu\bar{\nu}$  measurement is experimentally challenging due to the presence of two unobserved neutrinos in the final state. BaBar has performed a search for this decay using  $88 \times 10^6$   $B\bar{B}$  pairs using two techniques: Where one  $B$  in the event is reconstructed hadronically,  $B^- \rightarrow D^0 X_{\text{had}}$ , or where the  $B$  is reconstructed semileptonically,  $B^- \rightarrow D^0\ell^-\bar{\nu}X$ . The system recoiling against this reconstructed meson is considered for consistency with the  $B^+ \rightarrow K^+\nu\bar{\nu}$  signal. Candidate events are required to contain one charged kaon with CM momentum greater than  $1.5\text{ GeV}/c$  and less than  $250\text{ MeV}$  of additional neutral energy,  $E_{\text{extra}}$ , measured in the calorimeter.

Combining the two statistically independent analyses yields an upper limit on the branching fraction at the 90% confidence level of:

$$B(B^+ \rightarrow K^+ \nu \bar{\nu}) < 7.0 \times 10^{-5}, \quad (2)$$

which represents the best upper limit on this channel. This analysis is similar to that discussed in section 5.1.

### 3 Radiative $B$ decays

Radiative decays, such as  $b \rightarrow s\gamma$ , proceed at leading order in the SM through one loop penguin diagrams. The new fields predicted by many extensions to the SM can contribute with additional amplitudes to this process appearing as virtual particles in the penguin loop diagrams. A comparison of the measured inclusive branching ratio (world average  $B(B \rightarrow X_s \gamma) = 3.3 \times 10^{-4}$  <sup>5)</sup>) with respect to the SM theoretical predictions ( $(3.6 \pm 0.3) \times 10^{-4}$  <sup>6, 7)</sup>) has already provided some constraint on the new physics beyond the SM <sup>8)</sup>.

#### 3.1 $b \rightarrow s\gamma$

Using a sample of  $152 \times 10^6$   $B\bar{B}$  decays Belle recently measured the  $b \rightarrow s\gamma$  branching fraction using a fully-inclusive approach. A detailed description of the analysis can be found elsewhere. In this analysis the  $b \rightarrow s\gamma$  signal spectrum was extracted by collecting all high-energy photons, vetoing those from  $\pi^0$  and  $\eta$  decays to two photons. The contribution from continuum events was subtracted using the off-resonance data sample. The remaining backgrounds from  $B\bar{B}$  events are subtracted using Monte Carlo (MC) distributions scaled by data control samples. After subtracting the backgrounds the photon energy spectrum is corrected for the signal selection efficiency function obtained from signal MC after applying the correction determined by data control samples.

The efficiency-corrected spectrum is shown as a function of CM photon energy in Figure 1. The two error bars for each point show the statistical and the total error, including the systematic error which is correlated among the points. As expected, the spectrum above the 3 GeV endpoint for decays of  $B$  mesons from the  $\Upsilon(4S)$  is consistent with zero. Integrating this spectrum from 1.8 to 2.8 GeV a partial branching fraction is obtained of  $B(b \rightarrow s\gamma) = (3.59 \pm 0.32_{-0.31}^{+0.30} \pm 0.11_{-0.07}^{+0.11}) \times 10^{-4}$ , where the errors are statistical, systematic and theoretical respectively. This result is in good agreement with the latest theoretical calculations <sup>9)</sup>. The moments of the distribution are also measured yielding  $\langle E_\gamma \rangle = 2.289 \pm 0.026 \pm 0.034$  GeV and  $\langle E_\gamma^2 \rangle - \langle E_\gamma \rangle^2 = 0.0311 \pm 0.0073 \pm$

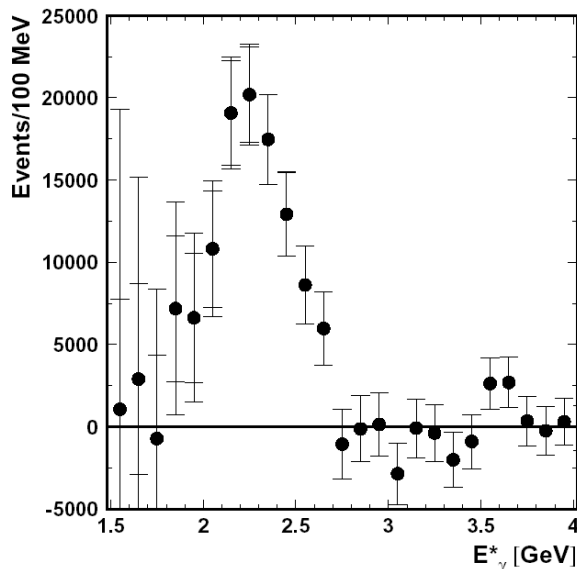


Figure 1: *Efficiency-corrected photon energy spectrum. The two error bars show the statistical and total errors.*

$0.0063 \text{ GeV}^2$  for  $E_\gamma^* > 1.8 \text{ GeV}$ , where the errors are statistical and systematic respectively.

### 3.2 $b \rightarrow d\gamma$

The  $b \rightarrow d\gamma$  process is suppressed with respect to  $b \rightarrow s\gamma$  by the Cabibbo-Kobayashi-Maskawa (CKM) factor  $|V_{td}/V_{ts}|^2$  with a large uncertainty due to the lack of precise knowledge on  $V_{td}$ .

In the analysis performed by the Belle collaboration (using the same sample as the  $b \rightarrow s\gamma$  analysis reported in the previous section) the exclusive reconstruction of the decays  $B^+ \rightarrow \rho^+\gamma$ ,  $B^0 \rightarrow \rho^0\gamma$  and  $B \rightarrow \omega\gamma$  is performed.  $B^+ \rightarrow K^{*+}\gamma$  and  $B^0 \rightarrow K^{*0}\gamma$  are reconstructed as control samples. The following decay chains are used to reconstruct the intermediate states:  $\rho^+ \rightarrow \pi^+\pi^0$ ,  $\rho^0 \rightarrow \pi^+\pi^-$ ,  $\omega \rightarrow \pi^+\pi^-\pi^0$ ,  $K^{*+} \rightarrow K^+\pi^0$ ,  $K^{*0} \rightarrow K^+\pi^-$  and  $\pi^0 \rightarrow \gamma\gamma$ . In each event a photon with the largest energy in the range  $1.8 \text{ GeV} < E_\gamma < 3.4 \text{ GeV}$  is selected in the  $e^+e^-$  center-of-mass frame (CM). Vetoes are applied to suppress backgrounds from  $\pi^0$  and  $\eta$  decays to pairs of photons.  $B$  candidates are formed by combining a  $\rho$  or  $\omega$  candidate and the primary photon using two variables: the beam-energy constrained mass  $M_{bc} = \sqrt{(E_{\text{beam}}^*/c^2)^2 - |p_B^*/c|^2}$  and the energy difference  $\Delta E = E_B^* - E_{\text{beam}}^*$ , where

$p_B^*$  and  $E_B^*$  are the measured CM momentum and energy, respectively, of the  $B$  candidate, and  $E_{\text{beam}}^*$  is the CM beam energy. The photon energy is replaced by  $E_{\text{beam}}^* - E_{\rho/\omega}^*$  if the momentum  $p_B^*$  is calculated. The signal region is defined as  $-0.1 \text{ GeV} < \Delta E < 0.08 \text{ GeV}$  and  $5.273 \text{ GeV}/c^2 < M_{bc} < 5.285 \text{ GeV}/c^2$ .

There are two major sources of background from  $B$  decays:  $B \rightarrow K^*\gamma$  and  $B \rightarrow \rho/\omega\pi^0$ . To suppress  $B \rightarrow K^*\gamma$ , we calculate  $M_{K\pi}$ , where the kaon mass is assigned to one of the pion candidates, and reject the candidate if  $M_{K\pi} < 0.96(0.92) \text{ GeV}/c^2$  for the  $\rho^0\gamma(\rho^+\gamma)$  mode. To reject  $B \rightarrow \rho/\omega\pi^0$ , a helicity angle cut is applied such that  $|\cos \theta_{\text{hel}}| > 0.8(0.6)$  for  $\rho^0\gamma$  and  $\omega\gamma(\rho^+\gamma)$  modes. Here,  $\theta_{\text{hel}}$  is the angle between the  $\pi^+$  and  $B$  momentum vectors in the  $\rho$  rest frame or between the normal to the  $\omega$  decay plane and the  $B$  momentum vector in the  $\omega$  rest frame.

The background from continuum  $e^+e^- \rightarrow q\bar{q}(q = u, d, s, c)$  events is rejected using event topology information. A Fisher<sup>10)</sup> discriminant is constructed from 16 modified Fox-Wolfram<sup>11)</sup> moments and the scalar sum of transverse momenta. The decay vertex of the candidate  $B$  meson is also used along with the origin of the remaining tracks in the event. The difference between these vertices along the  $z$ -axis discriminates continuum events that have a common decay vertex and signal events whose decay vertices are displaced in the laboratory frame.

To obtain the signal yield an unbinned maximum likelihood fit to  $M_{bc}$  and  $\Delta E$  is performed. The fit is performed simultaneously to three signal modes ( $B \rightarrow (\rho, \omega)\gamma$ ) plus the two  $B \rightarrow K^*\gamma$  modes assuming isospin relations  $B(B \rightarrow (\rho, \omega)\gamma) \equiv B(B^+ \rightarrow \rho^+\gamma) = 2\frac{\tau_{B^+}}{\tau_{B^0}}B(B^0 \rightarrow \rho^0\gamma) = 2\frac{\tau_{B^+}}{\tau_{B^0}}B(B \rightarrow \omega\gamma)$  and  $(B^+ \rightarrow K^{*+}\gamma) = 2\frac{\tau_{B^+}}{\tau_{B^0}}B(B^0 \rightarrow K^{*0}\gamma)$ , where  $\frac{\tau_{B^+}}{\tau_{B^0}} = 1.083 \pm 0.017$ <sup>5)</sup> is used. The five branching fractions, five background normalizations and five background  $\Delta E$  slopes are floated in the fit.

Preliminary results of the simultaneous fit are shown in Table 1. The simultaneous fit gives a significance of  $3.5\sigma$ , where significance is defined as  $\sqrt{-2\ln(L_0/L_{\text{max}})}$ ,  $L_{\text{max}}$  is the maximum likelihood in the  $M_{bc}$  fit, and  $L_0$  is the likelihood of the best fit when the signal yield is constrained to be zero.

#### 4 CP violation in radiative $B$ decays

The measurement of CP violation can shed new light on the structure of this flavor-changing neutral-current both testing the SM predictive powers and constraining the parameter space of SM extensions. Time-dependent CP asymmetries in radiative penguin decays have been covered elsewhere<sup>12)</sup> and are not discussed here due to lack of space.

Table 1: *Results of the efficiency, signal yield, significance and branching fraction from simultaneous and individual fits. All numbers are preliminary.*

Mode	efficiency ( $\pm$ syst.)	signal yield ( $\pm$ stat., $\pm$ syst.)	significance	branching fraction ( $\pm$ stat., $\pm$ syst.) $\times 10^6$
$B^+ \rightarrow \rho^+\gamma$	$(5.6 \pm 0.4)\%$	$15.5^{+7.1}_{-6.3} \pm 1.5$	2.5	$(1.8^{+0.8}_{-0.7} \pm 0.1)$
$B^0 \rightarrow \rho^0\gamma$	$(5.0 \pm 0.3)\%$	$3.6^{+3.6}_{-2.8} +0.7_{-0.9}$	1.2	$(0.5^{+0.5}_{-0.4} \pm 0.2)$
$B \rightarrow \omega\gamma$	$(4.7 \pm 0.5)\%$	$8.9^{+4.8}_{-4.0} \pm 1.2$	2.3	$(1.3^{+0.7}_{-0.6} \pm 0.2)$
$B \rightarrow (\rho, \omega)\gamma$	–	–	3.5	$(1.8^{+0.6}_{-0.5} \pm 0.1)$

#### 4.1 Direct CP violation in $\bar{B} \rightarrow X_s\gamma$ decays

In the SM the CP violation in the inclusive process  $\bar{B} \rightarrow X_s\gamma$  can be reliably predicted<sup>9)</sup>:

$$A_{\text{CP}} = \frac{\Gamma(\bar{B} \rightarrow X_s\gamma) - \Gamma(B \rightarrow X_{\bar{s}}\gamma)}{\Gamma(\bar{B} \rightarrow X_s\gamma) + \Gamma(B \rightarrow X_{\bar{s}}\gamma)} = 0.0044^{+0.0024}_{-0.0014} \quad (3)$$

whereas in some supersymmetric scenarios sizable asymmetries ( $A_{\text{CP}} \sim 10\%$ ) are possible and natural.<sup>13)</sup>

BaBar has studied this<sup>14)</sup> using a sample of  $(88.9 \pm 1.0) \times 10^6$   $B\bar{B}$  pairs. The  $\bar{B} \rightarrow X_s\gamma$  sample is obtained by combining twelve fully reconstructed self-tagging decay channels:

$$B^- \rightarrow K^- \pi^0 \gamma, K^- \pi^+ \pi^- \gamma, K^- \pi^0 \pi^0 \gamma, K^- \pi^+ \pi^- \pi^0 \gamma \text{ and} \\ \bar{B}^0 \rightarrow K^- \pi^+ \gamma, K^- \pi^+ \pi^0 \gamma, K^- \pi^+ \pi^0 \pi^0 \gamma, K^- \pi^+ \pi^+ \pi^- \gamma \text{ and} \\ B^- \rightarrow K_s^0 \pi^- \gamma, K_s^0 \pi^- \pi^0 \gamma, K_s^0 \pi^- \pi^0 \pi^0 \gamma, K_s^0 \pi^- \pi^+ \pi^- \gamma.$$

Their charge conjugates are used to obtain the  $B \rightarrow X_{\bar{s}}\gamma$  sample. Fully reconstructed  $B \rightarrow X_{\bar{s}}\gamma$  decays are characterized by two kinematic variable  $m_{ES}$  (which is analogous to  $M_{bc}$  defined in an earlier section) and  $\Delta E$ . The positive identification of charged kaons removes any contribution of  $b \rightarrow d\gamma$ .  $A_{\text{CP}}$  is obtained from the yield asymmetry between the  $B$  and  $\bar{B}$  sample correcting for flavor misidentification and detector asymmetry.

A CP asymmetry of  $(0.025 \pm 0.050 \pm 0.015)$  is measured, where the first error is statistical and the second is systematic, corresponding to an allowed range of  $-0.06 < A_{\text{CP}}(b \rightarrow s\gamma) < +0.11$  at the 90% confidence level and is in good agreement with SM predictions.

#### 4.2 Search for CP or isospin asymmetries in the $B \rightarrow K^*\gamma$ decays

The set of exclusive decays  $B \rightarrow K^*\gamma$  provide other opportunities to test the SM predictions for the isospin ( $\Delta_{0-}$ , Eq. 4) and the CP asymmetries ( $A_{\text{CP}}$ , Eq. 5):

$$\Delta_{0-} = \frac{\Gamma(B^0 \rightarrow K^{*0}\gamma) - \Gamma(B^+ \rightarrow K^{*+}\gamma)}{\Gamma(B^0 \rightarrow K^{*0}\gamma) + \Gamma(B^+ \rightarrow K^{*+}\gamma)} \quad (4)$$

$$A_{\text{CP}} = \frac{\Gamma(\bar{B} \rightarrow \bar{K}^*\gamma) - \Gamma(B \rightarrow K^*\gamma)}{\Gamma(\bar{B} \rightarrow \bar{K}^*\gamma) + \Gamma(B \rightarrow K^*\gamma)} \quad (5)$$

The SM predicts a positive  $\Delta_{0-}$  between 5 and 10% and  $A_{\text{CP}}$  less than 1%<sup>13)</sup>. New physics contribution can modify these values significantly.

The  $K^*$  is reconstructed in self-tagging decay channels  $K^{*0} \rightarrow K^+\pi^-$ ;  $K^{*+} \rightarrow K^+\pi^0$ ;  $K_s^0\pi^+$  and their charge conjugates. For the isospin analysis  $K^{*0} \rightarrow K_s^0\pi^0$  was also used.

The signal yield and  $A_{\text{CP}}$  for each decay mode are determined from a two-dimensional extended unbinned maximum likelihood fit to the  $m_{ES}$  and  $\Delta E^*$ .  $\Delta_{0-}$  is determined from the signal yields correcting for the differences in signal efficiency and lifetime between the neutral and charged  $B$ . The preliminary results are:

$$A_{\text{CP}} = -0.015 \pm 0.036(\text{stat.}) \pm (\text{syst.}) \quad (6)$$

$$\Delta_{0-} = +0.051 \pm 0.044(\text{stat.}) \pm 0.023(\text{syst.}) \pm 0.024(\text{R}^{+/0}) \quad (7)$$

the first error being statistical and the second the systematic error. The third error on  $\Delta_{0-}$  is related to the uncertainty on the ratios recently measured by the BaBar collaboration<sup>15)</sup> and accounts for the possibility of different production rates of charged and neutral  $B$ 's.

## 5 Leptonic $B$ decays

The study of purely leptonic  $B$  decays,  $B^+ \rightarrow \ell^+\nu_\ell$ , can provide sensitivity to poorly constrained SM parameters and also act as a probe for new physics. In the SM the reaction proceeds via the annihilation of the  $b$  and  $\bar{u}$  producing an intermediate  $W$  boson which subsequently decays to a lepton and neutrino, the branching ratio is given by:

$$B(B^+ \rightarrow \ell^+\nu) = \frac{G_F^2 m_B m_\ell^2}{8\pi} \left(1 - \frac{m_\ell^2}{m_B^2}\right)^2 f_B |V_{ub}|^2 \tau_B, \quad (8)$$

where  $G_F$  is the Fermi constant,  $m_\ell$  and  $m_B$  are the lepton and meson masses,  $f_B$  is the  $B$  decay constant,  $V_{ub}$  is the relevant CKM matrix element and  $\tau_B$  is the  $B^+$  lifetime. Currently  $f_B$  comes from lattice QCD calculations and is affected by a 15% uncertainty. Therefore, observation of  $B^+ \rightarrow \ell^+\nu$  could

provide the first direct measurement of  $f_B$ . Unfortunately, leptonic decays are strongly suppressed by helicity and there is, as yet, no experimental evidence for such decays.

### 5.1 $B^+ \rightarrow \tau^+ \nu$

Using 88.9 million  $B\bar{B}$  events BaBar has studied  $B^+ \rightarrow \tau^+ \nu$  using two statistically independent analysis techniques. Due to the presence of at least two neutrinos in the final state, the semileptonic ( $B^- \rightarrow D^0 \ell^- \bar{\nu} X$ ) and hadronic ( $B^- \rightarrow D^0 X_{\text{had}}$ ) decays of the other  $B$  have been reconstructed, as for the  $B^+ \rightarrow K^+ \nu \bar{\nu}$  analysis.

After reconstructing the other  $B$  in the event the signal signature is given by one or up to three charged tracks, depending on the  $\tau$  decay mode. Low remaining neutral energy,  $E_{\text{extra}}$ , is demanded to limit backgrounds from processes depositing considerable energy in the calorimeter. For the semileptonic tag analysis<sup>16)</sup>, only the single prong leptonic  $\tau$  decays are considered and a fit to  $E_{\text{extra}}$  is performed to extract the signal and background yields from data. In the analysis using the hadronic tag technique<sup>17)</sup>  $\tau$  decays into  $\pi^+ \bar{\nu}_\tau$ ,  $\pi^+ \pi^0 \bar{\nu}_\tau$  and  $\pi^+ \pi^- \pi^+ \bar{\nu}_\tau$  are also considered and the number of events with  $E_{\text{extra}} < 100$  MeV is counted. Combining the two samples yields a preliminary upper limit on the branching fraction at the 90% confidence level of

$$B(B^+ \rightarrow \tau^+ \nu) < 4.1 \times 10^{-4}, \quad (9)$$

which represents the best upper limit on this channel.

### 5.2 $B^+ \rightarrow \mu^+ \nu$

The  $B^+ \rightarrow \mu^+ \nu$  decay has been studied by BaBar using the same dataset as the  $B^+ \rightarrow \tau^+ \nu$  analyses. After identifying a muon, all remaining particles are associated with the decay of the other  $B$ . Once the other  $B$  is reconstructed, the muon momentum is calculated in the rest frame of the signal  $B$ . The signal muon momentum distribution peaks at 2.64 GeV/c. No significant signal excess has been observed and an upper limit on the branching fraction at the 90% confidence level of

$$B(B^+ \rightarrow \mu^+ \nu) < 6.6 \times 10^{-6}, \quad (10)$$

was set.

The Belle collaboration has also studied this channel using a similar method using  $60 \text{ fb}^{-1}$  of data and place a compatible limit of  $B(B^+ \rightarrow \mu^+ \nu) < 6.8 \times 10^{-6}$  at the 90% confidence level.

## 6 Conclusions

The unprecedented luminosities of the  $B$ -factories allows new extensive and detailed studies on processes involving flavor-changing neutral-current such as  $b \rightarrow s\ell^+\ell^-$ ,  $b \rightarrow s\gamma$  and  $b \rightarrow d\gamma$ . There is no experimental evidence for  $CP$  violation in  $b \rightarrow s\gamma$  at the 5% level and the SM predictions are confirmed. Both BaBar and Belle are collecting richer data samples that will permit more stringent tests of the SM through studies of radiative and leptonic  $B$  decays and there may be surprises in the very near future.

## References

1. B. Aubert *et al.*, The Babar Detector, Nucl. Instrum. Meth., A **479**,1-116, (2002).
2. K. Abe *et al.*, The Belle Detector, Nucl. Instrum. Meth., A **479**, 117 (2002).
3. B. Aubert *et al.*, Evidence for the rare decay  $B \rightarrow K^*\ell^+\ell^-$  and measurement of the  $B \rightarrow K\ell^+\ell^-$  branching fraction. Phys. Rev. Lett., **91**:221802, 2003, hep-ex/0308042.
4. B. Aubert *et al.*, Measurement of the  $B \rightarrow X_s\ell^+\ell^-$  branching fraction using a sum over exclusive modes. 2003, hep-ex/0308016.
5. K. Hagiwara *et al.*, Review of particle physics. Phys. Rev. **D66**:010001, 2002.
6. P. Gambino and M. Misiak, Quark mass effects in  $\bar{B} \rightarrow X_s\gamma$ . Nucl. Phys., **B611**:338-366, 2001.
7. A. J. Buras, A. Czarnecki, M. Misiak and J. Urban, Completing the NLO QCD calculation of  $\bar{B} \rightarrow X_s\gamma$ . Nucl. Phys. **B631**:219-238, 2002.
8. T. Hurth, Present status of inclusive rare  $B$  decays. Rev. Mod. Phys., **75** 1159-1199, 2003.
9. T. Hurth, E. Lunghi and W. Porod, Updated NLL results for  $\bar{B} \rightarrow X_{s,d}\gamma$  in and beyond the Standard Model. 2003, hep-ph/0310282.
10. R. A. Fisher, Ann. Eugen. 7, 179, (1936).
11. G. C. Fox and S. Wolfram, Phys. Rev. Lett. 41, 1581 (1978).
12. B. Aubert *et al.*, Measurement of time-dependent CP-violating asymmetries in  $B^0 \rightarrow K^{*0}\gamma(K^{*0} \rightarrow K_s^0\pi^0)$  decays, 2004, hep-ex/0405082.

13. A. L. Kagan, M. Neubert, Direct CP violation  $B \rightarrow X_s \gamma$  decays as a signature of new physics. Phys. Rev. **D58**:094012, 1998.
14. B. Aubert *et al.*, Measurement of the direct CP asymmetry in  $b \rightarrow s \gamma$  decays, hep-ex/0403035, 2004.
15. B. Aubert *et al.*, Measurement of the  $B^+/B^0$  production ratio from the  $\Upsilon(4S)$  meson using  $B^+ \rightarrow J/\psi K^+$  and  $B^0 \rightarrow J/\psi K_s^0$  decays. Phys Rev., **D69**:071101, 2004, hep-ex/0401028.
16. B. Aubert *et al.*, arXiv:hep-ex/0303034
17. B. Aubert *et al.*, arXiv:hep-ex/0303030

## ***SESSION XI – D Meson Spectroscopy***

- T. Barnes      Recent Developments in Charm Spectroscopy:  
X(3872),  $D_{sJ}^*(2317)^+$  and  $D_{sJ}(2463)^+$
- H. Guler      What Are the X(3872) and  $D_{sJ}$  Particles?
- R. K. Kutschke   Charmed Meson Spectroscopy



**RECENT DEVELOPMENTS IN CHARM SPECTROSCOPY:  
X(3872),  $D_{sJ}^*(2317)^+$  and  $D_{sJ}(2463)^+$**

T. Barnes

*Physics Div. ORNL, Oak Ridge, TN 37831, USA  
Dept. of Physics and Astronomy, University of Tennessee  
Knoxville TN 37996, USA*

ABSTRACT

The past year has seen reports of evidence for several remarkable hadronic states. Three of these new states, the X(3872),  $D_{sJ}^*(2317)^+$  and  $D_{sJ}(2463)^+$ , are mesons containing (as a minimum) charm quarks and strange or charm antiquarks. In this contribution I will concentrate on the X(3872) due to limitations of space, and will review what is known experimentally, what theorists have suggested regarding the interpretation of this state, and how future experimental studies might distinguish between the various theoretical assignments. The  $D_{sJ}^*(2317)^+$  and  $D_{sJ}(2463)^+$  will also be briefly discussed.

**1 Introduction: Heavy Quarkonium Spectroscopy**

To set the stage for our discussion of the new mesons, it is useful to recall our previous, apparently numerically accurate understanding of the spectrum of

heavy quarkonium, as it was known before 2003. (We will specialize to charmonium for this discussion.) Since the charm quark is moderately heavy, it is widely believed that a quark potential model provides a reasonable approximation to the charmonium system. In its simplest form this potential model picture assumes the nonrelativistic Schrödinger equation, with a color Coulomb potential at small  $c\bar{c}$  separations from OGE (one gluon exchange) and a linear confining potential at large distances,

$$V(r) = -\frac{4\alpha_s}{3} \frac{1}{r} + br. \quad (1)$$

This zeroth-order spin-independent potential is then augmented by the inclusion of spin-dependent forces. These are usually taken to be the Breit-Fermi Hamiltonian from OGE (which includes spin-spin, spin-orbit and tensor terms) and the inverted spin-orbit of linear scalar confinement. For the equal-mass  $c\bar{c}$  case this spin-dependent Hamiltonian is

$$H_I = \frac{32\pi\alpha_s}{9m_c^2} \delta(\vec{r}) \vec{S}_c \cdot \vec{S}_{\bar{c}} + \frac{2\alpha_s}{m_c^2 r^3} \vec{L} \cdot \vec{S} + \frac{4\alpha_s}{m_c^2 r^3} T - \frac{b}{2m_c^2 r} \vec{L} \cdot \vec{S}. \quad (2)$$

The strong effect of the spin-spin term on the wavefunctions of S-wave states at short distances is often treated by incorporating the spin-spin term in the “zeroth-order” potential  $V(r)$ . This contact interaction must then be replaced by a nonsingular distribution, which is typically a relatively narrow Gaussian with a width of  $1/\sigma$ . We follow this approach, which gives a potential model of charmonium with the four parameters  $\alpha_s, b, m_c$  and  $\sigma$ . Fitting this model to the masses of the 11 established charmonium states in the 2004 PDG <sup>1)</sup> (with equal weights) gives the spectrum shown in fig.1 and the parameter values  $\alpha_s = 0.5461$ ,  $b = 0.1425 \text{ GeV}^2$ ,  $m_c = 1.4794 \text{ GeV}$  and  $\sigma = 1.0946 \text{ GeV}$ . This fit is described in detail elsewhere, <sup>2)</sup> and gives a very reasonable rms error of 13.6 MeV. The well known potential models of Godfrey and Isgur <sup>3)</sup> and (for charmonium specifically) Eichten *et al.* <sup>4)</sup> assume very similar physics, but replace the nonrelativistic kinetic energy in the Schrödinger equation by a relativized form.

Recent developments in lattice gauge theory have led to reasonably well constrained mass predictions for the spectrum of heavy quarkonium states (*albeit* usually in the quenched approximation). As an example, in fig.2 we show the results of Liao and Manke, <sup>5)</sup> which are similar both to experiment and to the potential model. (Actually, since this potential model and quenched

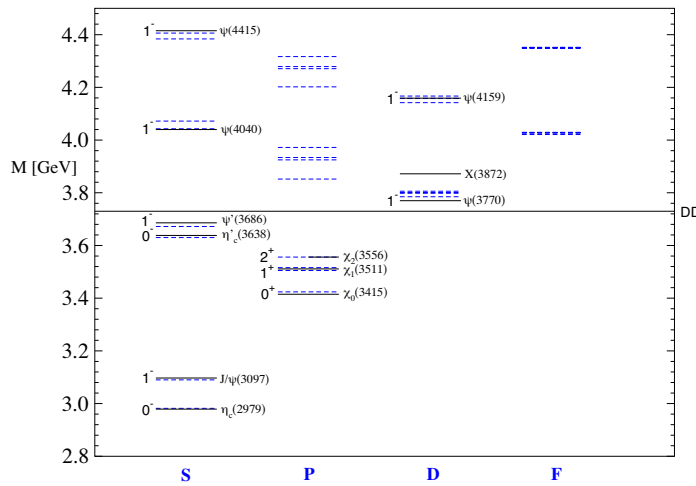


Figure 1: The spectrum of charmonium states predicted by the  $c\bar{c}$  potential model described in the text (dashed), fitted to the 11 well-established experimental states <sup>1)</sup> (solid). The  $X(3872)$  is also shown, although its identification with

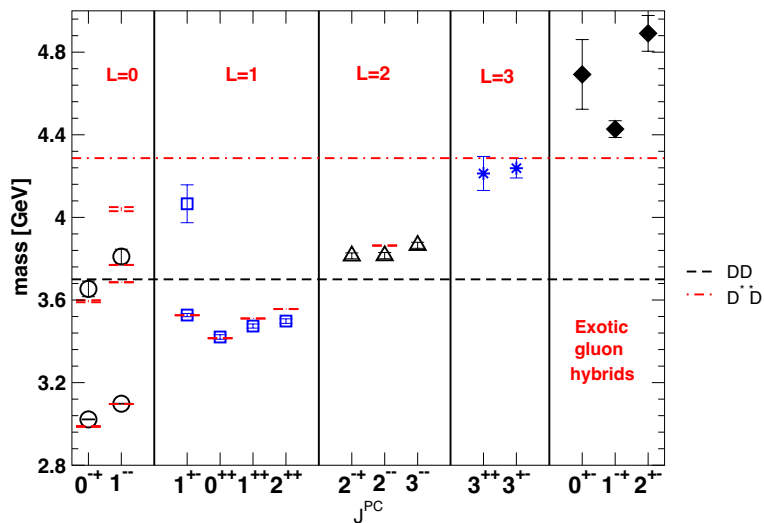


Figure 2: The spectrum of low-lying charmonium states predicted by lattice gauge theory in the quenched approximation. <sup>5)</sup> Compare with fig.1.

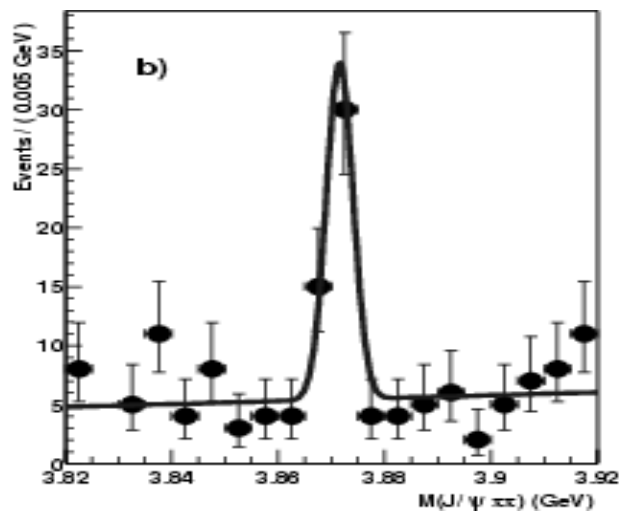


Figure 3: *The  $X(3872)$ , first reported by the Belle Collaboration in  $J/\psi \pi^+ \pi^-$ . <sup>6)</sup>*

LGT both neglect decay loops, both approaches may share similar systematic errors.) There are some indications that the higher-L charmonium states are predicted to lie at higher masses by LGT. Small higher-L multiplet splittings are evident in both approaches. The most interesting LGT prediction may be the mass of the  $J^{PC}$ -exotic  $1^{-+}$  charmonium hybrid, which is expected at about 4.4 GeV. (We note in passing that the experimental  $1^{+-}$   $h_c$  state shown near 3.52 GeV in the LGT figure has been withdrawn.)

## 2 The X(3872)

The recent discoveries of the X(3872),  $D_{sJ}^*(2317)^+$  and  $D_{sJ}(2463)^+$  have challenged our understanding of heavy quark meson spectroscopy, since these states are in serious disagreement with theoretical expectations. The X(3872) was originally discovered by the Belle Collaboration <sup>6)</sup> in B meson decay ( $B^{+-} \rightarrow K^{+-}\pi^+\pi^-J/\psi$ ) as a narrow peak in the  $J/\psi\pi^+\pi^-$  invariant mass distribution. The state had a very high statistical significance in the Belle data (in excess of  $10\sigma$ ), and has since been confirmed by CDF II, <sup>7)</sup> D0 <sup>8)</sup> and BABAR. <sup>9)</sup>

This decay mode suggested that the state might be one of the two missing narrow charmonium states in the  $L = 2$   $c\bar{c}$  multiplet, which have  $J^{PC} = 2^{-+}$  or  $2^{--}$ . These two  $c\bar{c}$  states are special in that they do not have open-flavor decay modes, unlike the other  $c\bar{c}$  states above DD threshold, and consequently are expected to have rather small total widths. (A total width of ca. 1 MeV is expected from annihilation and radiative decays.) Subsequent theoretical study has added the  $J^{PC} = 3^{-+}$   ${}^3D_3$   $c\bar{c}$  state to the list of X(3872) candidates; it can decay to DD, but the centrifugal barrier implies that this will nonetheless be a relatively narrow state. <sup>10, 11)</sup> Alternatively, the X(3872) might be a more complicated state such as a charm meson molecule, which contains a  $c\bar{c}$  pair that is combined with other (light) constituents.

The near equality of the reported mass of the X(3872) and the neutral  $D^0\bar{D}^{*0}$  threshold of  $3871.5 \pm 0.5$  MeV immediately suggested that the X(3872) could be a  $D^0\bar{D}^{*0}$  system (a bar is implicit here, such as  $D^0\bar{D}^{*0}$  or  $\bar{D}^0D^{*0}$  or a linear combination), either a weakly bound “molecule” <sup>12, 13, 14, 15, 16, 17)</sup> or perhaps simply a cusp phenomenon due to the opening of a new channel. <sup>18)</sup> Note that the mass of a charged ( $D^\pm D^{*\mp}$ ) pair is rather higher,  $3879.5 \pm 0.7$  MeV, so the X(3872) would presumably be a pair of neutral charmed mesons.

Table 1: *Experiments reporting the X(3872).*

Collab.	Mass (MeV)	Width (MeV)	mode
Belle <sup>6)</sup>	$3872.0 \pm 0.6 \pm 0.5$	$< 2.3, 95\% \text{ c.l.}$	$J/\psi \pi^+ \pi^-$
CDF II <sup>7)</sup>	$3871.3 \pm 0.7 \pm 0.4$		“
D0 <sup>8)</sup>	$3871.8 \pm 3.1 \pm 3.0$		“
BABAR <sup>9)</sup>	$3873.4 \pm 1.4$		“

Since this implies a very weakly bound system, with a binding energy of at most about 1 MeV (from the experimental mass uncertainties), the dominant binding mechanism would presumably be the longest-ranged strong interaction, one pion exchange. Fortunately we know the strength of the  $D^*D\pi$  coupling experimentally from  $D^*$  decay, so this effect can be estimated with only moderate uncertainty. One pion exchange does indeed provide an attraction in this system, and the forces are very close to the strength required to bind a  $D^0D^{*0}$  pair in S-wave. <sup>12, 16)</sup> With the addition of (also attractive) short-ranged quark-gluon forces, it does appear that a weakly bound  $D^0D^{*0}$  molecule is expected theoretically. <sup>16)</sup>

The naive expectation for strong decays of a weakly bound meson molecule is that it should decay as its constituents do. In this case only the  $D^*$  decay modes are relevant, so we would expect decays of a  $D^0D^{*0}$  bound state to populate the final states  $D^0D^0\pi^0$  and  $D^0D^0\gamma$ . However the  $D^{*0}$  has a rather small total width (not yet measured but probably only about 50 keV), so another decay mechanism, internal rescattering, is expected to dominate decays. The  $D^0D^{*0}$  pair can internally rescatter by constituent interchange into charmonium and a light meson, for example  $J/\psi \rho^0$  and  $J/\psi \omega$ . Evaluation of these rescattering amplitudes by Swanson <sup>16)</sup> leads to the prediction that they should be the dominant decay modes of a  $D^0D^{*0}$  molecule, (see Table 2) and that as a result  $J/\psi \pi^+ \pi^-$  and  $J/\psi \pi^+ \pi^- \pi^0$  should be the dominant final states populated by  $X(3872)$  decays. The remarkable prediction of comparable branching fractions to modes with different isospins ( $J/\psi \pi^+ \pi^- \pi^0$  and  $J/\psi \pi^+ \pi^-$  here are  $I = 0$  and  $I = 1$  respectively) is a simple consequence of the maximal isospin mixing implied by a  $D^0D^{*0}$  bound state. Additional predictions of branching fractions that follow from the  $DD^*$  molecule model have been given recently by Swanson. <sup>17)</sup>

Table 2: *The dominant decay modes of an S-wave  $1^{++}$   $D^0 D^{*0}$  molecule <sup>16)</sup> for  $E_B = 1$  MeV.*

mode	$D^0 \bar{D}^0 \pi^0$	$D^0 \bar{D}^0 \gamma$	$\pi^+ \pi^- J/\psi$	$\pi^+ \pi^- \pi^0 J/\psi$	$\pi^0 \gamma J/\psi$
$\Gamma^{thy}(\text{keV})$	66	36	1215	820	80

The prediction of comparable branching fractions to  $J/\psi \pi^+ \pi^-$  and  $J/\psi \pi^+ \pi^- \pi^0$ , through the intermediate states  $J/\psi \rho^0$  and  $J/\psi \omega$  respectively, is a remarkable prediction of the  $D^0 D^{*0}$  molecule model when combined with the assumption of an internal rescattering mechanism. A simpler question regarding  $J/\psi \pi \pi$  modes is whether there is a  $J/\psi \pi^0 \pi^0$  signal present with a comparable strength to  $J/\psi \pi^+ \pi^-$ . <sup>19)</sup> The presence of this  $J/\psi \pi^0 \pi^0$  mode would imply  $C=(-)$  quantum numbers, whereas the usual molecule assumption is that this is a  $C=(+)$  state. ( $J^{PC} = 1^{++}$ ). The mass distribution of the  $\pi \pi$  system in  $J/\psi \pi^+ \pi^-$  is also an interesting question, since there is evidence that it does peak at higher mass, but it is not yet clear whether the mass and width of the distribution are consistent with a  $\rho^0$  source. Similarly, in the molecule model the  $\pi^+ \pi^- \pi^0$  system in  $X(3872) \rightarrow J/\psi \pi^+ \pi^- \pi^0$  decays should be strongly peaked at high invariant mass, if the  $\pi^+ \pi^- \pi^0$  source is an  $\omega$  meson.

Although the near equality of the  $X(3872)$  mass and the  $D^0 D^{*0}$  threshold makes the molecule a very compelling picture (this is currently the favored assignment), the  $c\bar{c}$  option is also straightforward to test. The  $J^{PC} = 2^{-+}$  and  $2^{--}$   $^1D_2$  ( $h_{c2}$ ) and  $^3D_2$  ( $\psi_2$ )  $c\bar{c}$  assignments lead to predictions of relatively large radiative transitions to 1P charmonium states, for which Barnes and Godfrey <sup>10)</sup> found

$$\Gamma_{h_{c2} \rightarrow \gamma \chi_2} = 0.09 \text{ MeV} \quad (3)$$

and

$$\Gamma_{h_{c2} \rightarrow \gamma \chi_1} = 0.36 \text{ MeV} \quad (4)$$

for an initial  $^1D_2$   $h_{c2}(3872)$ , and

$$\Gamma_{\psi_2 \rightarrow \gamma h_c} = 0.46 \text{ MeV} \quad (5)$$

for a  $^3D_2$   $\psi_2(3872)$ . (See also Eichten, Lane and Quigg <sup>20)</sup> for radiative transition rates.) Since the total width of the  $X(3872)$  is below 2.3 MeV (95%

*c.l.*), a  $c\bar{c}$  assignment would evidently imply large branching fractions of at least  $\approx 20\%$  to radiative modes. These can be searched for through the large secondary radiative transitions of the P-wave mesons to S-wave charmonia,  $h_{c2} \rightarrow \gamma\chi_J \rightarrow \gamma\gamma J/\psi$  and  $\psi_2 \rightarrow \gamma h_c \rightarrow \gamma\gamma\eta_c$  respectively.

At present we only have an experimental limit for one of these radiative transitions. In their original paper Belle reported

$$\frac{B_{X(3872) \rightarrow \gamma\chi_1}}{B_{X(3872) \rightarrow J/\psi\pi^+\pi^-}} < 0.89, \quad 90\% \text{ c.l.} \quad (6)$$

Unfortunately, this is not constraining without an independent estimate of the partial width of the poorly understood dipion mode.

Another approach to testing possible assignments for the X(3872) is to search for other decay modes. For example, a D-wave  $c\bar{c}$  X(3872) will not appear in  $e^+e^-$ , and a  $2^{--} \ ^3D_2(\psi_2)$   $c\bar{c}$  will not be seen in  $\gamma\gamma$  collisions. Neither  $e^+e^-$  nor  $\gamma\gamma$  would show a  $1^{++}$  DD\* molecule (although  $\gamma\gamma^*$  would, with sufficient statistics). A  $2^{-+} \ ^1D_2(h_{c2})$   $c\bar{c}$  in contrast *will* be produced in  $\gamma\gamma$ , and the great sensitivity of current  $e^+e^-$  machines makes this a useful production channel to investigate. Unfortunately, the  $\gamma\gamma$  couplings of  $c\bar{c}$  states are expected to fall rapidly with increasing L; a hypothetical D-wave  $c\bar{c}$   $h_{c2}(3840)$  is predicted to have a  $\gamma\gamma$  width of only 20 eV. <sup>21)</sup>

There are now very strong recent experimental limits on production of the X(3872) in both  $e^+e^-$  and  $\gamma\gamma$ . Yuan, Mo and Wang <sup>22)</sup> used ISR data from BES to give an upper limit of

$$\Gamma_{e^+e^-}(X(3872)) \cdot B_{X(3872) \rightarrow J/\psi\pi^+\pi^-} < 10 \text{ eV}, \quad 90\% \text{ c.l.}, \quad (7)$$

and a new analysis of CLEO III data <sup>23)</sup> sets limits of

$$\Gamma_{e^+e^-}(X(3872)) \cdot B_{X(3872) \rightarrow J/\psi\pi^+\pi^-} < 8.0 \text{ eV}, \quad 90\% \text{ c.l.} \quad (8)$$

and

$$(2J+1)\Gamma_{\gamma\gamma}(X(3872)) \cdot B_{X(3872) \rightarrow J/\psi\pi^+\pi^-} < 12.9 \text{ eV}, \quad 90\% \text{ c.l.} \quad (9)$$

The X(3872) is not expected to appear in  $e^+e^-$  in either of the usual DD\* molecule or  $c\bar{c}$  assignments, since neither is  $1^{--}$ . The  $^3D_2$   $c\bar{c}$  assignment however does imply a (rather weak) coupling to  $\gamma\gamma$  of  $\Gamma_{e^+e^-}^{thy}(X(3872)) \approx 20 \text{ eV}$ , <sup>21)</sup> so this is a useful experimental limit. Unfortunately the branching fraction of

the  $X(3872)$  to  $J/\psi\pi^+\pi^-$  is unknown at present, however once this is established it may be possible to use this  $\gamma\gamma$  width limit to eliminate a dominantly  $c\bar{c}$  assignment.

### 3 $D_{sJ}^*(2317)^+$ and $D_{sJ}(2463)^+$

For completeness we will also briefly discuss the new charm-strange mesons  $D_{sJ}^*(2317)^+$  and  $D_{sJ}(2463)^+$ , since some aspects of these states are reminiscent of the  $X(3872)$ . Unfortunately there is insufficient space in this report for a detailed discussion, so only the basic issues will be noted.

The  $D_{sJ}^*(2317)^+$  was the first of the anomalous new charm mesons to be reported. It was discovered by the BABAR Collaboration <sup>24)</sup> as a very narrow peak in the final state  $D_s^+\pi^0$ , at a mass of 2.32 GeV. This discovery was quickly followed by the report of a second narrow state by the CLEO Collaboration, <sup>25)</sup> the  $D_{sJ}(2463)^+$  in  $D_s^{*+}\pi^0$ . In both cases the widths of the states were consistent with experimental resolution.

There were quark model states in the  $c\bar{s}$  sector that might *a priori* have been identified with these new discoveries, a  $0^+$   $^3P_0$  scalar and a  $1^+$  mixed  $^1P_1$  and  $^3P_1$  axial vector. The reported properties however were far from theoretical expectations; the  $0^+$   $^3P_0$   $c\bar{s}$  had been predicted by Godfrey and Isgur to have a mass of 2.48 GeV, and the two  $1^+$  states were expected near 2.55 GeV. <sup>3)</sup> In addition, both missing states were predicted to have very large total widths of 100s of MeV. <sup>29)</sup> Identification with the new experimental states would require that the potential model was in error by over 150 MeV, whereas past experience suggested errors of ca. 20 MeV in the  $c\bar{s}$  sector. If one could accept this mass discrepancy, the narrow widths could then be understood; at masses of 2.32 GeV and 2.46 GeV the  $0^+$  and  $1^+$   $c\bar{s}$  states would be below their lowest open-flavor decay modes (DK and  $D^*K$  respectively), and would have to decay to strongly suppressed modes such as the isospin-violating  $D_s^+\pi^0$  and  $D_s^{*+}\pi^0$ . Alternative explanations for these new states, such as a DK bound state for the  $D_{sJ}^*(2317)^+$ , were also proposed; it was noted that the very strong coupling predicted for a  $c\bar{s}$  quark model state to DK would induce a strong attraction in the DK channel, which might result in the formation of an S-wave bound state. <sup>26)</sup>

It may be that the mass errors in the potential model predictions for these states and their predicted large widths are related effects. It is well established

that virtual decays of mesons to two-meson continua can give rise to large, negative mass shifts in charmonium.<sup>27; 28)</sup> These effects should be very large for the  $0^+$  and  $1^+$   $c\bar{s}$  states, which were predicted to have especially large open-flavor decay couplings to DK and D\*K respectively. In this case the physical states would paradoxically be narrow because their decay couplings are so large; the resulting mass shifts have pushed the states below their open-flavor decay thresholds.

Whether this remarkable possibility is indeed numerically realistic given our current strong decay models, and what the resulting  $c\bar{s} \leftrightarrow DK$  mixing would predict for observables, are two of the most important questions raised by the discovery of the new narrow resonances.

#### 4 Acknowledgements

I am happy to acknowledge the kind invitation of Angel Lopez to attend the HQL2004 meeting in San Juan, and for the opportunity to discuss the exciting new developments in charmed meson spectroscopy with my fellow participants. The support of the organizers of HQL2004, the U.S. National Science Foundation through grant NSF-PHY-0244786 at the University of Tennessee, and the U.S. Department of Energy under contract DE-AC05-00OR22725 at Oak Ridge National Laboratory is also gratefully acknowledged. I would also like to thank F.E.Close, R.Kutschke, S.Godfrey, H.Lipkin, J.Quigg, J.Rosner, I.Shipsey and E.S.Swanson for discussions of various aspects of the material presented here.

#### References

1. S.Eidelman *et al.* (Particle Data Group), Phys. Lett. B**592**, 1 (2004).
2. T.Barnes, S.Godfrey and E.S.Swanson (in preparation).
3. S. Godfrey and N. Isgur, Phys. Rev. D **32**, 189 (1985).
4. E. Eichten, K. Gottfried, T. Kinoshita, K. D. Lane and T. M. Yan, Phys. Rev. D **21**, 203 (1980).
5. X. Liao and T. Manke, arXiv:hep-lat/0210030.
6. S. K. Choi *et al.* [Belle Collaboration], Phys. Rev. Lett. **91**, 262001 (2003) [arXiv:hep-ex/0309032].

7. D. Acosta *et al.* [CDF II Collaboration], arXiv:hep-ex/0312021.
8. V. M. Abazov *et al.* [D0 Collaboration], arXiv:hep-ex/0405004.
9. B. Aubert *et al.* [BABAR Collaboration], arXiv:hep-ex/0406022.
10. T. Barnes and S. Godfrey, Phys. Rev. D **69**, 054008 (2004) [arXiv:hep-ph/0311162].
11. C. Quigg, arXiv:hep-ph/0403187.
12. N. A. Tornqvist, Phys. Lett. B **590**, 209 (2004) [arXiv:hep-ph/0402237].
13. F. E. Close and P. R. Page, Phys. Lett. B **578**, 119 (2004) [arXiv:hep-ph/0309253].
14. M. B. Voloshin, Phys. Lett. B **579**, 316 (2004) [arXiv:hep-ph/0309307].
15. C. Y. Wong, Phys. Rev. C **69**, 055202 (2004) [arXiv:hep-ph/0311088].
16. E. S. Swanson, Phys. Lett. B **588**, 189 (2004) [arXiv:hep-ph/0311229].
17. E. S. Swanson, arXiv:hep-ph/0406080.
18. D. V. Bugg, arXiv:hep-ph/0406293.
19. S. Pakvasa and M. Suzuki, Phys. Lett. B **579**, 67 (2004) [arXiv:hep-ph/0309294].
20. E. J. Eichten, K. Lane and C. Quigg, Phys. Rev. D **69**, 094019 (2004) [arXiv:hep-ph/0401210].
21. E. S. Ackleh and T. Barnes, Phys. Rev. D **45**, 232 (1992).
22. C. Z. Yuan, X. H. Mo and P. Wang, Phys. Lett. B **579**, 74 (2004) [arXiv:hep-ph/0310261].
23. Z. Metreveli *et al.* (CLEO Collaboration), "Search for X(3872) in Untagged  $\gamma\gamma$  Fusion and Initial State Radiation Production with CLEO III", CLEO CONF 04-7, ICHEP04 ABS10-0768, to appear in the Proc. of the 32<sup>nd</sup> Internatl. Conf. on High Energy Physics (Beijing, Aug 2004).
24. B. Aubert *et al.* [BABAR Collaboration], Phys. Rev. Lett. **90**, 242001 (2003) [arXiv:hep-ex/0304021].

- 
25. D. Besson *et al.* [CLEO Collaboration], Phys. Rev. D **68**, 032002 (2003) [arXiv:hep-ex/0305100].
  26. T. Barnes, F. E. Close and H. J. Lipkin, Phys. Rev. D **68**, 054006 (2003) [arXiv:hep-ph/0305025].
  27. E. van Beveren, C. Dullemond and G. Rupp, Phys. Rev. D **21**, 772 (1980) [Erratum-ibid. D **22**, 787 (1980)].
  28. K. Heikkila, S. Ono and N. A. Tornqvist, Phys. Rev. D **29**, 110 (1984) [Erratum-ibid. D **29**, 2136 (1984)].
  29. S. Godfrey and R. Kokoski, Phys. Rev. D **43**, 1679 (1991).

## WHAT ARE THE $X(3872)$ AND $D_{sJ}$ PARTICLES?

Hulya Guler  
*University of Hawaii, Honolulu, Hawaii 96822*

### ABSTRACT

Recently, three new states, provisionally named  $D_{sJ}^*(2317)^+$ ,  $D_{sJ}(2460)^+$ , and  $X(3872)$ , were discovered by BaBar, CLEO, and Belle, respectively. None of the new states is readily accommodated by existing models of meson spectroscopy. While the two  $D_{sJ}$  states are suggestive of the hitherto-unobserved  $P$ -wave  $c\bar{s}$  doublet, this interpretation may require modification of standard interquark-potential models. The  $X(3872)$  may be a  $D^0\bar{D}^{*0}$  molecule, an excited  $c\bar{c}$  state, or a hybrid  $c\bar{c}g$  state. This paper surveys the experimental evidence and considers various theoretical explanations for these novel states.

### 1 Introduction

The past year has seen the discovery of three new particles that challenge the current understanding of meson spectroscopy. First, the BaBar collaboration

observed a narrow resonance near 2.32 GeV in the  $D_s^+\pi^0$  spectrum <sup>1)</sup>. Shortly thereafter, the CLEO Collaboration announced the observation of a similarly narrow resonance near 2.46 GeV in the  $D_s^{*+}\pi^0$  spectrum <sup>2)</sup>. The intrinsic widths of the two states were measured by CLEO to be smaller than 7 MeV at 90% C.L. Although these new states have been named  $D_{sJ}^*(2317)^+$  and  $D_{sJ}(2460)^+$  and interpreted as the missing  $P$ -wave doublet of the  $c\bar{s}$  system, their masses are significantly lower than theoretical predictions.

Not long after these discoveries, the Belle Collaboration reported the observation of a 3.872-GeV  $J/\psi\pi^+\pi^-$  resonance in the exclusive decay  $B^+ \rightarrow K^+J/\psi\pi^+\pi^-$  <sup>3)</sup>. The signal, which was measured to have an intrinsic width smaller than 2.3 MeV at 90% C.L., had a statistical significance greater than  $10\sigma$  and could not be reproduced in generic Monte Carlo. While this state, provisionally named the  $X(3872)$ , may be charmonium, it does not exhibit the theoretically predicted properties of any of the missing  $c\bar{c}$  states.

The following sections will briefly review the spectroscopy of the  $c\bar{s}$  and  $c\bar{c}$  systems, survey the experimental evidence, and outline the difficulties in reconciling the observations with theory.

## 2 The $D_{sJ}^*(2317)^+$ and $D_{sJ}(2460)^+$ Particles

### 2.1 The $c\bar{s}$ System

Two different approaches can be used to predict the properties of  $P$ -wave charmed mesons <sup>4)</sup>. The first is a non-relativistic quark model with an interquark potential that is partly Coulombic. In the limit where the mass of one of the quarks approaches infinity, the light-quark angular momentum  $\mathbf{j}_l = \mathbf{s}_l + \mathbf{l}$  is conserved, and the  $P$ -wave states are split into two levels, with  $j_l = 3/2$  and  $1/2$ . Since the heavy quark in a real meson is not infinitely massive, its spin cannot be neglected completely. The conserved quantity thus becomes the total angular momentum  $\mathbf{J} = \mathbf{j}_l + \mathbf{s}_h$ , and the levels are split further, the  $j_l = 3/2$  into  $J = 2$  and  $J = 1$ , and the  $j_l = 1/2$  into  $J = 1$  and  $J = 0$ . Since  $j_l$  is only approximately conserved, the two states with  $J = 1$  can mix. The  $S$ -wave and  $P$ -wave states for the  $c\bar{s}$  system are shown in Fig. 1.

The second approach employs heavy-quark effective theory (HQET) <sup>6)</sup>. In the limit where the mass of the heavy quark approaches infinity, the spin of the heavy quark and the angular momentum of the light quark are separately

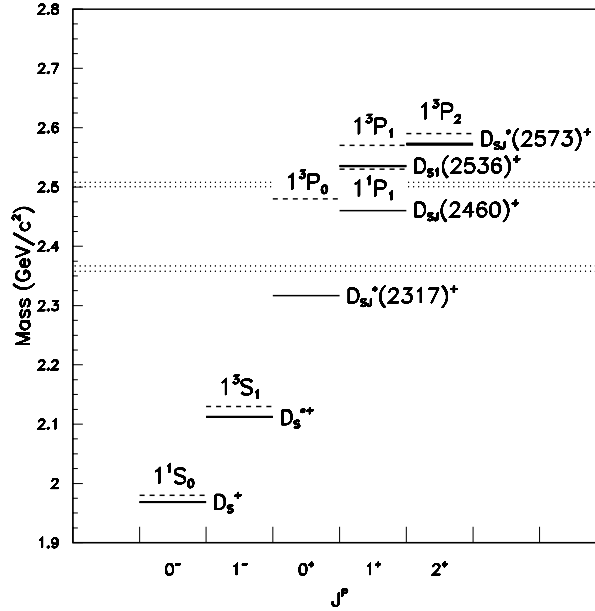


Figure 1: The  $S$ -wave and  $P$ -wave states of the  $c\bar{s}$  system. Dashed lines indicate the theoretical predictions of Godfrey and Isgur <sup>5)</sup>, and solid lines indicate the measured values. The dotted lines mark, from top to bottom, the  $D^{*+}K^0$ ,  $D^{*0}K^+$ ,  $D^+K^0$ , and  $D^0K^+$  thresholds. The spectroscopic notation used is  $n^{2s+1}L_J$ , where  $n$  is the principal quantum number,  $s$  is the total spin,  $L$  is the orbital angular momentum, and  $J$  is the total angular momentum. Note that since  $s$  is not a good quantum number, the  $1^3P_1$  and  $1^1P_1$  states can mix.

conserved by the strong interaction. This heavy-quark symmetry (HQS) is approximately true in the case of a heavy quark of finite mass and greatly simplifies QCD calculations.

These theoretical considerations have met with reasonable success in predicting the properties of the  $S$ -wave and  $P$ -wave  $j_l = 3/2$  states of the  $c\bar{s}$  system <sup>4)</sup>. The  $P$ -wave  $j_l = 1/2$  states were expected to be broad and to decay strongly to isospin-conserving  $DK$  and  $D^*K$  final states. The observation of two narrow states decaying to  $D_s^+\pi^0$  and  $D_s^{*+}\pi^0$  is therefore surprising. As Fig. 1 indicates, however, if the observed states are indeed the  $j_l = 1/2$  doublet, their unexpectedly low masses guarantee their small widths by closing the strong-decay channels. The masses of the new states are significantly

below potential-model expectations <sup>5, 7)</sup> and are nearly the same as their  $c\bar{u}$  counterparts recently observed by Belle <sup>8)</sup>.

## 2.2 Experimental Details

Following the initial observations by BaBar and CLEO, BaBar confirmed the  $D_{sJ}(2460)^+$  result of CLEO <sup>9)</sup>, and Belle reconstructed both particles in exclusive decays of the type  $B \rightarrow \bar{D}D_{sJ}$  <sup>10)</sup>. Belle further observed the  $D_{sJ}(2460)^+$  in its  $D_s^+\gamma$  and  $D_s^+\pi^+\pi^-$  final states. The masses measured for  $D_{sJ}^*(2317)^+$  and  $D_{sJ}(2460)^+$  by the three groups are listed in Table 1.

Table 1: *The  $D_{sJ}$  masses as measured by BaBar, Belle, and CLEO. Here and throughout, whenever two errors are quoted for a measurement, the first is statistical and the second systematic.*

	$D_{sJ}^*(2317)^+$	$D_{sJ}(2460)^+$
BaBar	$2317.3 \pm 0.4 \pm 0.8 \text{ MeV}/c^2$	$2458.0 \pm 1.0 \pm 1.0 \text{ MeV}/c^2$
Belle	$2317.2 \pm 0.5 \pm 0.9 \text{ MeV}/c^2$	$2456.5 \pm 1.3 \pm 1.3 \text{ MeV}/c^2$
CLEO	$2318.5 \pm 1.2 \pm 1.1 \text{ MeV}/c^2$	$2463.1 \pm 1.7 \pm 1.2 \text{ MeV}/c^2$

For the decays  $D_{sJ}^*(2317)^+ \rightarrow D_s^+\pi^0$  and  $D_{sJ}(2460)^+ \rightarrow D_s^{*+}\pi^0$  to conserve parity, the spin-parity of  $D_{sJ}^*(2317)^+$  must be natural (i.e.  $J^P = 0^+, 1^-, 2^+, \dots$ ) and  $D_{sJ}(2460)^+$  unnatural (i.e.  $J^P = 0^-, 1^+, 2^-, \dots$ ). The narrow width of the  $D_{sJ}(2460)^+$  in spite of its mass above  $DK$  threshold is consistent with an unnatural  $J^P$  assignment. The observation of  $D_{sJ}(2460)^+ \rightarrow D_s^+\gamma$  excludes  $J = 0$  for  $D_{sJ}(2460)^+$ , and Belle's angular analysis of this decay further rules out  $J = 2$  while being consistent with  $J = 1$ . The decay  $D_{sJ}(2460)^+ \rightarrow D_s^+\pi^+\pi^-$  strengthens these conclusions by eliminating  $J^P = 0^+$ .

If the interpretation of the new particles as the  $j_l = 1/2$  doublet of the  $c\bar{s}$  system is correct, certain decay modes that violate parity and angular-momentum conservation should not be seen. Table 2 shows several allowed and forbidden final states, along with measured branching ratios or upper limits.

Setting aside the low masses, the experimental evidence is entirely consistent with the interpretation of the new particles as the  $j_l = 1/2$  doublet of the P-wave  $c\bar{s}$  system.

Table 2: Measured branching ratios and upper limits at 90% C.L. for various possible  $D_{sJ}^*(2317)^+$  and  $D_{sJ}(2460)^+$  final states. Whether a given decay is allowed (A) or forbidden (F) by parity and angular-momentum conservation is also indicated. Values are given as a fraction of the branching ratio to  $D_s^+\pi$  and  $D_s^{*+}\pi^0$  for  $D_{sJ}^*(2317)^+$  and  $D_{sJ}(2460)^+$ , respectively.

Decay Mode	$D_{sJ}^*(2317)^+$		$D_{sJ}(2460)^+$	
$D_s^+\pi^0$	A	$\equiv 1.000$	F	Belle: $< 0.21$
$D_s^{*+}\pi^0$	F	CLEO: $< 0.11$	A	$\equiv 1.000$
$D_s^+\gamma$	F	BaBar: not observed CLEO: $< 0.052$ Belle: $\leq 0.05$	A	CLEO: $< 0.49$ Belle: $0.55 \pm 0.13 \pm 0.08$
$D_s^{*+}\gamma$	A	BaBar: not observed CLEO: $< 0.059$ Belle: $\leq 0.18$	A	CLEO: $< 0.16$ Belle: $\leq 0.31$
$D_s^+\pi^+\pi^-$	F	CLEO: $< 0.019$ Belle: $\leq 0.004$	A	CLEO: $< 0.08$ Belle: $0.14 \pm 0.04 \pm 0.02$
$D_s^+\gamma\gamma$	A	BaBar: not observed	A	–
$D_{sJ}^*(2317)^+\gamma$	–	–	A	CLEO: $< 0.58$

### 2.3 Theoretical Interpretations

Numerous theories have been proposed to explain the low masses of the new particles. These include attempts to improve standard HQET or quark-model arguments <sup>11)</sup>, as well as more exotic proposals such as a  $DK$  meson molecule, a  $D\pi$  atom, or a  $cq\bar{q}$  state <sup>12)</sup>. One possible explanation may be that the  $c\bar{s}$  mass spectrum is distorted as a result of coupling to the  $D_{(s)}^{(*)}K$  threshold <sup>13)</sup>. Searching for radiative decays may help distinguish between  $c\bar{s}$  and  $DK$ -molecule interpretations. <sup>14)</sup> Since the low masses may be symptomatic of a serious inadequacy of the current theory, it is important that more work be done to further specify the properties of the new particles.

## 3 The $X(3872)$ Particle

### 3.1 The $c\bar{c}$ System

The decay of the  $X(3872)$  to  $J/\psi\pi^+\pi^-$  suggests that it may be a  $c\bar{c}$  state. As the spectrum in Fig. 2 indicates, there are numerous  $c\bar{c}$  states that have not

yet been observed. In particular, the  $h_c(1^1P_1)$ ,  $\eta_{c2}(1^1D_2)$ , and  $\psi_2(1^3D_2)$  are expected to lie below  $D\bar{D}^*$  threshold and thus be narrow.

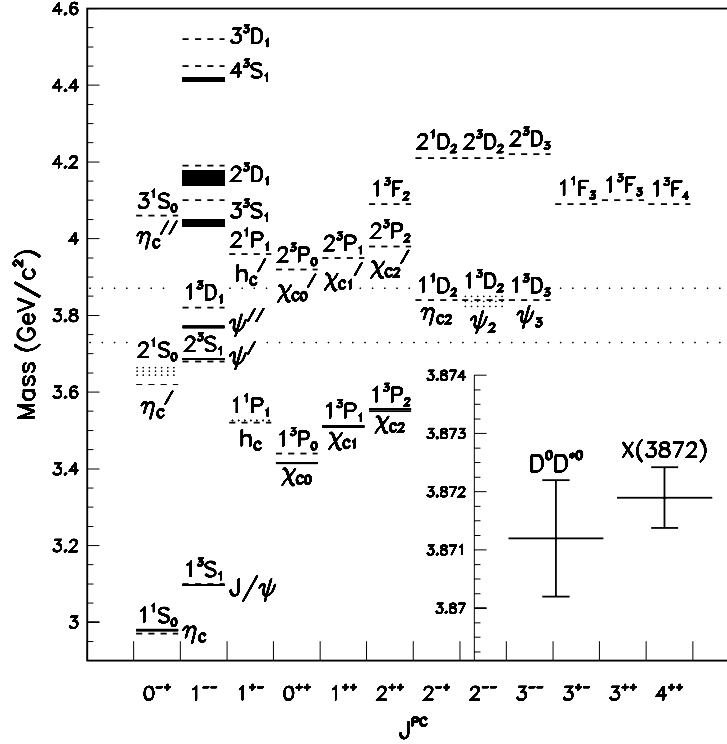


Figure 2: The  $c\bar{c}$  spectrum. Dashed lines indicate the theoretical predictions of Godfrey and Isgur <sup>5)</sup>, and solid lines indicate measured values according to the PDG <sup>15)</sup>. Measurements that need confirmation are indicated by dotted lines. The two dotted lines across the plot mark the  $D^0\bar{D}^0$  and  $D^0\bar{D}^{*0}$  thresholds. The inset compares the X(3872) mass (obtained by adding the statistical and systematic errors of each experiment in quadrature and calculating a weighted average of the four experiments) to the  $D^0\bar{D}^{*0}$  threshold. The spectroscopic notation is the same as that of Fig. 1.

### 3.2 Experimental Details

Belle's observation of the X(3872) has been confirmed by CDF <sup>16)</sup>, DØ <sup>17)</sup>, and BaBar <sup>18)</sup>. The masses measured are shown in Table 3.

Table 3: The  $X(3872)$  masses measured by BaBar, Belle, CDF II, and DØ.

	$X(3872)$
Belle	$3872.0 \pm 0.6 \pm 0.5 \text{ MeV}/c^2$
CDF	$3871.3 \pm 0.7 \pm 0.4 \text{ MeV}/c^2$
DØ	$3871.8 \pm 3.1 \pm 3.0 \text{ MeV}/c^2$
BaBar	$3873.4 \pm 1.4 \text{ MeV}/c^2$

The narrow width of the  $X(3872)$  despite its mass above  $D\bar{D}$  threshold suggests that its decay to  $D\bar{D}$  may be forbidden. Assuming that this is the case, all  $c\bar{c}$  states with small  $J$  and natural  $J^P$  may be ruled out<sup>19)</sup>. If known particles as well as states with predicted masses significantly different from that of the  $X(3872)$  are also excluded, six possibilities remain:  $\eta_c''(3^1S_0)$ ,  $\chi'_{c1}(2^3P_1)$ ,  $\eta_{c2}(1^1D_2)$ ,  $h'_c(2^1P_1)$ ,  $\psi_2(1^3D_2)$ , and  $\psi_3(1^3D_3)$ .

The first three of these states have even  $C$ -parity, while the remaining three have odd  $C$ -parity. A measurement of the  $C$ -parity of the  $X(3872)$  can thus be used to further reduce the number of possibilities. If the  $X(3872)$  is a  $c\bar{c}$  state with even (odd)  $C$ -parity, then  $X(3872) \rightarrow J/\psi\rho^0$  should be allowed (forbidden), and  $X(3872) \rightarrow J/\psi\pi^0\pi^0$  should be forbidden (allowed). The relative branching ratios of the  $X(3872)$  to  $J/\psi\pi^+\pi^-$  and  $J/\psi\pi^0\pi^0$  can also distinguish between a  $c\bar{c}$  state and something more exotic<sup>20, 21)</sup>. Belle has noted that the  $\pi^+\pi^-$  invariant-mass distribution tends to peak near the kinematic boundary, which is near the  $\rho^0$  mass. This suggests that the pion pair may come from a  $\rho^0$ , although a similar tendency to crowd the kinematic boundary is also seen in the dipion mass distribution of  $\psi' \rightarrow J/\psi\pi^+\pi^-$ . The observation is far from conclusive, and further study is required.

The  $\psi_2(1^3D_2)$  may be easy to observe at B-factories via its  $J/\psi\pi^+\pi^-$  final state<sup>22)</sup>. If the  $X(3872)$  is the  $\psi_2(1^3D_2)$ , however, its branching ratio to  $\chi_{c1}\gamma$  should be several times greater than its branching ratio to  $J/\psi\pi^+\pi^-$ <sup>23)</sup>. Belle has placed an upper limit on the ratio of partial widths to  $\chi_{c1}\gamma$  and  $J/\psi\pi^+\pi^-$  of 0.89 at 90% C.L.<sup>3)</sup>. Similarly, the  $\psi_3(1^3D_3)$  is expected to have an appreciable branching ratio to  $\chi_{c2}\gamma$ <sup>20)</sup>. Belle has placed an upper limit on the ratio of partial widths to  $\chi_{c2}\gamma$  and  $J/\psi\pi^+\pi^-$  of 1.1 at 90% C.L.<sup>24)</sup>.

The  $\eta_c''(3^1S_0)$  appears too large in mass and width to be the  $X(3872)$ . The  $\eta_{c2}(1^1D_2)$ ,  $\chi'_{c1}(2^3P_1)$  and  $h'_c(2^1P_1)$  are not expected to have significant

branching fractions to  $J/\psi\pi^+\pi^-$  (20). The  $h'_c(2^1P_1)$  is also ruled out by Belle's angular analysis of  $B^+ \rightarrow K^+J/\psi\pi^+\pi^-$ , the results of which are inconsistent with a  $J^{PC}$  assignment of  $1^{+-}$  (24).

These considerations are far from conclusive; in particular, coupling to open-charm channels can distort potential-model predictions for states above charm threshold (25). Nevertheless, there appears to be no obvious  $c\bar{c}$  candidate for the  $X(3872)$ .

### 3.3 Theoretical Interpretations

One striking coincidence is the overlap between the mass of the  $X(3872)$  and the  $D^0D^{*0}$  threshold (see Fig. 2). This mass degeneracy has led to speculation that the  $X(3872)$  may be a lightly-bound  $D^0\bar{D}^{*0}$  molecule (20, 21, 26). Such meson molecules were predicted as early as the 1970s (27).

It is also possible that the  $X(3872)$  is a  $c\bar{c}g$  hybrid state (28, 29). Such a state would be expected to have a narrow width and a large branching ratio to  $J/\psi\pi^+\pi^-$ , but a mass higher than 4 GeV.

## 4 Conclusion

The observation of the  $D_{sJ}^*(2317)^+$ ,  $D_{sJ}(2460)^+$ , and  $X(3872)$  have challenged the predictivity of current models of meson spectroscopy. While these new states may require no more than minor alterations to the theory, they may also be exotic particles that will lead to new breakthroughs in meson spectroscopy. Further experimental results on all three states will be important in resolving the situation.

## References

1. BaBar Collaboration, B. Aubert *et al.*, Phys. Rev. Lett. **90**, 242001 (2003).
2. CLEO Collaboration, D. Besson *et al.*, Phys. Rev. D **68**, 032002 (2003).
3. Belle Collaboration, S.K. Choi *et al.*, Phys. Rev. Lett. **91**, 262001 (2003).
4. J. Bartelt and S. Shukla, Ann. Rev. Nucl. Part. Sci. **45**, 133 (1995).
5. S. Godfrey and N. Isgur, Phys. Rev. D **32**, 189 (1985).

6. N. Isgur and M.B. Wise, Phys. Lett. B **232**, 113 (1989).
7. A. De Rujula, H. Georgi, and S.L. Glashow, Phys. Rev. Lett. **37**, 785 (1976); S. Godfrey and R. Kokoski, Phys. Rev. D **43**, 1679 (1991); N. Isgur and M.B. Wise, Phys. Rev. Lett. **66**, 1130 (1991); M. Di Pierro and E. Eichten, Phys. Rev. D **64**, 114004 (2001).
8. Belle Collaboration, K. Abe *et al.*, Phys. Rev. D **69**, 112002 (2004).
9. BaBar Collaboration, B. Aubert *et al.*, Phys. Rev. D **69**, 031101 (2004).
10. Belle Collaboration, P. Krokovny *et al.*, Phys. Rev. Lett. **91**, 262002 (2003); Belle Collaboration, Y. Mikami *et al.*, Phys. Rev. Lett. **92**, 012002 (2004).
11. W.A. Bardeen, E.J. Eichten, and C.T. Hill, Phys. Rev. D **68**, 054024 (2003); R.N. Cahn and J.D. Jackson, Phys. Rev. D **68**, 037502 (2003); P. Colangelo and F. De Fazio, Phys. Lett. B **570**, 180 (2003).
12. T. Barnes, F.E. Close, and H.J. Lipkin, Phys. Rev. D **68**, 054006 (2003); A.P. Szczepaniak, Phys. Lett. B **567**, 23 (2003); H. Cheng and W. Hou, Phys. Lett. B **566**, 193 (2003).
13. E. van Beveren and G. Rupp, Phys. Rev. Lett. **91**, 012003 (2003); T.E. Browder, S. Pakvasa, and A.A. Petrov, Phys. Lett. B **578**, 365 (2004).
14. S. Godfrey, Phys. Lett. B **568**, 254 (2003).
15. Particle Data Group, S. Eidelman *et al.*, Phys. Lett. B **592**, 1 (2004).
16. CDF II Collaboration, D. Acosta *et al.*, Phys. Rev. Lett. **93**, 072001 (2004).
17. DØ Collaboration, V.M. Abazov *et al.*, hep-ex/0405004; submitted to Phys. Rev. Lett.
18. BaBar Collaboration, B. Aubert *et al.*, hep-ex/0406022; submitted to Phys. Rev. Lett.
19. S. Pakvasa and M. Suzuki, Phys. Lett. B **579**, 67 (2004).
20. T. Barnes and S. Godfrey, Phys. Rev. D **69**, 054008 (2004).
21. N.A. Törnqvist, Phys. Lett. B **590**, 209 (2004).

22. P. Ko, J. Lee, and H.S. Song, Phys. Lett. B **395**, 107 (1997).
23. E.J. Eichten, K. Lane, and C. Quigg, Phys. Rev. Lett. **89**, 162002 (2002).
24. Talk presented by S.L. Olsen (Belle Collaboration) at the 8th International Workshop on Meson Production, Properties and Interaction (MESON2004), 4-8 June 2004, Krakow, Poland.
25. E.J. Eichten, K. Lane, and C. Quigg, Phys Rev. D **69**, 094019 (2004); E.J. Eichten, *et al.*, Phys. Rev. D **21**, 203 (1980).
26. E.S. Swanson, Phys.Lett. B **588**, 189 (2004).
27. See, for example, E. Eichten *et al.*, Phys. Rev. Lett. **34**, 369 (1975); M. Bander *et al.*, Phys. Rev. Lett. **36**, 695 (1976); A. De Rujula, H. Georgi, and S.L.Glashow, Phys. Rev. Lett **38**, 317 (1977); R. Zhang *et al.*, Phys. Rev. D **65**, 096005 (2002).
28. See S. Godfrey and J. Napolitano, Rev. Mod. Phys. **71**, 1411 (1999) and references therein.
29. See F.E. Close and P.R. Page, Phys.Lett. B **578**, 119 (2004) for an evaluation of the different interpretations of the  $X(3872)$ .

## CHARMED MESON SPECTROSCOPY

Robert K. Kutschke  
*Fermi National Accelerator Lab, P.O. Box 500, Batavia, IL 60510, USA*

### ABSTRACT

In the two years since HQL02, the long sought  $j_\ell = 1/2$  states have been observed. In the charmed non-strange sector, these states have the expected properties but, in the charmed strange sector, the states have masses below threshold for the otherwise dominant decay modes, allowing their observation in suppressed modes. Improved measurements of the masses and widths of the well established P-wave charm states have also been published.

### 1 Introduction

These proceedings will discuss new results in the P-wave sector of the  $c\bar{q}$  systems, where  $q$  is one of  $u$ ,  $d$  or  $s$ . The spectroscopy of these mesons is described by coupling of the spins of the quark and anti-quark,  $S_c$  and  $S_{\bar{q}}$ , with the orbital angular momentum,  $L$ , between the quark and anti-quark. When  $L = 1$  this coupling produces 4 states, with  $J^P = \{2^+, 1^+, 1^+, 0^+\}$ .

Until recently, all of the measured properties of the P-wave sector were well described by models which exhibit Heavy Quark Symmetry, HQS. In the limit that the mass of the charmed quark is  $\gg \Lambda_{QCD}$ , the spin of the charmed quark decouples from the dynamics, leaving the total angular momentum of the light quark,  $j_\ell = S_{\bar{q}} + L$ , as an effective quantum number. In this limit, the  $c\bar{u}$  and  $c\bar{d}$  P-wave states are grouped into two doublets. One doublet, with  $j_\ell = 3/2$ , has members with  $J^P = \{2^+, 1^+\}$ ; these states decay to  $D^{(*)}\pi$  in a D-wave and have natural widths of order 20 MeV. The other doublet, with  $j_\ell = 1/2$  has members with  $J^P = \{1^+, 0^+\}$ ; these states decay to  $D^{(*)}\pi$  in an S-wave and have natural widths of order a few hundred MeV. In the following the two  $J^P = 1^+$  states will be denoted as  $D_1$  and  $D_1(j_\ell = 1/2)$ , where the first notation is for the state with  $j_\ell = 3/2$ . To obtain the properties of the physical states, the finite mass of the charmed quark is introduced as a small perturbation on the HQS states.

The states with  $j_\ell = 3/2$  are well established and have the predicted properties. The states with  $j_\ell = 1/2$  have only recently been observed and are the topic of these proceedings. A more detailed discussion of HQS and a review of the data up to 10 years ago can be found in reference <sup>1)</sup>. The experimental results reviewed in these proceedings are the first significant new results since that time so the reference remains relevant.

Most models predicted a similar pattern for the  $c\bar{s}$  mesons and the  $j_\ell = 3/2$  states do indeed follow the pattern. There was, however, a model <sup>2)</sup> that predicted a rather different picture for the  $j_\ell = 1/2$   $c\bar{s}$  mesons. In this model, which combines chiral symmetry with HQS, the  $j_\ell = 1/2$   $c\bar{s}$  mesons were predicted to lie below threshold for decay to  $D^{(*)}K$ . The decay modes available in this case are:  $D_s^{(*)}\pi^0$ , which is isospin violating,  $D_s^{(*)}\pi\pi$ , which is is OZI suppressed, and  $D_s^{(*)}\gamma$ , which are electromagnetic transitions. All of these decay modes have small partial widths of, at most, a few MeV. Refer to the transparencies of this talk <sup>3)</sup> for a bibliography of recent theoretical work on the  $j_\ell = 1/2$   $D_s$  states.

## 2 P-wave Charmed Non-Strange Mesons

There are two new measurements in this sector. The FOCUS collaboration has presented measurements <sup>4)</sup> using the traditional method of looking at the inclusive  $D^+\pi^-$  and  $D^0\pi^+$  invariant mass spectra. The second set of new

measurements comes from the BELLE collaboration <sup>5)</sup>, who have pioneered a new technique, the measurement of excited charm resonances in the Dalitz plots of the decays  $B \rightarrow D\pi\pi$  and  $B \rightarrow D^*\pi\pi$ .

In the  $D\pi$  mass spectra presented by FOCUS one expects contributions from five processes plus combinatoric background. The five processes are:  $D_2^* \rightarrow D\pi$ , feed-down from  $D_2^* \rightarrow D^*\pi$ , feed-down from  $D_1(2420) \rightarrow D^*\pi$ ,  $D_0^* \rightarrow D\pi$ , and feed-down from  $D_1(j_\ell = 1/2) \rightarrow D^*\pi$ . In the feed-down processes, the  $D^*$ 's decay to a  $D$  plus unobserved neutrals, giving a final state of  $D\pi$ . Because of the small  $Q$  values in these decay chains, the peaks from the feed-down processes suffer little kinematic broadening. In previous inclusive measurements, the first three processes, which give rise to narrow peaks, have been well established, but the final two processes, which produce broad peaks, could not be resolved above the combinatoric background.

Following the earlier experiments, the FOCUS collaboration first tried to fit their  $D\pi$  mass spectra without including the last two processes. Their experiment, however, has an order of magnitude higher statistics than previous experiments and, after trying many models of the combinatoric background, none was able to produce a good fit to their data. Inspection of the residuals of the fits suggested that the fit would be improved by introducing a contribution from a broad resonance. Such a contribution was parameterized using S-wave Breit-Wigner<sup>1</sup> with a free mass, width and yield. This contribution is intended to model the sum of the contributions from an unknown mixture of  $D_0^*$  and feed-down from the  $D_1(j_\ell = 1/2)$ . When this term was added, the fit produced an acceptable  $\chi^2$ . However it was never possible to resolve separately contributions from the  $D_0^*$  and the  $D_1(j_\ell = 1/2)$ .

It has long been anticipated that the  $e^+e^-$  B-factory experiments would open a new window on charm spectroscopy through the analysis of the Dalitz plots in  $B$  decay. The first hint at the power of this technique was presented by CLEO <sup>6)</sup>, in which they used a partial reconstruction technique to perform a multi-dimensional fit to the decay  $B^- \rightarrow D^{*+}\pi^-\pi^-$ .

BELLE has presented the first example of this technique using full reconstruction of the final state. They presented a fit to the Dalitz plot of the decay

---

<sup>1</sup>This work does not give any information about the  $J^P$  of the broad states. The choice of an S-wave Breit-Wigner was driven by the expectation that any broad peak would be dominated by the  $D_0^*$ .

$B^- \rightarrow D^+ \pi^- \pi^-$  and a 4 dimensional fit to the decay  $B^- \rightarrow D^{*+} \pi^- \pi^-$ . A key component of their analysis is that the energy of the  $B$  mesons in the  $e^+e^-$  center-of-mass frame is fully determined and they require that the energy of their  $B$  candidates be consistent with this energy. This requirement removes the feed-down processes which complicate the FOCUS analysis. Compared with the FOCUS data, the BELLE data has an improved signal to background ratio, at the expense of signal yield.

The power of multi-dimensional fits is that interference among the contributing amplitudes gives rise to structures with distinctive shapes that are readily distinguished from backgrounds. For example the presence of the  $D_0^{*0}$  is established by observing its interference with the  $D_2^*$  in the  $D^+ \pi^- \pi^-$  Dalitz plot. Moreover these interference effects are powerful probes of the  $J^P$  of the intermediate states and BELLE establishes that the  $D_0^{*0}$  and  $D_1^0(j_\ell = 1/2)$  states do indeed have  $J^P = 0^+$  and  $J^P = 1^+$ , as expected. In neither fit does BELLE find a significant contribution from a constant amplitude; that is, the data are fully described by a sum of resonant contributions, including virtual processes via the  $D^*$  and  $B^*$ .

FOCUS and BELLE also presented new measurements of the parameters of the  $D_2^*$  mesons. These measurements have errors that are comparable to those of the previous world averages.

All of the masses and widths discussed above, along with the PDG 2002 averages and new world averages, are shown in figure 1. Inspection shows that the new results are consistent with the PDG 2002 values, albeit barely consistent in a few cases. It does seem that the new results do prefer broader widths for both the of the  $D_2^*$  charge states. Perhaps this indicates of a bias toward narrow widths in early, statistically weaker observations. Because the FOCUS measurements of the  $j_\ell = 1/2$  states are for an unknown mixture of the  $D_0^*$  and feed-down from the  $D_1(j_\ell = 1/2)$ , the author recommends that the best values for the properties of the  $D_0^{*0}$  are the BELLE results alone.

There are several reasons why the B decay results might differ systematically from the inclusive measurements. The line shape of the resonances is a matrix element squared multiplied by a phase-space factor. In the inclusive measurements it is difficult to write down the phase-space factor and it has always been ignored, motivated by the assumption that it varies only slowly over the region of interest. In  $B$  decays it is straightforward to write down

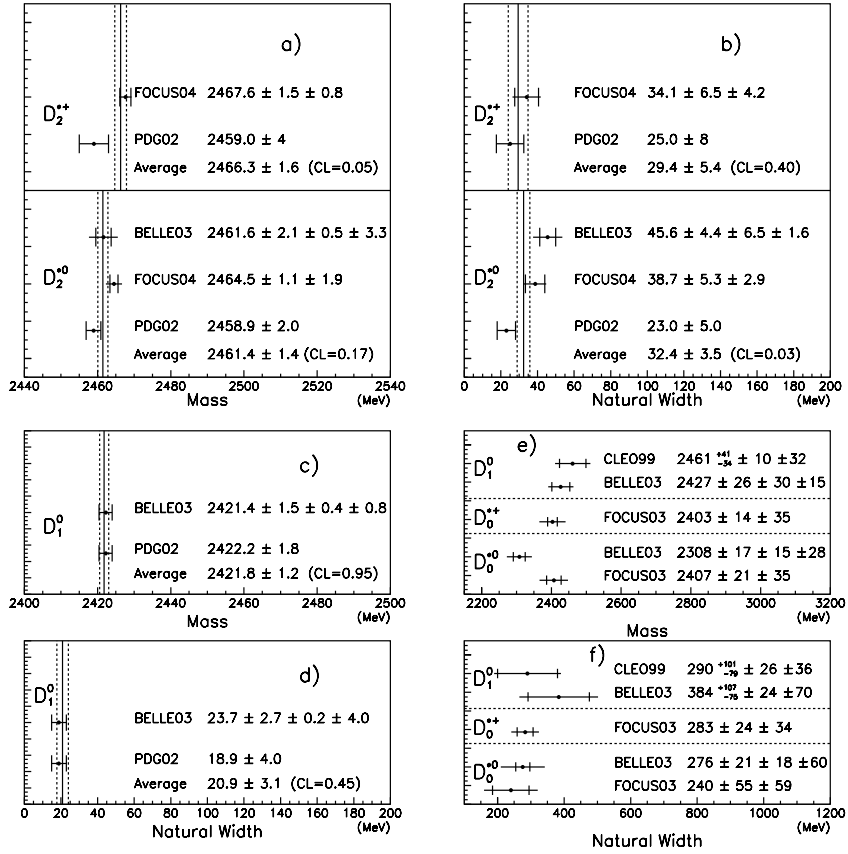


Figure 1: Masses and widths of charmed non-strange P-wave mesons. The first two errors are statistical and systematic. For BELLE the third error comes from the choice of contributions to the decay amplitude and for CLEO it comes from the parameterization of the strong phase. Parts a) through d) show the results for the well established  $D_2^*$  and  $D_1(2420)$  states. Parts e) and f) show the results for the newly observed broad  $D_1$  and  $D_0^*$  states. The averages are taken by the author; the CL notation gives the confidence level that the data are self consistent. As discussed in the text, no average is taken for the broad states and the BELLE results from the  $D_0^*$  should be preferred over the FOCUS ones.

the phase space factors and BELLE includes them. Presumably this is a small effect for the narrow states but an important effect for the broad states. A second difference is that the inclusive analyses always assume that the resonances are produced incoherently. While this is likely, is not certain.

The author looks forward to BaBar entering the field with Dalitz analyses of their B decays. He also looks forward to both B-factories presenting updated results with much larger datasets. In the longer term, both BTeV and LHC-b should contribute to charm spectroscopy through the Dalitz analysis of B decays.

### 3 P-wave Charmed Strange Mesons

In the charmed strange sector, the  $D_{s2}^*$  and the narrow  $D_{s1}(2536)$  have been well established for more than a decade. It was long presumed that the  $D_{s0}^*$  and the  $D_{s1}(j_\ell = 1/2)$  would lie above threshold for decay to  $DK$  and  $D^*K$ . In such a case this sector would look much like the non-strange sector, differing only in detail.

This picture was overthrown when the BaBar collaboration published the surprising observation of a new, narrow resonance at a mass of about 2317 MeV which decays to  $D_s\pi^0$  <sup>7)</sup>. Their paper also hinted at a second narrow resonance at a mass near 2456 MeV which decays to  $D_s^*\pi^0$ . Shortly afterward the first state was confirmed by CLEO <sup>8)</sup>, who also claimed a definite observation of the second state. Both BaBar and CLEO observed these states in continuum  $e^+e^-$  production. Both states were soon confirmed by BELLE, who observed them both in continuum  $e^+e^-$  <sup>9)</sup> and in B decay <sup>10)</sup>. BELLE observed new decay modes of the  $D_s(2456)$ , to  $D_s\gamma$  and  $D_s\pi^+\pi^-$ , and a new decay mode of one of the well established states,  $D_{s1}(2536) \rightarrow D_s\pi^+\pi^-$ . BaBar has since confirmed the  $D_s(2456)$  <sup>11)</sup>. Finally, FOCUS has observed the state at 2317 MeV in  $D_s\pi^0$ , which represents the first observation of either state outside of the  $e^+e^-$  <sup>12)</sup>. In the following these states will be referred to as the  $D_{s0}^*((2317))$  and the  $D_{s1}(2456)$ .

The analysis of the two states is more subtle than is hinted at by the previous paragraph. Consider the decay chain,  $D_{s1}(2456) \rightarrow D_s^*\pi^0$ ;  $D_s^* \rightarrow D_s\gamma$ . If the  $\gamma$  is missed and the state is reconstructed as  $D_s\pi^0$ , it produces a narrow feed-down peak in the  $D_s\pi^0$  mass spectrum at a mass very close to that of the  $D_{s0}^*(2317)$ . Now consider starting with the decay  $D_{s0}^*(2317) \rightarrow D_s\pi^0$ ,

adding a random photon, requiring that the  $D_s\gamma$  invariant mass fall within the experimental resolution on the  $D_s^*$  mass, and then plotting the  $D_s\gamma\pi^0$  invariant mass. This feed-up process will produce a narrow peak in the  $D_s^*\pi^0$  invariant mass spectrum at a mass close to that of the  $D_s(2456)$ . A typical mass peak in any of the BaBar, BELLE or CLEO analysis contains about 75% from the signal being looked for and about 25% from either the feed-up or feed-down background. The three experiments have developed different methods for unfolding the true signals from these backgrounds and all experiments get consistent results.

None of the experiments observe a non-zero natural width for these states and the best upper limit comes from BELLE <sup>9)</sup>,  $\Gamma(D_{s0}^*(2317)) < 4.6$  MeV and  $\Gamma(D_{s1}(2456)) < 5.5$  MeV, both at the 90% confidence level.

The quantum numbers of these states are already well constrained. The observation of  $D_{s1}(2456) \rightarrow D_s\gamma$ , forbids  $J = 0$  and the BELLE analysis of angular distributions in the decay  $B \rightarrow DD_{s1}(2456)$  prefers  $J = 1$  over  $J = 2$ . The decay  $D_{s1}(2456) \rightarrow D_s\pi^0$  is not observed, even though phase space favors it over  $D_s^*\pi^0$ . This is most easily explained if the  $D_s(2456)$  has  $J^P$  from the unnatural sequence,  $0^-, 1^+, 2^- \dots$ . So the spin parity assignment of  $J^P = 1^+$  is strongly preferred for the  $D_s(2456)$ . Because the  $D_s(2317)$  is observed to decay to two pseudo-scalars, and presuming that parity is conserved in its decay, the  $D_s(2317)$  must have  $J^P$  from the natural spin parity sequence,  $0^+, 1^-, 2^+ \dots$

#### 4 Summary and Conclusions

In the  $c\bar{u}$  and  $c\bar{d}$  sectors most of the  $j_\ell = 1/2$  states have been observed; only the  $D_1^+(j_\ell = 1/2)$  remains unobserved. These states have the properties predicted by HQS and the  $J^P$  quantum numbers are established using the multi-dimensional analysis presented by BELLE. The results from the old inclusive technique and the new exclusive technique agree with each other but, in a few cases, the agreement is only marginal. Perhaps this is an indication that small effects, which could be ignored in the past can no longer be ignored in high statistics, high precision experiments. The author looks forward to many years of new results in charm spectroscopy from the multi-dimensional analysis of B decays.

In the  $c\bar{s}$  sector both  $j_\ell = 1/2$  states have now been established. The  $D_{s1}(2456)$  has  $J^P = 1^+$  strongly favored while the  $D_{s0}^*(2317)$  is known to have

$J^P$  from the natural sequence, consistent with the expectation of  $0^+$ . Although many people considered the low masses of these states a surprise, if you accept the masses then all of the other properties of these states make sense. For example the narrow widths arise because only suppressed decay modes are kinematically allowed.

## 5 Acknowledgments

The author would like to thank the organizers of the conference for an exciting program, presented in comfortable and pleasant surroundings. He also thanks them for their patience in waiting for these proceedings.

## References

1. J. Bartelt and S. Shukla, *Ann. Rev. Nucl. Part. Sci.* **45**:133 (1995).
2. W.A. Bardeen and C.T. Hill, *Phys. Rev. D* **49**, 409 (1994). W.A. Bardeen, E.J. Eichten and C.T. Hill, *Phys. Rev. D* **68**:054024 (2003).
3. R.K. Kutschke, <http://charma.uprm.edu/hql04/particip.bymail/kutschke@fnal.gov/TAL-robert.k.kutschke.ppt>.
4. J.M. Link *et al* (FOCUS Collab.), *Phys. Lett.* **B586**:11 (2004).
5. K. Abe *et al* (BELLE Collab), *Phys. Rev.* **D69**:112002 (2004).
6. S. Anderson *et al* (CLEO Collab), Report CLEO CONF 99-6 (1999).
7. B. Aubert *et al* (BaBar Collab), *Phys. Rev. Lett.* **90**:242001 (2003).
8. D. Besson *et al* (CLEO Collab), *Phys. Rev. D* **68**:032002 (2003).
9. Y. Mikami *et al* (BELLE Collab), *Phys. Rev. Lett.* **92**:012002 (2004).
10. P. Krokovny *et al* (BELLE Collab), *Phys. Rev. Lett.* **91**:262002 (2003).
11. B. Aubert *et al* (BaBar Collab), *Phys. Rev. D* **69**:031101 (2004).
12. E.W. Vaandering, "Charmed Hadron Spectroscopy at FOCUS", In the Proceedings of the XXXIXth Rencontres de Moriond, hep-ex/0406044, (2004).





Frascati Physics Series Vol. XXXV (2004), pp. 455  
HEAVY QUARKS AND LEPTONS - San Juan, Puerto Rico, June 1-5, 2004

**IMPLICATIONS OF THE NEW RESULTS ON  $g-2$**

W. M. Morse

*BNL - Brookhaven National Laboratory, P.O. Box 5000, Upton, NY 11973-5000*

Written contribution not received



## MEASUREMENT OF THE TOTAL HADRONIC CROSS-SECTION AT $e^+e^-$ MACHINES

Ivan Logashenko

*Budker Institute of Nuclear Physics, Novosibirsk, 630090, Russia*  
*Boston University, Physics Department, Boston, MA 02215, USA*

### ABSTRACT

The current status of measurements of the cross-section  $e^+e^- \rightarrow hadrons$  at low energies ( $\sqrt{s} < 2$  GeV) is reviewed. Recent results of direct and ISR measurements are discussed.

### 1 Introduction

Measurement of the total cross-section  $e^+e^- \rightarrow hadrons$ , often expressed as the dimensionless ratio

$$R(s) = \frac{\sigma(e^+e^- \rightarrow hadrons)}{\sigma(e^+e^- \rightarrow \mu^+\mu^-)}, \quad (1)$$

has been an important topic of the high energy physics since early 70s.  $R(s)$  plays a special role in many high precision theoretical calculations of fundamental quantities such as the Higgs mass, the running QED and QCD coupling

constants,  $c$  and  $b$  quark masses. The most demanding current application for  $R(s)$  is the calculation of  $a_\mu$ , the anomalous magnetic moment of muon. The E821 experiment in BNL has measured the value of  $a_\mu$  to the 0.5 ppm precision <sup>1)</sup>. The SM prediction for the same value is known to 0.7 ppm, where the uncertainty is dominated by the knowledge of  $R(s)$  <sup>2)</sup>. The measured difference of 2-3 standard deviations between the experimental result and the theoretical value is on the edge of discovering forces beyond the Standard Model. This makes the improvement of the accuracy of  $R(s)$  determination very important.

The hadronic contribution to  $a_\mu$  is calculated via numerical integration of  $R(s)$  with the proper kernel function:

$$a_\mu^{had} = \left(\frac{\alpha m_\mu}{3\pi}\right)^2 \int_{4m_\pi^2} \frac{R(s)K(s)}{s^2} ds. \quad (2)$$

At high energies ( $\sqrt{s} > (5 - 10)$  GeV) the value of the integral can be calculated within the framework of pQCD with high precision. At lower energies the only source of  $R(s)$  is the experimental measurement of the cross-section  $e^+e^- \rightarrow hadrons$ . The energy region below 2 GeV gives by far the dominant contribution both to the value of the integral (2) and to its uncertainty. Moreover, it turns out that the systematic error of the measurements, not the statistical one, limits the final uncertainty.

In the following section we'll describe the on-going and near-future experiments focused on the high precision measurement of  $R(s)$  at  $\sqrt{s} < 2$  GeV. Measurements of  $R(s)$  at higher energies are described elsewhere <sup>3, 4)</sup>.

## 2 Measurement at Novosibirsk

The energy range  $0.36 < \sqrt{s} < 1.4$  GeV has been studied at the electron-positron collider VEPP-2M (Novosibirsk, Russia). Two experiments, the CMD-2 and the SND, started in 1992 and 1995, respectively, and continued up to 2000, when the collider was shut down. Two energy scans, covering the whole available energy range  $0.36 < \sqrt{s} < 1.4$  GeV with small steps were performed over these years. Measurement of  $R(s)$  was one of the major physics goals for both experiments.

In the VEPP-2M energy range the number of modes and the multiplicity of  $e^+e^- \rightarrow hadrons$  events are small, while the kinematic distributions for different modes are quite different. That makes an exclusive approach, where the

cross-section for each channel  $e^+e^- \rightarrow hadrons$  is measured independently with unique acceptance, radiative and other corrections, the only viable option. The inclusive approach, where the total cross-section  $e^+e^- \rightarrow hadrons$  is measured directly, becomes usable at  $\sqrt{s} > 2$  GeV<sup>3)</sup>. In the energy range under consideration the dominant contribution to  $R(s)$  comes from the  $e^+e^- \rightarrow \pi^+\pi^-$  mode. Above  $\sqrt{s} > 1$  GeV the contribution from  $e^+e^- \rightarrow 4\pi$  becomes important and, eventually, dominant. Other modes,  $e^+e^- \rightarrow 3\pi, KK$ , etc., give an important contribution at the narrow  $\omega$  and  $\varphi$  resonances.

The high precision measurement of the  $e^+e^- \rightarrow \pi^+\pi^-$  cross-section was performed at the CMD-2 detector. Design features of the detector allowed for a factor 2-3 reduction in the systematic error compared to the previous experiments in the same energy range. The results of the measurement in the energy range  $0.6 < \sqrt{s} < 1$  GeV were already published<sup>5, 6)</sup>. The analysis of much larger data set, covering the whole VEPP-2M energy range  $0.36 < \sqrt{s} < 1.4$  GeV, is in progress.

The analysis scheme is the following. Events with two tracks in the final state,  $e^+e^- \rightarrow e^+e^-, \mu^+\mu^-, \pi^+\pi^-$ , are selected simultaneously in the same fiducial volume. The background events, mainly from the cosmic background, are separated using the spatial distribution of the vertex. Then the three final states are separated with the help of the unbinned likelihood fit using either the momenta information (at energies  $\sqrt{s} < 0.6$  GeV) or the energy deposition information (at energies  $\sqrt{s} > 0.6$  GeV). The pion formfactor is calculated as follows:

$$|F_\pi|^2 = \frac{N_{\pi\pi}}{N_{ee}} \cdot \frac{\sigma(e^+e^- \rightarrow e^+e^-)}{\sigma(e^+e^- \rightarrow \pi^+\pi^-)|_{F_\pi=1}}, \quad (3)$$

where  $N_{ee, \pi\pi}$  are the numbers of the corresponding final states detected and  $\sigma(e^+e^- \rightarrow e^+e^-, \pi^+\pi^-)$  are the calculated detection cross-sections, which include all the acceptance and radiative corrections. The cross-section for the  $2\pi$  final state is calculated for point-like pions ( $F_\pi = 1$ ). Since muons and pions cannot be separated by their energy deposition, at  $\sqrt{s} > 0.6$  GeV the ratio  $N_{\mu\mu}/N_{ee}$  was fixed in the fit to the value calculated within the QED with acceptance and radiative corrections taken into account. At energies  $\sqrt{s} < 0.6$  GeV all three final states are separated, therefore, in addition to the  $e^+e^- \rightarrow \pi^+\pi^-$  cross-section, the  $e^+e^- \rightarrow \mu^+\mu^-$  cross-section is also measured, providing an additional consistency test. The ratio  $(N_{\mu\mu}/N_{ee}) \cdot (\sigma_{ee}/\sigma_{\mu\mu})$  is shown in Fig. 1. The experimental value ( $0.989 \pm 0.015$ ) is consistent with the expected value

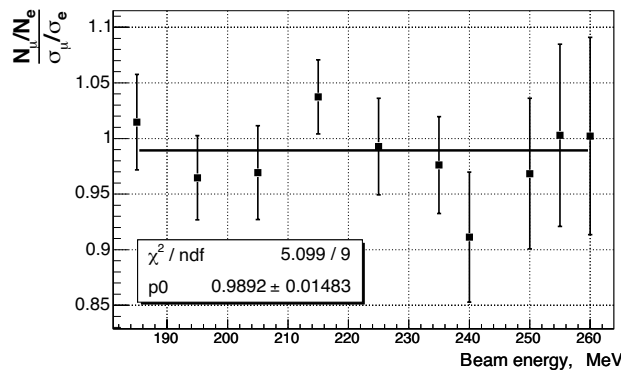


Figure 1: Ratio  $(N_{\mu\mu}/N_{ee}) \cdot (\sigma_{ee}/\sigma_{\mu\mu})$ , measured at CMD-2. The average value,  $0.989 \pm 0.015$ , is consistent with the expected value of 1.

of 1 within 0.8 statistical deviation.

The hadronic cross-section used for the calculation of  $R(s)$  and the hadronic cross-section used to extract parameters of the resonances are two different entities. The first is the “bare” one, although the final state radiation (FSR) is considered as apart of the cross-section; the latter is the “dressed” one, but the FSR effects should be excluded. Therefore, for the purpose of the pion formfactor measurement, the radiative corrections to the  $e^+e^- \rightarrow \pi^+\pi^-$  cross-section take into account the initial and the final state radiation, but not the vacuum polarization (VP). When  $R(s)$  is calculated, the “bare” cross-section is calculated from the “dressed” one by applying corrections for VP and FSR.

The cross-sections of other hadronic modes are calculated in the following way:

$$\sigma_f = \frac{N_f - N_b}{L \cdot (1 + \delta_f) \cdot \varepsilon_f}, \quad (4)$$

where  $N_f$  is the number of detected events of a particular final state,  $N_b$  is the number of background events,  $L$  is the luminosity,  $\delta_f$  is the radiative correction and  $\varepsilon_f$  is the detection efficiency. The luminosity is measured using the large angle Bhabha scattering with the systematic precision of 1-3%. The radiative correction takes into account the effects of the initial state radiation. The typical systematic uncertainty of the calculation is 1%. The detection effi-

ciency is calculated with the help of Monte-Carlo simulation, and its systematic uncertainty varies between 2% and 10% for different final states.

The main cross-sections measured at VEPP-2M are listed in Table 1 and are shown in Fig. 2. The data analysis is still under way, therefore some of the results are preliminary.

Table 1: The cross-sections  $e^+e^- \rightarrow hadrons$ , measured at VEPP-2M with CMD-2 and SND detectors. Some results are preliminary. References to the published results are shown in the third column.

Mode	Systematic error	References
$e^+e^- \rightarrow \pi^+\pi^-$	0.6%–5% (0.6% at $\rho$ -meson)	5), 6)
$e^+e^- \rightarrow 3\pi$	1.3%–5% (1.3% at $\omega$ -meson)	7), 8)
$e^+e^- \rightarrow 4\pi$	5%–10%	9), 10)
$e^+e^- \rightarrow K^+K^-$	3%–6%	11)
$e^+e^- \rightarrow K_S K_L$	1.7%–8% (1.7% at $\varphi$ -meson)	6), 11), 12)

The VEPP-2M collider was decommissioned in 2000 to prepare the experimental hall for the new collider, VEPP-2000<sup>13)</sup>. Direct high-precision measurement of the  $e^+e^- \rightarrow hadrons$  cross-section up to  $\sqrt{s} < 2$  GeV is one of its main goals. The CMD-3 and the upgraded SND detectors are expected to start data taking in 2006-2007.

### 3 Radiative return experiments

In addition to the direct measurements there were indirect measurements of  $e^+e^- \rightarrow hadrons$  cross-sections at  $e^+e^-$  colliders. It is possible to connect the vector spectral functions of hadronic  $\tau$  decays with the isovector part of  $e^+e^- \rightarrow 2\pi, 4\pi$  cross-sections. The large  $\tau$  data set collected by ALEPH, CLEO and OPAL allowed for the high precision measurements of these cross-sections from the threshold up to 1.8 GeV. There is significant discrepancy between these results and the direct measurements, unexplained at the moment. The details of comparison are described elsewhere<sup>14)</sup>.

The radiative return is another approach to a measurement of the  $e^+e^- \rightarrow hadrons$  cross-section at  $e^+e^-$  factories, complementary to the traditional en-

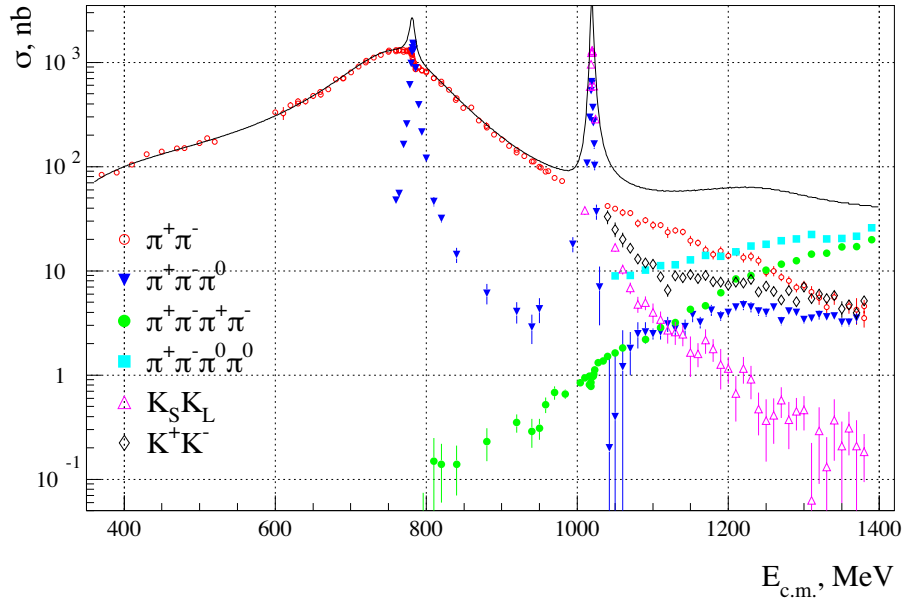


Figure 2: The cross-sections of different modes  $e^+e^- \rightarrow \text{hadrons}$ , measured at CMD-2. The line represents the total cross-section  $e^+e^- \rightarrow \text{hadrons}$ .

ergy scan<sup>15)</sup>. In this new method one measures the distribution of the invariant mass of the hadronic system in  $e^+e^- \rightarrow \gamma + \text{hadrons}$ , where a photon is radiated by the initial state electrons. The cross-section  $\sigma(e^+e^- \rightarrow \text{hadrons})$  is then calculated as:

$$\sigma(e^+e^- \rightarrow \text{hadrons}) \cdot H(M_{\text{hadrons}}^2) = M_{\text{hadrons}}^2 \cdot \frac{d\sigma(e^+e^- \rightarrow \gamma + \text{hadrons})}{dM_{\text{hadrons}}^2}. \quad (5)$$

The radiator function  $H(M_{\text{hadrons}}^2)$  is obtained from theory.

Two reasons make this approach promising at the particle factories. First, it allows to measure the cross-section in the wide energy range while the collider stays at single energy. This is particularly important at the factories designed to operate in the narrow energy range. Second, the high luminosity of the factories allows to overcome  $O(\alpha)$  suppression due to a requirement for the ISR photon in the final state.

The KLOE collaboration has recently announced the first results of the

$e^+e^- \rightarrow \pi^+\pi^-$  cross-section measurement using the ISR approach<sup>16)</sup>. The c.m. energy for the DAFNE  $\varphi$ -factory is 1.02 GeV, which makes the ISR photon relatively soft. In this case the FSR presents significant background to the main, ISR, process. In order to reduce its contribution, the analysis is restricted to events with low-angle, undetected ISR photons ( $\Theta_\gamma < 15^\circ$  or  $\Theta_\gamma > 165^\circ$ ). This and other kinematic restrictions limit the measurement of  $\sigma(e^+e^- \rightarrow \pi^+\pi^-)$  at KLOE to  $0.35 < s < 0.95$  GeV<sup>2</sup>.

The statistical uncertainty of the KLOE measurement is negligible. The total systematic uncertainty is 1.3%, with main contributions from the experimental technique (0.9%), the luminosity measurement (0.6%) and the calculation of the radiator function (0.5%). The comparison of the KLOE and CMD-2 results is shown in Fig. 3. While the contributions to the dispersion integral (2) from two data sets are consistent, the differential cross-sections differ beyond the claimed systematic errors. This discrepancy is not yet understood.

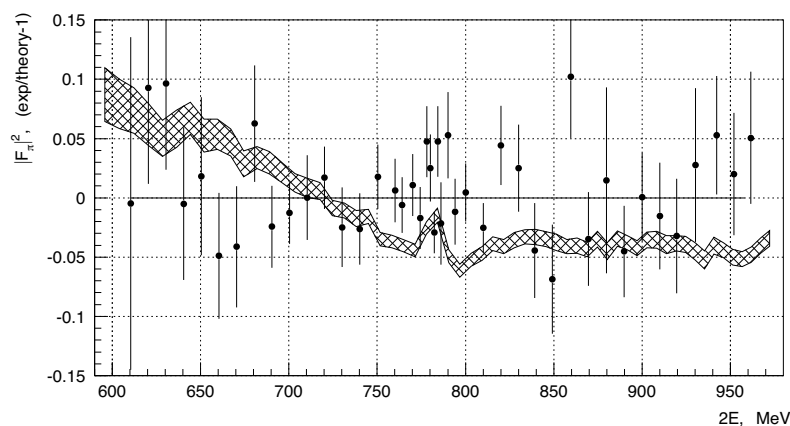


Figure 3: Comparison of the pion formfactor measured at CMD-2 and KLOE. The quantity shown is  $|F_\pi|^2(\text{exp.})/|F_\pi|^2(\text{theory}) - 1$ , where  $|F_\pi|^2(\text{theory})$  is the fit to the CMD-2 data. Data points show the CMD-2 data, the hatched corridor represents the KLOE results. Only statistical errors are shown. The CMD-2 data are corrected for the vacuum polarization.

The BaBar collaboration actively pursues the measurement of  $\sigma(e^+e^- \rightarrow \text{hadrons})$  at low  $s$  using ISR approach<sup>17)</sup>. There are two significant differences

between BaBar and KLOE techniques. First, the c.m. energy for the PEP-II collider is 10.58 GeV, while the interesting energy range for the cross-section measurement starts at the  $2\pi$  threshold. That makes the ISR photon very hard and FSR negligible for most hadronic states. Unlike the KLOE approach, the ISR photon is detected and is well separated from the hadronic state. Second, in BaBar analysis the  $e^+e^- \rightarrow \mu^+\mu^-\gamma$  is used as the monitoring process. The cross-section is calculated as:

$$\sigma(e^+e^- \rightarrow \text{hadron}) = \frac{N(\text{hadron} + \gamma) \cdot \varepsilon_{\mu\mu}(1 + \delta_{FSR}^{\mu\mu})}{N(\mu\mu\gamma) \cdot \varepsilon_{\text{hadron}}(1 + \delta_{FSR}^{\text{hadron}})} \sigma(e^+e^- \rightarrow \mu^+\mu^-), \quad (6)$$

where  $N$  is the number of detected events,  $\varepsilon$  is the detection efficiency and  $\delta_{FSR}$  is the correction for the final state radiation. In this approach many effects, such as the vacuum polarization, the radiative correction to the initial state, some detector inefficiencies, are cancel out. This should work particularly well for the  $e^+e^- \rightarrow \pi^+\pi^-$  channel, where the hadronic state and the monitoring process have a very similar signature.

The BaBar collaboration plans to measure exclusively all main hadronic cross-sections from the threshold up to 3-4 GeV. The first results have already been published (18).

#### 4 Conclusions

Recent years showed a significant progress in the measurement of  $\sigma(e^+e^- \rightarrow \text{hadrons})$  at low  $s$ . The data analysis of the direct measurements performed at VEPP-2M is getting finalized and most of the results are expected to be published in the next 1-2 years. The first results from the new approach, the radiative return measurements, were presented by the KLOE and BaBar collaborations. The new technique shows its great potential and these results will most likely dominate the field for the next 5-7 years. The new high precision results are expected from the VEPP-2000 collider once it starts the operation. These efforts, if successful, will allow to reach a precision below 0.4 ppm for the hadronic contribution to  $(g-2)_\mu$ .

#### 5 Acknowledgments

The author would like to thank S.I. Eidelman, F.V. Ignatov, B.I. Khazin and E.P. Solodov for their help in preparation of this paper. This work is supported

in part by grants RFBR-03-02-16280, RFBR-04-02-16217 and RFBR-04-02-16223.

### References

1. G. W. Bennett *et al.*, Phys. Rev. Lett. **92** (2004) 161802.
2. M. Davier *et al.*, Eur. Phys. J. C **31** (2003) 503.
3. J.Z. Bai *et al.*, Phys. Rev. Lett. **88** (2002) 101802.
4. S.A. Dytman, Nucl. Phys. B (Proc. Suppl.) 131 (2004) 32.
5. R.R. Akhmetshin *et al.*, Phys. Lett. **B527** (2002) 161.
6. R.R. Akhmetshin *et al.*, Phys. Lett. **B578** (2004) 285.
7. R.R. Akhmetshin *et al.*, Phys. Lett. **B476** (2000) 33.
8. M.N. Achasov *et al.*, Phys. Rev. **D66** (2002) 032001; M.N. Achasov *et al.*, Phys. Rev. **D68** (2003) 052006.
9. R.R. Akhmetshin *et al.*, Phys. Lett. **B466** (1999) 392; R.R. Akhmetshin *et al.*, Phys. Lett. **B595** (2004) 101.
10. M.N. Achasov *et al.*, J. Exp. Theor. Phys. 96 (2003) 789.
11. M.N. Achasov *et al.*, Phys. Rev. **D63** (2001) 072002.
12. R.R. Akhmetshin *et al.*, Phys. Lett. **B551** (2004) 27.
13. S.I. Eidelman and S.I. Serednyakov, Nucl. Phys. B (Proc. Suppl.) 131 (2004) 19.
14. M. Davier *et al.*, Eur. Phys. J. C **27** (2003) 497.
15. S. Binner, J.H. Kühn and K. Melnikov, Phys. Lett. **B459** (1999) 279; M. Benayoun *et al.*, Mod. Phys. Lett. **A14** (1999) 2605.
16. A. Aloisio *et al.*, hep-ex/0407048
17. M. Davier, Nucl. Phys. B (Proc. Suppl.) 131 (2004) 82.
18. B. Aubert *et al.* Phys. Rev. **D69** (2004) 011103.



Frascati Physics Series Vol. XXXV (2004), pp. 467-472  
HEAVY QUARKS AND LEPTONS - San Juan, Puerto Rico, June 1-5, 2004

## ELECTRIC DIPOLE MOMENT MEASUREMENTS IN A STORAGE RING

William M. Morse for the EDM in Storage Ring Collaboration  
*Brookhaven National Laboratory*

### ABSTRACT

Sensitive measurements of the electric dipole moment of charged particles in a storage ring experiment are discussed.

### 1 Introduction

Extensive studies have been made of electric dipole moments (EDM) of neutral particles: the neutron and atoms. We are proposing a new sensitive method of measuring the EDM of charged particles in a storage ring. The storage ring provides a clean environment with intense, highly polarized, stable beams with low emittance. The dominant systematic errors for the traditional neutral particle EDM measurement techniques are absent, or highly suppressed.

First we discuss the problems inherent in the traditional neutral particle EDM experimental method, and then introduce the new storage ring method.

The spin precession for a particle with  $\vec{v} = 0$  is:

$$\frac{d\vec{S}}{dt} = \mu\vec{S} \times \vec{B} + d\hat{S} \times \vec{E} \quad (1)$$

where the magnetic moment  $\mu = ge/2mc$ , and  $d$  is the electric dipole moment. For the neutron,  $e/m$  of the proton is used; and  $g_n = -3.8$ . Neutron EDM experiments have been ongoing since the 1950s<sup>1)</sup>. The experiments have been performed in a weak magnetic field, typically  $\simeq 1 \mu\text{T}$ , and a strong electric field, typically  $\simeq 2 \text{ MV/m}$ . The spin precession frequency is measured with the electric field parallel and anti-parallel to the magnetic field. A change in the measured spin precession frequency would be evidence for an EDM.

A systematic error can originate from any stray magnetic field, such as caused by leakage currents from the electric field electrodes, which changes when the electric field is flipped. In a real neutral particle EDM experiment with  $\vec{v} \neq 0$ , the spin precession is given by

$$\frac{d\vec{S}}{dt} = \mu\vec{S} \times (\vec{B} + \vec{v} \times \vec{E}) + d\hat{S} \times (\vec{E} + \vec{v} \times \vec{B}) \quad (2)$$

The  $\mu(\vec{S} \times (\vec{v} \times \vec{E}))$  term represents a systematic error to the EDM measurement since this term changes sign when the electric field changes sign. The  $d(\hat{S} \times (\vec{v} \times \vec{B}))$  term increases the EDM signal, but it is negligible compared to the electric field term.

## 2 The Storage Ring Case

Next we discuss the situation for a charged particle in a storage ring<sup>2)</sup> where there are both magnetic and electric fields. The spin precession due to the magnetic dipole moment is:

$$\frac{d\vec{S}}{dt} = \frac{e}{mc}\vec{S} \times \left[ \left( a + \frac{1}{\gamma} \right) \vec{B} - a \frac{\gamma}{\gamma+1} (\vec{\beta} \cdot \vec{B}) \vec{\beta} - \left( \frac{g}{2} - \frac{\gamma}{\gamma+1} \right) \vec{\beta} \times \vec{E} \right] \quad (3)$$

where  $a = (g - 2)/2$  is the anomalous magnetic moment. The spin precession due to the electric dipole moment is simply:

$$\frac{d\vec{S}}{dt} = d(\hat{S} \times (c\vec{\beta} \times \vec{B})) \quad (4)$$

We have neglected the  $d\hat{S} \times \vec{E}$  term in the above equation, since this change in the EDM signal is small compared to the magnetic field term. The spin precession due to the electric dipole moment is about the  $\vec{\beta} \times \vec{B}$  vector. This is easily understood as follows. The charge displacement given by  $\vec{d} = q\vec{\delta}$  creates a torque due to electric field created because the charged particle is moving in a circular orbit under the influence of the Lorentz force:

$$\vec{\tau} = q\vec{\delta}c\vec{\beta} \times \vec{B} = d\vec{S}/dt . \quad (5)$$

For the simple case of  $\vec{\beta} \cdot \vec{B} = \vec{\beta} \cdot \vec{E} = 0$ , the precession of the spin with respect to the momentum is given by  $\vec{\omega} = \vec{\omega}_a + \vec{\omega}_{edm}$  where

$$\vec{\omega}_a = \frac{e}{mc} \left[ a\vec{B} + \left( \frac{1}{\gamma^2 - 1} - a \right) \frac{\vec{\beta} \times \vec{E}}{c} \right] \quad (6)$$

is the rotation about the vertical ( $\vec{B}$ -field direction) direction that arises because there is an anomalous part to the magnetic moment. The motion about the radial direction

$$\omega_{edm} = d \frac{2}{\hbar} \left( \vec{E} + c\vec{\beta} \times \vec{B} \right) \quad (7)$$

comes from the torque produced by the EDM. The EDM signal is a changing vertical polarization produced by a non-vanishing  $\omega_{edm}$  precession. The size of this polarization is

$$P \frac{\omega_{edm}}{\Omega} \sin(\Omega t + \phi) \quad (8)$$

where  $P$  is the vector polarization of the particle beam and  $\Omega = \sqrt{\omega_{edm}^2 + \omega_a^2}$ . Thus it behooves us to minimize  $\omega_a$ , although for systematic error management  $\omega_a$  should be small but not zero. This can be done by applying a radial electric field of magnitude

$$E_r \simeq aBc\beta\gamma^2 \quad (9)$$

to cancel the  $a\vec{B}$  contribution to  $\omega_a$  in equ. 7. A sensitive EDM measurement requires large electric fields with a small anomalous magnetic moment.

### 3 Choice of Beams

Unfortunately, there are no particles with  $a = 0$ . Leptons have  $a \simeq 0.001$ . The electron in a storage ring generates a large amount of synchrotron radiation, which introduces an additional systematic error: an electron beam in a storage ring develops a polarization component along the direction of the magnetic field vector. The situation is better for the muon since synchrotron radiation intensity falls as  $1/m^4$ . The Storage Ring EDM collaboration has submitted an LOI to JPARC <sup>3)</sup> for a muon EDM experiment at the level of  $10^{-24} e \cdot cm$  statistical and  $\simeq 10^{-27} e \cdot cm$  systematic error. The large statistical error is because the muon beam derives from a secondary pion beam and is created with very large emittance. Its lifetime also limits the time for observing the EDM precession. The challenge of a MW proton beam creating an intense muon beam means that this experiment is at least one decade, and perhaps two decades away from physical realization. Thus other cases that can reach the same level of sensitivity in a shorter time are preferred.

The deuteron has a small anomaly,  $a = -0.143$ . Intense, low-emittance beams with high polarization and efficient polarimeters are readily available. We are proposing a measurement of the deuteron EDM with statistical and systematic errors  $\simeq 10^{-27} e \cdot cm$ .

### 4 Systematic Errors

The EDM measurement systematic error from leakage currents from the electric field electrodes which produce a weak magnetic field gives a negligible systematic error since the magnetic field is strong ( $\simeq 10^{-1}T$ ), not weak ( $\simeq 10^{-6}T$ ), as in the neutral beam EDM experiments. Furthermore, in the Storage Ring EDM measurement, the  $\vec{v} \times \vec{E}$  precession term is not a systematic error, but rather a tool to control the  $g - 2$  precession rate to increase the statistical sensitivity to the EDM. In order to control systematic errors, the  $g - 2$  precession rate is varied, as discussed below.

We have extensively studied spin dynamics systematic errors <sup>4)</sup>. We have found only one first-order spin dynamics systematic effect for the Storage Ring EDM experiment: if the electric field applied around the ring is not in a plane

Table 1: *Symmetry of E/B Systematic Effects and their Estimated Size. Only (1) is a first order effect. The symbol  $\otimes$  means in conjunction with. Errors 2-3 are non-commutation errors due to rotations about the longitudinal and vertical axis.*

<i>Systematic Effect</i>	<i>cc/ccw</i>	<i>Integrate Ring</i>	<i>Flip Polar. Direction</i>	$\delta\omega_\alpha$ <i>Depend.</i>	<i>Error [e · cm]</i>
(1) Non Planar E-field	-	+	+	+	$\approx 10^{-27}$
(2) $B_L \sin(k2\pi s/L) \otimes \Delta B_V \cos(k2\pi s/L)$	-	+	+	+	$< 10^{-29}$
(3) $B_L \sin(k2\pi s/L) \otimes \delta\omega_\alpha$	-	-	-	-	$< 10^{-29}$
(4) $(\vec{E} \cdot \vec{B} \neq 0 \otimes \delta\omega_\alpha)$	+	-	+	-	$< 10^{-29}$
(5) $E_V / (\beta\gamma^2) \otimes \Delta p/p$	-	+	+	+	$< 10^{-29}$

with respect to itself, then the spin will precess about the radial direction:

$$\omega_{syst} \simeq \frac{\mu E_V}{\beta c \gamma^2} \quad (10)$$

where  $E_V$  is the component of the electric field which is not in the plane. This effect, relative to the EDM effect, changes sign when injecting clock-wise (CW) vs. counter-clockwise (CCW). Thus, conceptually, the EDM signal is a difference in the measured deuteron spin precession rate about the  $\vec{\beta} \times \vec{B}$  direction when injecting CC vs. CCW. The deuteron has a small electric quadrupole moment. The systematic effect due to the deuteron electric quadrupole moment has been evaluated for the EDM storage ring method:  $\sigma_d < 10^{-30} e \cdot cm$ , and thus is negligible. Our experiment is not sensitive to the polarizability of the deuteron, since the torque  $\vec{d} \times \vec{E} = 0$ .

Second order systematic errors, which require two errors in the electric/magnetic fields, are given in Table 1 along with their symmetry characteristics. The sign (+) means the systematic error has the same symmetry as the EDM and is thus indistinguishable from it under the applied symmetry. The sign (−) means the opposite, i.e. the effect has the opposite sign as the EDM and thus can be minimized under the applied symmetry. The tests, besides CW/CCW are: that detectors around the ring measure the same precession rate, flipping the initial polarization direction of the beam, and that the asymmetry have the correct  $\delta\omega_a$  dependence. Obviously, the second order systematic effects which act only in conjunction with  $\delta\omega_a$  have an incorrect dependence. All second order systematic errors are less than  $10^{-29} e \cdot cm$ , ie. two orders of magnitude less than the non-planar electric field systematic error.

## References

1. N.F. Ramsey Annu. Rev. Nucl. Part. Sci. **40**, 1 (1990).
2. J.D. Jackson, Classical Electrodynamics, John Wiley and Sons, Inc.
3. <http://www.bnl.gov/edm/>
4. F. Farley et al., accepted for publication in Phys. Rev. Lett., hep-ex/0307006.

## FRASCATI PHYSICS SERIES VOLUMES

### Volume I

*Heavy Quarks at Fixed Target*

Eds. S. Bianco and F.L. Fabbri

Frascati, May 31–June 2, 1993

ISBN—88-86409-00-1

### Volume II – Special Issue

*Les Rencontres de Physique de la Vallée d'Aoste –*

*Results and Perspectives in Particle Physics*

Ed. M. Greco

La Thuile, Aosta Valley, March 5–11, 1995

ISBN—88-86409-03-6

### Volume III

*Heavy Quarks at Fixed Target*

Ed. B. Cox

University of Virginia, Charlottesville

October 7–10, 1994, 11

ISBN—88-86409-04-4

### Volume IV

*Workshop on Physics and Detectors for DAΦNE*

Eds. R. Baldini, F. Bossi, G. Capon, G. Panzeri

Frascati, April 4–7, 1995

ISBN—88-86409-05-2

### Volume V – Special Issue

*Les Rencontres de Physique de la Vallée d'Aoste –*

*Results and Perspectives in Particle Physics*

Ed. M. Greco

La Thuile, Aosta Valley, March 3–9, 1996

ISBN—88-86409-07-9

### Volume VI

*Calorimetry in High Energy Physics*

Eds. A. Antonelli, S. Bianco, A. Calcaterra, F.L. Fabbri

Frascati, June 8–14, 1996

ISBN—88-86409-10-9

**Volume VII***Heavy Quarks at Fixed Target*

Ed. L. Köpke

Rhinefels Castle, St. Goar, October 3–6, 1996

ISBN—88-86409-11-7

**Volume VIII***ADONE a milestone on the particle way*

Ed. V. Valente 1997

ISBN—88-86409-12-5

**Volume IX – Special Issue***Les Rencontres de Physique de la Vallée d'Aoste –  
Results and Perspectives in Particle Physics*

Ed. M. Greco

La Thuile, Aosta Valley, March 2–8, 1997

ISBN—88-86409-13-3

**Volume X***Advanced ICFA Beam Dynamics**Workshop on Beam Dynamics Issue for  $e^+e^-$  Factories*

Eds. L. Palumbo, G. Vignola

Frascati, October 20–25, 1997

ISBN—88-86409-14-1

**Volume XI***Proceedings of the XVIII International Conference on  
Physics in Collision*

Eds. S. Bianco, A. Calcaterra, P. De Simone, F. L. Fabbri

Frascati, June 17–19, 1998

ISBN—88-86409-15-X

**Volume XII – Special Issue***Les Rencontres de Physique de la Vallée d'Aoste –  
Results and Perspectives in Particle Physics*

Ed. M. Greco

La Thuile, Aosta Valley, March 1–7, 1998

ISBN—88-86409-16-8

**Volume XIII***Bruno Touschek and the Birth of the  $e^+e^-$* 

Ed. G. Isidori

Frascati, 16 November, 1998

ISBN—88—86409—17—6

**Volume XIV – Special Issue***Les Rencontres de Physique de la Vallée d'Aoste –**Results and Perspectives in Particle Physics*

Ed. M. Greco

La Thuile, Aosta Valley, February 28–March 6, 1999

ISBN—88—86409—18—4

**Volume XV***Workshop on Hadron Spectroscopy*

Eds. T. Bressani, A. Feliciello, A. Filippi

Frascati, March 8–2 1999

ISBN—88—86409—19—2

**Volume XVI***Physics and Detectors for DAΦNE*

Eds. S. Bianco, F. Bossi, G. Capon, F.L. Fabbri,

P. Gianotti, G. Isidori, F. Murtas

Frascati, November 16–19, 1999

ISBN—88—86409—21—4

**Volume XVII – Special Issue***Les Rencontres de Physique de la Vallée d'Aoste –**Results and Perspectives in Particle Physics*

Ed. M. Greco

La Thuile, Aosta Valley, February 27–March 4, 2000

ISBN—88—86409—23—0

**Volume XVIII***LNF Spring School*

Ed. G. Panzeri

Frascati 15–20 May, 2000

ISBN—88—86409—24—9

**Volume XIX***XX Physics in Collision*

Ed. G. Barreira

Lisbon June 29–July 1st, 2000

ISBN—88-86409-25-7

**Volume XX***Heavy Quarks at Fixed Target*

Eds. I. Bediaga, J. Miranda, A. Reis

Rio de Janeiro, Brasil, October 9–12, 2000

ISBN—88-86409-26-5

**Volume XXI***IX International Conference on Calorimetry in  
High Energy Physics*

Eds. B. Aubert, J. Colas, P. Nédélec, L. Poggioli

Annecy Le Vieux Cedex, France, October 9–14, 2000

ISBN—88-86409-27-3

**Volume XXII – Special Issue***Les Rencontres de Physique de la Vallée d'Aoste –  
Results and Perspectives in Particle Physics*

Ed. M. Greco

La Thuile, Aosta Valley, March 4–10, 2001

ISBN—88-86409-28-1

**Volume XXIII***XXI Physics in Collision*

Ed. Soo-Bong Kim

Seoul, Korea, June 28–30, 2001

ISBN—88-86409-30-3

**Volume XXIV***International School of Space Science – 2001 Course on:  
Astroparticle and Gamma-ray Physics in Space*

Eds. A. Morselli, P. Picozza

L'Aquila, Italy, August 30–September 7, 2000

ISBN—88-86409-31-1

**Volume XXV**

*TRDs for the 3rd Millennium Workshop on  
Advanced Transition Radiation Detectors for  
Accelerator and Space Applications*

Eds. N. Giglietto, P. Spinelli  
Bari, Italy, September 20–23, 2001  
ISBN—88–86409–32–X

**Volume XXVI**

*KAON 2001 International Conference on CP Violation*

Eds. F. Costantini, G. Isidori, M. Sozzi  
Pisa Italy, June 12th 17th, 2001  
ISBN—88–86409–33–8

**Volume XXVII – Special Issue**

*Les Rencontres de Physique de la Vallée d’Aoste –  
Results and Perspectives in Particle Physics*

Ed. M. Greco  
La Thuile, Aosta Valley, March 3–9, 2002  
ISBN—88–86409–34–6

**Volume XXVIII**

*Heavy Quarks at Leptons 2002*

Eds. G. Cataldi, F. Grancagnolo, R. Perrino, S. Spagnolo  
Vietri sul mare (Italy), May 27th June 1st, 2002  
ISBN—88–86409–35–4

**Volume XXIX**

*Workshop on Radiation Dosimetry: Basic Technologies,  
Medical Applications, Environmental Applications*

Ed. A. Zanini  
Rome (Italy), February 56, 2002  
ISBN—88–86409–36–2

**Volume XXIX – Suppl.**

*Workshop on Radiation Dosimetry: Basic Technologies,  
Medical Applications, Environmental Applications*

Ed. A. Zanini  
Rome (Italy), February 56, 2002  
ISBN—88–86409–36–2

**Volume XXX – Special Issue**

*Les Rencontres de Physique de la Vallée d'Aoste –  
Results and Perspectives in Particle Physics*

Ed. M. Greco

La Thuile, Aosta Valley, March 9–15, 2003

ISBN—88-86409-39-9

**Volume XXXI**

*Frontier Science 2002 – Charm, Beauty and CP,  
First International Workshop on Frontier Science*

Eds. L. Benussi, R. de Sangro, F.L. Fabbri, P. Valente

Frascati, October 6–11, 2002

ISBN—88-86409-37-0

**Volume XXXII**

*19th International Conference on x-ray and Inner-Shell Processes*

Eds. A. Bianconi, A. Marcelli, N.L. Saini

Università di Roma La Sapienza June 24–28, 2002

ISBN—88-86409-39-07

**Volume XXXIII**

*Bruno Touschek Memorial Lectures*

Ed. M. Greco, G. Pancheri

Frascati, May 11, 1987

ISBN—88-86409-40-0

**Volume XXXIV**

*Les Rencontres de Physique de la Vallée d'Aoste –  
Results and Perspectives in Particle Physics*

Ed. M. Greco

La Thuile, Aosta Valley, February 29 – March 6, 2004

ISBN88-86409-42-7